

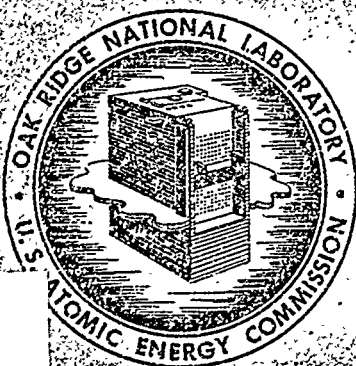
ORNL
MASTER COPY

60
580

ORNL-3697 *Wef*

UC-41 - Health and Safety
TID-4500 (34th ed.)

HEALTH PHYSICS DIVISION
ANNUAL PROGRESS REPORT
FOR PERIOD ENDING JULY 31, 1964



ChemRisk Document No. 580

OAK RIDGE NATIONAL LABORATORY
operated by
UNION CARBIDE CORPORATION
for the
U.S. ATOMIC ENERGY COMMISSION

Printed in USA. Price \$6.00. Available from the Clearinghouse for Federal
Scientific and Technical Information, National Bureau of Standards,
U.S. Department of Commerce, Springfield, Virginia

LEGAL NOTICE

This report was prepared as an account of Government sponsored work. Neither the United States, nor the Commission, nor any person acting on behalf of the Commission:

- A. Makes any warranty or representation, expressed or implied, with respect to the accuracy, completeness, or usefulness of the information contained in this report, or that the use of any information, apparatus, method, or process disclosed in this report may not infringe privately owned rights; or
- B. Assumes any liabilities with respect to the use of, or for damages resulting from the use of any information, apparatus, method, or process disclosed in this report.

As used in the above, "person acting on behalf of the Commission" includes any employee or contractor of the Commission, or employee of such contractor, to the extent that such employee or contractor of the Commission, or employee of such contractor prepares, disseminates, or provides access to, any information pursuant to his employment or contract with the Commission, or his employment with such contractor.

ORNL-3697
UC-41 - Health and Safety
TID-4500 (34th ed.)

Contract No. W-7405-eng-26

HEALTH PHYSICS DIVISION ANNUAL PROGRESS REPORT

For Period Ending July 31, 1964

K. Z. Morgan, Director
W. S. Snyder, Assistant Director
E. G. Struxness, Assistant Director

OCTOBER 1964

OAK RIDGE NATIONAL LABORATORY
Oak Ridge, Tennessee
operated by
UNION CARBIDE CORPORATION
for the
U. S. ATOMIC ENERGY COMMISSION

Summary

PART I. RADIOACTIVE WASTE DISPOSAL

1. Liquid Injection into Deep Permeable Formations

Movement of radionuclides through porous media is due to movement of the transporting water, but is also affected by the ion exchange properties of the medium. Calculations were made for the movement of the solution and radiostrontium through a slab of Berea sandstone and were confirmed by experimental data.

The behavior of chloride as a water tracer is complicated by its repulsion by negatively charged soil colloids. The relative exclusion of chloride is especially complicated when clay minerals are present and restricted in their degree of lattice expansion. However, these effects would be decreased as the concentration of electrolyte is increased and would probably be rather insignificant in "clean" sandstones having low specific surface and high porosity, especially if most of the surfaces were sufficiently separated to permit full development of an electric double layer.

Anion exclusion gives a good measure of lattice expansion and collapse of hydrobiotite systems, thereby providing a rather accurate method for measuring the distribution of surface charge density of these interstratified materials.

2. Disposal by Hydraulic Fracturing

Four water injections were made in the injection well at 986 and 966 ft. These tests confirmed other evidence that a fluid loss additive is not a necessary component of the mix to be used in the waste injections. Also, since in all cases the fracturing pressure was well above the overburden pressure, these tests furnished presumptive evidence that horizontal fractures were formed.

On the last water injection, the sand-erosion technique for slotting failed to cut the casing after 20 min at a jet pressure of 2600 psi. To determine the reason for this failure, tests were run by the Halliburton Company in their test well. During the tests, it was observed that considerable oscillation of the jetting tool was cutting a much wider slot than previous experience had suggested. This was probably responsible for failure of the slotting operation at Oak Ridge, since more time would be required to erode a wider slot and no allowance had been made for such a factor. In any case, these tests showed that the 5½-in. casing of the injection well could be cut despite the oscillation of the jet if a jet pressure of 4000 psi and a cutting time of 30 min were used.

An estimate of the probable operating cost of the shale fracturing plant shows that the cost of the mix and the well life are the significant variables. The well life can be significantly extended by making the batch size large. For this reason it seems probable that the direction of future work will be toward larger batch sizes than are being injected at the present time.

A hazards analysis of the shale fracturing experiment has been completed. It was concluded that the waste solution to be used in the first series of injections would be so low in specific activity that no significant hazard would result from its use. The other principal hazard involved in the shale fracturing experiment — that of working with high-pressure equipment — has been minimized where possible by installing this equipment in cells.

To verify that the Densometer system could be used to control the solids-to-solution ratio at very low proportions of cement, a mix test was run by the Halliburton Company. The Densometer controlled the density of the slurry to within 0.1 lb/gal of the desired density, which is entirely acceptable. It was found, however, that the

density indicated by the Densometer was uniformly 0.8 lb/gal lower than the true density. This error in calibration can be compensated for by a change in the Densometer setting.

Following construction of the surface plant, a series of five injections was made to determine the performance of the plant and the underground behavior of waste slurries of different compositions.

In the first injection (February 13), 37,000 gal of synthetic concentrated waste solution was mixed with 23,400 lb of attapulgite drilling clay and injected at a depth of 945 ft. This injection was made to check the operation of the surface plant and to evaluate a nonsetting mix.

In the second injection (February 21), 27,300 gal of synthetic concentrated waste solution with 30 curies of ^{198}Au tracer was mixed with about 170,000 lb of a cement-base mix and injected at a depth of 924 ft. This injection was made to evaluate a mix with a low cement concentration and to determine whether the activity in the grout sheet could be detected at the observation well.

In the third injection (April 3), 33,500 gal of a mixture of synthetic concentrated waste solution and actual intermediate-level waste was mixed with about 518,000 lb of a cement-base mix and injected at a depth of 912 ft. This injection was made to demonstrate that concentrated radioactive waste solutions similar to those to be produced by the ORNL waste evaporator can be fixed permanently underground.

In the fourth injection (April 17), 36,000 gal of intermediate-level waste solution was mixed with about 381,000 lb of a cement-base mix and injected at a depth of 900 ft. This injection was made to evaluate a mix for dilute waste solutions.

In the fifth injection (May 28), 148,000 gal of a mixture of synthetic waste solution and actual intermediate-level waste was mixed with about 1,040,000 lb of a cement-base mix and injected at a depth of 890 ft. This injection was made to test the surface plant during an extended (11-hr) disposal operation and to determine the underground behavior of large injections.

Minor difficulties were encountered with various components of the surface plant during the injections. These difficulties were corrected as they appeared. In general, the operation of the surface plant has been smooth and satisfactory; the disposal operation has become almost routine as experience has been accumulated.

Evaluation of the mixes used in the five injections and determination of the underground behavior of the grout sheets cannot be accomplished until cores of the formation have been recovered. Coring is expected to begin in July.

3. Disposal in Natural Salt Formations

Renovation of the topside facilities at the Carey Salt mine, Lyons, Kansas, is essentially complete. A new 7-ton capacity headframe has been erected; the existing hoist has been reworked, all electrical circuits and switchgear have been replaced, and the hoist house has been renovated. Drilling has started on the 19.1-in.-ID waste-charging shaft.

Mining equipment for the underground work has been purchased and installed in the mine. Cleanup of the main access tunnels in the mine is in progress. Layout of the experimental area has been completed, and mining should start early in July 1964.

Concurrent with the mine cleanup, plastic flow gages are being installed along the access tunnels and near the experimental area. The information from these gages will be used to determine the effect of increased temperature on stability of the mine.

Design of equipment for handling and storing the radioactive fuel assemblies is essentially complete. Fabrication of all handling and storage equipment is in progress, with the exception of the fuel element canisters. A draft of the hazards report on the shipment of fuel assemblies between Idaho and Lyons, Kansas, has been completed.

Laboratory tests of 1000-hr duration on pillar models made from Lyons salt have been run by the U.S. Bureau of Mines. Tests were run at pillar stresses ranging from 4000 to 10,000 psi. From the results of these tests, an empirical equation was derived which correlates well with measured vertical closure rates in the Lyons and Hutchinson mines in openings up to 70 years old.

The isolated $2 \times 8 \times 10$ ft heated model room (wall temperature approximately 140°C), after more than a year of heating, has a closure rate ten times higher than it had at ambient temperature.

4. Clinch River Study

Analyses of stable chemical constituents in discharge-weighted water samples from the Clinch and Tennessee Rivers show that variations in constituent concentrations are not great; bicarbonate is the predominant anion and calcium the predominant cation. Seasonal variations in concentration of several of the constituents were detected. Calculation of correlation coefficients for constituent pairs indicated that turbidity, apparent color, centrifuged color, suspended solids, iron, and manganese concentrations varied in a similar manner.

Measurement of gross gamma radioactivity in 146 cores of Clinch River bottom sediment has shown that radioactive sediment up to 8.7 ft thick is present in the river. Variations in radioactivity with depth were observed in several of the cores. The general pattern of variation is strikingly similar to the pattern of annual ^{137}Cs releases at White Oak Dam, and is assumed to be the result of continuous sedimentation of cesium-bearing clay particles suspended in the water.

Regulation of flow in the Clinch River due to power generation at Melton Hill Dam will produce greater daily changes in flow conditions than did similar operations at Norris Dam. Tracer studies were conducted to study the effect of releases from Melton Hill Reservoir on dispersion of radioactive releases from White Oak Dam. Pulses of tracers released twice daily from the creek, simulating summer conditions, were observed to occur at about 10 AM and noon each weekday at the ORGDP water treatment plant intake. During the normal weekend shutdown of operations at Melton Hill Dam, the mass of tracer released from the creek built up in the river. Power releases on Monday moved this maximum concentration of tracer downstream. The minimum dilution for the momentary peak on Monday at ORGDP water intake was computed to be 50. This minimum dilution is only about ten times less than the median dilution observed prior to construction of Melton Hill Dam.

Change in flow conditions due to Melton Hill Dam has necessitated a change to automatic proportional sampling of the river water.

Analyses of fish taken from the Clinch River show that about 2.5% of the maximum permissible intake (MPI) would be received from eating 37 lb

of fish per year. Radiation levels near filter beds in water plants upstream and downstream from White Oak Creek are at background.

Bottom sediments from the Clinch River were selectively leached. Salts between a pH of 6 to 8 removed less than 10% of the ^{60}Co , ^{106}Ru , and ^{137}Cs , though up to 80% of the ^{90}Sr . At lower pH's up to 80% of the ^{90}Sr and ^{60}Co were leached. At higher pH's up to 50% of the ^{106}Ru and up to 20% of the ^{60}Co are released.

5. Movement of Radionuclides in Terrestrial Environment

Core samples taken in and around waste pits 2 and 3 show that most of the ^{137}Cs and ^{90}Sr is concentrated in sludge and precipitates in the pits and on the first few inches of shale comprising the side walls and bottoms of the pits. By the use of tritiated water as a tracer, it has been observed that the normal rate of ground-water movement in the waste pit area is about 0.5 ft/day.

Most of the 700 curies of ^{137}Cs in the bed of White Oak Lake occupies highly selective exchange sites on the illitic clay fraction of the lacustrine sediment and can be desorbed only by disruption of the clay lattice structure.

Analyses of selected samples obtained from the upper 0.2 ft of White Oak Creek bottom sediment indicate that less than $5 \times 10^5 \mu\mu\text{c}$ of ^{137}Cs and substantially smaller quantities of ^{60}Co and ^{106}Ru are stored in this zone. The inference is drawn that the residence time for the less-than-63- μ sediment in this zone is relatively short and that the material is scoured during higher-than-normal stages and transported into White Oak Lake.

As an extension of information gained from laboratory studies on radionuclide sorption, field studies on deliberately contaminated plots, using ^{137}Cs , have been started in order to correlate areal and vertical redistribution of the nuclide with natural factors, including biologic, meteorologic, and pedologic factors.

6. Mineral Exchange Studies

In sorbing trace concentrations of strontium, ideal ion exchange behavior, based on mass action

expressions, was exhibited by several of the clay minerals under special conditions. Hydrrous sesquioxides sorbed strontium preferentially, and the strontium sorption curve did not yield the predicted slope for ideal behavior. Several soil materials were tested; the local Conasauga shale, whose sorption indicated strong influence of sesquioxides at alkaline pH, was shown to behave according to the mass action law when the free iron oxide was removed.

Ethylenediaminetetracetate (EDTA) forms a more stable complex with calcium than with strontium. In a waste solution containing calcium as a major ionic component, the major breakthrough of strontium through an ion exchange column can be delayed by complexing part of the calcium with EDTA. However, the delayed breakthrough of strontium is gained at the expense of increased "leakage" of strontium through the ion exchange column.

7. Engineering, Economics, and Safety Evaluations

Costs of permanent storage of calcined radioactive wastes in concrete vaults were five to seven times greater than those for storage in salt, and costs for storage in rooms mined out of granite formations were twice those for storage in salt mines. This economic advantage, plus greater safety, makes salt the preferred choice.

Study of the comparative costs for disposal in concrete vaults, hard-rock mines, and salt mines was based on the costs for disposal in salt developed in a previous study. In the preliminary study, costs for excavation of salt were assumed to be \$2/ton. During the year, work has continued on a final report of costs for disposal in salt. Excavation costs have been calculated as a function of the amount of salt mined yearly, and \$2/ton was found to be a reasonable figure for a relatively large operation. Costs per ton for small operations would be higher.

Estimates were made of the movement of ^{90}Sr , ^{106}Ru , and ^{137}Cs in Conasauga shale following a hypothetical release of reactor fuel-reprocessing waste from a tank. Computations were based on hydrologic and exchange characteristics of the local formation.

In Conasauga shale, ^{90}Sr would apparently move quite rapidly in an acid waste system, even if the

acid would be neutralized by calcite (CaCO_3) in the formation. Movement of ^{90}Sr in an alkaline waste solution would be much slower due to the formation of insoluble compounds, in addition to the greater holdup by ion exchange. Ruthenium-106 would be expected to move rapidly in either acid or neutralized waste systems, but it presents little long-term hazard due to its relatively short half-life. The movement of ^{137}Cs would be expected to be slow because of its strong fixation by the ion exchange sites of the illitic fraction of the Conasauga shale.

8. Related Cooperative Projects

The U.S. Geological Survey has continued to obtain partial-record base-flow and crest-stage records for the area. In addition, a geologic map of White Oak Creek Basin, with an explanatory text, has been issued. A generalized soils map of the basin is being prepared.

The work of the multiagency steering committee for the Clinch River Study has continued.

Three alien guests have been on assignment during the past year.

Several members of the Section have continued to participate in the following activities: the ASA Committee N5, the AEC Advisory Committee on Deep-Well Disposal, the ASCE Committee on Sanitary Engineering Aspects of Nuclear Energy, and various ORNL special committees. Members have also contributed to the journal *Nuclear Safety* and have served with the Nuclear Safety Information Center.

In addition, courses and lectures have been given for ORSORT, Vanderbilt University, University of Tennessee, and the U.S. Public Health Service.

PART II. RADIATION ECOLOGY

9. Radioactive Waste Area and Radiation Effects Studies

Statistical analyses of sedges growing on White Oak Lake bed indicated that length of inflorescence was mostly correlated with the air dose rate of gamma radiation at 1 m above ground surface. Some of the natural vegetation around the unshielded Health Physics Research Reactor exhibited the first visible effects of radiation

damage. After a period of winter dormancy, new growth produced in several species of forest trees contained many morphological abnormalities. The damaged vegetation occurred at distances of 10 to 20 m from the reactor, and total cumulated dose was approximately 600 to 140 rads (tissue dose in air) respectively. Radiation effects studies completed this year included fast-neutron exposures from the HP RR, and gamma-radiation exposures from both a ^{137}Cs field source and the White Oak Lake bed. Among the findings were that all acute fast-neutron doses ranging from 100 to 500 rads resulted in 100% mortality of pine seedlings although the time required to reach complete needle mortality varied widely within and between dose groups. Pine seedlings subjected to chronic gamma irradiation from White Oak Lake bed for 178 days exhibited 100% needle mortality, while controls averaged only about 10%. During the past fiscal year, a study was initiated to determine the seasonal changes in nuclear volumes of local tree species. Shoot apexes were measured monthly from 14 local species. An analysis of variance showed that most species increased significantly ($P < 0.01$) in size before shoot elongation. Initial spring activity of nucleic acids in shoot apexes is thus earlier in eastern Tennessee than would be anticipated from any external evidence. Continuing work on the use of metaphosphate glass dosimeters demonstrated that low-Z glass rods are subject to fading in sunlight. Predosed rods lost 37 to 46% of the dose during the first 6 hr of exposure to sunlight. Fading was also related to total predose since high predose rods had a significantly greater ($P < 0.01$) percentage loss than low predose rods.

Mud-dauber wasps that used radioactive mud from the liquid waste pits were found to be affected by the ionizing radiation. In the case of the species *Sceliphron cementarium*, the effect of the radiation is to reduce the successful emergence by a significant 40% ($P < 0.001$), and radioactive nest cells showed a higher mortality from parasites. The maximum integrated dose received by a developing wasp in this study was determined to be 10,630 rads. Continuing studies on radiocesium accumulation and elimination by various species of insects demonstrated the usefulness of these techniques for measuring food consumption and insect production under field conditions. Also, energy flow through the herbivorous insect population may now be estimated,

by using food consumption rates for herbivores calculated with steady-state equilibria for radiocesium. Preliminary studies of radiation response of several insect species including crickets and grain beetles were reported.

Hematological studies of native mammals initiated in 1962 were completed this year. The objective of these studies was to determine the effects of endogenous and environmental factors on the blood of indigenous species. Over 10,000 hematological measurements were made for over 2000 mammals of 41 species belonging to 11 families representing 7 orders. These studies have shown that factors such as age, sex, certain diseases, certain parasites, injuries, confinement, and season govern hematopoietic changes. The largest and most consistent change in normal serum patterns is characteristically demonstrated by albumin. Significant alterations in this component have been observed as a seasonal variation and as a result of numerous stress factors. One seasonal variation has been a higher albumin value for the sera of animals sampled in the water than from the same animals sampled in other seasons. Laboratory-bred cotton rats had higher albumin percentages than field-trapped members of the same species. A coefficient of correlation of -0.360 between total white cell count and albumin-globulin ratio was calculated for the white-footed mouse ($0.05 > P > 0.02$). If subsequent calculations show this relationship to be a general one, it would imply that a low albumin in combination with a high total globulin value might well serve as readily as a high white blood cell count as an indication of general infection or trauma in an individual or a wild population.

10. Processes and Components of Terrestrial Ecosystems

An inventory of total ^{137}Cs distribution among the tree-soil compartments of the tagged, tulip poplar ecosystem constructed from data collected during and at the end of the first growing season suggests that about 50% of the initial tag is found in the litter, soil, and smaller root components at the end of the first growing season. The maximum burden found in the canopy 4 to 6 weeks after inoculation was reduced by 60% in late September. This reduction is due to three processes: (1) export of cesium from foliage to woody tissue during

mature and senescent stages of leaf development, which accounts for the greatest amount of reduction; (2) removal of radiocesium from foliage by rain and dew leaching prior to mid-September, which accounts for about 4% of the total reduction; and (3) reduction in concentration (μC per gram of dry weight) by the formation of new tissue. Accumulation of surface income of ^{137}Cs within the organic litter layer and surface 2 cm of soil was measured in sample units which prevented root entry. Results from these sample units indicate that half of the surface income was contained within the organic layer and more than 80% was contained within the organic layer plus the surface 2 cm of mineral soil. Dispersion of ^{137}Cs outside the tagged forest ($20 \times 25 \text{ m}$) area by falling leaves was measured at the end of the second growing season. Sampling measurements indicated that 2.67 mc (representing $5.34 \mu\text{C}$ per m^2 of study site) of ^{137}Cs was transported outside the study area by falling leaves. Based on this figure and on canopy concentrations in both years, it is estimated that 20% of the leaves from the tagged trees fell outside the study area. Of this 20% more than three-fourths of this activity is located within a 10-m zone around the perimeter of the study area. A new phase of work in the ^{137}Cs -tagged forest was initiated this year to broaden the understanding of the behavior of this radionuclide in the various life stages of tulip poplar trees. Seeds collected from tagged trees were germinated, and patterns of translocation were followed through the early growth phases. These studies seem to indicate that cesium follows similar pathways to sugars and other foods which may be stored in tissue such as cotyledons used to sustain the early growth of seedlings. Transfers of this radionuclide in young seedlings are also rapid, as has been demonstrated for mature trees of this species.

Microbial uptake of stable cesium and cobalt was proportional to their concentrations in the environment over a concentration range of 2 to 3 orders of magnitude. There was no marked isotopic selection for either of these elements. Uptake of ^{134}Cs was proportional to the concentration of ^{134}Cs in the substrate. When microbes were separated from a tagged substrate by water, agar, or semipermeable film, microbial uptake was proportional to the concentration of ^{134}Cs in these intermediates. Microbial concentration factors for different substrates varied with the availability

of the tag. On fresh-leaf litter with readily available cesium, microbial concentration relative to the substrate was twice as high as on weathered, old litter with less readily available cesium.

11. Clinch River and Related Aquatic Studies

The series of analyses of stable strontium in white crappie (*Pomoxis annularis*) flesh and bone was completed, and it was possible to test the relation of the distribution of stable strontium and ^{90}Sr between the environment and the fish. The calcium and strontium concentrations in fish flesh and bone were relatively constant throughout the year with no seasonal variation and probably reflects the relative constancy of these elements in Clinch River water. Data on calcium and strontium concentrations in Clinch River water were published previously. There is a relatively good agreement between the specific activities in fish bone and water. These data suggest that for any constant release of ^{90}Sr to the river, it is possible to predict the consequent ^{90}Sr content of fish bone. The short biological half-life of strontium in fish flesh shows that measurements of ^{90}Sr in flesh will reflect the environmental concentrations at the time the fish were collected. The long biological half-life of strontium in fish bone suggests that ^{90}Sr concentrations in bone will reflect the average environmental concentrations during the lifetime of the fish. Studies on uptake and accumulation of strontium and calcium by algae and snails representing contrasting types of biogeochemical systems are reported. Uptake of calcium by the algae was found to be primarily a function of the media concentrations of calcium with a slight inverse influence by strontium in the media. A slight relative increase in calcium uptake at very low calcium concentrations indicates an increase in uptake efficiency at limiting levels of calcium and also suggests that calcium is required by the alga. Experiments also suggested that uptake is directly proportional to strontium in the media, with an enhancement in uptake at very low media concentrations of calcium, suggesting that strontium was used by the algae in place of calcium when calcium was in short supply. In snails the deposition of both calcium and strontium depends primarily on the respective concentrations of these elements in the immediate environment. The data also suggest

that there is a simple substitution of strontium uptake for that of calcium by snail shell when environmental calcium is deficient. Strontium uptake increased with increasing environmental strontium concentrations and decreased with increasing environmental calcium concentrations. Increased environmental strontium depresses strontium uptake and increased environmental calcium enhances strontium uptake.

Previously, it was reported that there is an increase of newly occurring chromosomal aberrations in the natural population of *Chironomus tentans* from White Oak Creek. This population of Diptera, which is receiving a calculated dose of 230 rads/year of chronic environmental radiation, has been sampled annually since 1960. Two new inversions, each involving several bands, were observed once in the additional collection from the irradiated area. No new inversions were observed in the additional collections from the control populations. The finding of these two new inversions supports the previous conclusion that there is an increase of newly occurring aberrations in the White Oak Creek population. These newly occurring aberrations are eliminated by selection or genetic drift and are not maintained in the gene pool of the population. The increased mutation rate produced by the chronic irradiation in the White Oak Creek population has not reduced the amount of chromosomal polymorphism in this natural population.

12. Theoretical Systems

To provide a conceptual basis for understanding radiation effects and the fate of nuclides in ecosystems, analog computer solutions of competition equations, both with and without radiation stress, were generated. The equations investigated were the Lotka-Volterra system which has received major attention in classical population ecology. There are four possible cases of outcome between two competing Lotka-Volterra species: (1) s_1 or s_2 , but not both, survives depending upon initial conditions; (2) s_1 survives to the exclusion of s_2 regardless of initial conditions; (3) s_2 only survives independent of initial conditions; and (4) both s_1 and s_2 coexist at equilibrium. For all four of these cases it was found that introducing radiation stress in the form of a rarefying term in the equations altered both transient and steady-state responses of the sys-

tem. Where the final result was determined in the unstressed cases only by the degree of competition between the two species, under radiation stress their respective reproductive potentials became an important factor. In addition, it was found that effects of radiation tend to be minimized when interactions between the competing species are greater; the stronger the coupling between two competing systems, the less the effect of an outside perturbing influence.

Previous compartment models for transfer of substances in ecological systems are generalized in the form of a system of differential equations. The system is $\dot{V} = VF$, where \dot{V} is instantaneous change in the state vector V , and F is a matrix of fractional transfer coefficients expressing the exchange of material between compartments. Estimations of F for a variety of real ecosystems are being made utilizing data from ecological and physiological sources to provide more realistic computer simulations.

PART III. RADIATION PHYSICS

13. Theoretical Radiation Physics

Distributions of dose and dose equivalent in anthropomorphic phantoms were computed for protons up to 400 Mev. A theory has been developed and a code written to give dose distributions in a proposed high-energy silicon dosimeter from isotropically incident protons of energies up to 400 Mev.

Dose distribution with linear energy transfer (LET) has been computed for a cylindrical anthropomorphic phantom irradiated with a beam of neutrons. A Monte Carlo code was used, and wide variations were found for the dose per unit LET at various points in the phantom for various neutron energies from thermal to 2.5 Mev.

A new fast-neutron spectrometer, the "Vectrometer," has been proposed. This device consists of two separated planar arrays of Geiger counters which measure the track lengths of recoil protons resulting from neutron irradiation of the hydrogen gas in the device. A simple expression yields the neutron energy from these track lengths. A prototype is under construction.

The simultaneous emission of bremsstrahlung and transition radiation from an electron-irradiated dielectric slab has been analyzed theoretically.

It has been shown that proper measurements of these radiations may be analyzed to yield the mean square scattering angle of electrons in the material. The mean free path of hot electrons in a free-electron gas has been determined from many-body perturbation theory. Previous workers have neglected exchange scattering processes altogether. It is found that such processes may make an important difference in the calculated energy and angular distribution of the hot electrons after collision. The effect of surface losses upon the stopping power of charged particles has been analyzed using a semiclassical approach. The dispersion and damping of surface plasmons have been computed from a semiclassical theory. The results are presented as a function of the wave vector of the surface plasmon. In connection with work done by the Experimental Radiation Physics Group, computer codes have been written to evaluate the optical constants of materials from measured reflectivities and transmittivities of plane parallel foils made of these materials.

The analysis of the dispersion for a medium in which a linear proton beam interacts with a stationary ionized medium indicates that there is a multiple instability. Physical conditions under which a multiple instability may occur were studied, and various types of plasma beam systems were investigated with particular reference to the frequency, ranges, and rates of growth of the excited waves.

An analysis was made of a dispersion equation for a medium in which a helical electron beam interacts with a stationary plasma. The interaction was investigated with particular reference to superluminous, subluminal, and counterstreaming instabilities.

The interaction of an ion beam of small intensity moving with velocity $c\beta$ (where c is the velocity of light) through a stationary plasma was investigated under the assumption that the beam and the waves resulting from the interaction are aligned along the direction of an impressed static magnetic field and that the frequencies of the excited waves are sufficiently high so that the motion of the ions perturbed by these waves can be neglected.

A plasma-beam system is investigated in which an electron beam of small intensity moving with velocity βc interacts with a cold plasma immersed in a magnetic field. It is assumed that the beam and the excited wave resulting from the interaction are aligned along the direction of the magnetic

field and that $(1 - \beta^2) \gg 1/\eta$, where η is the ion-to-electron mass ratio. The frequencies and growth rates of the excited waves are calculated.

14. Experimental Radiation Physics

The interaction of low-energy electrons with a number of benzene derivatives has been studied, using the swarm method. Control of the energy distribution in the electron swarm has been achieved, which allows discrimination between the different electron capture processes. The detailed study of the benzene derivatives aids in the understanding of the interaction of free electrons with more complicated organic molecules of great biological interest.

Improvements in the electron time-of-flight technique for electron diffusion measurements using a Geiger counter detector have been carried out by utilizing an empirical instrumental response characteristic to unscramble the drift time distributions observed in water vapor and ethylene. A new apparatus for drift measurements has been constructed and has undergone preliminary testing. This apparatus avoids problems associated with Geiger counter detectors by using an electron multiplier and differential pumping. A new method has been worked out and equipment has been constructed for determining oscillator strengths for electronic transitions in the vacuum ultraviolet region. This method uses pressure pulses of millisecond duration in the absorption cell and the pulsed light from a spark discharge source in order to avoid uncertainties in pressure and optical absorption associated with differential pumping. First application of the new method will be to determine oscillator strengths in argon.

An experiment is being developed which will determine the lifetime of temporary negative ions produced by unimolecular electron capture. The technique is designed to measure lifetimes from 10^{-9} to 10^{-6} sec and will be applied to the study of electron capture in water and other polar molecules. Monochromatic light from electron plasmon decay has been observed for the first time from aluminum foils a few hundred angstroms in thickness bombarded by 80-kev electrons. The sharp peak at 815 Å determines the plasma energy precisely at 15.3 eV. The optical constants of evaporated silver films were determined between 2500 and 3700 Å, the region of the Wood's

transparency. Optical transmission curves derived from these constants showed a minimum whose depth was proportional to the projection of the E vector of the incident light on the foil normal, thus indicating a resonant coupling of the radiation with electronic motion across the foil. No optical constants in the vacuum ultraviolet spectral region are available for indium, so these were measured also for use in evaluation of plasmon decay experiments.

The Keplertron was used to study Auger electron production in infinite isotropic radioactive copper media. The continuous slowing-down model neglects Auger production, which therefore must be studied experimentally. Further calibration data for the instrument were taken, and an electron slowing-down spectrum in gold was measured for the first time.

15. Physics of Tissue Damage

The optical reflectivity of hot-pressed pyrolytic graphite was measured from 1100 to 3000 Å, where no data were available. The optical constants showed that an electron resonance occurs at 6.9 eV, as predicted from energy loss experiments and as explained by Ichikawa as due to plasma excitation.

A new technique was developed for measuring charged-particle interactions in layers a few hundred atoms thick. These layers are vacuum evaporated on a thin silicon monoxide insulator and thus need not be self-supporting. Range measurements on protons from 2 to 10 keV were made with this method.

Further work on the time-of-flight electron beam monochromator resulted in a gun which produced a 2-nsec burst of electrons, an improved transistor amplifier, positive proof that the electron drift time is characteristic of its energy, and some preliminary observations of nitrogen vibrational excitation by 2-eV electrons.

Vacuum diffusion pump oil was irradiated in the LITR and then used in the pump. A trace amount of the radioactive oil escaped into the vacuum system, where it deposited on the walls to a maximum depth of 6 Å (less than a monomolecular layer). This technique should be useful in vacuum ultraviolet spectroscopy, where minute layers of oil change the optical properties of gratings, thin films, etc.

The so-called "gas effect" noted previously in thermoluminescence experiments was found to be a temperature effect with the gas playing the role of a heat transfer agent. Thus the doubt cast on previously obtained data is removed. Sample holders were fabricated from boron carbide since it is the only material we have found which is tissue equivalent, nonfluorescing, nonthermoluminescing, electrically and thermally conducting, structurally strong over a wide range of temperature, and capable of holding a high vacuum.

16. Professional Health Physics Training

A first-year graduate course, Applied Radiation Physics, was given at Vanderbilt University and the University of Tennessee for a total enrollment of 30 students. A course in Health Physics of 30 contact hr was given at ORSORT. Citizens of Pakistan, Austria, India, and Israel received training and experience with various sections of the Health Physics Division. Lectures were given at ORINS by a Health Physics Division staff member assigned to ORINS temporarily. Lectures and tours of the Laboratory were provided for personnel of the U.S. Public Health Service, the University of North Carolina, and the ORNL Orientation Program. Twenty holders of AEC Health Physics Fellowships completed a year of graduate training at Vanderbilt University and the University of Tennessee. Several fellowship holders elected to do their thesis work for the master's degree in the Health Physics Division at ORNL. A 1-year advanced graduate level course in radiation physics has been planned to be given at the University of Tennessee during the 1964-1965 academic year.

PART IV. RADIATION DOSIMETRY

17. Dosimetry Applications

The emphasis of the radiation dosimetry studies has been on the accumulation of human-exposure data, especially the dosimetry for the survivors of the nuclear bombings of Hiroshima and Nagasaki. Refinements were made in the "free-field" data and dose-distribution functions developed for typical Japanese houses. The equations were

developed by a "multiple regression and correlation" fit to the extensive data from Operation BREN. Computed values for the "shielding factor" at a point in a Japanese house, using these equations, were within 6% of the experimental values from weapons tests in 50% of the cases.

18. Dosimetry Research

Other areas of investigation included small detector research, spectrometry, instrumentation, and dosimetry for radiobiological research. Fading characteristics of metaphosphate detectors were measured, advancements were made in several types of spectrometers, energy response functions were determined for dosimetry systems, and accurate dose-conversion factors were determined for PuBe and PoBe sources.

19. HPRR Operations and Special Projects

The Health Physics Research Reactor was used in a wide assortment of radiobiological, dosimetric, physical, and ecological studies with participating researchers from numerous laboratories and several countries. A feasibility study was completed for the construction of an intense 14-Mev neutron source for the BREN tower; construction began in June 1964.

PART V. INTERNAL DOSIMETRY

20. Internal Dose Estimation

The program of the Internal Dose Estimation Section continues in the study and improvement of methods for assessment of exposure due to radioactive materials that may enter the body. As in the past, data have been gathered and interpreted to serve as a basis for estimation of dose from a source within the body. Although animal data are not disregarded, the principal emphasis is on direct data on man.

The work reported this year includes a study of the retention of HTO by an employee exposed in the course of his work. The retention is closely approximated by the sum of two exponentials, one showing an elimination half-time of about 9 days

and the other about 37 days. Although multiexponential retention functions have been observed in animals, this is the first direct observation of such a retention in man that has been reported; however, indirect evidence has been reported. This study involved members of the Health Physics Technology Section and Applied Health Physics Section, as well as members of the Internal Dose Estimation Section.

21. Stable Element Metabolism

Much useful data have been accumulated from the studies of trace elements in human tissues, diets, and excreta, although the newer studies involving diets and excreta are only partially complete at this time. Among other applications of these data, a distribution of stable strontium in the body has been studied and is found to differ rather significantly from the distribution of ^{226}Ra under chronic conditions of exposure. It is found that approximately 99% of the stable strontium is in the skeleton, whereas the skeleton burden of ^{226}Ra due to the natural background has been estimated to be only about 80% of the body burden.

22. A Two-Compartment Model with Random Variable Flows

Since estimates of dose depend upon a metabolic model, the Internal Dose Estimation Section must construct models for the metabolism of many substances and understand various factors that influence the retention of radionuclides in the body, particularly with a view to extrapolation from animals to man. Two such exploratory studies are reported here. A system of compartments has been constructed which are connected during periods of time distributed randomly, thus simulating bone sites that may be remodeling during various periods of time. Only the simplest of such systems, a two-compartment model, has been studied, and it is found that certain distributions of the time periods during which exchanges between compartments are permitted produce a power-function type of retention.

23. Studies on the Internal Exposure/External Exposure Equivalence Relation

A second study is reported which suggests a possible method of relating effects due to an internal source with effects due to external radiation. In effect, this amounts to a method for interspecies extrapolation at low levels of exposure.

24. Comments on Intake Guides for Various Isotopes and Isotopic Mixtures of Uranium

In the application of maximum permissible concentration (MPC) values, or intake guides, for uranium as provided by NCRP and ICRP, questions arise frequently concerning a "curie" of natural uranium, which has a special definition in these recommendations. Other questions relate to the fact that limiting values for some of the isotopes are based on considerations of chemical toxicity, while for other isotopes it is the radiological hazard that is limiting; thus uncertainties in the computation of values for mixtures of the isotopes are encountered. In this study simple formulas, additional MPC values, and explanations are given as an aid in resolving these and other similar problems.

25. On the Estimation of a Systemic Body Burden of Plutonium

Two studies are reported which test, to a very rough degree, the validity of a computer program reported previously which purports to estimate the intake and body burden of ^{239}Pu on the basis of urinary excretion. The one study uses data on an employee who had a long record of exposure to ^{239}Pu . From the urinary excretion data, an intake pattern and retention are estimated and compared with autopsy estimates of the tissue burdens. The study suggests that the metabolic model is not inconsistent with the data, but certain parameters of the model may be rather different for this individual and this material from the values given in ICRP Publication 2. The second study uses data on dogs given Pu-nitrate by intravenous injection and by inhalation. The program seems to predict a qualitatively plausible pattern of intake to blood, and the estimates of lung deposition obtained by the code are within a factor of 2 of the estimates by the experimenters.

PART VI. HEALTH PHYSICS TECHNOLOGY

26. Aerosol Physics

Surface contamination measurement techniques, described in previous annual reports, have been used in a study of particle resuspension in a room. A tracer dust is dispersed and allowed to settle in an area simulating a small work room of average cleanliness. Contamination samples are collected by a person wearing coveralls and a respirator. The number of tracer particles found on the respirator filter is related to the number that would have been inhaled without a respirator. Three tests using 3.1- μ -diam ZnS (fluorescence) and one test using 2- μ CuO (neutron activation analysis) indicate that a person working in the room is likely to inhale 1 particle/hr for every 2900 (CuO) to 5600 (ZnS) particles per square meter of surface.

Agglomerates of submicroscopic thorium dioxide particles, produced by exploding thorium metal wires, were allowed to settle on a stainless steel surface. The settled aggregates were approximately 1 to 10 μ in diameter. Laboratory-scale studies show that these agglomerates can be redispersed by air jets, by mechanical abrasion, and by adhesion to contacting surfaces; however, the redispersion efficiencies are lower than those observed for 1.5- and 5- μ -diam solid ThO_2 particles.

The question of what happens physically just prior to, during, and after a particle is reentrained in an airstream is being studied with the use of a small wind tunnel. Particles adhering to test surfaces are exposed to a known flow structure of air in the wind tunnel. The dynamics of the particles moving on the surface are observed by microphotography using a pulsed light beam. Borosilicate glass beads (28.9 μ CMD; $\sigma = 13\%$) on a glass surface display a variety of effects in an airstream of 5300 cm/sec average velocity ($\text{Re} = 24,400$). About half of the beads did not move during 2.5 sec of exposure, approximately one-third of the beads left the surface without having rolled, and the remainder moved along the surface in straight lines parallel to the direction of flow. Some of the beads that moved along the surface stopped, and some left the surface. There is an indication that the mechanisms involved in moving particles along the surface contributes a

time-dependent factor to the redispersion of particles in an airstream.

Basic interactions between particles and surfaces, which determine the scale of forces required for resuspension, are being studied by applying known forces to remove particles from various surfaces. Borosilicate glass beads (28.9 μ , CMD), dispersed by settling on quartz surfaces, are subjected to known removal forces by vibrating the test surface. Attempts to remove the glass beads by applying 2.8×10^{-3} dyne of force normal to the surface were unsuccessful. This level of force was repeated for nonradioactive beads on friction-charged and on uncharged quartz. In a third experiment, glass beads were activated by thermal neutrons (~ 0.4 curie/g) and were dispersed on an uncharged quartz plate. After aging for 2.5 days, the test plate and radioactive particles were found to have a net positive charge of 7×10^{-10} coulomb/cm². Despite the presence or absence of electrostatic charge, there were no glass beads removed by the application of forces up to 90 times gravity.

Tests have continued in exploration of the capabilities of the exploding-wire aerosol generator to produce and disperse a wide variety of submicron aerosols. Well-dispersed gold aerosols with reproducible mass density can be produced by the electrical explosion of gold wires. The aerosol yield is observed to depend on the wire length, wire diameter, and voltage used for explosion. In other tests, gold and platinum wires were twisted together and exploded simultaneously by the

electrical discharge. Particulate matter collected from the aerosol produced by such explosions consists of alloys of Au-Pt, giving some indication that metallic vapors were produced which mixed homogeneously.

27. Applied Internal Dosimetry

Emphasis of the ORNL whole-body counting program is on counting probable and potential exposure cases and on obtaining baseline counts on unexposed employees. During the past year, 1370 persons were counted for a total of 1568 human counts. Approximately 74% of the counts showed an essentially normal human spectrum. Several employees were counted for indications of ⁹⁰Sr-⁹⁰Y intake following three separate incidents of suspected exposure. One employee was estimated to have approximately 90% of the maximum permissible lung burden. Initial estimates in the other two incidents amounted to only 25 and 30% of the permissible total body burden; in both cases the estimates represent transient GI tract deposits which were eliminated rapidly. The computer program for processing whole-body count data has been made more flexible and can analyze data from about 75% of the routine counts. Computer plotting of in vivo spectra has been discontinued as not economical. Several different source-phantom configurations for calibrating the whole-body counter are being studied.

Contents

SUMMARY	iii
 PART I. RADIOACTIVE WASTE DISPOSAL	
1. LIQUID INJECTION INTO DEEP PERMEABLE FORMATIONS	3
Movement of Radionuclides Through Natural Porous Media	3
Comparison of Tritiated Water and Chloride Ion as Water Tracers.....	6
Interlayer Cesium Fixation by Biotite and Vermiculite Layers	9
2. DISPOSAL BY HYDRAULIC FRACTURING	10
Water Injection Tests	10
Hazards Analysis.....	11
Cost Analysis.....	12
Plant Construction.....	12
Waste Injections.....	12
3. DISPOSAL IN NATURAL SALT FORMATIONS	19
Demonstration of High-Level Waste Solids Disposal	19
Rheological Studies and Tests of Plastic Flow Instrumentation	27
Radiolytic Production of Chlorine from Salt	31
4. CLINCH RIVER STUDY	32
Chemical Composition of Clinch River Water	32
Bottom Sediment Studies.....	34
Dispersion Studies.....	35
Safety Analysis	37
Behavior of Nuclides Associated with Clinch River Sediments	40
5. MOVEMENT OF RADIONUCLIDES IN TERRESTRIAL ENVIRONMENT	43
Evaluation of Fission Product Distribution and Movement In and Around Chemical Waste Seepage Pits 2 and 3.....	43
Occurrence and Retention of Radionuclides in the Sediments of White Oak Lake.....	45
Hydrology of White Oak Creek Basin	46
Field Investigations of the Movement of Radionuclides Deposited on Soils	47

6. MINERAL EXCHANGE STUDIES	49
Sorption of Strontium by Clay Minerals.....	49
The Effect of EDTA on Calcium-Strontium Exchange by Hydrobiotite	52
7. ENGINEERING, ECONOMIC, AND SAFETY EVALUATIONS	54
Engineering and Economic Evaluation	54
Tank Safety Evaluation.....	56
8. RELATED COOPERATIVE PROJECTS	60
Geologic and Hydrologic Studies by U.S. Geological Survey	60
Cooperation of Other Agencies in ORNL Studies	60
Visiting Investigators from Abroad	60
Nuclear Safety Review	61
Committee Work	61
Participation in Educational Programs.....	61
Nuclear Safety Information Center.....	61
 PART II. RADIATION ECOLOGY 	
9. RADIOACTIVE WASTE AREA AND RADIATION EFFECTS STUDIES	65
Analysis of Growth Responses of Two Sedge Species on White Oak Lake Bed.....	65
Vegetation Studies Around the HPRR.....	66
Radiation Studies on Forest Tree Species.....	66
Plant Physiological and Biochemical Phenomena as Affected by Ionizing Radiation	68
Nuclear Volume Measurements.....	69
Environmental Influences on Responses of Metaphosphate Glass	70
Transport of Radioactive Materials by Mud-Dauber Wasps	71
Radiocesium Accumulation and Feeding by Willow Leaf Beetles (<i>Chrysomela knabi</i> Brown).....	73
Biological Half-Life for Radiocesium in Aphids.....	74
Measurement of Heterotrophic Productivity with Radioactive Tracers	74
Radiation Sensitivity of Insects	76
Metabolism of Crickets	76
Strontium-90—Yttrium-90 Beta Source	78
Hematology of Native Mammals	79
10. PROCESSES AND COMPONENTS OF TERRESTRIAL ECOSYSTEMS	85
First-Year Budget of ^{137}Cs in the Tagged <i>Liriodendron</i> Forest	85
Transfer of Radiocesium to Untagged Understory Plants in a Tagged Forest	86
Transfer and Distribution of ^{137}Cs Within the Forest Floor.....	87
Dispersion of ^{137}Cs Outside of Tagged Forest	89
Translocation of ^{137}Cs from Seed into New Growth of Tulip Poplar Seedlings.....	90
Microbial Mineralization and Immobilization of Radionuclides.....	92

Microbial Effect on Uptake of Radionuclides by Higher Plants	92
Soil Classification and Survey	93
11. CLINCH RIVER AND RELATED AQUATIC STUDIES	95
Calcium and Strontium in White Crappie Flesh and Bone	95
Uptake and Accumulation of Strontium and Calcium by Algae and Snails.....	96
Biological Half-Life of ^{134}Cs in Carp and Two Aquatic Insects.....	101
Population Genetics and Radiation Effects Studies on <i>Chironomus tentans</i>	102
Safety Evaluation of Clinch River Fisheries.....	103
12. THEORETICAL SYSTEMS	104
Effects of Radiation Stress on Interspecific Competition	104
A Generalized Compartment Model for Ecosystems	108
Related Activities	109

PART III. RADIATION PHYSICS

13. THEORETICAL RADIATION PHYSICS	113
Dose Calculations for High-Energy Protons	113
Response of Charged Particle Detectors to High-Energy Protons	115
Conceptual Design of a Dosimeter for High-Energy Protons.....	116
Distribution of Dose Resulting from Broad-Beam Irradiation of a Man-Sized Cylindrical Tissue Phantom	117
Charged Particle Vectrometer	124
Optical Bremsstrahlung and Transition Radiation from Irradiated Matter	125
Exchange Correction to the Mean Free Path of Hot Electrons and Holes in Metals	125
The Effect of Surface Losses in Stopping-Power Theory	125
The Dispersion and Damping of Surface Plasmons.....	126
Optical Properties of Metals	127
Multiple Instability in a Plasma-Beam System	127
Interaction of a Plasma with a Helical Electron Beam	128
Plasma-Beam Instability in the Hartree-Appleton Approximation.....	130
Interaction of a Stationary Plasma with an Electron Beam	130
14. EXPERIMENTAL RADIATION PHYSICS.....	131
Electron Capture in Organic Molecules	131
Electron Time-of-Flight Studies (Geiger-Mueller Detector).....	134
Electron Time-of-Flight Techniques.....	134
Oscillator Strength Measurements in the Vacuum Ultraviolet Region	136
Lifetimes of Negative Ions.....	136
Detection of Plasma Radiation from Electron-Bombarded Aluminum Foils.....	138
The Optical Constants and Resonance Absorption of Vacuum Evaporated Silver Films	139
Spherical Electrostatic Analyzer and Slowing-Down Spectra in Copper and Gold	142

15. PHYSICS OF TISSUE DAMAGE.....	144
Optical Properties of Pyrolytic Graphite	144
Range of Charge for Low-Energy Protons in Aluminum	145
Time-of-Flight Electron Beam Monochromator.....	147
Tracer Studies of Diffusion Pump Oil Deposition.....	150
Importance of Thermal Equilibrium in Thermoluminescence Measurements	150
16. PROFESSIONAL HEALTH PHYSICS TRAINING	152

PART IV. RADIATION DOSIMETRY

17. DOSIMETRY APPLICATIONS	155
Dose Distribution Functions for Japanese Houses.....	155
Air-Ground-Interface Effects	157
Metaphosphate-Glass Microdosimeters	158
18. DOSIMETRY RESEARCH	159
Response of a Neutron-Insensitive Gamma-Ray Dosimeter as a Function of Photon Energy.....	159
Neutron Dose Conversion Factors for PuBe and PoBe Sources	160
Experimental Calibration of Fission-Foil Threshold Detectors	160
A Feasibility Study for a Proposed Neutron Spectrometer.....	162
Neutron Leakage Normalizing Channel for HPRR.....	162
DOSAR Portable Scaler.....	162
HPRR Fast-Neutron Spectrum Using the ${}^6\text{Li}(n,\alpha){}^3\text{H}$ Reaction.....	163
19. HPRR OPERATIONS AND SPECIAL PROJECTS	165
Thermal-Neutron Pile	165
Operation HENRE	165
Health Physics Research Reactor Operations.....	168

PART V. INTERNAL DOSIMETRY

20. INTERNAL DOSE ESTIMATION	173
Urinary Excretion of Tritium Following Exposure of Man to HTO – A Two-Exponential Model	173
21. STABLE ELEMENT METABOLISM	178
Tissue Analysis Laboratory Progress Report	178
Trace Elements in Human Tissue: Rib and Vertebra	179
Trace Elements in Diets and Excreta – Preliminary Study.....	185
Distribution of Stable Strontium in Bone and Soft Tissues and its Application to Metabolism of Strontium-90	189
22. A TWO-COMPARTMENT MODEL WITH RANDOM VARIABLE FLOWS.....	193
Two-Compartment Model	194

23. STUDIES ON THE INTERNAL EXPOSURE/EXTERNAL EXPOSURE EQUIVALENCE RELATION	199
24. COMMENTS ON INTAKE GUIDES FOR VARIOUS ISOTOPES AND ISOTOPIC MIXTURES OF URANIUM	202
A Curie of Natural Uranium	202
Chemical Toxicity vs Radiation Damage as a Basis for Estimating Permissible Intake Values.....	203
Maximum Permissible Exposure Values for Mixtures of the Uranium Isotopes.....	204
Single Intake Guides for Uranium	206
25. ON THE ESTIMATION OF A SYSTEMIC BODY BURDEN OF PLUTONIUM	207

PART VI. HEALTH PHYSICS TECHNOLOGY

26. AEROSOL PHYSICS	213
Redispersed of Settled Particles in a Room.....	213
Measurement of Agglomerate Contaminants on Surfaces	215
Observation of Particle Reentrainment from Surfaces	216
Adhesion of Particles to Surfaces.....	218
Production of Gold and Gold-Platinum Aerosols by Exploding Wires	220
International Symposium on Surface Contamination	222
27. APPLIED INTERNAL DOSIMETRY	222
ORNL in Vivo Gamma-Ray Spectrometry Facility	222
In Vivo Detection and Measurement of ^{90}Sr - ^{90}Y Internal Contamination.....	223
Computer Program for in Vivo Counting Data.....	225
Developments in the ORNL in Vivo Gamma-Ray Spectrometry Facility.....	225
Iodine-131 in Milk and in Cattle Thyroids	226
Bioassay and Environmental Monitoring.....	226

PAPERS, PUBLICATIONS, AND LECTURES

PAPERS	229
PUBLICATIONS.....	223
LECTURES.....	241

Part I. Radioactive Waste Disposal

F. L. Parker

—

}
-
-

)

1. Liquid Injection into Deep Permeable Formations

D. G. Jacobs

M. U. Shaikh¹

MOVEMENT OF RADIONUCLIDES THROUGH NATURAL POROUS MEDIA

D. G. Jacobs O. M. Sealand
M. U. Shaikh

Movement of radionuclides through porous media is due to movement of the transporting water but is also affected by ion exchange properties of the medium. In order to relate the migration and dispersion of radionuclides to the calculated movement of the transporting water, experiments have been conducted using a 6 ft by 6 ft by 6 in. slab of gray Berea sandstone (obtained from the Cleveland Quarries Company, Amherst, Ohio).

Analytical solutions for streamlines, equipotential contours, and speed of water movement in the sandstone slab under conditions of an "inverted five-spot" system of injection and relief wells were obtained and plotted by computer-solving of the complex potential equations for the system (Fig. 1.1).² In Table 1.1 the measured pressures at various grid points on the sandstone slab agree quite closely with the calculated values.

The delay of cation movement due to ion exchange was determined using a cylindrical, consolidated core, 10 in. by 1 3/4-in. diameter, enclosed in an aluminum pipe with the space between the core and pipe filled with epoxy. Calcium chloride solution (0.01 *N*) tagged with ³H and ⁸⁵Sr was pumped through the core at a constant rate of 3 ml/min until over 95% breakthrough was observed for ⁸⁵Sr. The strontium *K_d* and the delay factor due to ion exchange were calculated from both the

saturation and leaching data. The delay factor is determined from the proportional amounts of the solute in the solution phase compared to the total amount of solute present and is given by the equation

$$\text{delay factor} = \frac{\bar{v}_{\text{H}_2\text{O}}}{\bar{v}_R} = 1 + \frac{K_d p_b}{f}, \quad (1)$$

where $\bar{v}_{\text{H}_2\text{O}}$ is the mean velocity of water, \bar{v}_R is the mean velocity of the radionuclide, *K_d* is the distribution factor for the radionuclide in milliliters per gram, *p_b* is the bulk density of the sorbent, and *f* is the porosity of the sorbent. A mean value of strontium *K_d* of 0.75 ml/g was found, corresponding to a delay factor of 8.5.

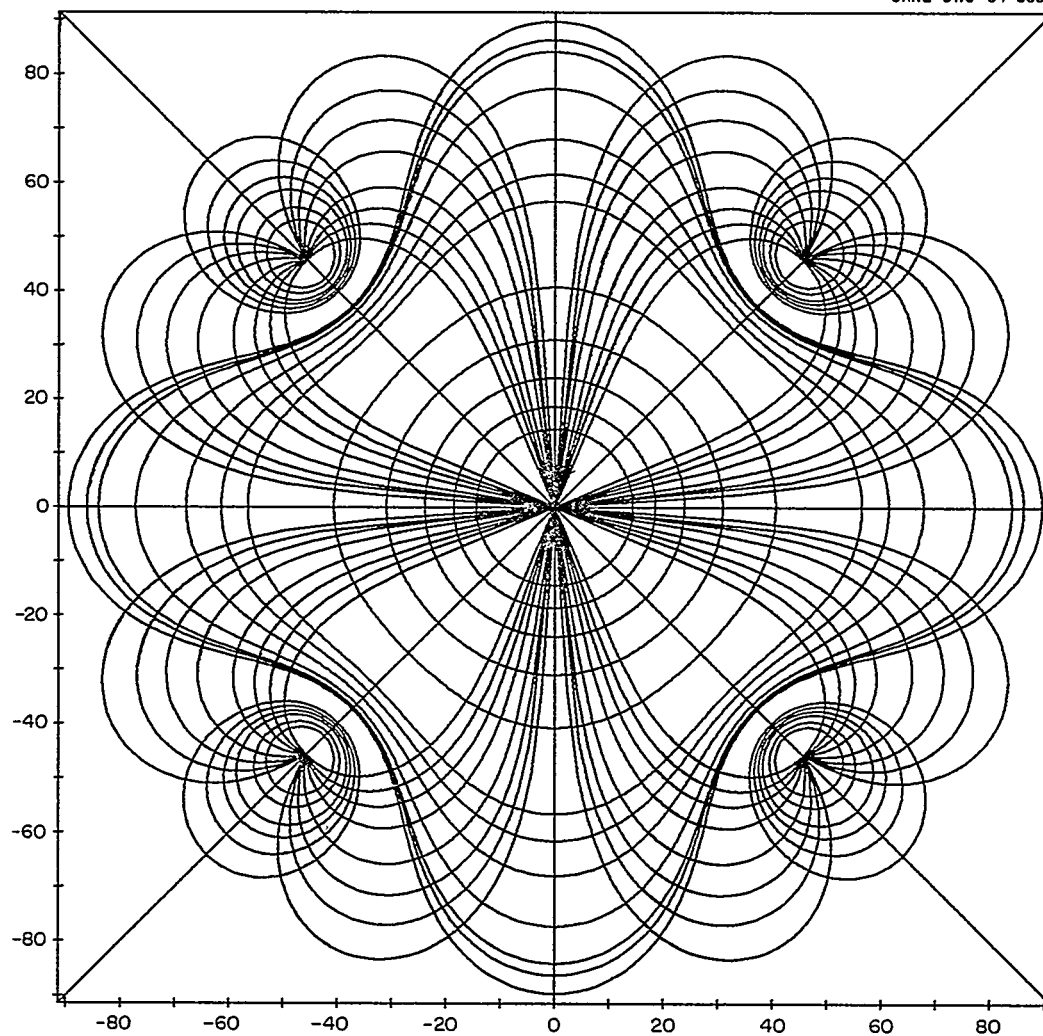
Studies of solution dispersion as a function of velocity were also made with the linear-flow cores. The breakthrough curves shown in Fig. 1.2 were obtained at flow rates of (A) 7.2×10^{-3} cm/sec, (B) 21.7×10^{-3} cm/sec, and (C) 41.9×10^{-3} cm/sec. The measured dispersion coefficients were proportional to the 1.7 power of solution velocity, in close agreement with the 3/2 power obtained by Hashimoto *et al.*,³ rather than the linear relationship found by Rifai *et al.*⁴ Calcium chloride (0.01 *N*) tagged with ³H, ⁴⁵Ca, and ⁸⁵Sr was pumped into the center well of the sandstone slab at a rate of 50 ml/min and withdrawn at the

¹Alien guest.

²L. M. Milne-Thompson, *Theoretical Hydrodynamics*, Macmillan, New York, 1950.

³I. Hashimoto, K. B. Deshpande, and H. C. Thomas, *Peclet Numbers and Retardation Factors for Ion Exchange Columns*, unpublished paper.

⁴M. N. E. Rifai, W. J. Kaufman, and D. K. Todd, *Dispersion Phenomena in Laminar Flow Through Porous Media*, I.E.R. Series No. 93, Issue No. 2, Sanitary Engineering Research Laboratory, Division of Civil Engineering, University of California, Berkeley (July 1, 1956).

UNCLASSIFIED
ORNL-DWG 64-3855

$$R^4 = (A^4/4) (\lambda \sin 4\theta - 4 \cos 4\theta)$$

$$-\phi = \frac{M}{2} \ln \left[\frac{R^8}{R^8 + A^8} + 2R^4 A^4 \cos 4\theta \right]$$

λ	ϕ	
0.03490	0.24000	-1.00000
1.07180	0.27500	-0.80000
2.03800	0.30000	-0.60000
3.35840	0.40000	-0.50000
5.71240	0.60000	-0.40000
8.20000	0.80000	-0.30000
10.98800	1.00000	
15.03200	2.00000	
	3.00000	
	4.00000	
	5.00000	
	6.00000	

Fig. 1.1. Equipotential Contours and Streamlines for an Inverted Five-Spot System with an Injection Well at the Center, Four Relief Wells, and Water Boundaries.

Table 1.1. Comparison of Grid Pressures Measured During Solution Injection with Those Calculated from Theory

Well No. (Equivalent Wells)	Position from Center		Measured Pressure (cm Hg)	Calculated Pressure (cm Hg)
	R (cm)	θ (deg)		
18, 32, 24, 26	22.80	0	4.1	4.0
17, 19, 31, 33	32.23	45	2.8	2.6
11, 27, 23, 39	45.60	0	2.1	1.6
4, 22, 28, 46	68.40	0	0.68	0.56
5, 47, 3, 45, 15 29, 21, 35	72.30	18.4	0.32	0.28
8, 36, 14, 42, 2, 44, 6, 48	82.41	33.7	-0.24	-0.21
16, 30, 20, 34, 10, 12, 38, 40	51.10	26.6	0.72	0.88
1, 7, 49, 43	97.0	45	-0.18	-0.22

four corner relief wells at a rate of 12.5 ml/min per well. Pumping rates were well balanced so that there was no buildup or drawdown of solution in the side pans. Temporary counting difficulties made it impossible to separate the spectra of ^3H and ^{45}Ca , but the observed movement of ^{85}Sr was related to the movement predicted from the geometric flow of water corrected for the delay afforded by ion exchange. The agreement between calculated and observed movement was quite good (Fig. 1.3).

In a second experiment an injection rate of 100 ml/min at the center well was used, but the relief wells were not pumped. This has nearly the same geometric effect on flow as operation of the inverted five-spot on a scale magnified eight times. Calcium-45 was not added to the 0.01 N CaCl_2 solution, but ^3H and ^{85}Sr were assayed at grid points after various time intervals. The migration of ^3H , corrected for the delay afforded by ion exchange, gives an adequate prediction of ^{85}Sr migration (Fig. 1.4). Evidently, in the sandstone slab, the exchange of ^{85}Sr is sufficiently rapid that it causes no measurable dispersion in addition to that observed for ^3H .

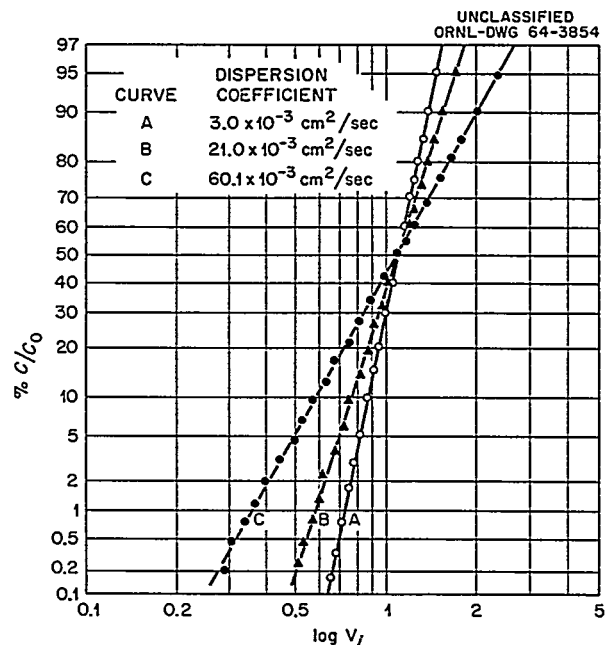


Fig. 1.2. Solution Dispersion in a Sandstone Core at Various Rates of Flow.

UNCLASSIFIED
ORNL-DWG 64-4601A

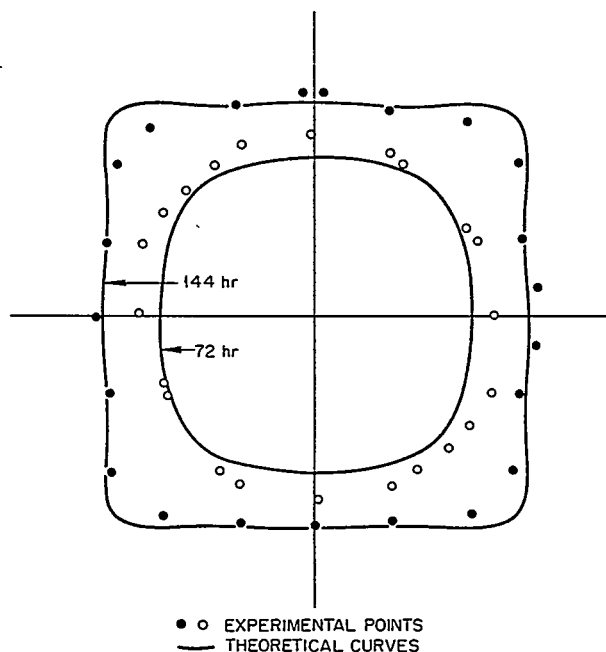


Fig. 1.3. Contours of Mean ^{85}Sr Movement in Sandstone Block as a Function of Time. (●, O = experimental points; — theoretical points).

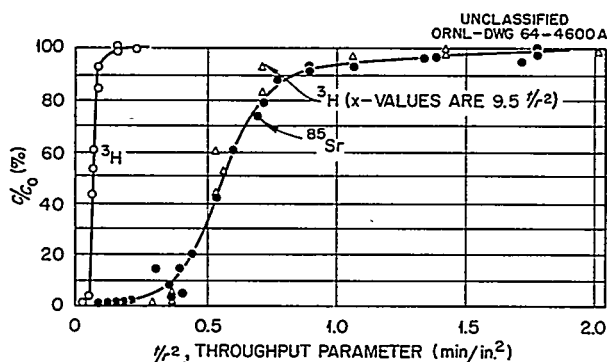


Fig. 1.4. Breakthrough of ^3H and ^{85}Sr as a Function of Time and Distance in Sandstone Block.

COMPARISON OF TRITIATED WATER AND CHLORIDE ION AS WATER TRACERS

D. G. Jacobs M. U. Shaikh O. M. Sealand

One of the properties of an ideal water tracer is that it must not react with the porous medium

through which it is being injected.⁵ Chloride ion has been used as a water tracer and found to move at a greater apparent velocity than does tritium. The present study was undertaken to describe the relative behavior of chloride and tritium tracers on the basis of electrical repulsion of the chloride ion by the negatively charged surfaces of the soil colloids. The basis is that distilled water is approximately $55 M \text{ H}_2\text{O}$, while only about $10^{-7} M$ with respect to H^+ and OH^- ; hence attraction or repulsion of ionic tritium by the charged surface of the clays should not affect the overall behavior of the tritium tracer to any extent. Furthermore, attraction of water dipoles to the surfaces of the soil colloids should occur equally as well with stable water as with the tritium tracer.

Clay minerals generally have a net negative charge which cannot be satisfied locally, since the counterions (ions having the opposite sign of charge from that of the surface) cannot penetrate the dense lattice. Thus the charge can be thought to effectively reside on the surface of the clay lattice, and an electric double layer is established with an accumulation of counterions and a deficit, or negative sorption, of coions (ions having the same sign of charge as the surface). The variation of the electrical potential, ψ , with distance from the surface, X , is given by the standard Gouy-Chapman theory,⁶

$$\frac{d\psi}{dX} = \left(\frac{32\pi n_0 k t}{\epsilon} \right)^{1/2} \sinh \left(-\frac{ze\psi}{2kt} \right), \quad (2)$$

where

- n_0 = the number of ions per cubic centimeter at a point far removed from the charged surface,
- k = the Boltzmann constant,
- t = the absolute temperature,
- ϵ = the dielectric constant of the medium,
- z = the valency of the ions, and
- e = the charge on an electron.

The local concentration of a given type of ion is given by the Boltzmann expression:

$$C_i = C_{i0} \exp \left(-\frac{ze\psi}{2kt} \right). \quad (3)$$

⁵W. J. Kaufman and G. T. Orlob, *J. Am. Water Works Assoc.* 48(5), 559 (1956).

⁶H. R. Kruyt, *Colloid Science*, vol. 1, p. 129, Elsevier, Amsterdam, 1952.

When these equations are combined and integrated over the electric double layer, the amount of coion excluded from the double layer can be calculated. Schofield and Talibuddin⁷ have shown that the integrated expression can be given approximately as:

$$\frac{\Gamma^-}{C} = \frac{q}{\sqrt{z\beta C}} + \frac{4}{z\beta\Gamma}, \quad (4)$$

where

Γ^- = the surface deficit of anions,

q = a factor determined by the ratio of valency of the counterion and the coion (and is equal to 2 for symmetrical salts),

$\beta = 8\pi F^2/1000\epsilon RT = 1.06 \times 10^{15}$ cm/meq when water is used as the solvent at 25°C,

F = the faraday,

ϵ = the dielectric constant of the medium,

R = the molar gas constant,

T = absolute temperature, and

Γ = the charge density of the surface in meq/cm².

The value Γ^-/C obtained from Eq. (3) has units of length and is the effective distance from which coions are excluded from the charged surface. The exclusion volume can be calculated if the surface area is known, or it can be determined experimentally from the slope of the curve when exclusion volume is plotted vs $q/\sqrt{z\beta C}$.

When two successive electric double layers overlap, a correction must be applied. If the surfaces are sufficiently close, however, the exclusion of anions can be adequately depicted by Donnan membrane theory.⁵

Experimental Procedure

For these studies, sodium-saturated hydrobiotite was used as the column filler. It was chosen because its high exchange capacity would accent the effects of anion repulsion and because it has good water transmitting characteristics. Hydrobiotite exists as a mixed-layer mineral, having a rather random mixing of collapsed biotite-type layers, with no interlamellar water, and vermiculite-type layers, with two layers of interlamellar water. The spacing between the charged faces of sodium-

saturated vermiculite layers is 5.55 Å (ref. 8); thus Donnan membrane theory can be applied to the interlamellar region.

The vermiculite columns were preequilibrated with untagged NaCl solutions of the desired concentration. Tritiated water solutions of NaCl of the same concentration and tagged with ³⁶Cl were passed through the column at a constant flow rate. Each run consisted of a saturated and a leaching step, and the same column was used for all runs. Samples were counted simultaneously for ³H and ³⁶Cl, using a Packard Instruments Tri-Carb counter.

A computer program, written by George Atta, Mathematics Division, was used to correct the overlap of the two beta spectra and to fit the experimental data to a chromatographic breakthrough curve of the type^{3,4,9}

$$C/C_0 = \frac{1}{2} \left[1 - \operatorname{erf} \left(\sqrt{P} \frac{V - \bar{V}}{\sqrt{V \bar{V}}} \right) \right], \quad (5)$$

where

C/C_0 = the fraction breakthrough of the tracer,

P = the Peclet number for the column ($P = \frac{N}{2} = \frac{v l}{4D}$, where N is the number of theo-

retical plates in Glueckauf's notation, v is velocity, l is column length, and D is the dispersion coefficient in the notation of Rifai *et al.*),⁴

V = the throughput volume, and

\bar{V} = the equivalent column volume.

Results

Experimental data (Table 1.2) show that the apparent pore volume for tritium remains relatively constant with changes in NaCl concentration. For chloride there is a steady drop in the apparent pore volume with decreasing NaCl concentration. If the charged surfaces of the hydrobiotite were sufficiently separated to permit full development of an electric double layer, a plot of the measured exclusion volume vs the right side of Eq. (3) would yield a straight line with an intercept of zero and

⁷R. K. Schofield and O. Talibuddin, *Discussions Faraday Soc.* 3, 51 (1948).

⁸R. E. Grim, *Clay Mineralogy*, p. 74, McGraw-Hill, New York, 1953.

⁹E. Glueckauf, *Trans. Faraday Soc.* 51, 34 (1955).

Table 1.2. Behavior of Tritiated Water and Chloride Ion Used as Water Tracers in a Column of Hydrobiotite

Concentration of NaCl (M)	Measured Pore Volumes (ml/g)		Measured Anion Exclusion Volume (ml/g)	Calculated Anion Exclusion Volume ^a (ml/g)
	Tritium	Chloride		
1.0	0.656	0.554	0.102 ± 0.004	0.107
0.1	0.628	0.506	0.122 ± 0.005	0.127
0.01	0.628	0.494	0.134 ± 0.006	0.134
0.001	0.628	0.479	0.149 ± 0.005	0.149
0.0004	0.624	0.462	0.162 ± 0.005	0.162

^aBased on an external surface area of 1.15 m²/g and an interlamellar volume of 0.127 ml/g with a volume charge density of 5.93 N.

a slope corresponding to the surface area. The linear portion of the curve (Fig. 1.5) has a slope corresponding to 1.15 m²/g, but the X intercept is 0.127 ml/g, which is a measure of the interlamellar volume where the electric double layers overlap.

The measured exchange capacity is 0.753 meq/g, and the total accessible internal and external surface area is calculated from the experimental data to be 4.59×10^6 cm²/g; thus the mean surface charge density is 1.64×10^{-7} meq/cm². Using this value, the second term of Eq. (4) is evaluated as 2.3×10^{-8} cm, and the volume charge density of the internal pore volume is 5.93 N. These numerical values were then used in recalculating the anion exclusion volumes given in Table 1.2.

To ensure that the above explanation of internal and external effects was correct, another series of experiments was conducted in which the hydrobiotite was subjected to potassium treatment for collapse of the vermiculite layers or to sodium tetraphenyl boron treatment for expansion of the biotite layers. In this series 0.01 M NaCl solutions were used. The results, compiled in Table 1.3, provide evidence that the model does provide an accurate description of the system, because, as the biotite expands, the exclusion volume increases, and as the vermiculite collapses, the volume decreases.

In the case of expanded hydrobiotite, corrections for interlamellar exclusion of anions are predominant. This is due to nearly complete exclusion of anions from the interlamellar spacings which con-

tribute up to 30% of the total pore volume, while the electric double layer established at the external surface of the hydrobiotite excludes chloride for an average distance of 59 Å, corresponding to about 0.007 ml/g.

It was also noted that the breakthrough curves were steeper for chloride than for tritium, which is reasonable, since the tritium must penetrate

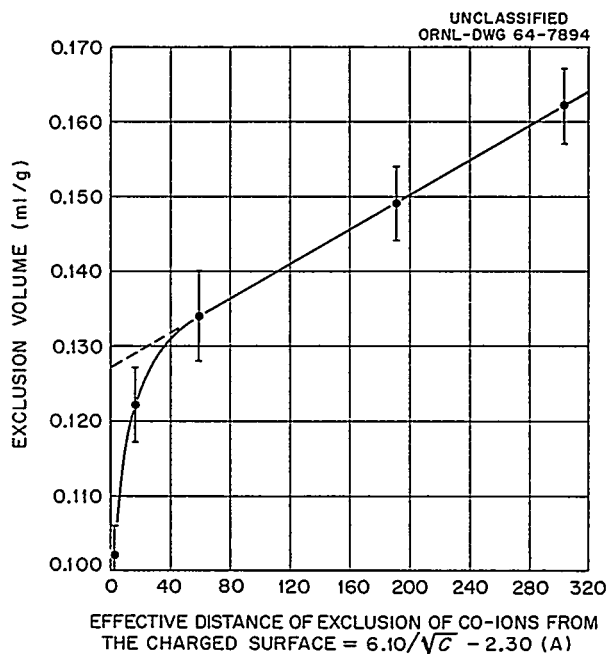


Fig. 1.5. Chloride Exclusion by Hydrobiotite.

Table 1.3. Effect of Lattice Collapse on Anion Exclusion by Hydrobiotite

Hydrobiotite Treatment	Exchange Capacity (meq/g)	Measured Chloride Exclusion Volume (ml/g)
Sodium tetraphenyl boron (5 times)	1.31	0.207
Sodium tetraphenyl boron (4 times)	1.29	0.201
Sodium tetraphenyl boron (3 times)	1.12	0.190
Sodium tetraphenyl boron (2 times)	1.12	0.188
Sodium tetraphenyl boron (1 time)	1.09	0.176
Sodium chloride	0.740	0.129
0.075 meq KNO ₃ /g	0.661	0.095
0.188 meq KNO ₃ /g	0.556	0.089
0.375 meq KNO ₃ /g	0.399	0.082
0.75 meq KNO ₃ /g	0.183	0.056
1.5 meq KNO ₃ /g	0.084	0.022
Potassium saturated	0.064	0.016

the restricted interlamellar space from which chloride is excluded.

It was assumed that difference in the experimental plate heights (obtained from the slopes of the ³H and ³⁶Cl breakthrough curves) would be due to a slow diffusion of tritium into the interlamellar spacing. Using Glueckauf's simplified model for the contribution of particle diffusion to total plate height, the particle diffusion coefficient for tritium into the interlamellar spacing was estimated to be $(4.6 \pm 2.7) \times 10^{-7}$ cm²/sec.¹⁰ These values are of the same order of magnitude as those obtained by Keay and Wild¹¹ for self-diffusion of barium ions in vermiculite.

INTERLAYER CESIUM FIXATION BY BIOTITE AND VERMICULITE LAYERS

D. G. Jacobs O. H. Myers

When hydrobiotite lattices are opened by treatment with sodium tetraphenyl boron, the exchange of trace quantities of cesium is similar to those

clays having only freely accessible exchange sites and the sorbed cesium is easily displaced by other salts. This provides additional proof that for trace quantities of collapse-inducing cations, fixation must occur at the edges of previously existing collapsed lattices.

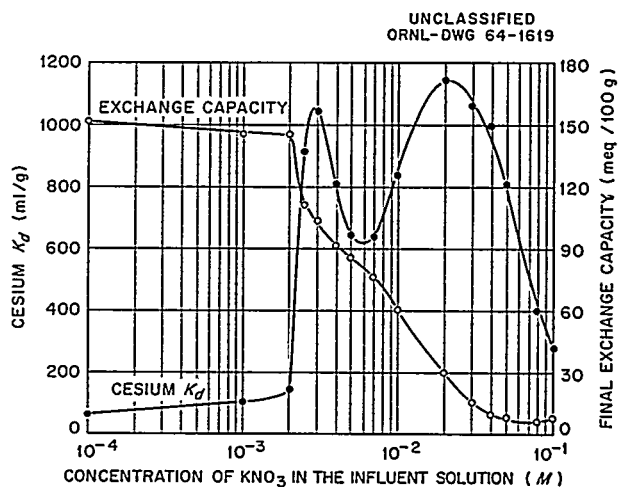


Fig. 1.6. The Effect of Potassium on the Sorption of Cesium from 0.5 M NaNO₃ by Sodium Tetraphenyl Boron Treated Hydrobiotite.

¹⁰F. Helfferich, *Ion Exchange*, p. 453, McGraw-Hill, New York, 1962.

¹¹J. Keay and A. Wild, *Soil Sci.* 92, 54 (1962).

When the concentration of potassium in the equilibrium solution is increased, two distinct peaks occur in the interlayer cesium fixation curve (Fig. 1.6), rather than the single fixation peak previously found for sodium chloride-treated hydrobiotite.¹² Each peak is accompanied by a distinct inflection in the exchange capacity curve. The sharp peak occurring between 10^{-3} and 10^{-2} M KNO_3 reflects the recollapse of the opened biotite layers, while the broader peak occurring between 10^{-2} and 10^{-1} M KNO_3 is due to collapse of vermiculite layers.

From the data presented in Table 1.3, it can be estimated that the average charge density is $(2.00 \pm 0.14) \times 10^{-7}$ meq/cm² for the biotite layers and

$(1.50 \pm 0.51) \times 10^{-7}$ meq/cm² for the vermiculite layers. It seems that the position and width of cesium fixation curves reflect the charge density distribution of the collapsible lattices. The higher the surface charge density, the more susceptible is the lattice to collapse; hence a smaller K^+/Na^+ ratio is required to induce collapse. The distinct peaks arising from the biotite and vermiculite type layers indicate that this hydrobiotite does not consist of an even gradation from low-charge-density vermiculite to high-charge-density biotite, but that there are two distinct mineral species in the material.

The difference in behavior of the biotite and vermiculite layers was also observed in time studies of potassium release in which it was noted that the collapsed vermiculite lattices had a much greater tendency for reexpansion than the biotite lattices.¹²

¹²D. G. Jacobs, *Proceedings of International Clay Conference held at Stockholm, Sweden, August 12-16, 1963*, pp. 239-48, Pergamon, 1963.

2. Disposal by Hydraulic Fracturing

Wallace de Laguna
R. C. Sexton¹

E. G. Struxness
T. Tamura

H. O. Weeren²

WATER INJECTION TESTS

Wallace de Laguna

B. L. Houser

Cores from the Joy No. 1 test well had been compared with the logs from wells 1 and 2. With this information it had been concluded that inclination of the bedding planes between wells 1 and 2 is low — approximately 6°.

A series of water injections was made in the injection well shortly after the completion of the well. Each test of the series consisted of the injection of a fixed volume of water, a 48-hr

pause to observe pressure variations, and a measurement of the rate and volume of bleed-back when the well was opened.

Four injections were made, three at a depth of 986 ft, and the fourth at a depth of 966 ft. The total volume of the first injection was 2000 gal; this injection served primarily to establish the test procedure.

The volume of the second injection was 50,000 gal. The fracturing pressure was 3240 psi, which fell to 900 psi during the injection. A total of 23,000 gal was recovered over a period of 60 days when the well was opened. A plot of the volume recovered is shown in Fig. 2.1.

The volume of the third injection was 23,000 gal — a volume identical to the bleed-back of the previous injection. The purpose of this injection

¹Plant and Equipment Division.

²Chemical Technology Division.

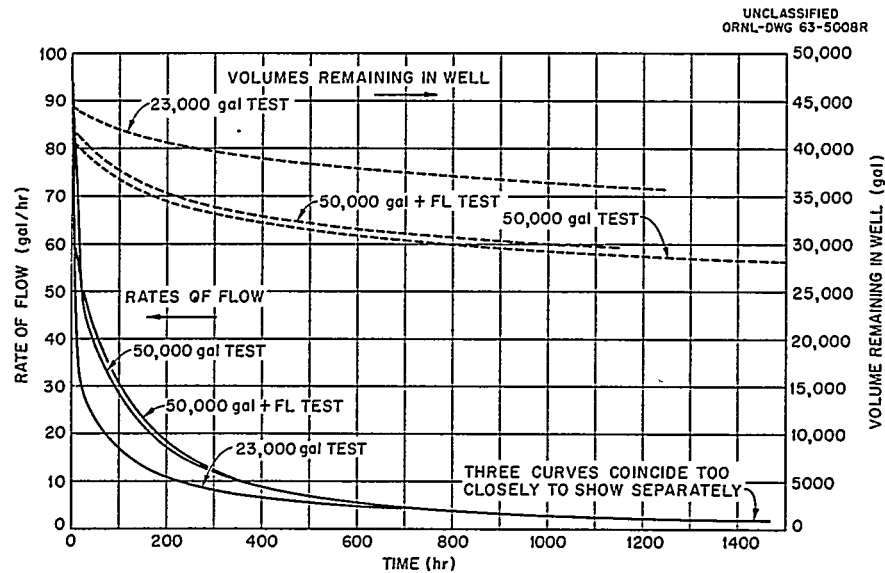


Fig. 2.1. Water Injection Test Phase 5 Final Backflow.

was to discover if the original fracture would be re-formed or if the injection of 23,000 gal would behave like a new injection. A total of 13,500 gal was recovered over a period of 50 days when the well was opened. This injection, therefore, behaved essentially like a new injection, leading to the conclusion that the water remaining in the well after the second injection had migrated beyond the original fracture.

The fourth injection was an injection into a new fracture of 50,000 gal of water mixed with a chemical that would retard fluid loss through small cracks or porous rock. The purpose of this injection was to discover if the mechanism of water loss was such that the chemical would significantly reduce it. A total of 23,000 gal was recovered over a period of 50 days when the well was opened. This injection, therefore, behaved almost identically like the previous injections, leading to the conclusion that the mechanism of water loss in these injections is such that the addition of a fluid-loss additive has no observable effect.

The water injection tests confirmed other evidence that a fluid-loss additive is not a necessary component of the mix to be used in the waste injections. Too, since in all cases the fracturing pressure was well above the overburden pressure, these tests furnished presumptive evidence that horizontal fractures were formed.

HAZARDS ANALYSIS

H. O. Weeren²

A hazards analysis of the shale fracturing experiment has been completed. It was concluded that the waste solution to be used in the first series of injections would be so low in specific activity that no significant hazard would result from its use. The other principal hazard involved in the shale fracturing experiment — that of working with high-pressure equipment — has been minimized where possible by installing this equipment in cells.

The unique hazard associated with the injections is the possibility that, during the course of an injection, the fittings at the wellhead may break off at the wellhead, thereby permitting some or all of the waste grout that has been injected into the well to flow back up the well into the wellhead cell with no way of shutting off the flow. Depending on the nature of the break at the wellhead, this flow could be up the tubing string, up the annulus between the tubing and the casing, or up both the tubing and the annulus. The expected maximum flows in each case are 535 gpm, 1010 gpm, and 1545 gpm respectively. In the event of such an occurrence, the grout will be washed through an 18-in. line to the nearby

emergency waste trench. Here the grout can be allowed to set up and be covered.

A rupture of a high-pressure line at any place except the wellhead would not constitute a major hazard. The line would be valved off or the injection pump would be stopped after, at most, a few hundred gallons had been spilled into one of the cells. A spill of this magnitude could be cleaned up quite readily.

A power failure at the facility would affect the waste pump, water pump, Densometer pump, and lights. Failure of these items would force a halt in the injection, but would not cause a serious hazard. If the power failure were temporary, the wellhead could be valved off and the injection pump shut down until pumping could be resumed. Alternatively, if the power were likely to be off for a considerable time, the injection could be terminated.

COST ANALYSIS

H. O. Weeren²

An estimate has been made of the probable operating cost of the shale fracturing plant if operated on a routine basis for the disposal of 400,000 gal/year of concentrated intermediate-level ORNL waste solution. This estimate shows that two variables are of particular significance – the cost of the mix and the well life. Other costs are either relatively small or fixed. The effect of these variables on the operating cost is shown in Fig. 2.2. It can be seen that the proportion

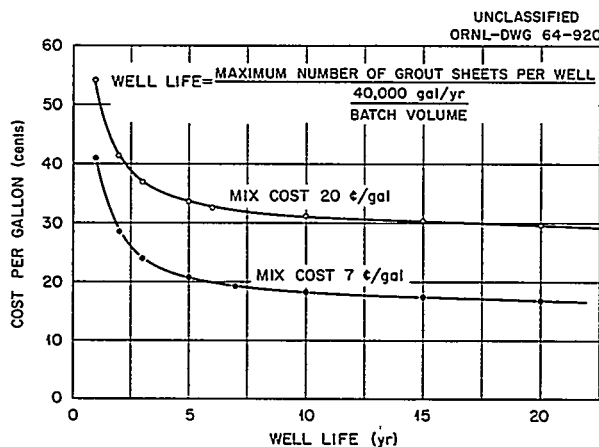


Fig. 2.2. Cost Estimate for Injection of ORNL Waste. 400,000 gal injected per year.

of the total cost attributable to the well cost becomes very large if the well life is less than 5 years. The factors that limit well life are not now known with certainty; it seems probable, however, that vertical uplift is one such factor. If this should prove to be the controlling factor, the well life will be limited to a fixed number of grout sheets and can be extended only by injecting larger and fewer batches. If, for example, the batch size were changed from 40,000 to 200,000 gal, the well life would be extended by a factor of 5. It seems probable, therefore, that the direction of future work will be toward large batch sizes.

PLANT CONSTRUCTION

R. C. Sexton¹ H. O. Weeren² B. L. Houser

Construction of the injection facility was completed. Views of the completed facility are shown in Figs. 2.3–2.5.

WASTE INJECTIONS

Wallace de Laguna Tsuneo Tamura
R. C. Sexton¹ B. L. Houser
E. G. Struxness H. O. Weeren²
F. S. Brinkley

A series of five injections was made to determine the performance of the surface plant and the underground behavior of the slurries of different compositions.

In the first injection (February 13) 37,000 gal of synthetic concentrated waste solution was mixed with 23,400 lb of attapulgit drilling clay and injected at a depth of 945 ft. This injection was made to check the operation of the surface plant and to evaluate a nonsetting mix.

In the second injection (February 21) 27,300 gal of synthetic concentrated waste solution with 30 curies of ¹⁹⁸Au tracer was mixed with about 170,000 lb of a cement-base mix and injected at a depth of 924 ft. This injection was made to evaluate a mix with low cement concentration and to determine whether the activity in the grout sheet could be detected at the observation well.

In the third injection (April 8) 33,500 gal of a mixture of synthetic concentrated waste solution and actual intermediate-level waste was mixed



Fig. 2.3. Overall View of the Cells and the Solids Handling Equipment. Shown are the bulk storage tanks, the wellhead cell, the injection pump (to the right of the wellhead cell), the standby injection pump (to the right of the injection pump), and the water storage tank (beyond the standby pump). The valve handles that can be seen protruding from the wall of the wellhead cell are part of the high-pressure valve rack.

with about 518,000 lb of a cement-base mix and injected at a depth of 912 ft. This injection was made to demonstrate that concentrated radioactive waste solutions similar to those to be produced by the ORNL waste evaporator can be fixed permanently underground.

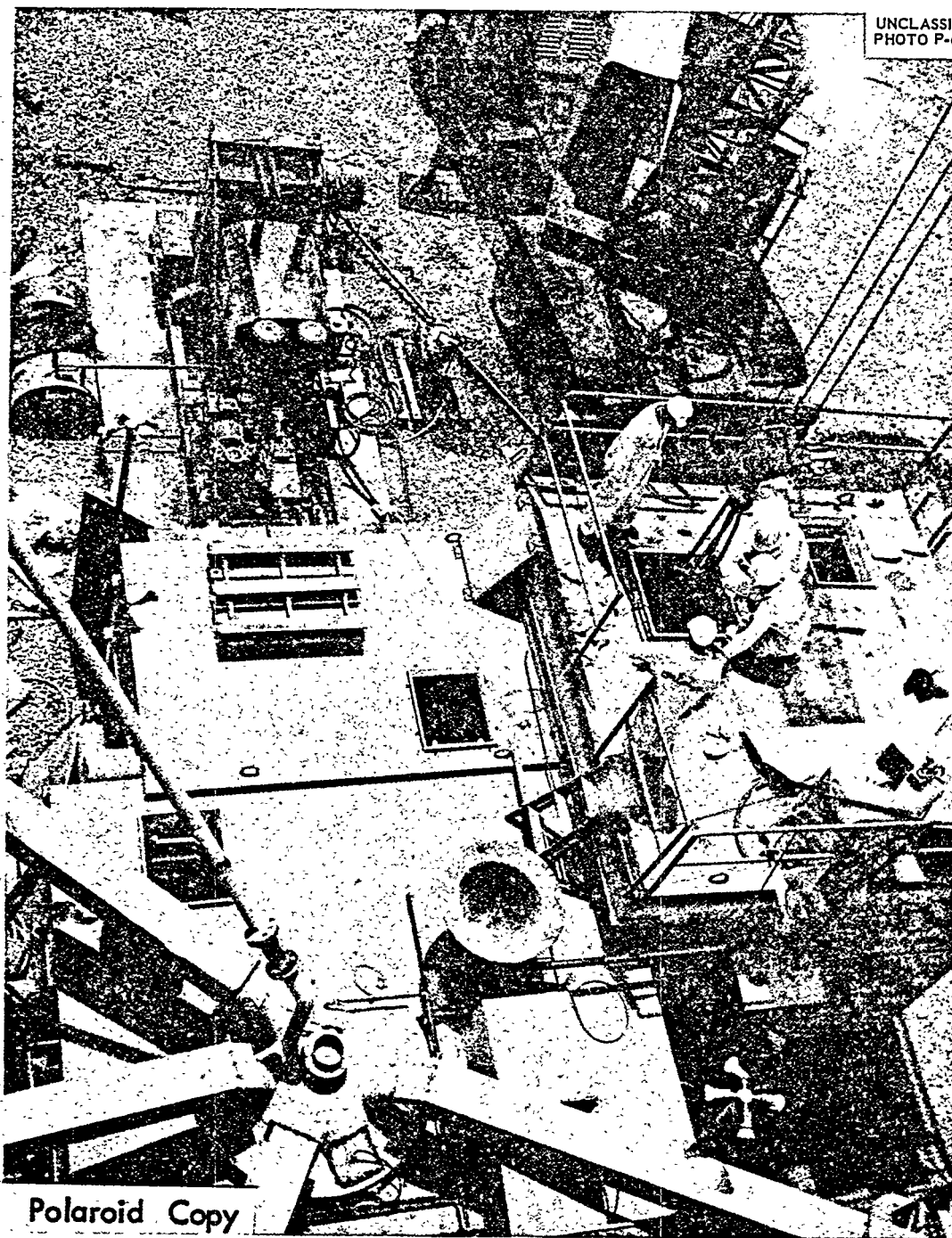
In the fourth injection (April 17) 36,000 gal of intermediate-level waste solution was mixed with about 381,000 lb of a cement-base mix and injected at a depth of 900 ft. This injection was made to evaluate a mix for dilute waste solutions.

In the fifth injection (May 28) 148,000 gal of a mixture of synthetic waste solution and actual intermediate-level waste was mixed with about 1,040,000 lb of a cement-base mix and injected at a depth of 890 ft. This injection was made to

test the surface plant during an extended (11 hr) disposal operation and to determine the underground behavior of large injections.

Minor difficulties were encountered with various components of the surface plant during the series of injections. These difficulties were corrected as they appeared. In general the operation of the surface plant has been smooth and satisfactory; the disposal operation has become almost routine as experience has been accumulated.

Evaluation of the mixes used in the five injections and determination of the underground behavior of the grout sheets cannot be accomplished until cores of the formation have been recovered. Coring is expected to begin in July.



UNCLASSIFIED
PHOTO P-65495

Polaroid Copy

Fig. 2.4. View of the Top of the Injection Plant During a Slotting Operation. The injection pump — a Halliburton HT-400 triplex positive displacement pump — is at the top left of the picture. The mobile crane at the top right of the picture is supporting the tubing string in the injection well. The mixing cell is at the lower left of the picture. The air slides that carry cement from the bulk storage tanks feed into the top of the mixer hopper. Slightly to the right of the mixer hopper is the top of the slurry tub; the boxlike structure on top of the slurry tub is a housing for a mirror so arranged that the interior of the tub can be viewed from the operating platform (just out of sight beneath the picture) without exposure to radiation.

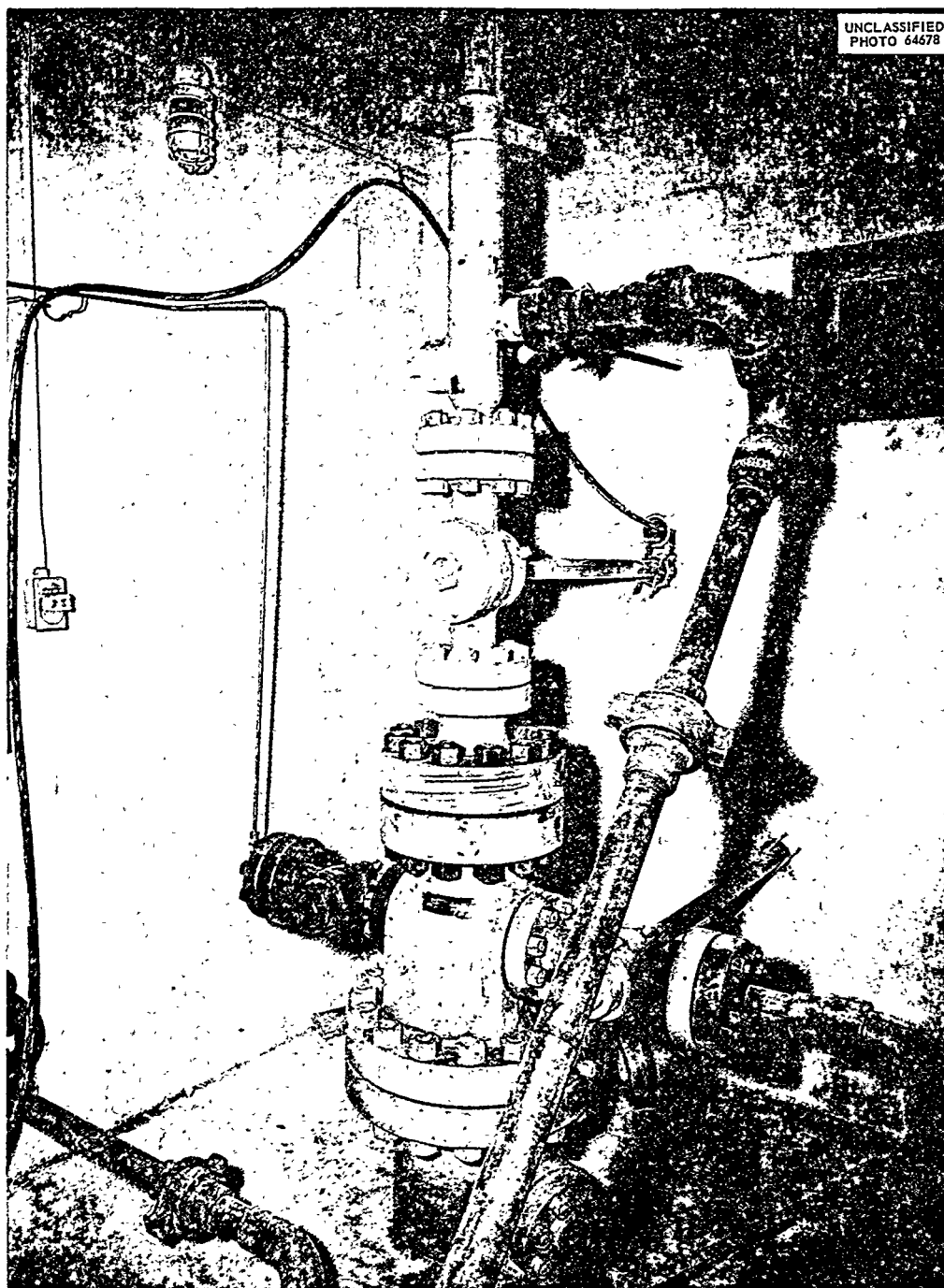

 UNCLASSIFIED
 PHOTO 64678

Fig. 2.5. View of the Wellhead of the Injection Bed with the Piping Arranged for Injection. The bottom fitting is the casing head of the $9\frac{5}{8}$ -in. surface casing. The next fitting above is the tubing head which provides connections to the $5\frac{1}{2}$ -in. casing. The flanged valve on the left connects to a pressure gage; the flanged valve on the right connects to the valve rack and to either the injection pump or the waste pit. Above the tubing head is the adapter flange which supports the tubing string. Above the adapter flange is the master valve and above the master valve is the plug container, which holds a wiper plug for wiping surplus cement from the inside of the tubing string at the end of a run. The connection on the plug container leads to the valve rack and the injection pump. All piping shown is rated at 10,000 psi.

Injection No. 1

Preliminary Preparations. — No solids mixing was required for this run, since attapulgitic drilling clay was the only solid to be added. The charge of 23,400 lb of attapulgitic was put into one of the bulk storage tanks prior to the injection. The synthetic waste solution in the storage tanks (40,500 gal) was evenly distributed among the three tanks by pumping from one tank into another. A dye (pontacyl brilliant pink) was added to the waste in each tank.

The well was slotted at a depth of 945 ft on February 11 by circulating a slurry of sand and water through the jet tool for approximately 40 min at an average pressure of about 5200 psi. The tool had two jets, each $\frac{3}{16}$ in. in diameter. The sand consumption was 37 sacks of 10–30 round sand.

After slotting was judged to be complete, the jet tool was pumped to the surface and held in the jet catcher. The well was backwashed to clear the sand from the well. The swivel and slick joint (equipment necessary for slotting) were removed from the wellhead assembly, several joints of tubing were removed to bring the bottom of the tubing string approximately 20 ft above the level of the slot, and the master valve and plug container were installed on the wellhead.

Pressure was applied to the well and increased until the formation fractured at 2150 psi. Flow was then increased to extend the fracture; a total of 3000 gal of water was pumped into the fracture at this time. A total of 37,300 gal of waste was mixed with 23,400 lb of attapulgitic and injected at an average rate of 250 gpm. The average mix proportion of 0.63 lb of clay per gallon of waste was acceptably close to the desired proportion of 0.66 lb/gal. The injection was uneventful.

Injection No. 2

Preliminary Preparations. — The waste storage tanks were refilled with synthetic 10X waste solution; four loads of solids were mixed. A dye (rhodamine B) and approximately 10 curies of ^{198}Au were added to the waste in each tank. The solution in each tank was mixed by air sparging.

The well was slotted at a depth of 924 ft on February 19 by circulating a slurry of sand and water through the jet tool for approximately 1 hr

at an average pressure of 3800 psi. A new jet tool was used for this job; the tool had four jets $\frac{3}{16}$ in. in diameter instead of the two jets used previously. A total of 37 sacks of 10–30 round sand was used.

Pressure was applied to the well and increased until the formation fractured at 3800 psi. Flow was then increased to extend the fracture; a total of about 2400 gal of water was pumped into the fracture at this time.

Injection. — The injection was started the afternoon of February 20. It quickly became apparent that the waste pumps were not delivering the necessary volume of waste solution and it was not possible to mix the solids being fed to the mixer with sufficient waste to obtain the desired slurry density. The injection was terminated by overflushing the slot in the casing with 500 gal of water. Approximately 1000 gal of waste solution, 3600 gal of water, and 32,600 lb of solids mix were consumed.

A check of the waste pumps revealed that the intake lines of these pumps were plugged at their common strainer. The strainer was removed and found to be plugged by an accumulation of small particles. The strainer was replaced by one with a much coarser screen.

Injection. — The injection was restarted February 21. All major components operated satisfactorily, and the injection continued until the supply of solids was exhausted. Approximately 27,300 gal of waste was pumped at an average rate of 227 gpm. The average cement content of the slurry was 5.87 lb/gal.

After approximately 8000 gal of waste had been pumped, the waste activity was detected in the cased observation well at a depth of 904 ft. After the initial appearance of the waste, it apparently channeled upward 30 or 40 ft alongside the well through the weak cement that had been used to cement the bottom 300 ft of the observation well.

Injection No. 3

Twelve loads of solids were mixed and blended over a four-day period and stored in the four bulk storage tanks. Bulk storage tanks 1, 2, and 3 each contained about 135,000 lb of cement (and other materials in proportion); bulk storage tank 4 contained about 110,000 lb of cement.

Approximately 13,000 gal of synthetic 10X waste solution remained in the waste storage

tanks after injection No. 2. This waste was mixed with 7500 gal of actual laboratory waste and about 15,800 gal of synthetic concentrated waste solution to produce 36,100 gal of solution. The activity of the solution averaged 0.0024 curie/gal.

The well was slotted at a depth of 912 ft on April 6 by circulating a slurry of sand and water through the jet tool for approximately 25 min at an average wellhead pressure of 3300 psi. A slotting jet with nozzles $\frac{1}{4}$ in. in diameter was used instead of the jet with nozzles $\frac{3}{16}$ in. in diameter that was used previously.

After slotting had been completed and the well had been backwashed, the formation was fractured. Breakdown pressure was approximately 2400 psi (wellhead measurement). A total of 1020 gal of water was injected at this time to establish that the formation had fractured sufficiently and to reduce the volume of water in the waste pit so that subsequent washup operations would not overfill the pit.

Injection. — The injection was made on April 8. Two equipment malfunctions occurred during this run — the mixing jet was partially plugged and the packing of the injection pump overheated. Neither malfunction was serious enough to require that the injection be terminated. The injection was continued until the supply of solids was exhausted. A total of 33,500 gal of waste solution was injected at an average rate of 195 gpm.

Readings of the intensity of the direct radiation were taken during the run at several points. In the valve pit and immediately adjacent to the waste pumps, the reading was 20 to 40 mr/hr. At the slurry sampler station the reading was 20 mr/hr. At the solids observation window on the operating platform, the reading was 1 mr/hr; the same reading was obtained at the other observation windows. Airborne contamination in the air withdrawn from the hopper and slurry tub was also measured; no activity was found. No activity was detected on the hopper off-gas filter at the end of the run.

No indication of the grout sheet was detected in the observation well on the day of the injection or on the following day. On April 13, however, a weak indication was found at a depth of about 890 ft. Since the grout had almost certainly set by this time, this indication was probably caused by migration of water containing a small amount of activity. A likely source of this water is phase

separation from the improperly proportioned grout pumped during the last 30 min of the injection.

Calculation of the ratio of solids to liquid of the mix that was injected during the run had indicated that for the first 2 hr the mix ratio was 13.3 lb of cement per gallon; for the next hour the mix ratio averaged 12.95 lb/gal; during the water washup at the end of the run the mix ratio averaged 11.2 lb/gal.

Injection No. 4

Preliminary Preparations. — Eight loads of solids were mixed and blended over a three-day period and stored in the four bulk storage tanks. Bulk storage tank No. 1 contained about 94,000 lb of cement, tank No. 2 contained about 136,000 lb, tank No. 3 contained about 61,000 lb, and tank No. 4 contained about 90,000 lb.

Approximately 39,000 gal of actual intermediate-level waste solution was transferred to the site and mixed with the solution remaining in the waste storage tanks. Samples were taken of the waste solution in each tank. The activity of the solution averaged 2.3×10^{-4} curie/gal.

An attempt was then made to slot the casing at a depth of 900 ft. An excessive vibration of the tubing string developed, however, and the attempted slotting was stopped. Investigation showed that the injection pump was drawing air past the packing, thereby causing the vibration. The slotting operation was therefore postponed, pending repacking of the pump. The pump was partially disassembled for repacking on April 14. It was found at this time that misalignment and overheating had caused considerable damage to pistons, packing, seals, and other parts of the pump and that fairly extensive repairs would be necessary. The necessary replacement parts arrived on April 17. At this time the pump was reassembled and tested.

The well was slotted at a depth of 900 ft by circulating a slurry of sand and water for approximately 25 min at a wellhead pressure of 2900 psi. Forty sacks of 20–40 mesh sand were used.

After slotting had been completed and the well had been backwashed, the formation was fractured. Breakdown pressure was approximately 3800 psi (wellhead measurement). A total of 2670 gal of water was injected at this time to establish that the formation had fractured sufficiently and to reduce the volume of water in the waste pit so

that subsequent washup operations would not overflow the pit.

Injection. — The injection was made on April 17. All major components operated satisfactorily, and the injection continued until the supply of solids was exhausted. Approximately 36,000 gal of waste was pumped at an average rate of 222 gpm.

After approximately 15,000 gal of slurry had been injected, activity was detected in the observation well. The activity was found to be spread over about 30 ft of the well, with peaks of activity at depths approximately 10 ft apart.

Shortly after the injection started, the level of water in the monitoring well was observed to be rising. The level rose 14 ft and overflowed at some time over the weekend. Since this occurrence was not expected, no provision had been made to measure the overflow. No activity was detected in the water in this well.

A calculation of the ratio of solids to liquid of the mix that was injected indicates that for the first 45 min of operation, the mix ratio was 9.42 lb of cement per gallon of waste; for the next hour, the ratio was 9.5; and for the final hour and 15 min, the ratio was 9.6.

Injection No. 5

Preliminary Preparations. — Fourteen loads of solids were mixed prior to the injection, blended over a five-day period, and stored in the four bulk storage tanks and the two blending tanks. Bulk storage bin No. 1 contained 157,000 lb of cement; bin No. 2 contained 157,000 lb; bin No. 3 contained 158,000 lb; bin No. 4 contained 159,000 lb; and the blending tanks each contained 46,000 lb.

Approximately 37,000 gal of intermediate-level waste solution was transferred to the site and mixed with the solution remaining in the waste storage tanks. One tank of this waste was thought to contain a significant quantity of ^{144}Ce , but an analysis of the solution in the tank showed a specific activity of only 0.013 curie/gal. (Subsequent events have led to the conclusion that the ^{144}Ce had probably precipitated and settled in the tank and hence was not picked up in the sample.) The solution activity in the other two waste storage tanks averaged 0.003 curie/gal.

The emergency waste trench was lined with plastic sheet and filled with approximately 100,000 gal of synthetic waste solution.

The well was slotted at a depth of 890 ft by circulating a slurry of sand and water for 35 min at a wellhead pressure of between 3000 and 3700 psi. Forty sacks of 10–20 mesh sand were used.

After slotting had been completed and the well had been backwashed, the formation was fractured. Breakdown pressure was approximately 3800 psi (wellhead measurement). A total of 1700 gal of water was injected at this time to establish that the formation had fractured sufficiently.

Injection. — For the planned injection approximately 1,000,000 lb of cement and 155,000 gal of waste solution were required. Since neither the waste storage tanks nor the bulk storage bins had sufficient capacity to store this quantity of materials, special procedures were used to fill the tanks and bins during the injection. The emergency waste trench was filled with synthetic waste solution, and the standby pump truck was used to pump the synthetic waste from the trench to the waste storage tanks. In addition, plant waste was pumped through the transfer line to the waste tanks during most of the run; a total of approximately 12,000 gal was transferred.

As soon as the first bulk storage bin was emptied, the solids stored in the blending tanks were transferred to the empty bin. Seven loads of cement (315,000 lb) were then blended and transferred to the bulk storage bins. A total of 137,000 lb of cement was charged to bin No. 1, 135,000 lb to bin No. 2, 90,000 lb to bin No. 3, and 45,000 lb to bin No. 1 a second time.

In previous injections considerable difficulty in determining mix density resulted because the bulk storage bins were not empty when flow was switched to another bin. To avoid such confusion in injection No. 5, particular care was taken to make sure each bin was empty when flow was switched.

The injection was made on May 28. All components of the facility operated satisfactorily, and the injection continued until the supply of solids was exhausted at 5:50 PM. Approximately 148,000 gal of waste was pumped at an average rate of 240 gpm.

As each bulk storage bin was emptied of cement, the volume of waste that had been pumped to that time was determined by level readings of the waste tanks. The volume of waste and the weight of cement consumed were used to determine the accuracy with which the Densometer system was

controlling the proportioning of solids and liquid. These checks showed good correlation during the first part of the run but a progressively poorer correlation thereafter, probably as a result of partial plugging of the Densometers.

Activity levels were considerably higher in this run than in any preceding run. Particularly high readings were obtained when the waste solution

was pumped from the waste tank containing the ^{144}Ce . These readings were much higher after the tank had been emptied and refilled than when the tank was being emptied the first time. Presumably the ^{144}Ce had precipitated and settled and was resuspended when the tank was refilled. No activity was detected in the hopper off-gas downstream of the filters, and no dose rate higher than 5 mr/hr was observed in any operating area.

3. Disposal in Natural Salt Formations

W. J. Boegly, Jr.
R. L. Bradshaw
F. M. Empson

W. C. McClain
F. L. Parker
W. F. Schaffer, Jr.¹

Hisashi Kubota²

DEMONSTRATION OF HIGH-LEVEL WASTE SOLIDS DISPOSAL

W. J. Boegly, Jr.
R. L. Bradshaw
F. M. Empson

W. C. McClain
F. L. Parker
W. F. Schaffer, Jr.¹

Last year's report described the objectives, handling procedures, and equipment required for the demonstration experiment.³ The current year has been spent in detailed design of the experiment and equipment, and preparation of the Lyons mine for the experiment.

The current schedule for the operation of the experiment shows that the first transfer of fuel assemblies to the mine will occur in early 1965.

Renovation of Lyons Mine

W. J. Boegly, Jr. F. M. Empson
W. C. McClain

The Stearns-Roger Corporation was employed to survey the salt mine facilities and to design new

equipment required to increase the hoisting capacity from 3000 lb to 7 tons. It was determined that a new headframe, shaft collar, and man and equipment cages were required to handle the 7-ton loads. A contract was awarded to the Foy Construction Company of Hutchinson, Kansas, for the construction and installation of the new headframe, shaft collar, and cages. The bid price was \$56,703, and the estimated time to complete the job was 120 days. Excavation for the shaft collar and headframe foundations started on November 7, 1963. Figure 3.1 shows the new headframe. The basic headframe was completed by April 30, 1964, and access to the underground workings for gage drilling and mine cleanup was initiated.

Stearns-Roger also recommended a general renovation of the hoist, hoist motor, electrical services, safety systems, and the hoist house. The hoist house renovations are in progress; a new concrete floor has been installed to replace the existing wood floor; the electrical system, including the main mine switchgear, has been replaced; the hoist has been checked and repaired; and a new office area has been built in the hoist house.

During the checking of the hoist drive, it was noticed that the main 9-in.-diam hoist shaft deflected under load. A detailed analysis of this problem followed by an ultrasonic check of the

¹Chemical Technology Division.

²Analytical Chemistry Division.

³F. L. Parker *et al.*, *Health Phys. Div. Ann. Progr. Rept.* June 30, 1963, ORNL-3492, pp. 19-34.

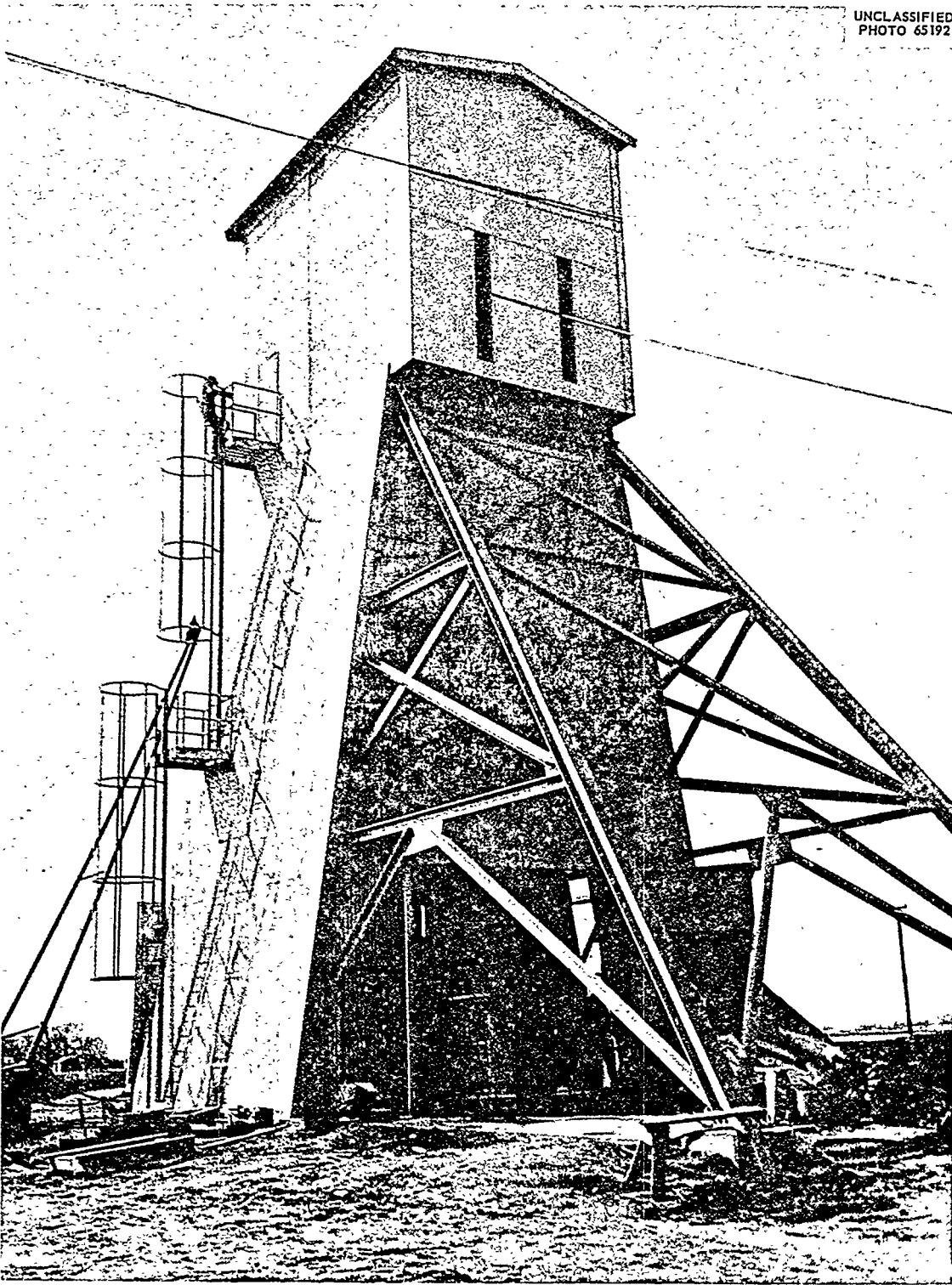
UNCLASSIFIED
PHOTO 65192

Fig. 3.1. New 7-ton-capacity Headframe.

integrity of the hoist shaft led to a recommendation for the installation of a center bearing to support the shaft. The installation of this bearing reduced the deflection and bending stresses in the shaft during the lowering and raising of large loads. The bearing was designed and installed by Doty and Sons of Pittsburg, Kansas.

As soon as access to the main shaft was attained, a complete check and repair of the hoist guides and shaft timbering in both hoisting compartments was initiated. Following this, a new main power cable and signal cable were installed in the north shaft compartment. The original power cable was left in place to serve as a standby.

Following completion of the headframe and grading around the shaft area and the hoist house, a security fence was installed to prevent unauthorized access to the shaft and hoist.

Underground work entails the clearing of approximately 2000 ft of mine passages and the mining of the experimental area. The experimental area will involve the removal of approximately 19,000 tons of salt. In order to perform this work within the scheduled time, it was decided to use conventional mining equipment. An inquiry for used mining machinery led to the purchase of a Joy loader and two Joy shuttle cars for the mining operations (Fig. 3.2). This equipment has been delivered, and one shuttle car and the Joy loader have been disassembled, lowered into the mine, and reassembled, and are now in operation. To date, approximately 300 ft of mine tunnel has been cleared. Power cables, transformers, circuit breakers, and power disconnects have been purchased and are ready for installation as the mine cleanup progresses.

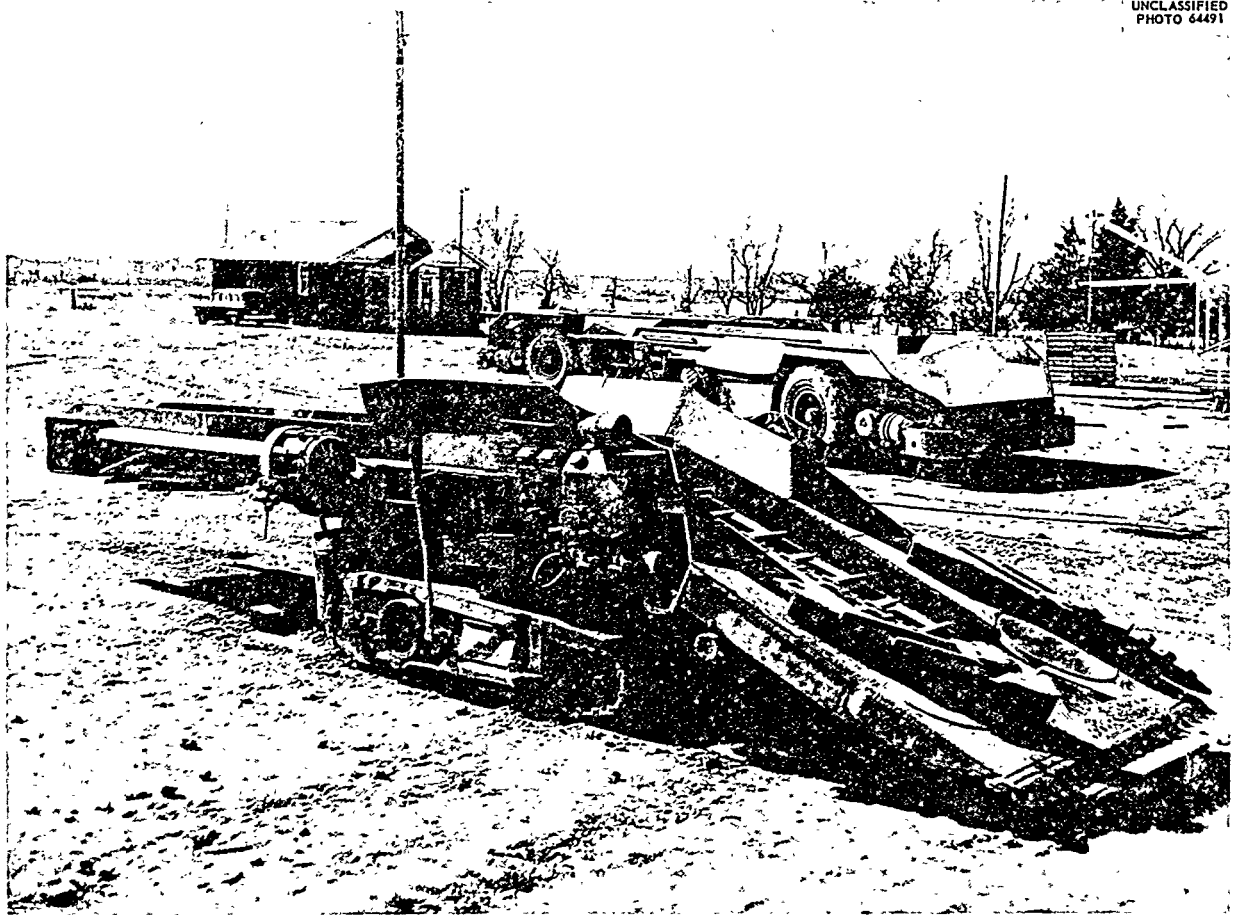


Fig. 3.2. Joy Loader (Foreground) and One of the Shuttle Cars for Use in Mining Experimental Area.

Design criteria for the waste-charging shaft have been completed, and the drilling is now in progress. The final inside diameter was set at 19.1 in., which will allow the transfer of 12-in. calciner pots and, if required, will serve as a secondary escape shaft. Detailed design of the surface facilities atop the waste shaft is now in progress.

Experimental Design

R. L. Bradshaw W. J. Boegly, Jr.
W. C. McClain

Preliminary design of the heating system and associated power supply for the demonstration has been completed. The same basic heating element (Incoloy sheathed) has been selected for use in all three of the arrays (two radioactive and one electrical control array), plus the pillar heating experiment (Fig. 3.3). Varying numbers of heating elements will be connected in parallel, and variable autotransformer control will be provided to supply the desired power to each of the heaters. Stabiline voltage regulators will ensure that proper power level is maintained during fluctuations in line voltage. Power will be supplied by a three-phase, 2400- to 240-v, 150-kva transformer bank.

Since heat output from the fuel assemblies decreases with time, the total heat output from the radioactive array holes will be maintained constant by increasing the power input to the supplementary electrical heaters attached to the hole liners. Automatic control of the power to the supplementary heaters was concluded to be unnecessarily complex, and thus control will be manual. Salt temperatures at points 6 in. away from the periphery of each hole in the radioactive array will be maintained at the same temperature as in the electrical control array. (Most of the beta decay heat will be released within the fuel assemblies and containers, and the gamma radiation dose rate will be down by a factor of 100 at a distance of 6 in. into the salt.)

It is planned to install about 450 thermocouples around the three arrays and the heated pillar. Two 144-point data loggers will routinely record temperatures from the experimental area. Critical temperatures (such as those on the fuel assemblies) will be printed on 24-point recorders. Some of the thermocouples in the salt will not be con-

nected to recording equipment, but will be read periodically with a portable instrument. The thermocouples will be inserted in plastic or Teflon tubes in the salt. The tubes will allow easier changeout of thermocouples in case of failure.

An important aspect of the demonstration is to determine the effect of heat and radiation on the plastic flow of salt and the resulting effect on stability of the mine. To obtain background information on room closure in the Lyons mine and also to obtain preexcavation flow rates, a number of plastic-flow measuring stations have been installed around the shaft bottom, along the access corridor, and around the experimental site. Additional gages will be installed as the experimental area is excavated.

At various locations in the mine, stress changes produced by excavation and heating will be monitored by "stressmeters" developed by Professor Potts (University of Newcastle-upon-Tyne). This information, plus the strain measurements, should

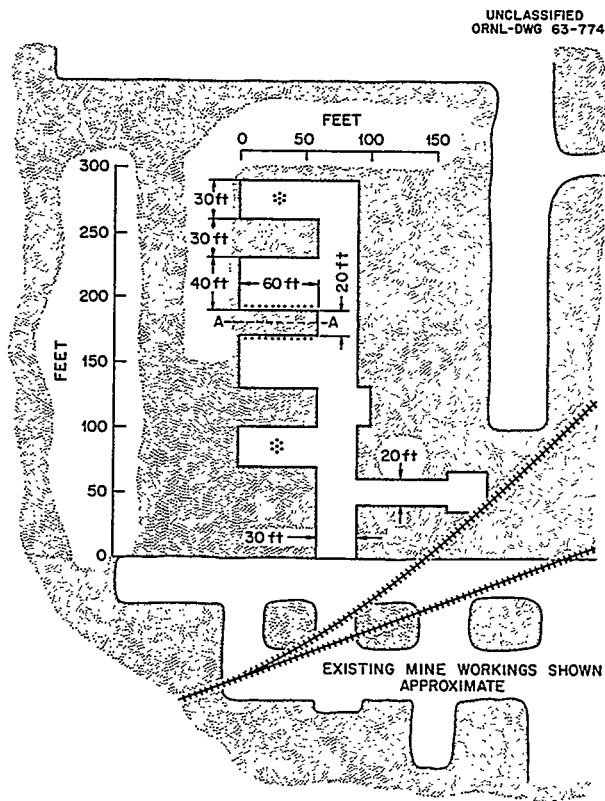


Fig. 3.3. Proposed Layout for Hot Demonstration Area. Room and pillar pattern.

provide sufficient information to describe the stability conditions in the mine before the experiment is started, and the effect of heating on stability of the mine.

Engineering Design

W. F. Schaffer, Jr.

Design of all major pieces of equipment for handling and storing the fuel assemblies has been completed. Procurement of most of the equipment has been initiated, and some deliveries have been made.

Fuel Assembly Canisters. — In order to prevent the escape of radioactive gases or particulates, design of the fuel assembly canisters was based on hermetically sealing the canister after fuel element insertion.

The final canister design provides four thermocouple monitoring points, two in the center of each fuel assembly. The shield consists of depleted uranium metal hermetically canned in stainless steel. The top section and shield are joined to the bottom plate by four bolts, allowing the shield to be removed remotely for use with replacement canister assemblies.

Casting of the depleted uranium shield plugs has been completed, and canning of the shields and fabrication of the lower canister sections and thermocouples will start in July 1964. A prototype canister has been fabricated (Fig. 3.4) and has been shipped to Phillips Petroleum Company,

Idaho Falls, Idaho, for use in their hot cell studies for encapsulation of the ETR fuel elements.

Hole Liner Assembly. — The purpose of the hole liner assembly is to prevent contact between the salt and the fuel assembly canisters, thereby ensuring the removal of the assemblies upon completion of the experiment and providing secondary containment.

As the salt is heated, it will flow plastically toward the liner. When the salt makes contact with the liner, pressures in excess of 1500 psi could occur. If the liner is designed to handle this pressure, the wall thickness would be great enough to produce a significant reduction in radiation dose to the salt. To overcome this problem, the design of the liner has been changed to allow the bottom half, which contains the canister, to be removable. Furthermore, an air annulus will be maintained between the liner and the salt at all times. Openings have been made to provide for the insertion of a caliper tool to gage the size of the annulus, and, if the salt approaches the liner, the lower half will be removed and a coring bit inserted to ream out the hole. The lower liner section will then be replaced and the experiment continued. It has been possible to design the liner with a minimum wall thickness consistent with the requirements for corrosion and internal pressure. Removal of the lower liner section also makes the replacement of heaters and thermocouples possible.

A prototype hole liner has been fabricated and is now being tested in Kansas. Orders have been placed and partial delivery made of the 14 hole

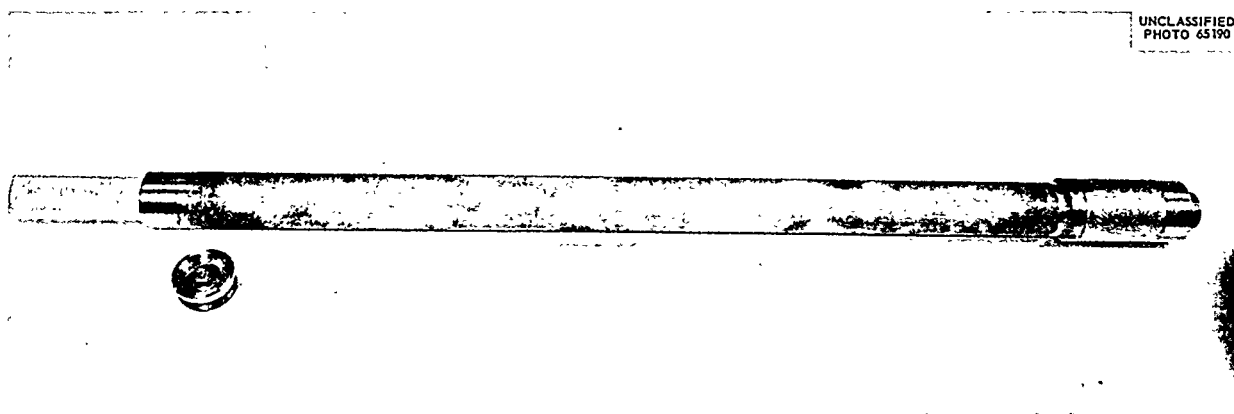


Fig. 3.4. Prototype Canister.

UNCLASSIFIED
PHOTO 65190

liners required for the floor and main arrays. Heaters and thermocouples for these liners will be ordered after results of the prototype test are available.

Surface Shipping Carrier. — Design drawings necessary to convert an existing SRE fuel shipping cask for the ETR fuel have been completed. Stress and heat transfer calculations indicate that the cask will meet the requirements of the proposed Federal shipping regulations for radioactive materials.⁴ The cask is shown in Fig. 3.5.

A shipping frame has been designed to secure the cask to a truck bed or rail car. The rack will also be used at the waste-charging shaft to allow elevation of the cask from the horizontal shipping position to a vertical charging position.

⁴Code of Federal Regulations, Title 10, Part 72, Regulation to Protect Against Radiation in the Shipment of Irradiated Fuel Elements, 10-CFR-72.

Underground Transporter. — The underground transporter has been designed and fabricated and has passed preliminary acceptance tests at the Athey Products Corporation, Chicago, Illinois, the fabrication subcontractor for Stowers Machinery Corporation. The transporter shown in Fig. 3.6 is powered by a standard Caterpillar two-wheel diesel tractor, coupled to a special trailer and vertically mounted cylindrical radiation shield. The transporter is capable of moving within the corridors and rooms of a mine storage facility. The vehicle was designed for disassembly into parts which weigh less than 7 tons and which can be passed through a 4- by 6-ft mine hoist shaft. The shield is unique and consists of a cylindrical steel shell into which 35 chevron-shaped rings of lead are inserted to provide shielding. The shield can be moved within a 3-ft-square area after rough positioning is made with the tractor. Shield movements are accom-

UNCLASSIFIED
ORNL-DWG 63-243

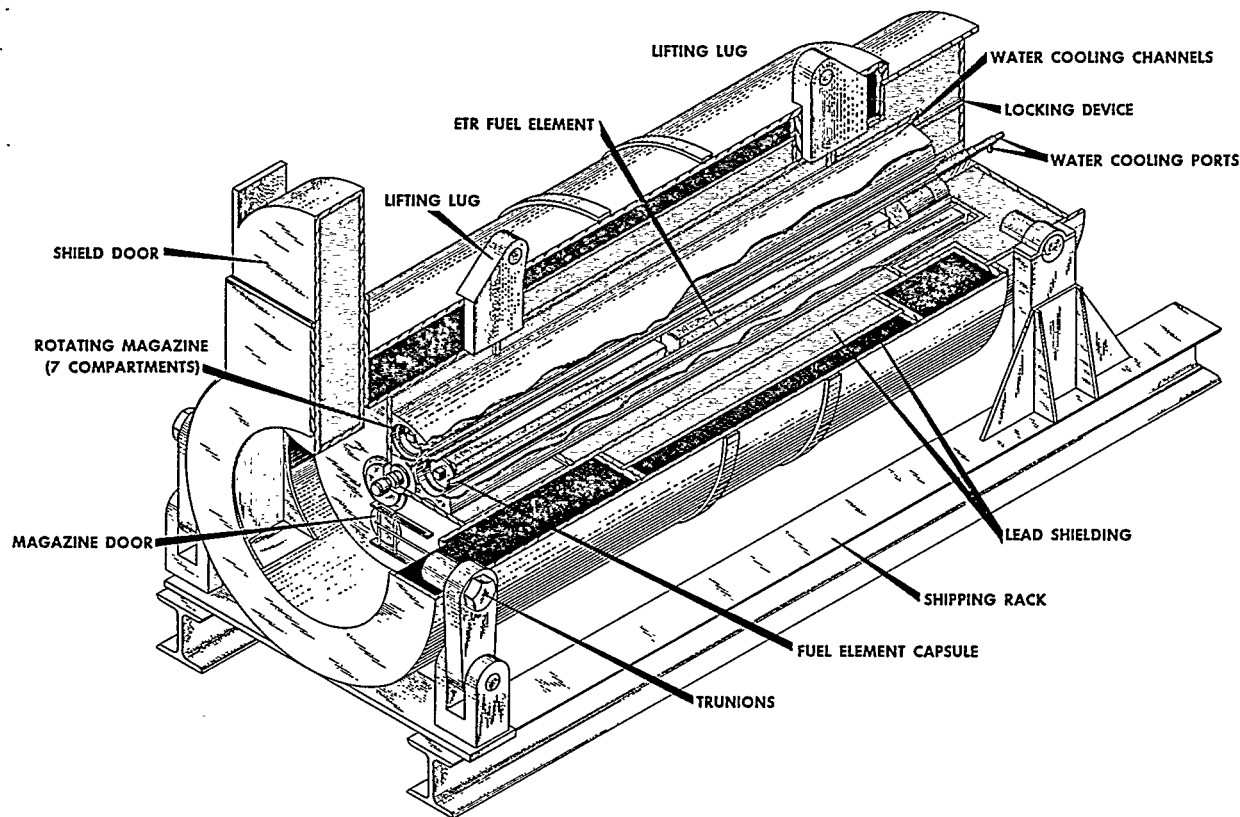


Fig. 3.5. Surface Shipping Carrier for ETR Fuel Assemblies.

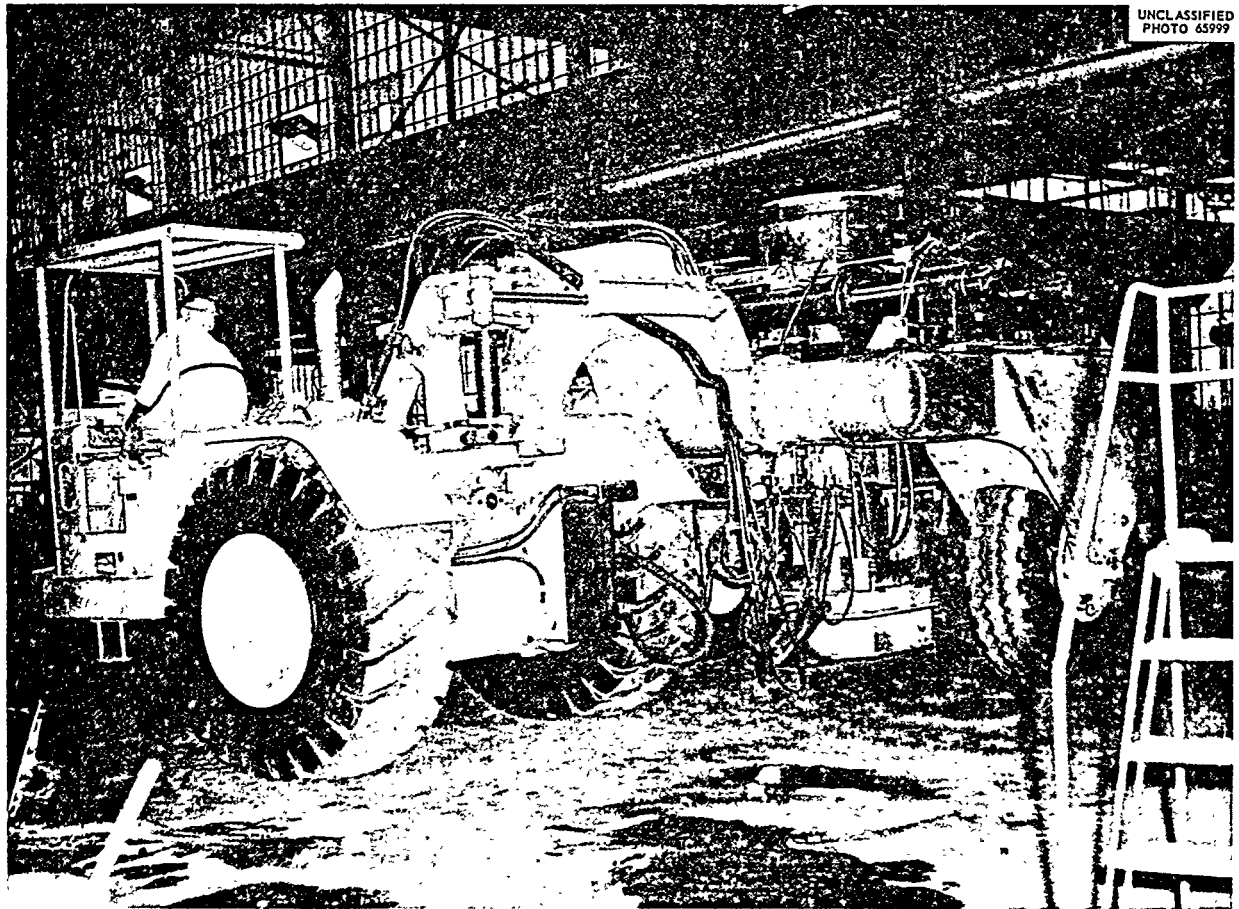
UNCLASSIFIED
PHOTO 65999

Fig. 3.6. View of Underground Transporter During Assembly at Athey Products Corporation.

plished by hydraulic cylinders or motors. Vertical movements of the shield and operation of the doors can be performed from a remote control panel or from the tractor operator's position.

Materials Selection

F. M. Empson

The corrosion test program has been completed. Based on laboratory tests, it has been decided to use 304L stainless steel for all critical components where contact with salt could cause problems. A test of 304L stainless steel in contact with salt in a ^{60}Co gamma-radiation field was performed and indicated that gamma radiation should have no effect on the corrosion rate.

Hazards Evaluation

W. F. Schaffer, Jr.

A draft of the hazards report on the fuel element shipments for the demonstration experiment is complete, and final editing of the report is under way.

Basically, the report shows that the surface carrier and its shipping rack will withstand the "G" loadings specified in *Title 10 - Code of Federal Regulations*.⁴ Sufficient shielding is available to limit the external dose from the carrier to less than 10 mr/hr at 1 m. Criticality review has shown that under no conditions could the material in the carrier achieve a critical configuration.

Analysis of the shipping carrier indicates that the *maximum credible accident* is one in which the cask is involved in a sustained fire, and loss of shielding results from rupture of the steel shell of the cask and the release of molten lead. In order to prevent the *maximum credible accident*, the shipping rig has been designed to minimize the chances of a sustained fire. The diesel fuel carried on the rig to operate the cooling system is one potential source of fuel for a sustained fire. Precautions have been taken to allow the fuel, in case of an accident, to drain rapidly from the shipping rig. Calculations have shown that

at least a 1-hr fire will be required to raise the temperature of the cask to the melting point of lead.

Prototype Test

R. L. Bradshaw W. C. McClain
F. M. Empson W. F. Schaffer, Jr.
Hisashi Kubota²

In order to check out techniques, a prototype test is being operated in the same room in which one of the radioactive arrays will be located. A vertical cross section of the prototype hole-liner installation is shown in Fig. 3.7.

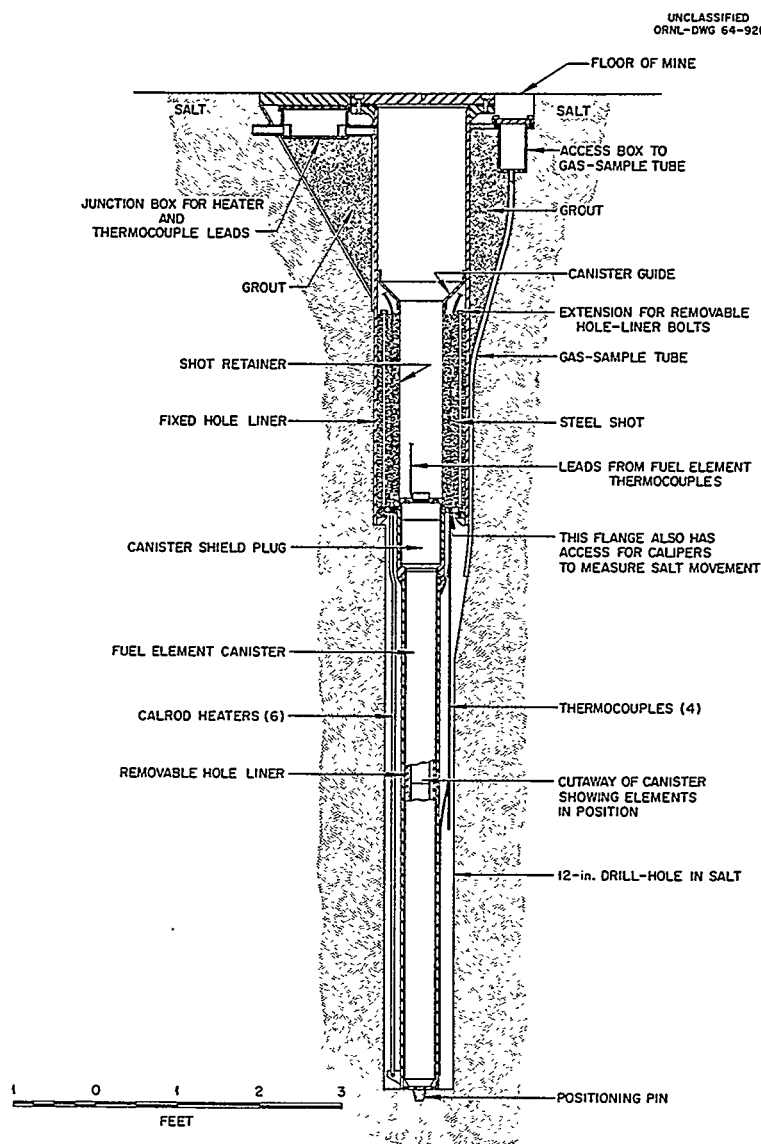


Fig. 3.7. Prototype Hole-Liner Installation.

Drilling of the 16-in.-diam upper portion and 12-in.-diam bottom portion of the hole was begun in April, and the upper portion of the liner was grouted into position. After the grout had set, auxiliaries and ancillary equipment were installed and operation (without a fuel canister, but with a metal plate closing the hole where the top of the canister should be) was started on June 2. To date, operation of the test has been approximately as expected. There has been some uplift of the floor (a few tenths of an inch as the salt temperature at the periphery of the hole approaches 200°C), and the first 10 days of operation have produced approximately 1 liter of water (released from shale interbedded with salt in the floor) in an off-gas condensate trap. This water has become progressively more concentrated in stainless steel corrosion products, and it is not yet known whether this is from corrosion of the hole liner or from the stainless steel condenser. Condenser corrosion seems a more likely possibility, but liner corrosion can only be assessed when the test is completed and the lower portion removed from the hole.

RHEOLOGICAL STUDIES

W. J. Boegly, Jr.	F. M. Empson
R. L. Bradshaw	T. W. Hodge, Jr.

Heated Model Room

W. J. Boegly, Jr.	F. M. Empson
R. L. Bradshaw	T. W. Hodge, Jr.

A rectangular room, 8 ft wide by 9½ ft high, geometrically similar to a mine room, was excavated in the face of a large pillar in the Hutchinson mine to study the effect of temperature on mine openings. Immediately after the opening was created, electrical transducer-type strain gages, capable of operating at 200°C, were installed to measure the floor-to-ceiling convergence, movement of the floor alone, and convergence of the side walls. Background closure rates and the data for the first 40 days of heating were presented in the 1963 Health Physics Division annual report.³ After about 50 days of heating, strain gages suddenly showed an apparent increase in the rate of convergence of the floor and ceiling. Investigation showed this to be due to bowing of the pipes supporting the strain gage

anchor bracket. This bracket is located in the haulageway, outside the cavity. Heat from the cavity was causing a vertical expansion of the haulageway floor, compressing the pipes between floor and ceiling. To correct for bowing of the pipes, a reference gage measuring the movement of the bracket toward the cavity was attached to the anchor bracket. The reference gage was installed after 93 days of heating. This gage indicated that movement of the bracket was somewhat erratic, and a slip joint was installed on the support pipes. This was done after 150 days of operation and appears to have corrected the difficulty; however, the closure rates determined for the period from 115 to 215 days are not believed to be reliable due to this difficulty.

After installation of the correction gage and the slip joints, the cavity closure rates as indicated by the strain gages should be correct; but, in order to get the total cumulative closure, it was necessary to extrapolate the deformation curves from 50 to 93 days. The corrected cumulative deformations, as indicated by the floor-to-ceiling gages at the end of 215 days of heating, are shown in Table 3.1. Shown in the right-hand column is the deformation rate during the period from 215 to 390 days. Also shown for comparison purposes are earlier rates and the rates before heating. It may be noted that the closure rates are now (390 days as of April 11, 1964) about ten times higher than the closure rates before heating. For the period from 215 to 390 days, the closure rates at various gage locations appear to be constant, or, if not constant, are decreasing at a rate such that it would take about another year of heated operation to establish the rate of decrease. The equipment is needed for the Lyons demonstration and the heating phase will thus be terminated. Creep rates will be monitored, however, as the cavity returns to ambient temperature.

The heating phase has shown that elevating the wall temperature of an isolated cavity by about 120°C (about 20°C rise at a distance of 9 ft from the cavity) resulted in a rapid reduction of about 5% in cavity dimensions, followed by a rapid decrease in closure rate. However, after more than a year at elevated temperature, the rate was still ten times higher than at ambient temperature. The effect appears to be approximately equivalent to that which would be obtained by doubling the load on the salt pillar.

Table 3.1. Closure of the Cavity During Heating

Gage No.	Cumulative Deformation at 215 Days (in.)	Prior to Heating	Rate of Movement in Units of 10^{-6} in. in. $^{-1}$ day $^{-1}$			
			During Heating			
			30 to 40 Days	40 to 115 Days	115 to 215 Days	215 to 390 Days
2	1.64	3.1	210	100	42	32
5	1.66	2.8	210	100	17	28
6	1.66	3.3	210	100	29	25
8	1.47	2.9	210	100	17	27
9	1.25	2.8	170	80	13	24

Bureau of Mines Pillar-Model Tests on Lyons Salt

R. L. Bradshaw

The Bureau of Mines Applied Physics Laboratory (APL) has performed creep tests at ambient temperature on pillar models prepared from a block of salt from the Lyons mine. In these models, the pillars were 1 in. high by 4 in. in diameter, and the models were loaded such that the average pillar stress was 4000, 5000, 6000, 7000, 8000, 10,000, and 12,000 psi. At 12,000 psi, flow was rapid and the pillar was considered to have failed due to excessive flow; however, there was no evidence of catastrophic (sudden or brittle) failure. The 10,000-psi model exceeded 20% deformation before the 1000-hr test was completed.

The Bureau of Mines Applied Physics Laboratory has supplied us with the cumulative deformation vs time curves obtained from the 1000-hr duration tests. Creep rates as a function of time were obtained by taking the tangents to the cumulative deformation curves. Data from the creep-rate curves can be fitted by an equation of the form:

$$\dot{\epsilon} = B\sigma^m t^n,$$

where

$\dot{\epsilon}$ = strain rate (vertical convergence, μ in. in. $^{-1}$ day $^{-1}$),

B = a constant (dependent on units of $\dot{\epsilon}$),

σ = average pillar stress (psi),

m = slope of $\dot{\epsilon}$ vs σ on a log-log plot (positive),

t = time (hr), and

n = slope of $\dot{\epsilon}$ vs t on a log-log plot (negative).

A reasonable fit is obtained with:

$$\dot{\epsilon} = 9 \times 10^{-8} \sigma^{3.1} t^{-0.6}.$$

Extrapolation of this equation to periods up to 70 years (in excess of 500,000 hr) produces creep rates which agree reasonably well with those actually measured in the Hutchinson and Lyons mines (see below).

Correlation of Creep Tests with Extrapolation of Pillar-Model Results

R. L. Bradshaw

W. J. Boegly, Jr.

F. M. Empson

T. W. Hodge, Jr.

Figure 3.8 shows the results of vertical convergence rate measurements in both the Hutchinson and Lyons mines and convergence rate curves plotted from the equation fitted to the pillar-model tests of APL. It should be noted that most of the gaging stations are located near the boundaries of the mined-out area, and thus the adjacent pillars would not be expected to be supporting the calculated dead weight of the overburden as would be the case if the pillars were in the center of a very large panel of rooms. That this is true (at least for openings up to a few years of age) is shown in Fig. 3.8 by the behavior of Hutchinson station No. 8. A short time after excavation in the area of station 8, mining was discontinued

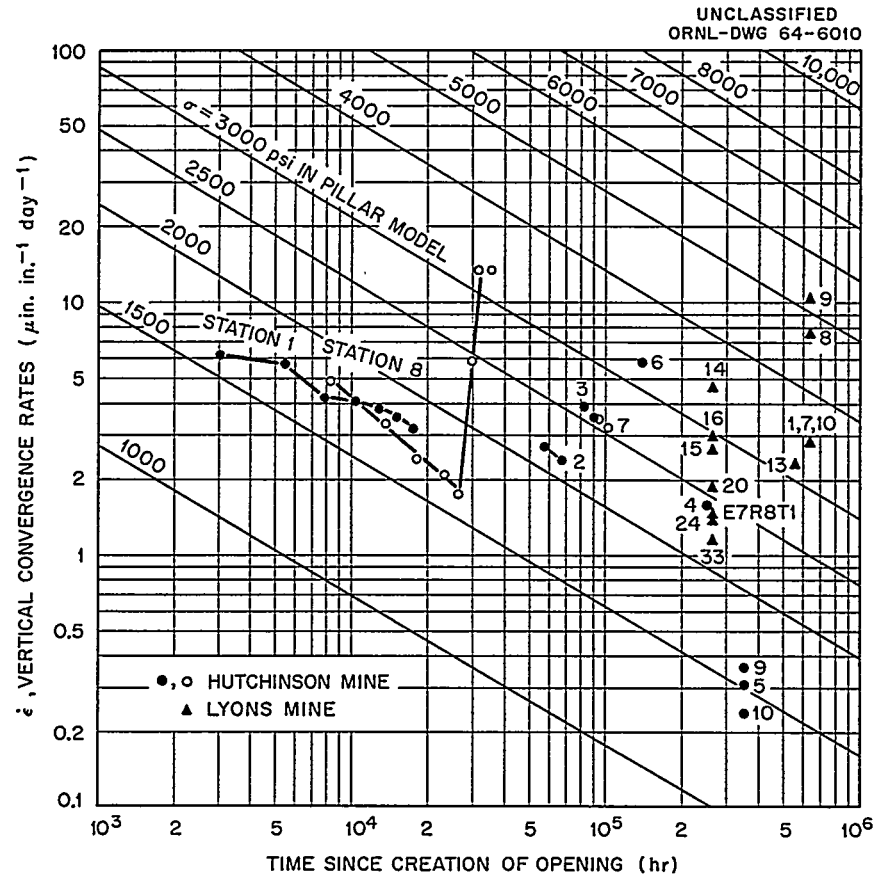


Fig. 3.8. Measured Mine Convergence Rates Superimposed on Plots of Equation Derived from Model Tests.

on the west side and shifted to the east side of the north panel. When the opening at station 8 was about 3 years old, the apparent stress in the pillar was about 1700 psi (see Table 3.2 and Fig. 3.8). At this time, mining was resumed near station 8 and the western boundary was extended. The rapid rise in vertical convergence rate indicates that the pillar had not been fully loaded after the initial mining; however, it should not be assumed that the load increased to more than 3000 psi (as might be inferred from Fig. 3.8), since the convergence rate would have been expected to show a considerable decrease as the pillar stabilized under its new load. Unfortunately, the gaging station had to be removed before this stage was reached.

In general, the stations located nearest the centers of large mined-out areas tend to approach

the stress calculated by assuming an infinitely large mined area (see Table 3.2). Hutchinson stations 5, 9, and 10, for example, are located near a northern boundary as well as the large irregular pillar left around the mine shaft. Hutchinson station 6, on the other hand, while located near the eastern boundary, is in the center of a panel which is very long in the north-south direction.

Lyons stations 1-13 are located in the area around the shaft (no large shaft pillar was left in this mine) where the mining pattern was very irregular and the estimated extraction ratio is no better than a guess. Therefore, the calculated pillar loads for these stations may be too high. The convergence rates at stations 8 and 9 are anomalous and are definitely known to be due to a parting separation and resultant ceiling sag.

Stations 16–33 are progressively nearer a western boundary, and the convergence rates seem to reflect this fact, although it is believed that there may be some ceiling sag contributing to the convergence at station 16 and possibly at station 20.

(It should be noted that the Lyons station numbers which were omitted are either different type measurements, have not yet been installed, or sufficient data have not been obtained to establish convergence rates.)

Table 3.2. Pillar Stresses Estimated by Different Methods

Station No.	Pillar Stress (psi)		
	Calculated from Dead Weight of Overburden	Calculated from Pillar-Model Extrapolation	Measured by USBM ^a (Stress Relief Method)
Hutchinson			
1	3000 ^b	1800	
2	2900 ^b	2100	
3	3000 ^b	2600	
4	2500 ^b	2400	
5	2200 ^c	1500	
6	3800 ^b	3300	
7	3950 ^b	2600	
8	2600 ^c	1700	1600
9	2200 ^c	1600	1300
10	2200 ^c	1400	1300
Lyons			
1	4000 ^d	3400	
7	4000 ^d	3400	
8	4000 ^d	4700	
9	4000 ^d	5200	
10	4000 ^d	3400	
13	4000 ^d	3200	
14	2900 ^d	3400	
15	2900 ^d	2800	
16	2500 ^b	3000	
20	2500 ^b	2600	
24	2500 ^b	2200	
E7R8T1	2500 ^b	2400	

^aReport APRL, E 40.1, *Stress Determinations and Borehole Deformation Studies*, by L. Obert, USBM, Applied Physics Research Laboratory, College Park, Md.

^bBased on actual measurement of room and pillar areas.

^cBased on nominal extraction ratio in the whole panel of rooms.

^dBased on estimated extraction ratio.

It should be noted that stress measurements made in the Hutchinson mine by APL tend to confirm the general validity of the pillar-model extrapolations (see Table 3.2). The 1300-psi figure was measured one pillar away from stations 9 and 10, and the 1600-psi figure was measured in a pillar near station 8, soon after station 8 was installed.

RADIOLYTIC PRODUCTION OF CHLORINE FROM SALT

Hisashi Kubota²

Last year³ it was reported that some oxidizing material was produced by radiolysis in solid salt upon exposure to ⁶⁰Co radiation, but that no release of chlorine to the surrounding atmosphere was detected. These studies were limited to reagent-grade salt of +20 mesh size. Since the salt surrounding disposal containers will consist of massive rock salt, as well as fine pieces of mined or otherwise crushed material, the effect of particle size on the extent of radiolysis was investigated. Finely ground salt (-100 mesh) was found to produce more oxidizer per unit weight than the unground material. Part of the ground powder was annealed at 500°C for 24 hr before irradiation in an effort to remove strains introduced by the grinding. There was a slight drop in oxidizer content as a result of this annealing; however, the amount of oxidizer found was still substantially higher than that of the unground salt. This suggested that surface effects might be involved.

Crystals of salt were grown from saturated salt solutions in two sizes. Precipitation with alcohol gave a product of -100 mesh which was carefully rid of alcohol by vacuum desiccation. Large crystals at least 2 to 3 mm to a side were grown by slow evaporation of saturated salt solution over a period of 3 months. Irradiation of these crystals gave the same radiolysis rate as that of the unground sample. Further annealing of ground material was then carried out, and the rate of radiolysis was found to approach that of the unground material after over 100 hr of annealing at 500°C. The G values for oxidizer production for the different conditions are shown in Table 3.3. It was

concluded that radiolysis takes place within the crystal itself and is quite independent of surface effects.

It should be pointed out that the G values were obtained by dissolving the salt samples, and, even though grinding or crushing of salt appears to produce higher G values, it would not be expected that any appreciable chlorine would be released under field conditions in a waste-disposal operation.

Past studies have shown that, under some conditions, water may be released to the disposal holes from either shale strata or halite. Thus, radiolysis of salt solutions is another possible hazard that needs to be considered. Laboratory studies show that production of chlorine takes place in acid chloride solutions with chloride concentrations greater than 1.4 M; however, all mine moisture samples tested to date have been slightly on the basic side, and thus no serious problems from this mode of radiolysis would be anticipated.

Table 3.3. G(Oxidizer) in Salt as a Function of Particle Size and Annealing

	Dose (rads)			
	3.2×10^6	10^7	3.8×10^8	10^9
	$\times 10^{-3}$	$\times 10^{-3}$	$\times 10^{-3}$	$\times 10^{-3}$
CP crystals (+20 mesh)	47	6.8	2	1.1
-100 mesh (ground)	147	37		
-100 mesh (annealed 24 hr at 500°C)			6	
-100 mesh (annealed 100 hr at 500°C)			2.9	
Synthetic crystals (+2 mm)			2.1	
Synthetic crystals (-100 mesh)			2.3	

4. Clinch River Study

F. L. Parker
K. E. Cowser
W. P. Bonner

P. H. Carrigan, Jr.¹
R. J. Pickering¹
B. J. Frederick¹

CHEMICAL COMPOSITION OF CLINCH RIVER WATER

R. J. Pickering E. R. Eastwood
J. E. Jackson

Collection of water samples from the Clinch and Tennessee Rivers for stable-chemical analysis was begun during the latter part of 1960 and was ended on December 1, 1962. The program was undertaken to determine the effect of the stable-chemical composition of river waters upon the fate of radionuclides released to the rivers.

Sampling stations were located at Clinch River Miles (CRM) 41.5 and 5.5 and Tennessee River Miles (TRM) 591.4, 529.9, and 471.0. Samples were taken at these stations once daily and composited weekly or monthly on the basis of daily discharge, except in the case of the station at TRM 591.4, where equal increments of the daily samples were composited. The composite water samples were analyzed by the chemical laboratory of the Tennessee Stream Pollution Control Board in Nashville, Tennessee. An additional sampling station was operated at CRM 14.4 from the latter part of 1960 until January 8, 1962. Samples collected at this station were composited according to discharge for the sampling interval and analyzed by the ORNL Analytical Chemistry Division.

Discharge-weighted mean concentrations of stable-chemical constituents at each sampling station for the entire period of record are listed in Table 4.1. The predominant constituent is the anion bicarbonate, and the predominant cation is calcium. Concentrations of the chemical constituents do not vary widely. The water from the Tennessee River contains somewhat less calcium, magnesium, bicarbonate, and suspended and dissolved solids, and somewhat more sodium and chloride than does the Clinch River water. Downstream stations generally show a lesser content of suspended materials than do upstream stations.

Discharge-weighted monthly concentrations of stable-chemical constituents have been computed for all stations (except TRM 591.4, for which time-weighted monthly concentrations were used), plotted, and examined for seasonal variations. Turbidity, apparent color, centrifuged color, suspended solids, and iron (largely controlled by seasonal variations in rainfall and runoff) varied in the same manner as discharge in the two rivers. Hardness, calcium, magnesium, sodium, chloride, and, in the Tennessee River only, dissolved solids and sulfate, showed maximum concentrations in the fall and minimum concentrations in the spring. The higher concentrations in the fall were probably due to the greater contribution of ground water to stream flow, as compared to surface runoff, at that time of year. Organic nitrogen reached a maximum in the early summer. Sporadic high concentrations of nitrate, which occurred in spring in the Clinch River and in summer in the Tennessee River, are assumed to reflect the use of nitrate fertilizers on farmland draining into the two rivers. Potassium showed maxima in both spring and fall in the Tennessee River, but only a single spring maximum in the Clinch River. Silica showed a maximum in the summer and a minimum in the winter in the Clinch River, but the pattern was reversed in Tennessee River water. It may be that the two constituents are present both in the form of suspended matter and in solution.

Statistical comparisons of variations in concentrations between constituent pairs were made for each station with the aid of a computer. Correlations were considered to be valid if the correlation coefficients were different from zero at the 99.7% confidence level and had relatively small standard errors of estimate. Turbidity, apparent color, and centrifuged color have a positive correlation with suspended solids, as expected. Iron and manganese, and at some stations silica and potassium, appear to vary in the same manner as the suspended material in the water, suggesting that those constituents are present in the water primarily as solid particles. The suspended sediment content, turbidity, and color of Tennessee

¹On loan from Water Resources Division, U.S. Geological Survey.

River water vary directly with discharge, but this pattern is not apparent in Clinch River water. At two stations, stable strontium shows a positive correlation with calcium, as one might expect if the two chemically similar elements were both derived from natural weathering processes. In

the lower Clinch River, however, stable strontium varied inversely with suspended sediment, suggesting that the strontium may have been associated with solids which were removed from the water during sedimentation, or diluted by low-strontium rainfall runoff.

Table 4.1. Summary of Discharge-Weighted Mean Values^a of Stable-Chemical Analyses^b of Clinch and Tennessee River Water^c

Constituent	CRM ^d 41.5	CRM ^e 14.4	CRM ^d 5.5	TRM ^f 591.4	TRM ^d 529.9	TRM ^d 471.0
Turbidity	28		17	14	6	7
Apparent color	197		114	88	53	59
Centrifuged color	20		20	23	24	31
pH	7.8	7.7	7.7	7.8	7.6	7.7
Bicarbonate	117	119	112	66	70	63
Acidity, as CaCO ₃	3		4	3	3	3
Hardness, as CaCO ₃	107		106	75	75	70
Calcium	27	21	27	21	20	19
Magnesium	9.4	7.7	9.4	5.5	5.8	5.5
Chloride	5	1.6	3	20	15	13
Sulfate	12	10	12	11	12	12
Nitrate	1.0	2.7	1.5	1.8	1.6	1.5
Iron	3.4	0.06	1.7	1.0	0.5	0.6
Phosphate	0.2	0.22	0.1	0.2	0.2	0.1
Potassium	1.7	1.3	1.6	1.3	1.8	1.3
Sodium	2.3	2.4	2.4	9.5	6.8	5.8
Silicon	2.9	1.5	2.7	3.5	3.1	3.4
Specific conductance	195	216	196	170	177	162
Suspended solids	185	25.3	55	22	15	9
Dissolved solids	125	129	133	121	112	101
Total solids	310	154	188	142	126	111
Organic nitrogen	0.7		0.5		0.5	0.4
Manganese	0.4		0.1	0.1	~0.0	~0.0
Chromium	0.02 ^g					
Strontium	0.073 ^h	0.070	0.069	0.063		
Discharge ⁱ	5088	4620	5585	21,419	31,340	38,876

^aConcentrations in parts per million, except pH in pH units, specific conductance in micromhos per centimeter, and discharge in cubic feet per second.

^bChemical analyses performed on filtered samples for CRM 14.1. For other stations, chemical analyses performed on unfiltered (raw) samples.

^cValues for TRM 591.4 are arithmetic averages of monthly samples which were not discharge-weighted when composited, as were samples for other stations.

^dSample period, Nov. 27, 1960–Dec. 1, 1962.

^eSample period, Nov. 28, 1960–Jan. 8, 1962.

^fSample period, August 1960–November 1962.

^gSample period, May 1961–November 1962 only.

^hSample period, Mar. 19, 1961–Jan. 6, 1962, only.

ⁱMean for the total sampling period.

BOTTOM SEDIMENT STUDIES

P. H. Carrigan, Jr.¹ E. R. Eastwood
R. J. Pickering¹ J. E. Jackson

Distribution of Radioactivity in 1962 Bottom Sediment Cores

During June, July, and August 1962, 163 bottom sediment cores were collected at 14 cross sections in the Clinch River and 4 cross sections in Poplar Creek and the Emory River. Variations in gross-gamma radioactivity with depth in 146 of the cores were determined by means of a specially constructed "core scanner."² Results of gross-gamma core scanning indicate that the entire thickness of radioactive sediment was sampled in most cores. The greatest thicknesses of radioactive sediment occur in the lower portion of the river, downstream from CRM 14. The single core showing the greatest thickness of radioactive sediment, 8.7 ft, was obtained at CRM 7.5. Upstream from CRM 14, radioactive sediment is largely confined to the sides of the stream channel. However, downstream from CRM 14, the sediment, while generally thickest on the less steep side of the stream channel, extends over a considerable portion of the channel, and at some sections, CRM 10.0, 11.9, and 12.1, extends

across almost the entire width of the channel. The depositional pattern of radioactive sediments in the study reach reflects the distribution of velocity in the river channel.

Similar distribution patterns of gross-gamma radioactivity were observed in several of the longer cores from the lower portion of the study reach. The general pattern which they exhibit is strikingly similar to the pattern of annual ¹³⁷Cs releases through White Oak Dam (Fig. 4.1). A computer program is being developed by which the similarities in the patterns will be statistically compared. It is assumed that the observed general pattern is the result of more or less continuous sedimentation of suspended sediment at the coring sites and the presence of ¹³⁷Cs as the predominant radionuclide in the bottom sediment. Cesium is known to be sorbed strongly on soil clay particles, and water sampling has shown that most of the ¹³⁷Cs passing through White Oak Dam is associated with solids suspended in the water.

Variations in content of the major radionuclides with depth in 11 cores have been determined by routing the "core scanner" output through a 512-channel pulse-height analyzer in order to obtain a gamma-ray spectrum for each 2-in. increment and, then, analyzing the gamma spectra by means of a digital computer program.

Summary of Progress - Processing of 1962 Bottom Sediment Cores. - (1) Variations in gross-gamma radioactivity with depth have been deter-

²F. L. Parker et al., *Health Phys. Div. Ann. Progr. Rept. June 30, 1963*, ORNL-3492, p. 38.

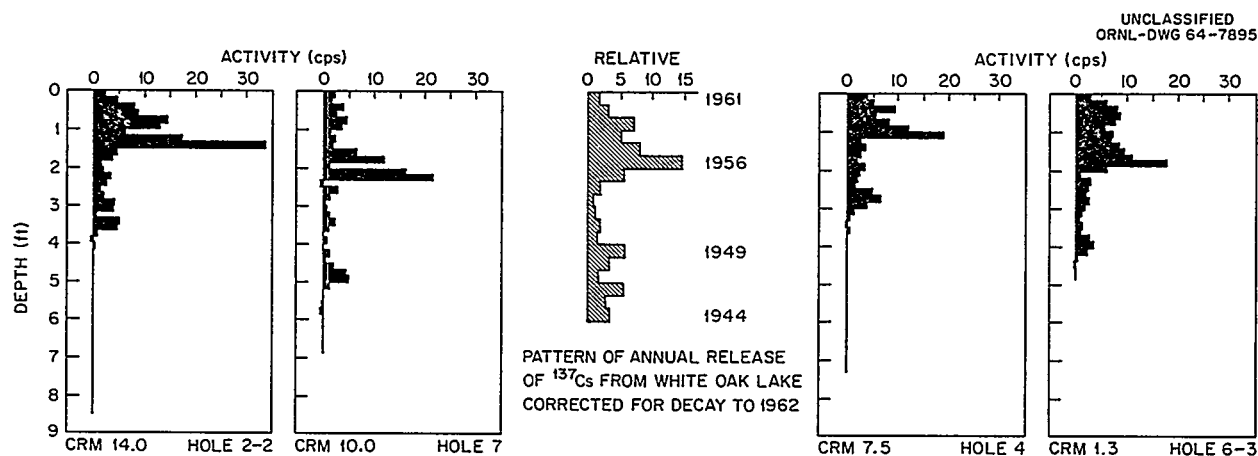


Fig. 4.1. Comparison of Vertical Distribution of Gross Gamma Activity in Clinch River Cores with Pattern of Annual Release of ¹³⁷Cs from White Oak Lake.

mined for 146 bottom sediment cores, and the results have been tabulated and plotted. (2) Gamma spectrum scans of 11 cores have been completed and are presently being analyzed. (3) Preparation of core, dredge, and SCUBA samples of Clinch River bottom sediment for use in calculating the total mass of each major radionuclide in the study reach has been completed. The samples have been submitted for radionuclide analysis and particle-size determination. (4) Alternate 2-in. slices from two bottom sediment cores have been submitted to ORNL and U.S. Geological Survey laboratories for analysis of their radionuclide content, particle-size distribution, mineralogy, cation exchange capacity, pH, calcium carbonate, organic matter, and free iron and aluminum oxides.

Influence of Releases on Radionuclide Concentration in Bottom Sediments of the Clinch and Tennessee Rivers

Changes with time in radionuclide concentrations in the upper portion of the bottom sediments of the Clinch and Tennessee Rivers follow the same general pattern as annual variations in the quantity of radioactivity released from White Oak Dam. This relationship is demonstrated by a comparison of annual releases for the years 1954 to

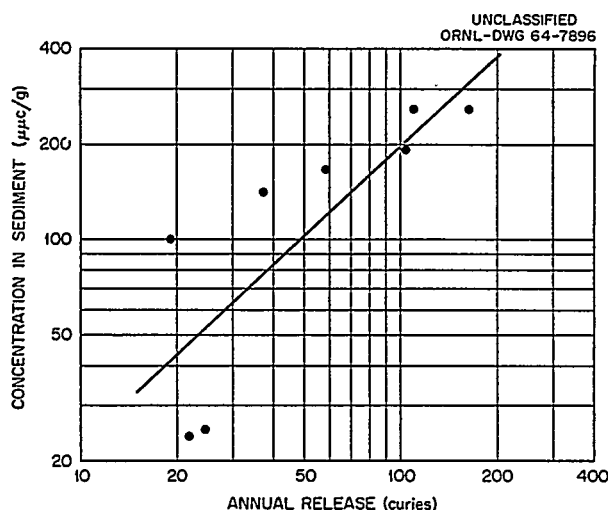


Fig. 4.2. Relationship of Annual Changes in ^{137}Cs Concentration in Bottom Sediments at CRM 1.1 to Changes in Annual Load of ^{137}Cs Released from White Oak Lake in Year Beginning July 1 and Ending June 30.

Table 4.2. Correlation of Annual Changes in Concentration in Bottom Sediments to Annual Load Released^a

Radionuclide	Correlation Index
^{137}Cs	0.80
^{106}Ru	0.89 ^b
^{144}Ce	0.66
^{90}Sr	0.72
Rare earths ^c	-0.48

^aCorrelation of logarithms of concentration and load; sediment samples collected at CRM 1.1; loads for year beginning July 1 and ending June 30.

^bBased on annual load released during calendar year.

^cRadiochemical analyses include ^{90}Y , but exclude ^{144}Ce .

1961 for each radionuclide with variations in the annually determined concentrations of each of the radionuclides in dredge samples of the bottom sediments. The comparison for ^{137}Cs is shown in Fig. 4.2. Similar comparisons have been made for other major radioactive constituents of the bottom sediments. Results of these comparisons are listed in Table 4.2. Data used in these comparisons were obtained by the Applied Health Physics Section in their continuing program of monitoring radioactive releases from White Oak Dam and of surveying radioactivity in bottom sediments each summer at selected sections of the Clinch and Tennessee Rivers. The annual samples of bottom sediments appear to have been composed primarily of sediment deposited during the previous year.

DISPERSION STUDIES

F. L. Parker P. H. Carrigan, Jr.¹
 B. J. Frederick¹ E. R. Eastwood
 J. E. Jackson

As a result of power generation at Melton Hill Dam, duration of flows in the Clinch River at the mouth of White Oak Creek may vary from 0 hr to 24 hr each day and flows in the river below the dam will change almost instantaneously from zero to several thousand cfs.

Some of the radioactivity released from White Oak Dam will accumulate in Clinch River waters in the vicinity of White Oak Creek during no-flow periods. During periods of power releases from Melton Hill, the radioactive mass accumulated in the still pool will be swept downstream in a mass.

A series of tracer tests were conducted in the Clinch River to study the effects of power re-

leases of water from Melton Hill Reservoir on dispersion in the Clinch River. Generating equipment was not fully installed at Melton Hill Dam at the time of the tests. As a consequence, variations in flow for the tests were simulated by releases through the gates. Cooperation of the Tennessee Valley Authority was required to perform these tests.

In the first test, Rhodamine B dye was steadily injected for a period of 24 hr into the flow over White Oak Dam. In the second test, injection was continued for a period of seven days.

The ebb and flood of water in White Oak Creek embayment (the reach of White Oak Creek downstream from White Oak Dam), due to large changes in water level in the Clinch River produced by the power releases, is much the same as flow in a tidal estuary. Using techniques of tidal flow analysis, it has been possible to compute the magnitude of peak concentrations of the dye pulse released on ebb flow from the creek at downstream sections in the river. A comparison of predicted and actual peak concentrations and

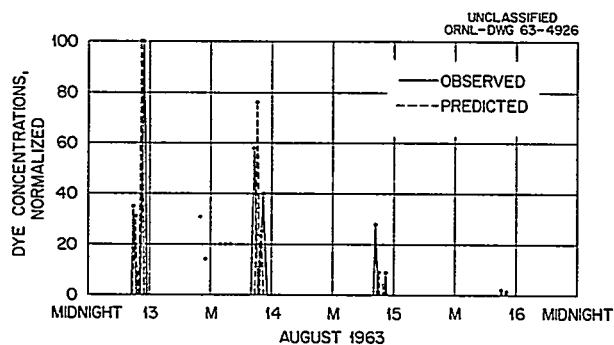


Fig. 4.3. Results of 24-hr Injection in Summer.

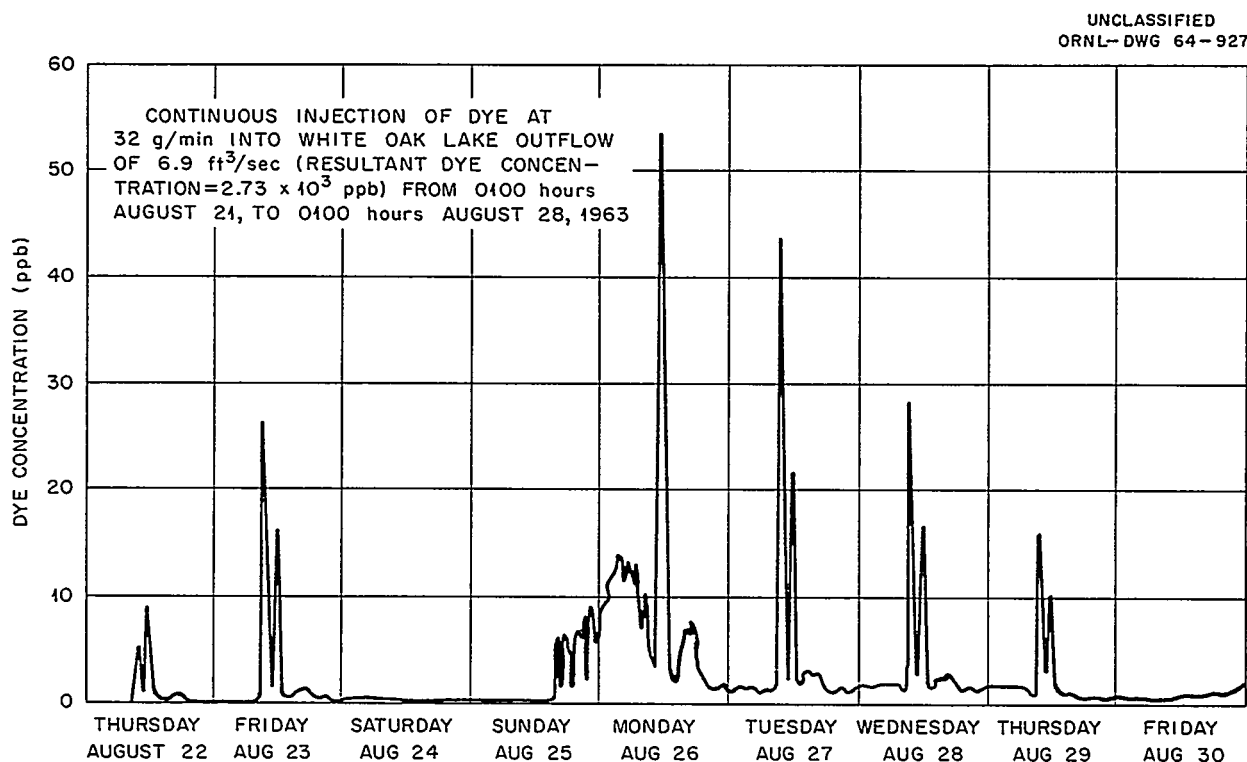


Fig. 4.4. Results of 168-hr Injection in Summer.

the times of arrival of these peaks are shown in Figs. 4.3 and 4.4.

As shown in Fig. 4.4, the twice-daily pulses of dye released from the creek were observed to occur at about 1000 and 1145 hr each weekday at the pumphouse for the Oak Ridge Gaseous Diffusion Plant (ORGDP) water treatment plant, CRM 14.4. The maximum concentration occurred on Monday morning, following the 58-hr weekend flow of tracer into the stilled river. On the basis of the concentration of tracer injected, and peak concentration observed on Monday, the minimum dilution for the momentary peak was computed to be 50.

Beginning on Sunday afternoon, as shown in Fig. 4.4, increased concentration of dye was observed at CRM 14.4. No releases were being made at Melton Hill Dam. It is believed that the mass of dye which passed the sampling section at CRM 14.4 at 1145 hr on Friday, and was stagnated about CRM 12, was slowly moved upstream during the weekend. This mass remained stagnated in the vicinity of CRM 14.4 until releases began on Monday morning. The upstream movement could have been caused by river control operations in the Tennessee River, by reestablishment of thermal stratification, or by a combination of both processes.

The median dilution of White Oak Creek releases by Clinch River waters was 570 for the period 1950 to 1960, a period unaffected by regulation from Melton Hill Reservoir. On the basis of the dye tests, the minimum momentary dilution due to power releases will be about ten times less than the median. At CRM 14.4 the radionuclide concentration during the last few years has been less than 1% of the maximum permissible occupational concentration. It is tentatively concluded, therefore, that the radionuclide concentrations will remain below $(MPC)_w$ even for the momentary peaks when power releases from Melton Hill Reservoir are begun.

SAFETY ANALYSIS

K. E. Cowser

The discharge of radioactive solutions to the Clinch River will result in exposure of man to ionizing radiation. Calculations have been made of the likely dose received due to exposure pathways deemed to be most important.^{3,4} This report includes additional calculations of the internal

and external exposure due to consumption of contaminated fish and exposure to the buildup of radionuclides in Clinch River water systems.

Contaminated Fish

Fish in the Clinch River and Tennessee River downstream from White Oak Creek assimilate some of the radionuclides released to the river system. Since fish is a dietary staple, radionuclides in the fish will contribute to the total dose received. Parker⁵ showed that catastrophic release of radionuclides from the biota of the Clinch River system was quite unlikely; the total inventory of radionuclides in the biota was estimated to be less than 1 curie,⁵ but a chronic intake is not excluded.

The data on radionuclide concentration in fish, used to estimate the dose individuals may receive, were developed by the Subcommittee on Aquatic Biology, Clinch River Study Steering Committee.⁶⁻¹¹ Fish were collected during

³K. E. Cowser, W. S. Snyder, and M. J. Cook, *Proceedings of Conference on Transport of Radionuclides in Fresh Water, January 30, 31, and February 1, 1963, Austin, Texas, U.S. Atomic Energy Commission, Washington, D.C., TID-7664, pp. 17-39 (July 1963).*

⁴K. E. Cowser, *Waste Treatment and Disposal-Progress Report for February-April 1963, ORNL-TM-603 (Dec. 16, 1963).*

⁵F. L. Parker, *Proceedings of Conference on Transport of Radionuclides in Fresh Water, January 30, 31, and February 1, 1963, Austin, Texas, U.S. Atomic Energy Commission, Washington, D.C., TID-7664, pp. 161-81 (July 1963).*

⁶A. G. Friend et al., *Fate of Radionuclides in Fresh Water Environments: Progress Report No. 2, Clinch and Tennessee Rivers, February 9-15, 1960, interim report to Clinch River Study Steering Committee, September 1960 (multilithed, 1962).*

⁷A. G. Friend et al., *Fate of Radionuclides in Fresh Water Environments: Progress Report No. 5, Clinch and Tennessee Rivers, May 15-30, 1960, interim report to Clinch River Study Steering Committee, October 1961 (multilithed, 1962).*

⁸A. G. Friend et al., *Fate of Radionuclides in Fresh Water Environments: Progress Report No. 6, Clinch and Tennessee Rivers, September 19-30, 1960, interim report to Clinch River Study Steering Committee, October 1961 (multilithed, 1962).*

⁹D. B. Porcella, *Data on Fish Collected in June and December 1961 and March 1962 (personal communication, May 8, 1963).*

¹⁰S. I. Auerbach (chairman) et al., *Progress Report No. 1, Subcommittee on Aquatic Biology, copies submitted to Clinch River Study Steering Committee, April 26, 1962 (unpublished).*

¹¹S. I. Auerbach (chairman) et al., *Progress Report No. 2, Subcommittee on Aquatic Biology, copies submitted to Clinch River Study Steering Committee, February 6, 1963 (unpublished).*

various seasons for the period 1960 to 1962, and were processed to approximate, in so far as possible, normal human utilization.^{7,11} The concentration of radionuclides in bottom feeders differed for the various species. The average concentration of radionuclides in the flesh of bottom feeders ranged from 240 to 540 $\mu\text{Ci/kg}$ ^{90}Sr , 480 to 1200 $\mu\text{Ci/kg}$ ^{137}Cs , 110 to 170 $\mu\text{Ci/kg}$ ^{106}Ru , and 32 to 42 $\mu\text{Ci/kg}$ ^{60}Co . Strontium-90 values were noticeably larger in the total fish analyses (830 to 5100 $\mu\text{Ci/kg}$ ^{90}Sr) due to its concentration in the bone. Sight feeders contained an average of 180 $\mu\text{Ci/kg}$ ^{90}Sr , 680 $\mu\text{Ci/kg}$ ^{137}Cs , 120 $\mu\text{Ci/kg}$ ^{106}Ru , and 22 $\mu\text{Ci/kg}$ ^{60}Co . Fish from the Tennessee River generally contained smaller amounts of these radionuclides, by factors ranging from about 2 to 5. Unexplained is the fact that sight feeders from the Tennessee River contained 50% more ^{90}Sr than sight feeders from the Clinch River.

An estimate was made of man's intake of radionuclides by assuming an annual rate of fish consumption of 37 lb.¹² This rate of fish consumption applied to commercial fishermen and, as a result, would estimate the intake of an admittedly high-exposure group. Radionuclide intake by the general population is likely to be influenced by all fish harvested in East Tennessee, in addition to the differences in radionuclide content among species of bottom feeders. Applying a fish dilution factor (weighted average for bottom feeders of 2.5) for East Tennessee fish, annual intakes were recalculated.

A maximum permissible intake (MPI) is calculated by assuming a daily intake of 2.2 liters of water containing the maximum permissible concentration (MPC) of the radionuclide of interest. Values used for MPC are discussed at length elsewhere.¹³ All $(\text{MPC})_w$ values used for data relating to the Clinch River are taken as one-tenth of the occupational $(\text{MPC})_w$ values for continuous exposure recommended by ICRP¹⁴ and NCRP.¹⁵ To obtain $(\text{MPC})_w$ values relating

to the Tennessee River, the $(\text{MPC})_w$ for continuous occupational exposure has been reduced by a factor of 1/100 for whole body as critical organ and by 1/30 with thyroid, bone, and gastrointestinal (GI) tract as the critical organs. Using the estimated intake, it is possible to calculate the fraction of MPI attained for the various critical organs as a result of eating contaminated fish (Tables 4.3 and 4.4). Estimates indicate that bone of the postulated high-exposure group may receive the largest dose; on the average, 28 to 34% of the MPI may be attained as a result of consuming bottom feeders (total fish) from the Clinch River. Strontium-90 is responsible for almost the entire bone dose. Consumption of 37 lb of "fishburgers" each year is certainly an overestimate, but better data of fish consumption is needed to arrive at a more reasonable intake. Use of the fish dilution factor is seen to reduce the estimated exposure.

Radionuclide Concentration in Water Systems

The presence of radionuclides in the raw water entering a water treatment plant may create, through processes of concentration, an external or internal dose problem. Three water systems that use Clinch River water as a source of supply were investigated. The Oak Ridge water plant has its raw water intake at CRM 41.5, well above the confluence of White Oak Creek and the Clinch River. The other two water treatment plants – the sanitary water plant serving the ORGDP and that serving the Kingston Steam Plant – have water intakes at CRM 14 and on the Emory River near CRM 4.4 respectively. The water treatment plants are basically similar, differing only in design details. Treatment processes include: prechlorination for algae control; coagulation with alum, soda ash (as dictated by raw-water alkalinity), and occasionally coagulant aids, for turbidity removal; settling; filtration (either sand or anthracite); and postchlorination for disinfection. Activated carbon is used when undesirable taste and other problems occur. Water used in boilers is treated further by zeolite softeners.

¹²P. Bryan and C. E. White, *Proceedings of the Twelfth Annual Conference, Southeastern Association of Game and Fish Commissioners*, pp. 128–32 (1958).

¹³C. P. McCammon (chairman) et al., *Progress Report No. 2, Subcommittee on Safety Evaluation*, copies submitted to Clinch River Steering Committee, February 6, 1963 (unpublished).

¹⁴*Recommendations of the International Commission on Radiological Protection*, ICRP Publication 2, Pergamon, 1959.

¹⁵*Maximum Permissible Body Burdens and Maximum Permissible Concentrations of Radionuclides in Air and in Water for Occupational Exposure*, U.S. Department of Commerce, National Bureau of Standards Handbook 69, June 5, 1959.

Table 4.3. Estimated Percentage of Maximum Permissible Intake That Man May Attain by Consuming Clinch River Fish

Fish Species	Critical Organ			
	Bone	Total Body	GI Tract	Thyroid
Bottom feeders ^a (flesh)	6.1 ± 1.6	1.5 ± 0.39	0.072 ± 0.0081	0.38 ± 0.072
Bottom feeders ^a (total) ^b	28 ± 4.5 (34) ^c	7.1 ± 1.2	0.14 ± 0.014	1.4 ± 0.19 (1.6)
Bottom feeders ^c (flesh)	2.4 ± 0.75	0.61 ± 0.19	0.03 ± 0.0039	0.16 ± 0.034
Bottom feeders ^c (total) ^b	9.5 ± 1.1 (12)	2.4 ± 0.33 (2.9)	0.053 ± 0.0047 (0.0058)	0.48 ± 0.051 (0.57)
Sight feeders ^d (flesh)	3.8 ± 1.7	1.0 ± 0.44	0.071 ± 0.012	0.31 ± 0.080

^aBottom feeders include carp, carpsucker, and buffalo.

^bTotal fish consist of flesh and bone.

^cIntake adjusted by fish dilution factor.

^dSight feeders include white crappie, bluegill, white bass, largemouth bass, sauger, drum, and catfish.

^eParenthetical values include four carpsuckers (composited) collected at CRM 19.6.

Table 4.4. Estimated Percentage of Maximum Permissible Intake That Man May Attain by Consuming Flesh of Tennessee River Fish

Fish Species	Critical Organ			
	Bone	Total Body	GI Tract	Thyroid
Bottom feeders ^a	7.2 ± 1.4	6.2 ± 1.2	0.11 ± 0.014	0.55 ± 0.084
Bottom feeders ^b	1.5 ± 0.28	1.3 ± 0.24	0.021 ± 0.0026	0.11 ± 0.017
Sight feeders ^c	16	14	0.11	0.83

^aBottom feeders include carp and carpsucker.

^bIntake adjusted by fish dilution factor.

^cSight feeders include white crappie, bluegill, white bass, largemouth bass, sauger, drum, and catfish.

The investigation consisted of external radiation surveys with a scintillation-type survey meter, and collection of samples of sludge from settling basins, condensers, hot water heaters, boilers, air conditioners, and an elevated tank; samples of sediment from filters and cores of filter media; and samples of zeolite softener regenerant and the softener media. Results of the analyses are incomplete and will be reported later.

There was little difference noted in dose rates at different units of the plants. Any increase in dose rate above background levels (referenced to the Oak Ridge water treatment plant) was, with one exception, undetectable. At a distance of 2 in. above a partially drained filter at the Kingston Steam Plant supply, a dose rate of 0.021 mr/hr was detected. The dose rate remained the same after the filter was backwashed. It is likely that the anthracite filter is to some extent concentrating radionuclides by ion exchange; this is currently being investigated by laboratory studies. The dose rate above the filters (0.015 mr/hr) of this supply is also influenced by the natural radioactivity present in the shale block used for construction of the building walls.

BEHAVIOR OF NUCLIDES ASSOCIATED WITH CLINCH RIVER SEDIMENTS

Tsuneo Tamura

W. P. Bonner

Desorption studies can provide the basis for defining the mechanisms of fixation of particular nuclides in naturally contaminated sediments. Desorption studies of Clinch River sediment should help to define the dominant factors responsible for the retention and migration of the radionuclides.

Using a Petersen dredge, bottom sediments were obtained from the mouth of White Oak Creek at CRM 20.8. Sediment from this location was sampled for the desorption tests because activity at this point had previously been reported to be relatively high. A sample of bottom sediment from CRM 15.3 and standard clay minerals obtained from Wards Natural Science Establishment were also used in these laboratory tests. Radioactive isotopes of cesium, strontium, and cobalt were used as tracers; ^{106}Ru from actual ORNL intermediate-level waste was used also.

Desorption of Radionuclides from Naturally Contaminated Sediment

The results of desorption treatments of the naturally contaminated sediment are shown in Table 4.5. Radionuclide content of the sediment was (dis/min per 50 g, oven-dry basis): ^{60}Co , 16,600; ^{137}Cs , 118,000; $^{103-106}\text{Ru}$, 129,000; ^{90}Sr , 2405; ^{144}Ce , 4145; and TRE, 24,190. Cesium-137, ^{103}Ru , and ^{106}Ru were the principal radioactive constituents; distribution of the radionuclides agreed with earlier results obtained on sediment sampled in the vicinity of CRM 20.8.

Up to 1 M solutions of salts, such as KCl, NaCl, and CaCl_2 , between pH 6 and 8, removed less than 10% of the ^{60}Co , ^{106}Ru , and ^{137}Cs ; on the other hand, between 30 and 77% of the ^{90}Sr was removed by the salts, depending on their concentration and pH. This behavior suggests that the strontium is held primarily by reversible ion exchange, whereas cobalt, ruthenium, and cesium are not. In strongly acid systems of HNO_3 or HCl, cobalt and strontium are released, but ruthenium and cesium resist desorption. In strongly alkaline systems, approximately one-half of the ruthenium and about 15% of the cobalt were desorbed. Neither cesium nor strontium was desorbed at the high pH; the 20% removal of strontium by NH_4OH at pH 8 was not confirmed by later tests.

If cesium or strontium is held in readily accessible sites, such as those found on montmorillonites or kaolinites, desorption can be accomplished by contacting with high-concentration salt solutions. Hence, even with illitic material, reversible ion exchange reactions can occur at or near the surface, and ions held at these sites are readily exchanged. It is believed that strontium is held primarily by this mechanism.

Data suggest that, in addition to clay exchange, another mechanism is operative when sorption occurs at high pH. From other tests, it became apparent that CaCO_3 was being formed and was responsible for the higher removals. The removal of strontium at higher pH may be likened to the lime-soda water-softening process whereby strontium is removed from solution by the formation of CaCO_3 .

Studies are continuing on the role of CaCO_3 formation on strontium retention. Tests with a sample from White Oak Lake suggest that CaCO_3 may play an even more important role in retaining

strontium than Clinch River sediment. With 1 M CaCl_2 only 35% of the strontium was removed; this can be compared to 77% removal from the sediment at CRM 20.8. The lower removal from the White Oak Lake sediment suggests that a greater percentage of the strontium is associated with CaCO_3 . Further evidence to support the role of CaCO_3 was found through analysis of the sediment; the sediment from White Oak Creek contained 4.22% CaCO_3 , while the sediment from CRM 20.8 contained 1.77%.

Desorption of Cobalt from Sediment – Our understanding of the fixation of cobalt and ruthenium is limited at this time. However, certain responses of the nuclides in water and sediment, as well as in resin exchangers, bear recording.

Tests of the sorption of cobalt from demineralized water by sediments revealed that optimum removal was obtained between pH 6 and 8; this behavior is similar to that of cobalt in demineralized water without sediment. With Dowex 50, however, maximum sorption occurred at pH 4 and the higher pH solutions showed a gradual reduction in sorption. Cobalt on the Dowex 50 was completely released with neutral sodium acetate; on the other hand, only about 80% of the cobalt was removed from ^{60}Co -tagged sediment with the same treatment. Since the neutral salts did not remove cobalt from the naturally contaminated sediment to an appreciable degree, reversible ion exchange may be eliminated from further consideration. Two possible factors which must

Table 4.5. Removal of Cobalt, Cesium, Ruthenium, and Strontium from Clinch River Sediment by Various Solutions

50 g (Oven-Dry Equivalent) CRM 20.8
400 ml Solution; 24 hr Contact

Reagent	Concentration (M)	pH	Percent Removed			
			^{60}Co	^{137}Cs	^{106}Ru	^{90}Sr
Tap water		6 (HNO_3)	2.8	a	3.0	21.3
Tap water		2 (HNO_3)	64.6	a	3.1	80.9
Tap water		1 (HNO_3)	78.1	3.3	5.5	
Tap water		6 (HCl)	a	a	3.5	19.4
Tap water		2 (HCl)	65.6	a	4.1	89.9
Tap water		7.7 (natural)	a	a	4.5	11.0
NaHSO_3	0.1	6	16.8	a	9.8	37.7
$\text{K}_2\text{Cr}_2\text{O}_7$	0.1	5.6	5.9	1.7	4.7	73.1
CaCl_2	0.1	7	6.4	a	4.1	58.6
CaCl_2	1.0	7	4.7	a	4.4	76.9
NaCl	0.1	6	3.5	0.8	4.1	39.2
NaCl	0.1	8	a	5.7	6.8	30.1
NaCl	1.0	6	a	0.7	3.9	63.1
NaCl	1.0	8	a	0.6	5.1	56.0
KCl	0.1	6.2	a	0.7	2.8	53.0
KCl	1.0	6.2	3.0	1.7	2.5	68.7
NaOH		8	a	0.4	5.9	6.0
NaOH		12	16.5	3.1	46.6	4.9
NH_4OH		8	a	0.7	8.2	20.0 ^b
NH_4OH		11.8	17.2	4.5	45.1	3.5
Ethyl alcohol					0.9	<1
Acetone					1.0	

^aRefers to concentrations below detectable limits.

^bNot confirmed by later tests.

be considered include the surface features of clays and sediments, and the properties of the cobalt ion at different pH. There is a possibility that monohydroxy cobalt is formed prior to the formation of the dihydroxy form.

The desorption of ruthenium sorbed on a sediment from actual ORNL intermediate-level waste mixed with tap water was determined. A sample of sediment from CRM 15.3 was contacted with a solution containing 2 ml of waste in 98 ml of tap water adjusted to pH 7. After 24-hr contact approximately 58% of the ruthenium was removed from solution (Table 4.6). The samples were then leached with solutions listed in Table 4.6. The relative effectiveness of the desorbing solutions was similar to that observed with the naturally contaminated sediment; however, the percentage desorbed was higher with the artificially contaminated sediment.

With 2 ml of waste and 98 ml of tap water adjusted to pH 7, a colloidal precipitate was ob-

served; centrifugation of the precipitate revealed that approximately 20% of the ruthenium was associated with it. Considering the chemical composition of ORNL intermediate-level waste, it was presumed that the precipitate was aluminum oxide hydrate; considerations of the solubility product precluded the formation of CaCO_3 at this pH. When the pH of the solution containing the precipitate was lowered to pH 2, 50% of the ruthenium returned to solution and the precipitate dissolved. If one assumes that 34% ($20 \div 58 \times 100$) of the ruthenium in the sediment is associated with the precipitate which releases one-half of its ruthenium as it dissolves at pH 2, then, of the amount desorbed at pH 2, 17% is due to the precipitate and about 6% is due to desorption from the sediment. The latter value agrees well with desorption of ruthenium from naturally contaminated sediment at pH 2. Further work is continuing to evaluate the solubility of the colloidal precipitate in 1 M CaCl_2 and pH 12 tap water.

Table 4.6. Sorption and Desorption of Ruthenium Using 10.0 g of CRM 15.3 Sediment and 100 ml Solution

	1	2	3
Sorption:			
Solution	(98 ml Tap water + 2 ml Waste from W-8)		
pH	7	7	7
4 hr (%)	52.5	56.0	54.1
24 hr (%)	58.8	60.1	55.3
Desorption:			
Solution	Tap water	1 M CaCl_2	Tap water
pH	2 (HNO_3)	7	12 (NaOH)
4 hr (%)	27.5	9.5	53.8
72 hr (%)	23.3	12.2	61.8

5. Movement of Radionuclides in Terrestrial Environment

T. F. Lomenick
Tsuneo Tamura
Ferruccio Gera²

W. M. McMaster¹
R. M. Richardson¹
D. A. Gardiner³

EVALUATION OF FISSION PRODUCT DISTRIBUTION AND MOVEMENT IN AND AROUND CHEMICAL WASTE SEEPAGE PITS 2 AND 3

T. F. Lomenick Ferruccio Gera
H. J. Wyrick

Quantity and Distribution of Radionuclides in the Area

Recent abandonment and subsequent filling of waste pits 2 and 3 has provided an opportunity to investigate in greater detail the nature and extent of fission product migration in the immediate environs. There are approximately 40,000 curies of ⁹⁰Sr and 180,000 curies of ¹³⁷Cs in the area.⁴

A series of 17 cores was taken in and around the two pits to determine the effectiveness of conventional sampling equipment and methods for obtaining representative samples of the various types of materials used as fill (lumber, metal drums, rock, etc.), of the soft sludges and precipitates in the bottoms of the pits, and of the weathered and unweathered Conasauga shale comprising the side walls and bottoms. A sufficient number of cores were taken and analyzed to grossly delineate radioactivity concentrations of the soil and materials in and around the area. Although core recovery was generally poor, radiochemical analyses of sections of the core indicated that apparently most of the activity, which is largely cesium and strontium, is associated with the soft sludges and precipitates and the first few inches of shale on the side walls and bottoms. It was also determined that the sludges and precipitates are not evenly distributed over the bottoms of the pits but have accumulated in irregularly shaped pockets. A

cross-sectional view of waste pit 3, showing the areas of high activity concentrations and the distribution of sludge, is presented in Fig. 5.1. It was noted in well 3 that the sludge is about 10 ft thick and is within 4 ft of the ground surface, while no sludge was found in hole 11 in the center of the pit. This is due to the highly mobile state of the sludge, which allowed it to be pushed ahead of the fill material until it was confined by timbers and was eventually covered. On a dry-weight basis, concentrations of ¹³⁷Cs and ⁹⁰Sr were as high as 96 and 17 $\mu\text{C/g}$, respectively, in the sludge, and 3 and 0.2 $\mu\text{C/g}$ in the weathered shale on the side walls and bottoms of the pits. There appears to be little difference in the concentrations of activity in the two pits, either in the sludge or the weathered shale, although the quantity of sludge in waste pit 2 is considerably less than that in waste pit 3.

Analyses of the sludge, which is produced in the low-level liquid treatment process at ORNL and routinely dumped into the pits during their operating life, show that from 20 to 50% of the material is in the form of CaCO_3 , while the remaining fraction is predominantly illitic-type clay. Practically all of the ⁹⁰Sr is contained in the CaCO_3 fraction, while the cesium occupies highly selective exchange sites on the illitic clay.

In order to determine adequately the quantity and define the distribution of the various radionuclides within the area, it is essential that the sludge and the shale that immediately underlies the bottoms and side walls be carefully sampled. A "freezing" method appears to be the most suitable for obtaining these samples. This method, which utilizes kerosene cooled with dry ice as a drilling fluid and a conventional core barrel for coring the frozen material, should allow almost 100% core recovery. The job, which is currently under way, will require at least 50 holes, fully cored from the surface to a minimum depth of 20 ft.

Ground Water Movement in the Area

In evaluating the effects of ground water on the movement of various radionuclides in and around

¹U.S. Geological Survey.

²Alien guest.

³Mathematics Division.

⁴F. L. Parker and R. E. Blanco, *Waste Treatment and Disposal Progress Report for May-October 1963*, ORNL-TM-757 (April 1964).

UNCLASSIFIED
ORNL-DWG 64-929
NE

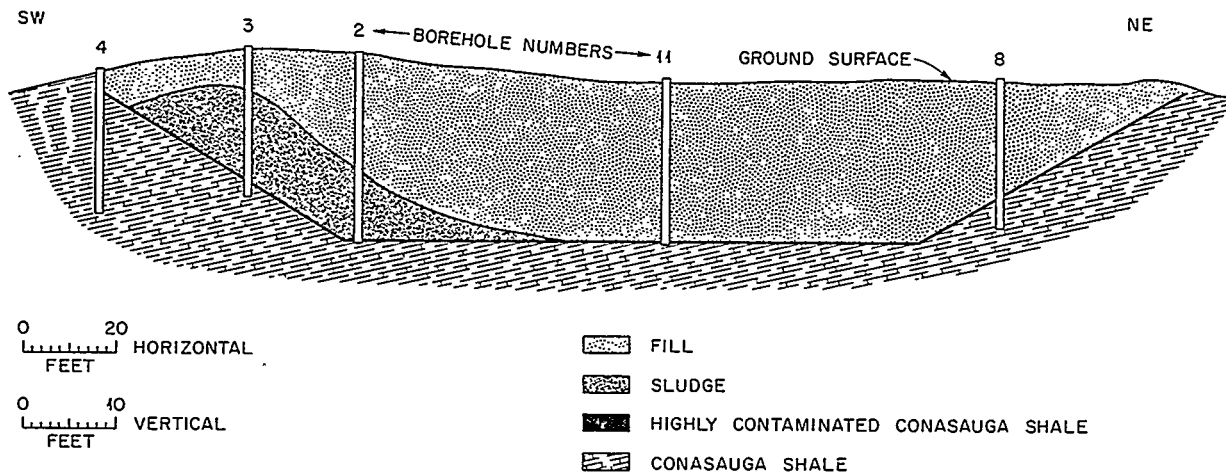


Fig. 5.1. Longitudinal Cross Section Through Waste Pit 3.

waste pits 2 and 3, it is essential that the directions and rates of subsurface-water movement be known. To aid in defining the movement of ground water in the waste pit area, a tracer test using tritium has been initiated. Twenty-one curies of tritiated water was injected into five 40-ft-deep holes, drilled on $1\frac{1}{2}$ -ft centers, along a line estimated to be at right angles to the strike of the geologic formation which underlies the area. By periodic sampling and analysis of the water from a series of observation wells, the rates and directions of movement of the tracer are being determined. After 6 months it has been established that the tritiated water has moved in a southwesterly direction with a minimum of lateral spread (see Fig. 5.2). The rate of flow of the peak concentration of the tritium, which may be referred to as the modal velocity of the water, was for the first 5 ft about 0.56 ft/day and only slightly less out to a distance of 10 ft.⁵ Because of the dilution of the tracer due to recharging rainfall, diffusion, etc., some difficulty has been experienced in defining the concentrations of tritium in the more

UNCLASSIFIED
ORNL-DWG 64-7897

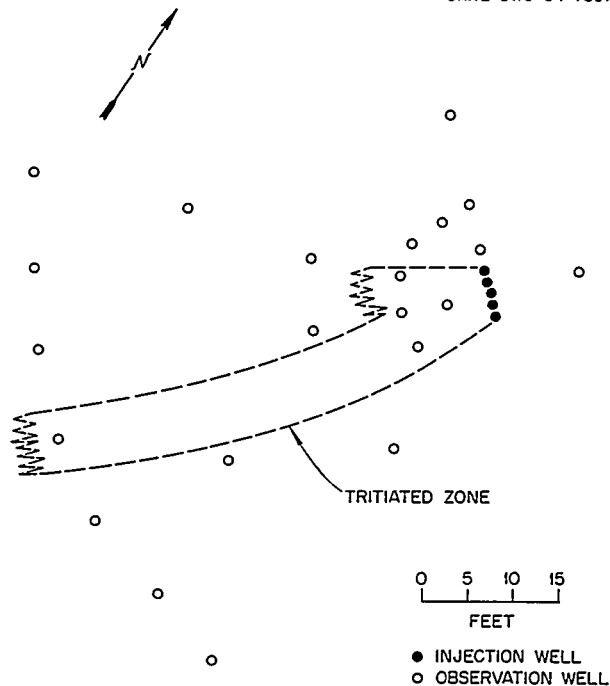


Fig. 5.2. Plan Showing Extent of Subsurface Migration of Tritium in Waste Pit Area Approximately Six Months After Tracer Injection.

⁵R. E. Blanco and F. L. Parker, *Waste Treatment and Disposal Progress Report for November 1963-January 1964*, ORNL-TM-830 (in press).

distant observation wells. However, it appears that the rate of flow of the tritiated water has not changed greatly from that observed in the observation wells close to the points of injection.

OCCURRENCE AND RETENTION OF RADIONUCLIDES IN THE SEDIMENTS OF WHITE OAK LAKE

T. F. Lomenick D. A. Gardiner³
H. J. Wyrick

The accumulation of the 700 curies of ^{137}Cs in the sediments of White Oak Lake illustrates clearly the effectiveness of a quiescent body of water in concentrating radionuclides in bottom sediments downstream from the point of continuous discharge of low-level liquid waste to surface streams. Nearly all the cesium in the lake bed is associated with lacustrine sediment. This is illustrated in Fig. 5.3, which shows the concentration of cesium in several cores taken throughout the lake bed. It is also noted that there is little difference in the concentration of cesium in the cores where the sediment is only a few inches thick and some of

the cores where the sediment is up to 12 in. thick. Thus, there is apparently no relationship between sediment thickness and cesium concentration. It is also observed that the concentration of cesium in the sediment varies greatly in some cores with depth, while in others it is relatively uniform. This is probably the result of variations in the cesium content of the sediment deposited at various times.

In order to define further the distribution of cesium in the sediments, several samples of the material were physically separated, using Jackson's method,⁶ into various particle size fractions, and then each fraction was analyzed to determine the quantity of cesium associated with it. The clay fraction of the sediment comprised only about 35% of the weight of the material, but more than 80% of the cesium was associated with it. In contrast, the silt fraction, which constitutes more than 60% of the weight of the sediment, was found to sorb only about 15% of the cesium. Only a trace of cesium was associated with the sand fraction of the sediment which made up less than 5% of the total weight of the sediment. It is obvious that the association of cesium with the sediment is due to the high affinity of the clay minerals for cesium. Through x-ray diffraction techniques, it has been found that the clay fraction of the sediment is predominantly illite. Leaching tests show that ^{137}Cs can be desorbed from the sediment only by disruption of the clay lattice structure. Thus it is unlikely that any large fraction of the cesium would move from the area except through a large-scale erosion of the sediment layer.

⁶M. L. Jackson, *Soil Chemical Analysis — Advanced Course*, published by author, Department of Soils, University of Wisconsin, Madison, 1956.

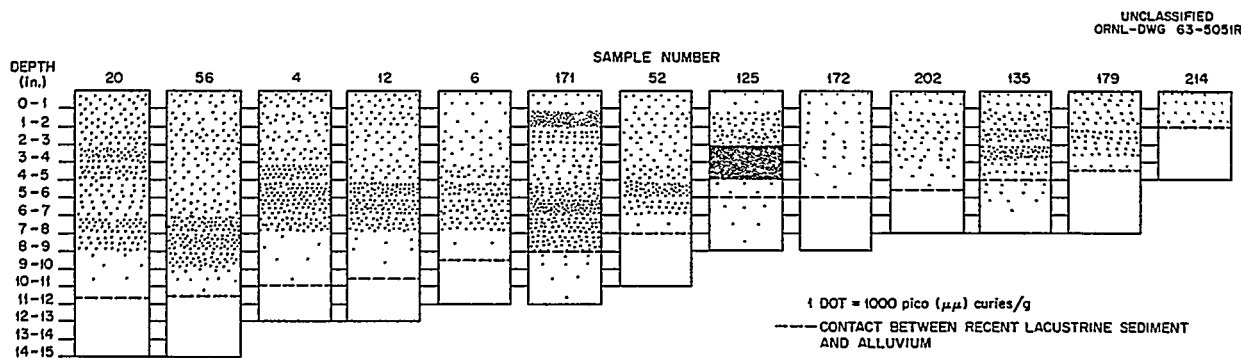


Fig. 5.3. Concentration of ^{137}Cs in White Oak Lake Core Samples.

HYDROLOGY OF WHITE OAK CREEK BASIN

W. M. McMaster¹R. M. Richardson¹

The objectives of the study of the hydrology of White Oak Creek Basin were to define and measure the hydrologic environment of the basin as it relates to the movement and retention of radionuclides released to the environment. Routine surface- and ground-water measurements were made in conjunction with special measurements such as surface-water time of travel for a wide range of flow conditions, correlation of rainfall-runoff data, sampling and analyzing channel bottom sediments and suspended sediments for particle size, mineralogy, and radionuclide content, and geologic mapping for correlation with hydrologic conditions.

During the 1964 fiscal year, a series of ten sediment ranges were established in White Oak Creek, two of which are above the Laboratory area, the remainder being distributed from the Laboratory to the head of White Oak Lake. At these sites, channel cross sections have been measured following significant high-water stages as an indication of scour and deposition. Samples have been collected from the upper 0.2 ft of bottom sediment at the sites in and below the Laboratory area for particle size analyses and for measurement of the content of associated radionuclides. As shown in Fig. 5.4, the distribution of radionuclides in the less than 63- μ fraction of the sampled zone varies considerably with place. The content of ^{137}Cs at all sections, except White Oak Creek

mile (WOCM) 2.56, is much greater than that of ^{60}Co or ^{106}Ru . The content of radioactivity decreases with distance from WOCM 2.35, about 0.21 mile below the Process Waste Water Treatment Plant effluent, to WOCM 1.12 near the head of White Oak Lake, where an increase in radioactivity occurs, chiefly in ^{137}Cs content.

The distribution of activity varies, not only along channel, but varies from side to side of the stream as shown in Fig. 5.4. The variations are caused by several factors, including channel characteristics such as pools and riffles and type of sediment present.

The bottom sediment of White Oak Creek is extremely variable with place, ranging from 50% finer than 63 μ at WOCM 2.22 to only 1% finer than 63 μ at WOCM 2.35. Throughout the channel the sediments consist of particles ranging from about 2 μ to several centimeters in diameter. The size composition of the sediments also varies widely. Particle size analyses show that, on the average, only 17% of the material was silt or smaller (less than 63 μ).

On the basis of analyses of bottom-sediment samples collected at the sediment ranges, the silt and finer sediment of the upper 0.2 ft of channel between WOCM 2.68 and 1.12 consists of about 1.22×10^8 g of material, bearing an average concentration of about 3.8×10^3 $\mu\mu\text{c/g}$ dry weight of ^{137}Cs , or a total of about 4.6×10^5 μc of ^{137}Cs . On this same basis, the sediment contains an average of 490 $\mu\mu\text{c/g}$ dry weight of ^{60}Co or a total of 5.9×10^4 μc ; these sediments contain an aver-

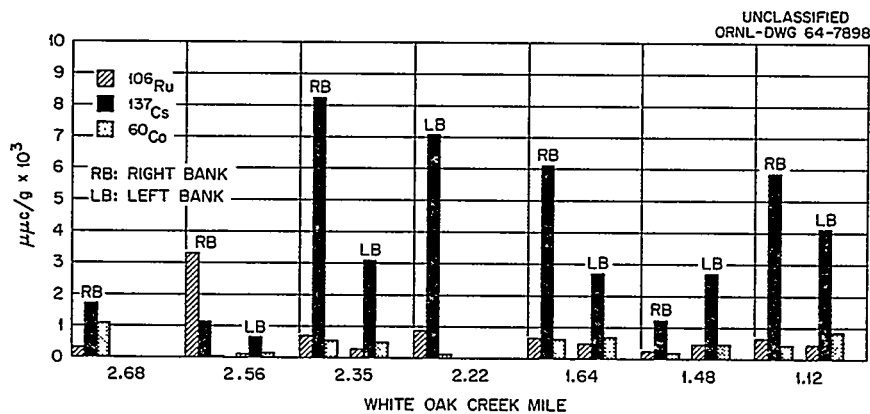


Fig. 5.4. Content of ^{106}Ru , ^{137}Cs , and ^{60}Co in Upper 0.2 ft of White Oak Creek Bottom Sediment (Silt and Smaller Fraction).

age of $720 \mu\mu\text{c/g}$ dry weight of ^{106}Ru or a total of $9.2 \times 10^4 \mu\text{c}$.

The low content of radioactivity in at least the upper 0.2 ft of channel sediments, as compared to the more than 450 curies in the upper 6 in. of White Oak Lake bed sediment as calculated by Lomenick,⁷ indicates that the residence time of near-surface contaminated sediments in White Oak Creek bed is probably fairly short. It is believed that most of the silt and finer material resides in this zone only between high stages before being washed into White Oak Lake, being replaced along the channel during stage recession by uncontaminated sediments carried in from the basin surface. These sediments in turn sorb activity from the stream during the period of base flow.

FIELD INVESTIGATIONS OF THE MOVEMENT OF RADIONUCLIDES DEPOSITED ON SOILS

Tsuneo Tamura R. M. Richardson¹
W. M. McMaster¹

The retention and movement of radionuclides have received much attention in the laboratory and in greenhouse studies. In particular, the two most hazardous nuclides, ^{90}Sr and ^{137}Cs , have been investigated with minerals or with air-dried soils brought into the laboratory.⁸⁻¹³ While laboratory studies have served to define the basic mechanisms involved in the retention of strontium and cesium, and the greenhouse studies have supported some of the findings in the laboratory, larger-scale field tests with these nuclides sorbed

on soils in equilibrium with their environment have been attempted only on a limited basis. Research in contaminated field areas such as the White Oak Lake bed has been the source of much valuable information; however, the doubtful origin, source, and original concentration of the contamination have made it difficult to draw conclusions regarding the eventual fate of the radionuclides in the sediment.

As increasing information is gained from laboratory studies on radionuclide sorption, it is becoming even more apparent that field studies are necessary, not only to resolve sometimes contradictory data between laboratory and greenhouse studies, but to investigate the reactions of fission products in soils which are in dynamic equilibrium with the biosphere and which are subject to daily, seasonal, and yearly changing natural forces of weathering. While radionuclide movement may be followed by percolating water or salt solutions through a packed column of soil material, in the field the soil will be subject to natural rainfall and erosional forces which alter the distribution of the nuclides. An even greater influence in field studies, which is seldom duplicated in the laboratory, is the biological condition of the soil, especially in the A horizon (organic rich), which will greatly affect retention and translocation.

Studies on the soil will provide valuable information on understanding the fate of the nuclide in the inorganic matrix (the minerals) and on understanding the behavior of nuclides in the entire ecological cycle. The more specific areas and avenues of research are outlined below; special emphasis is placed on the information which is unique to field situations.

1. The behavior of cesium (strontium studies will follow after experience and knowledge are gained with cesium) can be evaluated in the A_p horizon of a cultivated soil which is subject to the influence of normal environmental forces including precipitation, erosion, evaporation, percolation, and temperature variations.
2. The influence of the B and C horizons, including "plow pans," on the rate of movement downward from the A_p horizon may be evaluated by long-term experiments permitting many samplings.
3. Information on the influence of translocation by channeling and through roots will be obtained by selected sampling.

⁷T. F. Lomenick et al., *Health Phys. Div. Ann. Progr. Rept. June 30, 1963*, ORNL-3492, p. 51.

⁸T. Tamura and D. G. Jacobs, *Health Phys.* 2, 391-98 (1960).

⁹D. G. Jacobs, *Health Phys.* 4, 157-63 (1960).

¹⁰D. G. Jacobs and T. Tamura, *Trans. Intern. Congr. Soil Sci., 7th, Madison, Wis., 1960*, pp. 206-14.

¹¹T. Tamura and D. G. Jacobs, *Health Phys.* 5, 149-54 (1961).

¹²T. Tamura and E. G. Struxness, *Health Phys.* 9, 697-704 (1963).

¹³J. R. Miller and R. F. Reitemeier, "The Leaching of Radiostrontium and Radiocesium Through Soils," *Soil Sci. Soc. Am. Proc.* 27, No. 2 (1963).

4. Ion exchange information which will be obtained includes information on the rate of change in availability of cesium with time and the seasons. Included in this phase of the study is the concurrent measurement of the potassium status of the soil with time and season. Availability will be related to concentration in the crop (fescue grass) of both cesium and potassium.
5. The movement of cesium will be related to the moisture status and the geohydrologic factors.
6. Data from the field will be correlated with data from laboratory tests in order to establish the existence of a "coefficient."

To accomplish the objectives, samples will be collected periodically from the contaminated fields. Core samples will be removed periodically for assay of movement of the cesium using the gamma spectrometric core scanner which is already in operation. After scanning, the cores will be removed and analysis performed to determine the "fixation" and "availability" of the cesium, the available potassium content, the pH, and moisture content. Other core studies of a more permanent nature will be made by returning some of the cores to the field for longer exposure to the natural forces of weathering. It is also contemplated that with several of the cores, limestone and potash will be added on the surface in order to measure the influence of "normal" agricultural practices. By comparisons with cores which had not received the supplement treatment, it will be possible to differentiate effects of the amendments from normal changes occurring in the field. Bagged samples will be used primarily to determine the areal distribution of the nuclide. Selected samples will be analyzed for their ion exchange capacities, clay mineral, organic matter, and exchangeable ion content, particle size distribution, and other chemical and physical properties which could influence the fate of the nuclide. Synthetically assembled minerals will be used for comparison with field data.

Field Environmental Study Area

A rectangular area, 80 by 230 ft, was cleared, enclosed with 4-ft animal-proof fence, and seeded with rye and red fescue grass. Two 8- by 8-ft plots were enclosed with mesh panels, and provisions

have been made to collect and to measure all surface runoff from both plots.

After a suitable grass cover is established, the plots will be dosed with 5 mc of ^{137}Cs . Subsequently, water and sediment runoff from the plots will be collected, measured, and assayed for ^{137}Cs . In addition, cores of soil will be collected and assayed to determine the vertical distribution of ^{137}Cs in the soil profile. Measurements will also be made at the soil surface to determine whether an areal redistribution due to erosion and deposition has occurred.

Field Investigations of the Movement of Water Over and Through Soil

The principal agent which affects the movement of radionuclides deposited on soil is water, which is present in continually changing quantities in the atmosphere, on the earth's surface, and below ground. Surface runoff during and after storms may erode contaminated soil, causing an areal redistribution of radionuclides; the flux of soil moisture, which may be upward or downward, may cause a redistribution of radionuclides in the soil profile; finally, radionuclides which reach the water table may be transported by ground water.

In the plots, provisions have been made to collect and to measure all surface runoff, including sediment. The instruments that have been installed in the area include thermometers for measuring air and soil temperature at various points above and below land surface, tensiometers and soil moisture blocks to measure changes in soil moisture content, an observation well equipped with a water-stage recorder to measure fluctuations of the ground-water table, a rain gage to measure precipitation, an evaporation pan to measure evaporation, an anemometer to measure wind velocity, and a Livingston atomometer to measure evaporativity and solar radiation. The primary purpose of these measuring instruments is to obtain at first a clear qualitative picture of the physical processes involved in the exchange of water between soil and atmosphere. We hope ultimately to determine the quantitative importance of each process in the transfer of water between land surface and water table.

6. Mineral Exchange Studies

Tsuneo Tamura
D. G. Jacobs

Tohru Murano¹
W. P. Bonner

SORPTION OF STRONTIUM BY CLAY MINERALS

Tsuneo Tamura W. P. Bonner Tohru Murano

Sorption of strontium by the clay minerals has been considered to be an ion exchange reaction; on the other hand, sorption of this element by activated alumina and the hydrous sesquioxides is believed to be by a different mechanism than that for the clay mineral. To get a better understanding of the nature of the reaction of strontium, comparisons were made of the sorption of strontium with several sorbents using mass action considerations to depict ideal ion exchange behavior.

Ion Exchange Equilibria

Mass action expressions have been used by several investigators to describe ion exchange equilibria. In a system where the strontium is present in tracer quantities and the clay is essentially sodium saturated, the activity coefficients of the sodium clay, strontium clay, and strontium ion may be considered to be constant over a range of sodium concentration. One can write the equilibrium expression in the form

$$K' = \frac{(\text{SrC})[\text{Na}^+]^2}{(\text{Sr}^{2+})(\text{Na}_2\text{C})}, \quad (1)$$

whereby

K' incorporates the constant activity coefficients in the equilibrium constant,

() denotes concentrations, and

[] denotes activity.

By definition, the distribution coefficient (K_d) for strontium is defined as

$$K_d = \frac{(\text{SrC})}{(\text{Sr}^{2+})}, \quad (2)$$

and one may combine Eqs. (1) and (2) to form

$$K_d = K' \frac{(\text{Na}_2\text{C})}{[\text{Na}^+]^2}. \quad (3)$$

Since the clay remains essentially sodium saturated, Na_2C may be considered to be constant, and a $\log K_d$ vs $\log [\text{Na}^+]$ plot should yield a straight line. The slope of the line is a function of the exponent of Na^+ and K_d , and, in this case, the slope is -2 for an ideal system.

If one varies the sodium ion concentration over a wide range, the activity coefficient for the sodium ion changes and activity should be used in the plot. With clay size particles, dispersion of the material is observed below approximately 0.01 *M* sodium nitrate; and accurate measurements of (Sr^{2+}) are difficult to obtain below this concentration. For a more complete treatment of mass action equilibria in ion exchange reactions, one is referred to the paper by K. A. Kraus.²

Strontium Sorption by Clay Minerals

The $\log K_d$ vs $[\text{Na}^+]$ plot for montmorillonite and hydrobiotite is shown in Fig. 6.1. Note that in less than 0.02 *M* sodium ion concentration, the K_d appears constant for the montmorillonite sample; this behavior is believed to be due to the dispersion of the very fine particles of montmorillonite in the low salt concentration. On the other hand, the hydrobiotite sample is between 35 and 70 mesh, and very little dispersion was noted. These two materials represent the more classic examples of clays which exhibit ion exchange characteristics by isomorphic substitution, and they exhibit a slope of -2 as calculated. It is interesting to note that the K_d is greater for the hydrobiotite with approximately 70 meq/100 g of cation exchange capacity than for the montmorillonite with 90 meq/100 g.

¹Alien guest.

²K. A. Kraus, *Trace Analysis*, pp. 34–101, Wiley, 1957.

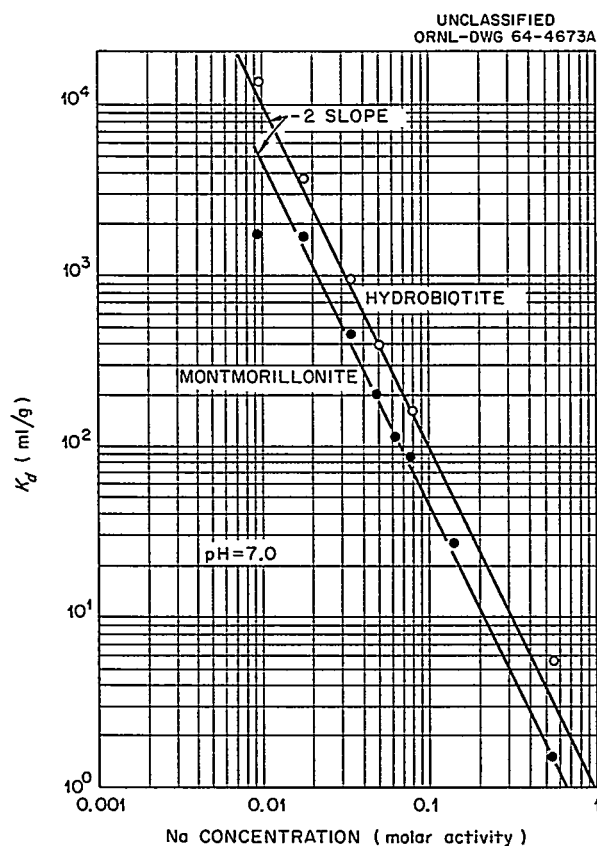


Fig. 6.1. Influence of NaNO_3 Concentration on Strontium Sorption by Montmorillonite and Hydrobiotite.

In Fig. 6.2 similar data are given for two illite samples. Tests show that the sample from Wisconsin differs from the one from Illinois in degree of crystallinity and exchange capacity. The former material gives a strong, sharp diffraction maximum at 10 Å in contrast to a weak diffuse maximum for the latter. The ion exchange capacity is approximately 22 meq/100 g for the Wisconsin sample and 17 meq/100 g for the Illinois sample. The data in Fig. 6.2 show that Wisconsin illite's response is similar to that of montmorillonite and hydrobiotite and that the response follows the predicted mass action reaction. The slope obtained for the Illinois sample is less than that predicted for ideal exchange; the reason for this difference in behavior is not yet known, though it is suspected to be related to the degree of crystallinity of the

clays. It is interesting to note again that despite a lower exchange capacity for the Illinois illite, the K_d is higher than for the Wisconsin illite at all levels of sodium nitrate concentration.

Strontium Sorption by Alumina

When alumina was similarly tested, the response curve differed greatly from that observed with clays. A plot of $\log K_d$ and \log sodium nitrate concentration produced a curve with a slope considerably less than -2 (i.e., a slope of -0.8 was calculated); and the K_d also was strongly dependent on the pH of the solution (Fig. 6.3). Similar response was noted for activated alumina (F-20 grade) from the Aluminum Company of America, the chief difference being much higher K_d values for the activated alumina because of the higher specific surface area of activated alumina.

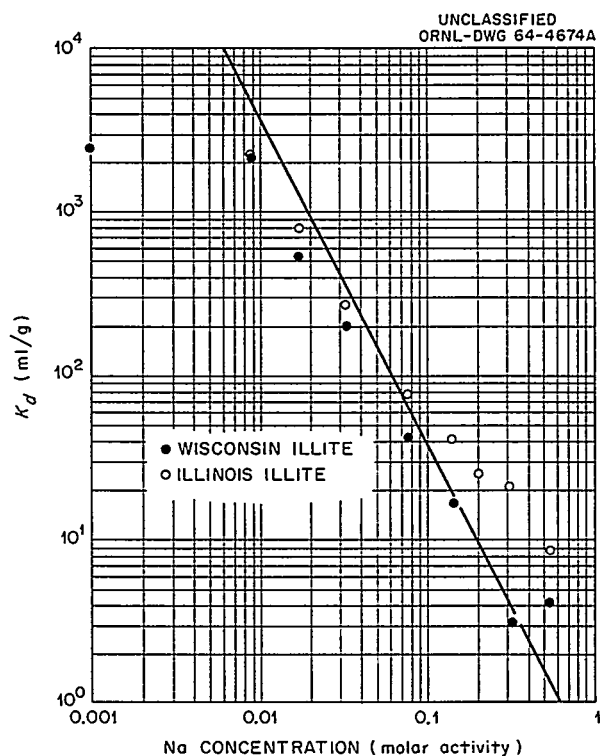


Fig. 6.2. Influence of Sodium Nitrate on Strontium Sorption by Illites.

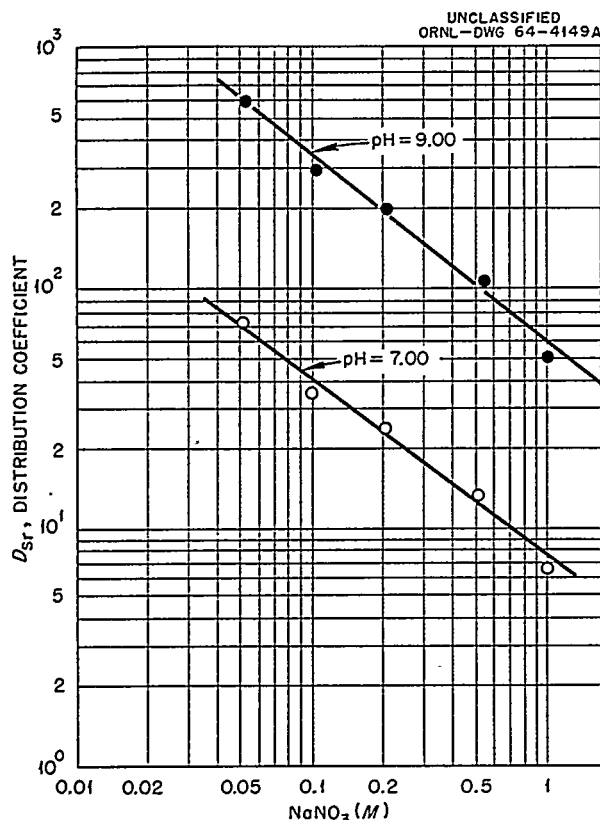


Fig. 6.3. Distribution Coefficient of Alpha Alumina in Sodium Nitrate Solutions.

At this time it may be useful to summarize some of the differences and similarities between alumina and the clay minerals from the standpoint of ion exchange reactions. Clay minerals, such as montmorillonite and hydrobiotite, exhibit ion exchange capacities by virtue of isomorphous substitution which gives rise to a charged particle and whose charge is neutralized by the exchange ions. Alumina, on the other hand, probably shows cation exchange reactions by neutralization of surface hydrogen ions; the degree of neutralization would be a function of pH.

Strontium Sorption by Muscovite

This mineral is similar to illites and represents a material of low exchangeable cation content. This material was selected for investigation, since studies with several soil materials from other

sections of the United States revealed muscovite as a relatively common constituent in them. The exchange capacity of the muscovite sample (less than 3.75 μ diameter) was approximately 4 meq/100 g when measured at pH 7.0 as compared to 17 meq/100 g for a sample of illite from Illinois tested under similar conditions.

The curve for muscovite is similar to that obtained with alumina; in both cases the slope of the $\log K_d$ vs \log sodium nitrate concentration is approximately -1 rather than -2 . At pH 9, muscovite removes strontium more effectively than montmorillonite at pH 9.0. This is surprising since montmorillonite particles are smaller and, therefore, expose more surface and could contribute more exchange by this mechanism. Tests with Illinoian illite also show that this material gives a -1 slope at pH 9. Considering all the materials tested, it appears that the ion exchange capacity of the clays and sesquioxides as measured by conventional methods is not the most significant index in defining the exchange characteristics for trace levels of strontium at alkaline pH.

Strontium Sorption by Soil Materials

The term *soil materials* is used to define natural fine-grained materials which have been subjected to natural weathering processes, and they generally differ from standard mineral samples, not only in being mixed mineral systems, but show different chemical and physical properties. Of particular interest at Oak Ridge is Conasauga shale from the upper mantle which has undergone weathering. This material is used as a disposal medium for liquid intermediate-activity waste; illite is the predominant clay mineral with vermiculite in lesser quantity. Tests at pH 7 show that ideal ion exchange behavior is obeyed (-2 slope); tests at pH 9 show that the slope is reduced and sorption increased (Fig. 6.4). The increase is expected at the higher pH because of the added capacity from the ionized hydrogens of the surface of the clay minerals. In addition to the sorption by the clay minerals, it was felt that the sesquioxides present in the shale could contribute to the removal of strontium at pH 9.0. To test this idea, the shale was treated for iron oxide removal by treatment with sodium dithionite and sodium nitrate. The resultant shale sample

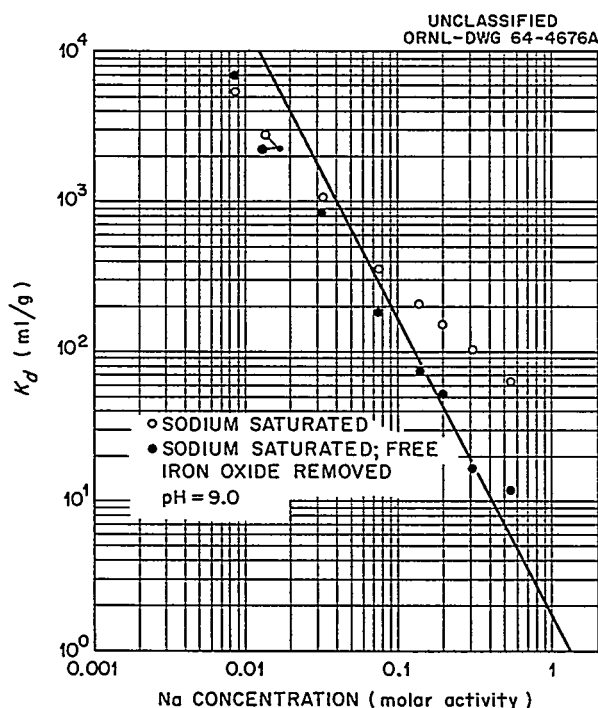


Fig. 6.4. Influence of Sodium Nitrate Concentration on Strontium Sorption by Conasauga Shale.

showed an increase in capacity from 13.0 meq/100 g to 17.7 meq/100 g, which suggests that the iron oxide had "blocked" the exchange site of the mineral. The increase in capacity, however, was not accompanied by an increase in sorption as might be expected from exchange capacity considerations, except for the sample at the lowest sodium nitrate concentration. The decrease is strong evidence of the direct participation of iron oxides in the sorption reaction at alkaline pH. This is of importance since disposal into this formation is accomplished in an alkaline system.

The influence of calcium ions, the types of exchange sites at pH 7 and 9, and the influence of dissolved salts on the production of exchange sites (Donnan effect) on the sorption of strontium are being investigated. Data obtained to date give evidence of the complex nature of soil materials in their reaction with strontium; information on the distribution and properties of the

reactive materials in soils will be helpful in understanding the sorption, fixation, and movement of this important nuclide in the environment.

THE EFFECT OF EDTA ON CALCIUM-STRONTIUM EXCHANGE BY HYDROBIOTITE

D. G. Jacobs Y. W. Kim¹
O. H. Myers S. M. Burke³
O. M. Sealand

Ethylenediaminetetraacetate (EDTA or Versene) forms stable soluble complexes with many metal cations, including the alkaline earths. For this reason EDTA is a common ingredient in solutions used for decontamination, and it is often found in low-level radioactive waste streams.

Sodium-based hydrobiotite was treated for removal of free iron by Jackson's method⁴ to prevent loss of EDTA due to its strong complexing with iron. Columns were filled with 10 g of the hydrobiotite and leached with 0.01 N EDTA at pH 9.5 overnight. Before a run was begun, the EDTA was washed from the column with a dilute solution of NaOH (pH 9.5).

Solutions were made of 0.01 N CaCl_2 , tagged with ^{45}Ca ; one batch was brought to the equivalence point with EDTA, and the other brought to 0.01 N NaCl. Strontium-85 was added to each of these solutions in equal concentration. Five columns were run using solutions prepared by mixing proper amounts of the solutions to give 0, 25, 50, 75, and 90% complexing of the calcium with EDTA.

In the column with no EDTA, the breakthrough of ^{45}Ca slightly precedes the breakthrough of ^{85}Sr , yielding a $K_{\text{Ca}}^{\text{Sr}}$ of 1.19 (Fig. 6.5). The ^{85}Sr breakthrough curve tails off slightly above 80% breakthrough because of conversion of the hydrobiotite from the sodium form to the calcium form. There is no apparent leakage through the column before the major breakthrough wave.

When the influent solution contains EDTA, there is immediate leakage of both ^{45}Ca and ^{85}Sr through the column which quickly builds up to an equilibrium value, determined by the stoichiometric equivalent of EDTA added (Fig. 6.6 and

³Summer employee.

⁴M. L. Jackson, *Soil Chemical Analysis*, Prentice-Hall, Englewood Cliffs, N.J., 1958.

Table 6.1). The ratio of the stability constant of the calcium-EDTA complex to that of the strontium-EDTA complex, $(K_{Ca-EDTA})_s / (K_{Sr-EDTA})_s$, can be determined from the leakage by the formula

$$\frac{(K_{Ca-EDTA})_s}{(K_{Sr-EDTA})_s} = \left(\frac{X}{100 - X} \right) \left(\frac{100 - Y}{Y} \right), \quad (4)$$

where

X = the percent calcium leakage, and

Y = the percent strontium leakage.

This ratio was determined experimentally to be 200, while the values given in the literature⁵ range from 91 to 138.

The major breakthrough wave is delayed, since the noncomplexed, ionic calcium (which controls the exchange reaction) is lower in concentration. Thus, in an ion exchange system the presence of some EDTA might be beneficial, provided a small leakage of strontium could be tolerated.

⁵A. E. Martell and M. Calvin, *Chemistry of the Metal Chelate Compounds*, Prentice-Hall, Englewood Cliffs, N.J., 1962.

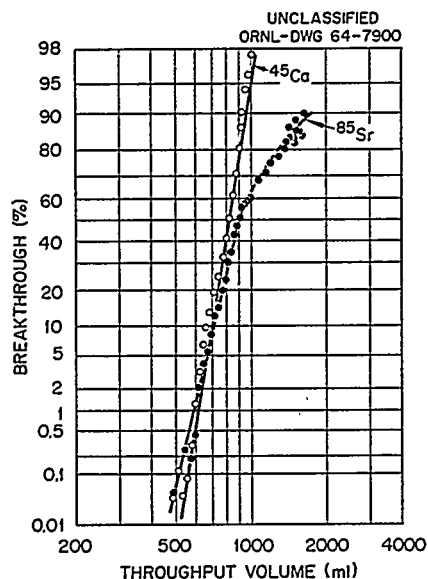


Fig. 6.5. Calcium-Strontium Exchange by 10 g of Hydrobiotite with a Trace of Strontium in 0.01 N $CaCl_2$ and 0.01 N NaCl.

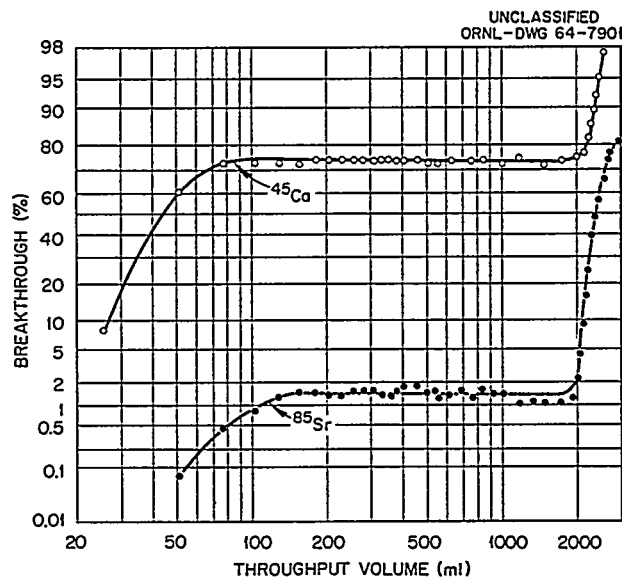


Fig. 6.6. Calcium-Strontium Exchange by 10 g of Hydrobiotite with a Trace of Strontium in 0.01 N $CaCl_2$ and 0.0075 N EDTA.

Table 6.1. Effect of EDTA on Calcium-Strontium Exchange by Hydrobiotite from 0.01 N $CaCl_2$ -0.01 N NaCl

	Column Number				
	1	2	3	4	5
Calcium complexed, %	0	24.48	49.81	74.85	90.00
Calcium leakage, %	0	24.89	50.38	74.41	92.04
Strontium leakage, %	0	0.19	0.49	1.45	4.29
$(K_{Ca-EDTA})_s / (K_{Sr-EDTA})_s$		174	203	204	201
SrK_d , ml/g	95	119	156	234	452
Apparent CaK_d , ml/g	74	71	66	57	38
Apparent K_{Ca}^{Sr}	1.28	1.68	2.36	4.11	11.9
Corrected ^a K_{Ca}^{Sr}	1.28	1.26	1.17	1.05	1.18

^aCorrected for the concentration of noncomplexed calcium.

7. Engineering, Economic, and Safety Evaluations

R. L. Bradshaw J. J. Perona¹
D. G. Jacobs J. O. Blomeke¹
K. E. Cowser

ENGINEERING AND ECONOMIC EVALUATION

R. L. Bradshaw J. J. Perona¹
J. O. Blomeke¹

This study, undertaken in cooperation with the ORNL Chemical Technology Division, has as its objective the evaluation of the economics and safety associated with radioactive waste management. All steps between final processing and ultimate disposal are being considered, and it is expected that an optimal combination of operations will be defined for different methods of disposal and, in addition, that the most promising areas for experimental study will be indicated.

Principal emphasis has been placed so far on the economics of a series of operations believed to represent an acceptably safe scheme for the management of highly radioactive liquid wastes. Estimated costs have been reported previously for interim storage of the wastes as liquids, conversion to solids by pot calcination, interim storage of solids, and shipment of solids. Also, the effect of fission product removal on waste management costs was estimated.

During the past year, studies were made of the comparative costs of permanent storage of solidified waste in concrete vaults, granite formations, and salt mines;² and work has continued on preparation of the final report on costs for disposal in salt mines. Additional heat-transfer calculations have been made; additional understanding of mine stability problems has been gained; and more accurate costs for salt excavation have been calculated.

Comparative Costs for Disposal in Vaults, Granite, and Salt

Although cavities mined in salt formations are believed to offer the best possibilities for the

permanent disposal of solidified wastes, the use of salt implies the probable need for shipping the wastes to a mine from a processing plant possibly many miles distant. Suitable deposits of granite or shale might be more accessible to a plant, and it is conceivable that high-integrity concrete vaults could be constructed at the plant site to serve the purposes of permanent containment. Lacking a formal safety analysis, a qualitative observation can be made that disposal in granite would, at best, be no safer than in salt and that concrete vaults would be less safe because of the limited period of integrity of the concrete and the proximity of the waste to the biosphere. Therefore, the costs for mining space in granite must be as low as for salt, and the costs for vaults must be lower than for salt, for these alternative methods to be competitive. As is seen below, this was found not to be the case. Costs for storage in concrete vaults were five to seven times as great as those for storage in salt, and costs for storage in granite were twice those for salt.

A basic assumption is that, after the waste has been placed in storage, all accesses to the storage area are sealed to provide the maximum containment and isolation from the environment. Under these circumstances, dissipation of the radioactive decay heat will occur only by conduction through the surrounding solid medium. Better heat transfer to permit more efficient utilization of storage space could be achieved by circulation of air through the storage area and discharging it back into the atmosphere after appropriate cleaning and monitoring. However, this would represent a less safe situation in that it would provide a direct route for the escape of the fission products into the environment in the event of sabotage or natural disaster.

Having available as a point of reference the more detailed preliminary analysis of the cost factors in the disposal of calcined wastes in salt mines,³ only a rather perfunctory analysis is

¹Chemical Technology Division.

²J. J. Perona et al., *Comparative Costs for Final Disposal of Radioactive Solids in Concrete Vaults, Granite, and Salt Formations*, ORNL-TM-664 (Oct. 23, 1963).

³R. E. Blanco and E. G. Struxness, *Waste Treatment and Disposal Progress Report for February and March 1962*, ORNL-TM-252, pp. 39-43 (Sept. 10, 1962).

needed to show the relative costs for disposal in vaults and granite. The procedure consisted in calculating the relative costs for storage space and then estimating space requirements as determined by heat transfer considerations. Handling procedures and operating costs were assumed to be identical to those used for disposal in salt.

As in previous cost studies in this series, a 6-tonne⁴ per day plant was assumed, processing 1500 tonnes of uranium converter fuel per year at a burnup of 10,000 Mwd/tonne and 270 tonnes of thorium converter fuel per year at a burnup of 20,000 Mwd/tonne. This hypothetical plant would process the fuel from a 15,000 Mw (electrical) nuclear economy, which may be in existence by 1975. Acid Purex and reacidified Thorex wastes, packaged in cylinders 6 to 24 in. in diameter, were chosen for this study, as they possessed the highest and lowest heat-generation rates per unit volume respectively.

The concrete-vault concept assumed the construction of concrete rooms completely buried with just sufficient earth cover to provide the necessary shielding. Based on a preliminary design of such a vault, equipped with a stainless steel liner and air-cooling system, Watson *et al.*⁵ estimated a cost of \$10.70 per cubic foot of storage space. The gross resemblance to the vaults provided for storage of liquid waste is striking, in that all are underground structures of reinforced concrete, are of about the same size and proportions, and have leak-tight metal linings over their interior surfaces. The cost per unit of storage space for tanks ranges from \$6 to \$22.50/ft³ at Hanford, Savannah River, and the Idaho Chemical Processing Plant.⁶ After deductions for cooling systems and metal linings, space in these underground concrete structures costs about \$3 to \$4/ft³. In the present study, the use of both ordinary and high-temperature concrete was considered, and the cost of space was taken to be \$3/ft³ and \$4.30/ft³ respectively. Salt is mined for about \$2/ton, which results in a cost for space in salt formations of about \$0.15/ft³.

The spacing between cylinders of waste in a storage system is controlled by the necessity to dissipate the heat generated by radioactive decay without reaching temperatures injurious to the storage system. These limiting temperatures were taken to be 1650°F for the waste, 400 to 500°F for ordinary concrete, 1000°F for special high-temperature concretes, and 400°F for salt. Space requirements for acid Purex and reacidified Thorex wastes situated in racks in concrete vaults were computed as functions of age at burial, assuming for heat-transfer estimates the case of a semi-infinite slab, initially at constant temperature, with a constant heat flux into one surface and heat loss from the other by convection. The greatest savings in space requirements for vaults compared with salt occurred for the storage of wastes aged from 10 to 30 years, and, over this range of ages, the requirements differed by constant factors. Hence, the comparison of costs was carried out only for the case of 30-year-old wastes, the storage area requirements for which varied from 1.8 ft² for 6-in.-diam cylinders of reacidified Thorex waste in high-temperature concrete to 1300 ft² for 24-in.-diam cylinders of acid Purex in salt.

Costs of storage space per cylinder in concrete vaults and salt were obtained from the area requirements and space costs, assuming a floor-to-ceiling height of 15 ft (Table 7.1). Costs for storage space in high-temperature concrete were 20 to 50% less than those for ordinary concrete, but the cost of space in vaults was at least eight times higher for both acid Purex and reacidified Thorex waste than the cost of space in salt formations. In calculating the total costs of storage in salt, 60 to 85% were for salt removal; and, since the other costs (e.g., for handling equipment and labor for storing the cans) would be about the same for all storage systems, the relative total costs would probably differ by factors of 5 to 7.

Excavation costs in hard rock (granite or metamorphosed basalt) have been reported to range from \$9 to \$15/yd³ at a number of recent Government projects.⁷ By way of comparison, excavation costs in salt are about \$4/yd³ (\$2/ton). This difference exists because heavier equipment is required to mine hard rock, drilling is more difficult and is slower, and costs of explosives are

⁴Metric ton.

⁵L. C. Watson *et al.*, *Method of Storage of Solids Containing Fission Products*, CRCE-736 (June 30, 1958).

⁶E. Doud, *Design of Underground Storage Tanks for Radioactive Wastes*, HW-57282 (March 1959).

⁷P. L. Russell, U.S. Dept. of the Interior, Bureau of Mines, personal communication to R. L. Bradshaw, ORNL, May 16, 1963.

Table 7.1. Cost of Space in Salt Formations and Concrete Vaults for Cylinders of Waste Aged 30 Years

	Cost of Space (\$/cylinder)	
	Acid	Reacidified
	Purex	Thorex
Salt Formations, 400°F Limit		
6-in.-diam cylinders	180	15
12-in.-diam cylinders	740	59
24-in.-diam cylinders	2,920	230
Vault, 500°F Limit		
6-in.-diam cylinders	2,300	185
12-in.-diam cylinders	9,100	720
24-in.-diam cylinders	36,500	2850
Vault, 1000°F Limit		
6-in.-diam cylinders	1,470	120
12-in.-diam cylinders	5,800	460
24-in.-diam cylinders	21,900	1850

higher. Since the thermal properties of salt (at 400°F) are within about 10% of those of granite, the space requirements in either medium would be about the same. Furthermore, the ratios of rock volume mined for storage space to that left as supporting pillars would also be comparable. Assuming all other costs (amounting to 15 to 40% of the total costs) to be also the same, storage in granite would cost about twice as much as storage in salt.

Additional Studies on Costs for Disposal in Salt Mines

Tentative costs were reported previously for storage of cylinders of calcined waste buried in a vertical position in the floors of rooms in salt mines.⁸ The primary purpose of the original study was to provide information on which parameters involved in the cost estimation were most important, and which items required further investigation. In making the original study, certain

assumptions were made for the cost of excavating salt and for the effect of temperature and mining patterns on the stability of a waste-disposal mine. This original study (based on \$2/ton for salt excavation) indicated that salt excavation costs accounted for 60 to 85% of the total cost, and that mine stability criteria (which were poorly understood at the time) could affect total costs by as much as a factor of 2.

Since the time of the original study, much knowledge has been gained concerning operations in salt mines, mine stability, etc. Much of this background information is reported in the previous reports in this series and in this report, under the heading: *Disposal in Natural Salt Formations*. Although the questions concerning mine stability have not yet all been answered completely, it was felt that sufficient information was available to refine the original study and to publish the results. This report is now nearing completion.

The costs of salt removal have been calculated as a function of the size of the mining operation, and it was found that the original estimate of \$2/ton is reasonable for a relatively large operation, but too low for operations in which the annual tonnage is small (less than 2×10^5 tons/yr).

The original heat calculations assumed an infinite array of waste containers covering the entire mine area and all placed in the mine simultaneously. Additional calculations have been performed for the more realistic case of waste containers in the floors of the rooms (i.e., none under roof-supporting pillars) and sequential filling of rooms with waste.

As a result of these new studies and other considerations, the original disposal-mine layout and concept have been modified. However, there have been no major changes, and, although the final cost figures have not yet been computed, it is believed that they will not be greatly different from the original figures and that none of the major previous conclusions will be changed.

TANK SAFETY EVALUATION

D. G. Jacobs

O. M. Sealand

Underground Movement of Fission Products

One possible route of radioactive waste solutions released by tank failure would be through

⁸F. L. Parker et al., *Health Phys. Div. Ann. Progr. Rept. July 31, 1962*, ORNL-3347, pp. 43-44.

the geologic formation lying between the tank site and the nearest surface drainageways. A hypothetical tank site at Oak Ridge is located in Conasauga shale on a promontory, with intermittent surface streams passing to the east, south, and west of the tank site. The shale formation is quite impermeable, and movement of water is restricted to flow along bedding planes, greatly limiting its velocity and direction.

Samples of the Conasauga shale were obtained below the highly weathered zone in a direct path toward the surface streams. These samples were acidified for removal of calcite, and the exchange capacities were determined by the calcium titration method of Jackson.⁹ A mean value of 11 ± 1 meq/100 g was obtained. Overnight refluxing in 7 M HNO₃ at 85°C showed hydrogen ion consumption of 260 meq/100 g, which would be sufficient to cause neutralization of the entire contents of an acid waste tank within 30 ft of the tank. In the case of acid waste, it was assumed that neutralization of the acid by calcite in the formation would result in a calcium salt system. In this system, strontium was assumed to compete with calcium without selectivity of either ion, though strontium might be slightly more selectively sorbed than calcium.¹⁰ For the sorption of strontium from neutralized wastes, and for the sorption of cesium and ruthenium, information on the sorption properties of Conasauga shale was obtained from previous laboratory studies.¹⁰⁻¹⁴

The quality of the ground water was assumed to be similar to that of Clinch River water, which has a total cation concentration of about 0.002 meq/ml, primarily calcium and magnesium.¹⁵

⁹M. L. Jackson, *Soil Chemical Analysis*, Prentice-Hall, Englewood Cliffs, N.J., 1958.

¹⁰D. G. Jacobs, pp. 43-53 in *International Colloquium on Retention and Migration of Radioactive Ions in Soils*, Centre d'Etudes Nucleaires de Saclay, France, October 16, 17, and 18, 1962 (1963).

¹¹R. L. Blanchard, B. Kahn, and G. G. Robeck, *Laboratory Studies on the Ground Disposal of ORNL Intermediate-Level Liquid Radioactive Wastes*, ORNL-2475 (March 15, 1958).

¹²W. J. Lacy, *Radioactive Waste Disposal Report on the Seepage Pit Liquid Waste - Shale Column Experiment*, ORNL-2415 (Nov. 1, 1957).

¹³D. G. Jacobs and T. Tamura, *Trans. Intern. Congr. Soil Sci.*, 7th, Madison, Wis., 1960 2, 206-14 (1961).

¹⁴D. G. Jacobs, *Health Phys.* 4, 157-63 (1960).

¹⁵R. J. Morton (ed.), *Status Report No. 3 on Clinch River Study*, ORNL-3370 (Nov. 21, 1962).

Seepage rates were assumed to be characteristic of the area surrounding waste pit 2, where the average seepage rate from 1953 to 1958 was 3900 gal/day through an average sidewall area of 9000 ft² (ref. 16). This corresponds to a mean superficial velocity of 0.064 ft/day. A mean ground-water velocity of 0.67 ft/day was used, which implies that ~10% of the formation had sufficient permeability to transmit solution. If the initial seepage rate were maintained, the daily seepage rate from the acid waste tank (filled to a height of 35 ft with 10⁶ gal of waste) would be 2275 gal. The seepage from the neutralized waste tank (filled to a height of 36 ft with 1.25×10^6 gal of waste) would be 2340 gal.

Dispersion properties of solution in the formation (Fig. 7.1) were estimated from the results of a chloride tracer test conducted at the site.¹⁶ These data indicate an effective plate height of 46.5 ft, according to the notation of Glueckauf.¹⁷

Calculation of Radionuclide Movement

In addition to the assumptions outlined above, it was further assumed that the waste would move

¹⁶K. E. Cowser, W. de Laguna, and F. L. Parker, *Soil Disposal of Radioactive Wastes at ORNL* (to be published as an ORNL-TM report).

¹⁷E. Glueckauf, *Trans. Faraday Soc.* 51, 34 (1955).

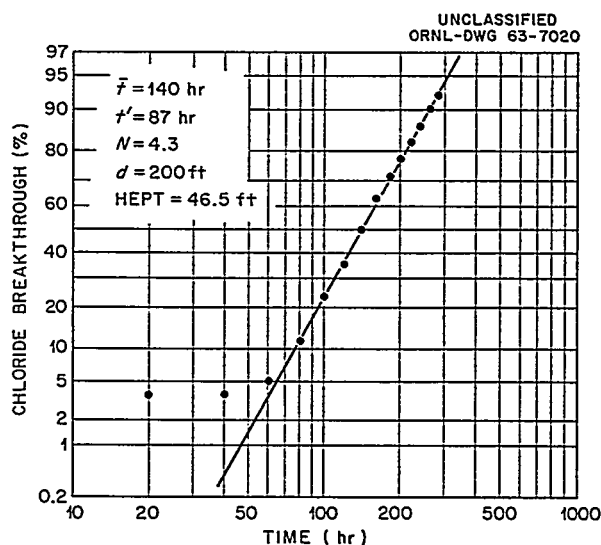


Fig. 7.1. Chloride Dispersion Properties of Conasauga Shale at 4-acre Site.

longitudinally through a zone 75 ft wide, with a height equal to the original liquid level in the waste tank, to surface water at a distance of 200 ft. No allowance was made for lateral dispersion, but the spread of the solute was assumed to occur according to Glueckauf's model for the elution of a band of solute through a linear ion exchange column.¹⁷ The porosity of the shale effectively contacted by solution was assumed to be 25%, with a grain density of 2.64 g/ml.

If a leak were to develop in a waste tank, the amount of solution lost to the formation would be limited by the ability of the formation to accept the solution. During percolation of the waste solution, the ground-water concentration in the zone of migration is increased, returning to normal when the waste solution is again displaced by the local ground water. Movement and dispersion of the specific radionuclides were estimated by using Glueckauf's model in order to describe the dispersion of the unsorbed anions and correcting for retention of the radionuclides by the formation, as discussed by Inoue and Kaufman.¹⁸ However, due to the changing electrolyte concentration of ground water, the retention factor is not constant with time. In addition, radioactive decay was considered.

The results of calculations for the movement of ⁹⁰Sr from an acid tank are shown in Fig. 7.2. The initial peak in ⁹⁰Sr activity at the surface drain-
ageway occurs at about 1 year and is due to the relatively slight sorption of strontium by the shale in the presence of high concentrations of electrolyte. With time, these high concentrations of salt are diluted and replaced by fresh ground water, and a second concentration peak occurs after about 150 years. The relative magnitude of these two peaks depends on the total quantity of electrolyte released to the formation. If, after a leak occurs, the waste solution is pumped from the ground, the initial rapid movement will not be observed, due to the removal of the excess electrolyte. Furthermore, in the case of ⁹⁰Sr in an acid waste system, an appreciable fraction of the total activity could be removed.

If the nitric acid of the Purex waste is reduced by treatment with formaldehyde¹⁹ or sugar,²⁰ there would be increased sorption of ⁹⁰Sr. The initial rate of movement would be reduced, and there would be more time for radioactive decay (Fig. 7.3).

For neutralized waste, the precipitation of strontium, in addition to the increased probability for ion exchange, prevents ⁹⁰Sr from attaining any significant concentration at the surface drain-
ageways. The high affinity of the Conasauga shale for cesium deters movement of ¹³⁷Cs so that radioactive decay occurs before significant concentrations would be observed in either acid or neutralized waste systems. The relatively rapid decay of ¹⁰⁶Ru (half-life = 1 year) would prevent it from attaining significantly high levels at surface seeps unless a very extensive leak were to occur.

Distribution of Fission Products in the Soil

The distribution of fission products in the soil is important because of the thermal problems that are likely to result from high concentrations of activity in a medium that has poor heat-conducting properties. The distribution of radionuclides in the soil was estimated by using Glueckauf's expression for the buildup of activity in an ion exchange column. The distribution of cesium in the soil was further modified because of its non-linear absorption isotherm, which gives a very sharp sorption front.²¹ With respect to neutralized wastes, both ¹³⁷Cs and ⁹⁰Sr are retained close to the leaking tank, but ¹⁰⁶Ru moves through the soil, causing a significant buildup of activity away from the tank. In acid wastes, the ⁹⁰Sr moves even faster than the ruthenium, and the entire 200-ft seepage zone is brought to a dangerously high level of contamination.

¹⁹R. C. Forsman and G. C. Oberg, *Formaldehyde Treatment of Purex Radioactive Wastes*, HW-79622 (Oct. 1963).

²⁰L. A. Bray, *Denitration of Purex Wastes with Sugar*, HW-76973 Rev., pp. 103, 542 (April 1963).

²¹E. Glueckauf, *Ion Exchange and Its Applications*, p. 34, Society of Chemical Industry, London, 1955.

¹⁸Y. Inoue and W. J. Kaufman, *Ground Disposal of Radioactive Wastes*, TID-7628, p. 303 (1962).

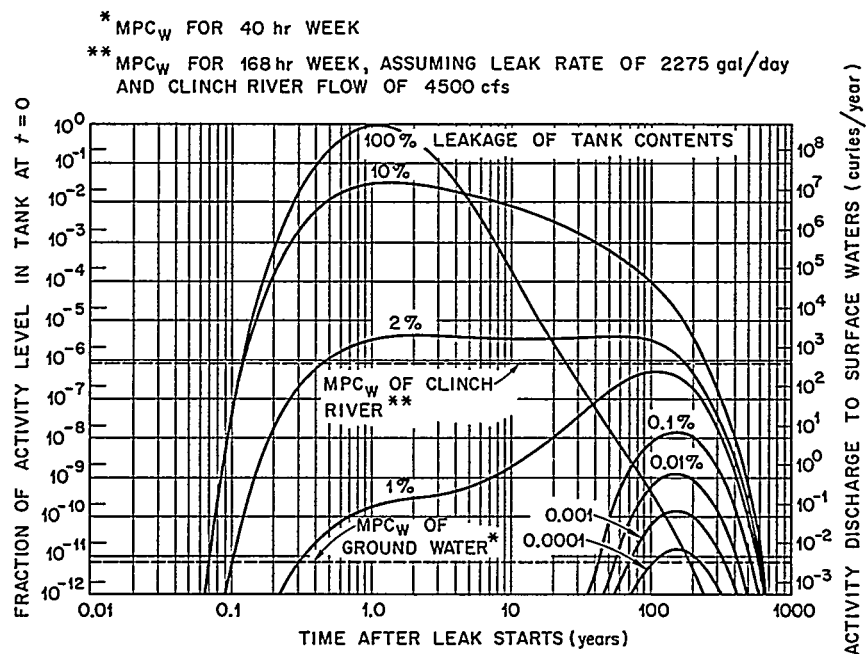
UNCLASSIFIED
ORNL-DWG 63-7022

Fig. 7.2. Strontium-90 Activity in the Ground Water at a Point 200 ft from a Leaking Tank of Acid Waste.

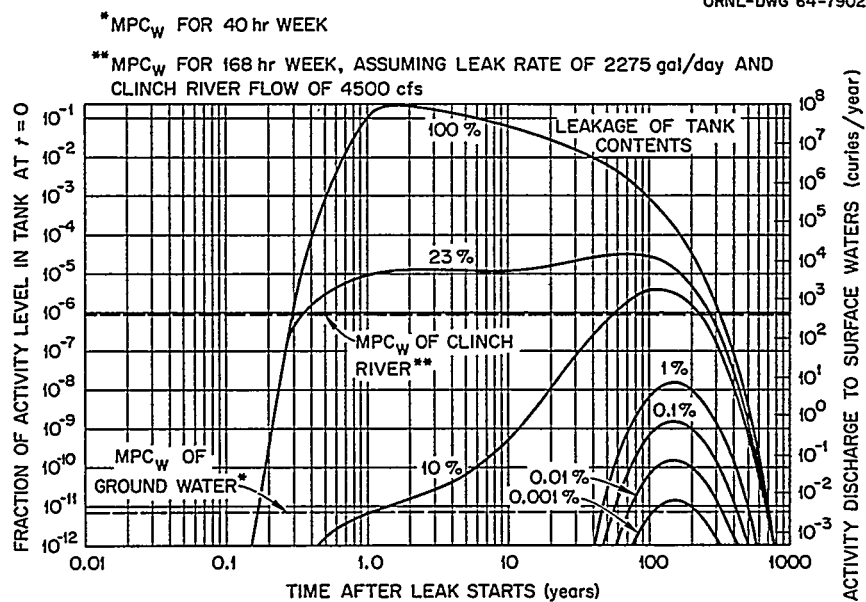
UNCLASSIFIED
ORNL-DWG 64-7902

Fig. 7.3. Strontium-90 Activity in the Ground Water at a Point 200 ft from a Leaking Tank of Acid-Killed Waste.

8. Related Cooperative Projects

GEOLOGIC AND HYDROLOGIC STUDIES BY U.S. GEOLOGICAL SURVEY

The U.S. Geological Survey continued to operate 13 continuous-record gaging stations and a network of 24 partial-record base-flow, and crest stage gages. The partial-record stations are being used to obtain information on base-flow and flood characteristics in the area and for quality of water sampling.

A geologic map and explanatory text of White Oak Creek Basin for the purpose of relating the basin geology to the hydrology of the basin was issued as an interim report. A generalized soils map of the White Oak Creek Basin and an explanatory text are being prepared in which the locations of the general soil types will be shown and the general soils characteristics and associations with geologic units will be described.

COOPERATION OF OTHER AGENCIES IN ORNL STUDIES

The research and development program of the Radioactive Waste Disposal Section of this Division is of special interest to various public and private agencies. Several study projects provide an opportunity for others to participate, both to supplement the Laboratory's research effort and to gain information and experience of value to the other agency. The ways in which another agency may cooperate include assignment of on-loan personnel as temporary additions to the ORNL staff, performance of specific work under cooperative agreements to augment ORNL programs, work authorized under ORNL subcontracts and performed by the contracting agency, or coordination of related work projects with ORNL projects for mutual benefit.

Clinch River Study

This is a cooperative study under the guidance of the Clinch River Study Steering Committee, which coordinates arrangements for participation of the agencies represented by membership on the committee. These include, in addition to ORNL, the

U.S. Geological Survey, the U.S. Public Health Service, the Tennessee Valley Authority, the Tennessee Department of Public Health and Stream Pollution Control Board, the Tennessee Game and Fish Commission, the Divisions of Reactor Development and Biology and Medicine of the U.S. Atomic Energy Commission, Washington, D.C., and the Biology Division of the U.S. Atomic Energy Commission, Oak Ridge Operations. The activities of the Steering Committee, participation by the several agencies, and the results during the past year are presented in a preceding section (see "Clinch River Studies," this chapter).

Disposal in Salt Formations

Agencies participating in this program during the past year have included the U.S. Bureau of Mines and the Carey Salt Company of Hutchinson, Kan., an ORNL subcontractor. The results of this cooperative program are given in a preceding section (see "Disposal in Salt Formations," this chapter.)

Disposal in Deep Wells

The subcommittee of the Committee on Research of the American Association of Petroleum Geologists continued its study of the deep sedimentary basins of the U.S. to identify those best suited to radioactive waste disposal. Cooperation between this group, the U.S. Geological Survey, and the Oak Ridge National Laboratory has been active but informal. Somewhat more formal collaboration has been developed between ORNL, the U.S. Geological Survey, the U.S. Bureau of Mines, and the University of California for the planning and eventual operation of certain field experiments and demonstrations in the disposal of liquid wastes into permeable formations. This work has been suspended pending the availability of a suitable site for the demonstration.

VISITING INVESTIGATORS FROM ABROAD

During the year, three noncitizen guests were on assignment as temporary members of the research staff of the Radioactive Waste Disposal Section.

Ferruccio Gera of Italy has used tritium tracers to determine the rate and direction of groundwater flow in the waste pit area. Mohammad Unis Shaikh of Pakistan has completed his thesis work on an experimental and theoretical study of the flow of fluids through porous media in a five-spot array. Tohru Murano of Japan has finished his studies of mechanisms of alumina sorption of strontium.

NUCLEAR SAFETY REVIEW

One member of the section served on the staff of *Nuclear Safety* as assistant editor. During the year, several individuals in the Section contributed review articles which were published under the category, "Consequences of Activity Release."

COMMITTEE WORK

American Standards Association

Several members of the staff of the Radioactive Waste Disposal Section have continued to serve on working groups of ASA sectional committee N5, Nuclear Fuel Cycle Engineering, its subcommittee N5.2, Radioactive Waste Disposal, and working group N5.2.2, Site Selection Criteria.

AEC Advisory Committee on Deep-Well Disposal

One staff member has served on the AEC Advisory Committee on Deep-Well Disposal. This committee is advising the AEC in the coordination of effort in the Deep-Well Disposal program and is reviewing plans for engineering-scale field tests.

ASCE - Committee on Sanitary Engineering Aspects of Nuclear Energy

The section leader served as a member of the Committee on Sanitary Engineering Aspects of Nuclear Energy of the American Society of Civil Engineers.

ORNL Committees and Special Working Groups

Two sanitary engineers of the staff have been designated to provide advisory service to engineering design groups regarding protection of the potable water supply of ORNL against "crossover" contamination where it is necessary to lay water mains and waste pipes across one another or in close proximity. Upon request of the design engineers during the year, a number of designs have been reviewed and discussed in the preliminary stages, and final plans have been checked for approval of the methods of protection provided.

PARTICIPATION IN EDUCATIONAL PROGRAMS

During the ten weeks of field training of the AEC Fellowship course in applied radiation physics at ORNL, three students were assigned to work five weeks in the Radioactive Waste Disposal Section under the supervision of four staff members.

The course in physical geology conducted by ORSORT, given again by one member of the Radioactive Waste Disposal staff, comprised approximately 30 lectures to a class of about 40 students, some American and some from other countries.

Four lectures and a field tour of the Laboratory's waste disposal facilities and ecological research activities were provided at ORNL by the staff of the section as part of the course conducted by the U.S. Public Health Service on "Reactor Safety and Environmental Health Problems," in September 1963 and May 1964.

NUCLEAR SAFETY INFORMATION CENTER

One member of the section served as a part-time staff member of the Nuclear Safety Information Center and completed a study of the current practices in the release and monitoring of ^{131}I at the National Reactor Testing Station, Hanford Atomic Products Operation, Savannah River Plant, and ORNL.¹

¹K. E. Cowser, *Current Practices in the Release and Monitoring of ^{131}I at NRTS, Hanford, Savannah River, and ORNL*, NSIC-3 (June 1964).

Part II. Radiation Ecology

S. I. Auerbach

100

100

100

100

100

9. Radioactive Waste Area and Radiation Effects Studies

S. I. Auerbach

G. N. Brown

D. A. Crossley, Jr.

P. B. Dunaway

J. M. Inglis¹

E. F. Menhinick

J. A. Payne

A. F. Shinn

J. P. Witherspoon, Jr.

Cynthia L. Corley

Gladys J. Dodson

B. E. Jacobs

Lovell Lawrence

G. D. Martin²

T. P. O'Farrell³

J. D. Story

F. G. Taylor, Jr.

ANALYSIS OF GROWTH RESPONSES OF TWO SEDGE SPECIES ON WHITE OAK LAKE BED

G. L. Plummer⁴

D. A. Crossley, Jr.

D. A. Gardiner⁵

Radiation-induced changes in natural populations living in contaminated environments are usually difficult to demonstrate, although radiation effects are readily produced in various types of experimental designs. On White Oak Lake bed, sedges (*Carex Frankii* Kunth and *C. vulpinoidea* Michx.) were found to have longer inflorescences than sedges growing on nearby uncontaminated sites.⁶ Because of variations in such factors as moisture, site fertility, and soil alkalinity, the differences in inflorescence length could not be ascribed to radiation dose with any certainty. Therefore, a further sampling of sedge inflorescences was made from seven areas (three on White Oak Lake bed and four on uncontaminated sites), various soil factors (pH, calcium, active phosphorus, exchangeable potassium, and organic matter) were measured at each area, and radiation dose rate was measured 1 m above ground surface. A statistical analysis was performed to investigate the possible contri-

bution of the soil factors to the observed increase in inflorescence length.

As a first approximation to a function relating soil factors and air dose rate to inflorescence length, we employed the linear function

$$Y = \alpha + \sum_{i=1}^k \beta_i X_i,$$

in which Y represents inflorescence length, α is a constant, β_i is a regression coefficient for the i th factor, X_i is an amount of the i th factor, and $k = 0, 1, 2, 3, 4, 5$, or 6 . There are 2^6 , or 64, possible models of this type, but in one of them ($k=6$) the model passes through the means, and its validity could not be assessed. The remaining 63 models were screened with a computer program which selected the best model with 1, 2, 3, 4, or 5 variables. For each sedge species, radiation dose rate gave the best single-term model, and dose rate appeared as a significant term in the 2-5 term models. For *C. vulpinoidea* the best general model was

$$Y = 63.66 \pm 0.2091R,$$

where Y = inflorescence length (mm), and R = radiation dose rate (mr/hr). For *C. Frankii* the best model suggested from the data was the three-term one:

$$Y = 157.83 + 0.5827R - 14.87 \text{ pH} + 0.4362 \text{ Ca},$$

where pH = hydrogen ion concentration in soil, and Ca = exchangeable calcium (lb/acre).

Thus air dose rate of gamma radiation measured at 1 m above ground surface provided the best

¹ORINS summer research participant.

²Temporary summer employee.

³ORINS fellow.

⁴ORINS summer participant, 1960.

⁵Mathematics Division.

⁶G. L. Plummer, *Biometric Analysis of a Growth Response of Two Plant Species in a Radioactive Waste Area*, ORNL-2903 (April 1960).

correlation with inflorescence length for the two sedge species. The absorbed dose received by the plants — particularly the root systems — was greater than the air dose rates would suggest. Kaye⁷ estimated that the exposure dose rate 3 cm below the soil surface was approximately five times the exposure dose rate above the soil, on White Oak Lake bed. Even at minimal estimates, the dose rates were sufficient to induce both generic and physiological disturbances in plants.⁸

Although soil factors considered here appear to affect inflorescence length, those influences were far from adequate to explain the increase in length found in the radioactive areas. The coefficient *R* doubtless includes other factors besides radiation, however. An experimental approach (in both field and laboratory) would seem to be needed to resolve whether the observed increase in length of inflorescence is a direct response to radiation, an indirect response, the consequence of some purely chemical aspect of waste disposal, or a combination of these.

VEGETATION STUDIES AROUND THE HPRR

J. P. Witherspoon, Jr.

F. G. Taylor, Jr.

This spring some of the natural vegetation around the Health Physics Research Reactor exhibited the first visible effects of radiation damage. After a period of winter dormancy, new growth in several species of forest trees contained many morphological abnormalities. The reactor has been in operation for approximately one year, and total power output has been about 60 kw-hr delivered in a variety of operational modes. The damaged vegetation occurred at distances of 10 to 20 m from the reactor, and total cumulated dose was approximately 600 to 140 rads (tissue dose in air) respectively. Although damage to vegetation was found over the entire 10- to 20-m range, a gradation of effects was observed. Most severely damaged were persimmon (*Diospyros virginiana* L.) and black gum (*Nyssa sylvatica* Marsh) saplings (0.5 to 1.2 m in height) growing 10 to 15 m from the reactor. Those at 10 m (600 rads) failed to produce apical growth, and many apices were dead. Leaf

production was limited to fasciated tufts of three to five leaves located laterally along the entire shoot length at 1- to 3-cm intervals. These leaves, by early June, were much reduced in size, ranging from 0.2 to 3.0 cm in length.

No dead apices were found in persimmon or black gum at 20 m from the reactor, but shoot growth averaged only half that of similar aged trees growing on control sites. Leaf size was also reduced in these plants. Pine seedlings (*Pinus virginiana* Mill.) growing here received ~140 rads (960 rems) total dose, and exhibited apical die-back in some cases and apical stem fasciation in other cases.

Samples of apices of several species of trees were collected at distances >20 m from the reactor. These are being examined histologically for early effects such as disorientation and death of cells in meristematic tissue. As reactor use continues, it is anticipated that the vegetation damage pattern will extend out several more meters during the remainder of this growing season.

RADIATION STUDIES ON FOREST TREE SPECIES

J. P. Witherspoon, Jr.

Radiation effects studies completed this year included fast-neutron exposures from the HPRR, and gamma-radiation exposures from both a ¹³⁷Cs field source and White Oak Lake bed. This spring an indoor ⁶⁰Co facility was completed which will deliver gamma radiation at a rate of from 800 to 1.5 r/hr, and studies on the interaction of environmental factors and radiation have begun. These latter studies utilize Virginia pine, mimosa, red oak, and tulip poplar.

Three-year-old seedlings of *Pinus virginiana* Mill. (Virginia pine) and 80-day-old seedlings of *Liquidambar straciflua* L. (sweet gum) received acute fast-neutron doses of 100 to 500 rads and 500 to 1100 rads respectively. All doses proved lethal to pines, but the length of time required to reach 100% needle mortality varied widely within and between dose groups. Mortality of apical needles and buds, and changes in growth rate gave much better correlations with dose than total needle mortality. Figure 9.1 shows the average length of time required to reach an LD₅₀ of apical needles in Virginia pine (*N* = 40) at several lethal

⁷S. V. Kaye, "Use of Miniature Glass Rod Dosimeters in Radiation Ecology," *Ecology* (in press).

⁸G. M. Woodwell, *Science* 138, 572-77 (1962).

doses, plants being maintained under greenhouse conditions. Sweet gum seedlings, maintained under controlled conditions in growth chambers, exhibited an LD_{50} in eight months at a dose of 800 rads (range 500 to 1100 rads), while those

maintained under greenhouse conditions showed the same effect at five months.

Pine seedlings were exposed to chronic irradiation for 178 days (last growing season) on White Oak Lake bed. Plants were placed on metal racks 3 ft above the soil surface to minimize contamination by uptake of soil radionuclides. Control plants were placed 65 m off the lake bed. During this period the lake bed pines received a total gamma dose of 470 rads delivered at an average dose rate of 2.6 rads/day. Absorbed dose was measured by shielded metaphosphate glass dosimeters placed on plant shoot apices. Control pines received 4.5 rads during this period. All plants received water only from rain and dew. By the end of the growing season, all pines in the lake bed group ($N = 32$) exhibited 100% needle mortality, while controls averaged only about 10%. Figure 9.2 shows some of the apical shoot growth characteristics at the end of the study. The length of terminal shoot growth in lake bed plants ($52.3 \pm SE 5.2$ mm) was significantly less ($p < 0.01$) than that in the controls (78.4 ± 5.1 mm). Significant differences also existed between White Oak Lake pine apical bud length (5.4 ± 0.3 mm) and controls (7.4 ± 0.6 mm). Lateral shoot and bud length and needle length also exhibited similar differences. Growth anomalies and lethality produced at this

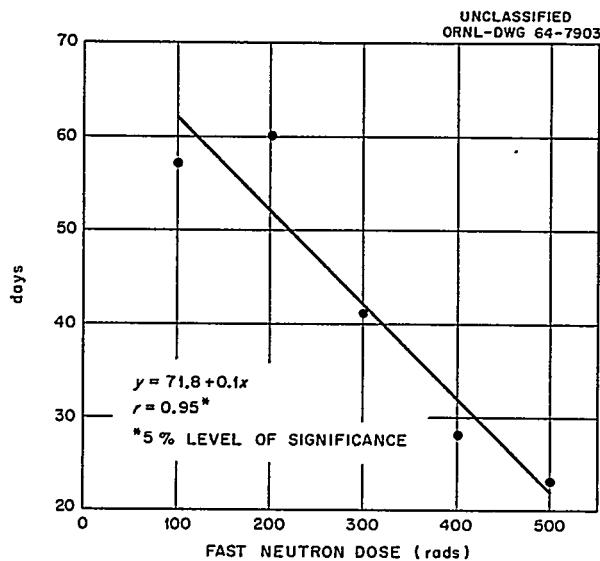


Fig. 9.1. Time Required to Get LD_{50} of Apical Needles (Virginia Pine).

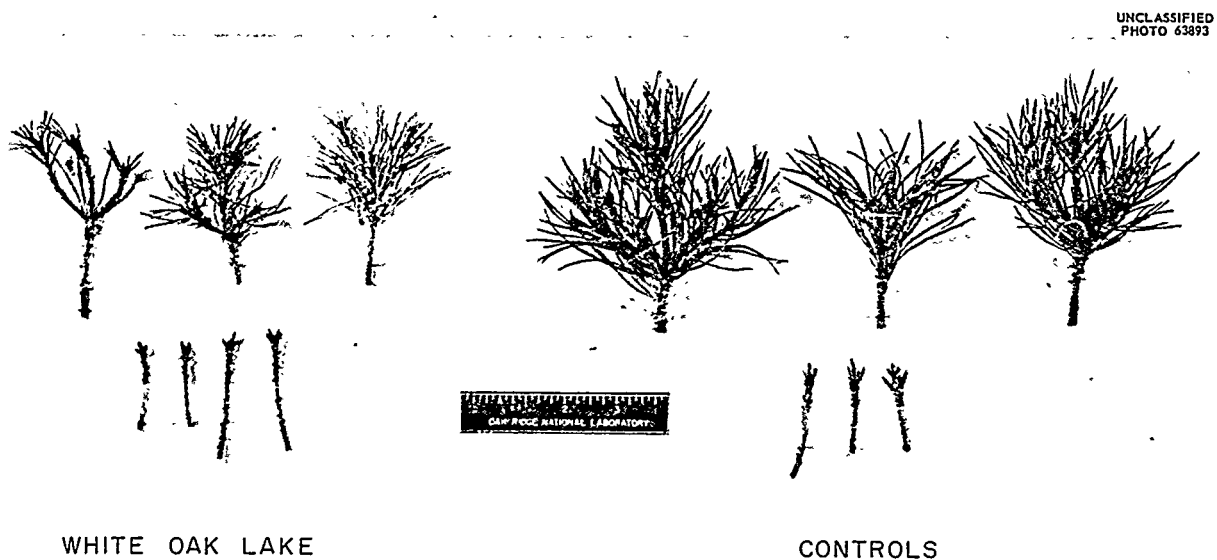


Fig. 9.2. Apical Shoots and Buds of Virginia Pine (Left - 178 Days on White Oak Lake, 470 Rads of Gamma Radiation).

relatively low total dose and low dose rate were greater than had been expected. These results are interpreted, therefore, as being due to a combination of radiation and soil moisture stress. Summer moisture levels were 7 to 8 in. below normal, and August precipitation was a record low for the area.⁹ This study, being repeated this year, illustrates how an environmental factor may serve to augment or intensify radiation effects in a field situation. Fiscal year 1965 experiments will be designed to sort out and evaluate the influence of such factors on the syndrome of effects and the recovery of irradiated forest tree species.

PLANT PHYSIOLOGICAL AND BIOCHEMICAL PHENOMENA AS AFFECTED BY IONIZING RADIATION

G. N. Brown

Various physiological phenomena vital to the metabolism of plants are influenced by ionizing radiation. These biochemical effects are ultimately manifested in growth responses such as the inhibition of stem growth. Fundamental in plant metabolism are nucleic acids, due to their roles as genetic material and in protein (and enzyme) synthesis. Little is known of levels of these acids in native forest tree species. Therefore, baselines are being established for species of local importance which will be used in studies aimed at understanding ionizing radiation-environmental interactions, and possible mechanisms underlying such interactions.

Mimosa seedlings (*Albizia julibrissin* Durazzini) were germinated at controlled rates by varying temperature conditions. Total and soluble RNA (SRNA) were extracted from each sample and expressed as percentages of soluble RNA/total RNA. Soluble RNA consists of low-molecular-weight RNA and is believed to be responsible *in vivo* for carrying amino acids to the site of protein synthesis within the cell.

Analyses of nine samples have been completed, and the percentages of SRNA to total RNA have averaged $13.94 \pm 1.77\%$ (1 SE). An ultraviolet light absorption analysis yielded a ratio between 0.48 and 0.50 for all samples of optical density at

280 to 260 m μ . This indicates a complete lack of protein contamination. Also, a modified diphenylamine test illustrated a negligible deoxyribonucleic acid content. Finally, a Beckman model E analytical ultracentrifuge was used to determine the sedimentation rate (S) of the SRNA. This value was calculated at 3.18S.

Base compositions of SRNA were determined for each sample (Table 9.1) by use of HCl hydrolysis and paper chromatography, followed by elution of the nucleotide spots from the paper and determination of nucleotide ultraviolet absorption at 260 m μ . A linear correlation exists between base compositions (individual bases of SRNA) and growth rates. However, growth rate apparently has little, if any, effect on the SRNA/total RNA percentages.

Groups of mimosa seedlings germinated at one optimal temperature condition are presently being irradiated in the ⁶⁰Co source room and will be used for RNA determinations similar to those for the controls germinated at the same temperature condition (Table 9.1). Thus far, only one extraction of SRNA has been obtained from irradiated mimosa seedlings. The SRNA/total RNA ratio (23.69%) varied considerably from that of the controls (average of 15.12%). The base compositions also showed some differences. Guanine (34.2%) and cytosine (30.6%) were both slightly higher than control figures (averages of 32.6 and 30.2% respectively), while adenine (18.0%) and uracil (17.1%) were both slightly lower than control figures (averages of 19.8 and 17.4% respectively). The dose received by the mimosa seedlings ranged from 500 to 1500 r over a four-day period preceding extraction.

Rate of ³²P incorporation into nucleic acids is an estimate of rate of nucleic acid synthesis. Since rate of synthesis is a phenomenon vital to the growth of the plant and is probably sensitive to certain sublethal levels of ionizing radiation, techniques have been developed to study the effects of radiation on these rates. A red cedar (*Juniperus virginiana* L.) tree was tagged with ³²P at the main stem, and leaf tissue was removed after one week. Total RNA was isolated, hydrolyzed, and the four bases separated by using paper chromatography. Quantitative determinations of the four bases by ultraviolet absorption agreed within 5% of the relative counts per minute measured for the incorporated ³²P. Therefore,

⁹USWB, *Climatological Data - Tennessee* 68 (8 & 9) (1963).

Table 9.1. Growth Rates in Ribonucleic Acid Characteristics in Mimosa Seedlings

Growth Rate ^a	Soluble RNA/Total RNA ^b (%)	Soluble RNA Base Ratios (%)			
		Adenine	Cytosine	Guanine	Uracil
8 ^c	13.75	20.4	28.6	33.3	17.6
8 ^c	18.21	19.4	31.4	33.1	16.1
9 ^c	13.39	19.7	30.5	31.3	18.5
Control mean (3 samples)	15.12 ± 1.66 ^d	19.8 ± 0.34	30.2 ± 0.97	32.6 ± 0.69	17.4 ± 0.83
12	13.18	21.1	26.2	37.2	15.4
12	6.88	21.8	29.8	32.9	15.5
13	13.20	21.1	27.9	32.8	18.1
13	22.61	17.5	32.0	34.5	16.1
16	16.63	20.9	30.6	28.9	19.8
21	7.58	21.2	26.7	30.3	21.8
Total mean (9 samples)	13.94 ± 1.77 ^d	20.3 ± 0.48	29.3 ± 0.65	32.7 ± 0.93	17.7 ± 0.72

^aDays to attain established size.^bAdjusted for excess deoxyribonucleic acid.^cUsed as controls for the irradiation study.^dOne standard error.

³²P incorporation into nucleic acids will be used as a rate measure of nucleic acid synthesis under various conditions of gamma irradiation.

NUCLEAR VOLUME MEASUREMENTS

F. G. Taylor, Jr.

Predictions of relative radiosensitivity have been made for various tree species based on nuclear volumes. Difference in radiation sensitivity between dormant and actively growing white pines on Long Island can be explained by the differences in interphase nuclear volumes between dormant and actively growing plants.¹⁰ To attain the proper perspective in constructing an index, it is necessary to anticipate the changes in nuclear volume if predictions of radiation sensitivity are to be reliable.

¹⁰A. H. Sparrow *et al.*, *Radiation Botany* 3, 169 (1963).

During the past year a study was initiated to determine the nuclear volumes, through time, of local tree species. Different procedures and techniques were tried. Shoot apices were collected monthly from 14 local species. The material was embedded, sectioned, and stained. The nuclei were measured, and from the mean diameter the nuclear volume was calculated. An analysis of variance showed that nuclei of most species increased in size ($P < 0.01$) before shoot elongation. Between January and March, *Pinus strobus* and *P. taeda* showed the greatest increase in nuclear volume, from $631 \mu^3 \pm 38.49$ SE to $1113 \mu^3 \pm 43.12$ SE and $638 \mu^3 \pm 26.67$ SE to $1026 \mu^3 \pm 23.41$ SE respectively. *Cornus florida* showed no response to the approach of spring activity, remaining unchanged from $99 \mu^3 \pm 2.85$ SE to $100 \mu^3 \pm 5.79$ SE, while four species of *Acer* showed increases (45 to $199 \mu^3$ in January, 83 to $264 \mu^3$ in March). Table 9.2 summarizes the volumetric changes of interphase nuclei for 14 local tree species during the first quarter of 1964.

Table 9.2. Summary of Interphase Nuclear Volumes Calculated from Mean Diameters of 14 Local Tree Species, Oak Ridge, Tennessee, First Quarter 1964

Order of listing is phylogenetic after Gray's *Manual of Botany*

Species	Nuclear Volume ($\mu^3 \pm SE$)		
	January	February	March
<i>Tsuga canadensis</i>		693 \pm 23.34	763 \pm 11.81
<i>Pinus strobus</i>	631 \pm 38.49	830 \pm 23.89	1113 \pm 43.12
<i>Pinus taeda</i>	638 \pm 26.67	792 \pm 28.03	1026 \pm 23.41
<i>Pinus echinata</i>	599 \pm 24.88	599 \pm 32.81	784 \pm 21.44
<i>Pinus virginiana</i>	357 \pm 10.42	457 \pm 38.04	735 \pm 19.87
<i>Juniperus virginiana</i>		493 \pm 21.78	517 \pm 26.68
<i>Liriodendron tulipifera</i>	107 \pm 4.86	148 \pm 5.80	152 \pm 2.90
<i>Liquidambar styraciflua</i>	45 \pm 1.43	69 \pm 1.39	82 \pm 2.63
<i>Acer saccharum</i>	45 \pm 2.13	69 \pm 2.59	83 \pm 2.46
<i>Acer rubrum</i>	199 \pm 9.46	254 \pm 10.81	264 \pm 6.24
<i>Acer saccharinum</i>	94 \pm 3.42	92 \pm 3.44	132 \pm 2.50
<i>Acer negundo</i>	49 \pm 1.88	85 \pm 2.85	119 \pm 1.13
<i>Aesculus octandra</i>	58 \pm 2.82	79 \pm 3.45	106 \pm 4.98
<i>Cornus florida</i>	99 \pm 2.85	91 \pm 2.08	100 \pm 5.79

Initial spring activity of nucleic acids in shoot apices is thus earlier in eastern Tennessee than would be anticipated from any morphological changes such as swelling of buds or separation of bud scales. Information of this nature is essential in predicting ranges of relative radiosensitivity and interpreting plant radiation effects. Continuing changes are being followed through the seasons.

ENVIRONMENTAL INFLUENCES ON RESPONSES OF METAPHOSPHATE GLASS

B. G. Blaylock J. P. Witherspoon, Jr.

Application of glass rod dosimetry is increasing in radiation ecology studies. To qualify certain of these uses, a study was made on the influence of temperature and sunlight on radiation response

(fluorescence) of Toshiba low-Z glass rods. Shielded and unshielded rods were exposed to beta and gamma radiation from solutions of ^{137}Cs after the method of Tapper *et al.*,¹¹ over a temperature range of 3.5 to 53.5°C. No change in response to beta radiation was observed, but the response to gamma radiation increased with increasing temperature. A linear expression describing this increase is:

$$Y = 4.32 + 0.014X, \quad r = 0.44 \quad (P < 0.05),$$

where Y is fluorometer units per rad (Bausch and Lomb microdosimeter reader), and X is temperature (°C).

¹¹D. N. Tapper *et al.*, *Health Phys.* 8, 207-16 (1962).

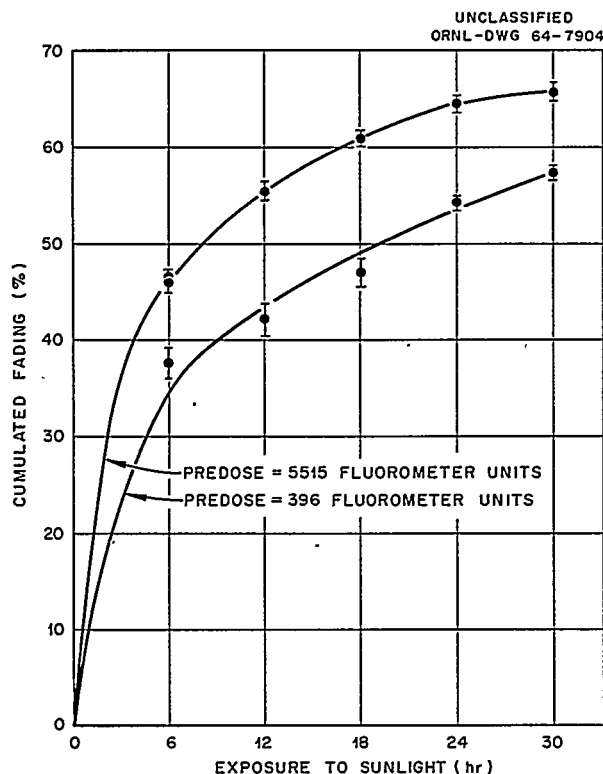


Fig. 9.3. Fading of Toshiba Low Z Rods in Sunlight.

Predosed rods were found to fade (lose fluorescence) rapidly when exposed to sunlight for 30 hr, exposed in 6-hr increments at about 10^4 ft-c. Figure 9.3 illustrates the cumulated loss (average ± 1 SE). Rods lost 37 to 46% of the predose during the first 6 hr. Fading was also related to predose, as high predose rods had a significantly greater ($P < 0.01$) percentage loss than low predose rods. The effectiveness of several kinds of shields was studied, and nylon plastic shields, painted black, were found to prevent fading when tested by 20-day exposures on White Oak Lake bed. White, opaque nylon shields were not effective in preventing fading, and indicated doses 41% lower than those measured with black shielded rods.

Field use of these dosimeters, then, demands shielding that will prevent sunlight from striking the glass, and compensation of response to large changes in temperature (i.e., summer vs winter use).

TRANSPORT OF RADIOACTIVE MATERIALS BY MUD-DAUBER WASPS

A. F. Shinn Gladys J. Dodson
Cynthia L. Corley

The Black-and-Yellow mud-dauber wasps (*Sceliphron cementarium*) construct nests using radioactive mud from radioactive waste pits and from White Oak Lake bed. The nests constitute a hazard to humans and to wasps, and suggest possible implications of changes in the ecosystem involved. The Pipe-Organ mud-dauber wasp (*Trypoxylon politum*), which is common in the same areas, never uses radioactive mud in constructing its nest.

Nests are often placed out of sight or in inaccessible locations such as open pipes, behind instrument panels, inside small instrument boxes, between house walls, and in numerous other places where discovery is difficult and decontamination virtually impossible. Mud is usually carried to the nest site from less than 150 ft away, but can be carried for distances up to 650 ft. A short flight range is also indicated by the fact that radioactive nests comprise from 89 to 95% of the nests at nesting sites where virtually all nearby mud is radioactive.

The practical solution to the problem of radioactive mud-dauber nests in unwanted places is to gasket doors of cabinets, close small holes larger than 2 mm in diameter, and screen air vents as well as spray them with repellent insecticide.

Several species of wasps, beetles, and flies use the mud nests constructed by *Sceliphron* in the role of parasites or tenants. The incidence of the more important parasites is shown in Fig. 9.4. Statistically significant differences in occurrence of eulophid wasps ($P < 0.001$), beetles ($P < 0.001$), and bee flies ($P < 0.05$) may reflect differences in natural distribution of the parasites in slightly different habitats or may possibly be a radiation-associated phenomenon.

The effect of the radiation on *Sceliphron* is to reduce successful emergence by a significant 40% ($P < 0.001$), and radioactive cells of the nests show a higher mortality from parasites ($P < 0.01$, see Fig. 9.4).

Radioactive nests gave survey meter readings from slightly above background to more than 1 r/hr of mixed gamma and beta radiation, but neither spiders stored as food nor developing wasps were

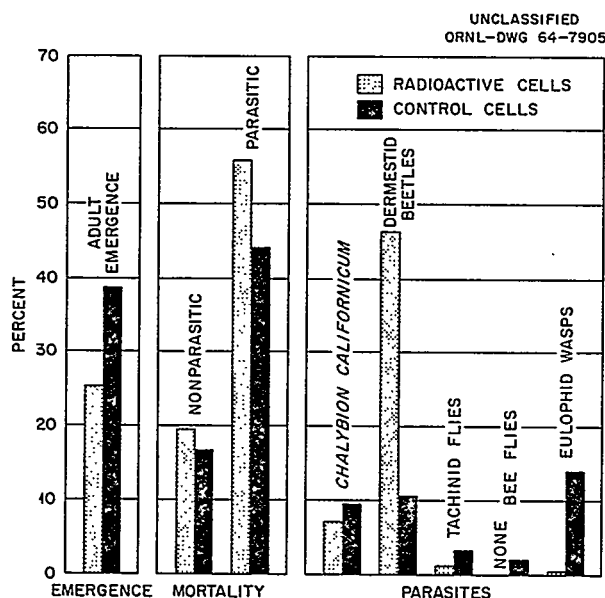


Fig. 9.4. Emergence, Mortality, and Parasites of Radioactive and Control Cells of the Nests of *Sceliphron cementarium*.

radioactive. Gamma emitters in the nests were identified as ^{137}Cs , ^{106}Ru , ^{60}Co , ^{65}Zn , and ^{144}Ce , along with the beta emitter ^{90}Sr . Gamma activities up to $77 \mu\text{c}$ per gram of dry mud were obtained, which would indicate about $221 \mu\text{c}$ per single cylindrical cell. The distribution of radio-nuclides in individual cells in a nest varied; for example, gamma spectrometry gave activities of 3, 8, and $12 \mu\text{c}$ per gram of dry weight on samples from a single nest. This nest delivered doses of 1146 and 7637 rads to two silver phosphate glass rod dosimeters exposed for a period of nine months. Variation in dose received by developing wasps in a single nest is shown in Fig. 9.5. The total dose received by a developing wasp in this study as determined from glass rod dosimetry was 10,630 rads: 110 rads to the egg (3 days), 520 rads to the larva while feasting on its spiders (14 days), and 10,000 rads to the overwintering larva in its cocoon (9 months).

Failure of the Pipe-Organ mud-dauber to use radioactive mud in making its nests may result from fundamental properties of the nonradioactive mud, or may be a radiation-associated or direct radiation effect. X-ray diffraction studies of the clays in the nests showed no significant structural

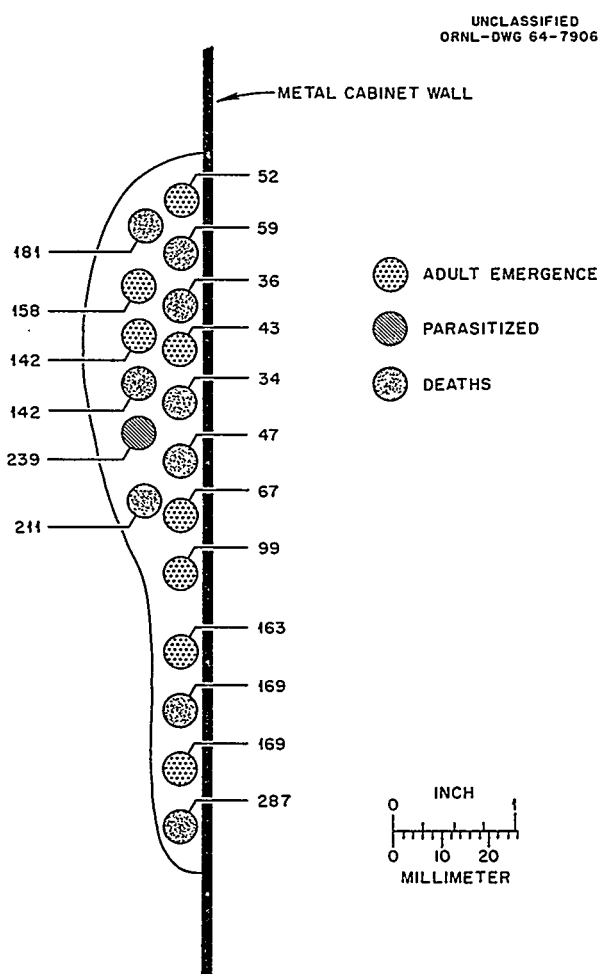


Fig. 9.5. Longitudinal Sectional View of Radioactive Black-and-Yellow Mud-Dauber (*Sceliphron*) Nest Giving Dose in Rads Received by Developing Wasps.

differences; neither pH nor cation exchange capacity was different. Odors of the wetted muds were not different. Kiln-firing of the nests did not disclose any significant differences between the nest series.

Future work will include rating the texture of muds used by the two species, and an evaluation of the repellency of ozone generated at the radioactive mud-air interface as possible explanations of this phenomenon. Radioactive mud will be offered to field-caged Pipe-Organ wasps to see if they will construct nests from it.

The ecological consequences of the different reactions of these two species of wasps to radioactive mud sources are plain: the *Sceliphron*

population will decline and the Pipe-Organ dauber will hold its population level or possibly increase it, as more nest site area becomes available.

The food web involving *Sceliphron* and its spider prey, parasites, and tenants will be altered, as well as that of the metallic-blue dauber, which provisions its cells in part with black widow spiders.

RADIOCESIUM ACCUMULATION AND FEEDING BY WILLOW LEAF BEETLES (*CHRYSOMELA KNABI* BROWN)

D. A. Crossley, Jr.

Gladys J. Dodson

Radioisotope accumulation by insects on White Oak Lake bed vegetation has been used to estimate their rates of feeding, by applying laboratory-derived elimination rates for cesium to equilibrium concentrations of ^{137}Cs in field populations.¹² Larvae of the beetle species *Chrysomela knabi*

Brown have been used to test the validity of this extrapolation, in experiments which followed radio-cesium accumulation in the laboratory and measured food consumption under controlled conditions. This insect species is well suited to such studies, in that the larvae feed only on willow leaves, remain on the host plant, and are easily collected. However, there is but one generation per year, and it was necessary to collect data for several field seasons in order to make a valid comparison of the observed ^{137}Cs accumulation with that predicted from laboratory experiments.

Table 9.3 shows ^{137}Cs concentrations in willow leaves and in various stages of *Chrysomela knabi* for the years 1962–64, in collections made during May–June from White Oak Lake bed. Samples in 1963 and 1964 had to be taken by use of a boat,

¹²D. A. Crossley, Jr., pp. 43–54 in *Radiation and Radioisotopes Applied to Insects of Agricultural Importance*, IAEA, Vienna, 1963.

Table 9.3. Cesium-137 Content of Leaf Beetles (*Chrysomela knabi*) and Willow Leaves (*Salix nigra*) from White Oak Lake Bed, May 1962–1964

(I, II, and III = first, second, and third instars; radiocesium determinations shown as mean \pm standard error)

	Number	Fresh Weight (g)	Mean Weight (mg)	^{137}Cs (picocuries/g)
1962				
III larvae	88	1.046	11.9	25 \pm 5.2
<i>Salix</i> leaves	a	5.464		21.2 \pm 1.3
1963				
I + II larvae	406	1.628	4.0	11.9 \pm 1.1
III larvae	410	5.820	14.2	11.0 \pm 1.1
Adults	13	0.313	24.0	10 \pm 4.5
<i>Salix</i> leaves	a	17.13		14.3 \pm 0.2
1964				
I + II larvae	102	0.211	2.1	5 \pm 7
III larvae	113	1.570	13.9	14.4 \pm 1.3
Pupae	53	1.255	23.7	8.2 \pm 0.8
Adults	50	1.013	20.3	6.5 \pm 1.0
<i>Salix</i> leaves	a	29.30		17.9 a

^aNot enumerated.

due to the reflooding of the lake bed. Comparing 1962 with later years shows that flooding had little influence on willow leaf concentrations of ^{137}Cs , but concentrations in larvae may have decreased after flooding. Food consumption rates were estimated for third-instar larvae from their radiocesium content (Table 9.3) and from laboratory estimates of biological half-lives in larvae (8 hr). For 1962, 1963, and 1964 data, feeding rates were estimated to be 29, 23, and 23 mg of fresh weight per larva per day respectively. Larvae of this size maintained in the laboratory ate 28 mg per day. This agreement confirms the previous results on insect food chains and emphasizes the utility of this method for estimating food consumption.

Radiocesium concentrations in samples of other life-history stages of the beetle species (Table 9.3) were consistent with results obtained in laboratory experiments, but close comparison was not possible. Biological half-lives were difficult to estimate for the younger larvae. The reduction in ^{137}Cs concentration in pupae was also found in laboratory experiments, and appears to result from clearance of stored metabolites from the larva immediately prior to pupation. Adult stages were more active than larvae, had more rapid elimination rates, and reached lower equilibrium concentrations of ^{137}Cs .

BIOLOGICAL HALF-LIFE FOR RADIOCESIUM IN APHIDS

D. A. Crossley, Jr. Cynthia L. Corley

Special attention is being directed toward the measurement of biological half-lives for radiocesium in insects with sucking mouthparts. These form a significant number of the insects which occur in grassland successional stages such as the White Oak Lake bed and the proposed ^{137}Cs contaminated old-field site, and are numerous in the canopy layer in the ^{137}Cs -tagged *Liriodendron* stand. Previous laboratory studies have concerned only insects with chewing mouthparts, and a different class of size-elimination rate relationships might be expected because of differences in physiology. Experimentation was initiated to determine whether the available information on biological half-lives could be applied meaningfully to sucking insect species.

Aphis fabae, the bean aphid, was used in the experiment. Bases of nasturtium (*Tropaeolum majus*) twigs infested with aphids were inserted in aqueous solutions of $^{134}\text{CsCl}$. After three days of feeding, approximately 30 aphids were transferred to each of three unlabeled nasturtium twigs. The twigs plus aphids were then counted in a small animal counter at approximately 4-hr intervals, to estimate biological half-lives. This procedure of counting aphids and plant together was necessary, because aphids will not resume feeding immediately if removed from the plant (for counting) and then replaced. Also, chances of injury to the insects were reduced. The only disadvantage we noted was that some of the excrement containing radiocesium accumulated on the nasturtium twigs, and consequently some of the last counts had to be discarded.

Estimates of biological half-lives at 8, 18, and 28°C were 42, 23, and 11 hr respectively. The changes with temperature indicate a Q_{10} of 2, that is, a doubling of the elimination rate for each 10° increase. Biological half-lives were longer than expected for insects of this size (average live weight, 0.51 mg). Small beetle larvae (*Chrysomela knabi*) weighing about 2 mg had biological half-lives for cesium in excess of 6 hr (at 24°C), so that the aphid measurements do not follow the cesium turnover rates expected from size. Current work is using milkweed bugs (*Oncopeltus fasciatus*), which are larger insects with sucking mouthparts, to pursue differences in size-elimination rate relationships.

MEASUREMENT OF HETEROTROPHIC PRODUCTIVITY WITH RADIOACTIVE TRACERS

D. A. Crossley, Jr.

Rates of energy storage by animals (heterotrophic production) are of central importance in analyses of food chains in natural ecological systems, but are difficult to measure in field situations. Radioactive tracer techniques, especially applications of biological half-lives for radioisotopes, have been developed previously to measure feeding rates of insect populations.^{13,14} These tech-

¹³D. A. Crossley, Jr., pp. 427-30 in *Radioecology*, ed. by Vincent Schultz and A. W. Klement, Jr., Reinhold, New York (1963).

¹⁴D. A. Crossley, Jr., pp. 43-54 in *Radiation and Radioisotopes Applied to Insects of Agricultural Importance*, IAEA, Vienna (1963).

niques can be extended to provide estimates of energy flow and energy storage in food chains, when used in conjunction with conventional ecological methods. Data obtained for the plant-insect herbivore-insect predator food chain on White Oak Lake bed were used for the estimation of heterotrophic production and energy flow at the herbivore level, by combining information on radiocesium movement and information on biomasses, respiration rates, and caloric content of plants and insects.

Figure 9.6 illustrates a net increase in biomass (and therefore in stored energy) in herbivorous insects on White Oak Lake bed for a nine-week period from late June through August 1961. The net change in weight (140 mg of dry weight per m^2) merely represents the excess of production over mortality of insects during this period. In other years, there was no such increase in biomass during the summer, production and mortality being approximately equal. Total production, then, can be estimated from change (if any) in biomass, plus loss due to mortality. In these insect populations mortality due to predation is a large proportion (about 80%) of the total mortality, except at the end of the growing season.¹⁵ Predator biomass for the 1961 sampling period is shown at the bottom of Fig. 9.6. Radioisotope measurement of predator feeding provides an estimate of herbivore mortality and thus enables an estimate of total production for the population of herbivorous insects.

Food consumption by predators was estimated by using the ^{137}Cs concentrations on White Oak Lake bed and laboratory data on elimination rates, in a method described in detail elsewhere¹⁶ and discussed in previous reports.¹⁷ The equilibrium concentration of ^{137}Cs in predaceous insects (73 pc per g of dry weight) and an elimination constant for radiocesium corrected for the average size of the population (0.98 day^{-1}) suggest an intake rate of 72 pc per g of dry weight of predator per day. From the average ^{137}Cs concentration in herbivorous insects (78 pc/g), the food intake by predators was estimated to be 0.92 g eaten per g of predator per day. For the integrated biomass curve shown for predators (Fig. 9.6), this is 630

mg of herbivore consumed per m^2 during the sampling period. Assuming a nonpredatory mortality of 20%, total mortality would then be estimated as 788 mg per m^2 .

Total production for the herbivorous insect population during the nine-week sampling period is thus estimated to be 140 mg per m^2 net increase, plus 788 mg per m^2 loss to mortality, for a total of 928 mg per m^2 production. Net increase in biomass was only 15% of total production, and would be a poor estimate of production in this field population.

Energy flow through the herbivorous insect population may now be estimated by using food consumption rates for herbivores calculated with steady-state equilibria for radiocesium. Conversion from milligrams of dry matter to kilocalories was made by using bomb calorimeter measurements of energy content in insect and plant samples from White Oak Lake bed. Energy flow through herbivorous insects was 33.6 kcal per m^2 maintenance, 10.8 kcal per m^2 production, for a total of 44.4 kcal per m^2 , corrected to a 20-week growing season. These numbers appear to be in good agreement with published estimates of energy flow and production, but a further examination of procedures is necessary.

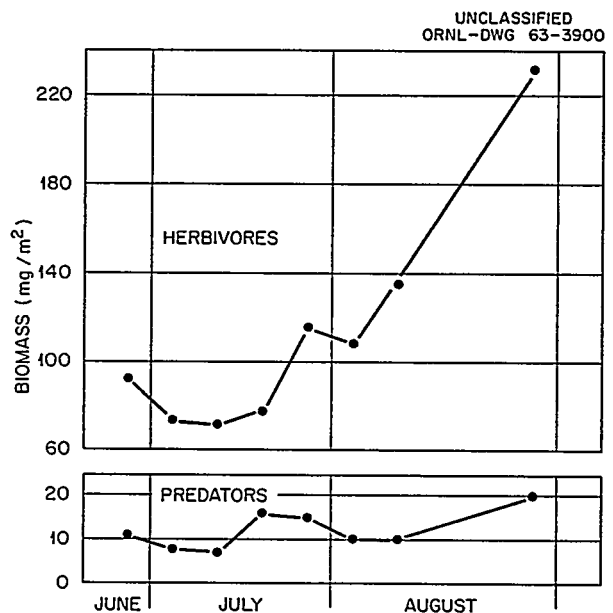


Fig. 9.6. Biomass of Herbivorous and Predaceous Insect Populations on White Oak Lake Bed Vegetation (Summer 1961).

¹⁵J. M. Teal, *Ecology* 43, 614-24 (1962).

¹⁶D. A. Crossley, Jr., *loc. cit.* pp. 103-5.

¹⁷S. I. Auerbach et al., *Health Phys. Div. Ann. Progr. Rept. June 30, 1963*, ORNL-3492, pp. 94-95.

RADIATION SENSITIVITY OF INSECTS

E. F. Menhinick Gladys J. Dodson

Changes in insect populations as a consequence of irradiation may be due to direct biological effects or indirect effects on food, predators, or environment. Laboratory studies describing the relative radiosensitivity of different species and of the various life history stages (radiation profiles) are a necessary first step in the interpretation of results from contaminated areas.

Five species of insects were irradiated in a ^{60}Co source at 3 or 30 kr/min, and given total doses of 1 to 512 kr in 100% increments. Insects were kept at 28°C, and records were kept on mortality until all organisms were dead. Effects were expressed as mean life expectancy in days. An LD_{50-30} has little comparative value for insects, as some species do not live 30 days, and in others the effects are not manifest until after 30 days.

Doses of 512 kr were immediately lethal to all species examined; 2 kr or less did not affect survival compared with controls. Mean survival time plotted against the log of dose was essentially a straight line from 4 to 512 kr (Fig. 9.7). Crickets

(*Acheta domestica*) were the most sensitive insects examined. First and second instar crickets were more radiosensitive than adults. Radiation profiles of grain beetles (*Tenebrio molitor*) showed pupae to live longer than adults or larvae at doses over 16 kr, but small larvae were more radio-resistant at doses below 8 kr (perhaps a function of their greater life expectancy as shown by controls). Milkweed bugs (*Oncopeltis fasciatus*) and roaches (*Parcoblatta* sp.) had a mean survival time similar to *Tenebrio*. Ants (Formicidae sp.) were the most resistant species examined. Data are now being acquired on radiosensitivity of additional life-history stages for these and other insects.

METABOLISM OF CRICKETS

E. F. Menhinick

The importance of a species in a community may best be determined by studying its food and energy requirements. Radiation would be expected to affect several aspects of metabolism. Lethal doses would of course increase mortality and decrease standing crop. Sublethal doses would probably decrease egg production and growth, resulting in decreased assimilation, but low doses may actually reduce mortality. Radiation has been shown to depress food intake and O_2 consumption.¹⁸ To determine the extent to which radiation may affect these energy requirements and thereby cause changes in community structure, a study was made of the feasibility of simultaneous measurements of different aspects of energy flow: ingestion, defecation, O_2 consumption, and production.

Crickets (*Acheta domestica*) 17 days old with an average dry weight of 5.0 mg were placed on a screen wire in a sealed chamber (Fig. 9.8). Food, shelter, and water were provided. A CaCl_2 desiccant kept humidity down to prevent molding of food and feces. KOH, added as a CO_2 absorbent, was titrated to determine CO_2 evolution. As O_2 was consumed, the CO_2 evolved was absorbed by KOH, creating a partial vacuum. This drew pure O_2 from a graduated cylinder into the chamber. Oxygen removed from the graduated cylinder was

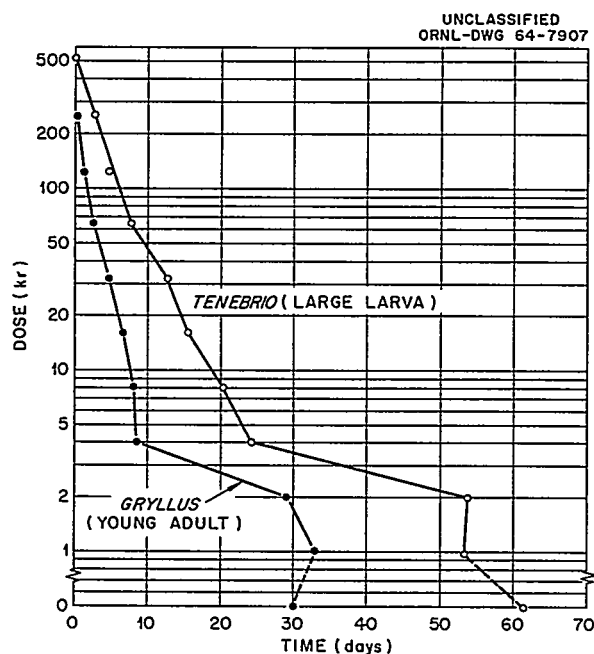


Fig. 9.7. Mean Life Expectancy of Cricket Adults and Mealworm Larvae.

¹⁸R. C. King and L. P. Wilson, *Radiation Res.* 2, 544-55 (1955).

replaced with water from a constant-water-level source. Increase in water level in the graduated cylinder was therefore a measure of oxygen consumption. Pressure in the chamber could be increased or decreased by raising or lowering the constant water level. Use of pure O_2 in the graduated cylinder allowed the percent O_2 in the chamber to remain at the original level. Composition of atmospheric gases (except CO_2) could thus be controlled at any desired level. All tests were run at 1 atm, using 21% O_2 . Temperature was held constant at 28°C. Corrections were made for barometric changes. Each test lasted for about eight days. Oxygen consumption for each period is given in Table 9.4.

Food consumption was determined by weighing food dried in a 105°C oven before and after each period. Feces, cast skins, and dead crickets were likewise dried and weighed. Some crickets were

sacrificed to determine wet weight-dry weight ratios for conversion of changes in standing crop to dry weight. Cannibalism was estimated from change in numbers and weight not accounted for by dead crickets. Energy flow for each period is given in Table 9.4.

Over a period of 42 days, the crickets consumed an average of 435 mg of meal per individual and 4 mg of dead crickets—a total ingestion of 439 mg. Of this, 160 mg was lost in feces, resulting in an assimilation of 279 mg. Standing crop increased 38 mg; skins weighed 2 mg; and mortality accounted for 8 mg; this gave a total production of 48 mg. Oxygen consumption for this period was 166 ml STP.

Future experiments coupled with calorimetry data will be used to study the effects of radiation on energy flow, and the relation of isotope uptake, loss, and equilibrium with energy flow.

UNCLASSIFIED
ORNL-DWG 64-7908

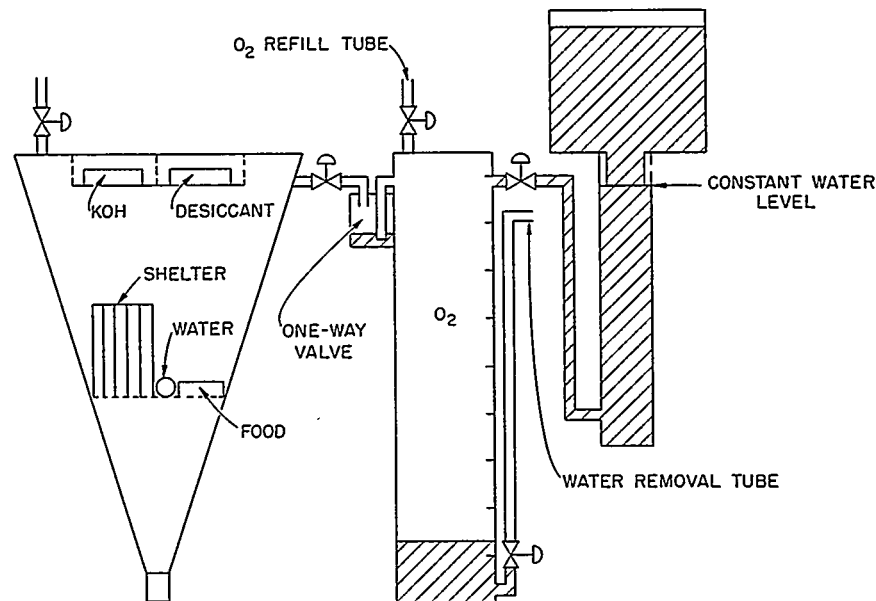


Fig. 9.8. Apparatus for Study of Cricket Metabolism.

Table 9.4. Calculation of Metabolism of Crickets (*Acheta domestica*) from Food Consumption, Defecation, O₂ Consumption, and Production

Age (days)	17	25	33	41	50	59
Mean dry weight (mg)	5.0	9.4	18.2	21.4	46.3	61.5
Meal consumption	2.47	3.51	6.27	10.61	11.97	16.82
Cannibalism	0.03	0.08	0.08	0.04	0.06	0.16
Food consumption	2.50	3.59	6.35	10.65	12.03	16.98
Feces	1.09	1.73	2.39	3.29	4.46	6.13
O ₂ consumption (ml STP)	0.64	1.30	2.74	3.71	4.38	7.04
Δ standing crop	0.42	0.65	0.98	0.95	1.01	0.55
Skins	0.03	0.03	0.12	0.11	0.00	0.00
Death	0.07	0.10	0.18	0.17	0.18	0.24
Production	0.52	0.78	1.28	1.23	1.19	0.79

STRONTIUM-90-YTTRIUM-90 BETA SOURCE

E. F. Menhinick

The effects of beta radiation on small arthropods have received minor attention compared with the effects of gamma radiation. Most studies have involved effects of beta radiation on insects raised in contaminated media, or fed contaminated food. Phosphorus-32 has been used in over 70% of the experiments, with attention also given to ³⁵S, ⁴⁵Ca, ⁹⁰Sr, ⁸⁹Sr, ¹⁴C, and others. In most cases the amount of isotope in the food or medium is given, but no attempt is made to estimate absorbed dose. Absorbed dose would have to be known to compare the effects of different radiations or to predict effects under different conditions. Most data on the RBE of beta radiation come from studies on the control of grain pests with accelerated electrons produced by a Van de Graaff generator or betatron. These studies indicate that the relative effect of beta and gamma radiation on insects varies with dosage and age of the organisms.

Because of close contact of insects to contaminated surface areas and to soil, beta radiation dose to insects may be a more important component of environmental contamination than gamma radia-

tion. Because of the low penetration of beta radiation, smaller organisms would receive higher tissue doses than larger ones; insect eggs would receive higher doses than adult insects. Other factors governing the effect of beta radiation concern the importance of chitinous shielding, the additive effects of beta and gamma radiations, dose rate effects, and techniques for measuring beta radiation.

Three plane beta sources of 100, 1000, and 10,000 r/hr on the surface have been constructed to answer some of these questions. Strontium-90 was chosen as the isotope to be used because of its long half-life (~30 years), its strong daughter isotope (⁹⁰Y = 2.2 Mev), and its low cost (\$10.00/curie). Materials with low atomic number were used to minimize bremsstrahlung. The bremsstrahlung spectrum through 4 mils of aluminum and ³/₈ in. of plywood as determined with multi-channel analyzer and NaI crystal indicated that most energy was less than 200 kev, and was concentrated around 14 kev (Fig. 9.9). Complete shielding of beta particles is obtained by 0.35 in. of wood or 0.20 in. of glass. However, ³/₄ in. of plywood and ¹/₂ in. of glass were needed to reduce bremsstrahlung to 0.1% of the exposure dose of both beta and bremsstrahlung with only 5 mils of aluminum shielding. Feather analysis and dose

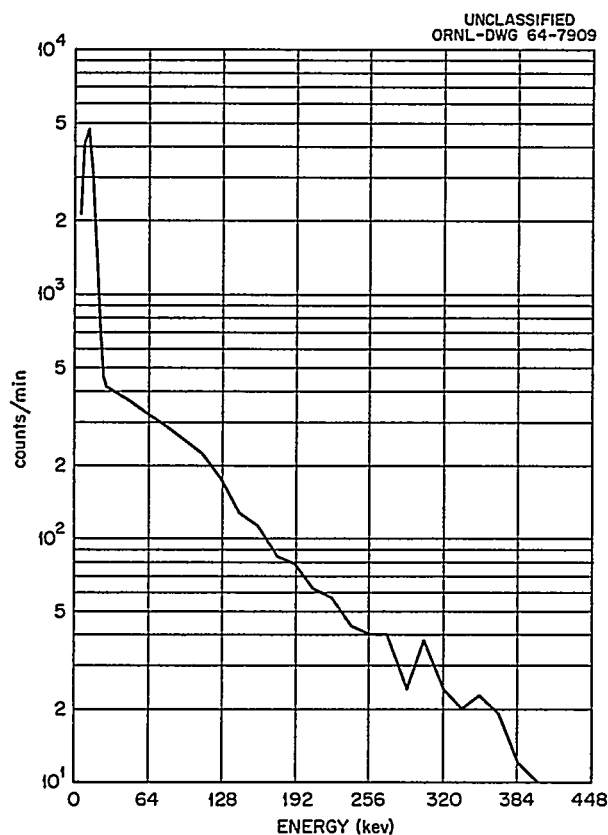


Fig. 9.9. Bremsstrahlung Spectrum of ^{90}Sr - ^{90}Y over Transite. Radiation passing through 4 mils of aluminum and $\frac{3}{8}$ in. of plywood (multichannel analyzer).

rate studies indicated that 5 mils of aluminum shielded out most of the 0.54-Mev ^{90}Sr , and at the same time transmitted a large percentage of the 2.2-Mev ^{90}Y beta rays, which was desirable in order to obtain more uniform tissue doses.

A plane source rather than a point source was made to simulate surface contamination. A source 13 in. in diameter was found to give uniform surface dose rates from the center up to 1 in. from the edge. Transite asbestos sheeting was used for the plaques because of its low atomic number and because it would not deteriorate with radiation as would plastic or wood. The ^{90}Sr was mixed with 30 ml of sodium silicate, an inorganic compound not affected by radiation, to bind it to the transite surface. The pitted surface of the transite enabled uniform application of ^{90}Sr with a brush; uniform application was not possible with aluminum sheeting. Seventy millicuries of ^{90}Sr

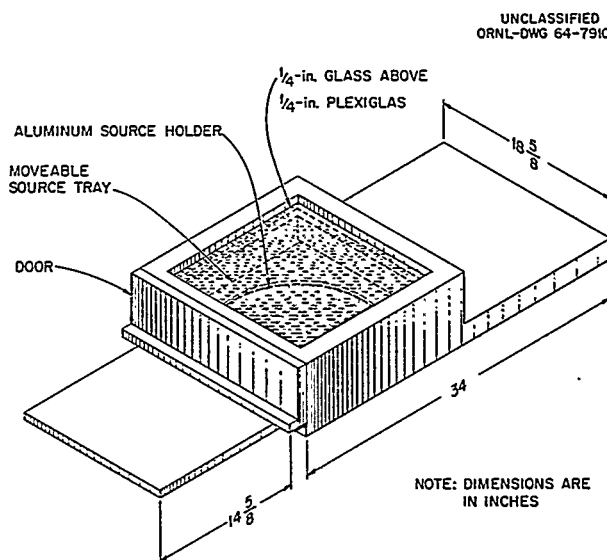


Fig. 9.10. Strontium-90 Source in Irradiate Position.

^{90}Y gave surface dose rates of 100 r/hr through the 5 mils of aluminum; 0.7 curie gave 1000 r/hr, and 7.0 curies gave 10,000 r/hr. After application of the isotope, the transite plaques were placed in leak-tested aluminum containers, consisting of 5 mils of aluminum at the top and $\frac{1}{4}$ in. of aluminum on the bottom. The aluminum containers were then placed in a concavity in the far end of a sliding plywood tray. The tray was placed in a plywood container, and stop plugs were added to prevent its removal (see Fig. 9.10 for design of the container). To irradiate a series of insects, the source was slid into the shielded position (Fig. 9.10) and the door (which can only be opened when the source is in the shielded position) opened. The insects were placed in a plastic container with a thin milar bottom, then placed on another milar sheet directly above the source tray. The door was then closed and the source slid out into irradiate position, directly below the insects.

HEMATOLOGY OF NATIVE MAMMALS

P. B. Dunaway	B. E. Jacobs
Lovell Lawrence	J. D. Story
J. A. Payne	T. P. O'Farrell
G. D. Martin	

The hematological studies of native mammals initiated in 1962 were completed this year. The

objective of these studies was to determine the effects of endogenous and environmental factors on the blood of indigenous species before research is started on the effects of ionizing radiation on the blood of these species. Consequently, it was necessary to establish normal blood values for mammals of this area as well as to ascertain some of the factors which cause changes in blood. Animals from other parts of North America were sampled because of taxonomic, altitudinal, and latitudinal implications.¹⁹ Over 10,000 hematological measurements were made for over 2000 mammals of 41 species belonging to 11 families representing 7 orders.

Most of the instruments and techniques for these studies have been discussed previously.^{20,21} However, hemoglobin determinations and electrophoretic measurements were initiated during the past year. Two innovations were developed for these tests: (1) a technique was developed whereby the dilution for leucocyte counting is utilized also for the hemoglobin determinations, and (2) the plasma from the microhematocrit tubes is used also for the electrophoresis runs. These innovations make possible a more efficient use of small quantities of blood and also reduce the number of manipulations.

Taxonomic relationships among the various species of mammals must be considered in planning experiments on radiation effects on blood. An interrelation was shown previously between erythrocyte count, mean corpuscular volume, and body weight of species within several families of mammals; that is, erythrocyte count is inversely related to the body weight of the species within a family, and mean corpuscular volume is directly related to body weight.^{20,21} Additional work with more species and families of mammals supports this finding. This interrelation is clearly apparent in the seven species of the family Cricetidae

(native rats and mice) and the four species of the Sciuridae (the squirrel family) trapped on the Oak Ridge reservation (Figs. 9.11 and 9.12). It appears also that a similar relationship exists in other families examined, but not enough species in these families were available to obtain definitive familial curves.

Many species of mammals acclimated to high altitudes have elevated erythrocyte counts, hematocrit percentages, and hemoglobin concentrations.²² Conversely, other investigators have reported that measurements of these blood values in other species are much the same at different altitudes.^{23,24} Our research with mammals from higher altitudes indicates that certain hematopoietic functions in some species (red squirrels, redback mice, and deer mice) may be under genetic control to a considerable degree, but that in other species (least chipmunks and white-footed mice) physiological responses to changes in altitude cause hematopoietic changes. Latitude also may be an important factor governing erythrocyte number in mammals. Species from more northern latitudes had erythrocyte counts above the RBC/weight curves plotted for the respective families in the Oak Ridge area. Erythrocyte counts for species from more southern latitudes were below the curve for Oak Ridge cricetids.

Mean corpuscular volume (MCV) seems to be less variable in some families than in others. For instance, the MCV for each species of sciurid from areas other than the Oak Ridge area (including those species from high altitudes) lies close to the MCV/weight curve for the Oak Ridge animals, but the MCV values for cricetids from other areas are all appreciably less than the curve plotted for the Oak Ridge cricetids. In general, MCV values for the smallest species of mammals are much less than the values for the larger species examined. For instance, the shrews, bats, small cricetids, and small sciurids have small cells (22 to 46 μ^3), whereas the opossum, the monkeys, the rabbit, the larger cricetids, and the larger sciurids have relatively large cells (71 to 79 μ^3).

¹⁹Thanks are due to the following persons for their donations of animals or blood from animals from other areas: R. H. Baker, Michigan State University; C. H. Brink, University of Alaska; D. deL. Condon, Great Smoky Mountains National Park; P. Eide, Oak Ridge Institute of Nuclear Studies; J. M. Inglis, Texas A & M College; I. C. S. McArthur, University of Saskatchewan; D. P. Snyder, University of Massachusetts; and C. A. Tryon, Jr., University of Pittsburgh.

²⁰S. I. Auerbach et al., *Health Phys. Div. Ann. Progr. Rept. July 31, 1962*, ORNL-3347, p. 52.

²¹S. I. Auerbach et al., *Health Phys. Div. Ann. Progr. Rept. June 30, 1963*, ORNL-3492, p. 84.

²²C. L. Prosser and F. A. Brown, Jr., *Comparative Animal Physiology*, 2d ed., p. 222, Saunders, Philadelphia, 1961.

²³F. G. Hall, *J. Mammal.* 18, 468-72 (1937).

²⁴N. J. Kalabuchov, *J. Anim. Ecol.* 6, 264-72 (1937).

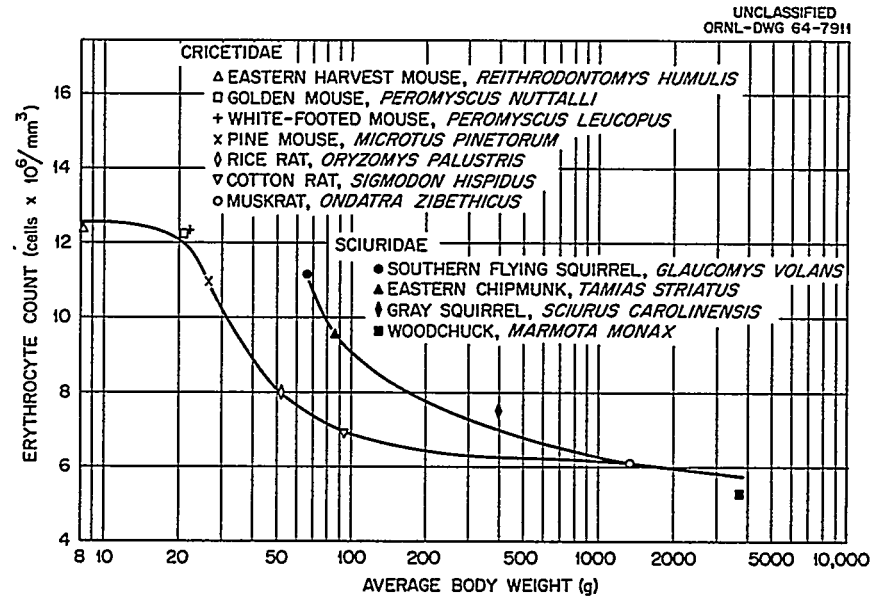


Fig. 9.11. Relation of Erythrocyte Count to Body Weight in the Cricetidae and Sciuridae.

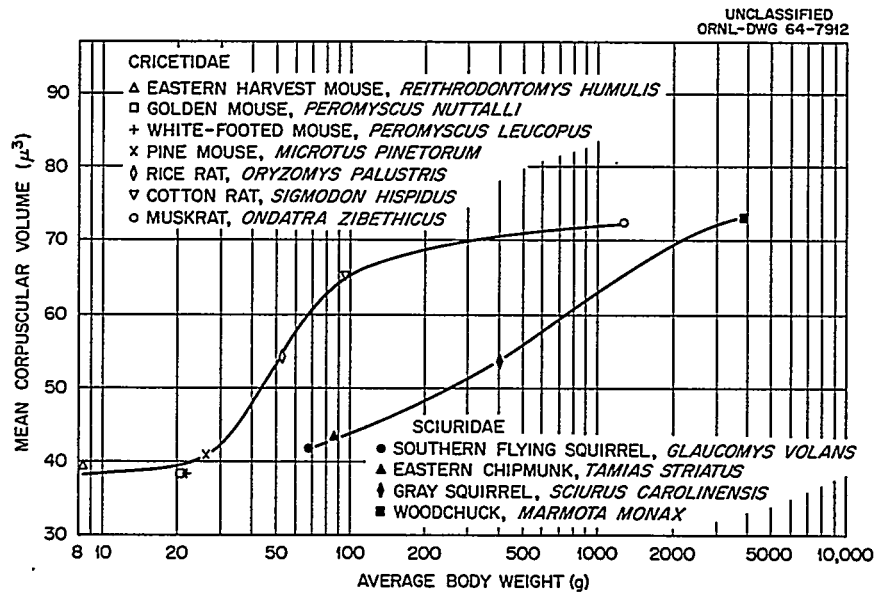


Fig. 9.12. Relation of Mean Corpuscular Volume to Body Weight in the Cricetidae and Sciuridae.

The amount of hemoglobin in the species studied does not vary greatly (12 to 19 g/100 ml of blood). The values for shrews, bats, and several small cricetids seem to be relatively high (>16 g/100 ml of blood), whereas the values for opossums, tamarins, woodchucks, and skunks are relatively low (<13 g/100 ml of blood). Also, it appears that several species of animals from higher elevations have relatively high concentrations of hemoglobin (>16 g/100 ml of blood), even after several months of captivity at a lower elevation.

The total leucocyte count appears to be lowest in the smaller species ($<5 \times 10^3$ cells/mm³) and highest in the larger species ($>10 \times 10^3$ cells/mm³). The tendency for larger species to have higher leucocyte counts may not be related to body size per se, but may be related more to increasing parasite loads and disease in the larger species, which, in general, tend to live longer than the smaller species and thus have more time to develop disease and accumulate parasites. Parasites, diseases, and injuries can cause drastic changes in the blood of various species. Some of the hematological effects of botfly myiasis in white-footed mice are shown in Table 9.5 as an example. It is obvious from the data that erythrocyte count, hematocrit percentage, and hemoglobin concentration are reduced and that the leucocyte count is elevated. Mice captured within a month or less after emergence of the bots had completely normal blood values. Studies during the seasons of last year indicated that, in general, synchronous changes cannot be expected to occur in all blood parameters of all species during the course of a year. However, within a given species it is

apparent that seasonal changes in blood do occur. These changes are more attributable to such factors as population age structure and parasitism than to climate per se. The only consistent seasonal pattern seen for all species tested was that the hemoglobin concentration was lowest in the summer, highest in the winter, and decreased from winter to spring.

In summary, these hematological studies have shown that such factors as age, sex, certain diseases, certain parasites, injuries, confinement, and season govern hematopoietic changes. Obviously, all of the factors causing changes in the blood of these mammals from wild populations could not be determined during the period of this study. However, we feel that sufficient data are available for studies to begin on the effects of ionizing radiation on local species.

Electrophoretic Analyses of Wild Mammal Blood

Species specificity and alterations due to a variety of stress conditions are reflected by serum and plasma protein electrophoretic patterns. Electrophoretic analyses of wild mammal blood were begun as an adjunct to other hematological studies in process.

Paper electrophoresis was carried out on a Spinco model R cell. The paper strips were stained in bromophenol blue and colorimetrically analyzed in a Spinco model R Analytrol. Thereby the relative mobilities and percent total serum protein for the various moieties were quantitatively obtained as well as the albumin-globulin ratios. Differential

Table 9.5. Hematological Effects in *Peromyscus leucopus* Infested with *Cuterebra angustifrons* Larvae

	RBC (Cells $\times 10^6$ /mm ³)	HCT (%)	HGB (g/100 ml)	WBC (Cells $\times 10^3$ /mm ³)
Summer, 1963				
Animals without bots	11.82 (32) ^a	46 (30)	15.6 (31)	6.2 (32)
Animals with bots	9.49 (10)	37 (7)	12.8 (10)	11.9 (10)
Fall, 1963				
Animals without bots	12.55 (35)	45 (29)	16.2 (33)	7.0 (35)
Animals with bots	9.21 (5)	37 (5)	13.0 (5)	9.6 (4)

^aNumber in parentheses indicates number of samples.

staining techniques specific for lipoproteins (beta globulins and gamma globulins) and for glycoproteins (alpha globulins) are being used as a basis for identification of the various globulins. The total protein concentrations of the samples are being determined by the biuret method. Analyses are being completed on sera of animals belonging to 33 species representing 8 families belonging to 6 different orders.

Some systematic similarities in serum protein patterns are readily apparent. For instance, the average albumin percentage of all cricetids thus far studied was within the range of 50 to 55%, whereas the range for the sciurids was appreciably lower (31 to 34%).

The largest and most consistent change in normal serum patterns is characteristically demonstrated by the albumin. Significant alterations in this component have been observed as a seasonal variation and as a result of numerous stress factors. One seasonal variation has been a higher albumin value for the sera of animals sampled in the winter than from the same animals sampled in other seasons. Bot fly (*Cuterebra angustifrons*) and nematode (*Litomosoides sigmodontis*) infestations are two conditions which have resulted in reduced relative and absolute albumin components. This change is consistent with that seen in a variety of infections and pathological conditions.

Additional relationships which may be of significance have been noted. Laboratory-bred cotton rats had higher albumin percentages than field-trapped members of the same species. A coefficient of correlation of -0.360 between total white cell count and albumin-globulin ratio was calculated for the white-footed mouse ($0.05 > P > 0.02$). If subsequent calculations show this relationship to be a general one, it would imply that a low albumin in combination with a high total globulin value might well serve as readily as a high white blood cell count as an indication of general infection or trauma in an individual or a wild population.

Analyses of these data are at present incomplete, but work is continuing in an effort to clarify the correlations noted and to elucidate additional relationships.

Incorporation of 5-¹³¹Iodo-2'-deoxyuridine into the DNA of Indigenous Mammals

The chemical 5-¹³¹Iodo-2'-deoxyuridine (¹³¹IUDR) is an antimetabolite, which, upon *in vivo* injection, is incorporated into the DNA (deoxyribonucleic acid) of rapidly proliferating cells and serves as an index to cell proliferation and DNA synthesis.²⁵ The fact that as little as 10 r of ionizing radiation will alter the rate of incorporation suggests a potential use of ¹³¹IUDR as a physiological dosimeter.²⁶ The objectives of experiments designed to test this potential are to establish normal ¹³¹IUDR retention curves for three species of native mammals (*Sigmodon hispidus*, cotton rat; *Microtus pinetorum*, pine mouse; and *Peromyscus leucopus*, white-footed mouse), and to quantify the effects of acute and chronic radiation on incorporation in *Sigmodon*.

Experimental animals were injected intraperitoneally with 1 μ c of ¹³¹IUDR and counted periodically in a small-mammal whole-body counter. The percent radioactivity remaining was plotted on a semilogarithmic scale from the counter data. Control animals of each species received an injection of 1 μ c of Na¹³¹I to establish retention curves for radioiodine, the major product of ¹³¹IUDR metabolism.

Retention curves for white-footed mice and pine mice are illustrated in Fig. 9.13, along with the curves for two subspecies of *Rattus norvegicus*, brown rat and Sprague-Dawley strain laboratory rat, which were obtained in a pilot experiment. Each curve had approximately three major components. The first component had a steep slope that reached a point of inflection about 24 hr after injection. This component corresponds to an elimination phase during which most of the unincorporated ¹³¹IUDR was broken down and eliminated. The second component was a line of less extreme slope and indicated loss of incorporated ¹³¹IUDR from the labeled cohort. The second component, however, was partially masked by the third component. This last portion of the curve, which began ~ 192 hr postinjection, approached a slope of 0 and closely paralleled the retention curve for Na¹³¹I. It appeared that the

²⁵M. B. Wheeler *et al.*, *Exp. Cell Res.* 33, 39-45 (1963).

²⁶D. Gitlin *et al.*, *Science* 133(3458), 1074-75 (1961).

final component was mainly a measure of the ^{131}I retained as a metabolic by-product in the skin and hair. To test this hypothesis, three white-footed mice and six pine mice were killed at the termination of whole-body counting, their tissues were removed and weighed, and radioactivity was determined with a scintillation spectrometer. Between 88 and 91% of the remaining radioactivity was found in the skin and hair of *P. leucopus*, and about 77% was in the same compartment of *M. pinetorum*.

The amount of radioactivity 48 hr after injection was used as an index to the incorporation of

^{131}I IUDR. This time period was chosen because it occurred at an interval when the curve representing ^{131}I IUDR loss would not be masked by either the elimination component or the curve of ^{131}I retention. The average incorporation for the species tested was: pine mouse, 2.2%; white-footed mouse, 1.2%; brown rat, 0.19%; and Sprague-Dawley rat, 0.08%. It appeared from these data that animals with higher rates of metabolism incorporated a greater amount of ^{131}I IUDR and apparently had a higher rate of DNA synthesis.

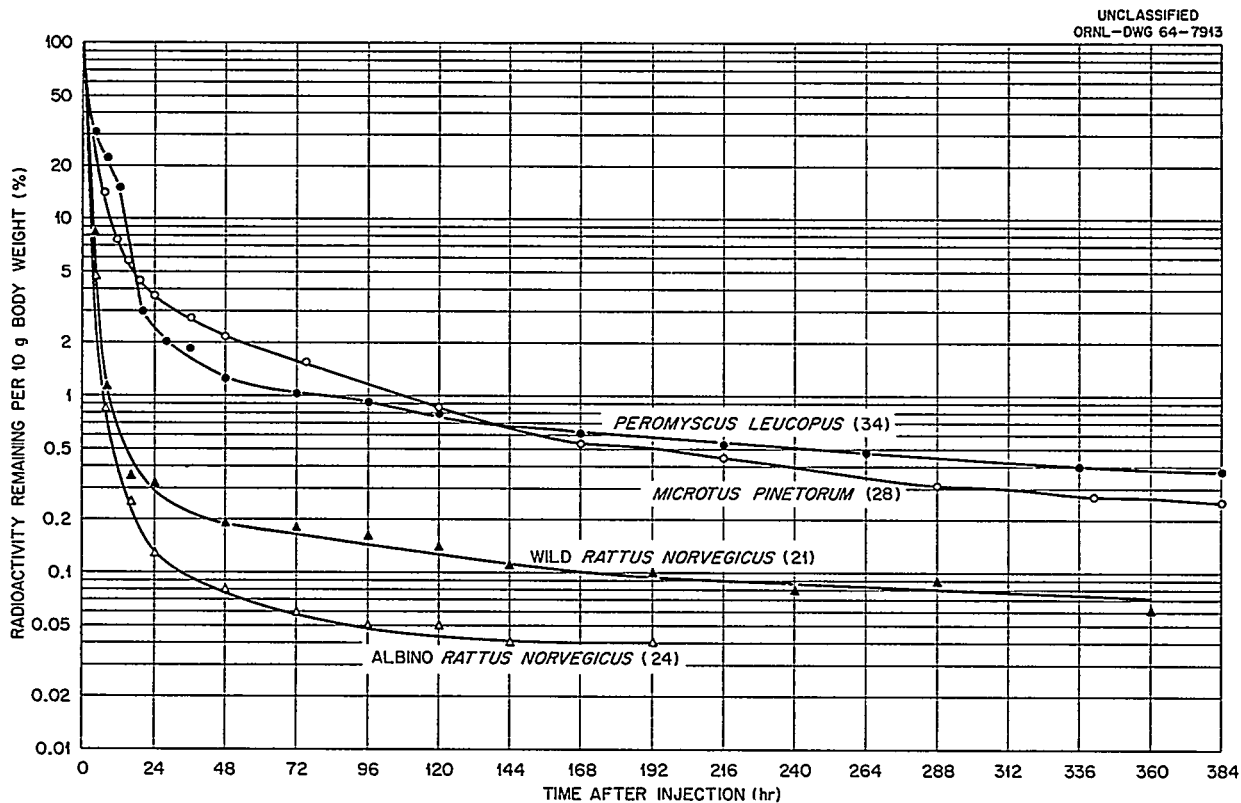


Fig. 9.13. Average Radioactivity Retained Following an Injection of $1\ \mu\text{c}$ of $5\text{-}^{131}\text{I}$ odo-2'-deoxyuridine. Numbers in parentheses indicate sample size for each species.

10. Processes and Components of Terrestrial Ecosystems

J. S. Olson
G. N. Brown
G. M. Van Dyne
H. D. Waller
J. P. Witherspoon, Jr.

Martin Witkamp
Regina M. Anderson
W. C. Cate
Marilyn L. Frank
F. G. Taylor, Jr.

FIRST-YEAR BUDGET OF ^{137}Cs IN THE TAGGED LIRIODENDRON FOREST

H. D. Waller Regina M. Anderson
J. S. Olson W. C. Cate

An inventory of total ^{137}Cs distribution among the tree-soil compartments of the tulip poplar forest system (tagged May 1962) was constructed from data collected during the first growing season. About one-half of the initial inoculant was found

in the litter, soil, and smaller root components by October (Fig. 10.1). Transport of cesium from leaves was discussed last year. The maximum burden found in the canopy about four weeks after inoculation ($248 \mu\text{C}/\text{m}^2$ of ground area) was reduced to $117 \mu\text{C}/\text{m}^2$ of ^{137}Cs by late September, that is, about a 60% reduction. This reduction is due to three processes: (1) export of cesium from foliage to woody tissue during mature and senescent stages of leaf development, which accounts for the greatest amount of reduction; (2) removal

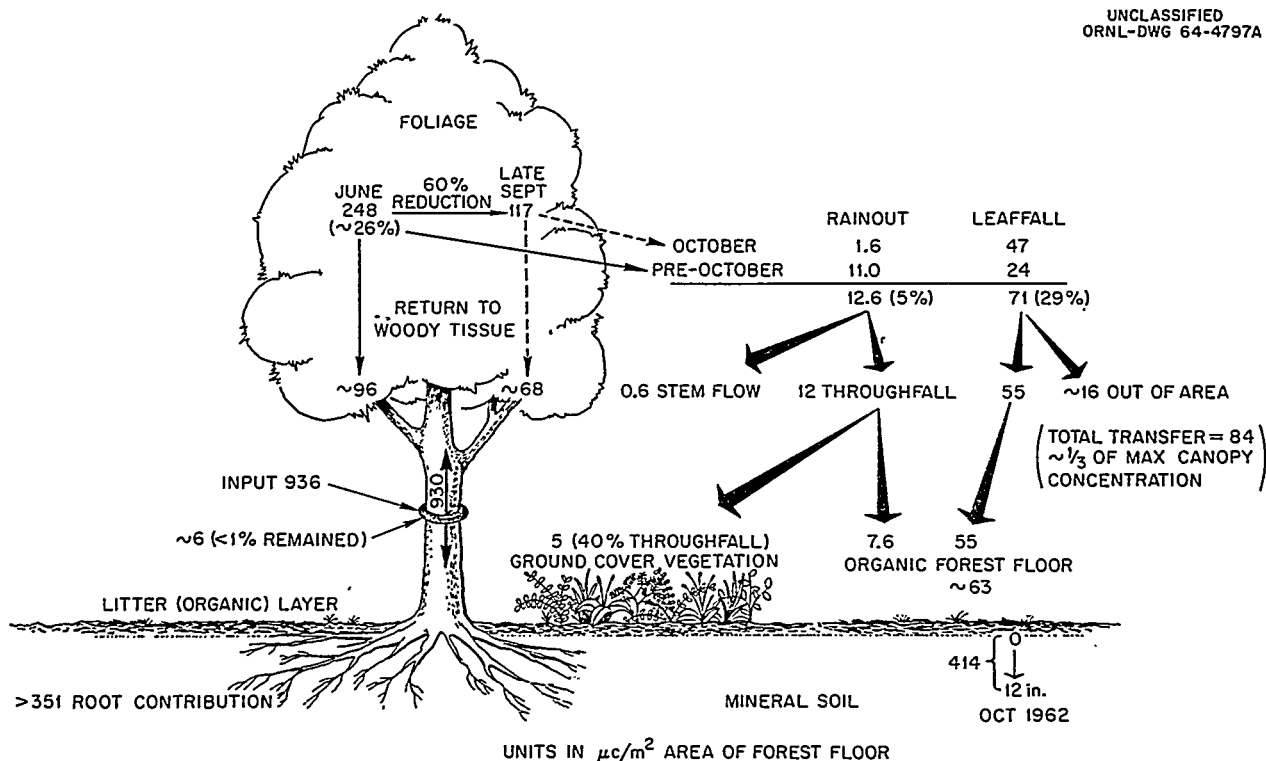


Fig. 10.1. Flow Diagram Depicting the Input of ^{137}Cs per Square Meter of Area of Forest Floor and Translocation or Transfer After the First Growing Season. Maximum movement into foliage occurred in June ($248 \mu\text{C}/\text{m}^2$, 26% of total inoculant). During October there was a remobilization of cesium just prior to leaf fall; more than one-half of the cesium in the foliage in late September moved back into woody tissue, and the remainder (~40%) was transferred to other components of the forest system either by rainout or by leaf fall.

of radiocesium from foliage by rain and dew leaching prior to mid-September, which accounts for about 4% of the total reduction; and (3) reduction in concentration (μC per g of dry weight) by the formation of new tissue. Stenlid¹ reported similar transfers from mature leaves for other mineral elements, especially potassium, phosphorus, and nitrogen.

Of the $248 \mu\text{C}/\text{m}^2$ of ^{137}Cs estimated to be in the canopy during the June maximum, almost two-thirds moved back into woody tissue by autumn. An estimated $96 \mu\text{C}/\text{m}^2$ was transferred from leaf tissue to woody tissue during the summer (June to late September). In October, prior to leaf drop, an additional $68 \mu\text{C}/\text{m}^2$ was transferred from canopy component to woody component (stems and roots) of the tagged trees.

The important paths of transfer of ^{137}Cs from tagged trees to the forest floor were found to be rain leaching, leaf fall, and passage through the roots. Losses from the foliage and stems through litter fall and rain leaching accounted for almost 9% of the total inoculant introduced into the tree boles (Fig. 10.1). However, soil (including roots $< \frac{3}{4}$ -in. diam) and litter sampling during October indicated a much larger quantity: $414 \mu\text{C}/\text{m}^2$ already in the top 12 in. of mineral soil. Estimates of rainout (almost $13 \mu\text{C}/\text{m}^2$) plus leaf fall in the plot ($55 \mu\text{C}/\text{m}^2$) indicate $68 \mu\text{C}/\text{m}^2$ transferred from aerial components of tagged trees to the ground inside the plot. About $5 \mu\text{C}/\text{m}^2$ of this was intercepted by untagged ground-cover vegetation, so the surface contribution of radiocesium was only $63 \mu\text{C}/\text{m}^2$. Approximately half of this surface income remained in the organic surface layer (leaving half as income for mineral soil), therefore, roots from tagged trees must be contributing over $350 \mu\text{C}/\text{m}^2$ (about 90%) of the total soil burden.

TRANSFER OF RADIOCESIUM TO UNTAGGED UNDERSTORY PLANTS IN A TAGGED FOREST

H. D. Waller Regina M. Anderson
J. S. Olson W. C. Cate

One of the objectives of the tagged forest experiment is to quantitatively describe the main

pathways of transfer of ^{137}Cs from the tagged tulip poplar trees to the untagged understory plants. There are two primary pathways for this transfer. The most direct is the interception of cesium rainout from the canopy and subsequent foliar uptake by the untagged understory. The second pathway is the transfer of the cesium from tagged trees to the forest floor (via rain leaching of canopy components, roots, and litter fall), and subsequent root uptake by the understory plants. Although there were no direct measurements separating foliar absorption from root uptake during the first growing season, the data listed in Table 10.1 suggest foliar absorption to be about 10^3 to 10^4 times more important in the transfer than uptake from soil. Comparing plant/soil ratios [$(\mu\text{C}$ per gram of plant)/(μC per gram of soil)] obtained with understory vegetation and soil substrate, we get ratios of about 100 (Table 10.1). Previous work at ORNL on plant uptake of cesium through root systems suggest plant/soil ratios to be of the order of 0.01 if uptake from soil is the pathway of entry to the vegetation.^{2,3} Therefore, root uptake was considered to be of little significance for the first growing season.

After two growing seasons, the transfer of ^{137}Cs to untagged understory was primarily from rainout through the overhanging crowns. Twenty samples (each with an area of 0.1 m^2) were taken in August 1963 to ascertain the amount transferred into the small ground-cover plants. Soils within each 0.1-m^2 ring were sampled to obtain the radiocesium concentration of the plant's growing medium. Eight species showed plant/soil activity ratios ranging from 0.23 to 6.7, suggesting that foliar absorption was 40 to 400 times greater than root uptake near the end of the second growing season.

A complementary experiment was initiated in April 1964 in a nearby area to obtain a soil-to-plant uptake value for cesium in this forest system.

¹G. Stenlid, *Encyclopedia of Plant Physiology* 4, 615-37 (1958).

²J. P. Witherspoon et al., *Cycling of Cesium-134 in White Oak Trees on Sites of Contrasting Soil Type and Moisture*, ORNL-3328 (October 1962).

³R. E. Shanks and H. R. DeSelm, pp. 97-103 in *Radioecology* (ed. by V. Schultz and A. W. Klement, Jr.), Reinhold, New York, 1963.

Table 10.1. Ground-Cover Vegetation
Foliar absorption vs root uptake in the ^{137}Cs -tagged forest (first growing season)^a

	Weight (g/m ²)	Distribution of ^{137}Cs by Species (%)	Plant Concentration of ^{137}Cs (μc/g)	Soil Concentration of ^{137}Cs (μc/g)	Plant/Soil Ratio
			$\times 10^{-2}$	$\times 10^{-4}$	
Christmas fern (<i>Polystichum acrostichoides</i>)	28.44	35	5.62 ± 1.17	7.63	76.3
Hydrangea (<i>Hydrangea aborescens</i>)	39.46	53	5.55 ± 1.35	7.63	75.4
Virginia creeper (<i>Parthenocissus quinquefolia</i>)	3.84	3	9.13 ± 1.43	7.63	124.0
Others species, including <i>Botrychium virginianum</i> , <i>Lonicera japonica</i> , <i>Smilax</i> <i>glauca</i> , <i>Galium circaeazans</i> , <i>Desmodium</i> sp., <i>Goodyera</i> <i>pubescens</i> , <i>Viola</i> sp., <i>Convolvulus</i> sp., <i>Agrimonia gryposepala</i>	14.6	9	11.64 ± 3.85	7.63	158.1

Note: Previous work at ORNL on plant uptake of ^{134}Cs for woody plants (white oak, *Quercus alba*, saplings using tagged leaves placed around the base of stem) by Witherspoon (*Cycling of Cesium-134 in White Oak Trees on Sites of Contrasting Soil Type and Moisture*, ORNL-3328, October 1962) gave uptake values of 0.77% (plant/soil ratio of 0.008). Shanks and DeSelm (*Radioecology*, pp. 97-103, ed. by V. Schultz and A. W. Klement, Jr., Reinhold, New York, 1963) listed average uptake values of 0.77% (plant/soil ratio of 0.008) for ^{137}Cs for herbaceous species growing on White Oak Lake bed.

^aAll weights are oven-dry weights.

TRANSFER AND DISTRIBUTION OF ^{137}Cs WITHIN THE FOREST FLOOR

H. D. Waller F. G. Taylor, Jr.
J. S. Olson Regina M. Anderson
W. C. Cate

Accumulation of surface income of ^{137}Cs (rain leaching of canopy and litter fall) within the organic litter layer and surface 2 cm of soil was measured in sample units designed to prevent root entry. Interpretation of distribution of surface income would otherwise have been very difficult, since so much cesium reached the soil through roots. Results indicate that half of the surface income was contained within the organic layer, and more than 80% was contained within the organic layer plus the surface 2 cm of mineral soil (Fig. 10.2, surface income).

Although surface income is the most direct transfer pathway, it contributes only a small portion to the total burden of ^{137}Cs measured within the surface 12-in. layer of mineral soil (Fig. 10.2). When only the surface 2 in. are considered, surface income accounts for less than 20% of the measured burden of ^{137}Cs (Fig. 10.2, mineral soil burden in surface foot). Although roots from tagged trees contribute more than 80% of the cesium burden to the 12-in. mineral soil layer, there is an orderly reduction of ^{137}Cs concentration in each successively deeper layer of mineral soil, ranging from 20 to more than 40% (Fig. 10.2, mineral soil burden in surface foot).

Statistical analysis of the distribution showed significant differences between the six depths within 1-ft soil cores, between 20 subplots in the 20 × 25 m tagged plots, and between 10 cores within each 5 × 5 m subplot.

In view of earlier results on high root activities, the depth profiles [averaging 161, 106, 64, 36, 27, and 20 $\mu\text{C}/\text{m}^2$ in successively deeper 2-in. (5-cm) layers] can be interpreted as representing contributions primarily from irregularly distributed roots in the lower portions of the profile, and higher root contributions (plus surface income) in the surface layers. The gross spatial variations fitted a reasonable pattern relative to chance distribution of tagged trees, ranging from 125 and 169 $\mu\text{C}/\text{m}^2$ (profile only) in two edge subplots with no tagged trees to 672 $\mu\text{C}/\text{m}^2$ (west corner) and 742 $\mu\text{C}/\text{m}^2$ (southeast edge of the plot). The variability within subplots was high and skewed, apparently because of sporadic root distribution. The coefficients of variation of profile totals ranged from 40 to 109% of the plot means. Square-root and logarithmic transformations helped to normalize the data and indicated that the inten-

sive sampling provided means within a few percent of the actual radiocesium content, in spite of the high variance and nonnormal distribution.

With the roots apparently contributing such a high percentage of ^{137}Cs activity to the soil system, it became necessary to attempt an association of the radionuclide with the different components of the soil system. Results of mechanical separation of soil components with a 2-mm sieve and hand removal of seven 1-mm fragments and subsequent separation by using flotation and chemical leaches as indices for distribution of ^{137}Cs are given in Fig. 10.3. Final results from the successive separations suggest that only 166 $\mu\text{C}/\text{m}^2$ (of the total 293 $\mu\text{C}/\text{m}^2$) is associated with organic tissue within the soil profile. The remaining 127 $\mu\text{C}/\text{m}^2$ is associated with the surface litter layer or inorganic fraction of the soil. Surface income of ^{137}Cs from rain

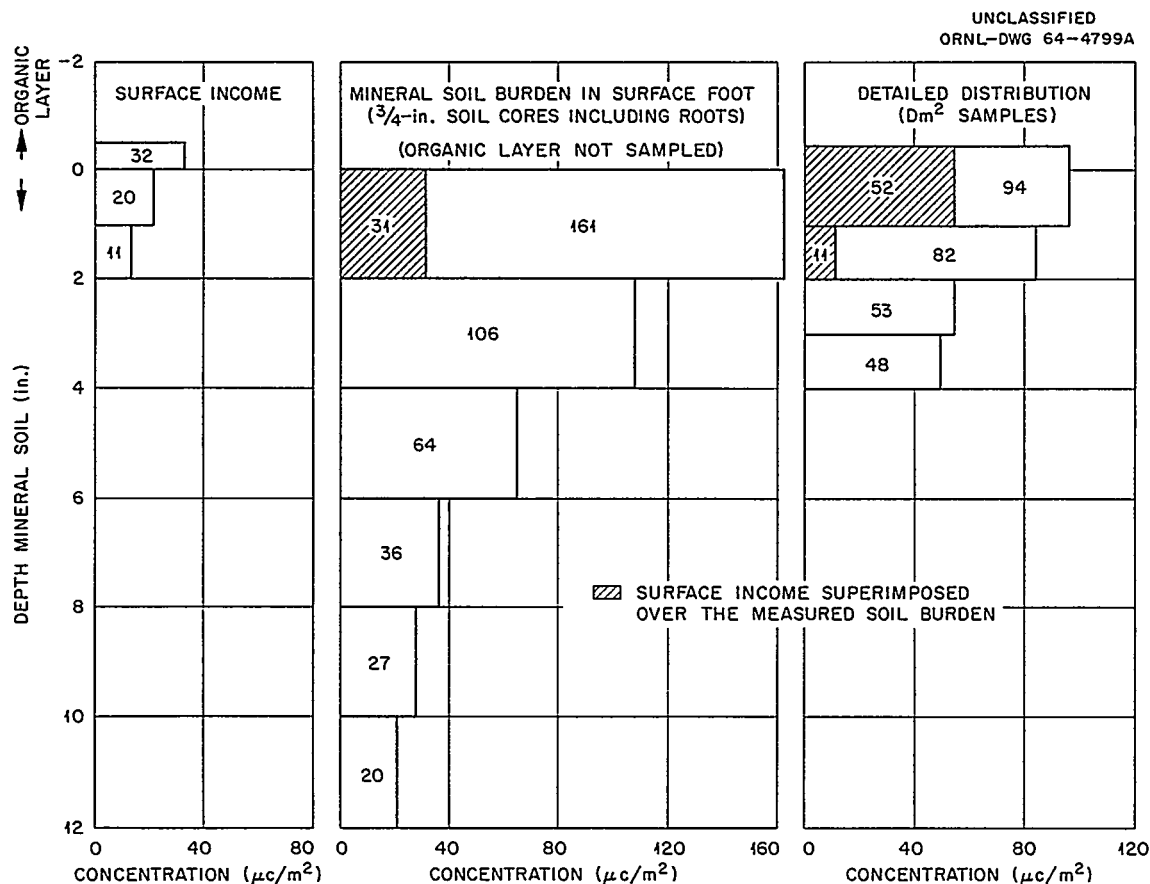


Fig. 10.2. Vertical Distribution of ^{137}Cs Within Forest Floor.

	LITTER	>2mm ROCK	>1mm ROOT	<1mm ROOT	FINE ORGANIC MATERIAL	<2mm REMAINDER SOIL	TOTAL
$\mu\text{c}/\text{m}^2$	16	9	57	25	84	102	293
PERCENT	5	3	20	8	28	36	100

SURFACE INCOME (RAIN and LEAF FALL)	63 $\mu\text{c}/\text{m}^2$
SUBSURFACE INCOME (> 1mm ROOTS)	57 $\mu\text{c}/\text{m}^2$
ACCOUNTED FOR (<1mm ROOTS)	25 $\mu\text{c}/\text{m}^2$
(FINE ORGANIC MATTER)	84 $\mu\text{c}/\text{m}^2$
TOTAL	229 $\mu\text{c}/\text{m}^2$
SOIL SAMPLING	293 $\mu\text{c}/\text{m}^2$
(-) MEASURED INCOME	229 $\mu\text{c}/\text{m}^2$
	64 $\mu\text{c}/\text{m}^2$ *

*DEFICIT THAT MAY BE ACCOUNTED FOR BY CESIUM ENTERING THE SOIL SYSTEM THROUGH ROOT EXUDATION, DIE-OFF OF MINUTE HAIR ROOTS, AND LEACHING OF ROOTS BY SOIL SOLUTION.

SUBSURFACE TRANSFER \geq SURFACE TRANSFER.

Fig. 10.3. Distribution of ^{137}Cs Between Soil Components.

leaching and from litter fall of canopy components accounts for a total of 63 $\mu\text{c}/\text{m}^2$, which is associated primarily with the surface litter layer or with the inorganic fraction of the soil. The remaining 64 $\mu\text{c}/\text{m}^2$ associated with the inorganic fraction is apparently ^{137}Cs which may have already reached mineral soil through root exudation, root leaching, or death of root materials. The above suggests that mineral turnover (at least for some elements) may be as great below ground surface as above ground surface in this forest ecosystem.

DISPERSION OF ^{137}Cs OUTSIDE OF TAGGED FOREST

H. D. Waller Regina M. Anderson
J. S. Olson W. C. Cate

Dispersion of ^{137}Cs outside the 20 x 25 m study area by falling leaves from tagged trees was not

measured until the end of the second growing season (October 1963). Figure 10.4 shows leaf-fall pattern of tagged leaves falling outside the delineated 20 x 25 m study area and indicates that few leaves fell beyond 10 m from the outside boundary. Although this leaf-fall pattern was not determined until the end of the second growing season, the nature of this pattern should not differ greatly from one year to the next because of location of this forest in a sinkhole area protected from strong wind movement. Results from 174 samples (each 0.1 m in area), collected at 5-m intervals along transects extending 20 m beyond the east and west boundary of the study area and 10 m beyond the north and south boundary, indicate that 2.67 mc (representing 5.34 $\mu\text{c}/\text{m}^2$ of study site) of ^{137}Cs was transported outside the study area by leaves from tagged trees during the second growing season.

If one assumed that leaf-fall pattern and total weight of tagged leaves falling outside the de-

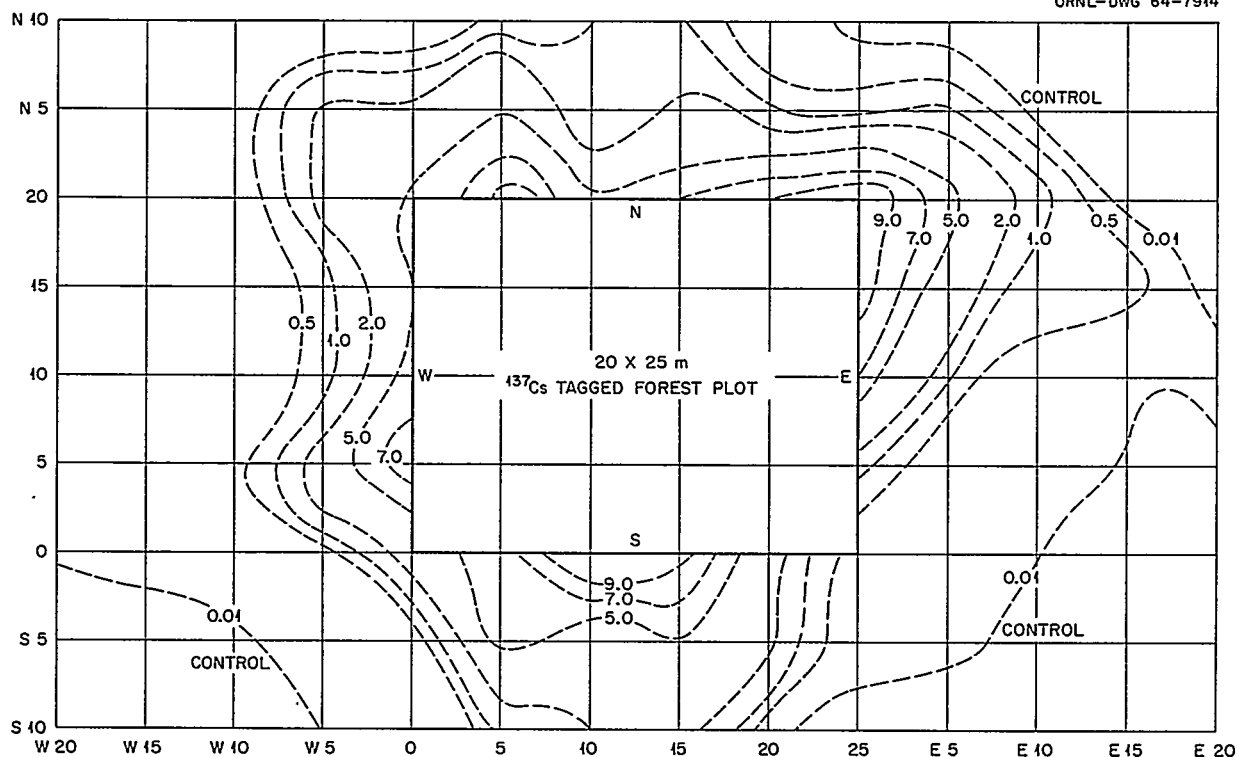
UNCLASSIFIED
ORNL-DWG 64-7914

Fig. 10.4. Dispersion of ^{137}Cs Outside of Plot by Leaf Fall (Units in Microcuries per Square Meter of Ground Area).

lineated study area were similar in both seasons, an estimate of ^{137}Cs transported outside the experimental area may be obtained. The foliage concentration per unit weight prior to leaf fall (Sept. 29, 1962) in the first growing season averaged $0.6 \mu\text{c/g}$, and the concentration per unit weight prior to leaf fall (Oct. 3, 1963) in the second growing season averaged $0.2 \mu\text{c/g}$. Therefore, ^{137}Cs deposited outside the study area through leaf fall for the first growing season should have been about three times the $5.3 \mu\text{c/m}^2$ removed through leaf fall at the end of the second growing season.

This $16 \mu\text{c/m}^2$ deposition of ^{137}Cs is a significant amount when compared with the $55 \mu\text{c/m}^2$ that was estimated in collections of litter inside the experimental study plot, and suggests that about one-fifth of the leaves from the tagged trees fall outside the $20 \times 25 \text{ m}$ area. However, more than three-fourths of this activity is located within a 10-m zone around the perimeter of the study area.

TRANSLOCATION OF ^{137}Cs FROM SEED INTO NEW GROWTH OF TULIP POPLAR SEEDLINGS

J. P. Witherspoon, Jr. G. N. Brown

A new phase of work in the ^{137}Cs -tagged forest was initiated this year to broaden understanding of the behavior of this radionuclide in the various life stages of tulip poplar trees. Seed collected from tagged trees was stratified, germinated, and grown under controlled environmental conditions. After stratification for 70 days in moist sand at 5°C , seed was planted in germination flats maintained at 30°C (day) to 20°C (night). Germination percentages were checked against controls collected from trees of similar age and size growing on a similar site. Seed from the tagged trees received a radiation exposure throughout their entire development (170 days) from both internal concentrations of ^{137}Cs and external radiation from other parts of the trees. A total dose of

250 rads (beta:gamma = 19.5) was computed for the development period of the seed. After a 60-day germination test in sand flats, 9.3% of the tagged forest seed ($N = 2200$) had germinated, while only 3.5% ($N = 1400$) of controls germinated. It is not known whether increased germination (5% is average for this species)⁴ was due to the small amount of radiation received or to other factors. This work will be repeated with this season's seed in a factorial experiment designed to weigh the importance of additional environmental factors.

Seedlings germinated from tagged seed were harvested at intervals, and weight and ^{137}Cs content were determined for seedling components. Table 10.2 illustrates the translocation of radiocesium into plant parts during a ten-week growth period. Plants were maintained on a 16-hr day (3500-fc light intensity), day temperature of

30°C, night temperature of 20°C, in flats containing topsoil of the Bolton soil series. Total plant dry weight increased linearly with time and is described by the expression

$$Y = -8.46 + 1.53X, \quad r = 0.97 \quad (p < 0.01),$$

where Y is total dry weight in mg, and X is seedling age in days. From the first to the third week of growth the cotyledons lost about half of their ^{137}Cs content to other rapidly growing tissues. During the next four weeks, additional radiocesium was translocated into new leaf growth, while stem and root levels tended to remain stable. From the 7th to the 10th week a large influx to roots occurred, with all other components losing some of their radiocesium. These data seem to indicate that cesium follows pathways similar to those of sugars and other foods stored in tissue, such as cotyledons used to sustain the early growth of seedlings. Transfers of this radionuclide in young seedlings are also rapid, as has been demonstrated for mature trees of this species.

⁴Woody Plant Seed Manual, USDA Misc. Publ. No. 654, 222-23 (1948).

Table 10.2. Translocation of ^{137}Cs from Seed into Seedling Components

Plant Component	Percent of Total Plant Dry Weight	Percent of Total Plant ^{137}Cs	Age (weeks)	Total Dry Weight (mg)	Shoot:Root		
					^{137}Cs	Weight	N
Roots	32.6	32.9	1	4.3 ± 0.3	2.04	2.07	25
Stem	13.9	16.0					
Cotyledons	53.5	51.1					
Roots	54.9	46.5	3	26.4 ± 2.2	1.15	0.82	25,
Stem	7.2	15.6					
Cotyledons	15.6	24.5					
Leaves (2)	22.3	13.4	7	55.1 ± 4.6	1.12	1.21	25
Roots	45.2	47.1					
Stem	7.6	14.3					
Cotyledons	8.4	16.8					
Leaves (4)	38.8	21.8	10	106.8 ± 5.0	0.43	1.07	25
Roots	48.2	70.1					
Stem	9.4	8.2					
Cotyledons	4.9	7.4					
Leaves (6)	37.5	14.3					

MICROBIAL MINERALIZATION AND IMMOBILIZATION OF RADIONUCLIDES

Martin Witkamp Marilyn L. Frank

Microbial breakdown of organic materials containing radionuclides results in release of these nuclides from decomposing substrate and aging microbes (mineralization). Simultaneously, incorporation of nuclides in microbial tissue takes place (immobilization). Results of numerous experiments concerning microbial effects on movement of radionuclides were reported two years ago. Additional experiments on the influence of ion concentrations, temperature, and moisture were performed last year.

Microbial uptake of stable cesium and cobalt was proportional to their concentrations in the environment over a concentration range of 2 to 3 orders of magnitude. There was no marked isotopic discrimination for either of these elements. Thus uptake of ^{134}Cs was proportional to the concentration of ^{134}Cs in the substrate. When microbes were separated from the tagged substrate by water, agar, or semipermeable film, microbial uptake was proportional to the concentration of ^{134}Cs in these intermediates. Microbial concentration factors for different substrates varied with the availability of the tag. On fresh litter with readily available cesium, microbial concentration relative to the substrate was twice as high as on weathered, old litter with less readily available cesium. Mushrooms collected in a tagged forest stand showed concentration factors for ^{137}Cs (0.05 to 44) similar to those two years before. Thus concentrations of ^{137}Cs in the mushrooms had increased in proportion to the concentrations of ^{137}Cs in the natural substrates. Substrate concentrations of potassium ranging over 2 orders of magnitude did not affect microbial uptake of ^{137}Cs , but when potassium became deficient, uptake of cesium increased by 2 orders of magnitude. Dilution of ^{134}Cs in litter substrate with untagged litter did not affect microbial uptake and release of the nuclide.

Leaching of nuclides from sterile litter was positively correlated with temperature. Four times more ^{137}Cs and 30% more ^{60}Co were leached at 50°C than at 2°C . Increasing temperature also increased microbial immobilization of ^{134}Cs and decreased the amount of ^{134}Cs in the leachate. After burning of oak leaves (80% loss of weight),

only 6% of the initial ^{134}Cs was easily leached, and 7% was lost with the smoke. The remaining 87% became adsorbed onto the charred 20% residue.

Leaching of ^{134}Cs from oak litter increased with increasing moisture content (35 to 67% H_2O). Leaching of dried oak leaves caused a high release of ^{134}Cs because of preceding death of the microflora by drought. Increasing rates of leaching removed increasing amounts of ^{137}Cs from sterile tulip poplar leaves, but leaching efficiency (percent of initial nuclide per ml of leachant) was highest at around a rate of leaching equivalent to precipitation of 50 cm/year. Microbial immobilization of ^{134}Cs was highest on leaf litter with 25 to 60% moisture.

MICROBIAL EFFECT ON UPTAKE OF RADIONUCLIDES BY HIGHER PLANTS

Martin Witkamp Marilyn L. Frank

Soil microbes affect uptake of radionuclides by higher plants mainly in two ways: (1) by accumulating in microbial tissue the same minerals as utilized by higher plants (immobilization), and (2) by liberating minerals from organic materials or mineral compounds for subsequent plant uptake (mineralization). Results of experiments on immobilization and mineralization of radionuclides by microbes growing on leaf litter in the absence of higher plants are reported in a separate section.

Influence of microbes on uptake of the radionuclides ^{32}P , ^{60}Co , and ^{137}Cs by green plants was evaluated by comparing their uptake in sterile and nonsterile cultures of mustard plants. Plants grown in the presence of a mixed microbial flora accumulated less than half of the ^{32}P accumulated by sterile plants. Presence of microbes increased accumulation and concentration of ^{137}Cs as well as plant growth. Immobilization of nuclides by soil microbes reduced the nuclide content in the soil solution. This immobilization increased in the order $^{137}\text{Cs} < ^{60}\text{Co} < ^{32}\text{P}$.

Soil sterilization methods using steam, ethylene oxide, or radiation from a ^{60}Co source (3 to 5×10^6 r) were tested for future use in sterile plant cultures. Ethylene oxide was successful as a soil sterilant, but left, after reaction with soil moisture, a phytotoxic residue (ethylene glycol) which could only be removed after repeated evacuation of the soil. Subsequent use of ethylene oxide

will be limited to sterilizing containers and apparatus. For soil sterilization, gamma irradiation will be used. A complication is the occasional reduction of seed germination in sterile cultures which occurs several days postirradiation. This reduction presumably is caused by breakdown products formed by residual soil enzymes.

SOIL CLASSIFICATION AND SURVEY

H. D. Waller J. S. Olson

Soil analysis and mapping within the reservation was concentrated in the White Oak Creek watershed. Previous field mapping of soils has been restricted to small study areas and geological belts of special contrast.⁵ More recently the trend has been toward analyzing larger landscape units as a preliminary to future field investigations. White Oak Creek watershed was chosen for the first survey because of its use in radioactive waste disposal operations. The major soil series were plotted on a topographic map of the watershed (Fig. 10.5).

Soils occurring within the White Oak Creek drainage basin belong largely to the broad groups of red-yellow podsollic, reddish-brown lateritic, and lithosols. These soils occur extensively in the southeastern U.S. over most of the coastal plain, much of the Piedmont and southern end of the Appalachian Plateau, and the Valley and Ridge province. In general, soils in this area are strongly leached, acid in reaction, low in organic matter, and have exchange capacities generally less than 10 meq per 100 g of dry weight.⁶

The soils occurring within the drainage basin have a wide range of physical and chemical properties. Depth of the soil profile varies from 6 in. in some of the shale and sandstone areas to depths of 15 ft or more in some of the dolomitic limestone areas and alluvial deposits along drainage ways. The pH ranges from near neutrality in the Bland and young alluvial soils to strongly acid in some of the weathered upland shale and sandstone soils such as Litz and Lehew (Fig. 10.5). Texture of the surface is dominantly silt loam or cherty silt loam; but in eroded areas, such as commonly found in the Bland soils, the surface may be a silty clay. Texture of the subsoil ranges from cherty silt loam (Clarksville soils) to a firm, plastic clay (Talbot and Colbert soils). Entrance of surface water into the soil profile varies from rapid (up to 10 in./hr) in Clarksville soils to slow (less than 0.2 in./hr) in Colbert and Bland soils. Internal soil drainage ranges from poorly drained in Melvin series to excessively drained in the Clarksville and Muskingum series. Other soils such as Pace and Leadvale have fragipan layers (occurring at 24- to 30-in. depths) which impede or prohibit the downward percolation of soil water.

The soils derived from the Knox dolomite contain kaolinite as their principal clay mineral, those from the Conasauga shale contain illite and vermiculite as principal clay minerals, and the soils derived from the Chickamauga limestone contain a mixture of kaolinitic and illitic minerals with some units probably having a significant amount of montmorillonitic clay minerals. The clay minerals are undersaturated with bases, leaving H^+ in the exchange positions of the clay. Base saturation varies from less than 10 to more than 60%.⁷

⁵J. S. Olson *et al.*, *Forest Ecology at the Oak Ridge National Laboratory*, ORNL-3189 (1961).

⁶H. D. Waller and B. C. Cox, *Soil Handbook for Anderson County, Tennessee*, Soil Conservation Service Rept. 1963, 292 pp. (unpublished).

⁷Dorothy Carrol, *Soils and Rocks of the Oak Ridge Area, Tennessee*, U.S. Geological Survey Report 785 (1961).

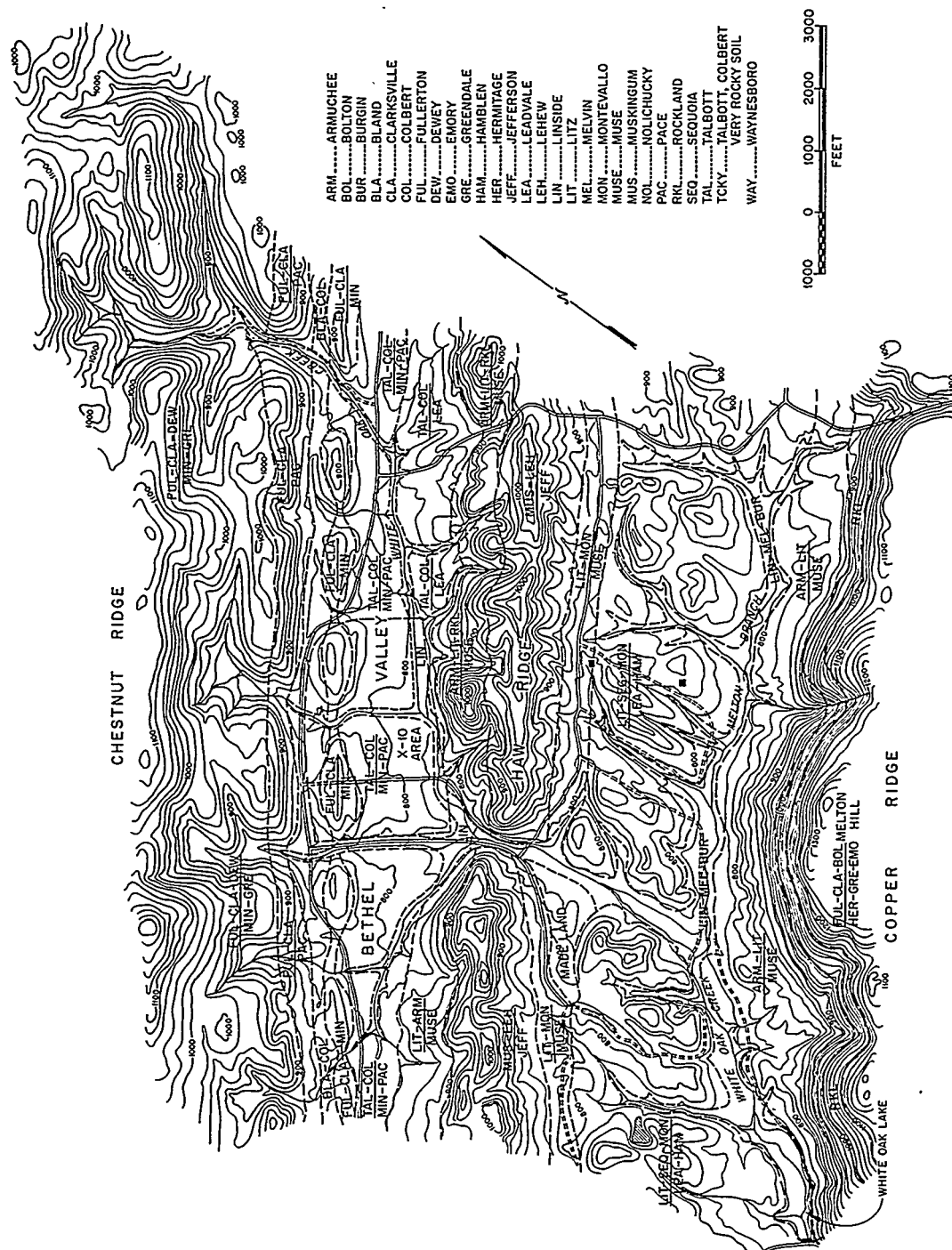


Fig. 10.5. Soil Association Map of White Oak Creek Drainage Basin. Commonly occurring soils within each geologic belt, geologic unit, or topographic unit are listed according to relative abundance (most abundant appear to the left) and toposquence (upland soils in the numerator and colluvial-bench soils or bottom land soils in denominator).

11. Clinch River and Related Aquatic Studies

D. J. Nelson
S. I. Auerbach
B. G. Blaylock

N. R. Kevern
B. C. Patten
G. M. Rosenthal¹

R. C. Early
N. A. Griffith
Tom Grizzard²

CALCIUM AND STRONTIUM IN WHITE CRAPPIE FLESH AND BONE

D. J. Nelson N. A. Griffith
R. C. Early

The series of analyses of stable strontium in white crappie (*Pomoxis annularis*) flesh and bone was completed, and it was possible to test the relation of the distribution of stable strontium and ⁹⁰Sr between the environment and the fish.³ Samples were taken at monthly intervals to determine whether there were seasonal changes in strontium concentrations in fish flesh and bone. Bone and flesh samples were also analyzed for calcium, while bone samples were also analyzed for ⁹⁰Sr.

The calcium and strontium concentrations in fish flesh and bone were constant throughout the year; average annual concentrations are reported

in Table 11.1. Relatively constant calcium and strontium concentrations were expected in bone because of the long biological half-life of these elements in bony tissue. A seasonal variation in the calcium and strontium concentration was not detected and probably reflects the relative constancy of these elements in Clinch River water.⁴ Of particular interest is the fact that the average concentration of strontium in fish flesh is essentially the same as that of river water.

To test whether specific activity ratios of ⁹⁰Sr in fish tissue were related to those in water, the concentrations of ⁹⁰Sr and strontium in bone were compared by use of the proportion:

$$\frac{{}^{90}\text{Sr}}{\text{Sr}} \text{ water} = \frac{{}^{90}\text{Sr}}{\text{Sr}} \text{ fish bone},$$

$$\frac{4.3 \times 10^{-3} \mu\text{c/ml}}{6.8 \times 10^{-2} \mu\text{g/ml}} \cong \frac{1.446 \times 10^1 \mu\text{c/g}}{2.684 \times 10^2 \mu\text{g/g}},$$

$$6.23 \times 10^{-2} \mu\text{c}/\mu\text{g} = 5.39 \times 10^{-2} \mu\text{c}/\mu\text{g}.$$

¹ORINS summer research participant.

²Temporary summer employee.

³R. J. Morton (ed.) *Status Report No. 4 on Clinch River Study*, ORNL-3409 (Sept. 11, 1963).

⁴R. J. Morton (ed.) *Status Report No. 3 on Clinch River Study*, ORNL-3370 (Nov. 21, 1962).

Table 11.1. Calcium and Strontium Concentrations in White Crappie Flesh and Bone and Clinch River Water

All values ± 1 standard error

	No. of Samples	Calcium	Concentration Factor ^a	Strontium	Concentration Factor ^a
White crappie					
Flesh ($\mu\text{g/g}$)	113	135 \pm 2.43	6.34	0.0687 \pm 0.035	1.01
Bone (mg/g)	105	365 \pm 7.77	17,136	0.268 \pm 0.064	3941
Clinch River					
Water ($\mu\text{g/g}$)		21.3 \pm 3.0		0.068 \pm 0.0094	

^aConcentration factor = $\frac{\text{concentration/g wet tissue}}{\text{concentration/ml water}}$.

The data on ^{90}Sr concentrations in water were obtained from the Applied Health Physics Section of the Health Physics Division and are for the period of time these fish lived in the river water. Data on calcium and strontium concentrations in Clinch River water were published previously.⁴ There is relatively good agreement between the specific activities in fish bone and water. These data suggest that for any constant release of ^{90}Sr to the river, it is possible to predict the consequent ^{90}Sr content of fish bone.

The short biological half-life of strontium in fish flesh, reported last year, shows that measurements of ^{90}Sr in flesh will reflect the environmental concentration at the time the fish is collected. The long biological half-life of strontium in fish bone suggests that ^{90}Sr concentrations in bone will reflect the average environmental concentrations during the lifetime of the fish. This information is of considerable importance in connection with the operating mode of Melton Hill turbines and releases of radioactivity from White Oak Creek.

UPTAKE AND ACCUMULATION OF STRONTIUM AND CALCIUM BY ALGAE AND SNAILS

N. R. Kevern G. M. Rosenthal, Jr.
N. A. Griffith D. J. Nelson

Studies of the comparative uptake of strontium and calcium in an alga, *Oocystis eremosphaeria*, and snails, *Physa heterostroph*a, initiated last year,⁵ were completed. Algae represent a biological system in which there is a rapid turnover and equilibrium of strontium and calcium between the environment and the cell, while snails are a biogeochemical sink, and the newly deposited shell materials reflect the strontium and calcium concentration in the environment. The objective of the experiments was to obtain information on the behavior of strontium in aquatic environments, particularly with respect to the comparative effects of calcium and strontium in the environment on strontium uptake.

These experiments differed significantly from other strontium and calcium experiments because the strontium and calcium concentrations of the experimental media were rigidly controlled by assay of the strontium and calcium content of all chemicals utilized. Furthermore, highly purified calcium carbonate was used to avoid significant quantities of adventitious strontium which occur in reagent calcium compounds.

In the algal study, the range of environmental calcium and strontium concentrations was 1 to 100 ppm and 0.002 to 0.20 ppm respectively. These concentrations include the range of calcium and strontium most commonly found in fresh water. Algal cells from a stock culture were transferred to a series of flasks established according to a 3 Sr by 3 Ca factorial design with two replications, thus giving nine media combinations of strontium and calcium. Carrier-free ^{85}Sr and ^{45}Ca , with negligible carrier, were added in equal amounts to each flask as tracers. The uptake of the tracers by the algae was determined by using standard counting procedures, and the uptake of the stable elements was calculated by using specific activities as follows:

$$\text{Sr in algae} = \frac{{}^{85}\text{Sr in algae} \times \text{Sr in medium}}{{}^{85}\text{Sr in medium}}$$

Figure 11.1 shows the uptake of calcium by the algae to be primarily a function of the media concentrations of calcium, with a slight inverse influence by strontium in the media. A slight relative increase in calcium uptake at very low calcium concentrations indicates an increase in uptake efficiency at limiting levels of calcium, and also suggests that calcium is required by the alga. The response plane for strontium (Fig. 11.2) reveals that uptake is directly proportional to strontium in the media, with an enhancement in uptake at very low media concentrations of calcium, suggesting that strontium was used by the algae in place of calcium when calcium was in short supply. The uptake of ^{85}Sr was not significantly different when tested statistically by the three concentrations of strontium, but the uptake was significantly greater ($P = 0.05$) at the lowest calcium concentration than at the two higher calcium concentrations. Accordingly, a significant reduction of total strontium or ^{90}Sr uptake by adding calcium to the medium would be possible only if the existing calcium concen-

⁵S. I. Auerbach et al., *Health Phys. Div. Ann. Progr. Rept.* June 30, 1963, ORNL-3492, p. 109.

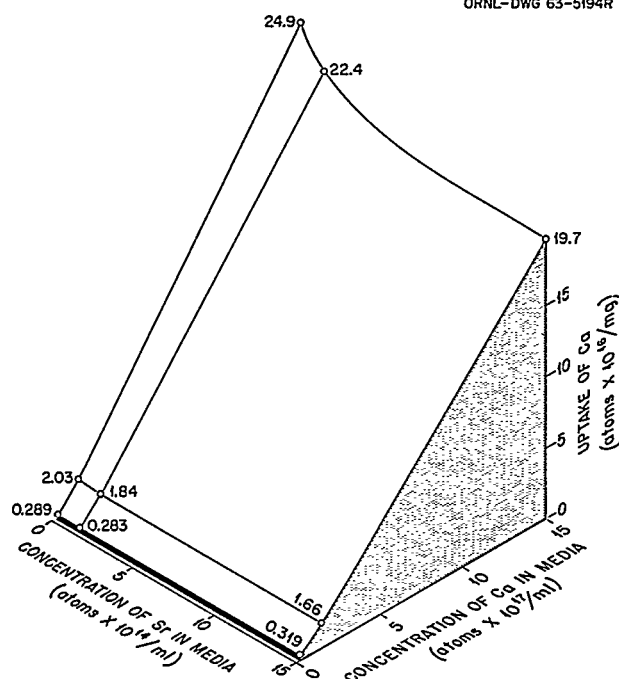
UNCLASSIFIED
ORNL-DWG 63-5194R

Fig. 11.1. Mean Uptake of Calcium per Milligram Dry Weight of Algae as a Function of Environmental Concentrations of Strontium and Calcium. 0.15×10^{14} atoms Sr/ml = 2.18 ppb Sr, 0.15×10^{17} atoms Ca/ml = 1.0 ppm Ca.

tration was limiting. Regression formulas satisfying the response planes of Figs. 11.1 and 11.2 are:

$$\ln Sr_{\text{uptake}} = 0.693 + 0.990 \ln Sr_{\text{input}} - 0.098 \ln Ca_{\text{input}},$$

$$s_b = \pm 0.017, \quad \pm 0.017,$$

$$\ln Ca_{\text{uptake}} = 0.432 + 0.932 \ln Ca_{\text{input}} - 0.013 \ln Sr_{\text{input}},$$

$$s_b = \pm 0.058, \quad \pm 0.058,$$

where strontium uptake is in atoms $\times 10^{12}$ per mg of dry weight of algae, calcium uptake is in atoms $\times 10^{15}$ per mg of dry weight of algae, strontium input is in atoms $\times 10^{13}$ /ml, calcium input is in atoms $\times 10^{16}$ /ml, and s_b is the standard error.

In the snail study, strontium and calcium amendments in the form of chlorides were added to the

experimental solutions according to a hexagonal design with the center point duplicated. The final strontium and calcium concentrations of the media (Table 11.2) were determined by scaling the vertices of the hexagon so that they were within ranges of 0 to 10 ppm strontium and 0 to 200 ppm calcium, essentially the extreme range of concentrations of the elements in natural waters. The pH of the media was adjusted to neutrality by the addition of small amounts of NaOH, and 200 ml of solution was placed in 400-ml Pyrex beakers. Carrier-free ^{85}Sr and ^{45}Ca with negligible carrier were added as tracers to all beakers in constant amounts.

The deposition of calcium and strontium by snails is illustrated graphically in Figs. 11.3 and 11.4 respectively. These are response surfaces

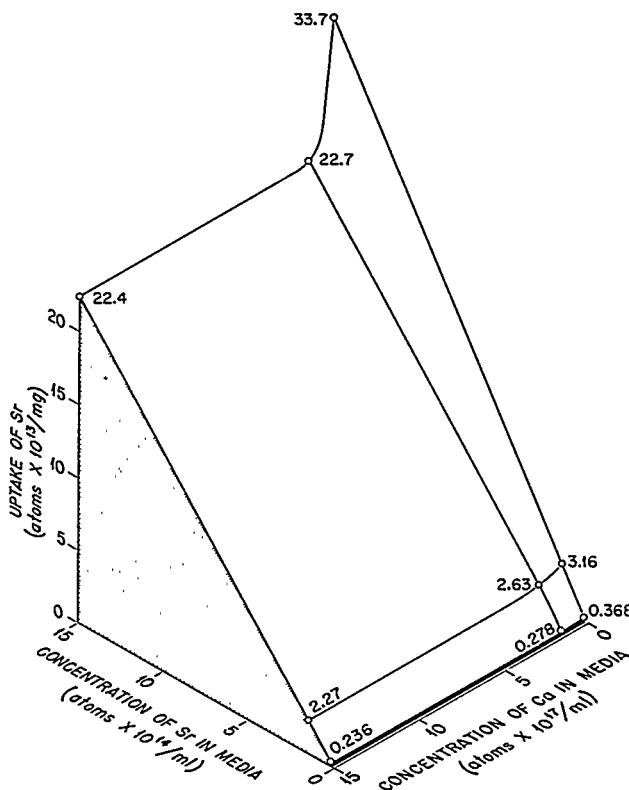
UNCLASSIFIED
ORNL-DWG 63-5193R

Fig. 11.2. Mean Uptake of Strontium per Milligram Dry Weight of Algae as a Function of Environmental Concentrations of Strontium and Calcium. 0.15×10^{14} atoms Sr/ml = 2.18 ppb Sr, 0.15×10^{17} atoms Ca/ml = 1.0 ppm Ca.

Table 11.2. Strontium and Calcium Concentrations in the Experimental Solution and Uptake of Strontium and Calcium by Snails

Experimental Point	Concentration in Medium (atoms/ml)		Uptake (atoms/g of shell)		Number of Snails
	Sr	Ca	Sr	Ca	
	$\times 10^{-16}$	$\times 10^{-16}$	$\times 10^{-18}$	$\times 10^{-20}$	
1	5.555	274.7	1.347	2.444	5
2	0.0111	162.5	0.005319	2.784	6
3	5.069	14.64	8.793	1.182	6
4	3.545	150.6	1.387	2.235	7
5	6.430	160.3	3.670	3.760	2
6	1.904	49.31	1.771	2.029	6
7	2.304	261.6	0.7676	3.145	8
8	3.545	150.6	1.326	2.011	7

UNCLASSIFIED
ORNL-DWG 64-557R

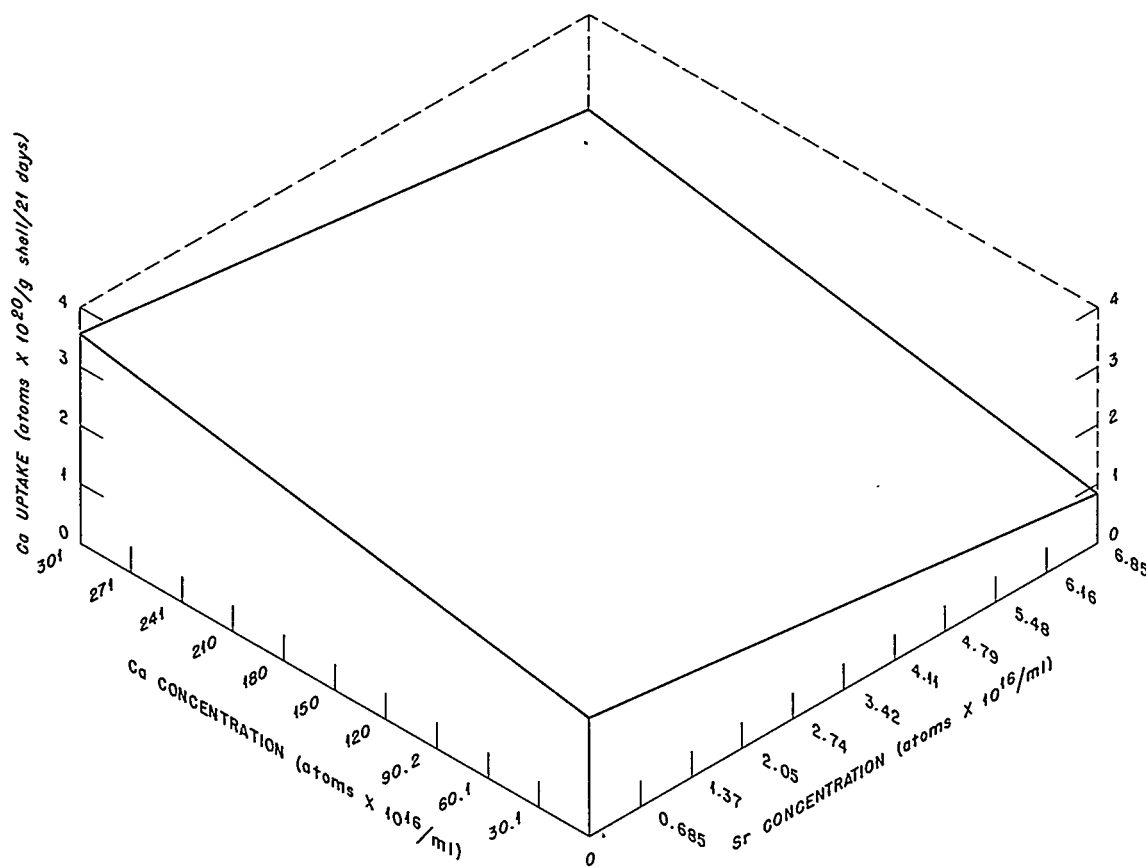


Fig. 11.3. Calcium Deposition in Snail Shell as a Function of Environmental Calcium and Strontium Concentrations. 30.1×10^{16} atoms Ca/ml = 20 ppm Ca; 0.685×10^{16} atoms Sr/ml = 1 ppm Sr.

UNCLASSIFIED
ORNL-DWG 64-558R

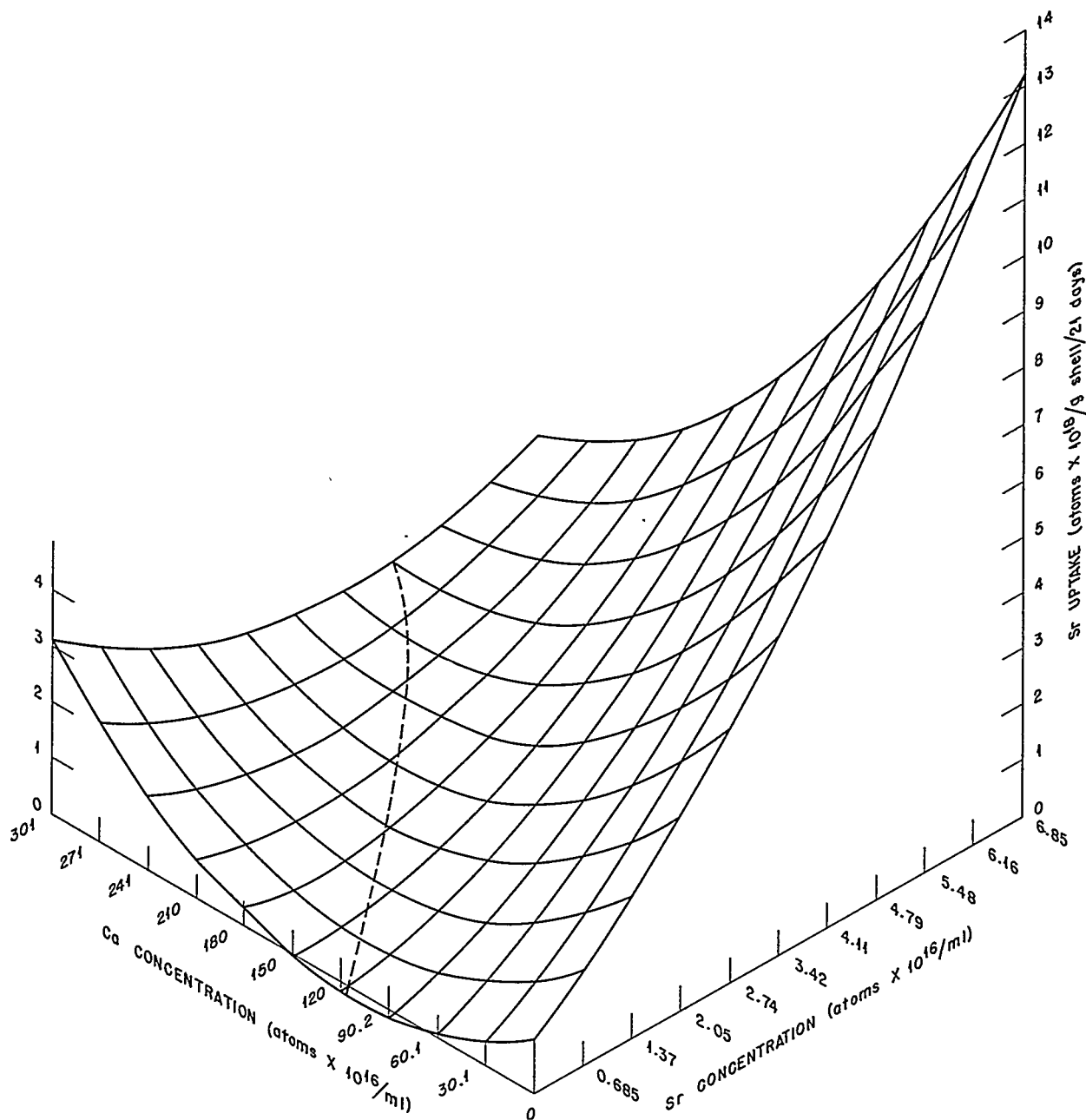


Fig. 11.4. Strontium Deposition in Snail Shell as a Function of Environmental Calcium and Strontium Concentrations. 30.1×10^{16} atoms Ca/ml = 20 ppm Ca; 0.685×10^{16} atoms Sr/ml = 1 ppm Sr.

calculated from a least-squares fit of the data. Concentrations of calcium and strontium at the experimental points and respective uptakes are listed in Table 11.2. Calcium uptake is represented best by a plane surface which is expressed mathematically as follows:

$$\text{Ca}_{\text{uptake}} = 19,800 + 54.14 \text{Ca}_{\text{input}} - 1713 \text{Sr}_{\text{input}}, \\ s_b = 4970, \pm 15.94, \pm 968,$$

where uptake is in atoms $\times 10^{16}$ per g of shell per 21 days, input is in atoms $\times 10^{16}$ /ml, s_b = standard error. Calcium carbonate is the basic structural component of mollusk shell, and a slight increase in growth is indicated by an increasing uptake of calcium with increasing calcium concentrations. However, growth differences in the seven experimental environments, as measured by calcium deposition, were only 0.17 times as much as the differences in the environmental calcium concentrations. While growth increased directly with the calcium concentration, the increases were relatively small when compared with the differences in environmental calcium concentrations.

The uptake of calcium is conservative when compared with that of strontium. Strontium uptake is represented best by a quadratic expression:

$$\text{Sr}_{\text{uptake}} = 98.78 - 2.12 \text{Ca}_{\text{input}} + 97.74 \text{Sr}_{\text{input}} + 0.009 (\text{Ca}_{\text{input}})^2 \\ (s_b = 63.2, \pm 0.59, \pm 15.2, \pm 0.002) \\ + 11.88 (\text{Sr}_{\text{input}})^2 - 0.659 (\text{Ca}_{\text{input}})(\text{Sr}_{\text{input}}) \\ (s_b = 3.37, \pm 0.134),$$

where uptake is in atoms $\times 10^{16}$ per g of shell per 21 days, input is in atoms $\times 10^{16}$ /ml, s_b = standard error. The range of strontium deposition in the snail shells was 2.9 times the range of environmental concentrations.

The surfaces depicting the deposition of calcium and strontium in Figs. 11.3 and 11.4 are based on goodness of fit of the data in Table 11.2. Inspection of the data and Figs. 11.3 and 11.4, viewed grossly as plane surfaces, indicates that deposition of both calcium and strontium in the shell of *P. heterostropha* depends primarily on the respective concentrations of these elements in the immediate environment. Failure of the planes to intersect the zero axis is a geometric artifact

arising from the extrapolation of the equations to zero; obviously there can be no incorporation of calcium or strontium when none is present. A slight negative interaction, that is, of environmental strontium on calcium deposition, and vice versa, is also evident from the skewed appearance of the incorporation planes. Biologically this interaction is probably best explained in the conventional terms of competition for incorporation sites.

The dotted line in Fig. 11.4 represents the minimum strontium deposition for the various combinations of strontium and calcium in the environmental media. To the right of the dotted line there is essentially a linear increase in strontium uptake with increasing environmental strontium concentrations. At lower calcium concentrations (in this portion of the surface) there is a relatively greater uptake of strontium. This suggests a simple substitution of strontium uptake for that of calcium by snail shell when environmental calcium is deficient. At all points to the right of the dotted line, strontium uptake increases with increasing environmental strontium concentrations, and decreases with increasing environmental calcium concentrations. To the left of the dotted line the opposite behavior is noted; that is, increased environmental strontium depresses strontium uptake, and increased environmental calcium enhances strontium uptake.

This phenomenon, the reversal of the relation of strontium deposition rate to strontium and calcium concentrations, is unexpected. Three possible explanations may be offered: (1) it is a statistical artifact; (2) it is brought about by different reactions, purely chemical in nature, based largely on concentration differences; (3) it is primarily biological and probably associated with a threshold or compensatory effect. We do not believe the first explanation is likely, and there is no evidence, either specific or general, for accepting the second. The effect would seem to be related to some physiological property of mantle cells, possibly to membrane phenomena or secretory activity, and warrants further investigation. Correlation coefficients calculated from this experiment show the relative merit of various ratios: $\text{Sr (uptake)} \times \text{Ca (medium)} = 0.36$; $^{85}\text{Sr (uptake)} \times \text{Ca (medium)} = 0.47$; $^{85}\text{Sr (uptake)} \times \text{Sr (medium)} = 0.75$; $\text{Sr (uptake)} \times \text{Sr (medium)} = 0.79$; $^{85}\text{Sr (uptake)} \times \text{Sr/Ca (medium)} = 0.92$; $\text{Sr (uptake)} \times \text{Sr/Ca (medium)} = 0.95$. There is a

relatively poor correlation between either strontium or ^{85}Sr uptake and environmental calcium concentrations. The correlation between either strontium or ^{85}Sr uptake and environmental strontium is considerably better, but the best correlations are of strontium or ^{85}Sr uptake and the ratio of Sr/Ca in the environment. The results of these experiments indicate the need for consideration of stable strontium concentrations in any interpretation of the behavior of ^{90}Sr in biological systems.

BIOLOGICAL HALF-LIFE OF ^{134}Cs IN CARP AND TWO AQUATIC INSECTS

N. R. Kevem N. A. Griffith
Tom Grizzard

One phase of the aquatic food-chain study is concerned with determining the feeding rate of organisms. This can be accomplished by using radionuclides and the following formula:

$$Q = a \frac{q}{p + b},$$

where Q is the body burden of the radionuclide maintained by the organism, a is the fraction of the ingested radionuclide deposited in the organism, p is the physical decay of the radionuclide, b is the biological turnover (half-life) of the radionuclide in the organism, and q is the amount of radionuclide that the organism must ingest to maintain Q . The value of Q is being determined for ^{137}Cs in carp (*Cyprinus carpio*) living in White Oak Lake. A laboratory study was initiated to determine the uptake a and the biological half-life b of cesium in carp as influenced by water temperature.

Two groups of carp were fed a single dose of organic detritus tagged with ^{134}Cs . One group of ten fish was held at 12.5°C , and the other group of five fish was held at 20.0°C . Retention curves derived from whole-body counts of the carp are given in Figs. 11.5 and 11.6. The curves are described by the sum of two exponential rate functions and demonstrate an initial rapid elimination of the ^{134}Cs followed by further elimination at a reduced rate. The retention equation for carp at 12.5°C is

$$R = 3.0e^{-0.06242t} + 3.79e^{-0.00396t},$$

and for carp at 20.0°C ,

$$R = 3.27e^{-0.10505t} + 3.30e^{-0.00706t},$$

where R is the percent of the ingested ^{134}Cs retained, and t is time in days. The sum of the two coefficients in each equation indicates the percent of the ingested ^{134}Cs initially deposited in the fish (a in the feeding rate equation), 6.79% in the cold water, and 6.57% in the warm water. Expressed as the biological half-life, the initial rate function was 11.1 days for carp at 12.5°C and 6.6 days for carp at 20.0°C ($Q_{10} = 2.0$). The second rate was 174 days for carp in cold water and 98.1 days for the fish in warm water ($Q_{10} = 2.15$). The higher metabolic rate of fish in the warmer water is demonstrated by a more rapid elimination of the ^{134}Cs .

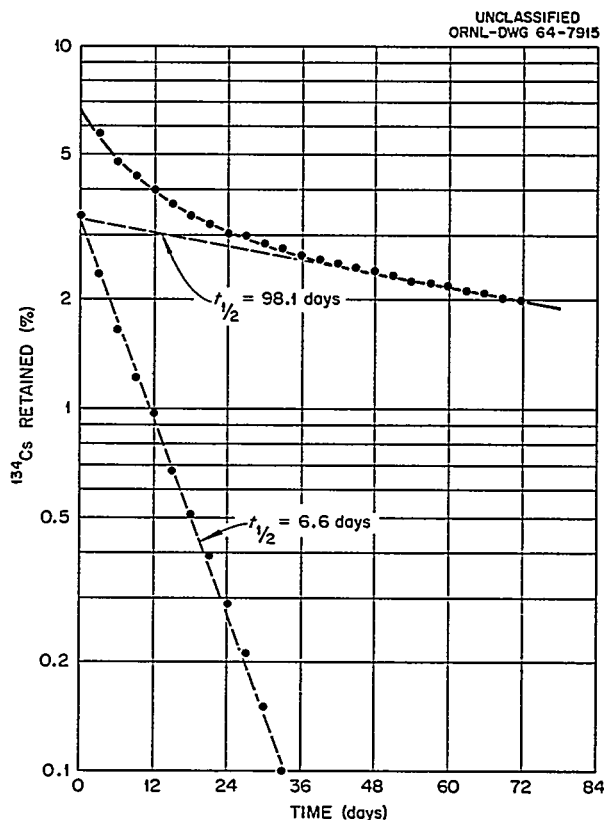


Fig. 11.5. The Mean Percentage of ^{134}Cs Retained by Carp Held in Water at 20.0°C . The retention curve is the sum of two exponential rate functions (dashed lines).

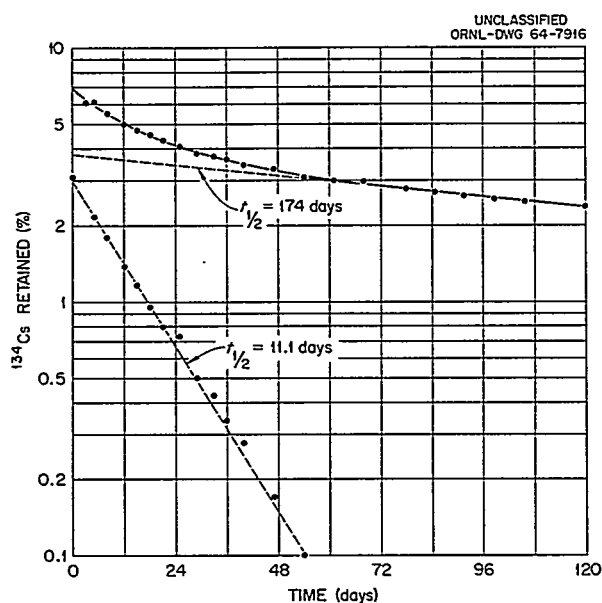


Fig. 11.6. The Mean Percentage of ^{134}Cs Retained by Carp Held in Water at 12.5°C . The retention curve is the sum of two exponential rate functions (dashed lines).

Similar studies have been completed for a mayfly nymph (*Ephemera varia*) and a midge larva (*Chironomus commutatus*). Mayfly nymphs initially retained 16.8% of the ingested ^{134}Cs and demonstrated a biological half-life of 8.3 days. Midge larvae, while initially assimilating 39% of the ingested isotope, had a shorter biological half-life of 3.5 days.

POPULATION GENETICS AND RADIATION EFFECTS STUDIES ON *CHIRONOMUS TENTANS*

B. G. Blaylock

R. C. Early

Previously⁶ it was reported that there is an increase of newly occurring chromosomal aberrations in the natural population of *Chironomus tentans* from White Oak Creek. This population of Diptera which is receiving a calculated dose of 230 rads/year from chronic environmental radiation has been sampled annually since 1960. The

analysis of the 1963 collection for chromosomal aberrations in the salivary gland chromosomes increased the number of larvae analyzed from the irradiated population to 578 and the controls to 568 (Table 11.3). Two new inversions, each involving several bands, were observed one time in the additional collection from the irradiated area. No new inversions were observed in the additional collections from the control populations; however, one inversion that occurs in the irradiated area was found for the first time in the control area. The finding of these two new inversions supports the previous conclusion that there is an increase of newly occurring aberrations in the White Oak Creek population. These newly occurring aberrations are eliminated by selection or genetic drift and are not maintained in the gene pool of the population.

A relatively high degree of chromosomal polymorphism is found in the population of *C. tentans* from White Oak Creek. Chromosomal polymorphism, which is found in most species of Diptera, is a way that highly adapted gene arrangements can be held together. These highly adapted blocks of genes are carried in the gene pool of the population to help meet changing environmental conditions. A population receiving chronic irradiation would have an increased mutation rate, and lethals accumulating in these blocks of genes could reduce or eliminate these highly adapted gene arrangements. There has not been a significant statistical change in the frequency of three endemic inversions during July for the past four years (1960–1963) in the White Oak Creek population of *C. tentans* (Table 11.4). Also, there was no significant difference in the frequencies of these three inversions from a sample of 578 larvae from White Oak Creek when compared to 568 larvae from control areas. The increased mutation rate produced by the chronic irradiation in the White Oak Creek population has not reduced the amount of chromosomal polymorphism in this natural population. Consequently, the plasticity of the population does not appear to have been reduced. On the other hand, this is a very large population of *Chironomus*, and migration from nearby populations could maintain the frequencies of these inversions.

Toshiba low-Z metaphosphate rods were used to estimate the radiation dose to *Chironomus* larvae in White Oak Lake. Twelve Lucite shielded and unshielded rods were submerged in the radioactive mud for four weeks. The average dose for the 12

⁶S. I. Auerbach et al., *Health Phys. Div. Ann. Progr. Rept.* June 30, 1963, ORNL-3492, p. 112.

Table 11.3. Number of Chromosomal Aberrations Observed in Irradiated and Control Populations of *Chironomus tentans*

Populations	Number of Larvae Analyzed	Aberrations Found in Both Populations	Aberrations Found in Only One Population	Total Aberrations Observed
Irradiated	578	6	11	17
Control	568	6	0	6

Table 11.4. Four-year Comparison of Three Endemic Inversions Found in the White Oak Creek Population of *Chironomus tentans*

	Dates				χ^2	P (3 degrees of freedom)
	7-8-60	6-23-61 7-23-61	7-12-62 7-30-62	7-8-63 7-26-63		
	No. of Larvae					
	31	51	31	57		
Inversion 1Ra	8	12	3	6	6.83	7.08
Inversion 2Lab	7	6	4	15	4.74	7.25
Inversion 3Ra	3	5	1	1	4.44	7.25

shielded rods (gamma rays) was 3 rads for the four-week period. The beta dose was calculated by the difference between shielded and unshielded rods. Calculations were based on experiments where shielded and unshielded rods were submerged in a solution of ^{137}Cs and the response of Toshiba low-Z rods to cesium beta rays was determined. Since the average beta energy from a composite sample of the radionuclides from White Oak Lake was approximately the same as the average ^{137}Cs beta energy, the rod response to cesium was used to estimate the beta dose of the mixed radionuclide sample. The beta dose was calculated as 15.4 rads for the four-week period. The total dose was 239.2 rads/year, based on the metaphosphate rod response. This is in close agreement with a previous dose rate of 230 rads/year, calculated on the basis of radio-

nuclide concentrations. However, these concentrations were based on samples collected three years ago, and the percent of nuclides in the samples could have changed.

SAFETY EVALUATION OF CLINCH RIVER FISHERIES

S. I. Auerbach R. C. Early
D. J. Nelson N. A. Griffith

An additional series of commercial food-fish species (carp, carpsucker, smallmouth buffalo, and redhorse) was collected and analyzed for their radionuclide content as part of the cooperative Clinch River Study (participating agencies: ORNL, U.S. Public Health Service, U.S. Geological

Survey, Tennessee Valley Authority, Tennessee Game and Fish Commission, and Tennessee Department of Public Health). Fish were collected from both the Clinch and the Tennessee River, downstream from the confluence of the Clinch River. As was done last year, the fish were analyzed jointly by ORNL and the USPHS laboratories in Cincinnati. Radiochemical procedures and results were compared, and the agreement

of analytical results with fish tissues was relatively good. The Tennessee Game and Fish Commission also obtained information on the consumption of fish in the local area. These investigations are providing data for the Subcommittee on Safety Evaluation of the Clinch River Steering Committee; the data will be used to ascertain the intake by humans of radionuclides via the aquatic food chain.

12. Theoretical Systems

B. C. Patten

J. S. Olson

G. M. Van Dyne

EFFECTS OF RADIATION STRESS ON INTERSPECIFIC COMPETITION

B. C. Patten

The fate of radioisotopes in ecosystems is determined in part by the dynamics of organisms present. These dynamics are subject to radiation effects which can be expected to vary depending upon how the community is organized. Consequently, the subject of organism interactions is basic to two major areas of radioecological responsibility — effects and fate of nuclides. To provide a conceptual basis for understanding effects of radiation on interacting systems, analog computer solutions of competition equations, both with and without radiation stress, were generated.

The classical concept of competitive interaction between two species is given by the Lotka-Volterra equations:

$$\begin{aligned}\dot{N}_1 &= r_1 N_1 [1 - (1/K_1)N_1 - (\alpha/K_1)N_2], \\ \dot{N}_2 &= r_2 N_2 [1 - (1/K_2)N_2 - (\beta/K_2)N_1],\end{aligned}\quad (1)$$

where N_i ($i = 1, 2$) is population size of species i ($0 \leq N_i \leq K_i$), r_i is the "biotic potential" if

population growth were exponential ($\dot{N}_i = r_i N_i$), $1/K_i$ is the inhibition of species i by one individual of itself, α/K_1 is the inhibition of species 1 by one individual of species 2, and β/K_2 is the inhibition of species 2 by one individual of species 1. The system is in equilibrium when $\dot{N}_1 = \dot{N}_2 = 0$, in which case r_i , N_i , or the terms in brackets must vanish. Setting $(K_1 - N_1 - \alpha N_2)/K_1 = 0$ and $(K_2 - N_2 - \beta N_1)/K_2 = 0$, the zero isoclines are

$$\begin{aligned}N_1 &= K_1 - \alpha N_2, \\ N_2 &= K_2 - \beta N_1.\end{aligned}\quad (2)$$

When the system is not in equilibrium, all values of N_1 for which $dN_1/dN_2 = 0$ must lie on the line $K_1 - \alpha N_2$, and all values of N_2 for which $dN_2/dN_1 = 0$ must fall on $K_2 - \beta N_1$. When these lines are graphed on an (N_1, N_2) plane, the N_1 intercept of the N_1 isocline is K_1 , and the N_2 intercept is K_1/α ; the N_1 intercept of the N_2 isocline is K_2/β , and the N_2 intercept is K_2 (Fig. 12.1a). From any point on the plane, the system will move in such a direction that the curve of its transient response will cross the N_1 isocline vertically and the N_2 isocline horizontally. A

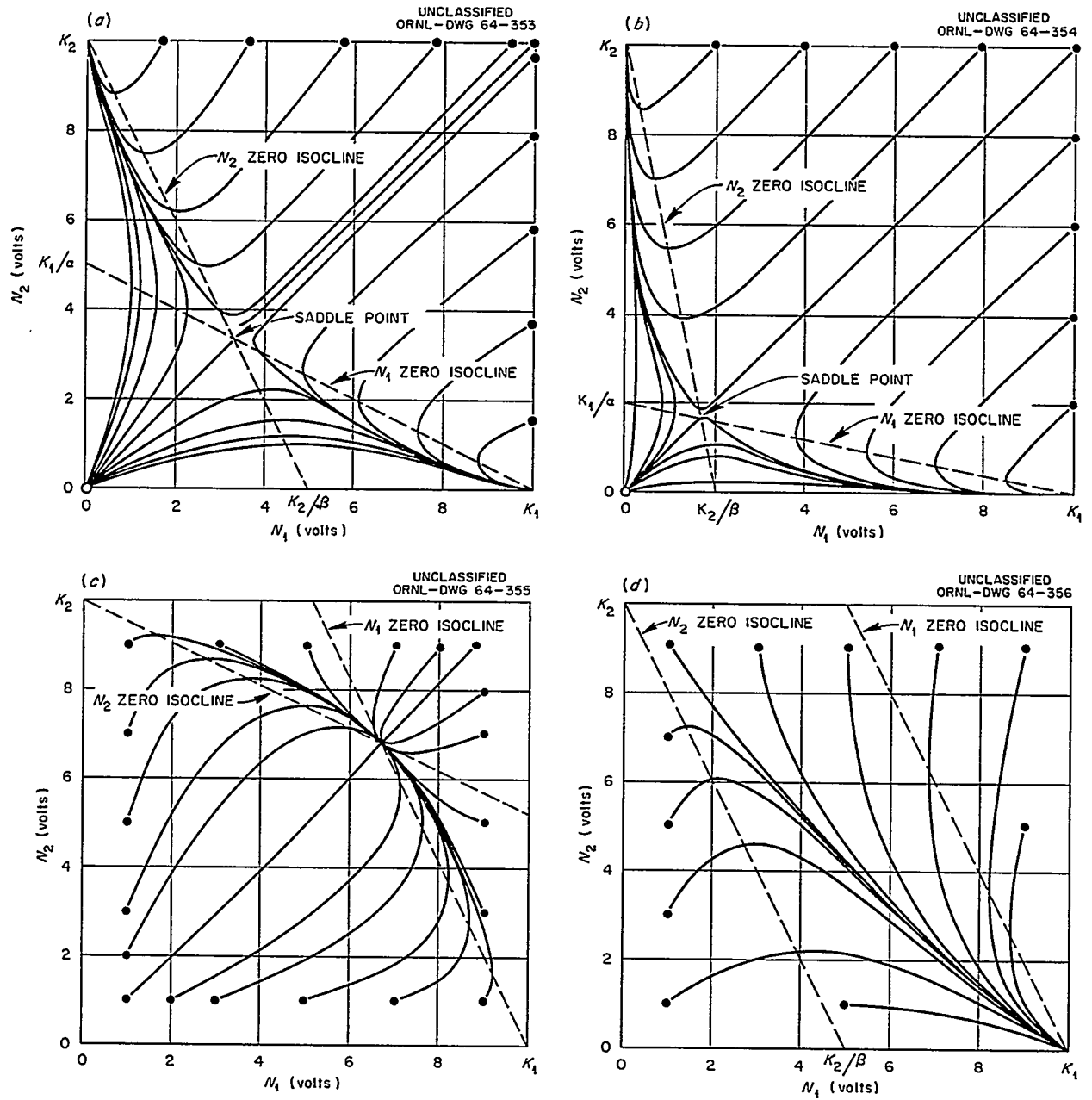


Fig. 12.1. Phase Diagrams of Responses of Unirradiated Lotka-Volterra Systems [Eqs. (1)]. The initial position of each locus is indicated by a solid circle, and equilibrium points which are not obvious are indicated by arrows: (a) Case 1 with $r_1 = r_2 = 1$, $\alpha = \beta = 2$, and $K_1 = K_2 = 10$ v; (b) Case 1 with $r_1 = r_2 = 1$, $\alpha = \beta = 5$, and $K_1 = K_2 = 10$ v; (c) Case 2 with $r_1 = r_2 = 1$, $\alpha = \beta = 0.5$, and $K_1 = K_2 = 10$ v; (d) Case 3 with $r_1 = r_2 = 1$, $\alpha = 0.5$, $\beta = 2$, and $K_1 = K_2 = 10$ v.

saddle point of unstable equilibrium occurs where the two isoclines intersect:

$$\begin{aligned} N_1 &= \frac{1}{\beta}(K_2 - K_1 - \alpha N_2), \\ N_2 &= \frac{1}{\alpha}(K_1 - K_2 - \beta N_1). \end{aligned} \quad (3)$$

Four kinds of stable equilibria are possible: Case 1 ($\alpha/K_1 > 1/K_2$, $\beta/K_2 > 1/K_1$); one species only survives at the level $N_i = K_i$, which one being determined by the initial population sizes (Fig. 12.1a). When the values of α and β are increased, the outcome is not changed, but the transient behavior is altered (Fig. 12.1b). The biotic potentials r_i have no influence on the form of the graphs or on the equilibrium result, but they do determine the time to reach equilibrium. Case 2 ($\alpha/K_1 < 1/K_2$, $\beta/K_2 < 1/K_1$); both species coexist, the equilibrium point being determined by the interaction coefficients α and β (Fig. 12.1c). Case 3 ($\alpha/K_1 < 1/K_2$, $\beta/K_2 > 1/K_1$); species 1 is the sole survivor at the level $N_1 = K_1$ for all initial conditions and for all possible relationships between r_1 and r_2 (Fig. 12.1d). Case 4 ($\alpha/K_1 > 1/K_2$, $\beta/K_2 < 1/K_1$); species 2 always survives with $N_2 = K_2$.

Radiation stresses ρ_1 and ρ_2 can be introduced into the model by modifying the basic equations (1) as follows:

$$\begin{aligned} \dot{N}_1 &= r_1 N_1 [1 - (1/K_1)N_1 - (\alpha/K_1)N_2] - \rho_1 N_1, \\ \dot{N}_2 &= r_2 N_2 [1 - (1/K_2)N_2 - (\beta/K_2)N_1] - \rho_2 N_2, \end{aligned} \quad (4)$$

where the ρ_i represent rates of population reduction due to radiation. The zero isoclines become

$$\begin{aligned} N_1 &= K_1 [1 - (\rho_1/r_1) - (\alpha/K_1)N_2], \\ N_2 &= K_2 [1 - (\rho_2/r_2) - (\beta/K_2)N_1], \end{aligned} \quad (5)$$

from which conditions for the outcomes of competition corresponding to the four cases described above can be specified: Case 1

$$\left(\frac{\alpha}{1 - \rho_1/r_1} > \frac{K_1/K_2}{1 - \rho_2/r_2}, \frac{\beta}{1 - \rho_2/r_2} > \frac{K_2/K_1}{1 - \rho_1/r_1} \right);$$

species 1 or species 2 survives at reduced equilibrium population sizes ($N_i < K_i$) provided the stresses are less than the biotic potentials ($\rho_i < r_i$) (Fig. 12.2a). Increasing the interaction coefficients α and β has no effect on the equilibrium population levels, but it does reduce the influence of differential radiation effects in determining survivorship. This is illustrated in Fig. 12.2b, which shows that species 1, which was more vulnerable to radiation ($\rho_1 = 0.5$, $\rho_2 = 0.2$), can now prevail over species 2 from many more initial starting points in the (N_1, N_2) plane than was possible under the lower levels of interspecific competition (Fig. 12.2a). In other words, Fig. 12.2b is more symmetrical (like Figs. 12.1a and 12.1b) than Fig. 12.2a. Hence, the greater the competitive interaction between two Lotka-Volterra species, the less the influence of differential radiation effects in determining the outcome of competition.

Although reproductive ability has no effect other than on the rate at which equilibrium is attained in nonirradiated populations under conditions of radiation stress, the coefficients r_i become of prime significance in determining the outcome of competition. In Fig. 12.2c all parameters were the same as in Fig. 12.2a except that r_1 and r_2 were reduced from 1 to 0.5. This change drastically altered the phase diagram so that success of species 2 was assured for most starting positions in the plane. The equilibrium populations were also reduced, from $N_1 = 5.1$ v and $N_2 = 8.1$ v (Fig. 12.2a) to $N_1 = 1.6$ v and $N_2 = 6.25$ v (Fig. 12.2c). Thus, in competition between irradiated Lotka-Volterra species, reduced biotic potentials enhance both the suppressing effect of the radiation on the steady-state population levels and the influence of differential radiation effects in determining the winning species. Conversely, high biotic potentials reduce the effect of differential responses to radiation stress in determining the surviving species, and increase the equilibrium level of the winning population.

Case 2 is defined by

$$\left(\frac{\alpha}{1 - \rho_1/r_1} < \frac{K_1/K_2}{1 - \rho_2/r_2}, \frac{\beta}{1 - \rho_2/r_2} < \frac{K_2/K_1}{1 - \rho_1/r_1} \right);$$

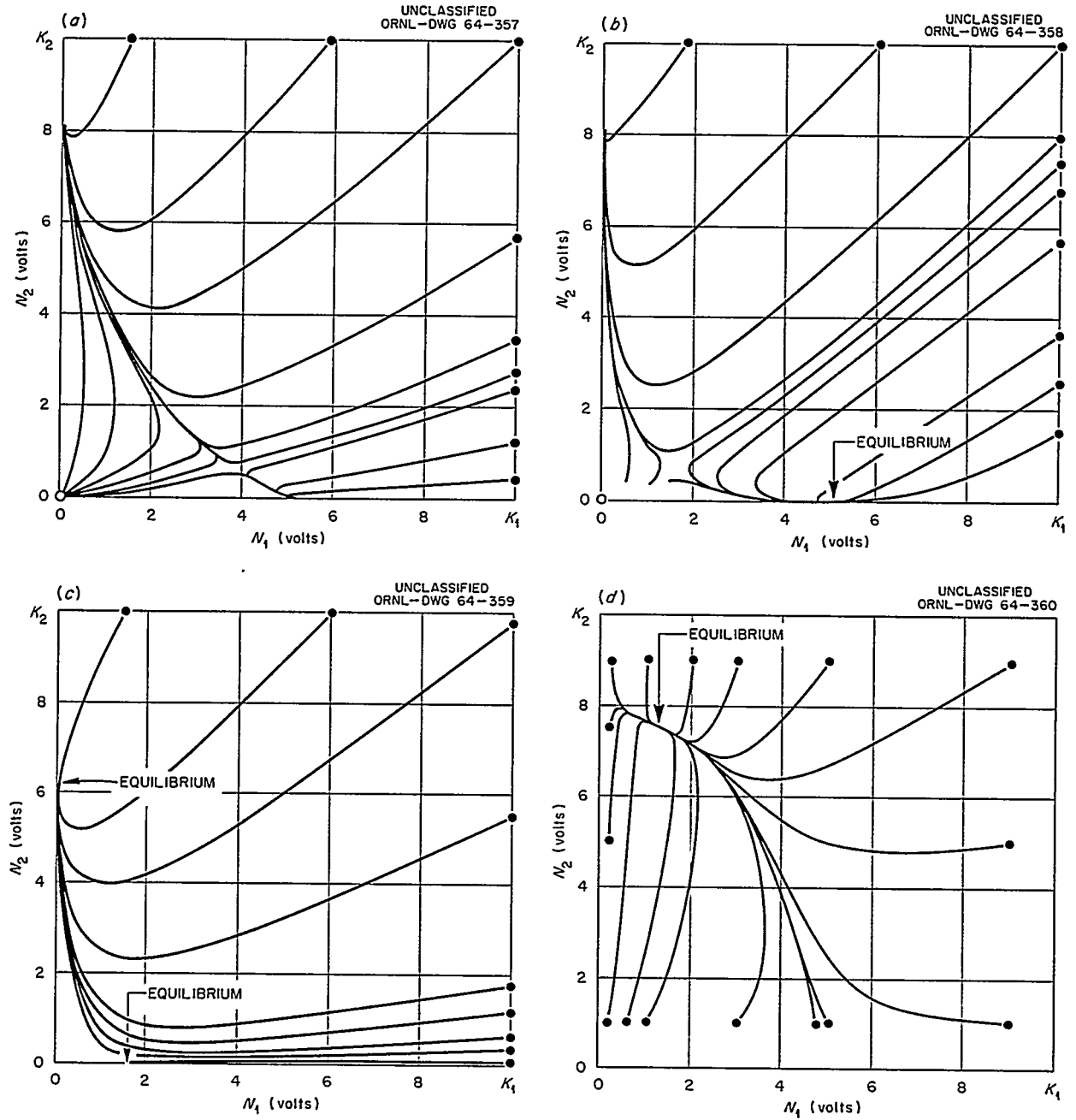


Fig. 12.2. Phase Diagrams of Lotka-Volterra Systems Under Chronic Radiation Stress as Defined by Eqs. (4). (a) Case 1 with $r_1 = r_2 = 1$, $\alpha = \beta = 2$, $K_1 = K_2 = 10$ v, $\rho_1 = 0.5$, and $\rho_2 = 0.2$; (b) Case 1 with $r_1 = r_2 = 1$, $\alpha = \beta = 5$, $K_1 = K_2 = 10$ v, $\rho_1 = 0.5$, and $\rho_2 = 0.2$; (c) Case 1 with $r_1 = r_2 = 0.5$, $\alpha = \beta = 2$, $K_1 = K_2 = 10$ v, $\rho_1 = 0.5$, and $\rho_2 = 0.2$; (d) Case 2 with $r_1 = r_2 = 1$, $\alpha = \beta = 0.5$, $K_1 = K_2 = 10$ v, $\rho_1 = 0.5$, and $\rho_2 = 0.2$.

case 3 by

$$\left(\frac{\alpha}{1-\rho_1/r_1} < \frac{K_1/K_2}{1-\rho_2/r_2}, \frac{\beta}{1-\rho_2/r_2} > \frac{K_2/K_1}{1-\rho_1/r_1} \right);$$

and case 4 by

$$\left(\frac{\alpha}{1-\rho_1/r_1} > \frac{K_1/K_2}{1-\rho_2/r_2}, \frac{\beta}{1-\rho_2/r_2} < \frac{K_2/K_1}{1-\rho_1/r_1} \right).$$

A variety of computer solutions for each of these conditions demonstrated that, as for case 1, the final state of competing Lotka-Volterra systems subjected to chronic reduction by radiation depends on the relationships between initial conditions, biotic potentials, the competition coefficients, and (through K_1 and K_2) the environment. The outcome of a case 2 experiment which differed from that of Fig. 12.2c only in the values of ρ_i is shown in Fig. 12.2d. Other results for cases 2, 3, and 4 are presented in an ORNL report.¹

A GENERALIZED COMPARTMENT MODEL FOR ECOSYSTEMS

J. S. Olson

Several previous models for transfer of substances within ecosystems have been encompassed within a more general model. A framework for studies of landscape contamination may be provided by including transfers between systems, as from some "inner" system of special interest, to some "border" system or to an "outer" system (indexed by subscript $H = 1, 2, 3$, for example). It includes diverse types of variables (indexed by I) such as radionuclides and their elements, which together constitute total mass, and the energy associated with that mass in various parts of the system. Additional variables, if needed, can describe the configuration of these quantities and the environmental factors which control transfers of the preceding quantities from compartment J to compartment K of the system (Fig. 12.3). When the fraction of a given material I transferred

from part J to part K is expressed as an instantaneous rate, f_{JK} , then the dynamic structure of transfers is summarized by nondiagonal terms in a matrix F :

$$F \equiv \begin{pmatrix} -f_{11} & f_{12} & \dots & f_{1N} \\ f_{21} & -f_{22} & \dots & f_{2N} \\ \vdots & \vdots & \ddots & \vdots \\ f_{N1} & f_{N2} & \dots & -f_{NN} \end{pmatrix} \quad (1)$$

Each negative term on the diagonal

$$f_{J\cdot} = - \sum_{K \neq J} f_{JK} \quad (J \neq K)$$

is here defined as the sum of all fractional loss rates for a given compartment (i.e., the sum of nondiagonal terms in a row). This determines the turnover time, and essentially controls the steady state which can be attained by a given compartment for a given level of input to that compartment. The state of the system is expressed

UNCLASSIFIED
ORNL-DWG 64-7917

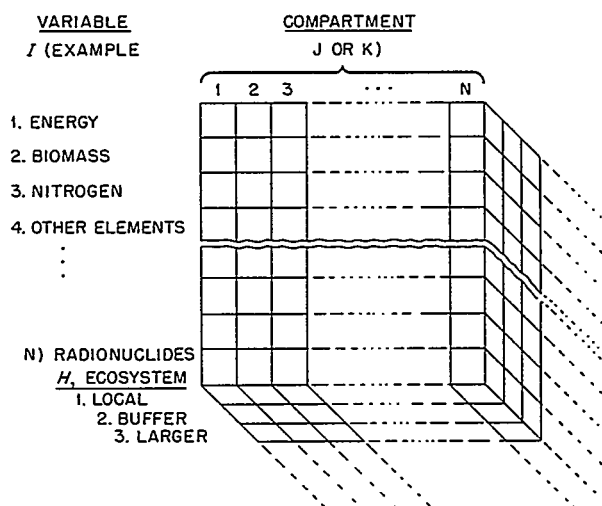


Fig. 12.3. Diagram of a Generalized Model for Transfer of Variable Quantities of Materials (I) Between Compartments (J, K) of a Series of Nested or Coupled Ecosystems (H).

¹B. C. Patten, *Community Organization and Energy Relationships in Plankton*, ORNL-3634 (1964).

as the row vector $V \equiv (V_1 \ V_2 \ \dots \ V_N)$. Given Eq. (1) and the initial state $V|_{t=0}$, the system of differential equations for further rates of change in V , summarized as sums of income and loss terms in previous reports, may be conveniently abbreviated

$$\dot{V} = VF. \quad (2)$$

A review of terrestrial productivity² attempted to relate a variety of data from ecological and physiological sources to the estimation of transfer rates f_{JK} so that continuing simulation studies can more closely approximate behavior of various classes of real ecosystems.

RELATED ACTIVITIES

The section chief served on a special National Academy of Sciences study group on civil defense. This study, "Project Harbor," evaluated all phases of the present civil defense posture of

the U.S. and prepared a report analyzing the civil defense program.

Members of the section participated as faculty in a summer institute in radiation ecology sponsored by ORNL and ORINS. This institute was attended by 20 college and university teachers.

Graduate and undergraduate classes in plant ecology and mammalogy from the University of Tennessee, and an undergraduate class in ecology from Middle Tennessee State College toured the laboratory and field facilities and were briefed on the ORNL ecology program. Likewise, a group of university scientists in the field of microbiology and plant pathology visited the section.

One member of the section participated in the ORNL-University of Tennessee educational program and presented a graduate seminar course in microbial ecology in the University's Institute of Radiation Biology.

One member of the section served as a U.S. delegate for plant ecology on a National Academy of Sciences Committee which met in Paris, France, with similar committees from other European countries to plan for the proposed International Biological Program.

One person served as a member of a review team for a Division of Biology and Medicine offsite project review at the University of Minnesota.

²J. S. Olson, *J. Ecol.* 52(Suppl), 99-118 (1964).

Part III. Radiation Physics

G. S. Hurst

13. Theoretical Radiation Physics

Jacob Neufeld
R. H. Ritchie

V. E. Anderson¹
J. C. Ashley²
W. F. Boone³
W. G. Connor⁴

J. Crowell⁵
R. N. Hamm
G. S. Hurst
A. L. Marusak⁴
H. A. Wright

W. S. Snyder
T. D. Strickler⁴
J. E. Turner
C. L. Wiginton⁴

DOSE CALCULATIONS FOR HIGH-ENERGY PROTONS

Dose calculations for protons with energies up to 400 Mev have been completed.⁶ Results for protons normally incident on a tissue slab appeared in ORNL-3492 (ref. 7).

The techniques described in ORNL-3492 were applied to the calculation of dose in a tissue phantom having the shape of a parallelepiped of dimensions $20 \times 30 \times 60$ cm. Monoenergetic protons with an isotropic flux distribution were considered. It was found that the radiation dose is essentially uniform in the phantom for incident proton energies above about 200 Mev. At these higher energies, proton ranges in tissue are large compared with the average track length of a primary proton in the phantom. Below 200 Mev

the dose near the surface of the phantom is considerably higher than that in the interior. Figures 13.1, 13.2, and 13.3 show the quantitative results for incident proton energies of 100 and 150 Mev. In Fig. 13.1 the parallelepiped is divided into sections by slices parallel to the XYZ axes as shown. Figure 13.2 shows the total rad and rem dose for an incident proton energy of 100 Mev plotted as a function of position along the Y axis in both of the sections perpendicular to the X axis, 0-5 and 5-10 cm. Figure 13.3 shows the same data for protons with an incident energy of 150 Mev. At 100 Mev there is about 50% more dose along the edges of the 0-5 cm section than elsewhere. In the 5-10 cm slice there is about five times as much dose at the edges as there is in the interior. At 150 Mev the dose is almost uniform over the 0-5 cm section and is about 50% higher at the edges of the next section relative to the interior of that section.

Work has continued on the preparation of codes for the calculation of dose from incident protons and neutrons with energy up to several Bev. Various detailed interactions are being studied from the standpoint of assessing their possible contribution to dose. The codes are being written for a tissue phantom of arbitrary geometry for use in analyzing specific experiments to assist in making estimates of RBE values.

¹On loan from Central Data Processing Facility (ORGDP).

²Temporary leave.

³Summer employee.

⁴Consultant.

⁵Oak Ridge Graduate Fellow.

⁶J. E. Turner *et al.*, "Calculation of Radiation Dose from Protons to 400 MeV," to be published in *Health Physics*.

⁷J. Neufeld *et al.*, *Health Phys. Div. Ann. Progr. Rept.* June 30, 1963, ORNL-3492, p. 119.

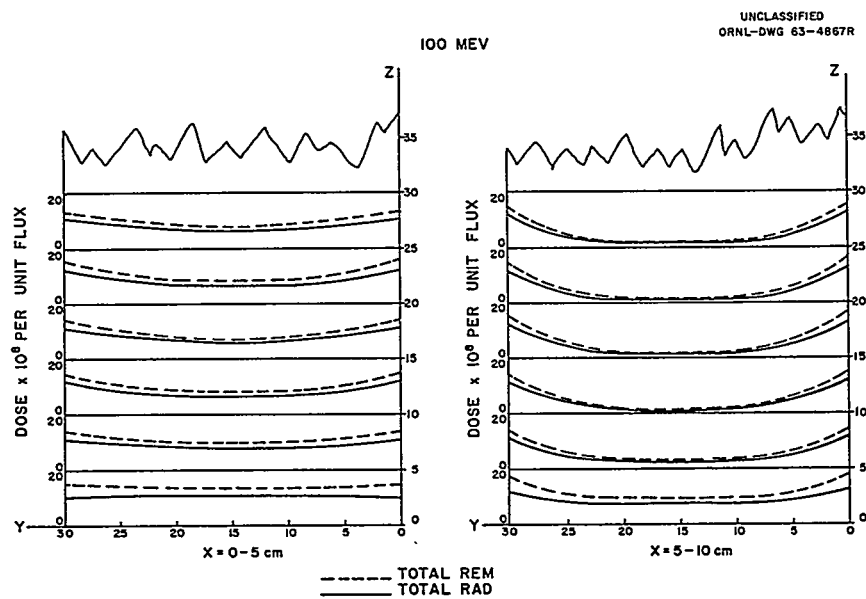


Fig. 13.1. Reference Axes and Sectioning of Parallelepiped for Figs. 13.2 and 13.3.

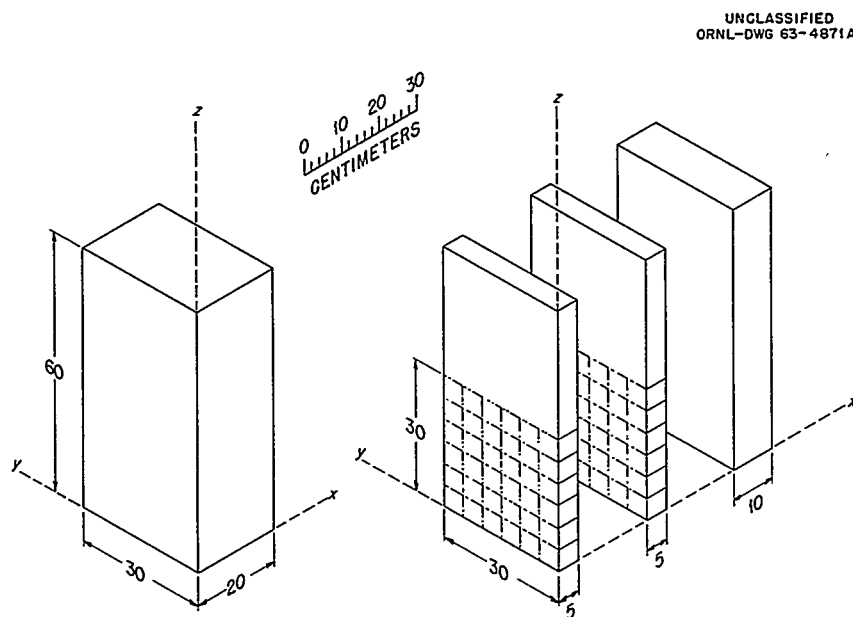


Fig. 13.2. Total Rad and Rem Dose in Tissue Parallelepiped from 100-Mev Isotropic Protons.

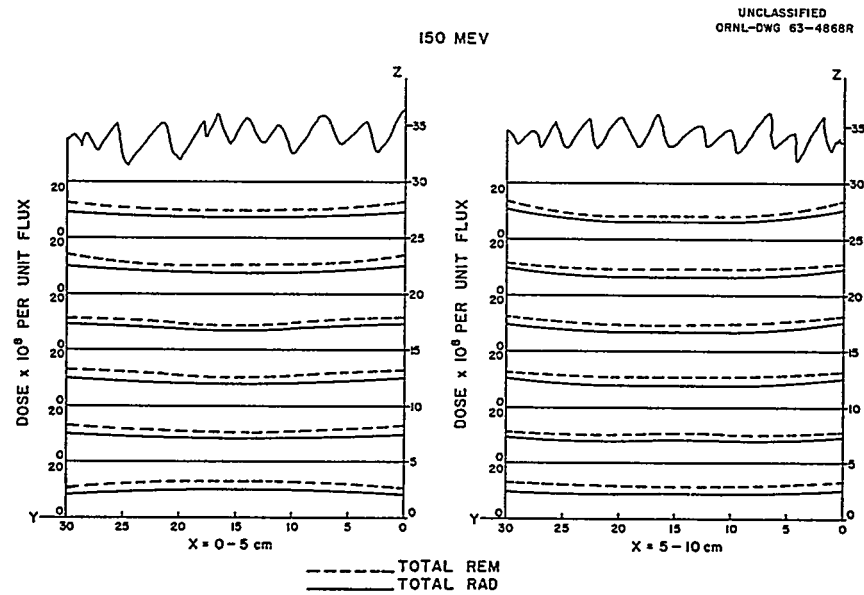


Fig. 13.3. Total Rad and Rem Dose in Tissue Parallelepiped from 150-Mev Isotropic Protons.

RESPONSE OF CHARGED PARTICLE DETECTORS TO HIGH-ENERGY PROTONS

A code has been written to determine the distribution of energy losses of an isotropic flux of monoenergetic protons in an array of silicon detectors consisting of a main crystal of dimensions $d \times d \times t$ cm bounded on each of its six faces by a crystal of 0.1-cm thickness. A proton penetrating such an array will lose energy by ionization (nuclear collisions have been neglected up to the present time but may be taken into account later) in various of the crystals. Let E be the energy of the incident proton and ϵ the energy lost in traversing the crystal. The number $n(\epsilon, E)$ of protons of incident energy E having losses between ϵ and $\epsilon + d\epsilon$ can be plotted as a function of ϵ . The code is sufficiently general to give such an energy loss distribution for those particles that enter one face and exit through the opposite face, that enter one face and exit through

an adjacent face, or that enter one face and stop within the array. Also, the distribution may be for the total energy loss, the energy loss in the main crystal, the energy loss in the side crystals of dimensions $0.1 \times d \times d$ cm, or the side crystals of dimensions $0.1 \times d \times t$ cm.

A typical example of the type of results that can be obtained from this program is shown in Fig. 13.4. Curves are drawn for 30,000 protons incident isotropically at each of the three energies, $E = 400, 200$, and 100 Mev. The abscissa is the energy loss ϵ Mev with the increment $d\epsilon = 0.2$ Mev, and the ordinate $n(\epsilon, E)$ is the number of incident protons which enter one face and exit through the opposite face and have energy loss between ϵ and $\epsilon + d\epsilon$. The dimensions of the main crystal are $1 \times 1 \times 1$ cm.

An application of the results obtained by this program is discussed in the next section, "Conceptual Design of a Dosimeter for High-Energy Protons."

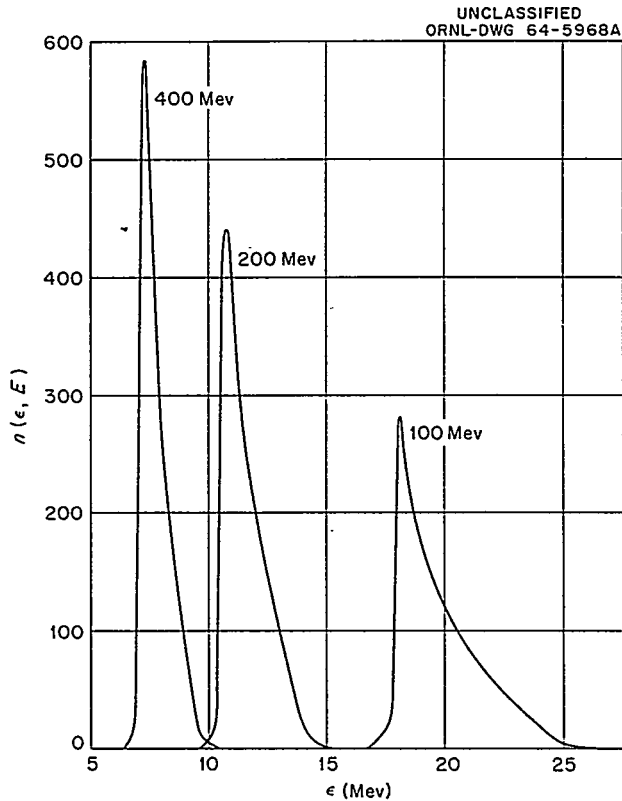


Fig. 13.4. Unnormalized Distribution of the Total Energy Losses of Those Protons Which Enter One Face and Exit Through the Opposite Face of a Detector Array Having a Main Crystal of Dimensions $1 \times 1 \times 1$ cm.

CONCEPTUAL DESIGN OF A DOSIMETER FOR HIGH-ENERGY PROTONS

We wish to illustrate the use of the generalized concept for radiation dosimetry⁸ in the dosimetry of high-energy protons. In the present case we wish to find an energy loss operator $O(\epsilon)$ such that an energy loss distribution function $n(\epsilon, E)$ will be transformed into a dose function $D(E)$ within small limits δ ; that is,

$$|O(\epsilon) n(\epsilon, E) - D(E)| \leq \delta.$$

From the calculations of the previous section, it is seen that for a charged particle detector made in the form of a cube whose edge dimensions are equal to the range of a 50-Mev proton

⁸G. S. Hurst and R. H. Ritchie, *Health Phys.* 8, 117 (1962).

it is convenient to define two groups of energy loss distributions; for group 1 the proton energy is less than 50 Mev, and for group 2 the proton energy exceeds 50 Mev. Consider, for illustration, counting channels for the group 1 case as shown in Table 13.1. The last column of the table gives the fraction of the proton losses appearing in the counting channels for selected proton energies. The distribution of energy losses for the group 2 cases is slightly more complex, and it is seen that an inversion occurs; that is, the greater the incident proton energy, the smaller is the energy loss in the detector. See Fig. 13.4 for proton energies $E = 100, 200$, and 400 Mev. In the high-energy group we define channels as shown in the second part of Table 13.1.

An operator well suited to the analysis of these distributions is of the matrix element weighting type; thus,

$$\sum_j a_j N_{ij} = D_i,$$

where $D_i \equiv$ dose in rems (see Fig. 13.5) for 1 proton/cm² when the proton energy is E_i , $N_{ij} \equiv$ number of pulses created in channel j due to 1 proton/cm² when the proton energy is E_i , and $a_j \equiv$ weighting factor for channel j . Thus, finding the a_j 's leads to the exact determination of the rem dose at selected energies with $\delta = 0$. In our simple example, only the diagonal matrix elements

Table 13.1. Fraction of Energy Losses in Various Channels for Selected Proton Energies

Channel No.	Energy Span (Mev)	Fraction of Proton Energy Losses in Channel and Incident Proton Energy
Group 1		
1 ^L	0-9	1.00 at 5 Mev
2 ^L	9-15	1.00 at 10 Mev
3 ^L	15-30	0.90 at 25 Mev
Group 2		
1 ^H	0-10	0.11 at 400 Mev
2 ^H	10-16	0.11 at 200 Mev
3 ^H	16-26	0.11 at 100 Mev

need be considered. These are shown in Table 13.2.

In Fig. 13.6 we illustrate an electronic circuit which performs the above energy selection and matrix weighting. The pulses corresponding to the high-energy proton data are routed to the proper section of the data processor by means of circuitry that senses coincidence between opposite side detectors and then routes the output to a linear gate that passes this output only when

the gate is activated simultaneously by a signal from the main detector. The pulses corresponding to the low-energy proton data are routed to the proper section of the data processor by means of a circuit which senses anticoincidence between all six side detectors, and if this circuit shows an output in only one side detector, this output is added linearly (by means of a linear mixer and linear gates) to any signal that may be present in the main detector. After this selection has occurred, matrix weighting and addition are performed in suitable data processing equipment.

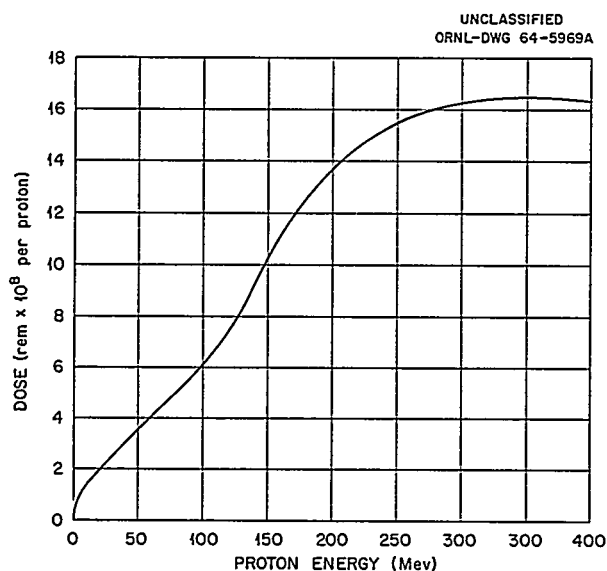


Fig. 13.5. Dose in Rems per Proton Incident Isotropically on a 30-cm Tissue Slab.

Table 13.2. Weighting Coefficients for Various Counting Channels

E_p	Channel	N_{ij}	a_{ij} (rem/pulse)
$\times 10^{-8}$			
5	1 ^L	1.0	1.1
10	2 ^L	1.0	1.5
25	3 ^L	0.9	2.4
400	1 ^H	0.11	150
200	2 ^H	0.11	130
100	3 ^H	0.11	55

DISTRIBUTION OF DOSE RESULTING FROM BROAD-BEAM IRRADIATION OF A MAN-SIZED CYLINDRICAL TISSUE PHANTOM

The effectiveness of ionizing radiation in inducing various radiation effects in tissue is generally considered to be influenced by the rate of energy loss along the tracks of the various ionizing particles. Many experiments have been performed to study the relation between relative biological effectiveness (RBE) and linear energy transfer (LET) for a variety of effects in many species. Moreover, the ICRP and the NCRP have included a quality factor defined in terms of LET in the definition of the rem, the basic unit of exposure to ionizing radiation for man. However, in spite of this interest in the relation between biological effectiveness and the physical parameter LET, there has been no detailed analysis of the LET distribution of dose for irradiation of mammals by neutrons; attempts to correlate RBE and LET generally have used average values of LET, although it is evident that there would be considerable variation in the distribution in the case of large mammals.

To meet the need for more thorough investigation in this area, codes employing Monte Carlo methods have been developed for the CDC 1604 computer which provide detailed information on the LET distribution of dose in various volume elements of a tissue phantom. These codes produce individual neutron "histories" in which the parameters of the neutron — its energy, location, and direction; the nucleon with which it interacts; its angle of recoil; etc. — are determined in a random fashion but in conformity with established physical theory. When taken together, a large number of these particle histories provide an

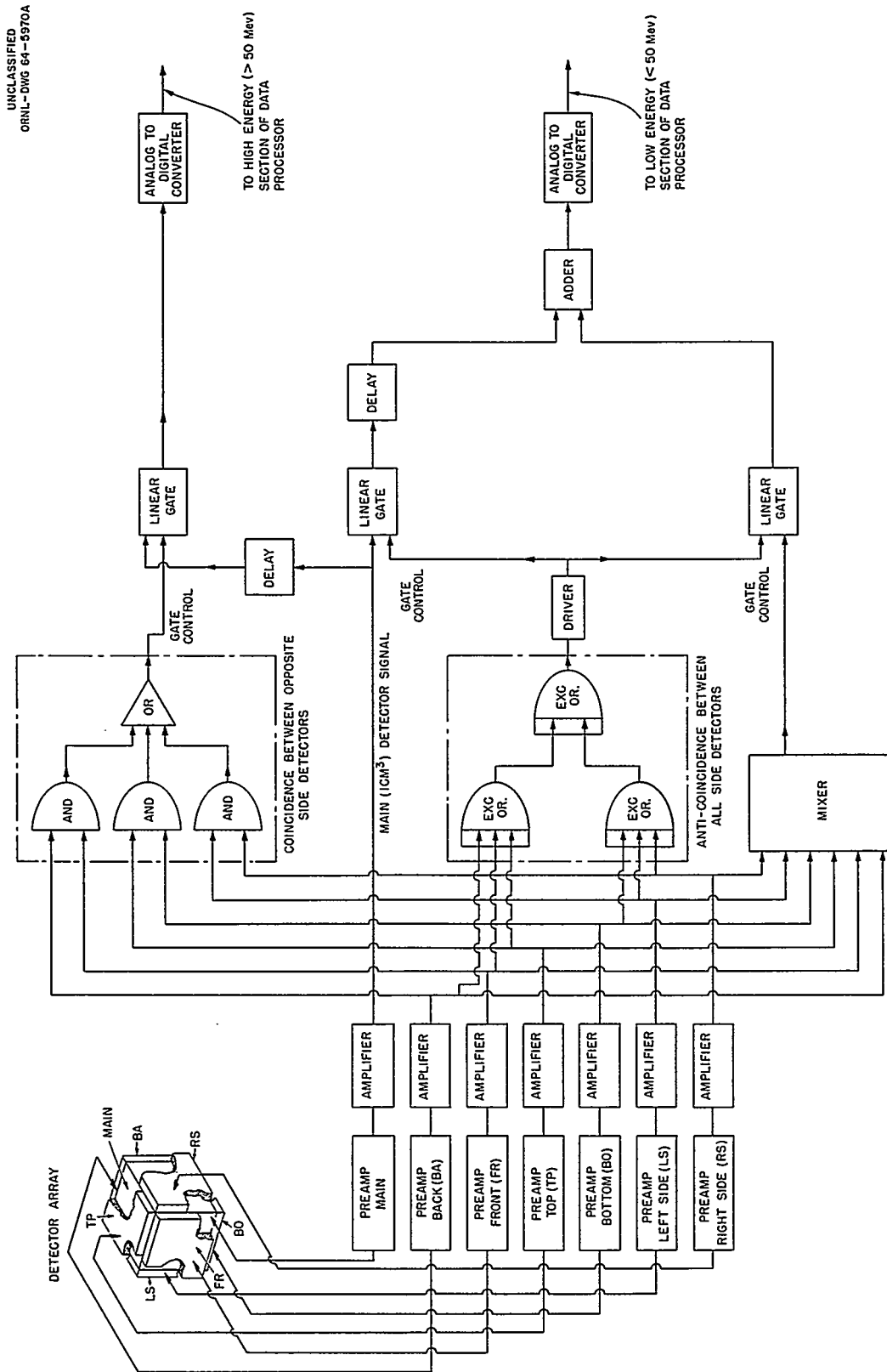


Fig. 13.6. Electronic Circuitry for Energy Selection and Matrix Weighting.

adequate representation of the behavior of an actual radiation field in the phantom. Analysis of these histories provides more precise knowledge of the variation of dose with location in the phantom, and the fraction of dose in specified ranges of LET can be estimated also. A good account of the techniques employed in this type of Monte Carlo calculation is given by Cashwell and Everett.⁹ The cross-section data used by the code are taken from BNL-325, 2d ed., and anisotropy of angular scattering is handled according to procedures developed by Kalos and Goldstein¹⁰ for carbon, by Lustig¹¹ for oxygen, and by Lustig, Goldstein, and Kalos¹² for nitrogen.

When a neutron is absorbed by a hydrogen nucleus in the $n\text{-}\gamma$ interaction, a photon with energy 2.2 Mev is produced. A representative sample of such photons is analyzed by using these photons as the source for a second Monte Carlo code which computes photon histories and interactions. This code uses cross-section data given by Grodstein.¹³ The energy absorbed in the phantom from the photons is thus obtained. The dose from the protons produced by the $n\text{-}p$ reaction with nitrogen nucleons is also taken into account.

The results presently available are computed for a homogeneous cylindrical phantom having a diameter of 30 cm, a height of 60 cm, and the composition of standard man¹⁴ with density 0.96 g/cc. The phantom is divided into 150 regions, referred to below as "boxes," as shown schematically in Fig. 13.7. A total of 10,000 neutrons of a given energy are assigned points of entry distributed over the surface of the cylinder, corresponding to a uniform broad beam of neutrons with velocity vector parallel to the

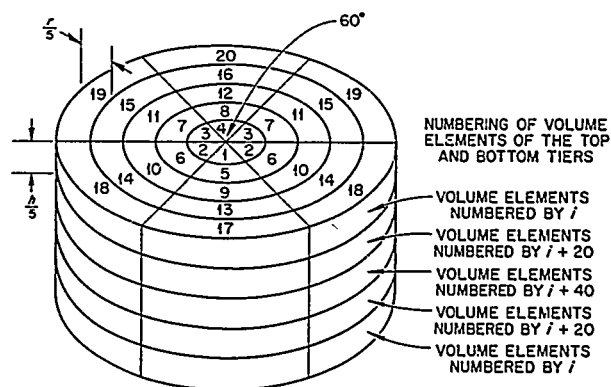


Fig. 13.7. Numbering of Volume Elements in the Cylindrical Phantom.

bisector of the acute angle shown for box 1. The total dose, including the dose from photons, the dose from the protons produced by the $n\text{-}p$ reaction with nitrogen, and the energy imparted by elastic scattering to the various recoil nuclei of the phantom, is averaged over each box. This average dose in each box is subdivided into doses delivered in various ranges of LET; the formulas used for this analysis are given in ref. 15. The points of subdivision of the LET scale are 0, 3.5, 7, 15, 25, 35, 50, 62.5, 75, 87.5, 100, and 200 keV/ μ .

The resulting dose distributions in boxes 17, 1, and 20 are presented in Figs. 13.8–13.10 for the case of monoenergetic 2.5-Mev neutrons. An interval four standard deviations in length also is shown for each value. The average dose in each range of LET corresponds to the area of the column for the respective interval, and the height of the column represents the dose per unit of LET for that interval. It is clear that there is considerable variation in the amount of dose delivered to the three boxes and also a significant difference in the LET distribution of dose in the boxes. These distributions are normalized in Figs. 13.11–13.13 in order that the difference in quality can be studied apart from the magnitude

⁹E. D. Cashwell and C. J. Everett, *A Practical Manual of Monte Carlo Methods for Random Walk Problems*, Pergamon Press, New York, 1959.

¹⁰M. Kalos and H. Goldstein, *Neutron Cross Section Data for Carbon*, NDA 12-16 (Mar. 31, 1956).

¹¹H. Lustig, *Differential Elastic Neutron Scattering Cross Section of Oxygen*, NDA 2111-3, vol. A (Nov. 1, 1959).

¹²H. Lustig, H. Goldstein, and M. H. Kalos, *The Neutron Cross Sections of Nitrogen*, NDA 86-1 (June 30, 1957).

¹³G. W. Grodstein, *X-ray Attenuation Coefficients from 10 kev to 100 Mev*, Natl. Bur. Std. (U.S.), Circ. 583 (Apr. 30, 1957).

¹⁴Protection Against Neutron Radiation Up to 30 Million Electron Volts, Natl. Bur. Std. (U.S.), Handbook 63, p. 8 (Nov. 22, 1957).

¹⁵W. S. Snyder, "The LET Distribution of Dose in Some Tissue Cylinders," p. 3 in *Biological Effects of Neutron and Proton Irradiations*, vol. 1, p. 3, IAEA, Vienna, 1964.

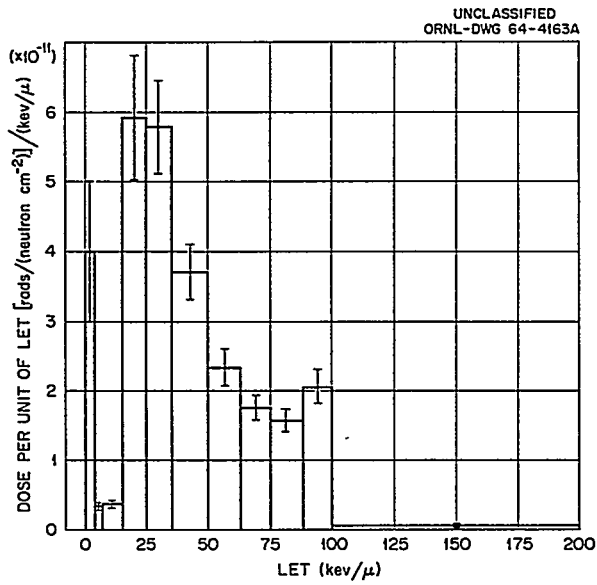


Fig. 13.8. Distribution of Dose with LET (Box 17, 2.5-Mev Neutron Beam).

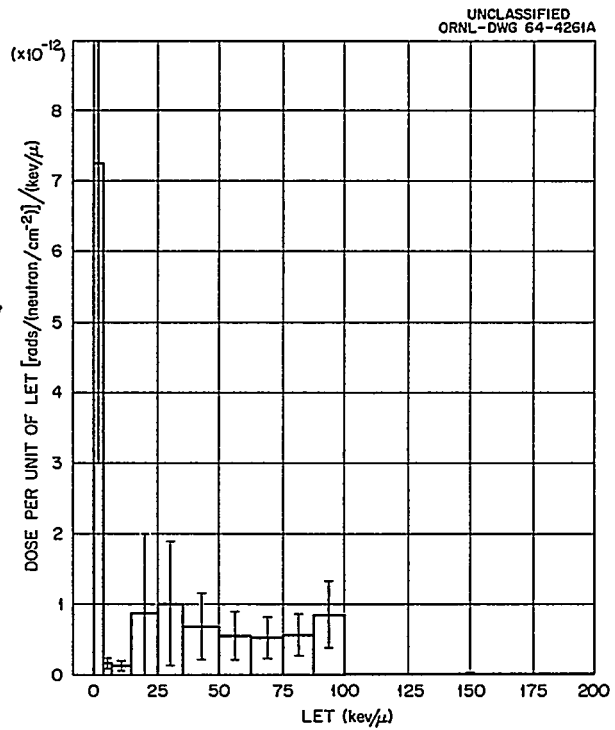


Fig. 13.10. Distribution of Dose with LET (Box 20, 2.5-Mev Neutron Beam).

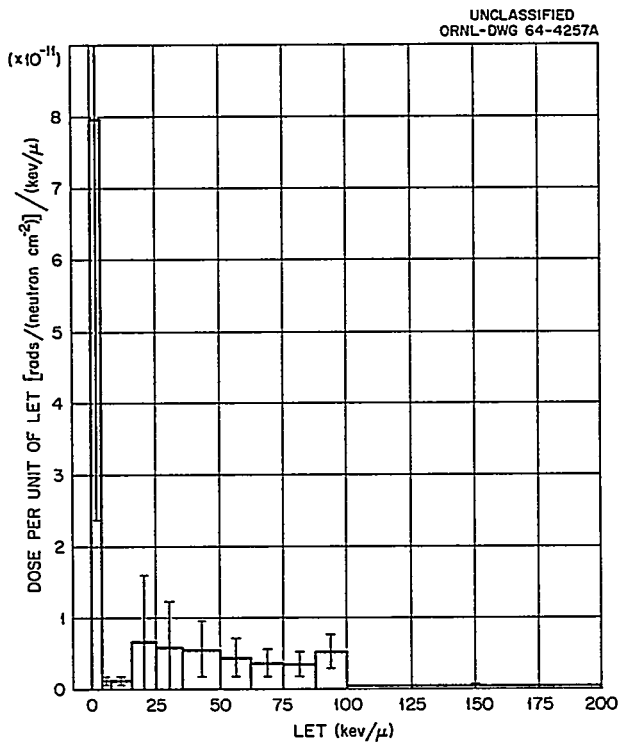


Fig. 13.9. Distribution of Dose with LET (Box 1, 2.5-Mev Neutron Beam).

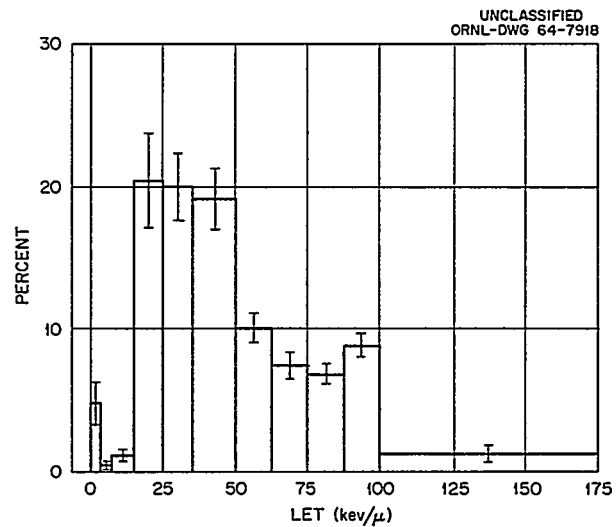


Fig. 13.11. Normalized Distribution of Dose with LET (Box 17, 2.5-Mev Neutron Beam).

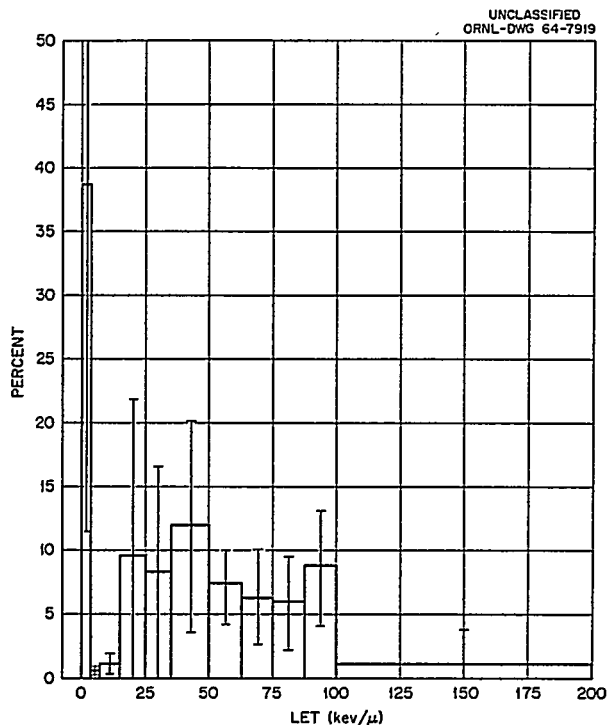


Fig. 13.12. Normalized Distribution of Dose with LET (Box 1, 2.5-Mev Neutron Beam).

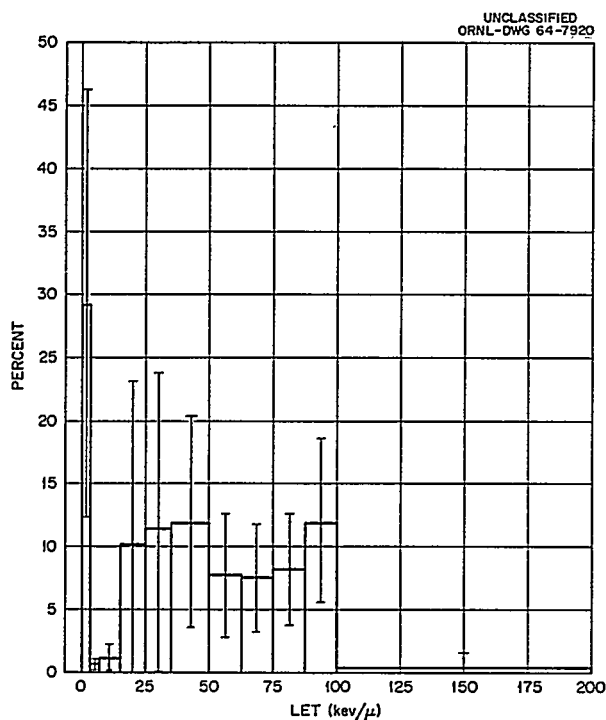


Fig. 13.13. Normalized Distribution of Dose with LET (Box 20, 2.5-Mev Neutron Beam).

of the dose. Note that in these figures the height of the column represents the dose deposit in the particular LET interval rather than the dose per unit LET as in Figs. 13.8–13.10. Similarly, Figs. 13.14–13.17 present the LET distribution of dose in box 17 for neutron energies of 1, 0.1, and 0.005 Mev and for thermal neutrons. The normalized distributions are presented in Figs. 13.18–13.21. A comparison of total dose in the slab as given in NBS Handbook 63¹⁶ with total dose along a diameter parallel to the direction of the incident neutrons is shown for various energies in Fig. 13.22. It is clear that there are significant differences in some of the cases, although the statistical uncertainties of the results are still considerable.

These results indicate that there is a marked variation in the LET distribution of dose as well as in the magnitude of dose within the phantom when it is irradiated by monoenergetic neutrons and that the LET distribution of dose varies markedly with neutron energy. Thus a large mammal irradiated unilaterally experiences a pattern of dose which cannot be represented adequately by a single dose value. Different organs and tissues receive doses which differ widely in magnitude and quality. With effects which depend directly upon the exposure of a

¹⁶Protection Against Neutron Radiation Up to 300 Million Electron Volts, Natl. Bur. Std. (U.S.), Handbook 63, pp. 46–61 (Nov. 22, 1957).

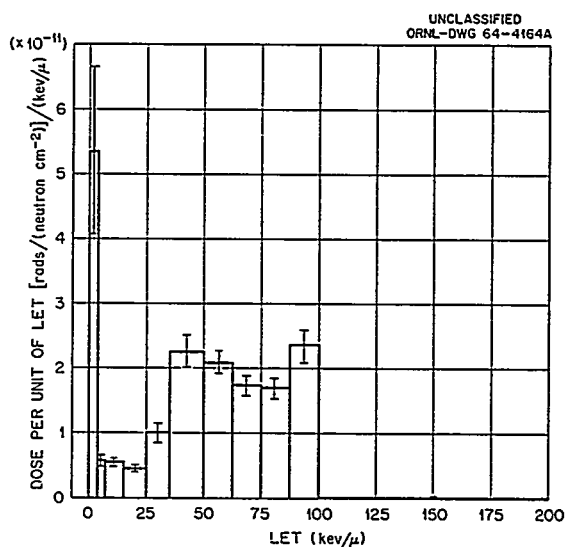


Fig. 13.14. Distribution of Dose with LET (Box 17, 1-Mev Neutron Beam).

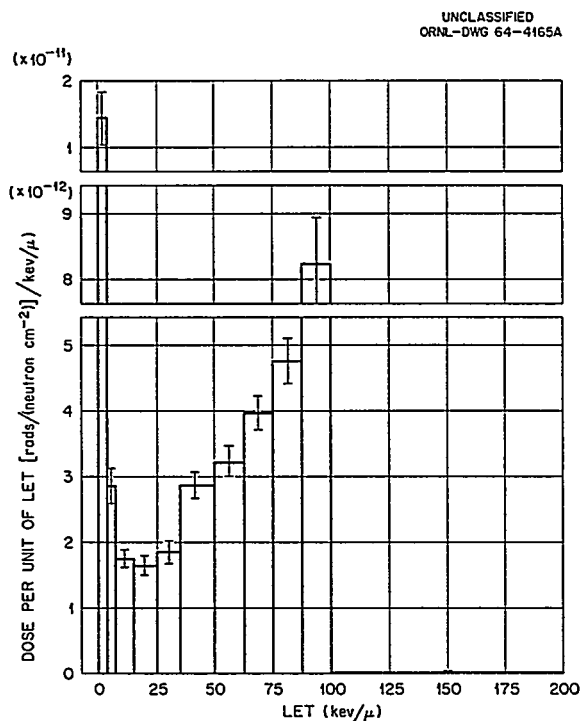


Fig. 13.15. Distribution of Dose with LET (Box 17, 0.1-Mev Neutron Beam).

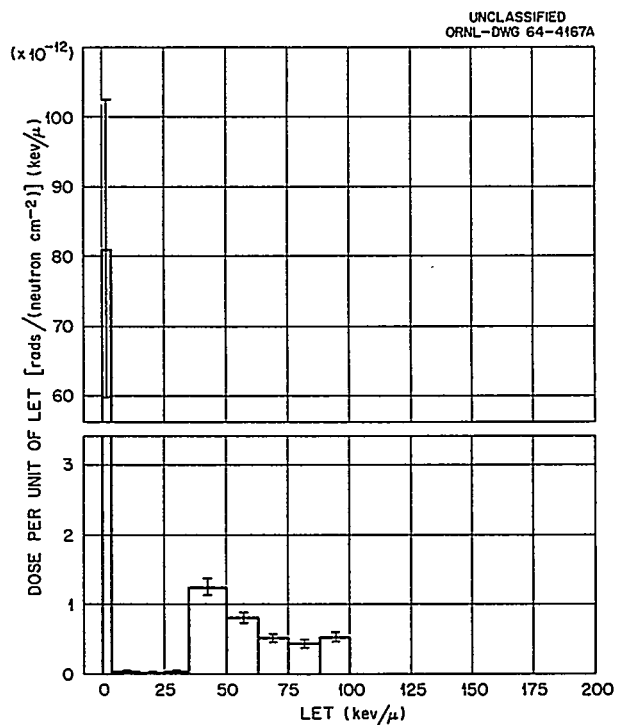


Fig. 13.17. Distribution of Dose with LET (Box 17, Thermal-Neutron Beam).

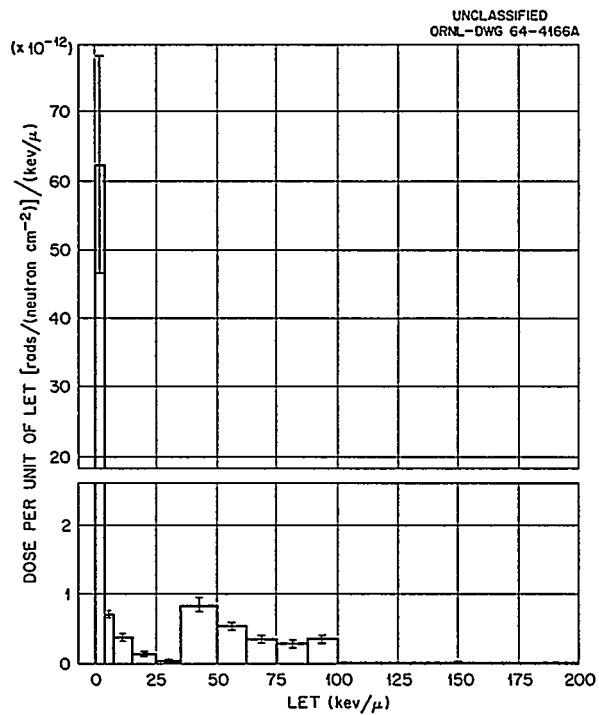


Fig. 13.16. Distribution of Dose with LET (Box 17, 0.005-Mev Neutron Beam).

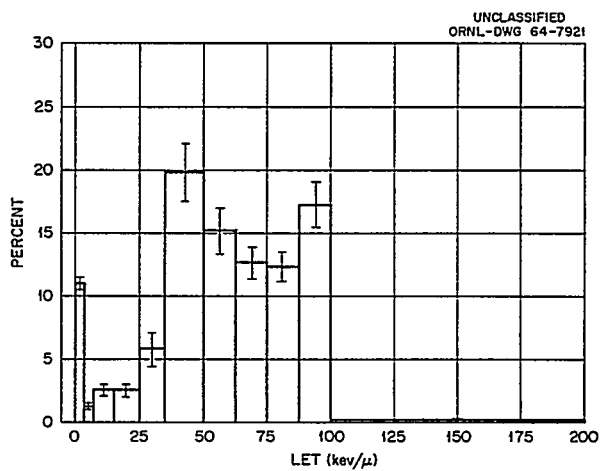


Fig. 13.18. Normalized Distribution of Dose with LET (Box 17, 1.0-Mev Neutron Beam).

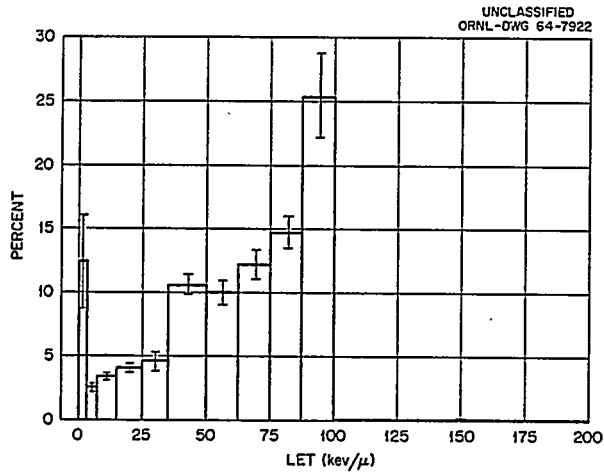


Fig. 13.19. Normalized Distribution of Dose with LET
(Box 17, 0.1-Mev Neutron Beam).

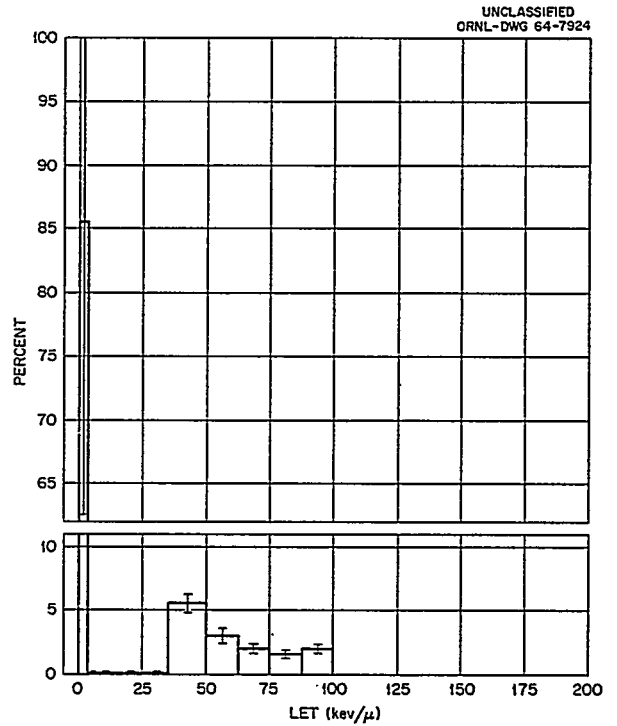


Fig. 13.21. Normalized Distribution of Dose with LET
(Box 17, Thermal-Neutron Beam).

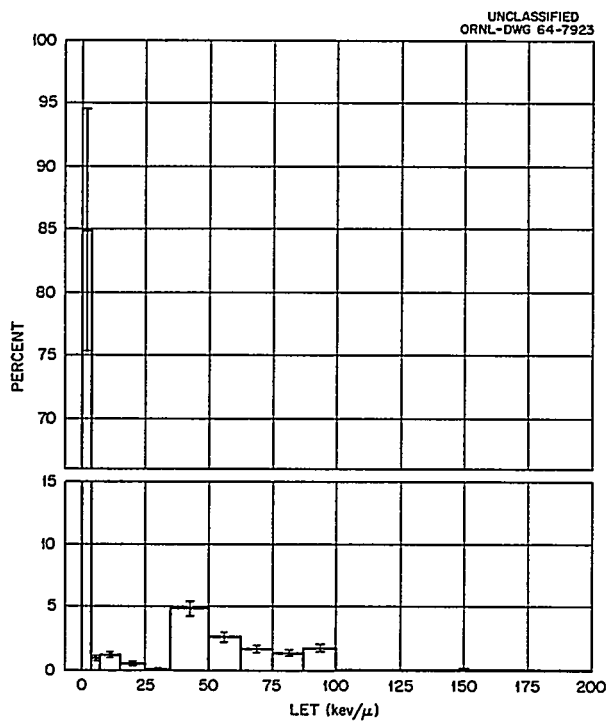


Fig. 13.20. Normalized Distribution of Dose with LET
(Box 17, 0.005-Mev Neutron Beam).

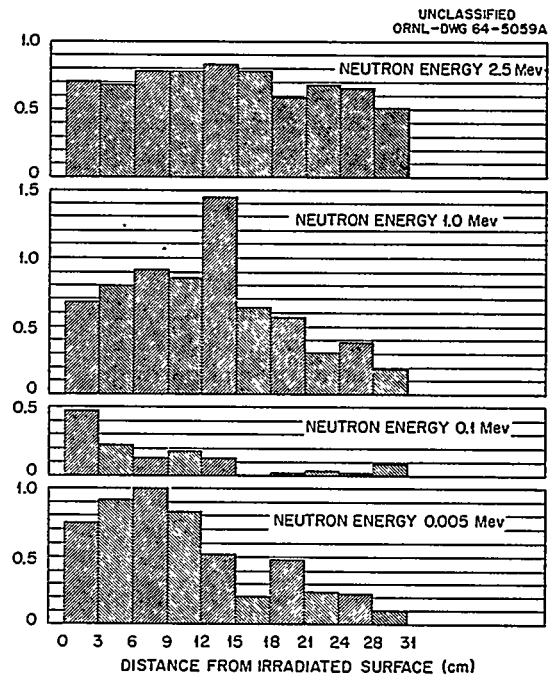


Fig. 13.22. Estimated Ratio of Dose in Cylinder to
Dose in Slab from Monoenergetic, Monodirectional Broad
Beams of Neutrons.

particular organ, the quality and magnitude of the local dose are important. For other effects, such as the depression of white-blood-cell count, a global interpretation might be more appropriate. The radiobiologist or physician concerned with the study or treatment of human exposure to neutrons usually will need the entire pattern of dose to interpret adequately the effects of the radiation. In general, when new types of radiation fields are encountered, as in the exploration of space, consideration of the LET distribution of dose provides the best available guide for predicting the biological effects of exposure.

CHARGED PARTICLE VECTROMETER

A device for measuring the direction and length of the ionization track produced by a charged particle in a gas has been designed. A model of this device, called a "vectrometer," is being assembled and will be tested to determine the operating characteristics and feasibility of the design.

Basically, the device consists of two coplanar sets of parallel wires at right angles to each other; each wire forms the anode of a G-M counter and is located at the center of a cylindrical cavity in a brass plate. Narrow slits in the brass plate in front of the wires allow electrons to enter the G-M tubes and be counted. This rectangular array of G-M counters forms one side of a cubical box representing an ionization chamber.

A field is applied to the ionization chamber in a direction that causes electrons to drift toward the G-M counters, and another potential is applied between the anode wires and the surface of the cavities surrounding the wires. The outputs of all G-M counters in one direction, say the y direction, are paralleled and, separately, all the counters in the x direction are paralleled. If a charged particle entering the chamber produces an ionization track, the secondary electrons are drawn to the collecting array and, in general, will intercept G-M counters in both sets. The x and y components of the ionization track length are determined by the number of counters which fire in each set. If the track is straight, this information appears as a succession of equally spaced pulses at the output of each set of counters, and from the time spread of these pulses the z component of the track length can be determined.

Thus, if the separation between wires is s , and n_x counters fire in the x direction and n_y counters fire in the y direction, and if w is the drift velocity of electrons in the chamber, the x, y, and z components of the track length are given by:

$$x = n_x s,$$

$$y = n_y s,$$

$$z = w T,$$

where T is the total time between the first and last pulse (in either set of counters). The total track length l is then given by:

$$l^2 = x^2 + y^2 + z^2.$$

A typical use for such a vectrometer would be as a neutron spectrometer where, if the chamber is filled with hydrogen, an analysis of the length and direction of proton recoil tracks provides information as to the energy of the incident neutrons. Thus, if neutrons of energy E_0 are incident on the chamber in the x direction, the recoil proton energy is $E_p = E_0 \cos^2 \theta$, where θ is the polar angle of scatter. The track length l is related to the proton energy by $l = kE_p^n$, where k and n are determined from the range-energy relationship. The neutron energy is then given by:

$$E_0 = \frac{(x^2 + y^2 + z^2)^{1/2n}}{k^{1/n} x^2}.$$

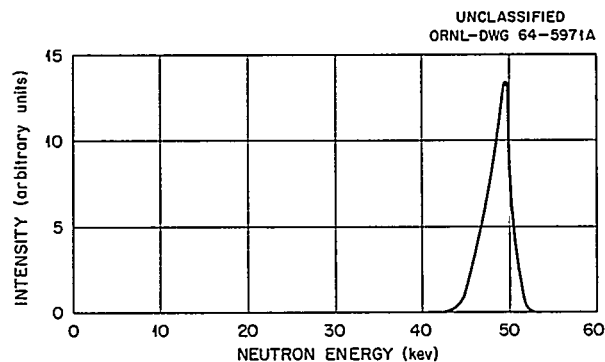


Fig. 13.23. Theoretical Response of Vectrometer to Incident 50-keV Neutrons.

A calculation of the energy resolution to be expected from the vectrometer has been made for the case of monoenergetic neutrons of energy 50 kev, using a slit separation $s = 3.81$ cm and a pressure of 2.5 mm Hg (neglecting diffusion in the ion track) by computer. Although this depends somewhat on the exact point of origin of the track with respect to the counter slits, a typical resolution curve is shown in Fig. 13.23.

OPTICAL BREMSSTRAHLUNG AND TRANSITION RADIATION FROM IRRADIATED MATTER

A semiclassical theory has been used to analyze the process by which light is generated when energetic electrons bombard a semi-infinite dielectric and undergo multiple elastic scatter in its interior. The electrons are taken to be normally incident from vacuum upon a plane surface bounding the dielectric. Parameters characterizing the material are (1) its complex dielectric permittivity $\epsilon(\omega)$ for light of frequency ω , (2) $\sigma(\omega)$, the cross section for elastic scatter of electrons on a single scattering center in the dielectric, and (3) N , the density of scattering centers, which are taken to be randomly distributed throughout the medium. Light generated due to electric polarization induced in the medium (transition radiation) is considered together with that due to acceleration of the electron in collisions with nuclei. The distribution function describing the emitted light includes transition radiation, bremsstrahlung from multiple elastic small-angle electron scattering, and interference between these two kinds of radiation.

Observation of such radiations, together with information on optical constants of the solid, may be used to deduce the mean square scattering angle per unit length for such electrons scattering on the ion cores in the medium. This quantity is not easy to obtain from direct electron scattering experiments, especially at low and intermediate electron energies, and is of importance since it may be used to obtain information on the effective electron-ion interaction in the dielectric. The method may also be of value in plasma diagnostics.

This work will be published in *The Physical Review*.

EXCHANGE CORRECTION TO THE MEAN FREE PATH OF HOT ELECTRONS AND HOLES IN METALS

As part of a program to extend the calculation of the hot electron mean path in a free electron gas to the region of real metal electron densities, contribution of the simplest exchange processes to this mean free path has been evaluated using many-body perturbation theory. The exchange effect has been neglected entirely in previous mean free path calculations, although results appropriate to a high-density system have been used recently as a basis for treatments which emphasize solid state effects and which are intended for application to real densities.^{17,18} We find that the exchange contribution is small compared with the result neglecting exchange in the high-density limit. However, at metallic densities the calculated exchange contribution is comparable with the contribution from the direct process. This is analogous to the results of Gell-Mann and Brueckner on the contribution of exchange to the correlation energy of a free electron gas. The distribution in energy of a carrier after having scattered on an electron gas is quite different at all densities compared with the result neglecting exchange. The energy loss rate and lifetime of a carrier are thus different from the values quoted in the literature.

The angular and energy distributions of the primary excited electron and the secondary electron after a collision have been evaluated. The effect of exchange is found to be very important in determining these quantities.

THE EFFECT OF SURFACE LOSSES IN STOPPING-POWER THEORY

The Bethe-Bloch stopping-power formula was derived assuming that an energetic charged particle interacts with atoms randomly distributed in an infinite medium. The existence of charged particle energy losses of a special type associated

¹⁷J. J. Quinn, *Appl. Phys. Letters* 2, 167 (1963).

¹⁸S. L. Adler, *Phys. Rev.* 130, 1654 (1963).

with the presence of boundaries has been postulated¹⁹ and confirmed experimentally.²⁰ Such surface losses result in a larger total energy loss in a foil of given thickness than one would predict using conventional stopping-power theory. One expects these corrections to stopping power to be small in most practical situations. However, in view of the accuracy with which modern experimental work is carried out in this area ($\sim \pm 1\%$), it is desirable to have quantitative criteria for deciding when the effect is negligible. Also, in certain special experimental situations the effect may not be negligible.

One may employ electromagnetic theory to calculate W , the energy change of a particle having charge Ze and velocity \vec{v} incident normally on a foil of thickness a characterized by a complex dielectric permittivity $\epsilon(\omega)$. One finds that part of W due to the presence of foil surfaces may be written, in the asymptotic limit ($a \rightarrow \infty$), as

$$-\left(\frac{W}{a}\right)_{\text{surface}} = \frac{4(Ze)^2}{\pi a} \int_0^\infty k^3 dk \int_0^\infty \frac{d\omega}{\omega} f(k, \omega),$$

where

$$f(k, \omega) = \text{Im} \left\{ \left(\frac{1}{\nu\epsilon + \nu'} \right) \times \left[\frac{\omega^2}{\epsilon\nu^2} (\epsilon\Lambda_1 - \Lambda_2)^2 - \nu\nu'(\Lambda_1 - \Lambda_2)^2 \right] \right\},$$

where

$$\nu = \sqrt{k^2 - \omega^2/c^2},$$

$$\nu' = \sqrt{k^2 - \epsilon\omega^2/c^2},$$

$$\beta = v/c,$$

$$\Lambda_1 = [k^2 + (\omega^2/v^2)(1 - \beta^2)]^{-1},$$

$$\Lambda_2 = [k^2 + (\omega^2/v^2)(1 - \epsilon\beta^2)]^{-1}.$$

Comparing this with the conventional Bethe-Bloch formula for the energy lost per unit length in the foil, one sees that $-(W/a)_{\text{surface}}$ must become negligible in comparison as $a \rightarrow \infty$. Employing

values of $\epsilon(\omega)$ for various elements taken from the work of Sternheimer on the density effect,²¹ one finds that $-(W/a)_{\text{surface}}$ is less than 0.01 ($-dE/dx$) in most materials in the nonrelativistic limit as long as a is larger than a few hundred angstroms. The effect is largest in those materials in which conduction electrons account for an appreciable fraction of the total oscillator strength. Work is proceeding to evaluate $-(W/a)$ numerically in the case where $\beta \sim 1$.

THE DISPERSION AND DAMPING OF SURFACE PLASMONS

The dispersion of surface plasmons has been considered by Kanazawa²² using the random-phase approximation, and by Ritchie²³ using a hydrodynamical theory of the free electron gas. Recent experimental work by Schmüser²⁴ on the dispersion relation for surface plasmons in a very thin foil has confirmed earlier theoretical work by Ritchie²⁵ and has shown that it is possible to measure such quantities. In view of these developments, surface plasmon dynamics in thick foils has been analyzed using a semiclassical approach which is more rigorous than that used in ref. 23. This approach is equivalent to the use of a Boltzmann-Vlasov equation for the perturbed electron distribution function at a metal surface, assuming that electrons are reflected therefrom in a specular mode and that they constitute a free electron gas.

One finds that the equation which determines the eigenfrequency $\omega(K)$ of a surface plasmon in this approximation is

$$1 + \frac{2}{\pi} \int_0^{\pi/2} \frac{d\theta}{\epsilon(K \sec \theta, \omega)} = 0, \quad (1)$$

where $\epsilon(k, \omega)$ is the longitudinal dielectric constant of the infinite free electron gas and K is the wave vector of the surface plasmon parallel

¹⁹R. H. Ritchie, *Phys. Rev.* 106, 847 (1957).

²⁰C. J. Powell, J. L. Robin, and J. B. Swan, *Phys. Rev.* 110, 657 (1958); C. J. Powell and J. B. Swan, *Phys. Rev.* 115, 869 (1959); C. J. Powell and J. B. Swan, *Phys. Rev.* 116, 81 (1959); and C. J. Powell and J. B. Swan, *Phys. Rev.* 118, 640 (1960).

²¹R. M. Sternheimer, *Phys. Rev.* 88, 851 (1952).

²²H. Kanazawa, *Progr. Theoret. Phys. (Kyoto)* 26, 851 (1961).

²³R. H. Ritchie, *Progr. Theoret. Phys. (Kyoto)* 29, 607 (1963).

²⁴P. Schmüser, *Solid State Commun.* 2, 41 (1964).

²⁵R. H. Ritchie, *Phys. Rev.* 106, 876 (1957).

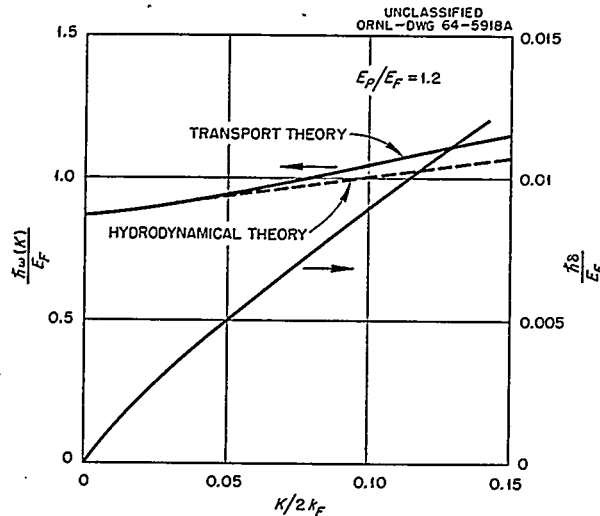


Fig. 13.24. Dispersion and Damping of Surface Plasmons. The solid (nearly horizontal) curve shows the relation between the frequency of a surface plasmon and its wave number, while the dotted line gives this relation obtained from hydrodynamic theory. The remaining curve shows the damping frequency of this surface plasmon as a function of wave number. All calculations were made for an electronic density such that $E_P/E_F = 1.2$.

with the bounding plane. Note that ω in general possesses both a real and an imaginary part, the latter corresponding to damping of the surface plasmon.

Figure 13.24 shows numerical results for the solution of Eq. 1. Plotted are values of $\hbar\omega(K)/E_F$. Here E_P is the volume plasmon energy and E_F is the energy of the free electron gas, which is taken to be at the absolute zero of temperature. The quantity k_F , the Fermi wave vector, is given by $\sqrt{2mE_F/\hbar}$. On the same graph is shown the prediction of the hydrodynamical theory for the relation $\omega(K)$. One sees that for $K \sim 0$ agreement is good but there are differences as K increases. Also shown is $\delta(K)$, the imaginary part of $\omega(K)$, as a function of $K/2k_F$. The hydrodynamical theory predicts zero damping of surface plasmons.

OPTICAL PROPERTIES OF METALS

In connection with work done by the Experimental Radiation Physics Group, equations have been

derived relating reflectivity, transmittance, and absorption to the optical constants of isotropic materials. Computer codes have been written to calculate these quantities and to evaluate optical constants from measured reflectivities.

This approach is being extended to anisotropic media. Computer codes are being written to evaluate optical constants for such media from measured quantities. Also, studies are being made to determine the possibility of evaluating optical properties from measured transition radiation.

MULTIPLE INSTABILITY IN A PLASMA-BEAM SYSTEM

A "multiple instability" in a plasma-beam system occurs when several waves having different frequencies and aligned in the same direction are simultaneously excited. Such an instability is investigated for a system in which a cold and uniform ionized medium immersed in a static magnetic field B_0 interacts with a beam of protons aligned in the direction of B_0 . The excited waves considered in this investigation are transverse and move in the direction parallel to B_0 . The multiple instability occurs when the velocity βc (c is the velocity of light) of the proton beam satisfies the inequality $\beta_a < \beta < \beta_b$, where β_a and β_b depend on the plasma parameters A and α . The parameter $A = \omega_i/\Omega_i$, where $\omega_i = (4\pi ne^2/M_i)^{1/2}$, Ω_i is the ion gyrofrequency, e is the electronic charge, n is the plasma density, M_i is the mass of a plasma ion, $\alpha = M_i/M_p$, and M_p is the mass of a proton. The relationship between β_a and β_b and the parameter A is shown in Fig. 13.25 for $\alpha = 1, 2, 4$, and 32 , which correspond to stationary plasma ions being protons, deuterons, helium ions, and molecular oxygen ions respectively.

The typical qualitative behavior of the system for a fixed value of A and α is given in Fig. 13.26, which shows the frequency of the excited waves as a function of the beam velocity β . Fig. 13.27 shows the typical qualitative behavior of the growth rate, $|\text{Im } \delta|$, of the excited wave for the same plasma-beam system shown in Fig. 13.26. It can be seen from Fig. 13.26 that for $\beta < \beta_a$ or $\beta > \beta_b$ the instability is "single." In the region of a multiple instability, if the frequencies of

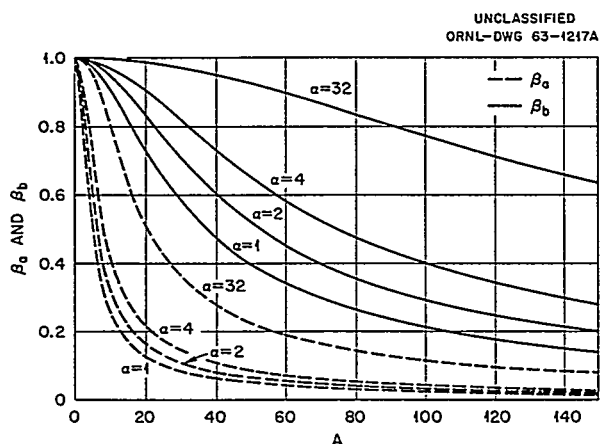


Fig. 13.25. Upper and Lower Limits (β_b and β_a respectively) of Beam Velocity for a Multiple Instability as a Function of A for Various Values of α .

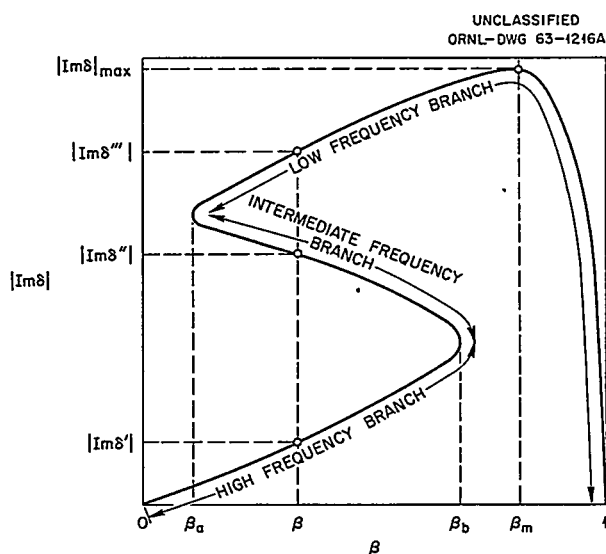


Fig. 13.27. Qualitative Relationship Between the Frequency and Beam Velocity for a Typical Plasma-Beam System.

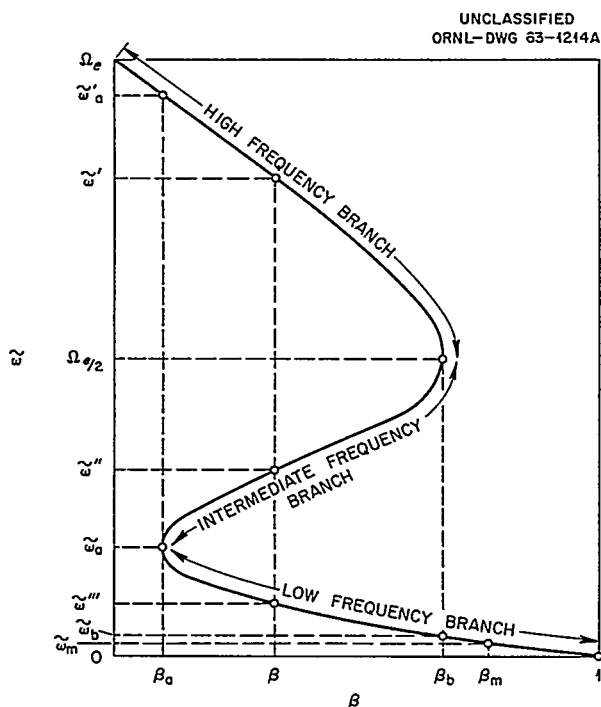


Fig. 13.26. Qualitative Relationship Between the Growth Rate and Beam Velocity for a Typical Plasma-Beam System.

the excited waves satisfy the inequality $\omega' > \omega'' > \omega'''$, the corresponding growth rates, designated $|Im \delta'|$, $|Im \delta''|$, and $|Im \delta'''|$, respectively, satisfy the inequality $|Im \delta'| < |Im \delta''| < |Im \delta'''|$. Thus, the wave having the lowest frequency has the highest rate of growth and represents the dominant instability. In the region of single instability for $\beta < \beta_a$, the frequency of the excited wave is in the neighborhood of electron gyrofrequency. If $\beta > \beta_b$, the frequency is relatively low, usually much below the gyrofrequency of plasma ions.

INTERACTION OF A PLASMA WITH A HELICAL ELECTRON BEAM

This investigation deals with the interaction of a stationary plasma and an electron beam in the presence of a static magnetic field B_0 . It is assumed that the electrons in the beam have helical trajectories coaxial with B_0 . Each of these electrons has a velocity component $v_{||} = \beta_{||}c$ (c is the velocity of light) in the direction of B_0 and a velocity component $v_{\perp} = \beta_{\perp}c$ in the direction perpendicular to B_0 . The beam formed by these electrons is designated as "helical" and it moves with velocity $v_{||}$ (or $\beta_{||}$) in the direction parallel to that of B_0 .

The interaction of a plasma with a helical beam is of relatively frequent occurrence in astrophysics, geophysics, thermonuclear research, etc. In the early stages of the development of radio astronomy it was suggested by Kiepenheuer²⁶ that the nonthermal radio emissions from the sun are due to electron beams produced at the sunspots and directed at an arbitrary angle to the magnetic field. These helical beams spiral out of the sunspots into the surrounding plasma which forms the solar corona. Similar types of interactions occur under terrestrial conditions in the outer regions of the ionosphere (exosphere). They are caused by helical beams which comprise electrons and protons gyrating around the earth's magnetic field and are believed to produce auroral effects. These beams interact with the plasma in the exosphere and generate very-low-frequency electromagnetic radiations which are detected at the earth's surface in the form of continuous noise and whistlers.²⁷

The plasma-beam system is examined for instabilities which result in growing transverse waves aligned in a direction parallel to that of B_0 . Two classifications of instabilities are introduced. The first classification is based on the comparison of excited waves in the plasma-beam system with stationary waves which may be propagated through the undisturbed plasma (in the absence of the beam). This classification deals with two types of instabilities which will be designated, respectively, as a P instability and a B instability. In a P instability the growing waves (P waves) result from the excitation of corresponding stationary waves in an undisturbed plasma. If the intensity of the beam is sufficiently small, the frequency of an excited P wave differs very little from the frequency of a corresponding stationary wave in an undisturbed plasma. If the beam is linear, that is, if the electrons in the beam have trajectories aligned along the direction parallel to that of B_0 ($B_1 = 0$), there is only one type²⁸ of instability (P instability). On the other hand, if the beam is helical ($B_1 \neq 0$), there is an additional instability (B instability) which gives

rise to excited B waves. A B instability occupies a relatively wide frequency range in the neighborhood of a P instability and represents a continuation of the P instability along the frequency axis.

If the intensity of the helical beam is sufficiently small, the P instability is "strong" and the B instability is "weak," that is, the rate of growth of P waves is relatively large, whereas the rate of growth of B waves is relatively small.²⁹

The second classification of plasma-beam instabilities is based on the relationship between the velocity of the beam and the phase velocity of the excited waves. In accordance with the second classification, the instabilities will be labeled as "superluminous," "subluminous," or "counterstreaming." In a superluminous instability the velocity of the beam exceeds the phase velocity of the excited wave; in a subluminous instability it is less than the phase velocity of the excited wave; and in both cases the direction in which the excited wave moves is the same as that of the beam. In a counterstreaming instability, the excited wave moves in the direction opposite to that of the beam.

It is found in this investigation that a P instability is always multiple, that is, there are either two or four excited transverse waves having different frequencies which are aligned in the direction of the beam. If there are two excited waves, one represents a superluminous and the other a counterstreaming instability. If there are four excited waves, one represents a superluminous instability, another represents a counterstreaming instability, and the two remaining waves represent a subluminous instability.

A multiple P instability occurs only if the electron beam is helical; that is, a multiple instability does not occur if the electron beam is linear.

A discussion is given on the relative rates of growth of the excited waves representing a multiple P instability. The study of the relative rates of growth is useful in ascertaining which one of the multiply occurring instabilities is "dominant," that is, has the largest rate of growth.

It is also found that subluminous and superluminous instabilities are convective, whereas counterstreaming instabilities are nonconvective.

²⁶K. O. Kiepenheuer, *Nature* 158, 340 (1956).

²⁷L. R. O. Storey, *Phil. Trans. Roy. Soc. (London)* A246, 113 (1953).

²⁸Jacob Neufeld and Harvel Wright, *Phys. Rev.* 129, 1489 (1963).

²⁹Jacob Neufeld, *Phys. Rev.* 124, 1 (1961).

PLASMA-BEAM INSTABILITY IN THE HARTREE-APPLETON APPROXIMATION

The interaction of an ion beam of small intensity moving with velocity $c\beta$ (where c is the velocity of light) through a stationary plasma is investigated under the assumption that the beam and the waves resulting from the interaction are aligned along the direction of an impressed static magnetic field and that the frequencies of the excited waves are sufficiently high so that the motion of the ions perturbed by these waves can be neglected. It is found that the beam is capable of exciting waves only if $\beta < \beta_{max}$, where $\beta_{max} = [\eta(\eta + 4A^2)]^{1/2}$ (η is the ion-to-electron-mass ratio, and $A^2 = \eta\omega_e^2/\Omega_e^2$, where ω_e is the plasma frequency and Ω_e is the electron gyrofrequency). For each value of $\beta < \beta_{max}$, there are two excited waves having frequencies $\omega = \Omega_e(1 + R)/2$ and $\omega = \Omega_e(1 - R)/2$, where $R = [1 - 4\beta^2 A^2/(1 - \beta^2)\eta]^{1/2}$. The rates of growth $|\text{Im } \delta_I|$ and $|\text{Im } \delta_{II}|$ corresponding to the frequencies ω_I and ω_{II} are

$$|\text{Im } \delta_I| = \sigma^{1/2} \omega_e (1 - \beta^2) \times$$

$$(1 - R)/[2\eta^{1/2} A(1 - R\beta^2)^{1/2}]$$

and

$$|\text{Im } \delta_{II}| = \sigma^{1/2} \omega_e (1 - \beta^2) \times$$

$$(1 + R)/[2\eta^{1/2} A(1 + R\beta^2)^{1/2}]$$

respectively. Certain characteristic features of the above instabilities are investigated for a "relatively dense" plasma ($A > 1$) and for a "rarefied" plasma ($A \leq 1$). In a "relatively dense" plasma for which $A \ll \eta/4$, a low-velocity ion beam characterized by $(1/A) \ll \beta^2 \ll 1$ excites simultaneously an electron-cyclotron wave and a low-frequency wave similar to the one associated with whistling atmospherics. For sufficiently low velocities of the beam, the rate of growth of the low-frequency wave is considerably higher than the rate of growth of the electron cyclotron wave.

INTERACTION OF A STATIONARY PLASMA WITH AN ELECTRON BEAM

A plasma-beam system is investigated in which an electron beam of small intensity moving with velocity βc (c is the velocity of light) interacts with a cold plasma immersed in a magnetic field. It is assumed that the beam and the excited wave resulting from the interaction are aligned along the direction of the magnetic field and that $(1 - \beta^2) \gg 1/\eta$, where η is the ion to electron mass ratio. It is found that the frequency $|\tilde{\omega}|$ of the excited wave is $|\tilde{\omega}| = \Omega_i[1 - (1 + 4R)^{1/2}]/2R$, where $R = A^2\beta^2/\eta^2(1 - \beta^2)$, $A^2 = \eta\omega_e^2/\Omega_e^2$, ω_e is the plasma frequency, and Ω_i and Ω_e represent, respectively, the ion and the electron gyrofrequency. The expression showing the explicit relationship between the growth rate $|\text{Im } \delta|$ of an excited wave and the velocity β of the beam is obtained as follows:

$$|\text{Im } \delta| = \sigma^{1/2} \omega_i \beta U^{1/2},$$

$$U = \frac{1}{R} \left[1 + \frac{2R^2}{1 + 4R - (1 + 2R)(1 + 4R)^{1/2}} \right],$$

$\omega_i = \omega_e/\eta$, and σ is the fractional part of the plasma density represented by the density of the beam. It is shown that $|\text{Im } \delta|$ attains a maximum for an appropriate value $\beta = \beta_m$ and that β_m increases with A/η . For many typical plasmas one has $A/\eta \ll 1$, and in such a case the maximum is attained for beam velocities β_m in the relativistic range. One obtains then $|\text{Im } \delta|_{max} \sim 0.4 \sigma^{1/2} A\Omega_i$, corresponding to a frequency $|\tilde{\omega}| \sim 0.59 \Omega_i$. When $R \ll 1$, the electron beam excites ion cyclotron waves, and in such a case $|\tilde{\omega}| = \Omega_i(1 - R)$, that is, the quantity R represents the departure in frequency from the condition of gyroresonance. The relationship between the rate of growth of an ion cyclotron wave and the beam velocity can be expressed as $|\text{Im } \delta| = \sqrt{2} \sigma^{1/2} A\Omega_i\beta$.

14. Experimental Radiation Physics

R. D. Birkhoff

E. T. Arakawa

T. E. Bortner¹

Ada E. Carter

J. G. Carter

L. G. Christophorou

R. N. Compton²

J. T. Cox

F. J. Davis

L. C. Emerson

D. J. Erickson³R. E. Glick¹P. M. Griffin⁴

J. A. Harter

R. J. Herickhoff²

H. H. Hubbell, Jr.

R. H. Huebner^{3,5}

G. S. Hurst

A. G. Kenerly⁶

W. J. McConnell

J. E. Parks¹

Devon Pittman

P. W. Reinhardt

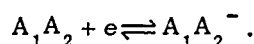
A. L. Roecklein⁵J. L. Stanford²J. A. Thompson³

E. B. Wagner

ELECTRON CAPTURE IN ORGANIC MOLECULES

The interaction of low-energy electrons with organic molecules has been investigated, using the swarm method previously described by Bortner and Hurst⁷ (with a modified parallel plate ionization chamber). Control of the energy distribution in the electron swarm can now be achieved over an interesting range of electron energies. Figure 14.1 shows the effect of the carrier gas and of E/P on the distribution of electron energies. This control of electron energies aids in the discrimination between the different processes by which free electrons are captured to molecules in the gas phase. Three such processes can be distinguished.

1. Temporary nondissociative electron capture,



The lifetimes of the temporary ions are determined by internal rearrangement or by molecular collisions that involve energy transfers of the order of kT . If an equilibrium is reached, the ion density, n_i/n_e , is determined by the electron affinity, E_0 , of the molecule,

$$n_i/n_e = \text{const } e^{E_0/kT}.$$

¹Consultant.

²Oak Ridge Graduate Fellow.

³Summer employee.

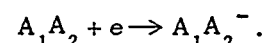
⁴Physics Division.

⁵AEC Health Physics Fellow.

⁶Instrumentation and Controls Division.

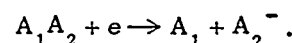
⁷T. E. Bortner and G. S. Hurst, *Health Phys.* 1, 39 (1958).

2. Permanent nondissociative electron capture,



The excited negative ion has to be stabilized by collisions. The capture cross section, $\sigma_c(\epsilon)$, is determined as a function of electron energy.

3. Dissociative electron capture,



No collisional stabilization is required, and the only effect of the carrier gas is to determine the distribution function, $f(\epsilon, E/P)$.

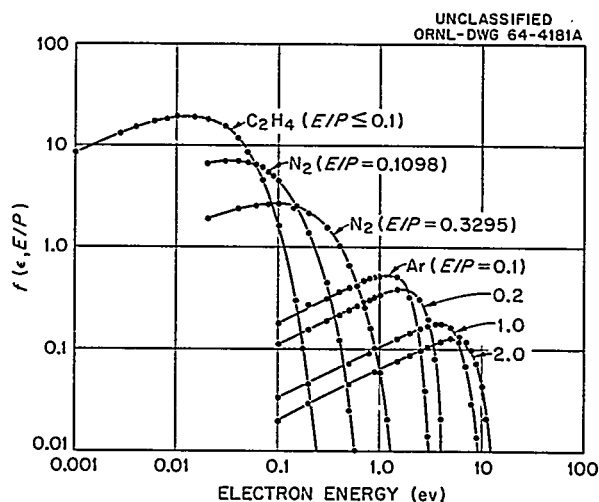

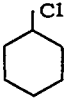
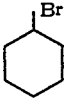
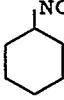
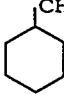
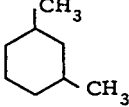
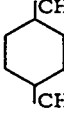
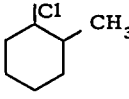


Fig. 14.1. Energy Distribution in Electron Swarms for Different Carrier Gases and E/P .

Table 14.1. Electron Capture in Organic Molecules

Molecule	Formula	Capture at Low E/p^a	Dissociative Electron Capture	$\alpha(E/P) \times w(E/P)$ (for low E/P) [(mm Hg) $^{-1}$ μ sec $^{-1}$]	ϵ_1 (for dissociative electron capture) (ev)	$\int_0^\infty \sigma_c(\epsilon) d\epsilon$ (for dissociative electron capture) (cm 2 ev)
Benzene		Yes	No	4×10^{-3}		
Chlorobenzene		Yes	Yes	9×10^{-2}	0.76	1.4×10^{-17}
Bromobenzene		Yes	Yes	38×10^{-2}	0.7	5.7×10^{-17}
Nitrobenzene		Yes	?	Very high, >15	(~0.0) ?	Very high ?
Toluene		Yes	Yes	6×10^{-3}	0.75	1.4×10^{-20}
<i>m</i> -Xylene		Yes	No	Very small		
<i>p</i> -Xylene		Yes	No	Very small		
<i>o</i> -Chlorotoluene		Yes	Yes	$\sim 10 \times 10^{-2}$	~ 1.4	$\sim 3.5 \times 10^{-17}$

^aNear thermal energy.

Dissociative Electron Capture by Benzene Derivatives

Dissociative electron capture by some benzene derivatives — chlorobenzene (C_6H_5Cl), bromobenzene (C_6H_5Br), toluene ($C_6H_5CH_3$), *o*-chlorotoluene ($C_6H_4ClCH_3$) — has been observed. From the experimental data the attachment coefficient, $\alpha(E/P)$ (the probability of capture per centimeter traveled in the field direction per torr of the sample gas), has been calculated. On the assumption that the capture cross section (for dissociation) peaks strongly at a particular energy, ϵ_1 , the energy-integrated cross section,

$$\int_0^\infty \sigma_c(\epsilon) d\epsilon,$$

was obtained. Values of

$$\int_0^\infty \sigma_c(\epsilon) d\epsilon$$

and ϵ_1 for the above compounds are given in Table 14.1. When C_6H_5Cl and C_6H_5Br were studied with a Bendix negative ion time-of-flight mass spectrometer, Cl^- and Br^- were found as products of the dissociative electron capture.

The capture cross section for nitrobenzene ($C_6H_5NO_2$) is not found to peak at a particular energy, although electrons are expected to be captured by a dissociative process with NO_2^- as a product. This, most probably, is because NO_2 has a high value for E_0 and even thermal electrons can dissociate $C_6H_5NO_2$.

No dissociative electron capture has been observed for *m*-xylene and *p*-xylene.

Nondissociative Electron Capture by Organic Molecules

Using ethylene as a carrier gas and restricting ourselves to low E/P 's, we were able to have an electron swarm with pure thermal energies (Fig. 14.1). Benzene, chlorobenzene, bromobenzene, toluene, *m*-xylene, *p*-xylene, *o*-chlorotoluene, and naphthalene were studied in mixtures with ethylene, and in all cases a small electron capture was observed at low E/P . Figure 14.2 shows the small decrease in pulse height due to thermal electron capture in mixtures of toluene-ethylene. The product $\alpha(E/P) \times w(E/P)$, where $w(E/P)$ is the drift velocity, which gives the fraction of

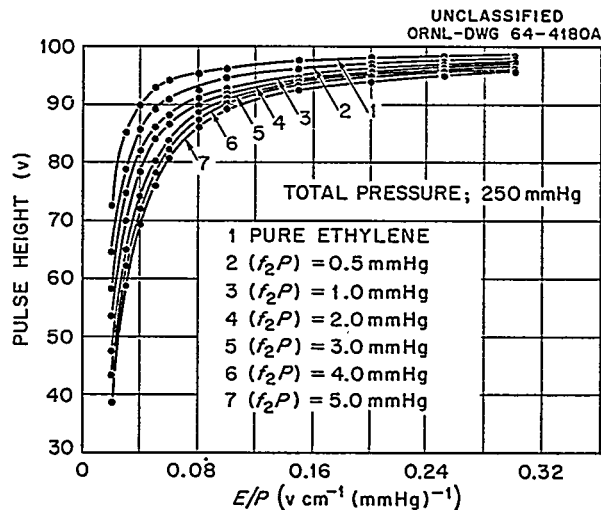


Fig. 14.2. Toluene in Ethylene.

electrons removed by capture per microsecond from a swarm in ethylene per torr of the sample gas, is given in Table 14.1.

Our results indicate that a small nondissociative thermal electron capture may be a general phenomenon in organic molecules. Further information is required to determine whether these negative ions are stable or temporary.

Electron Capture by Compounds of Biological Interest

By applying the swarm method to the study of the interaction of low-energy electrons with organic molecules, our attention is focused on molecules of biological interest. The ability of a molecule to capture thermal electrons to form temporary or stable negative ions is a measure of its electron transport properties, which are considered to play an important role in the biological activity of molecules. Since we are able to discriminate between the different capture processes and to control the energy distribution in the electron swarm, we hope to be able to give a quantitative answer to the electron capture ability of organic molecules and to test the idea that various characterizations of electron capture are related to specific biological function.

ELECTRON TIME-OF-FLIGHT STUDIES (GEIGER-MUELLER DETECTOR)

As previously mentioned, some difficulty has been experienced in measuring electron diffusion coefficients with the electron time-of-flight apparatus in which a Geiger-Mueller counter is used for a detector.⁸⁻¹⁰ Most of the difficulty has been attributed to error fluctuations in instrumentation and a method of taking these errors into account has been worked out.

If $E(t)$ represents the distribution of the time of arrival of the electrons at the detector hole, and if $T_0(t)$ represents the error fluctuations, it can be shown that, in attempting to measure $E(t)$, actually a convolution integral of the two functions, $E'(\tau)$, is measured, that is,

$$E'(\tau) = \int_0^T E(t) T_0(\tau - t) dt.$$

The problem of measuring $T_0(t)$ was resolved by finding a way to supply electrons at the detector hole at time zero, that is, electrons with zero drift time. The method employed made use of reflected ultraviolet light to the inside of the detector where photoelectrons were created. This then simulated electrons with zero drift time in the reaction region.

An analytical expression for T_0 was neither assumed nor sought, but the data were used in numerical form to integrate the function $E'(\tau)$ in making a least-squares fitting of the data to this function.

Data have been taken using C_2H_4 at E/P 's where the half-width of $E(t)$ is small and the half-widths of $T_0(t)$ and $E'(\tau)$ are comparable. Preliminary results indicate that the main error in determining the electron diffusion coefficient was in fact due to instrument fluctuations, and that the present method should substantially reduce these errors.

An experiment is planned to verify that the detecting of single electrons using a Geiger-Mueller counter in the time-of-flight technique follows Poisson statistics. If the instrumentation error is negligibly small, it can be shown that the measured

electron time-of-flight distribution $E''(t)$ is given by

$$E''(t) = E(t) e^{-\int_0^t E(\tau) d\tau}.$$

In this equation $E''(t)$ differs from $E(t)$ due to counts lost during counter dead time, which is assumed to be greater than the transport time spread. Verification of the last equation will provide a reliable basis for making corrections for distortion due to counter losses.

This more accurate time-of-flight method is being applied to the study of electron transport in mixtures of ethylene and H_2O in order to further elucidate the interesting idea previously reported of long-duration collisions with H_2O .

ELECTRON TIME-OF-FLIGHT TECHNIQUES

Construction of a new electron time-of-flight apparatus, described previously,⁹ has been completed, and the testing and evaluation are well advanced. The apparatus, as shown in Fig. 14.3, has been tested by first studying the performance of the individual major components of the system and then examining their functioning as a part of the complete apparatus comprised of (1) the overall vacuum system, (2) the electron lens, and (3) the electron detection system.

The vacuum system was tested by flowing nitrogen gas through a leak valve into the reaction chamber so as to allow different equilibrium pressures to be attained in the reaction chamber, and then the resultant pressures in the first and second differential pumping stages were monitored. The results of these tests are shown in Table 14.2.

The data indicate that the vacuum is satisfactory for the electron multiplier with pressure up to 10 torr in the reaction chamber, but that for a pressure of 5 torr in the reaction chamber the pressure in the first differential pumping stage becomes somewhat marginal.

Initial testing of the electron lens was carried out in a small test vacuum chamber which had a large side window to allow the viewing of a phosphorescent screen. A tungsten filament was used to generate electrons, and both a Faraday cup and a phosphorescent screen were used to evaluate the optimum parameters and quality of focusing. Both three- and four-element electrostatic quadrupole

⁸R. D. Birkhoff et al., *Health Phys. Div. Ann. Progr. Rept. July 31, 1962*, ORNL-3347, p. 81.

⁹R. D. Birkhoff et al., *Health Phys. Div. Ann. Progr. Rept. June 30, 1963*, ORNL-3492, p. 135.

¹⁰G. S. Hurst et al., *J. Chem. Phys.* 39, 1341 (1963).

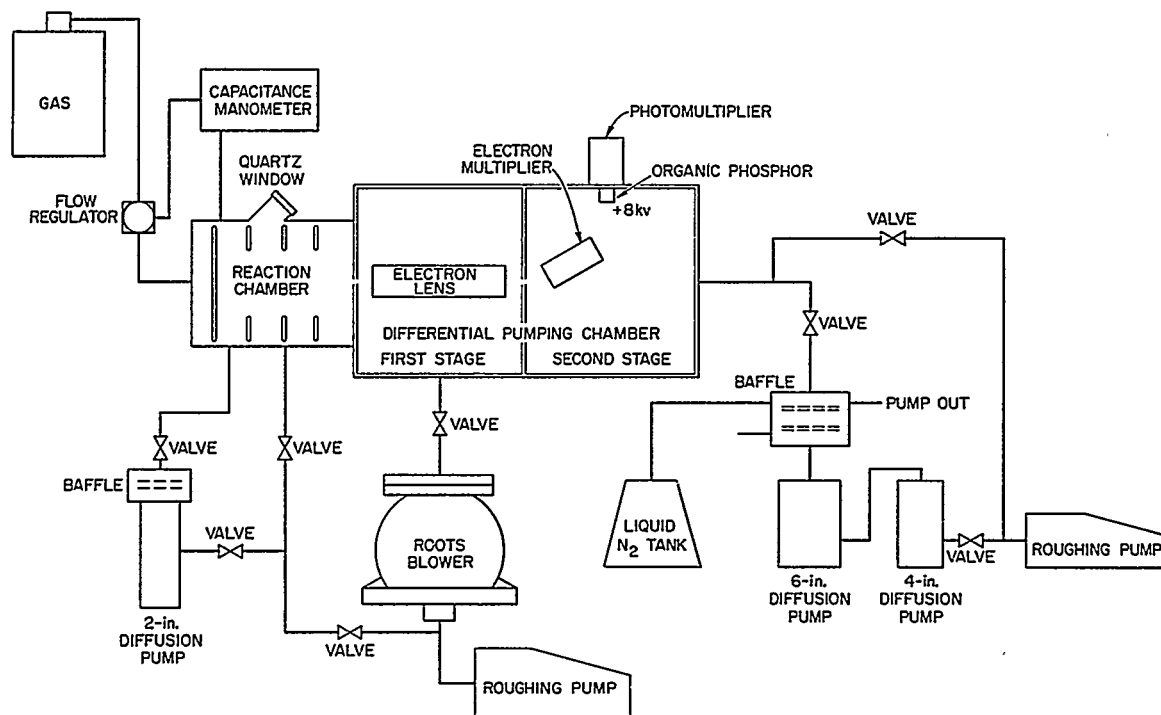


Fig. 14.3. Schematic Diagram of Electron Time-of-Flight Apparatus.

lenses were evaluated, and a three-element lens based on design criteria as described by Enge¹¹ appeared to be the most satisfactory. With this lens a beam of less than 1 mm diameter was observed on the phosphorescent screen placed at the image focal distance.

Three methods of electron detection are being considered. The first simply uses an electron multiplier with an amplifier to count the single electrons. Using a similar scheme, Allen¹² claims a 100% counting efficiency for electrons of 500-ev energy. The second method, which has not been tried, employs an arrangement which accelerates the electrons to a 30-kv potential, and the electrons are detected by a thin plastic scintillator coupled to a photomultiplier with a light pipe. The third method is basically a combination of the first two methods and is described in ref. 9.

An RCA model C7185J 14-stage copper-beryllium-dynode, open-window electron multiplier is being

used at present for the electron detection. Electron time-of-flight spectra have been measured with nitrogen. However, sufficient data have not been collected and analyzed to allow a comprehensive appraisal of the experiment.

Table 14.2. Pressure in First and Second Differential Stages as a Function of Gas Pressure in the Reaction Chamber

Pressure in Reaction Chamber (torr)	Pressure in First Differential Stage (torr)	Pressure in Second Differential Stage (torr)
1	1×10^{-3}	6×10^{-7}
2	2×10^{-3}	2×10^{-6}
5	4.5×10^{-3}	2.4×10^{-6}
10	9×10^{-3}	3.4×10^{-6}

¹¹H. A. Enge, *Rev. Sci. Instr.* 32, 662 (1961).

¹²J. S. Allen, *Rev. Sci. Instr.* 18, 739 (1947).

OSCILLATOR STRENGTH MEASUREMENTS IN THE VACUUM ULTRAVIOLET REGION

In collaboration with the Institute of Molecular Biophysics, Florida State University, a new method has been found for determination of the oscillator strengths of electronic transitions in the vacuum ultraviolet region. A spark source emitting photons over a continuous range of frequencies provides a pulse of light which illuminates gas in a windowless absorption cell. The gas is pulsed into the absorption cell, and the light pulse is time correlated with the pressure pulse in such a manner that the light passes through when no gas has diffused through the thin slits on either side of the cell.

The pressure pulse¹³ (pressure as a function of time) can be shown to be

$$P(t) = \frac{P_0}{[(V + v)/v] - (c'/c)} \left\{ e^{-c't/V} - e^{-[c(V + v)/vV]t} \right\},$$

where the volumes V and v refer to the volume of the absorption cell and the volume of a small supply cell respectively; c and c' are the input and output conductances respectively. Based on this equation and assuming purely viscous flow, it may be seen that for a typical input conductance c the pressure P will reach a maximum in a few milliseconds. For a typical spectrometer slit, whose dimensions determine c' (e.g., 50- μ separation and 1-cm length), P will drop by 1% in 15 msec. Thus, it is quite convenient to pulse a light source at a time when the pressure in the cell is known and is at the maximum. The cycle, that is, pressure charging followed with a light pulse, can be repeated each 30 sec and the usual uncertainties in pressure associated with differential pumping are avoided. The pulse light source showing the most promise of providing a continuum in the vacuum ultraviolet region is a "sliding spark discharge" and, fortunately, requires a discharge in a vacuum. Such a source has been constructed from information in the literature¹⁴ and with suggestions from G. L. Weissler (University of Southern California). The source gives an

"apparent continuum" over at least the range from 500 to 2000 Å and gives an intense pulse of light of about 3- μ sec duration. Electronic circuits for controlling the pressure and light pulses have been completed. A code has been written which will convert film blackening as a function of frequency into oscillator strength at various frequencies. Work is in progress to determine the oscillator strengths for the argon atoms in which use is made of a vacuum ultraviolet monochromator of 1-m focal length.

LIFETIMES OF NEGATIVE IONS

The interaction of low-energy electrons with many molecules is known to produce temporary negative ions. Unimolecular electron capture into a temporary negative ion state takes place in such a manner that the excess kinetic energy of the electron is distributed among the several modes of vibration and/or rotation of the molecule. This would conceivably allow the negative ion intermediate to exist in an excited state for a time which may be long compared with the vibration time before the energy could be concentrated in a mode which would result in the ejection of the electron. An approximate equation relating the lifetime of a negative ion intermediate to the number of internal degrees of freedom (N), the electron affinity (E_B), and the actual energy of the complex (E) has been given by Burton and Magee¹⁵ to be

$$\tau = 10^{-13} (1 - E_B/E)^{1-N}.$$

The range of lifetimes for temporary negative ions may range from approximately 10^{-13} sec for a diatomic molecule to greater than 10^{-6} sec for many of the perfluorocarbon molecules. However, despite this wide range of times, temporary negative ion lifetimes have never been measured directly.

An experiment is being developed which will determine the lifetimes of short-lived negative ions produced by unimolecular electron capture. A technique, shown in Fig. 14.4, is designed to determine lifetimes from 10^{-9} to 10^{-6} sec and will be applied to the study of electron capture

¹³Based on calculations of C. E. Normand, consultant not under subcontract.

¹⁴J. Romand, *J. Quant. Spectry. Radiative Transfer* 2, 691 (1962).

¹⁵M. Burton and J. L. Magee, *J. Phys. Chem.* 56, 842 (1952).

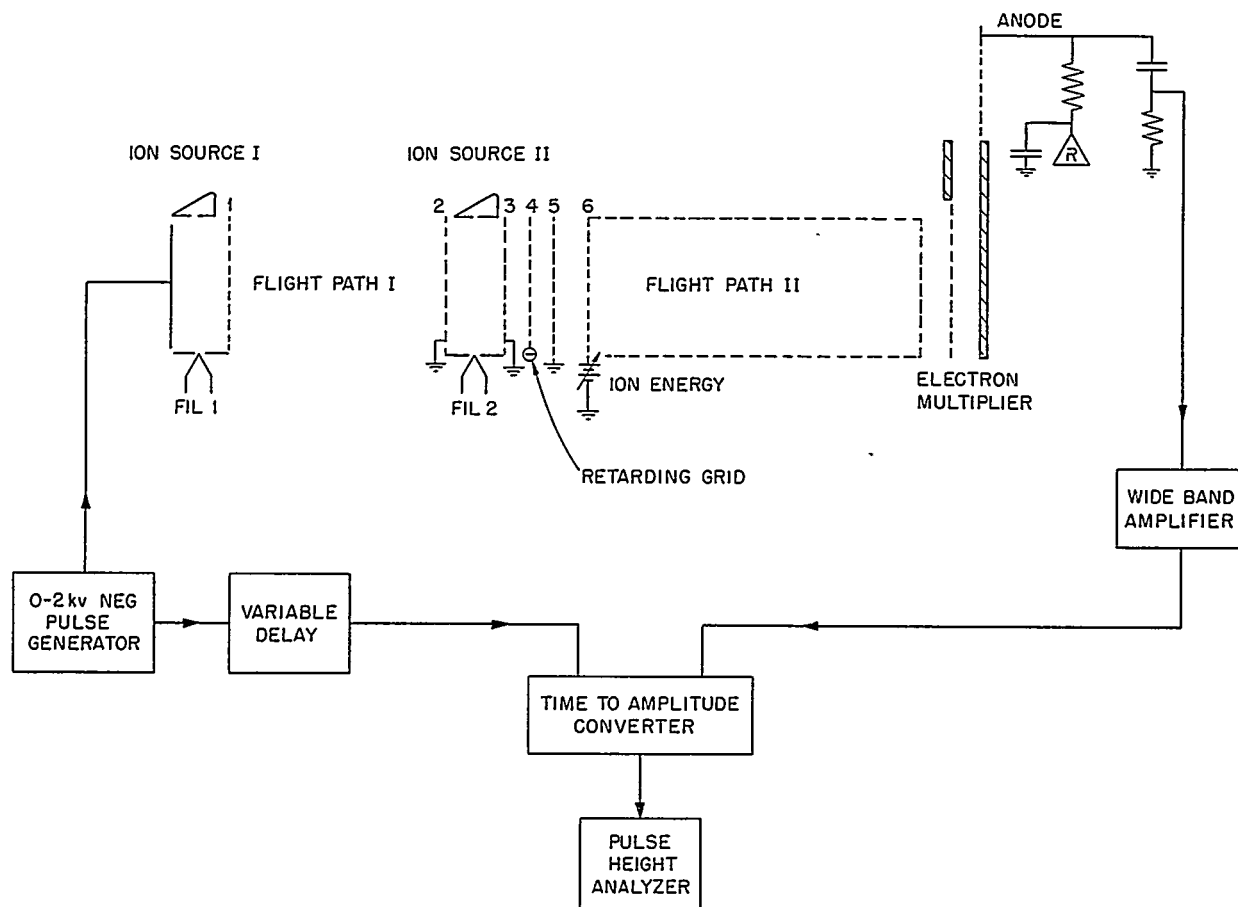


Fig. 14.4. Schematic Diagram of Negative Ion Lifetime Apparatus.

in polar molecules. Of special interest is the possible formation of short-lived negative ions of H_2O .¹⁶ Low-energy electrons produced by filament 1 enter ion source I and are temporarily captured by molecules into an excited negative ion state. The temporary negative ion is accelerated by a 2-kv pulse with a nanosecond rise time to an energy determined by the lifetime of the negative ion. Specifically, a negative ion of mass m which ejects its electron after a time t (lifetime) will

gain energy from a uniform electric field E and this kinetic energy is given by

$$\text{K.E.} = \frac{e^2 E^2}{2m} t^2.$$

Thus, if the kinetic energy can be determined, the lifetime of the negative ion can be calculated. This kinetic energy is determined from the time of flight from ion source I to ion source II in the following manner. The neutral molecule leaves ion source I with a few electron volts kinetic energy and enters ion source II where it is ionized by a second electron beam. Positive ions of

¹⁶G. S. Hurst, J. A. Stockdale, and L. B. O'Kelly, *J. Chem. Phys.* 38, 2572 (1963).

thermal energies will also be produced by the background gas in ion source II. The thermal positive ions will be separated from the energetic ions by a slightly negative retarding potential on grid 4. The energetic ions will then penetrate a 6-kv field and will travel down a second flight tube and be detected by an electron multiplier. The total flight time will be determined from the electronics shown in Fig. 14.4. Since the flight time from ion source II to the electron multiplier can be calculated, the flight time from ion source I to ion source II can be determined.

One further refinement to the discussion results from the fact that the lifetimes of the negative ions are statistical in nature. Since there will be a distribution of negative ion lifetimes, there will be a corresponding distribution in flight times. Using the exponential decay law, it is easy to show that the number of ions arriving at the ion source II with a flight time T within an interval ΔT is

$$\Delta N = \lambda N_0 \frac{mL \Delta T}{eET^2} e^{-\lambda mL/eET},$$

where $1/\lambda$ is the mean lifetime of the ions, and N_0 is the number of negative ions present at $t = 0$. The first estimate of the mean lifetime can then be calculated from the maximum of the plot of ΔN vs T .

DETECTION OF PLASMA RADIATION FROM ELECTRON-BOMBARDED ALUMINUM FOILS

An alternative method of studying characteristic energy losses by observing the light emitted from electron bombarded foils was suggested by Ferrell¹⁷ in 1958. The conventional method requires measurement of the difference between two large quantities, the energy of fast electrons before and after they have passed through the foil, each of which exceeds the quantity of interest by a factor of at least 10^2 . The explanation of the characteristic loss lines by Bohm and Pines¹⁸ as due to plasma oscillations led Ferrell to predict the existence of observable radiation from the decay of the plasma oscillations. Since the detection of this radiation would be a direct measure of the

energy loss, the optical method would provide a much more accurate means of measuring the plasma frequency than would the conventional method. A peak in the silver spectrum at 3300 Å has been observed previously¹⁹ but the interpretation is complicated by interband effects.²⁰ The band structure of aluminum has been shown to be nearly free-electron-like and should provide a better test for the plasma oscillation theory. Electron energy loss experiments show sharp discrete losses in aluminum at multiples of 15.3 eV.²¹ The decay of this plasmon should be accompanied by the emission of photons at approximately 800 Å.

Self-supported aluminum foils 500 to 800 Å in thickness were bombarded with 60- to 100-keV electrons. The light emitted at 30° from the foil normal was analyzed with a 50-cm Seya-Namioka vacuum ultraviolet spectrometer. The detector was an EMI 6256B photomultiplier whose quartz window was coated with sodium salicylate. A sharp peak at 815 ± 15 Å was found in the aluminum spectrum (Fig. 14.5) in good agreement with the characteristic energy loss experiments and with theoretical predictions. The theoretical spectrum was calculated by inserting the optical constants of aluminum determined by Hunter²² into the transition radiation equation given by Ritchie and Eldridge.²³

In order to verify the fact that the peak in the aluminum spectrum was 815-Å radiation and not due to scattered photons, an LiF filter which only transmits radiation of wavelengths longer than 1100 Å was inserted into the light path. The peak at 815 Å disappeared when the filter was inserted.

The improved resolution obtainable by measuring photon energies instead of electron energies makes possible detailed investigations of characteristic energy losses heretofore limited by the difficulty

¹⁹W. Steinmann, *Phys. Rev. Letters* 5, 470 (1961); R. W. Brown, P. Wessel, and E. P. Trounson, *Phys. Rev. Letters* 5, 472 (1961); H. Boersch, C. Radeloff, and G. Sauerbrey, *Phys. Rev. Letters* 7, 52 (1962); A. L. Frank, E. T. Arakawa, and R. D. Birkhoff, *Phys. Rev.* 126, 1947 (1962).

²⁰H. Ehrenreich and H. R. Philipp, *Phys. Rev.* 128, 1622 (1962).

²¹C. J. Powell and J. B. Swan, *Phys. Rev.* 118, 640 (1960).

²²W. R. Hunter, *J. Opt. Soc. Am.* 54, 208 (1964).

²³R. H. Ritchie and H. B. Eldridge, *Phys. Rev.* 126, 1935 (1962).

¹⁷R. A. Ferrell, *Phys. Rev.* 111, 1214 (1958).

¹⁸D. Bohm and D. Pines, *Phys. Rev.* 82, 625 (1951).

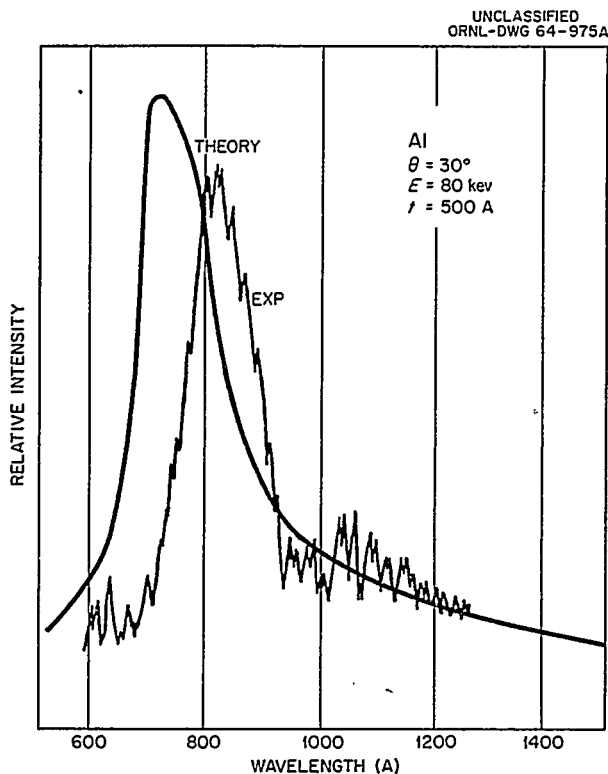


Fig. 14.5. Photon Emission from Electron-Bombarded Aluminum Foil 500 Å in Thickness. Spectrum uncorrected for spectrometer response.

in making accurate electron energy loss measurements.

THE OPTICAL CONSTANTS AND RESONANCE ABSORPTION OF VACUUM EVAPORATED SILVER FILMS

Recent investigations of optical emission from electron-bombarded thin silver foils^{24,25} and of the resonance absorption of light in thin silver films^{26,27} have demonstrated a need for further

²⁴E. T. Arakawa et al., *J. Phys. (Paris)* 25, 129 (1964).

²⁵R. W. Brown, P. Wessel, and E. P. Trounson, *Phys. Rev. Letters* 5, 472 (1960); A. L. Frank, E. T. Arakawa, and R. D. Birkhoff, *Phys. Rev.* 126, 1947 (1962); W. Steinmann, *Phys. Rev. Letters* 5, 470 (1960).

²⁶S. Yamaguchi, *J. Phys. Soc. Japan* 17, 1172 (1962); *J. Phys. Soc. Japan* 18, 266 (1962).

²⁷A. J. McAllister and E. A. Stern, *Phys. Rev.* 132, 1599 (1963).

study of the optical properties of silver. The observed effects were found to be less intense than the theoretical predictions based on optical constants of bulk silver. These discrepancies occur primarily in the wavelength region 2500 to 3700 Å.

The optical constants of vacuum-evaporated silver films were evaluated from reflectance data by means of a program which has been written for the CDC 1604A computer. The equations derived from Fresnel's equations relating reflectance to n and k were used in the program:

$$r_s = \left| \frac{[(n + ik)^2 - \sin^2 \phi]^{1/2} - \cos \phi}{[(n + ik)^2 - \sin^2 \phi]^{1/2} + \cos \phi} \right|^2,$$

$$r_p = \left| \frac{[(n + ik)^2 - \sin^2 \phi]^{1/2} - (n + ik)^2 \cos \phi}{[(n + ik)^2 - \sin^2 \phi]^{1/2} + (n + ik)^2 \cos \phi} \right|^2,$$

where r_s and r_p are reflectances for light with the electric vector normal to and parallel to the plane of incidence respectively; ϕ is the angle of incidence; and n and k are the real and imaginary parts of the complex index of refraction of the reflecting material. When r_p and r_s were measured directly for one angle of incidence, an analytic solution of the two equations was used. When r_s or R , the unpolarized reflectance, was measured for two different angles of incidence, n and k were determined from the appropriate equations by an iterative process. The accuracy of the calculated n and k values depended essentially upon the precision of the reflectance input data.

Reflectance curves for unpolarized light incident at 20 and 70° are shown in Fig. 14.6. The real and imaginary parts of the complex index of refraction, n and k , respectively, were evaluated using the computer program described earlier from reflectance data for a number of films. Reflectances were measured to $\lambda = 6000$ Å by using a tungsten filament source, but the small differences in reflectance between the 20 and 70° incidence data for wavelengths greater than 3700 Å lead to large uncertainties in n and k determinations. Consequently, the optical constants were evaluated from 2500 to 3700 Å, which was the region of primary interest.

The n and k values presented in Fig. 14.7 are a composite of values found for a number of evaporated silver films. The n and k values for the films exposed to air are shown as circles. These

optical constants were compared with those reported by Ehrenreich and Philipp²⁰ for electropolished bulk silver. Below 2800 Å the optical constants for bulk and evaporated silver surfaces are in good agreement. The most significant dif-

ferences in the optical constants for bulk and evaporated silver surfaces were observed primarily in the vicinity of the minimum in k at 3224 Å. At the minimum the k value (0.299) for evaporated silver was nearly a factor of 2 greater than k (0.162) evaluated for bulk silver. The values of n for bulk and evaporated silver were essentially the same in this region. The differences in the k values may be attributed to characteristics of the metal surfaces introduced by the two methods of preparation.

The real part of the complex dielectric constant, $\epsilon_1 = n^2 - k^2$, the imaginary part, $\epsilon_2 = 2nk$, and the energy loss function, $\text{Im}(1/\epsilon)$, calculated from the n and k values of Fig. 14.7, are shown in Fig. 14.8. The condition for collective electron oscillation is satisfied where the damping term ϵ_2 is small and ϵ_1 passes through zero. This occurs for vacuum-evaporated silver films at 3285 Å or 3.78 eV. The damping term ϵ_2 for evaporated silver was found to be greater than ϵ_2 for bulk

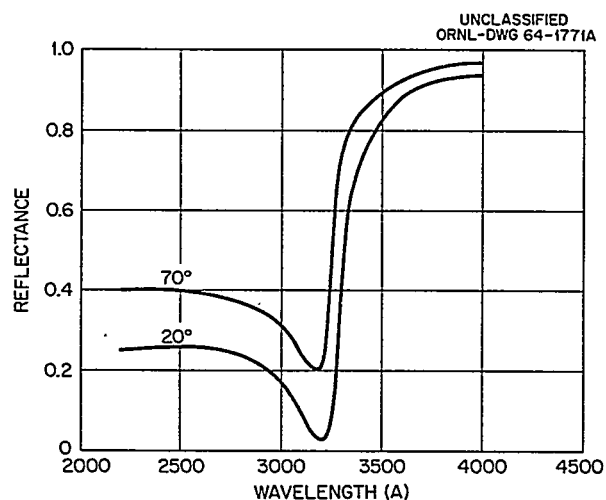


Fig. 14.6. Measured Reflectance of Unpolarized Light from a Vacuum-Evaporated Silver Film for Light Incident at 20 and 70°.

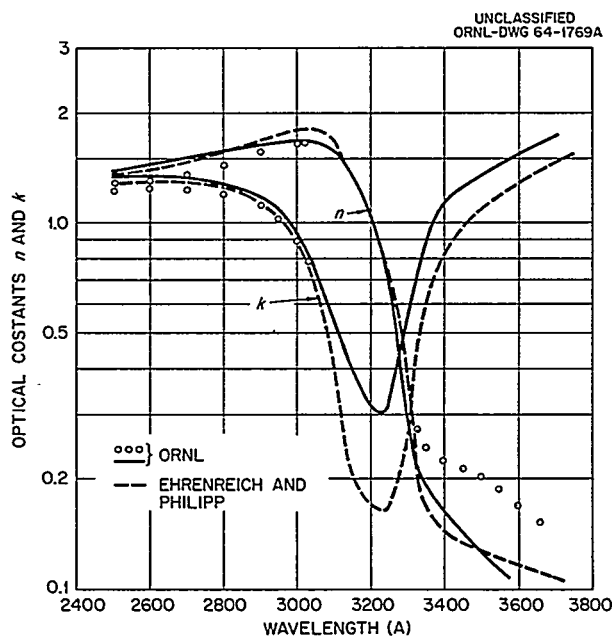


Fig. 14.7. The Real and Imaginary Parts of the Complex Index of Refraction for Bulk and Vacuum-Evaporated Silver.

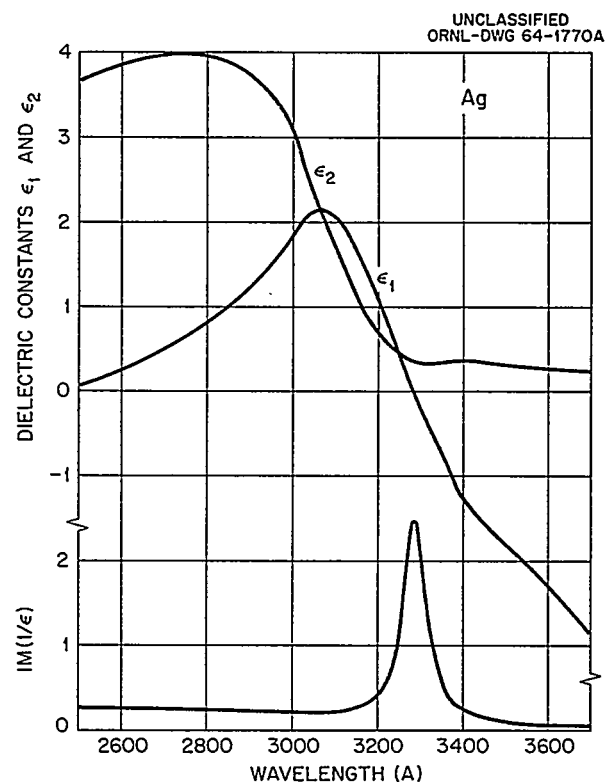


Fig. 14.8. The Real and Imaginary Parts of the Complex Dielectric Constants and the Energy Loss Function $\text{Im}(1/\epsilon)$ for Vacuum-Evaporated Silver.

silver in the region where ϵ_1 passes through zero. Likewise, the magnitude of the maximum in the energy loss function was determined to be 2.47 for evaporated silver, which is less than the $\text{Im}(1/\epsilon)$ value of 4.0 for bulk silver in this region.

The agreement between the experimentally observed photon emission from electron-bombarded silver films²⁴ and the transition radiation theory²³ is much better when the present results are used in the calculations instead of the n and k values of bulk silver (Fig. 14.9). The spectral distribution of photons was measured at 30° from the normal to the film surface for silver foils 660 Å in thickness bombarded by 40-keV electrons.

Ferrell²⁸ predicted that electromagnetic radiation of the proper frequency and polarization at nonnormal incidence should couple strongly with the collective electron oscillation modes in thin metal films to produce an optical resonance effect. This process was suggested as a purely optical means for studying the collective electron resonance in metals. An optical study which yielded the energy loss function $\text{Im}(1/\epsilon)$ was carried out by Yamaguchi,²⁶ and his results for thin silver films were related to the absorption resonance. A minimum in the transmission spectrum of parallel polarized light through thin silver films at various angles of incidence was reported by McAllister and Stern²⁷ and described as the excitation of the "surface plasma mode." They found discrepancies between their experimental results and theoretical values of the resonance effect calculated using bulk silver optical constants.

We reinvestigated the resonance minimum in the transmittance spectrum of silver. Theoretical expressions for the transmission of polarized light through a thin absorbing film on a transparent backing were derived from Fresnel's equations for reflection and transmission at a single surface and were programmed for numerical evaluation. Transmittance of parallel polarized light measured for a 415-Å silver film on quartz at various angles of incidence was compared with theory (Fig. 14.10). The theoretical transmittance curves calculated from evaporated silver n and k values give good agreement with observed values.

The optical constants of evaporated indium films were evaluated from reflectance data in the vacuum ultraviolet region. No other optical constants for

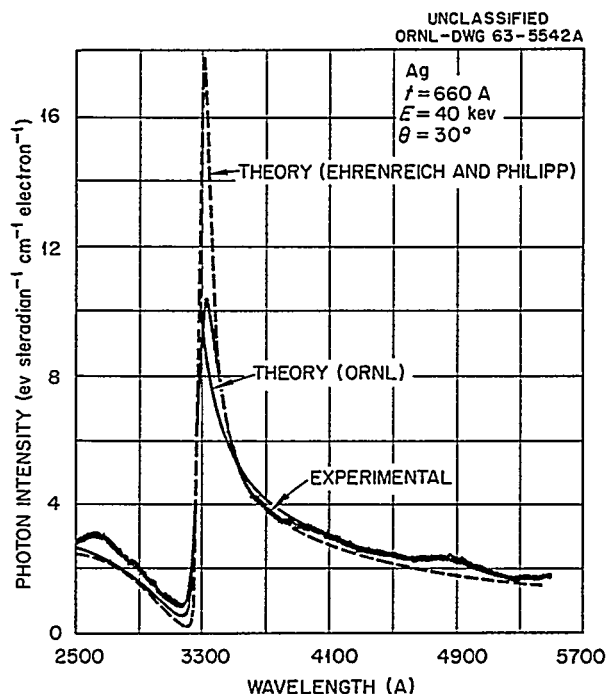


Fig. 14.9. Comparison of the Experimentally Observed Photon Emission from Electron-Bombarded Silver Foil with Transition Radiation Theory Using n and k Values of ORNL and Ehrenreich and Philipp.

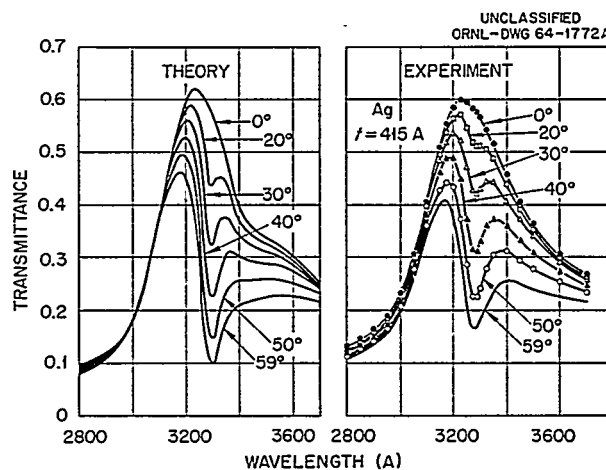


Fig. 14.10. Transmission Spectra for Parallel Polarized Light of Silver Film 415 Å in Thickness for Various Angles of Incidence.

²⁸R. A. Ferrell and E. A. Stern, *Am. J. Phys.* 31, 810 (1962).

indium are available in the wavelength region investigated. At present optical measurements on evaporated magnesium films are in progress.

SPHERICAL ELECTROSTATIC ANALYZER AND SLOWING-DOWN SPECTRA IN COPPER AND GOLD

The spherical electrostatic beta-ray analyzer (the Keplertron) described previously^{29,30} underwent further tests and development. Steps found previously³⁰ in the electron slowing-down spectrum in copper were identified, and the electron slowing-down spectrum in gold was obtained. The transmission for ^{152}Sm Auger electrons resulting from beta decay in ^{152}Eu reported previously³⁰ was determined more accurately. The line profile for the ^{152}Sm Auger electrons (actually a superposition of six lines) is shown in Fig. 14.11. The theoretical line was constructed by adding lines having the shape predicted by the theory of the Keplertron, and with relative intensities extrapolated from experimental data given by Nijgh, Wapstra, and Van Lieshout.³¹ It was assumed that the peak height of each line was 25% of the number of electrons emitted into a 4π solid angle. The composite line was normalized to one KLL Auger electron emitted. The experimental data were corrected for source activity, gamma-ray background, electrical leakage in the Keplertron, and continuum background. The transmission calculated from these data is $(25 \pm 7)\%$.

Additional tests were made to locate the sources of and reduce the effects of spurious electrons. Figure 14.12 shows line profiles obtained using an electron gun consisting of a hemispherical grid of wires over a circular filament (old sphere, gun No. 4) and using a gun consisting of a double grid with a positive bias voltage applied to the inner grid (old sphere, gun No. 6). In addition to suppressing secondary electrons from the gun, gun No. 6 was designed to simulate the cavity sources used in slowing-down experiments.

²⁹R. D. Birkhoff et al., *Health Phys. Div. Ann. Progr. Rept.* July 31, 1962, ORNL-3347, p. 82.

³⁰R. D. Birkhoff et al., *Health Phys. Div. Ann. Progr. Rept.* June 30, 1963, ORNL-3492, p. 141.

³¹G. J. Nijgh, A. H. Wapstra, and R. Van Lieshout, *Nuclear Spectroscopy Tables*, p. 83, North-Holland, Amsterdam, 1959; Interscience, New York, 1959.

The lowest curve in Fig. 14.12 shows a line profile obtained using gun No. 6, a new inner sphere with antiscatter ridges, and sooting the whole Keplertron and both sides of each of the grids in the gun. The high-energy wing on the peak is gone, the low-energy wing is reduced to less than 10% of the central peak, and the secondary emission peak is only 0.2% of the central peak. Since every component of a continuum contributes to this secondary peak, it is very important to have the peak as small as possible for any one component.

A detailed discussion of the construction and calibration of the Keplertron is given in the literature.³²

³²H. H. Hubbell, Jr., W. J. McConnell, and R. D. Birkhoff, "The Spherical Condenser as a High Transmission Particle Spectrometer - III. Construction and Calibration," submitted for publication in *Nuclear Instruments and Methods*.

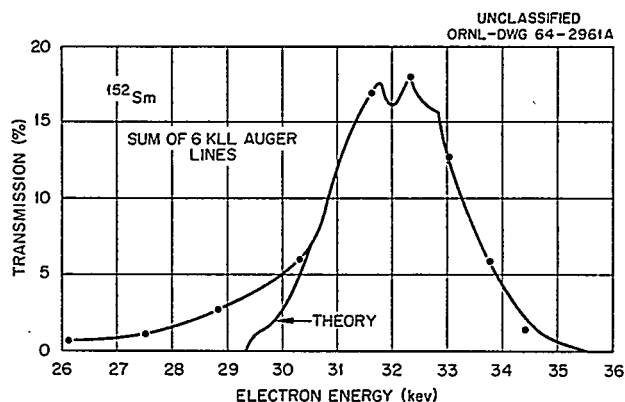


Fig. 14.11. Keplertron Line Profile for ^{152}Sm Auger Electrons.

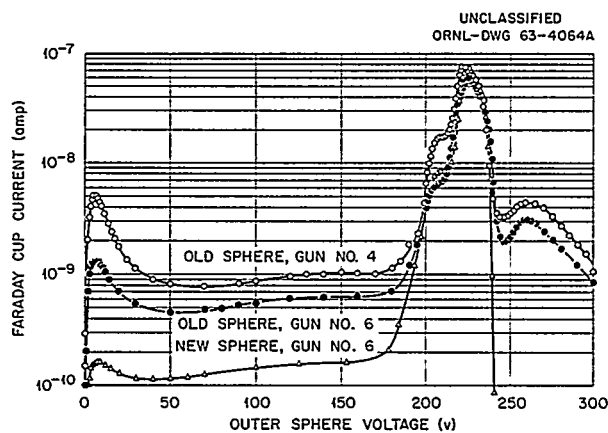


Fig. 14.12. Keplertron Line Profiles Illustrating Successive Reductions in Secondary Emission Effects.

Steps previously reported³⁰ in the slowing-down spectrum of ^{64}Cu beta rays in copper are believed to be due to Auger electrons, photoelectrons, and Compton scattered electrons. The large step at about 7 keV is caused by *KLL* Auger electrons and K_{α} photoelectrons. The Auger electrons are composed of 6.55-keV nickel *KLL* Auger electrons caused by electron capture in ^{64}Cu and 7.03-keV copper *KLL* Auger electrons from the filling of *K* vacancies in copper atoms caused by beta rays. The photoelectrons are produced by 7.47-keV K_{α} x rays from nickel and 8.04-keV K_{α} x rays from copper. Since the linear absorption coefficient for a 7.5-keV x ray is 568 cm^{-1} in copper, only a negligible fraction of the x rays escape from the 0.05-cm-thick source. Also, since the probability for the photoelectric effect is higher for the tightly bound shells, most of the photoelectrons will be from the *L* shells and appear with energies of 6.55 keV and 7.03 keV. As a result of these processes the ratio of electrons with *KLL* energies to *K* vacancies is approximately 1. The less prominent step at about 800 eV is probably caused by *LMM* Auger electrons and L_{α} photoelectrons in processes similar to those described above. Although the photoeffect is dominant in copper at the K_{α} energies, Compton scattering can still occur. The small step at about 250 eV may be the edge of the Compton distribution caused by the K_{α} x rays.

The electron slowing-down spectrum from a gold cavity source was measured and is shown with the theory in Fig. 14.13. The contributions of the primary and secondary electrons to the theoretical flux are also shown. At least a part of the difference between the theory and experiment is due to self-shielding of the gold during neutron activation. This would cause the inner walls of the cavity to have a lower activity than the outer walls. A rough calculation gave a value of 0.5 for the ratio of the inner wall activity to the outer wall activity. The data shown here were normalized to the total activity as determined by a gamma scintillation spectrometer. The proper activity for normalization would be somewhat less and tend to bring the data closer to theory. Figure 14.14 shows a comparison of the gold and copper spectra. The open circles represent the gold data and the dots represent the copper data.

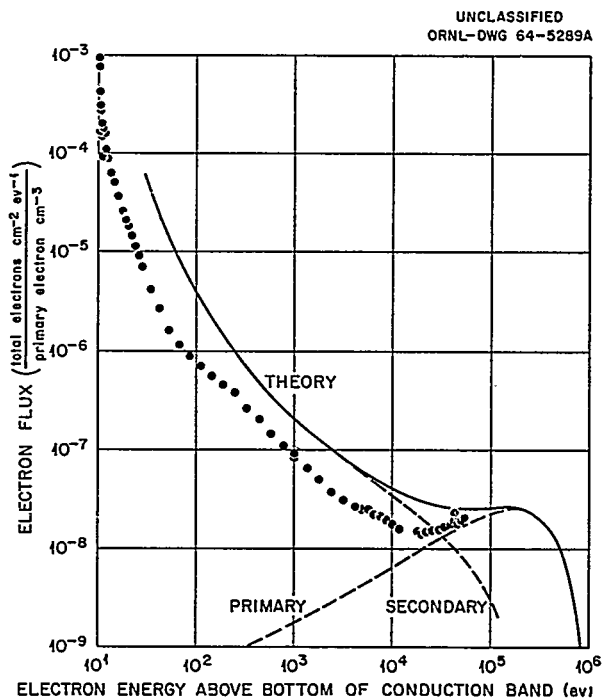


Fig. 14.13. Electron Flux Spectrum of ^{198}Au Beta Rays Absorbed in Gold.

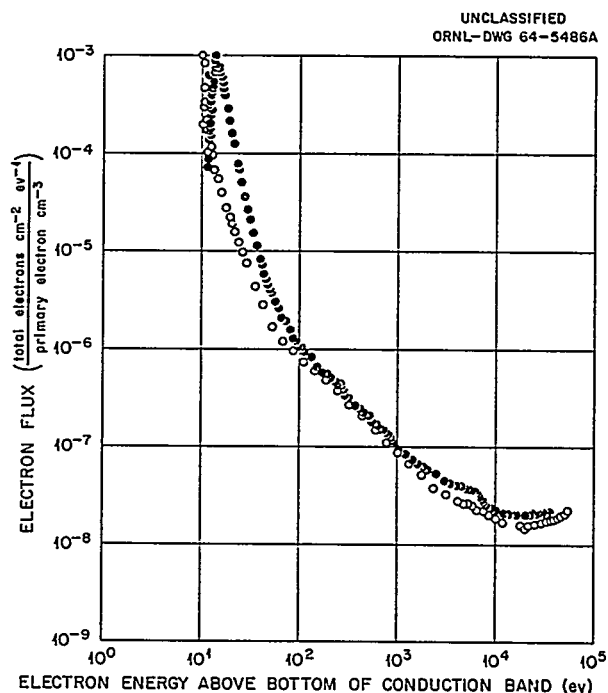


Fig. 14.14. Comparison of Electron Flux Spectra in Gold and Copper.

15. Physics of Tissue Damage

R. D. Birkhoff

J. G. Carter

R. A. MacRae¹D. R. Nelson²

M. Y. Nakai

OPTICAL PROPERTIES OF PYROLYTIC GRAPHITE

The electronic properties of graphite, as determined by its molecular structure, are of particular interest in biophysics because this material represents a "series limit" to the sequence of many ring aromatic molecules. That is, the geometrical arrangement of carbon atoms in rather widely spaced parallel planes within which the atoms are in hexagonal array gives a good representation of an organic molecule containing many benzene rings. Accordingly, we have measured the optical reflectance of hot-pressed pyrolytic graphite in the 1100- to 3000-Å spectral region and determined the energy-loss function in an effort to obtain information on the predicted collective electron oscillation at 7.5 eV.

The hot-pressed pyrolytic graphite used in our studies was manufactured by the Carbon Products Division of Union Carbide Corporation. The sample was taken from a half cylinder approximately 3½ in. in diameter and 1½ in. thick. The half cylinder was prepared by pressing several sheets of pyrolytic graphite in the c direction at a very high temperature. The structure of the material was determined by x-ray diffraction and electron transmission and diffraction studies. The texture of this pyrolytic graphite is much like a highly oriented fiber texture with all (001) type directions aligned parallel to the compression axis, and all possible rotations about this axis uniformly distributed. Thin strips 2 cm wide by 5 cm long of the pyrolytic graphite were peeled from the sample and attached to a holder for the reflectivity measurements involving the plane of incidence perpendicular to the basal surfaces. For the measurements with the plane of the incident light parallel to the basal surfaces, a section of the half cylinder was attached to the holder.

Reflectance curves for unpolarized light incident at 20 and 70° are shown in Fig. 15.1, where the ba-

sal surfaces were oriented perpendicular to the plane of incidence. In Fig. 15.2 the real (n) and imaginary (k) parts of the complex index of refraction are presented for this orientation. In Fig. 15.3 the reflectance curves of unpolarized light incident at 20 and 70° are presented for the orientation of basal surfaces parallel to the plane of incidence. Figure 15.4 shows the corresponding n and k values for this orientation. The real and imaginary parts of the dielectric constant may be computed from the relations $\epsilon_1 = n^2 - k^2$ and $\epsilon_2 = 2nk$ respectively. These are plotted for the perpendicular data as shown in Fig. 15.5. Also plotted is the imaginary part of the reciprocal dielectric constant which is known as the energy-loss function and is proportional to the energy loss an electron beam would experience in passing through graphite. This function can be seen to peak at 6.9 eV, a value which agrees well with energy-loss data.

The reflectance data were analyzed by the CDC 1604 computer using a computer code, based on the Fresnel coefficients, which solves for n and k from reflectances at two angles of incidence. In

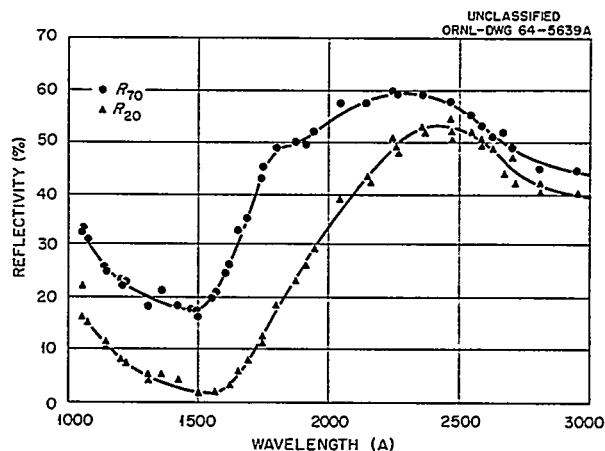


Fig. 15.1. Measured Reflectance of Unpolarized Light from Pyrolytic Graphite for Light Incident at 20 and 70°. Basal surfaces oriented perpendicular to the plane of incidence.

¹Summer employee.

²Temporary leave.

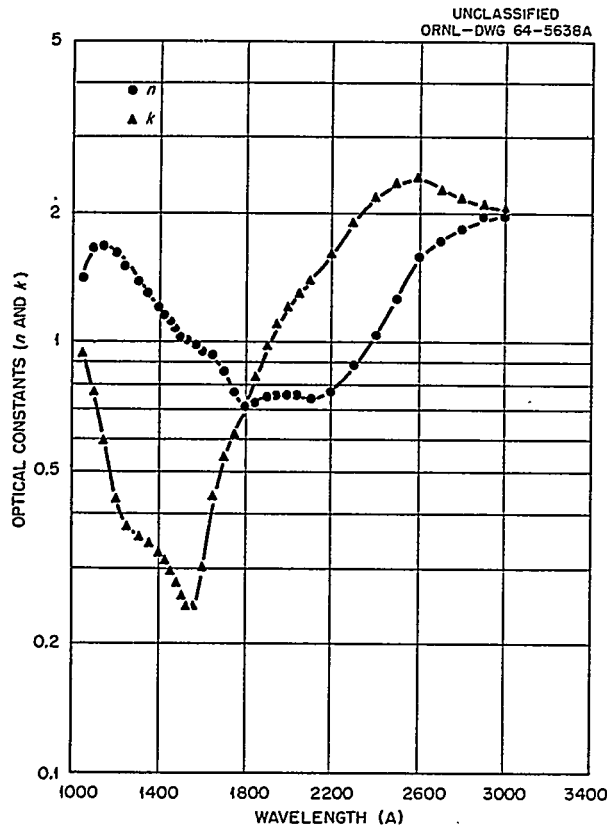


Fig. 15.2. The Real and Imaginary Parts of the Complex Index of Refraction for Pyrolytic Graphite. Basal surfaces oriented perpendicular to the plane of incidence.

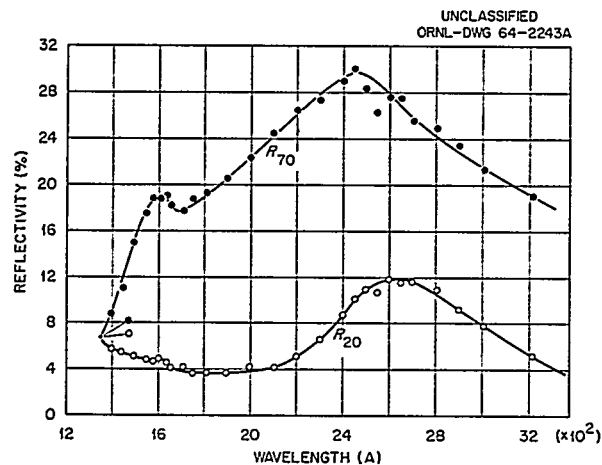


Fig. 15.3. Measured Reflectance of Unpolarized Light from Pyrolytic Graphite for Light Incident at 20 and 70°. Basal surfaces oriented parallel to the plane of incidence.

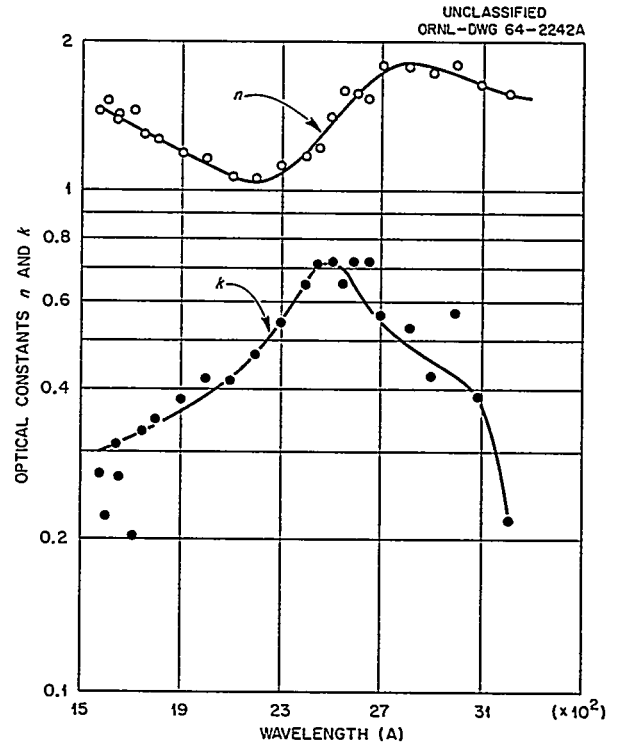


Fig. 15.4. The Real and Imaginary Parts of the Complex Index of Refraction for Pyrolytic Graphite. Basal surfaces oriented parallel to the plane of incidence.

the results presented here the simplifying assumption is made that the graphite is isotropic. Since graphite is actually anisotropic, a more complete analysis will be made taking this into account; and, for the same reason, the reflectances will be remeasured using polarized light. By measuring the optical constants more accurately, it is hoped to establish definitely whether or not collective electron oscillations occur at 1800 and 500 Å as predicted from electron energy-loss data.

RANGE OF CHARGE FOR LOW-ENERGY PROTONS IN ALUMINUM

A new technique was investigated for studying the absorption of charged particles in solids. This method utilizes a thin layer of the material to be studied which has been vacuum evaporated onto the surface of an insulator. The latter provides mechanical support for the film, thus permitting use of films of as little as 100 Å thickness, and

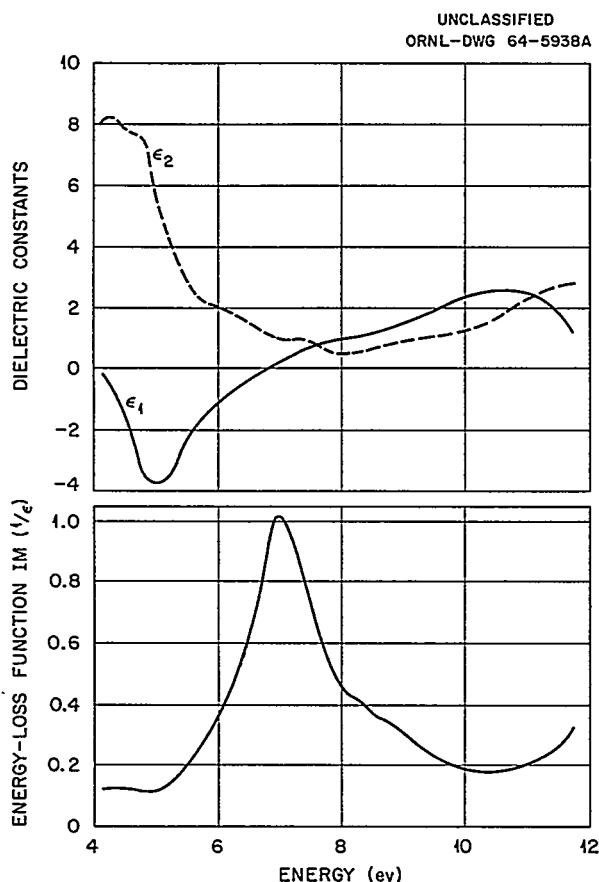


Fig. 15.5. (Top) The Real and Imaginary Parts of the Complex Dielectric Constant for Pyrolytic Graphite (Perpendicular Orientation); (Bottom) the Energy Loss Function $\text{Im}(1/\epsilon)$ for Pyrolytic Graphite (Perpendicular Orientation).

separates the film electrically from the conducting substrate so that currents to both from an incident beam may be monitored with low-resistance galvanometers. The currents may be analyzed to yield the "charge transmission," that is, the product of the particle transmission of the film and the average charge of the particle as it left the film and entered the insulator. Since the average charge is always ≤ 1 , the charge ranges measured by this method are smaller at any particle energy than the actual particle ranges.

A layer of SiO_2 about 75 Å thick was vacuum evaporated onto the substrate to form the insulator. The thickness of this layer was determined both

by a neutron activation-beta counting procedure and by use of a thin film thickness monitor during evaporation. The resistance of the insulator had to exceed 1000 ohms before the resulting diode was usable (i.e., its resistance \gg galvanometer resistances). However, it was frequently found to exceed 1 megohm. Some success was achieved in rejuvenating diodes which were leaky because of insulator imperfections, metallic bridges, radiation damage, etc., by discharging a 40- μf condenser through the insulator.

The thin film was vacuum evaporated from a filament specially designed to reduce emission of atomic clumps. Film thickness was determined by optical interferometry and by the film thickness monitor. Thicknesses ranging from 200 to 1050 Å were produced.

A complete diode was placed in the proton beam from a small proton accelerator constructed for these studies. A beam of protons of about 0.1 μA and of energy variable from 2 to 35 keV was produced with an H_2^+ content of only a few percent. A suppressor electrode above the diode prevented loss of secondary electrons.

Typical curves of top (i.e., film) current and bottom (i.e., substrate) current as a function of proton beam energy are shown in Fig. 15.6 for a 200-Å film of aluminum. The currents are normalized to unit current. It may be seen that the bottom current becomes slightly negative at higher proton energies. This is attributed to the presence

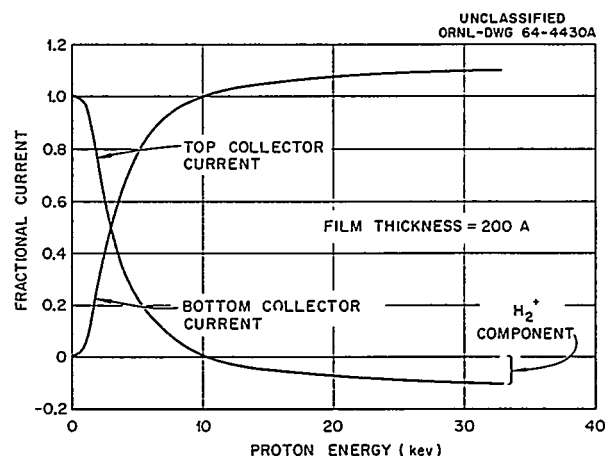


Fig. 15.6. Fractional Current Distribution in the Aluminum Layers vs Proton Energy for an Aluminum Thickness of 200 Å.

in the beam of H_2^+ which dissociates on striking the film into H^0 and H^+ with the former then losing its electron to the film before both particles cross the insulator. The distortion to the data may be removed by use of the ideas that each atomic fragment has half the energy of the H_2^+ and that the product of transmission $T(E)$ and charge at leaving the film $f^+(E)$ is asymptotically zero for small E .

The product $T(E) f^+(E)$ is shown in Fig. 15.7. The energy at which 50% transmission occurs is taken from these curves and plotted in Fig. 15.8 along with data of Hines³ for a 50% value of $T(E)$ and with the data of Young⁴ for $T(E) = 0$. The reciprocal electronic stopping power of Lindhard and Scharff⁵ integrated over all proton energies is shown also, and it is seen to greatly exceed all experimental values because it does not include proton scattering which has the effect of shortening the proton range. The ratio at any energy of our curve to those of Hines and Young gives the average charge $f^+(E)$ of the protons as they leave the film. It may be seen that this charge approaches unity at the higher proton energies. It is clear that considerably more data are required before this quantity is established with precision, however.

³R. L. Hines, *Phys. Rev.* 132, 701 (1963).

⁴J. R. Young, *J. Appl. Phys.* 27, 1 (1956).

⁵J. Lindhard and M. Scharff, *Phys. Rev.* 124, 128 (1961).

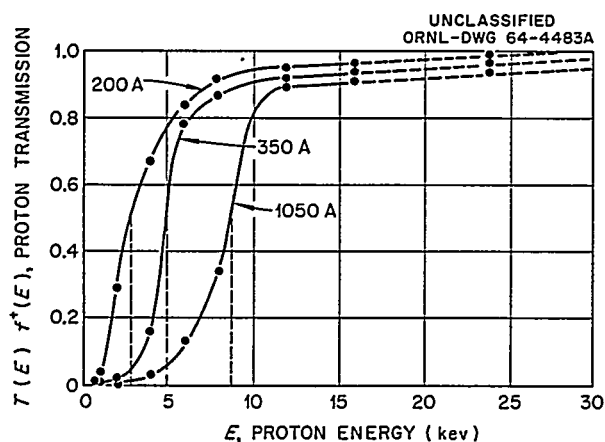


Fig. 15.7. Proton Transmission as a Function of Energy for Several Aluminum Thicknesses.

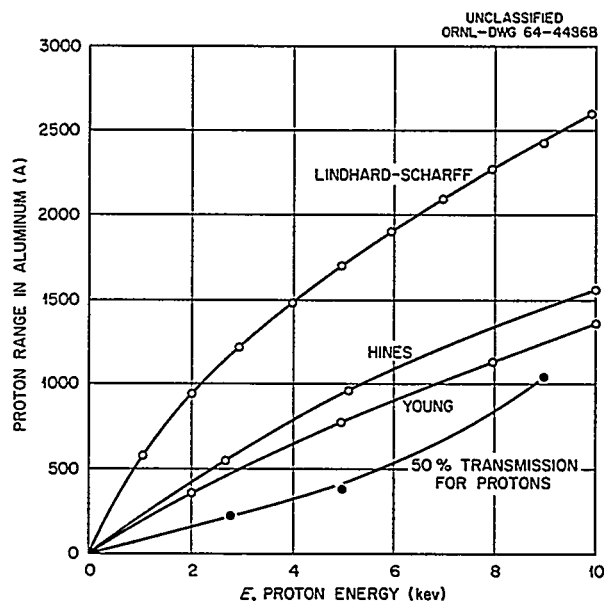


Fig. 15.8. Comparison of Theoretical and Experimental Range-Energy Curves.

TIME-OF-FLIGHT ELECTRON BEAM MONOCHROMATOR

One of the most important effects of ionizing radiation is the generation of low-energy electrons in the bombarded medium. These electrons then move through the medium, interacting with atoms and molecules in specific ways with probabilities which depend on the electron energies and the characteristic atomic and molecular absorption energies. Detailed studies of these absorption processes involve generating highly monoenergetic electrons whose energy may be varied at will and then using them to explore the characteristic energy levels of the absorbing medium. Experiments of this type have been severely hampered in part by the difficulty of obtaining a truly monoenergetic electron beam. Ideally, one would wish an energy spread of no more than 0.01 eV, but this has not been achieved as yet although G. J. Schultz,⁶ H. Boersch *et al.*,⁷ and J. A. Simpson

⁶G. J. Schultz, *Phys. Rev.* 125, 229 (1962).

⁷H. Boersch, J. Geiger, and H. Hellwig, *Phys. Letters* 3, 64 (1962).

and U. Fano⁸ have reduced the energy spread to about 0.1 eV using electron optical techniques. Because of the known difficulties of these techniques, we decided to try a different approach which utilized the time-of-flight of electrons as a measure of their energy.

Further work on the time-of-flight electron beam monochromator centered on producing a better electron gun, improving the broad-band transistor amplifier, studying the energy distribution of the pulsed beam by stopping-potential techniques, and making preliminary observation of resonance levels in the residual gases of the vacuum system. A portion of this work has been described in a recent ORNL report.⁹

Several more electron guns were designed, constructed, and tested. The objective was to provide proper cable termination to prevent the pulse on the grid from ringing and to increase the number of electrons emitted per pulse. The first was accomplished by going to a coaxial geometry, as shown in Fig. 15.9. The structure to the right supports a hairpin filament which protrudes into the coaxial gun through a hole in the outer grounded cylinder. The filament reaches into a specially shaped cavity in the center electrode (the "grid") which carries the pulse from an avalanche transistor pulser. Electrons emitted when the grid is pulsed pass through a hole in the grid and exit through a hole in the left side of the coaxial shield. The gun is properly terminated at its top with a commercial 50-ohm termination. It was found that if the grid were biased positively by about 75 V, electrons were apparently stored near the grid, with the result that when the 7-V pulse appeared, a considerable enhancement of emission occurred. The shape of the electron pulse was examined with a collector 15 cm from the gun as shown in Fig. 15.10 and was found to have a width of 10 nsec as compared with a pulse on-time of 2 nsec for ~4-eV electrons. This discrepancy is consistent with the dispersion in time introduced by the spread in velocity of the electrons emitted at the gun; that is, at $t = 0$, $\Delta t \cong 0$ also. After drifting 84 cm the electrons have been dispersed further to a width at half height of 80 nsec.

⁸J. A. Simpson and U. Fano, *Phys. Rev. Letters* 11(4), 158 (1963).

⁹D. A. LaBar, J. A. Harter, and R. D. Birkhoff, *Time-of-Flight Studies of Electrons in Vacuum*, ORNL-3484 (1964).

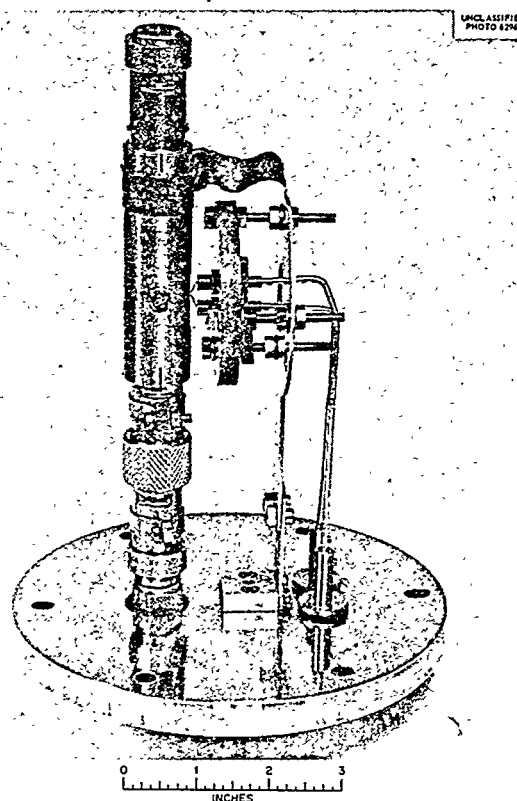


Fig. 15.9. Photograph of the New Coaxial Electron Gun.

That the drift time was properly related to electron energy is illustrated in Fig. 15.11. A triple-grid arrangement was introduced at the collector such that the outer grids were at ground and the inner grid could take on various potentials. It is clear that the electrons taking the longest time to reach the collector are removed from the pulse by increasing the grid bias from 6 to 9 V. The finite slope of the right side of the pulse is due to field penetration through the grids and the signal induced on the collector plate by electrons moving from the third grid to the plate.

The nanosecond-pulse amplifier is a three-stage amplifier using the design proposed by Williams and Neiler.¹⁰ Each stage is basically a cascode

¹⁰C. W. Williams and J. H. Neiler, *IRE Trans. Nucl. Sci.* 9(5), 1 (1962).

amplifier buffered by input and output emitter-followers. The overall gain of the amplifier is $3500\times$ with a rise time response to a step function input of 5 nsec, although the 2N769 transistors used throughout have an f_t of 800 Mc. The response is illustrated in Fig. 15.12 for a 10-nsec

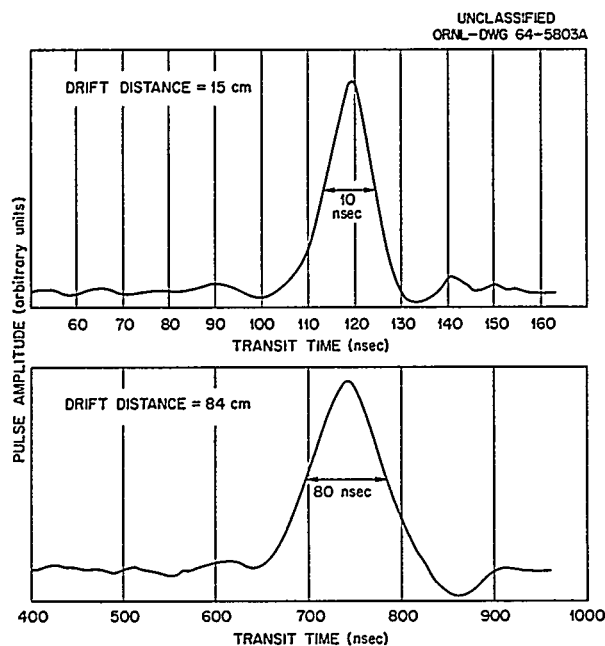


Fig. 15.10. Time-of-Arrival Distribution of Pulsed Electron Gun at 15 and 84 cm.

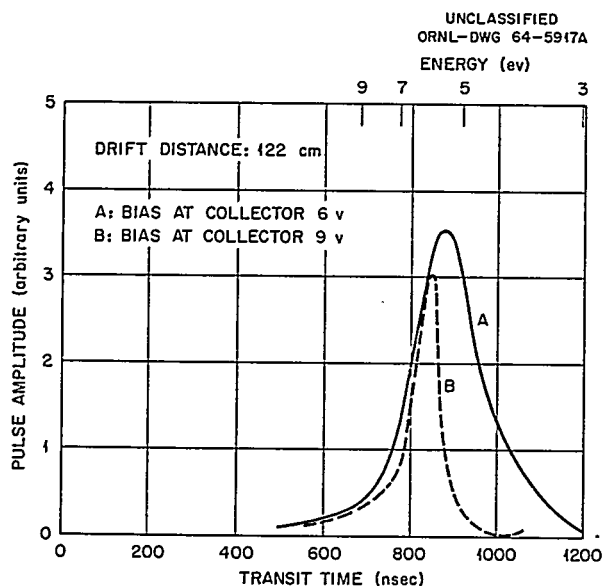


Fig. 15.11. Effect of Collector Bias on Pulse Shape.

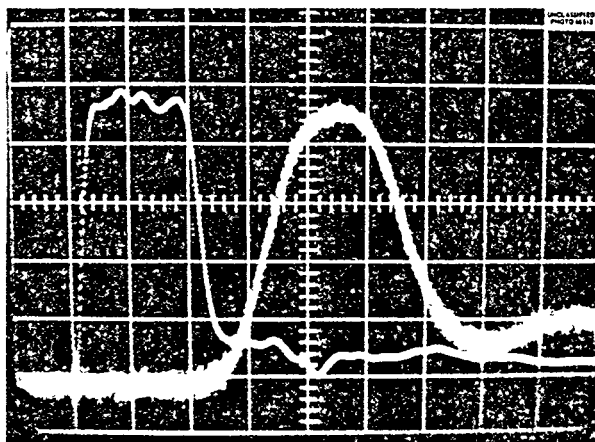


Fig. 15.12. Nanosecond Amplifier Response: Representative Input and Output Pulses.

pulse shown at left and the same pulse amplified at the right. Time scale is 5 nsec/cm. With the present components and layout the amplifier seems capable of still better bandwidth if point-to-point wiring and printed circuit layout techniques are used.

As all components of the gun, drift chamber, and electronics were improved, we noticed that "bumps" began to appear on the time-of-arrival distributions. One minimum which appeared quite consistently at 1600 nsec drift times is believed to correspond to the excitation of vibrations in the residual N_2 in the system, even though the total pressure of all gases was about 1×10^{-7} mm Hg. This identification was made on the high probability of the presence of N_2 and the energy of 2.5 ev associated with the drift time, which corresponds closely to the accepted^{11,6} value of 2 to 3 ev. Typical data are shown in Fig. 15.13. Other minima at 3.2 and 4 ev are present but as yet unidentified.

Because of the difficulties of making an effective electrostatic gate with which to select a monochromatic electronic component from the swarm (the original purpose of this research) and because of the unexpected observance of the electron-gas interaction, we have decided to alter the concept of the experiment to include more studies of the latter type. Thus the experiment as now

¹¹R. H. Neynaber et al., *Phys. Rev.* 129, 2069 (1963).

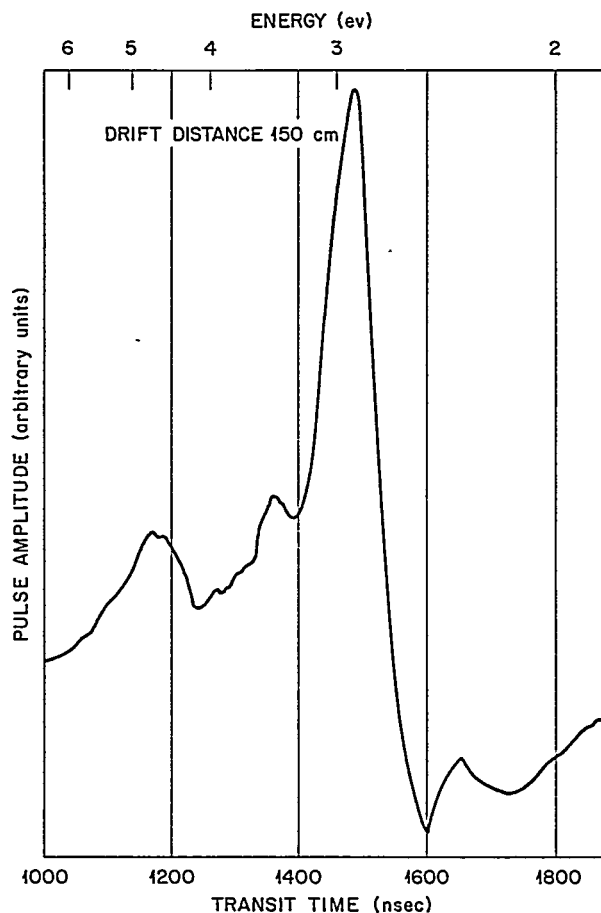
UNCLASSIFIED
ORNL-DWG 64-5949A

Fig. 15.13. Time-of-Arrival Distribution with a Minimum at 2.5 ev.

conceived is completely analogous to an infrared absorption experiment with electrons from the gun replacing photons from a black body, and the drift time replacing the wavelength. The pressures here are many orders of magnitude lower than those used in infrared absorption cells, and it may be possible to duplicate much of the work of infrared spectroscopy with this new technique.

TRACER STUDIES OF DIFFUSION PUMP OIL DEPOSITION

A radioactive tracer technique has been used as a quick, simple, nondestructive method for

measuring the deposition of diffusion pump oil in a vacuum system. Dow-Corning 704, which is a silicon base oil, was used in these activation studies. In the preliminary experiments 5 ml of the oil was irradiated in the Low Intensity Test Reactor (1.25×10^{-12} neutrons $\text{cm}^{-2} \text{sec}^{-1}$) at ORNL for 2.6 hr. The ^{30}Si , comprising 0.54 wt % of the oil, becomes activated to ^{31}Si , which has a half-life of 2.6 hr, and emits a beta ray of 1.48 Mev end-point energy. The oil was diluted to 225 cm^3 and added to a 300 MCF Consolidated Electrodynamics Corporation diffusion pump that evacuated a bell jar (18×12 in. diam), 4-in. valve, and optical baffle assembly. After pumping on this assembly for 1 hr, the bell jar was removed, and the inside was scanned with a Geiger counter. The ratio of counts/ cm^2 in the top of the jar to the counts/ cm^3 of the bulk oil gave a thickness of 6 Å. Use of larger radioactive samples and higher reactor fluxes may increase the sensitivity by more than 2 orders of magnitude. Further experiments will be conducted utilizing baffles cooled with H_2O and liquid nitrogen.

This particular method should be extremely useful in determining thin layers of pump oil deposition on various components in vacuum systems. One example where this method would have considerable advantages over more conventional methods of measuring oil contamination involves the measurement of oil deposition on diffraction gratings in vacuum ultraviolet spectrometers. In general, wherever there are components in a system that are affected by minute quantities of pump oil, and it is desired to quickly and simply determine the extent of this contamination without moving or touching components, this method appears to offer advantages.

IMPORTANCE OF THERMAL EQUILIBRIUM IN THERMOLUMINESCENCE MEASUREMENTS

Initial experiments involving the thermoluminescence spectra and glow curves of organic macromolecules gave erratic results that were attributed to the condensation of some atmospheric gases on the samples. Subsequent experiments conducted with the samples in high vacuum led to the conclusion that it was necessary to have a gas present during the irradiation and the

subsequent warmup in order to obtain the characteristic light emissions from the samples. Following experiments proved that the sole function of the gas was to produce temperature equilibrium between the sample and the bottom of the sample holder, although the sample was almost completely surrounded by walls at the sample holder temperature.

Heat transfer in vacuum between the sample and its environment takes place mainly by radiation. According to the well-known Stefan-Boltzmann law, the total rate at which energy is emitted in all wavelengths is proportional to the 4th power of its absolute temperature. The heat absorbed by the liquid-nitrogen-cooled walls per unit solid angle and per square centimeter will be much less than the heat supplied by the port into the optical spectrometer at room temperature. Therefore, the sample will be at equilibrium when its temperature is somewhere between room temperature and liquid-nitrogen temperature. Now if one equates the amount of heat gained by the sample via radiation from the room-temperature observation port and the amount of heat given up to the liquid-nitrogen-temperature surfaces by radiation from the sample, one obtains the equilibrium temperature the sample reaches. From the geometry of the sample holder, the fraction of solid angle subtended by walls at room temperature in our experiment is only 1%, and, if the holder is assumed to radiate like a black body, it is estimated that the sample will be in temperature equilibrium when its temperature is about -150°C .

To experimentally determine the sample temperature in vacuum a 0.003-in. iron-constantan thermocouple was attached to a thin copper disk which was embedded in a dry amino acid (tyrosine) sandwich. This sandwich was then placed in the sample holder, and the system was evacuated to 10^{-6} torr. In Fig. 15.14, one sees the sample temperature plotted as a function of time. It can be seen from the graph that the sandwich reached an equilibrium temperature of approximately -105°C . After the sample was at this temperature for 130 min, helium was introduced into the system at a pressure of 50 torr, and the powder temperature fell to liquid-nitrogen temperature in about 30 sec. If the sample is cooled in a gaseous atmosphere to -196°C and then the gas is evacuated, the temperature of the sandwich will rise until an equilibrium temperature warmer than -196°C is reached.

From these results it is obvious that the above-mentioned gas-pressure dependency is actually due to a temperature-regulating mechanism. When we irradiated an amino acid, tyrosine for example, at -196°C in a gaseous atmosphere, the sample was at liquid-nitrogen temperature, and the normal low-temperature trapping in metastable energy states could occur. Then, upon warming the sample, this trapped energy was released in the form of visible light. For tyrosine this release occurred at approximately -160°C . However, when the sample was excited in a vacuum of 10^{-6} torr, it never reached a low enough temperature for the trapping to occur. That is, the tyrosine powder in vacuum attained a temperature of approximately -150°C instead of -196°C ; consequently, when the holder was heated to room temperature, the characteristic light emission was not observed. These results are particularly important because they remove the doubt that has been associated with data obtained using powdered samples in a

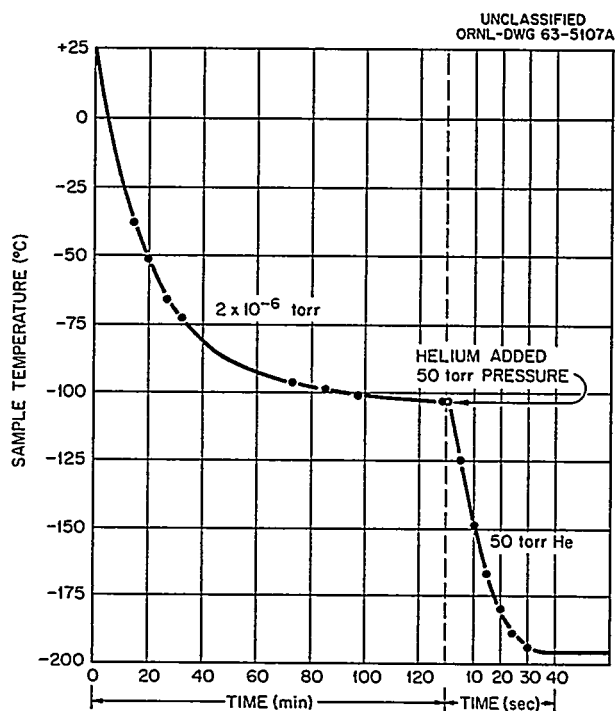


Fig. 15.14. Sample Temperature as a Function of Time After Sample Holder Is Cooled to -196°C . Helium is added at 130 min and time scale is changed as shown.

gaseous atmosphere. Also these results point to a possible source of error in thermoluminescence dosimetry.

A sample holder for thermoluminescence measurements was designed and fabricated for the first time out of boron carbide. The holder should be tissue equivalent for dose measurements, non-fluorescing and nonthermoluminescing, electrically and thermally conducting, structurally strong over a wide range of temperature, and capable of hold-

ing a high vacuum. After evaluating many materials with regard to the above requirements, a holder was designed and fabricated from boron carbide. Dose measurements in the holder using Fricke dosimeters and Victoreen meters indicated agreement with air dose values. All other requirements were satisfied by this holder. It is the only material we have found that satisfies all these requirements and may have important applications in dosimetry.

16. Professional Health Physics Training

K. Z. Morgan¹
M. F. Fair²

L. C. Emerson
H. H. Hubbell, Jr

Twenty-two students at Vanderbilt University and seven students at the University of Tennessee completed the course in Applied Radiation Physics in May 1964. Of the students at Vanderbilt, 18 were AEC Fellows and 4 were Vanderbilt students. The group at the University of Tennessee consisted of 3 AEC Fellows, 1 Advanced Health Physics Fellow, 1 citizen of India, and 2 University of Tennessee students.

Twenty AEC Fellows reported to the Health Physics Division in June for Applied Health Physics training. (One of the Vanderbilt Fellows elected to terminate his Fellowship after the academic training since he had had 3 years of applied work prior to accepting the Fellowship.) In addition to the AEC Fellows, two Public Health trainees from the University of Minnesota reported in June for 3 months training in the Applied Health Physics Section.

Twenty students for the 1964-1965 AEC Fellowship program were selected in March 1964. Sixteen

will enroll at Vanderbilt University and four at the University of Tennessee in September 1964.

A 30-hr course in Health Physics was presented by the Division for the ORSORT Program. The course consisted of lectures and tours covering various aspects of health physics.

Four of the AEC Fellows (1963-1964) who received extensions of their Fellowships elected to do their research work for the Master's degree at ORNL. Three were supervised by Health Physics Division personnel, and one was supervised by a member of the Solid State Division.

One citizen of Pakistan, one from Austria, and one from India have received training in the various sections of the Health Physics Division. One citizen of Israel completed 1 year of training in the Applied Health Physics Section in November 1963.

One member of the Education and Training Section was temporarily assigned to ORINS for 1 year and in this capacity presented the ORINS lectures ordinarily given by a member of the ORNL Education and Training Section. In addition, lectures and tours of the Laboratory were given for the U.S. Public Health Service, Cincinnati, Ohio; the University of North Carolina, Raleigh, North Carolina; and the ORNL Orientation Program.

¹Acting Chief, Education and Training Section.

²On temporary assignment with ORINS.

Part IV. Radiation Dosimetry

J. A. Auxier

17. Dosimetry Applications

J. A. Auxier

J. S. Cheka

C. G. Conn¹

J. L. Ellis¹

F. F. Haywood

W. R. Hendee¹

D. R. Johnson

T. D. Jones

J. W. Poston

DOSE DISTRIBUTION FUNCTIONS FOR JAPANESE HOUSES

Analysis of Japanese house shielding data was continued using, initially, the coordinate projector previously described.² Because of the large quantity of data and the multiplicity of parameters occurring in the experimental arrangements, progress was slow.

The method was replaced by a process known as "multiple regression and correlation," which works well with a digital computer. This process is used to obtain the best fit of a set of observations of dependent and independent variables by an equation of the form:

$$Y = b_0 + b_1x_1 + b_2x_2 + \dots + b_nx_n, \quad (1)$$

or any equation which can be transformed to this form by substitution such as $x_i = P_1P_2, P_1^n, \cos P_1, e^{\pm P_1}$, or $\log P_1$, where P_1 and P_2 are parameters.

A multiple regression solution gives the least-squares "best" value of the coefficients for a particular sample of observations. The solution also gives a measure of the reliability of each of the coefficients so that inferences can be made regarding the parameters of the population from which the sample of observations was taken, and insignificant parameters are eliminated.

¹Summer employee.

²J. A. Auxier, J. S. Cheka, and F. W. Sanders, WT-1725 (1961) (classified).

Multiple regression equations were derived for neutron dose, reactor-produced gamma-ray dose, and the dose resulting from a ⁶⁰Co source, which was assumed to approximate fission product gamma rays which failed to emerge from the reactor core. Nine parameters were found to be significant.

The following equations were found to predict dose with a probable error of less than 6%, that is, 50% of the predicted values deviated from the observed values by not more than 6%. This is analogous to a 50% confidence interval such that the maximum error is less than or equal to 6%.

Neutrons

$$\begin{aligned} D/D_{\text{air}} = & 0.33 + 0.0118FN + 0.675e^{-SP} \\ & - 0.00855IFW + 0.0456e^{-FS} + 1.597e^{-(US+HF)} \\ & - 0.0332FSS - 0.0267LS - 0.0116ILW, \quad (2) \end{aligned}$$

Hard Gamma

$$\begin{aligned} D/D_{\text{air}} = & 1.258 + 0.112FN - 0.00467SP \\ & - 0.00690FS, \quad (3) \end{aligned}$$

Soft Gamma (no front opening influencing readings)

$$\begin{aligned} D/D_{\text{air}} = & 0.382 + 0.625e^{-SP} + 0.242e^{-FS} \\ & + 0.111e^{-IFW}, \quad (4) \end{aligned}$$

Soft Gamma (front opening influencing readings)

$$D/D_{\text{air}} = 0.214 + 0.367e^{-SP} + 0.0535US + 4.006e^{-(US+HF)}. \quad (5)$$

In these equations

US (unshielded) = distance from front window, by 5-ft zones. If zone is fractional, use next integer. If no window, use 100.

HF = height above floor (ft). Use fractions.

FS = frontal shielding. Use: 0, if no shield; 1, if a wall in front; and 2, if one or more houses in front.

SP = slant penetration (ft).

FN = floor number. Use: 1, if single-story house; 2, if lower floor of two-story house; and 3, if upper floor of two-story house.

FSS = front shield size. Use: 0, if no shield; 1, if single-story house; and 2, if two-story house.

LS = lateral shielding. Use: 0, if size window and no external shield; 1, if no window and no external shield; 2, if lateral shield (house) and in zone 2; and 3, if lateral shield (house) and in zone 3. (See Fig. 17.1.)

ILW = number of internal lateral walls shielding locations.

IFW = number of internal front walls shielding locations.

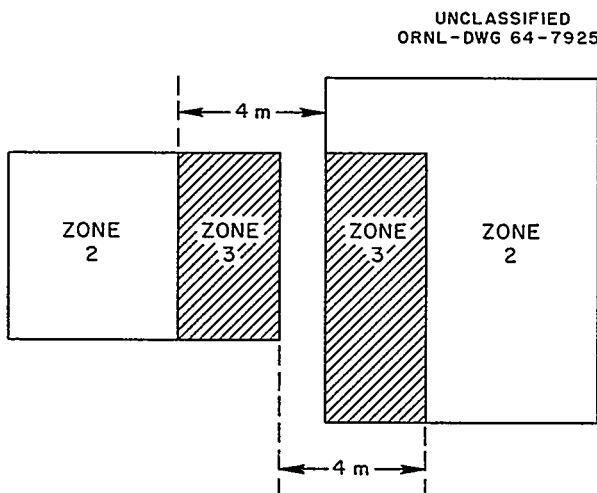


Fig. 17.1. Delineation of LS Zones.

Although this method was not derived to fit the physical parameters of this problem, it (1) selected variables relative to their importance, eliminating insignificant ones, (2) predicted dose values such that the probable error in the agreement between calculated magnitudes and instrumental observations was less than 6%, (3) yielded equations which were based on measured parameters, and (4) provided a means whereby Japanese technicians can evaluate dose values speedily and with no computational equipment other than a slide rule.

Equations (2-5), having been derived on the basis of Bare Reactor Experiment Nevada (BREN) data, were then tested on data from Hardtack, phase II. The neutron field data checked out within $\pm 6\%$ probable error, as defined above. The gamma-ray data, however, required a combination of the formulas for the hard and soft spectra, since with a weapon, the fission product gamma radiation is not attenuated as with the core of the reactor.³ It was found by trial and error that if these were combined on the assumption of a relative distribution of 45% hard and 55% soft gamma, the calculated or predicted values agreed to within $\pm 6\%$ with the majority of the field measurements.

It was assumed that this division of the gamma spectrum would be a good approximation to that at Nagasaki. Since the neutron-gamma ratio at Hiroshima was somewhat higher, a 55 to 45% hard-to-soft gamma ratio was assumed to fit that city better.

The combined equations for use at Nagasaki are as follows:

$$D/D_{\text{air}} = 0.587 + 0.344e^{-SP} + 0.133e^{-FS} + 0.0609e^{-IFW} + 0.0504FN - 0.00210SP - 0.00284FS \quad (6)$$

if the point of interest is not near a window, and

$$D/D_{\text{air}} = 0.684 + 2.209e^{-US+HF} + 0.202e^{-SP} + 0.294US + 0.0504FN - 0.00210SP - 0.00284FS \quad (7)$$

if the point of interest is near a window.

³S. Glasstone (ed.), *The Effects of Nuclear Weapons*, Chap. 8, sect. 8.13, USAEC, Washington, 1962.

The corresponding equations for Hiroshima are:

$$D/D_{\text{air}} = 0.708 + 0.281e^{-SP} + 0.109e^{-FS} \\ + 0.049e^{-IFW} + 0.0616FN \\ - 0.00257SP - 0.00946FS \quad (8)$$

if the point of interest is not near a window, and

$$D/D_{\text{air}} = 0.787 + 1.803e^{-US+HF} \\ + 0.165e^{-SP} + 0.0241US + 0.0616FN \\ - 0.00257SP - 0.00346FS \quad (9)$$

if the point of interest is near a window.

Equation (2) is used for neutrons in both cities.

The Japanese technicians in the ABCC shielding groups in Hiroshima and Nagasaki were instructed in the application of these formulas. With the use of case histories, criteria for applicability of the various parameters were defined, and detailed instructions were written for the use of the equations by technicians.

The results are to be coded on IBM cards, so that final figures for exposure of individuals can be easily obtained on establishment of good radiation yield values for the two weapons.

Studies of Cobalt Activation in Steel

Ten steel samples were obtained from concrete buildings in Hiroshima for cobalt activation analysis. In each case, the sample was attached to an exterior wall, but outside the concrete surface. Location and geometry of each specimen had been documented. Cobalt content was determined spectroscopically; cobalt activation was determined by placing samples in a well NaI crystal spectrometer and measuring the cobalt peaks. An estimate of the neutron field will be obtained on calibration of cobalt samples exposed to the fission spectrum at simulated geometry.

Another study of cobalt activation in steel is being conducted in collaboration with the Institute of Radiological Sciences in Japan. In this case, only specimens embedded at least 8 cm deep in concrete are being considered. The comparison of the specimens in the two geometries will show whether cobalt measurements in air give neutron

field values which are in agreement with those made on the moderated spectrum inside concrete.

AIR-GROUND-INTERFACE EFFECT

A series of gamma-ray and neutron dose measurements were made in an air-over-ground geometry during Operation BREN (Bare Reactor Experiment Nevada).⁴⁻⁶ Measurements of dose were made in radiation fields from steady-state operation of the ORNL Health Physics Research Reactor and from a ⁶⁰Co source whose apparent activity was 800 curies.

It is generally stated that the presence of the air-ground interface tends to increase the measured dose near the source and decreases it at large distances. That is, at a certain distance (R) from the source, the dose in an air-over-ground geometry is equal to what it would be at the same distance in an infinite air medium. At distances less than (R) the measured dose is greater than that in the infinite medium, and at distances larger than (R) the measured dose is less than that for the infinite medium. This behavior can be demonstrated best by plotting the ratio, dose in the finite medium to dose in the infinite medium ($D_{\text{finite}}/D_{\infty}$), as a function of slant range (R) for several source-detector configurations.

In Fig. 17.2, the variation of $D_{\text{finite}}/D_{\infty}$ with slant range is presented for the HPRR support at 27 ft above the interface and neutron detectors lying on the interface. This is compared with computed data by Ritchie⁷ for a 3-Mev neutron source supported at 33 ft above the interface and detector on the interface. These two curves are found to be in good agreement over a range of several hundred yards.

This ratio ($D_{\text{finite}}/D_{\infty}$) is frequently referred to as a boundary correction factor (K). Berger⁸ has computed boundary correction factors for several

⁴F. W. Sanders et al., *Operation Plan and Hazards Report - Operation BREN*, CEX-62.02 (1962).

⁵J. A. Auxier, F. F. Haywood, and L. W. Gilley, *General Correlative Studies - Operation BREN*, CEX-62.03 (1963).

⁶F. F. Haywood, J. A. Auxier, and E. T. Loy, *Neutron and Gamma-Ray Dose Distributions Above Air-Ground Interface - Operation BREN*, CEX-62.14 (to be published).

⁷R. H. Ritchie, *Health Phys. Div. Ann. Progr. Rept. July 31, 1961*, ORNL-3189, pp. 145-48.

⁸M. J. Berger, *J. Appl. Phys.* 28, 1502-8 (1957).

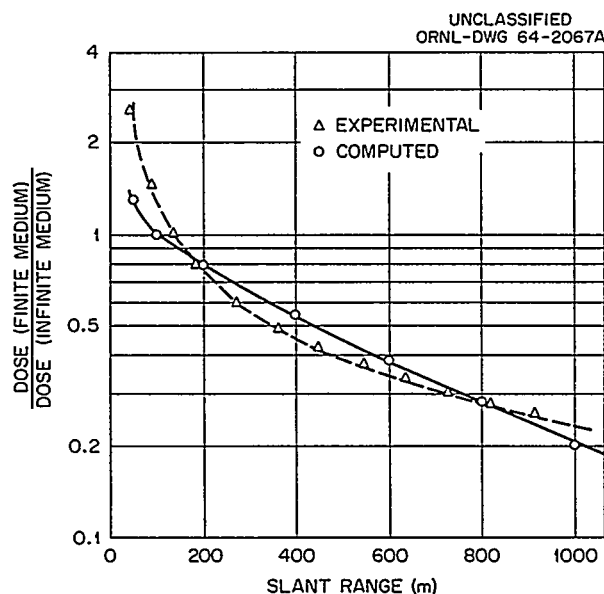


Fig. 17.2. Comparison of Experimental Boundary Correction Factor $K_{(exp)}$ to Computed Boundary Correction Factor for Neutron Dose as a Function of Slant Range (R).

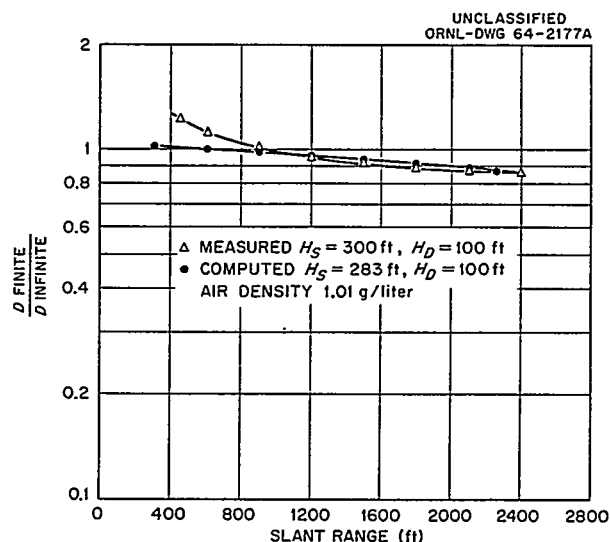


Fig. 17.4. Comparison of $K_{(exp)}$ for a ^{60}Co Source Height of 300 ft and Detector Height of 100 ft, to K for a ^{60}Co Source Height of 283 ft and Detector Height of 110 ft, as a Function of Slant Range (R).

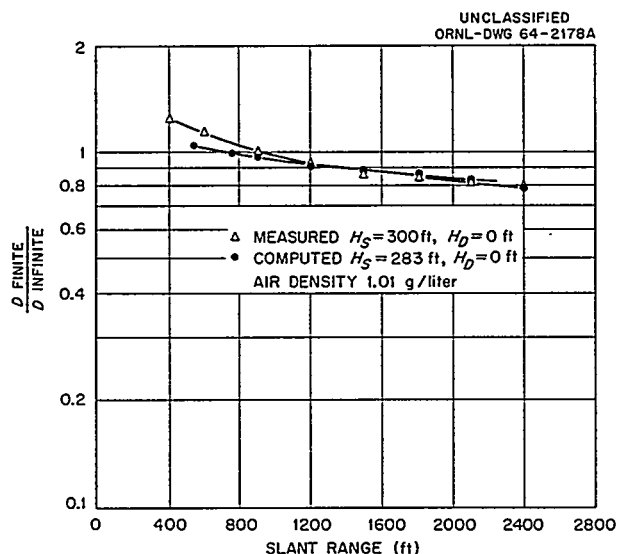


Fig. 17.3. Comparison of $K_{(exp)}$ for a ^{60}Co Source Height of 300 ft and Detector Height of 0 ft, to K for a ^{60}Co Source Height of 283 ft and Detector Height of 0 ft, as a Function of Slant Range (R).

source-detector configurations. Computed values of (K) are compared with experimentally determined boundary correction factors [$K_{(exp)}$] in Figs. 17.3 and 17.4. In Fig. 17.3, the variation of $K_{(exp)}$ with slant range for a ^{60}Co source supported at 300 ft above the air-ground interface and detector lying on the interface is compared with the variation of K with slant range for a ^{60}Co source supported at 283 ft (one-half the mean free path at 1.01 g/liter) and detector lying on the interface. In Fig. 17.4, a similar comparison is presented; but in this case, the detectors are supported at 100 ft above the interface.

In each of the three figures above, it is seen that D_{finite}/D_{∞} is >1 near the source and <1 at large distances, hence supporting the general air-ground-interface theory.

METAPHOSPHATE-GLASS MICRODOSIMETERS

The investigation of change of fluorescence of three types of metaphosphate glass with time in

dark storage after single exposures to gamma radiation^{9,10} has been reported.¹¹ The types used comprised the Bausch and Lomb high-Z, the Bausch and Lomb low-Z, and Toshiba II, also a low-Z glass. The exposures ranged from 100 r to 100 kr. Time elapsed between exposure and readout ranged from 1 day to 1 year.

Two types of centers (fluorescent and absorption) are formed in the glass by irradiation. Both of these increase with irradiation; but the latter, producing a visible discoloration and opacity at about 10 kr, interferes with readout of fluorescence, causing a drop from linearity, and at sufficiently high exposures, a reversal.

⁹J. A. Auxier et al., *Health Phys. Div. Ann. Progr. Rept. July 31, 1962*, ORNL-3347, p. 93.

¹⁰J. A. Auxier et al., *Health Phys. Div. Ann. Progr. Rept. June 30, 1963*, ORNL-3492, p. 153.

¹¹J. S. Cheka, *Health Phys.* 10, 303 (1964).

After irradiation, the fluorescent centers build up, pass through a maximum, and then reverse. The maximum is attained in 10 to 20 hr in high-Z glass and about 3 months in both of the low-Z types. At the end of 1 year, the high-Z glass reads ~78% of the 24-hr reading for moderate exposures (≤ 1000 r). The low-Z types attained maxima of less than 10% above 24-hr readings in about 100 days, then dropped slowly, being approximately equal to 24-hr readings at the end of 1 year.

The opacity subsides at a faster rate, so that at 100 kr the high-Z rods maintained readings of approximately unity through 1 year, while the low-Z rods increased in fluorescence output throughout the year, reaching +42% for Bausch and Lomb low-Z and +28% for the Toshiba II glass.

The fluorods were tested for the effect of sunlight on readout. Two hours of direct sunlight reduced the fluorescence output by ~20% in all three types. This implies that for use in dosimeters, the glass must be shielded from light.

18. Dosimetry Research

J. H. Thorngate

M. D. Brown¹

W. L. Croft²

D. R. Johnson

J. F. Lemontt²

J. E. Parks¹

P. T. Perdue

RESPONSE OF A NEUTRON-INSENSITIVE GAMMA-RAY DOSIMETER AS A FUNCTION OF PHOTON ENERGY

A gamma-ray dosimeter with low neutron sensitivity has been described previously by Wagner and Hurst.³ This dosimeter uses a small Geiger-Mueller counter suitably shielded with tin and lead to make its response more uniform at gamma energies below 200 kev. Wagner found that the

response of the dosimeter from 200 kev to 1.25 Mev was approximately proportional to exposure in roentgens.

The dosimeter response above 1.25 Mev has been determined with gamma rays obtained from a number of proton-induced resonance reactions which were run at the ORNL 5-Mev Van de Graaff accelerator.

The dosimeter response in counts per photon per square centimeter is shown in Fig. 18.1 as a function of photon energy. When these data are weighted to a first-collision tissue-dose curve, such as that given in *NBS Handbook 75*, the results shown in Fig. 18.2 are obtained. The average response up to 2 Mev is 4.26×10^6 counts

¹Graduate student (2 days/week).

²Summer employee.

³E. B. Wagner and G. S. Hurst, *Health Phys.* 5, 20-26 (1961).

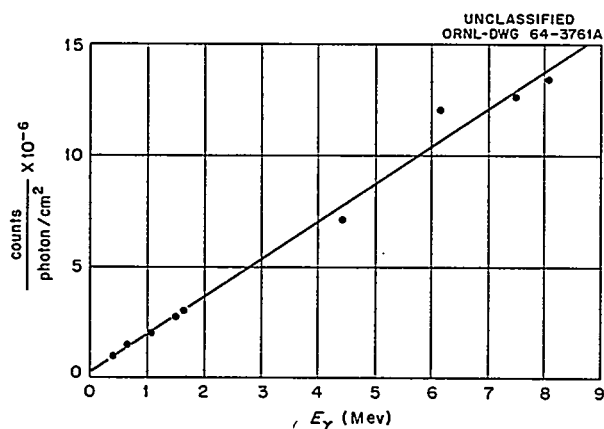


Fig. 18.1. Dosimeter Fluence Response.

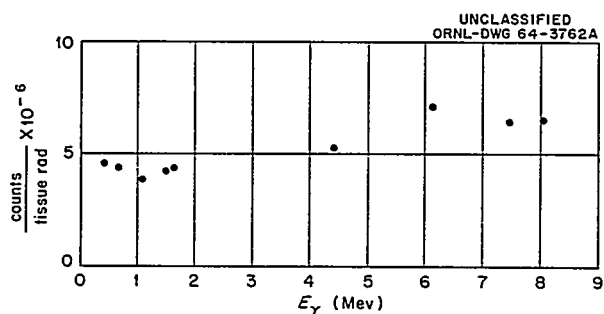


Fig. 18.2. Dosimeter Dose Response.

per tissue rad, which is in good agreement with data published previously by Wagner. An average of all the points is $(5.17 \pm 1.26) \times 10^6$ counts/rad, which is equivalent to 86 counts/min per millirad per hour.

NEUTRON DOSE CONVERSION FACTORS FOR PuBe AND PoBe SOURCES

A calculational and an experimental program were conducted to determine the average first-collision tissue dose in rads neutron⁻¹ cm⁻² produced by PuBe and PoBe neutron sources. Calculated values were obtained using eight previously published PoBe spectra and four PuBe

spectra which were weighted according to the first-collision tissue dose as a function of neutron energy. In addition, a direct measurement was made of the energy deposited by the neutrons in a polyethylene-lined, cyclopropane-filled proportional counter.⁴ Calculated values were $(4.08 \pm 0.20) \times 10^{-9}$ rad neutron⁻¹ cm⁻² for PoBe and $(3.90 \pm 0.06) \times 10^{-9}$ rad neutron⁻¹ cm⁻² for PuBe sources. The corresponding experimental values were $(4.0 \pm 0.2) \times 10^{-9}$ for PoBe and $3.9 \pm 0.2 \times 10^{-9}$ for PuBe sources. A value of 4×10^{-9} rad neutron⁻¹ cm⁻² was chosen for use with both PuBe and PoBe sources.

EXPERIMENTAL CALIBRATION OF FISSION-FOIL THRESHOLD DETECTORS

A surface-barrier detector was used with thin fissile targets to calibrate the fission foils used in the Hurst threshold-detector system. The detector efficiency was determined by irradiating it in a known thermal-neutron fluence using ²³⁵U and ²³⁹Pu targets. Efficiencies for measuring fast-neutron fluences using ²³⁹Pu, ²³⁸U, and ²³⁷Np targets were calculated by multiplying the efficiency for counting thermal neutrons by the ratios of fast to thermal fission cross sections. Then the detector was mounted in a cadmium cup and a Hurst-type ¹⁰B sphere (as shown in Fig. 18.3) and exposed to fast neutrons from the HPRR using the various fissile targets. Standard-size fission foils, also shielded by a cadmium cup and a ¹⁰B shield, were irradiated simultaneously in the same geometry. New fission product decay curves were determined using the fast-neutron fluences as measured with the diode detector and the weights and gamma count rates of the standard fission foils. The new decay curves, which are shown in Fig. 18.4, describe as a function of time the gamma activities of the foils per gram per 10¹⁰ neutrons/cm² above their threshold energies. The overall differences between the former decay curves as they appear in the literature and the present $N(t)$ curves can amount to differences of ~10 to 20% when used to calculate fast-neutron fluences. These differences are due both to cross-section revisions and to refinements made by the present research.

⁴E. B. Wagner and G. S. Hurst, *Rev. Sci. Instr.* 29, 153-58 (1958).

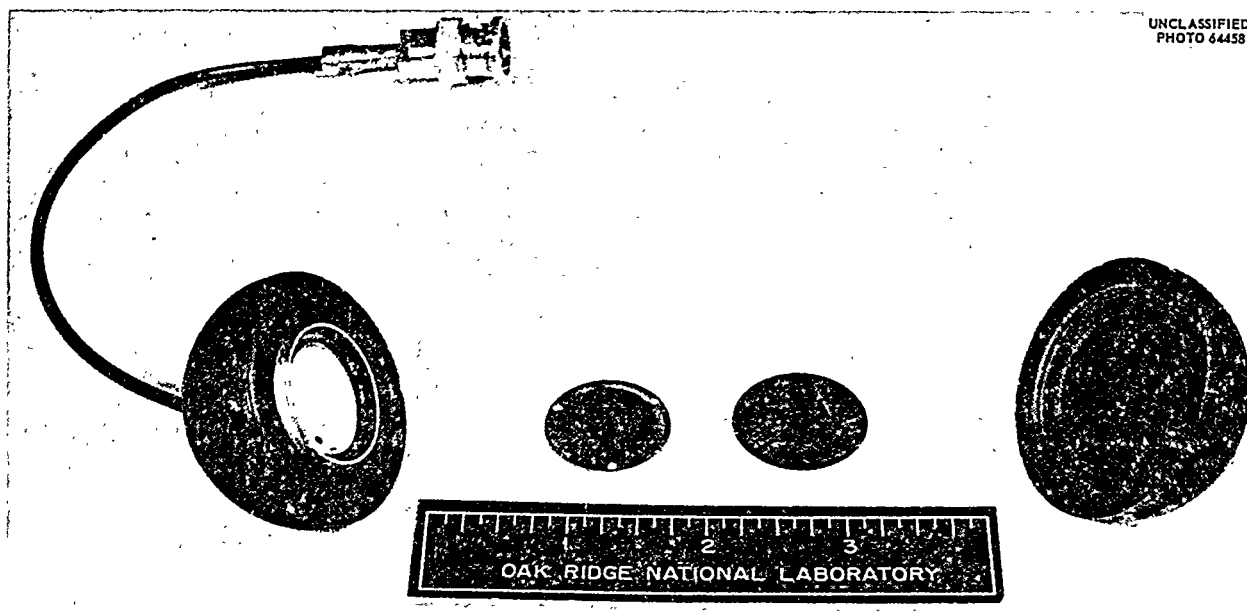


Fig. 18.3. Surface Barrier Detector Mounted in Cadmium Cup and ^{10}B Shield.

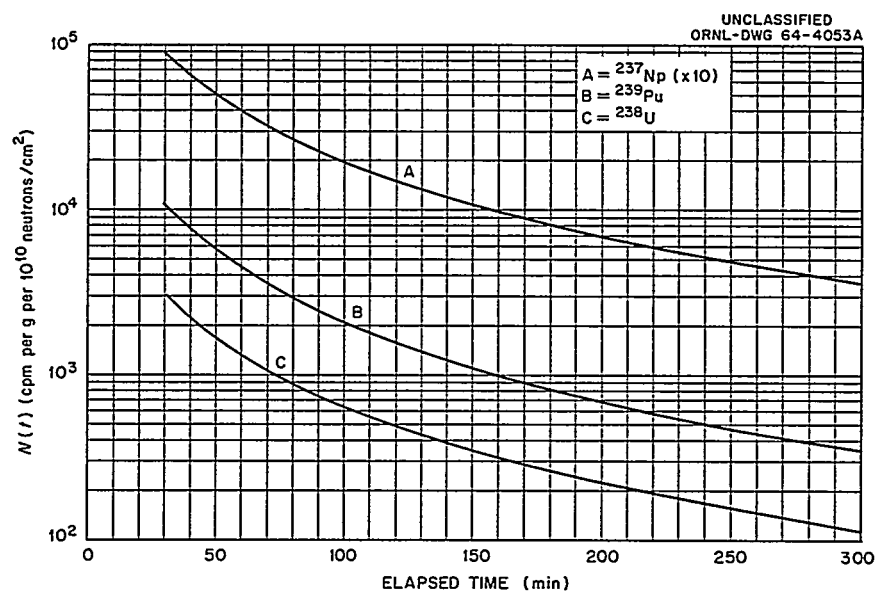


Fig. 18.4. Fission Product Decay Curves for ^{239}Pu , ^{238}U , and ^{237}Np .

FEASIBILITY STUDY FOR A PROPOSED NEUTRON SPECTROMETER

A neutron spectrometer was proposed in which a proportional counter was to be used to discriminate against recoil protons not scattered in the forward direction relative to the incident neutrons. Ion tracks which occur parallel to the center wire of a proportional counter produce a voltage pulse with a faster rise time than that of an extended track which is perpendicular to the wire⁵ so that those not parallel to the wire would have pulses with rise times slower than those of the parallel cases.

In order to test the idea in general, an analytical expression was found in which the pulse shape could be found for tracks of any orientation within a counter. The resultant expression is:

$$V(\tau) = \int_0^R N_0 B \left[\ln \left(1 + \frac{\tau - t}{t_0} \right) \right] (R - 1)^{(1/n)-1} dL,$$

where N_0 is the number of ion pairs formed by the recoil proton, B and t_0 are constants depending upon the counter geometry, R is the range of the recoil proton, n is the exponent in the range-energy relation, and L is a variable of integration over the range of the recoil proton. Here, t is a complicated expression taking into account range-energy relationships, the dE/dx factor, the polar angles, the azimuthal angles, the distance from the wire where the track originates, the electric field as a function of the distance from the center wire, the ionization time, the drift time of the electrons and the positive ions, and all the physical parameters of the counter. It was assumed that the drift velocity and positive-ion mobility were directly proportional to the electric field divided by the pressure, and no diffusion effects were introduced since they were assumed to be negligible.

The analytical expression was programmed for the computer, and pulse shapes due to oblique tracks were compared with ones due to parallel tracks. Upon making comparisons between pulses of parallel and oblique tracks, it was found that

similar pulse shapes occurred for a number of orientations.

No experimental evaluation was made, due to the significant number of similar pulse profiles for oblique tracks. In addition, a simple calculation of the effects of electron diffusion indicated that this would be a major problem.

NEUTRON LEAKAGE NORMALIZING CHANNEL FOR HP RR

At the ORNL Dosimetry Applications Research (DOSAR) facility, separate runs of the HP RR are normalized to one another with sulfur pellets which are placed in a reproducible position and changed for each run. Because such a system is not adequate for normalizing short exposures made at low power, a fission counter normalizing system has been designed for use with the reactor. The counter uses natural uranium as the fissionable material. A fast fission reaction decreases the sensitivity of the normalizing counter to environmental changes. In operation, the counter is shielded with cadmium to make the contribution due to thermal fissioning of ^{235}U in the target foil insignificant.

The counter is fastened in a fixed position on the reactor superstructure so that it will remain at a known distance from the core regardless of reactor orientation. The signal produced in the counter is amplified by a factor of 100 with a high-gain preamplifier designed to have low radiation sensitivity and good line-driving characteristics. A transistorized double-decay-line amplifier located in the control building further amplifies the signal and operates a high-speed discriminator. Counting is done on a scaler having a 10-nsec resolving time. High-speed electronic equipment is required since the fission counter is designed to produce 10 counts/sec per watt of reactor power; this results in a maximum of 10^5 counts/sec at maximum reactor power.

DOSAR PORTABLE SCALER

A versatile portable scaler has been built for field measurements. It uses three transistorized scales of 10 to provide a scale of 1000 followed by a mechanical register to provide four additional decades of count storage. The scaler has a double

⁵G. S. Hurst and R. H. Ritchie, *Rev. Sci. Instr.* 24(8), 664-68 (1953).

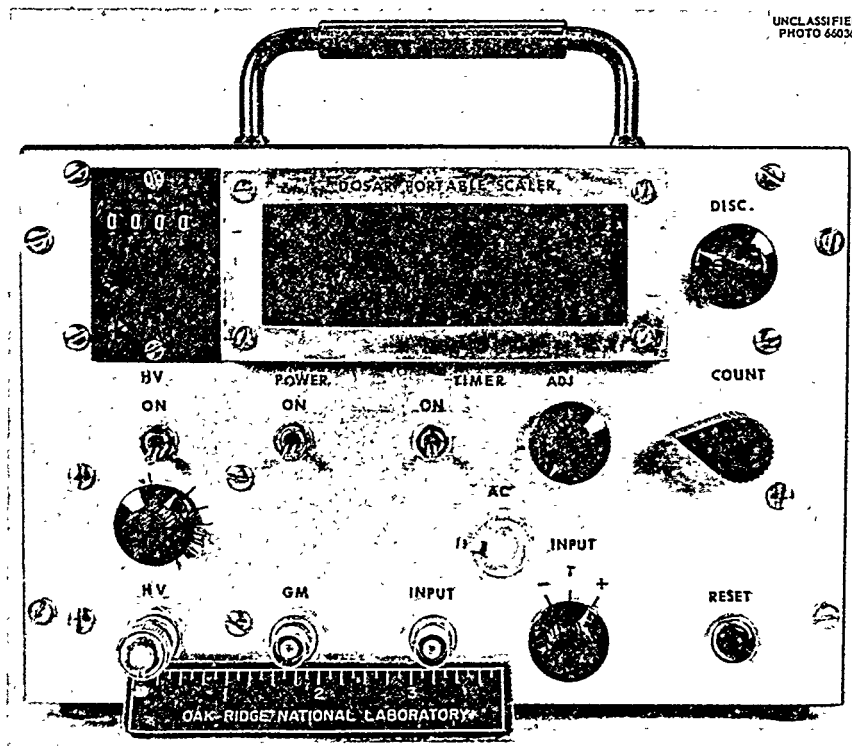


Fig. 18.5. DOSAR Portable Scaler.

pulse resolving time of 7 μ sec but is limited to a continuous count rate of 3×10^3 /sec by the mechanical register.

The pulse-height discriminator varies from 0.1 to 5 v for positive pulses and from 0.005 to 5 v for negative pulses; however, input pulses as large as 25 v will not cause circuit damage. An internal test signal is available for checking the circuits. Timed runs from 10 sec to 10 min are possible using an internal timer which is reproducible within 0.5%. High voltages from 200 to 1500 v at up to 100 μ a are available from a built-in regulated power supply. The scaler will operate for 24 hr on one charge of the nickel-cadmium battery. The scaler is shown in Fig. 18.5.

HPRR FAST-NEUTRON SPECTRUM USING THE ${}^6\text{Li}(n,\alpha){}^3\text{H}$ REACTION

The fast-neutron energy spectrum of the HPRR was determined using a spectrometer consisting

of two closely spaced surface-barrier detectors, one of which was coated⁶ with a thin layer of ${}^6\text{LiF}$. Fast neutrons incident on the spectrometer gave rise to ${}^6\text{Li}(n,\alpha){}^3\text{H}$ events, releasing a total energy equal to the neutron energy plus the reaction Q value of 4.78 Mev. The total energy shared by the particles was indicated by summing the output pulses from the two detectors. The large Q value of the reaction provided a bias against gamma rays and low-energy background events, while fast coincidence gating of the summed information reduced the spectrometer's response to undesired (n,p) and (n,α) reactions in the silicon detectors. A background unit which was identical to the neutron spectrometer except for having no ${}^6\text{LiF}$ coating was useful in subtracting these undesired background events.

⁶T. A. Love and R. B. Murray, *Use of Silicon Surface-Barrier Counter in Fast Neutron Detection and Spectroscopy*, ORNL-CF-60-5-121.

*circuit drawing
for this instrument
65-6641
65-6642*

The spectrometer's response to monoenergetic neutrons was observed using 2.95-Mev neutrons from the $D(d,n)^3\text{He}$ reaction and is shown in Fig. 18.6. The resolution was ~ 300 kev. The fast-neutron energy spectrum of the HP RR as measured with this spectrometer is shown in Fig. 18.7. The

shape of the spectrum is similar to that of Godiva II.⁷

⁷M. G. Chasanov and B. F. Wadding, *Analytical Fit for Godiva II Neutron Spectrum*, IBO-1584 (1958).

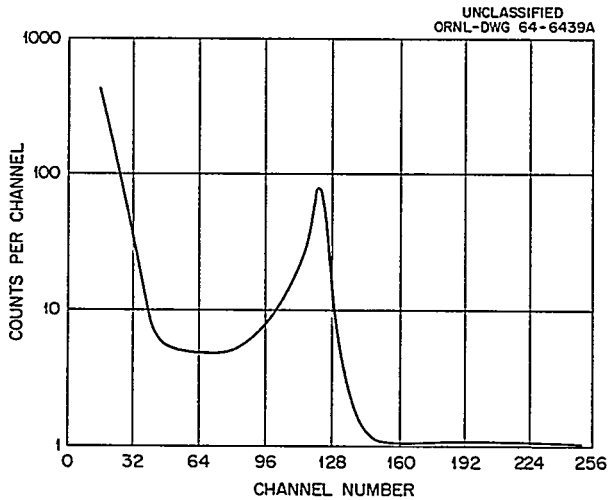
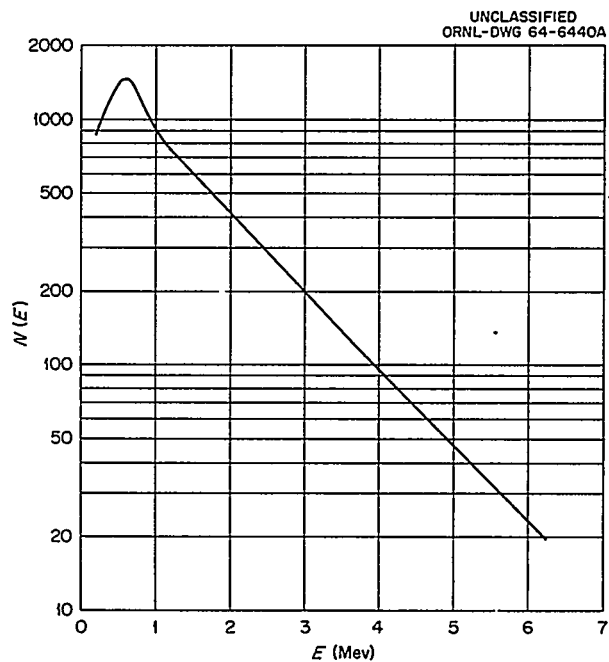


Fig. 18.6. Response of Spectrometer to 2.95 Mev Neutrons.

Fig. 18.7. Neutron Energy Spectrum of HP RR.



19. HPRR Operations and Special Projects

L. W. Gilley¹

C. R. McAmis²

H. T. Miller³

J. W. Poston

T. G. Provenzano³

F. F. Haywood

E. M. Robinson

W. H. Shinsaugh, Jr.

E. J. Story⁴

D. R. Ward¹

THERMAL-NEUTRON PILE

In an effort to regain some of the thermal-neutron calibration capability which was eliminated when the ORNL Graphite Reactor was retired, a thermal-neutron irradiation facility was designed and fabricated at the HPRR.

Several cubical configurations of graphite were examined to determine the physical size in which the optimum relation between neutron flux and cadmium ratio was observed. The final configuration consisted of a stack of graphite 156 cm wide, 165 cm deep, and 152 cm high (see Fig. 19.1). The reactor is operated either at steady state or in a burst mode with the core positioned 3 m from the front face of the graphite. A sample irradiation chamber $10 \times 10 \times 20$ cm is located ~ 95 cm deep along the horizontal center line of the graphite pile.

The ratio, thermal-neutron flux to "epi-cadmium" flux, was found to be 214 at a depth of about 1 m. The thermal-neutron fluence rate at this depth was 2×10^7 neutrons $\text{cm}^{-2} \text{sec}^{-1} \text{kw}^{-1}$. Because the HPRR may be operated at a steady-state power of 10 kw for short periods, the maximum attainable fluence rate is 2×10^8 neutrons $\text{cm}^{-2} \text{sec}^{-1}$. For a burst of 1×10^{17} fissions, a fluence rate of $\sim 10^{18}$ neutrons $\text{cm}^{-2} \text{sec}^{-1}$ is available for ~ 40 μsec . The thermal-neutron fluence rate as a function of reactor power and depth in the graphite pile is presented in Fig. 19.2.

¹On loan from Neutron Physics Division, ORNL.

²On loan from Instrumentation and Controls Division, ORNL.

³Visiting investigator from Armed Forces Radiobiology Research Institute, Bethesda, Md.

⁴Visiting investigator from Edgerton, Germeshausen, and Grier, Inc., Santa Barbara, Calif.

OPERATION HENRE

As a result of research accomplished during Operation BREN in 1962, it has been proposed that a monoenergetic point neutron source be constructed and operated on the same tower. The field experiment which would be conducted at this time has been designated as Operation HENRE (High Energy Neutron Reactions Experiment). In order to obtain a significant neutron fluence rate at distances to 1500 m, the most feasible method (because of weight and size limitations) is a positive-ion accelerator employing the $T(d,n)^4\text{He}$ reaction. The accelerating potential of the D_1^+ ions would be ~ 150 kv.

In January 1964, a group was formed at ORNL to undertake a detailed feasibility study concerning the design, construction, and operation of such a neutron source. This study group was made up of employees of the Health Physics Division, Thermonuclear Division, the U.S. Army, and Edgerton, Germeshausen, and Grier, Inc. Specifically, the feasibility study was to determine if an accelerator could be constructed so that it would (1) meet the weight and volume restrictions compatible with the present hoisting mechanism on the 1500-ft tower and (2) be capable of producing an average of 10^{13} neutrons/sec for a period of 4 hr. By May 1964, the study had resulted in the conclusion that it was feasible to build such an accelerator and have it perform satisfactorily.

Technology in the fields of target and ion source development have advanced markedly. Titanium-tritide targets have been tested, with a resulting neutron yield of 9.6×10^{10} neutrons/sec per ma of D_1^+ beam with a target half-life of 3 to 4 hr. An erbium-tritide target has been found to yield 1.1×10^{11} neutrons/sec per ma with a half-life of 1.85 hr. The absorbing film of these targets (titanium and erbium) was $\sim 4 \text{ mg/cm}^2$ thick. A highly

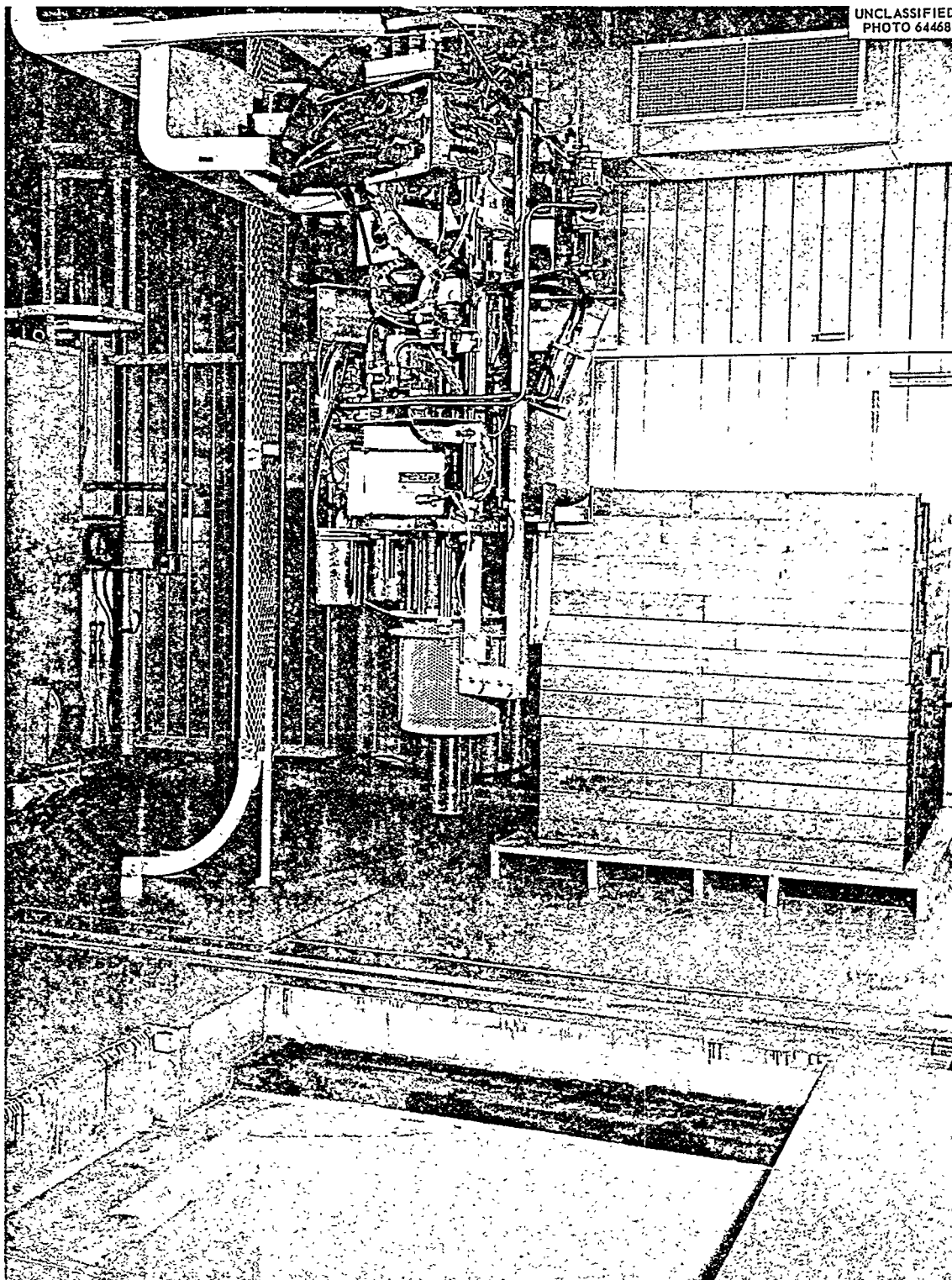


Fig. 19.1. HPRR Thermal Neutron Irradiation Facility.

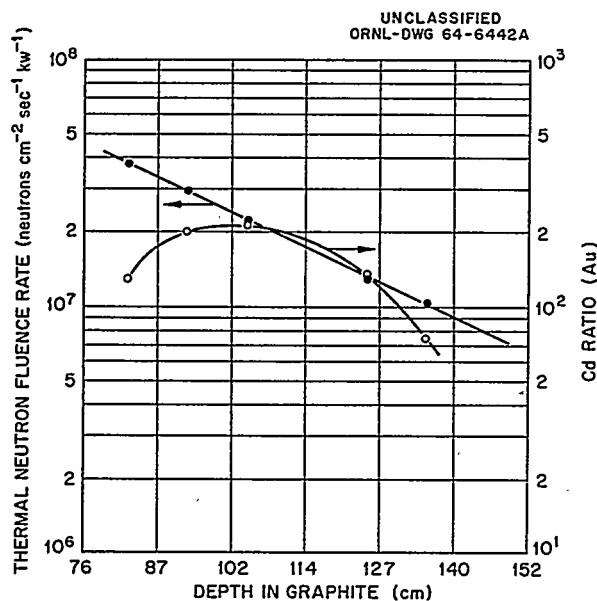


Fig. 19.2. Thermal Neutron Fluence Rate as a Function of Reactor Power and Depth in the Graphite Pile.

reliable duoplasmatron ion source has been developed by the Thermonuclear Division for the injection of high beam currents into the DCX-1 and DCX-2 machines. This type of ion source has been chosen for use in the HENRE neutron source because it has been operated at a beam current of 300 ma for 4 hr. Thus, a target yield of 7×10^{10} neutrons $\text{sec}^{-1} \text{ma}^{-1}$ with a 4-hr half-life, and an ion source operating at 300–500 ma would produce 2.1 to 3.5×10^{13} neutrons $\text{sec}^{-1} \text{ma}^{-1}$ so that the average neutron yield for 4 hr would be $\geq 1 \times 10^{13}$ neutrons/sec.

The major problem associated with the final design of the neutron source is that of target cooling. For an accelerating potential of 150 kv and a maximum beam current of 500 ma, 75 kw of heat must be removed from the target. Experiments have been conducted, and 68 kw have been dissipated from a mockup target assembly by circulating water through the target chamber and cooling the water by blowing air through standard automotive radiators. Refinements in this system must be made to minimize the physical size of the component package and to minimize the temperature of the water recirculated into the target chamber.

The experimental objective of Operation HENRE is to define the radiation fields at large distances from a point isotropic source of fast neutrons. Numerous computer calculations have been made to describe these radiation fields. This neutron source will then serve as a "fiducial" point for normalizing experimental data to computed data.

Specifically, the field experiments will be broken down into three main categories as follows.

HENRE Experimental Program

Free-Field Measurements

- A. Neutron dose as a function of slant range, height of neutron source, height of detector, and angle of incidence at detector.
- B. Gamma-ray exposure as a function of slant range, height of neutron source, height of detector, and angle of incidence at detector.
- C. Neutron fluence as a function of neutron energy and angle of incidence, for several source heights and for several slant ranges.
- D. Gamma-ray fluence as a function of gamma-ray energy and angle of incidence, for several source heights and for several slant ranges.
- E. Analysis of neutron-induced activity in soil as a function of depth in soil, neutron source height, and slant range.

Shielding

- A. Neutron dose and gamma-ray exposure, as a function of composition of shield, geometrical shape, thickness, neutron source height, and slant range.
- B. Neutron fluence as a function of neutron energy, angle of incidence, and other parameters in (A).
- C. Neutron dose and gamma-ray exposure inside "holes in the ground, with and without covers," as a function of depth into the hole for several neutron source heights and several slant ranges.
- D. Neutron fluence in these "holes" as a function of neutron energy and depth into the holes for several source heights and several slant ranges.
- E. Neutron dose and gamma-ray exposure inside Japanese houses.

Radiobiology

- A. Neutron dose and gamma-ray exposure in man-sized phantoms, as a function of depth in the phantom, slant range, and neutron source height.
- B. Analysis of neutron-induced activation of elements in biological systems.

HEALTH PHYSICS RESEARCH REACTOR OPERATIONS

The HPRR has been operated successfully for ~70 kwhr. Animal irradiations and dosimetry research account for the majority of experiments. Users of reactor time include ORNL divisions in addition to Health Physics, university groups, AEC contractors, private industry, and representatives of three foreign nations.

A second reactor core has been fabricated for the HPRR. This core is to be used in experiments in which it is necessary to maintain a high ratio of neutron to gamma-ray dose. It is often necessary to measure small values of gamma-ray exposure during reactor operation. Therefore, the contribution to total exposure by gamma rays from the fission product inventory must be insignificant. Because high-power, steady-state operations (to 10 kw) and burst operations (to 1×10^{17} fissions) are performed periodically, the residual fission product activity in one core can be high (0.2 to >1.0 r/hr at 1 m). It is then necessary to have two cores available to accommodate the variety of operational requirements.

The critical mass of core 2 was found to be within 1.5% of core 1. The two adjustable control rods (regulating and mass adjustment) were calibrated as a function of their position in the reactor.

A series of reactor physics experiments were performed for the HPRR in the burst mode of operation in order to calibrate the burst rod for fission yields up to 6×10^{16} fissions for the unreflected core. This was accomplished by measuring the fission yield as a function of $\Delta\rho$ of the core at the time the burst rod was fired into the core. This procedure is to be extended to 1×10^{17} fissions (maximum target burst). An experiment has been prepared and instruments have been installed so that the "wait time," or time between insertion of burst rod and initiation of burst, may be measured. In this same experiment the time

interval between initiation of burst and ejection of safety block will be measured. It is expected that this experiment will assist in further understanding the fundamental differences in burst shape and yield for a fixed critical mass.

A neutron and gamma-ray dose mapping experiment was conducted in order to gain information relative to dose as a function of distance from the reactor and as a function of reactor power. Such information is useful in determining the position of experiments and reactor power level. Measurements of dose were made at separations ranging from 0.5 to 14 m from the center of the core to the detector for several detector heights and corresponding reactor heights. The "Radsan" fast-neutron dosimeter and the "Phil" gamma-ray dosimeter were used for this experiment. Results of the experiment are shown in Figs. 19.3 and 19.4, where dose rate per unit reactor power is

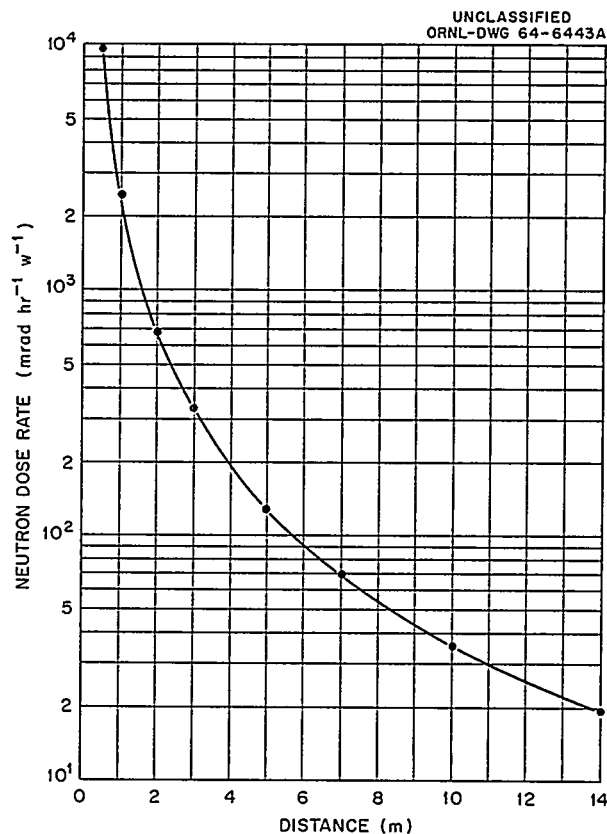


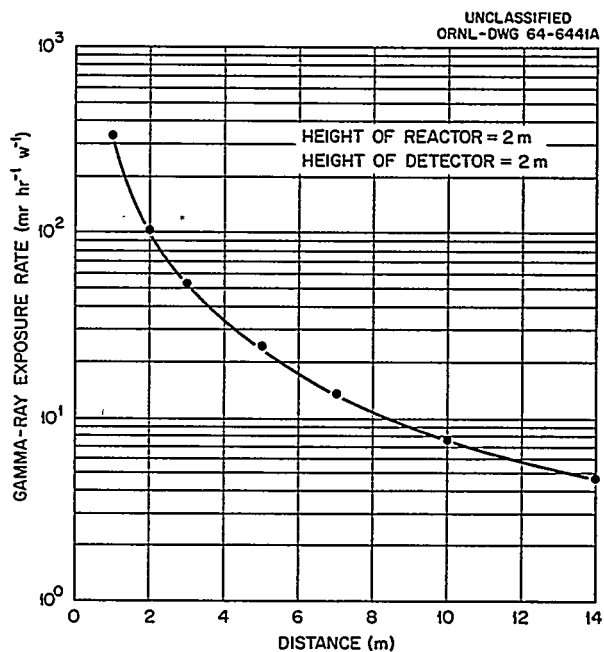
Fig. 19.3. Fast Neutron Dose Rate as a Function of Distance for Reactor and Detector 2 m Above the Floor.

plotted as a function of separation between source and detector for reactor and detector 2 m above the floor.

The source-detector geometry was varied such that runs were made with the reactor and detector at the same height above the floor and with the

reactor and detector at different heights. For a given power level and distance from the reactor, the dose appeared to be fixed regardless of source or detector height, but the scattering from floor and wall surfaces did not allow a $1/D^2$ reduction in dose as a function of distance (D).

Fig. 19.4. Gamma-Ray Exposure Rate as a Function of Distance for Reactor and Detector 2 m Above the Floor.



Part V. Internal Dosimetry

W. S. Snyder

20. Internal Dose Estimation

URINARY EXCRETION OF TRITIUM FOLLOWING EXPOSURE OF MAN TO HTO - A TWO-EXPONENTIAL MODEL

W. S. Snyder B. R. Fish

S. R. Bernard Mary R. Ford J. R. Muir

The metabolic course of HTO in the body may be considered to be relatively well understood. Numerous animal experiments supplemented by experiments on humans suggest that HTO introduced into the body becomes a part of the general pool of body fluids, and is eliminated from the body via the urine, perspiration, breath, and other avenues of elimination of water from the body. The experimental data prior to 1957 are summarized in the comprehensive review of the problem by Pinson and Langham.¹ In addition, there is a wealth of experience gained in working with tritium which has revealed other factors which influence the metabolism of HTO, in particular, age and seasonal variations.

Nevertheless, there are some data to suggest that the metabolic model which assumes HTO to enter and be nonpreferentially eliminated from the general pool of body water is not entirely accurate. Thompson² exposed mice and rats to HTO and observed that retention in a variety of tissues could be represented by a sum of two exponentials which were distinct from the single exponential representing the retention in body water. In addi-

tion to experimental work on mice which gave a multiexponential retention, Pinson and Langham report an experiment in which one human subject was exposed to tritium over a period of 8 months, and dried biopsy specimens of skin and fat taken 51 days after the end of the exposure showed a higher concentration of tritium than did urine at the time of the biopsy. Thus, there is the implication that in man, as in experimental animals, some fraction of the HTO entering the body is not eliminated at the rate characteristic of the elimination of water from the body, and that this fraction may be more closely incorporated in certain tissues of the body. Subsequent to the inhalation of HTO by a human subject, we have been able to measure the concentration of tritium in various body fluids and, in particular, have found that concentration in urine does follow a pattern described as a sum of two exponentials during 255 days following an intake.

The exposure occurred when an individual, working with a source of HTO in a hood, inhaled some of the material. The subject is a senior scientist, a male of age 41 years, weight 66.5 kg, height 161 cm, and apparently enjoying good health. He was aware of the general nature of the problem posed by HTO in the body, and we are indebted to him for his cooperation which made this extended study possible. After the first samples were evaluated, it was agreed that he would not attempt any drastic increase in his normal fluid intake, although he was encouraged to drink liberally.

During the first 11 days, samples of urine, blood serum, and sputum were obtained and analyzed for tritium. No significant difference in the levels found in these various body fluids was noted, and this is in line with measurements reported by Pinson and Langham.¹ Also, the data appeared to follow a single exponential as expected but indicated a half-time for elimination of something under

¹E. A. Pinson and W. H. Langham, *J. Appl. Physiol.* 10, 108-26 (1957).

²R. C. Thompson, *J. Biol. Chem.* 197, 81-87 (1952); *op. cit.* 200, 731-43 (1953).

9 days. The data for the first 13 days are shown in Fig. 20.1. An early evaluation of the dose to be expected was made and indicated no apparent need for measures to hasten elimination. After discussion with the subject, it was agreed that he would not attempt to deliberately alter his normal habits for the purpose of hastening the elimination of the tritium.

At the time of writing, urine specimens have been collected periodically and analyzed during 255 days postexposure and have been analyzed by liquid scintillation counting. All counting times were for 30 min. All the urine data are shown in Fig. 20.2, and all the postexposure data are given in Table 20.1. During these 255 days, the subject has not been working directly with tritium. However, prior to this incident, he had shown urine concentrations in excess of the later values reported here. For example, the last sample taken before the incident was on October 25, just 3 days before the incident, and a concentration of 6.1×10^4 dis $\text{min}^{-1} \text{ml}^{-1}$ was measured. It is possible that this earlier exposure may have some influence on the data.

From Fig. 20.2 it appears that two exponential terms are required to fit the urinary concentrations observed in this case. By the courtesy of Chester Richmond of LASL, we have obtained a least-squares fit of the data to a sum of two exponentials using the LASL code described in ref. 3 which does not require a logarithmic transformation of the concentrations. This fitting procedure yielded a formula for concentration in urine of

$$R(t) = 5.3 \times 10^6 e^{-\alpha t} + 2.3 \times 10^4 e^{-\beta t},$$

with

$$\alpha = \frac{0.693}{8.7} \quad \text{and} \quad \beta = \frac{0.693}{34}.$$

Cases of internal exposure at ORNL which warrant consideration of dose and intake on the basis of the characteristics of the individual are evaluated by an internal dose evaluation committee. This subject's total body water was estimated on the following bases:

1. On weight basis: for 66.5 kg of body weight the human contains 0.44 to 0.70 liter of water

³C. R. Richmond *et al.*, *Health Phys.* 10(1), 3-13 (1964).

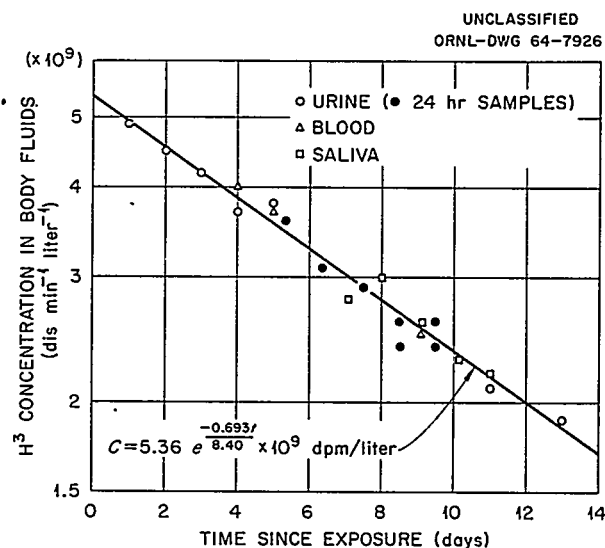


Fig. 20.1. Tritium Concentration in Body Fluids.

per kilogram (the mean, $0.52 \times 66.5 = 34.6 \approx 35$ liters).⁴

2. On age basis: humans 41 years of age contain from 0.44 to 0.65 liter of water per kilogram (the mean, $0.525 \times 66.5 = 34.9 \approx 35$ liters).⁴
3. On the basis of weight to height ratio: weight/height = 0.41 kg/cm, the male human body weight is 18 to 37% fat (mean 28%). Lean body weight (LBW) $\approx (1 - 0.28) \times 66.5 = 47.9$ kg.⁵ The same reference suggests: total body water = 0.72 LBW = 34.5 ≈ 35 liters.
4. On the basis of total potassium content: the subject was counted in the ORNL Whole-Body Counting Facility on November 8, 1963, with the following results: age - 41; weight - 66.5 kg; height - 161 cm; estimate 121 g of potassium based upon ^{40}K measurement.

Total potassium content = 0.28% of LBW; LBW = 121 g/0.0028 = 43.2 kg.⁶ This reference indicates that 72% of the lean weight and 20% of the fat weight is made up of water; thus,

⁴Biological Handbook - Blood and Other Body Fluids, Federation of American Societies for Experimental Biology, Washington, D.C., 1961.

⁵G. B. Forbes, J. Gallup, and J. B. Hursh, *Science* 133, 101-2 (Jan. 13, 1961).

⁶E. C. Anderson, *Brit. J. Radiol. Suppl.* 7, 27 (1957).

total body water = $0.72 \times 43.2 + 0.2 \times 23.3 = 35.76 \approx 36$ liters.

The Committee decided to use 36 liters as the amount of body water. Assuming a concentration of 5.3×10^6 dis min^{-1} ml^{-1} initially and that all the tritium is in the body water at early times post-exposure, this yields $5.3 \times 10^6 \times 36 \times 10^3 = 1.9 \times 10^{11}$ dis/min, or 86 mc, as the initial intake. The total dose to body water is then

$$D = \frac{51 \times f_2 \epsilon q(0)}{m \times 5.32 \times 10^6} \int_0^\infty dt R(t) = 15.5 \text{ rems},$$

where $f_2 = 1$, $m = 3.6 \times 10^4$ g, $\epsilon = 0.01$ Mev, $q(0) = 86 \times 10^3$ μC , and

$$\int_0^\infty R(t) dt = \frac{5.32 \times 10^6 \times 8.7}{0.693} + \frac{2.3 \times 10^4 \times 34}{0.693} \\ = 6.68 \times 10^7 + 1.13 \times 10^6 = 6.79 \times 10^7.$$

It is apparent that the second exponential term contributes only about 1.7% to the total dose. The dose in various body tissues may be somewhat less

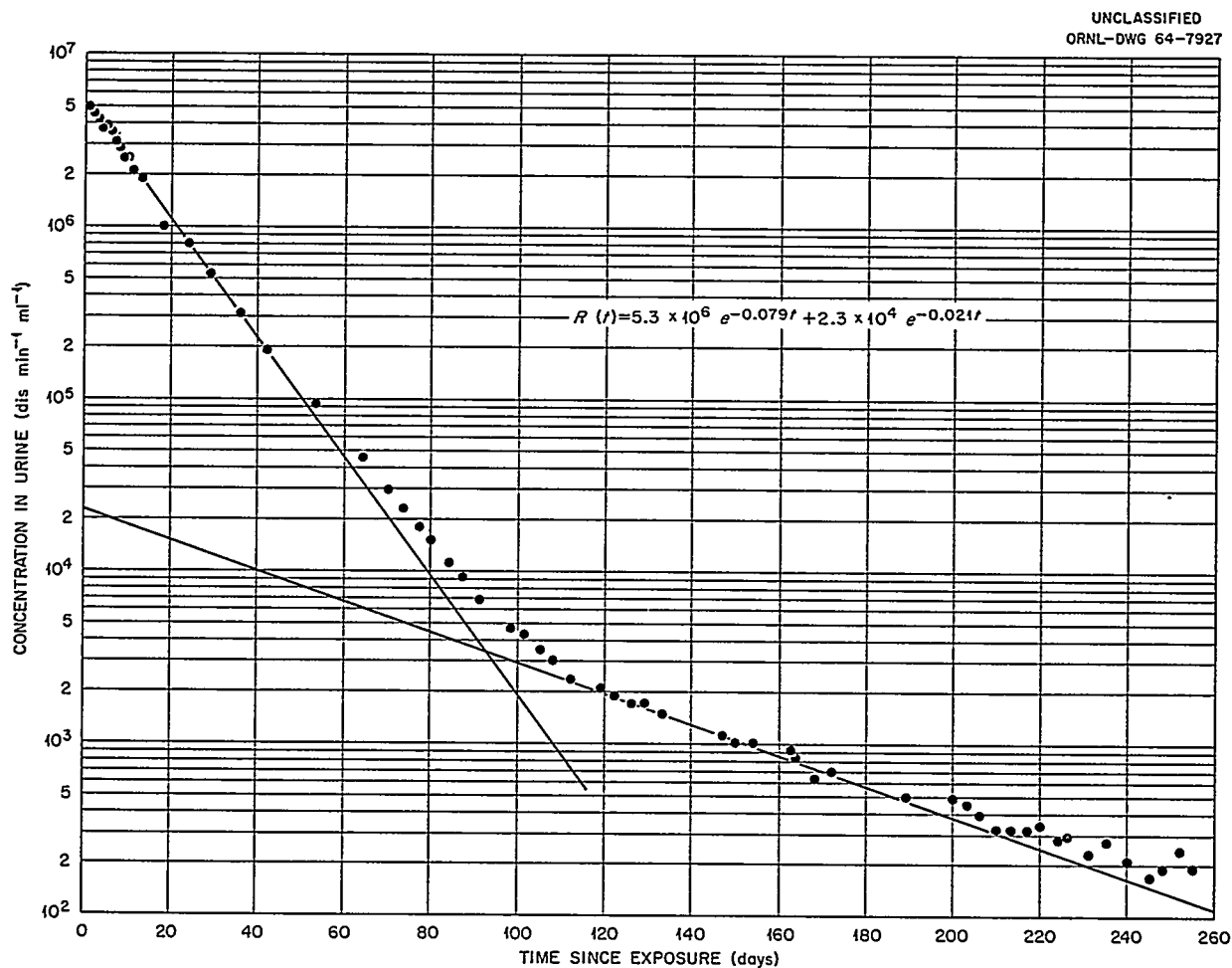


Fig. 20.2. Tritium Concentration in Urine.

since no allowance has been made for the presence of organic material. However, there are some tissues in which water constitutes a preponderant part of the mass, and so the estimate is substantially, although not precisely, correct for such tissues. On the other hand, there remains the probability that some tissue may accumulate a higher

concentration than body water, particularly at times much later than the exposure. However, the contribution of the second exponential term to the total dose is very small, and unless some tissue concentrates the material to a rather high degree, it seems unlikely that the dose would be significantly in excess of the dose to body water.

Table 20.1. Concentration of Tritium in Body Fluids

Time After Exposure (days)	Concentration (dis min ⁻¹ ml ⁻¹) ^a		
	Urine	Blood Serum	Sputum
1	$4.9 \times 10^6 \pm 5.1 \times 10^3$		
2	$4.5 \times 10^6 \pm 5.1 \times 10^3$		
3	$4.2 \times 10^6 \pm 3.5 \times 10^3$		
4	$3.7 \times 10^6 \pm 4.6 \times 10^3$	$4.0 \times 10^6 \pm 3.4 \times 10^3$	$3.3 \times 10^6 \pm 4.4 \times 10^3$
5	$3.8 \times 10^6 \pm 3.4 \times 10^3$	$3.7 \times 10^6 \pm 3.3 \times 10^3$	
6 ^b	$3.6 \times 10^6 \pm 3.3 \times 10^3$		
7 ^b	$3.1 \times 10^6 \pm 3.0 \times 10^3$		$2.8 \times 10^6 \pm 2.9 \times 10^3$
8 ^b	$2.9 \times 10^6 \pm 2.9 \times 10^3$		$3.0 \times 10^6 \pm 3.1 \times 10^3$
9 ^b	$2.6 \times 10^6 \pm 2.8 \times 10^3$	$2.5 \times 10^6 \pm 1.5 \times 10^3$	$2.6 \times 10^6 \pm 8.8 \times 10^2$
9	$2.4 \times 10^6 \pm 2.7 \times 10^3$		
10 ^b	$2.6 \times 10^6 \pm 2.8 \times 10^3$		$2.3 \times 10^6 \pm 3.8 \times 10^3$
10	$2.4 \times 10^6 \pm 3.9 \times 10^3$		
11	$2.1 \times 10^6 \pm 3.6 \times 10^3$		$2.2 \times 10^6 \pm 3.9 \times 10^3$
13	$1.9 \times 10^6 \pm 3.4 \times 10^3$		
18	$1.0 \times 10^6 \pm 2.0 \times 10^3$		
24	$7.9 \times 10^5 \pm 1.8 \times 10^3$		
29	$5.4 \times 10^5 \pm 1.0 \times 10^3$		
36	$3.2 \times 10^5 \pm 7.8 \times 10^2$		
42	$1.9 \times 10^5 \pm 6.2 \times 10^2$		
53	$9.4 \times 10^4 \pm 3.8 \times 10^2$		
64	$4.6 \times 10^4 \pm 2.8 \times 10^2$		
70	$3.0 \times 10^4 \pm 2.2 \times 10^2$		
73	$2.3 \times 10^4 \pm 2.0 \times 10^2$		
77	$1.8 \times 10^4 \pm 1.8 \times 10^2$		
80	$1.5 \times 10^4 \pm 1.7 \times 10^2$		
84	$1.1 \times 10^4 \pm 1.5 \times 10^2$		
87	$9.2 \times 10^3 \pm 1.7 \times 10^2$		
91	$6.7 \times 10^3 \pm 1.3 \times 10^2$		
98	$4.6 \times 10^3 \pm 1.3 \times 10^2$		
101	$4.2 \times 10^3 \pm 92$		
105	$3.5 \times 10^3 \pm 86$		
108	$3.0 \times 10^3 \pm 82$		$3.0 \times 10^3 \pm 47$
112	$2.3 \times 10^3 \pm 71$		
115	$2.2 \times 10^3 \pm 75$		
119	$2.1 \times 10^3 \pm 73$		
122	$1.9 \times 10^3 \pm 74$		
126	$1.7 \times 10^3 \pm 59$		

Table 20.1 (continued)

Time After Exposure (days)	Concentration (dis min ⁻¹ ml ⁻¹) ^a		
	Urine	Blood Serum	Sputum
129	$1.7 \times 10^3 \pm 58$		
133	$1.5 \times 10^3 \pm 56$		
147	$1.1 \times 10^3 \pm 47$		
150	$1.0 \times 10^3 \pm 46$		
154	$1.0 \times 10^3 \pm 49$		
163	$9.2 \times 10^2 \pm 30$		
164	$8.3 \times 10^2 \pm 29$		
168	$6.3 \times 10^2 \pm 28$		
172	$6.9 \times 10^2 \pm 28$		
189	$4.9 \times 10^2 \pm 24$		
200	$4.8 \times 10^2 \pm 26$		
203	$4.4 \times 10^2 \pm 25$		
206	$3.8 \times 10^2 \pm 24$		
210	$3.2 \times 10^2 \pm 23$		
213	$3.2 \times 10^2 \pm 23$		
217	$3.2 \times 10^2 \pm 24$		
220	$3.4 \times 10^2 \pm 25$		
224	$2.8 \times 10^2 \pm 23$		
226	$2.9 \times 10^2 \pm 25$		
231	$2.3 \times 10^2 \pm 23$		
235	$2.7 \times 10^2 \pm 22$		
240	$2.1 \times 10^2 \pm 17$		
245	$1.7 \times 10^2 \pm 17$		
248	$1.9 \times 10^2 \pm 16$		
252	$2.4 \times 10^2 \pm 16$		
255	$1.9 \times 10^2 \pm 17$		

^aMean disintegration rate \pm one standard deviation.^b24-hr samples; all others are spot samples.

21. Stable Element Metabolism

W. S. Snyder
Cyrus Feldman¹
Isabel H. Tipton²
Peggy L. Stewart²

Mary Jane Cook
F. S. Jones¹
Jane J. Shafer²

Because a radionuclide follows the metabolic pathway of a stable element, one may predict the distribution pattern of a radionuclide under chronic conditions from the analysis of grossly normal human tissues for stable elements. Allowing for radioactive decay, the concentration of stable elements indicates the tissues where the corresponding radionuclide would deposit under chronic exposure and thus indicates the dose that tissues might receive under chronic exposure. Due to the heterogeneity of the human population, a sufficiently large sample is needed in order to permit an estimate of the variability of dose that might be received, and to correlate this variability with age, sex, occupation, geographical location, etc. Such dose estimates are essential because efficient use of atomic energy requires accurate estimates of maximum permissible concentrations (MPC) of radionuclides in air, in water, and in food, not only for atomic energy workers but also for the general population which includes babies, children, teen-agers, etc.

Under chronic conditions inorganic elements are taken into the body through food, water, and air, but little attention has been devoted to the amount of daily intake of the majority of trace elements. Also, very little is known about the quantities excreted in the urine or in the feces. In applied health physics programs, samples of urine of radiation workers are collected and analyzed routinely to determine the presence of various radionuclides to which the worker may have been exposed. The interpretation of such data requires a metabolic model for the handling of such substances by the body, and trace element analysis of tissues supplies evidence bearing directly on major sites for deposition of the material and indirectly on various parameters of the metabolic model. Such metabolic models are the basis for

estimation of daily intakes that might be expected to produce a specified body burden of a radionuclide. Thus, studies of this kind are one of the major sources of data utilized for control of exposure to environmental contamination by radioactive material.

TISSUE ANALYSIS LABORATORY PROGRESS REPORT

Cyrus Feldman F. S. Jones

Spectrographic analysis of samples of human tissue collected in earlier years was continued using the previously described procedures.³ Approximately 430 soft tissues were analyzed for 23 stable elements. These tissue samples were predominantly the smaller organs such as thymus, gall bladder, and ovary, and small tissue samples from the larger organs such as kidney.

To test the possibility of analyzing tissues for thorium, three tissues were analyzed by radioactivation analysis. Equal portions of ash from several kidney samples from Atlanta were mixed, and duplicate analyses were made. This same procedure was followed for other kidney, bone, and lung samples. The analytical results and the mean values are presented in Table 21.1.

For the past several months, Consumers Union has been analyzing for ⁹⁰Sr, ⁸⁹Sr, Ca, and ¹³⁷Cs in teen-age diets collected from several cities in the United States.⁴ Because the elemental composition of the diet is of importance in calculating MPC values and very little such data are available, samples of these diets were obtained from Consumers Union in order to analyze them for other

¹Analytical Chemistry Division.

²Department of Physics and Astronomy, University of Tennessee.

³S. R. Koirtzohann and C. Feldman, "The Spectrographic Determination of Trace Elements in Human Tissue," *Analytical Chemistry in Nuclear Reactor Technology, Fourth Conference, Gatlinburg, Tennessee, Oct. 12-14, 1960*, TID-7606, pp. 51-63.

⁴Irving Michelson, *Health Phys.* 9, 944-50 (1963).

Table 21.1. Results of Radioactivation Analyses for Thorium in Human Tissues^a

Samples	Micrograms of Th per gram of Ash		
	1st Analysis	2d Analysis	Mean
Kidney, Atlanta	0.10	0.096	0.073
Kidney, San Francisco	0.06	0.07	
Kidney, New York	0.06	0.05	
Bone, Atlanta	0.07	0.07	0.067
Bone, San Francisco	0.05	0.06	
Bone, New York	0.08	0.07	
Lung, Atlanta	0.12	0.12	0.114
Lung, San Francisco	0.12		
Lung, New York	0.10	0.11	

^aAnalyses performed by E. I. Wyatt.

trace elements. To date, 75 of these diet samples have been analyzed. Some preliminary results are presented in Table 21.2. These data are being compared with similar data on diets of adults as reported by other investigators and are being studied in relation to questions of population exposure to a variety of radionuclides.

In order to speed the analytical procedure and to eliminate the human errors of handling data, an automatic data-acquisition computer system was installed. The data output from the Quantometer consists of recorder deflections which, when compared with standards of known composition, are converted and printed out in parts per million of ash. This was done previously by plotting curves on transparent overlays and interpreting the recorder chart deflections.

TRACE ELEMENTS IN HUMAN TISSUE: RIB AND VERTEBRA

Isabel H. Tipton

Jane J. Shafer

Since the gross composition of bone is quite different from that of soft tissue, a different set of standards and a somewhat different method are required in the spectrographic analysis of bone. For this reason, in the program for spectrographic analysis of human tissue, all the samples of bone which were collected from individuals both from within and outside the United States were

held for analysis as a group. This group of bone samples included rib, vertebra, sternum (only from Dallas), and unidentified bone. For this report, only the data for rib and vertebra are included. A summary of the total number of bone samples which were analyzed and the geographical distribution of these samples is given in Table 21.3.

The bone samples were analyzed in the spectrographic laboratory of the Analytical Chemistry Division of ORNL by methods which have been described.⁵ Data from these analyses were processed at the University of Tennessee Computing Center using nonparametric methods previously described.⁶ The Kruskal-Wallis test for two-way classification was used to test the hypothesis that two groups were from the same population.⁷

Descriptive statistics for rib and vertebra of adults from the United States are given in Tables 21.4 and 21.5 respectively. For the ash percent of wet, dry percent of wet, and ash percent of dry, the column "Fraction Observed" means the number of samples for which the parameter was calculated, divided by the total number of samples. For an

⁵W. S. Snyder et al., *Health Phys. Div. Ann. Progr. Rept. June 30, 1963*, ORNL-3492, p. 178.

⁶I. H. Tipton and J. J. Shafer, *Arch. Environ. Health* 8, 58 (1964).

⁷W. H. Kruskal and W. A. Wallis, *Am. Statist. Assn. J.* 47(260), 584 (1952).

Table 21.2. Preliminary Results of the Spectrographic Analysis of Teen-Age Diet Samples

(The values are the means of the number of determinations in parentheses. The numbers in brackets indicate the lower limit of detection.)

City	% Dry Ash	Al (ppm)	Ba (ppm)	Cu (ppm)	Mn (ppm)	Pb (ppm)	Sn (ppm)	Sr (ppm)	Ti (ppm)	Zn (ppm)	C (%)	Ca (%)	Fe (%)	K (%)	Mg (%)	Na (%)	P (%)	S (%)	Si (%)
Chicago, Ill.	18.8 (3)	0.86 (3)	297 (3)	33 (3)	56 (3)	98 (3)	380 (3)	61 (3)	21 (2)	557 (3)	54.6 (3)	6.14 (3)	0.11 (3)	15.5 (3)	1.41 (3)	17.9 (3)	7.76 (3)	0.19 (3)	0.23 (3)
Duluth, Minn.	19.4 (3)	0.79 (3)	540 (4)	28 (4)	66 (4)	113 (4)	144 (4)	76 (4)		455 (4)	53.8 (3)	6.36 (3)	0.09 (3)	18.1 (3)	1.42 (3)	16.3 (3)	7.93 (3)	0.18 (3)	0.57 (3)
Knoxville, Tenn.	21.1 (4)	0.90 (4)	338 (4)	35 (4)	59 (4)	123 (4)	333 (4)	60 (4)	184 (2)	445 (2)	53.8 (4)	6.82 (4)	0.06 (4)	15.1 (4)	1.39 (4)	16.9 (4)	8.41 (4)	0.16 (4)	0.38 (4)
Little Rock, Ark.	17.0 (2)	0.75 (2)	665 (2)	45 (2)	46 (2)	145 (2)	605 (2)	55 (2)	15 (1)	560 (4)	52.5 (2)	8.83 (2)	0.06 (2)	16.4 (2)	1.38 (2)	14.9 (2)	8.89 (2)	0.18 (2)	1.14 (2)
Los Angeles, Calif.	18.1 (3)	0.77 (3)	230 (3)	38 (3)	187 (3)	111 (3)	383 (3)	143 (3)	14 (2)	660 (3)	55.1 (2)	6.26 (2)	0.08 (2)	17.9 (2)	1.61 (2)	15.0 (2)	8.51 (2)	0.21 (2)	0.50 (2)
New Orleans, La.	15.8 (4)	0.71 (4)	470 (4)	54 (4)	109 (4)	143 (4)	855 (4)	92 (4)	38 (3)	545 (4)	51.8 (4)	8.01 (4)	0.07 (4)	15.2 (4)	1.42 (4)	16.4 (4)	8.27 (4)	0.18 (4)	0.52 (4)
New York, N.Y.	18.4 (2)	0.86 (2)	500 (2)	29 (2)	85 (2)	125 (2)	370 (2)	76 (2)	114 (2)	415 (2)	54.1 (2)	6.47 (2)	0.06 (2)	15.4 (2)	1.36 (2)	17.5 (2)	7.64 (2)	0.19 (2)	0.73 (2)
Portland, Ore.	19.0 (4)	0.86 (4)	355 (4)	49 (4)	62 (4)	145 (4)	498 (4)	86 (4)	17 (3)	455 (4)	52.4 (4)	6.46 (4)	0.08 (4)	15.5 (4)	1.55 (4)	17.3 (4)	8.01 (4)	0.18 (4)	0.47 (4)
San Francisco, Calif.	20.8 (4)	0.88 (4)	228 (4)	53 (4)	70 (4)	123 (4)	403 (4)	95 (4)	161 (4)	965 (4)	53.8 (4)	6.92 (4)	0.08 (4)	15.8 (4)	1.51 (4)	17.0 (4)	8.13 (4)	0.18 (4)	0.64 (4)
Sioux Falls, Ida.	19.8 (4)	0.86 (4)	710 (4)	144 (4)	60 (4)	108 (4)	463 (4)	92 (4)	98 (2)	443 (4)	53.8 (4)	6.83 (4)	0.08 (4)	14.9 (4)	1.45 (4)	17.9 (4)	7.87 (4)	0.18 (4)	0.2 (4)

element, the column "Fraction Observed" means the number of samples in which the element occurred in a concentration above the lower limit of detection (and was thus actually observed), divided by the total number of samples. For those elements which were not observed in concentrations above the lower limit of detection in every sample, it was impossible to calculate a mean value for concentration, since it could only be assumed that

the concentration of such an element lay somewhere between zero and the lower limit of detection. Therefore, the two limiting values of the mean were calculated for these elements, one assigning to those samples in which the element was not observed a value for the concentration equal to zero, and the other assigning a value equal to the lower limit of detection. These limiting values for the mean are given in the last

Table 21.3. Number of Samples of Rib and Vertebra

All Adult Subjects ≥ 20 Years	Total Number of Subjects	Rib	Vertebra
United States	150	91	53
Colorado, Denver		9	8
Illinois, Chicago		1	
Florida, Miami		19	1
Maryland, Baltimore		23	22
New York, New York			
Texas, Dallas			
Virginia, Richmond		22	20
Washington, Seattle		17	2
African Continent	54	1	
Near East	37	19	
India, Bombay		8	
India, Delhi		7	
India, Lucknow		4	
India, Vellore			
Lebanon, Beirut			
Far East	70	52	10
Formosa, Taipei		4	
Hong Kong		10	
Japan, Chiba		6	9
Japan, Kyoto		5	
Japan, Tokyo		8	
Philippine Islands, Manila		9	1
Thailand, Bangkok		10	
Switzerland, Bern	9	2	2
Alaska, Anchorage	2		
Hawaii, Honolulu	12	9	4
Males 20-59 Years			
United States	88	56	
African Continent	1	1	
Near East	24	14	
Far East	39	27	
Females 20-59 Years			
United States	30	16	

Table 21.3. (continued)

Children 0—<20 Years			
United States	23	11	7
Colorado, Denver		2	4
Illinois, Chicago			
Florida, Miami		3	
Maryland, Baltimore		2	1
New York, New York			
Texas, Dallas			
Virginia, Richmond		2	2
Washington, Seattle		2	
African Continent	5		
Near East	9	4	
India, Bombay		1	
India, Delhi		2	
India, Lucknow		1	
India, Vellore			
Lebanon, Beirut			
Far East	3	3	
Formosa, Taipei			
Hong Kong			
Japan, Chiba			
Japan, Kyoto			
Japan, Tokyo		2	
Philippine Islands, Manila		1	
Thailand, Bangkok			
Switzerland, Bern			
Alaska, Anchorage			
Hawaii, Honolulu			

column of the table as "Limits of Sample Mean." In some instances, when the element was observed in all but a few samples, (e.g., aluminum in vertebra), the difference between these two values for the mean lies in the second or third digit. The precision of the analytical method at this level is in general only good to one digit, and thus only one digit is reported; however, in such cases the two estimates of the mean do not differ significantly. The lower limit of concentration of those elements which were not observed in every sample is given as less than the lower limit of detection (< limit of detection). When an element was not observed in at least half the samples, the median value for concentration of that element

is given in the tables as less than the lower limit of detection. Cadmium and molybdenum were observed in only one sample of rib, and these elements and gold were not observed in any of the vertebrae.

On the basis of the Kruskal-Wallis test, the median values for the concentration in ash of iron, sodium, and potassium in vertebra were significantly ($p \leq 0.01$) higher than the median values for the concentration in ash of the same elements in rib. On the other hand, the median value for the concentration of calcium in ash was significantly higher in rib than in vertebra (Fig. 21.1). The median value for concentration of strontium was higher ($p = 0.02$) and of lead was

lower ($p = 0.05$) in rib than in vertebra. The ash percent of wet weight also was significantly higher in rib than in vertebra (Fig. 21.1). This reflects the difference in texture of the two types of wet bone, rib being compact and vertebra porous with the interstices filled with blood and "soft-type" tissue which ashes with a low residue and which is also high in iron, sodium, and potassium.

Since the concentration of certain elements in rib and vertebra showed a correlation with age, and since the concentrations of several of these elements in rib were also significantly different in adult male and female subjects (Fig. 21.2), only those values for males between the ages of 20 and 59 were used in the two-sample tests for geographic differences. In general, only rib

was collected from the foreign group, and so geographical comparisons have been made only in rib. (There were not enough samples of bone from African and Swiss subjects to consider them as subgroups in performing these tests.)

Geographic differences in the concentration in ash of calcium, strontium, and lead are shown in Fig. 21.3. The poor nutritional status of the Near Eastern subgroup is reflected in the significantly lower median value for the concentration of calcium in rib. The median value for strontium in rib in the Far Eastern subgroup was significantly higher than for either of the other two groups. Lead was in significantly higher concentration in the subgroup from the United States than in either of the other subgroups. In the Far Eastern subgroup this

Table 21.4. Concentrations of Elements in Bone – Rib for Adult Subjects from the United States

	Fraction Observed ^a	Total Range		Median	95% Confidence Interval for Median		Mean	Std Dev	Limits of Sample Mean ^a	
Ash % of Wet	91/91	7.6	50.	24.	22.	25.	24.	8.5		
Dry % of Wet	52/91	48.	79.	65.	62.	67.	63.	7.9		
Ash % of Dry	52/91	16.	56.	37.	34.	39.	36.	8.6		
Grams per 100 Grams of Tissue Ash										
Calcium	91/91	29.	39.	36.	36.	36.	36.	3.8		
Iron	91/91	0.01	0.16	0.04	0.03	0.05	0.04	0.03		
Magnesium	91/91	0.25	0.59	0.46	0.45	0.48	0.46	0.10		
Potassium	91/91	0.29	2.6	0.62	0.56	0.72	0.70	0.29		
Sodium	91/91	0.9	4.4	1.3	1.3	1.5	1.5	0.57		
Micrograms per Gram of Tissue Ash										
Lead	91/91	10.	140.	43.	41.	52.	47.	21.		
Strontium	91/91	38.	360.	110.	110.	120.	120.	49.		
Zinc	91/91	100.	450.	200.	190.	210.	210.	46.		
Aluminum	85/91	<5.	110.	10.	5.	10.			12.	13.
Cadmium	1/91	<5.	5.	<5.	<5.	<5.			0.	5.
Chromium	3/91	<2.	20.	<2.	<2.	<2.			0.	2.
Cobalt	4/91	<2.	21.	<2.	<2.	<2.			0.	2.
Copper	82/91	<2.	35.	3.	2.	3.			3.	4.
Gold	0/91	<2.	<2.	<2.	<2.	<2.			0.	2.
Manganese	87/91	<2.	10.	2.	2.	2.			2.	2.
Molybdenum	1/91	<2.	2.	<2.	<2.	<2.			0.	2.
Nickel	21/91	<2.	69.	<2.	<2.	<2.			2.	4.
Tin	7/91	<5.	20.	<5.	<5.	<5.			0.	5.

^aSee text for explanation.

Table 21.5. Concentrations of Elements in Bone – Vertebra for Adult Subjects from the United States

	Fraction Observed ^a	Total Range		Median	95% Confidence Interval for Median		Mean	Std Dev	Limits of Sample Mean ^a	
Ash % of Wet	53/53	7.5	27.	15.	14.	16.	15.	3.4		
Dry % of Wet	34/53	40.	62.	51.	49.	53.	51.	6.4		
Ash % of Dry	34/53	15.	41.	29.	26.	31.	29.	5.7		
Grams per 100 Grams of Tissue Ash										
Calcium	53/53	32.	37.	35.	35.	35.	35.	2.9		
Iron	53/53	0.02	0.40	0.09	0.07	0.11	0.10	0.07		
Magnesium	53/53	0.30	0.62	0.51	0.49	0.54	0.50	0.07		
Potassium	53/53	0.50	2.7	0.99	0.91	1.1	1.0	0.29		
Sodium	53/53	1.2	3.9	2.0	1.7	2.3	2.0	0.44		
Micrograms per Gram of Tissue Ash										
Lead	53/53	5.	130.	51.	45.	56.	54.	21.		
Strontium	53/53	58.	200.	100.	90.	110.	110.	34.		
Zinc	53/53	94.	340.	220.	210.	250.	220.	45.		
Aluminum	47/53	<5.	78.	5.	5.	10.			9.	9.
Cadmium	0/53	<5.	<5.	<5.	<5.	<5.			0.	5.
Chromium	1/53	<2.	5.	<2.	<2.	<2.			0.	2.
Cobalt	1/53	<2.	15.	<2.	<2.	<2.			0.	2.
Copper	52/53	<2.	10.	5.	2.	5.			4.	4.
Gold	0/52	<2.	<2.	<2.	<2.	<2.			0.	2.
Manganese	51/53	<2.	10.	2.	2.	3.			2.	2.
Molybdenum	0/53	<2.	<2.	<2.	<2.	<2.			0.	2.
Nickel	11/53	<2.	43.	<2.	<2.	<2.			2.	3.
Tin	7/53	<5.	20.	<5.	<5.	<5.			1.	5.

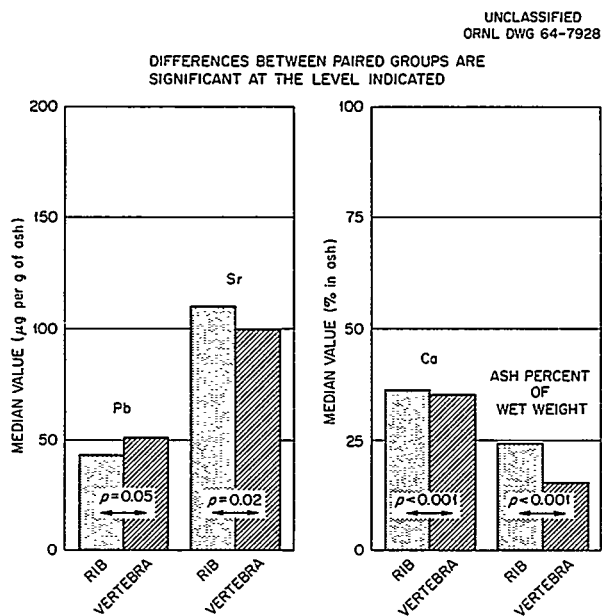
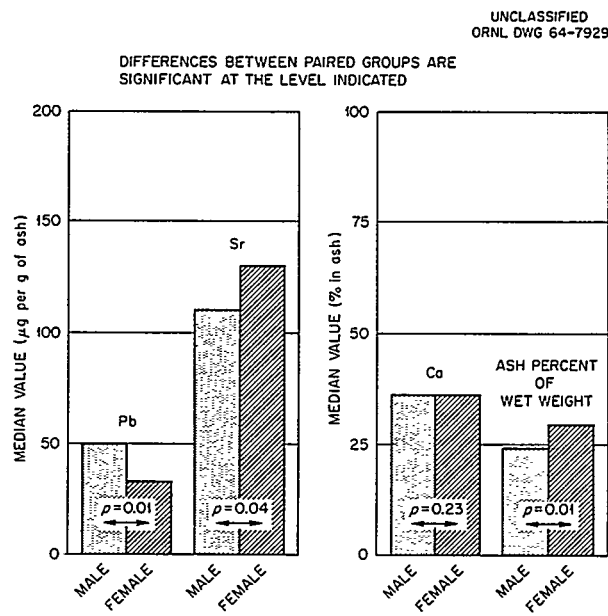
^aSee text for explanation.Fig. 21.1. Differences Between Rib and Vertebra, Adults ≥ 20 yr.

Fig. 21.2. Rib – Sex Differences, U.S. Adults 20–59 yr.

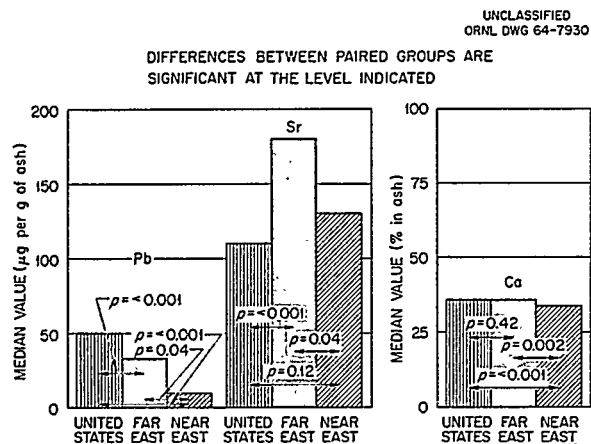


Fig. 21.3. Rib - Geographic Differences, Males 20-59 yr.

element was significantly higher than in the Near Eastern. This may reflect the differences in exposure to automobile exhaust fumes of these three subgroups, since at the time of collection of these samples, lead was a common additive in most gasoline.

TRACE ELEMENTS IN DIETS AND EXCRETA - PRELIMINARY STUDY

Isabel H. Tipton

Peggy L. Stewart

To obtain some idea of the average amounts and day-to-day variation of trace elements in ordinary diets, two subjects for a month saved duplicate samples of all food ingested and all excreta. The subjects were husband and wife, ages 35 and 34, respectively, who for several years have maintained weights of ~165 and 136 lb respectively.

All fluids except water, tea, and coffee were included in the daily samples of food. A record was kept of the daily intake of water, tea, and coffee, and samples of each also were supplied for analysis.

Complete 24-hr samples of urine were collected, and analyses were made on these daily samples. Feces were composited for a 3-day period since the chances of no fecal output during a 24-hr period are high.

The average daily intake of food and output of urine and feces are shown in Table 21.6. The

total intake was arrived at by adding the weight of food to the weight of drink (assuming a specific gravity of 1.0). The amount of water in the food samples was determined by distillation with toluene. Thus, it was possible to calculate the total intake of water.

The average daily intake and output of trace elements as shown in the table seem to indicate a positive balance for most elements. In some instances this is due to a limitation of the spectrographic method which was set up for the analysis of carefully controlled diets in a program where the range of variation for most elements was not very great. In the *ad libitum* diets the range was very great, and in many cases the measurements were made at and extrapolated beyond the upper limits of the method where exact values were difficult to obtain. This was especially true for the feces which had extremely high concentrations of trace elements. In urine the reverse was true - concentrations were so low that many values were uncertain. There is also the possibility that some of the excretion might be via perspiration, exhalation, etc.

For some elements (e.g., zinc, silver, and nickel) the concentration in food was too low to be detected by the spectrographic method employed in the study. More sensitive methods are being developed. The concentrations of these elements in feces (and of nickel in urine), however, were in good measurable range. For this preliminary report, the average daily intake of these elements has been assumed to be equal to the output.

The figures show the daily amounts of calcium (Fig. 21.4) and strontium (Fig. 21.5) ingested and excreted in the feces and urine by each of the subjects. Although the variation in intake is wide, the amounts vary around a mean which remains fairly constant with time.

The daily intake of stable strontium in these subjects was about twice that generally reported, but the mean intake of calcium was 1.1 g/day, which agrees with the generally accepted value of 1 g/day. Thus, the ratio of strontium to calcium in their diets was somewhat higher than the average values by other investigators.⁸ As indicated, this report is preliminary, and the data and analysis are not complete at this time.

⁸W. S. Snyder, M. J. Cook, and M. R. Ford, *Health Phys.* 10, 171-82 (1964) (especially Table 2).

Table 21.6. Balance Studies June 12–July 11, 1963 for Two Subjects, *ad libitum* Diets

	Female, Age 34, Weight ~ 136 lb			Male, Age 35, Weight ~ 165 lb		
	Intake	Output	Urine/Fecal Ratio	Intake	Output	Urine/Fecal Ratio
Total	2372 g/day ^a	1570 g/day ^a	26.0	2487 g/day ^a	1200 g/day ^a	15.0
Food (including milk, beer, etc.)	1278 g/day			1769 g/day		
Drink (water, tea, coffee)	1094 cc/day			718 cc/day		
Total water (food and drink)	1952 cc/day			1939 cc/day		
Dry solids	461 g/day			547 g/day		
Urine		1511 cc/day			1131 cc/day	
Feces		59 g/day			74 g/day	
Ca	1.1 g/day	0.78 g/day	0.32	1.7 g/day	1.4 g/day	0.39
Mg	0.23	0.23	0.55	0.40	0.13	0.11
Cu	2.9 mg/day	2.4 mg/day	0.31	2.2 mg/day	2.0 mg/day	0.11
Mn	6.4	4.8	0.0004	7.5	2.1	0.0005
Zn ^b	6.2	6.2	0.00	22.0	22.0	0.00
Ag ^b	0.082 mg/day	0.082 mg/day	0.03	0.11 mg/day	0.11 mg/day	0.05
Ba	1.4	1.2	0.06	1.5	0.62	0.11
Cr	0.033	0.006	0.50	0.007	0.005	3.0
Ni ^b	1.7	1.7	1.4	0.81	0.81	0.21
Pb	1.0	0.81	0.84	2.9	0.26	0.44
Sn	1.9	2.1	0.06	3.4	3.6	0.00
Sr	2.7	1.4	0.20	4.0	0.53	0.26
Ti	0.79	1.1	1.0	0.50	0.25	0.92

^aAssuming the specific gravity of water, tea, coffee, and urine to be 1.^bIntake assumed equal to output.

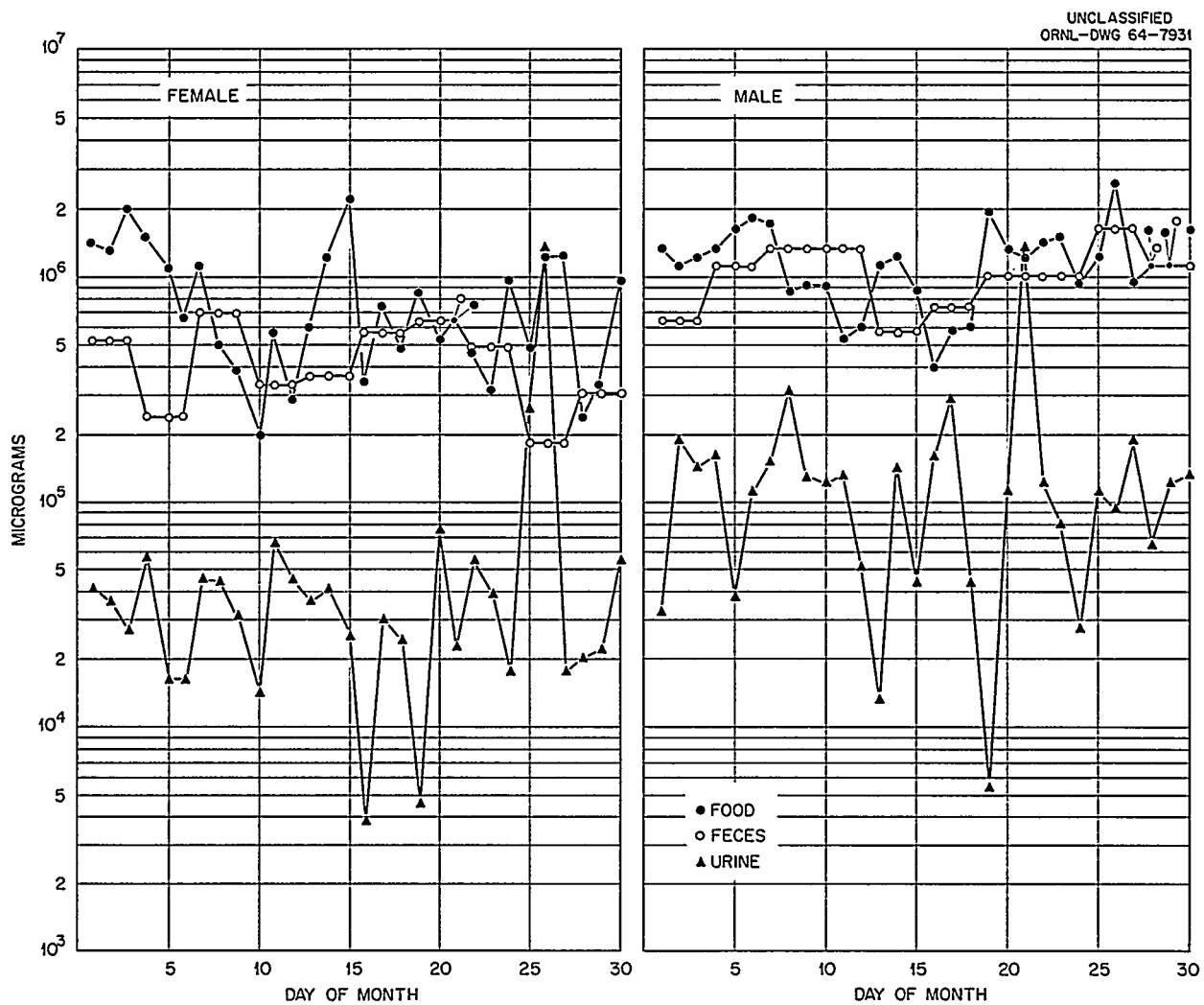


Fig. 21.4. Daily Intake and Excretion of Calcium.

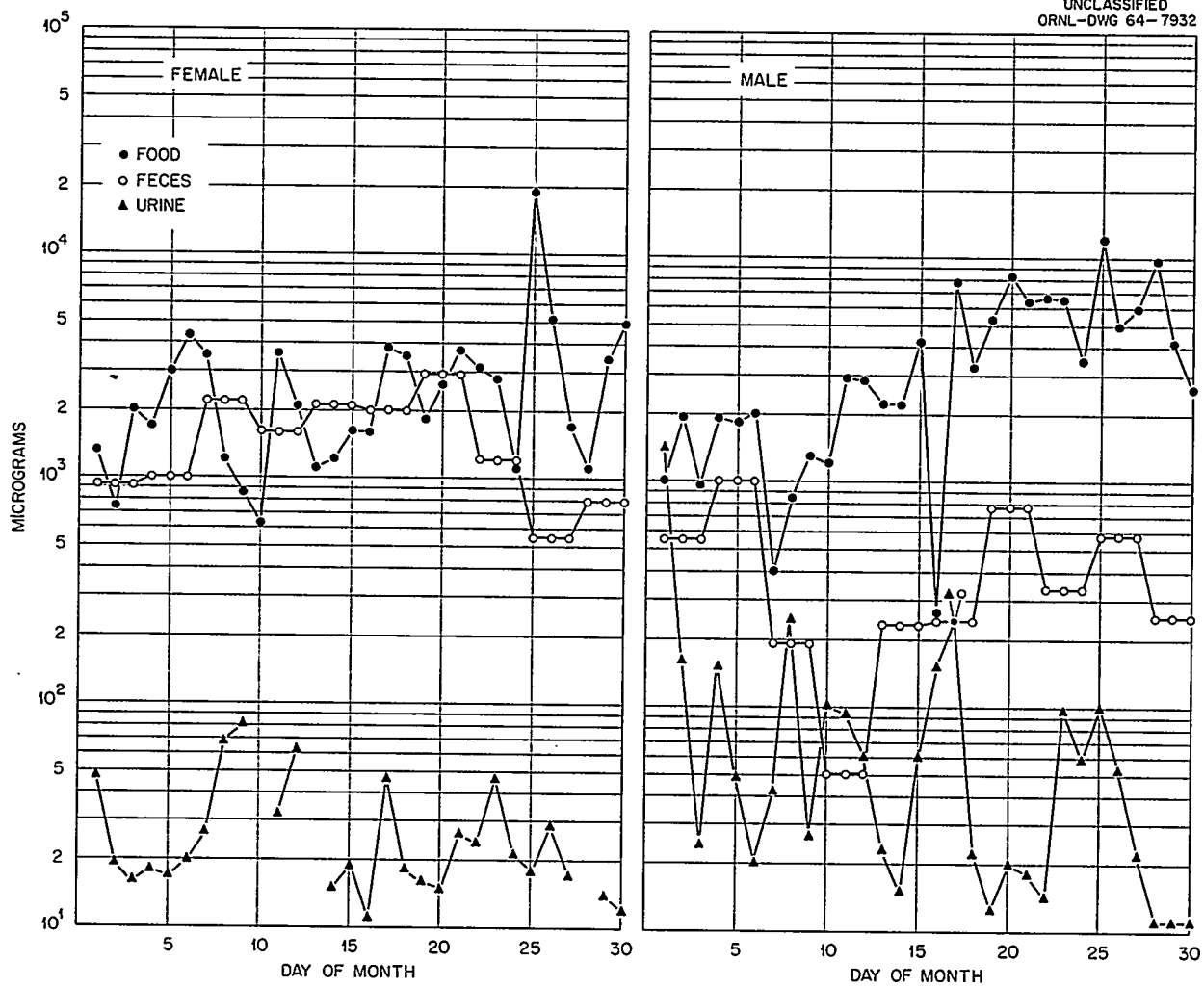
UNCLASSIFIED
ORNL-DWG 64-7932

Fig. 21.5. Daily Intake and Excretion of Strontium.

DISTRIBUTION OF STABLE STRONTIUM IN BONE AND SOFT TISSUES AND ITS APPLICATION TO METABOLISM OF STRONTIUM-90

W. S. Snyder

M. J. Cook

Strontium has been shown to be a bone seeker in both human and animal studies. Little attention has been focused upon the distribution of strontium in soft tissues; however, every tissue examined in our program on the analysis of human tissues has been found to contain a measurable amount of stable strontium. For this study the age of the individuals was restricted from 20 through 59 years, which would include the majority of working people. Over 2200 soft tissue samples and 160 bone samples were examined spectroscopically, and the data are analyzed here to estimate the distribution of strontium under near equilibrium conditions. It is found that bone contains ~99% of the strontium present in the body, thus differing significantly from ^{226}Ra for which estimates of as low as 80% of the body burden have been given for bone.⁹

In Fig. 21.6 are presented the means of the concentration for 27 different soft tissues and bone, with the number of samples of each tissue analyzed given in parentheses. The length of the vertical line is equal to two standard deviations on the vertical scale. If the vertical line representing the mean concentration of any tissue is turned 90° to either the right or left, plus or minus two standard deviations may be ascertained. Based on the concentration of strontium, the tissues seem to fall into three classes: (1) bone, which is in a class to itself; (2) trachea, larynx, and aorta, which are higher in calcium than the majority of soft tissues; and (3) the remaining soft tissues.

At the meeting of the International Commission on Radiological Protection (ICRP), December 2-5, 1963, Committee 2 proposed to calculate maximum permissible concentration (MPC) values for nuclides that are incorporated into gonadal tissue on the basis of mean dose equivalent delivered to the whole gonadal tissue. On this basis of averaging over the entire organ, it is found that at the 95% confidence limit the concentration of stable strontium in the ovary differs from that in

the testes. The mean concentration in the ovary is about $2\frac{1}{2}$ times that in the testes.

Since no whole bodies are available for analysis, the estimate of strontium for the whole body had to be based on samples available, and several compromises were necessary. First, many samples only contained a fraction of the entire organ or tissue being sampled, and the weight of the entire organ or tissue was not known. The amount of strontium in various organs was estimated by multiplying the weight of the organ as given for standard man¹⁰ by the mean concentration observed in the wet tissues. Second, it was not feasible to separate bone and marrow in the course of analysis; therefore, the analytical values reported for bone also include strontium present in the marrow. Since no samples of marrow were available, we have assumed that the concentrations of strontium in red and yellow marrow are comparable to the concentrations of strontium in spleen and fat respectively. The calculated estimate of strontium content of marrow was subtracted from the analytical values reported for bone plus marrow. Finally, some tissues were not sampled, and assigned weights could not be found in literature for some other tissues. However, these tissues only account for about 1200 of the 70,000 g of standard man. The average concentration of the soft tissues which were sampled and analyzed but for which no body weights could be assigned was used as the mean concentration value for the remaining tissues for which no weights were found and for tissues not sampled. By this method the total body burden of stable strontium was estimated to be ~0.33 g.

In calculating MPC and body-burden values for radioisotopes, the fraction of the body burden in an organ is needed. This factor is designated by f_2 in the ICRP¹⁰ and NCRP¹¹ internal dose reports. In Fig. 21.7 these values are presented. Of the stable strontium in the body, 98.5% is found in the bone. Although muscle has a very low concentration on a microgram per gram wet basis, it may be noted that due to its mass, which comprises

⁹J. B. Hursh and Arvin Lovaas, *Nature* 198, 265-68 (1963).

¹⁰Recommendations of the International Commission on Radiological Protection, ICRP Publication 2, *Report of Committee II on Permissible Dose for Internal Radiation* (1959), p. 151, Pergamon, London.

¹¹"Maximum Permissible Body Burden and Maximum Permissible Concentrations of Radionuclides in Air and in Water for Occupational Exposure," *Natl. Bur. Std. (U.S.), Handbook 69*, GPO, Washington, 1959.

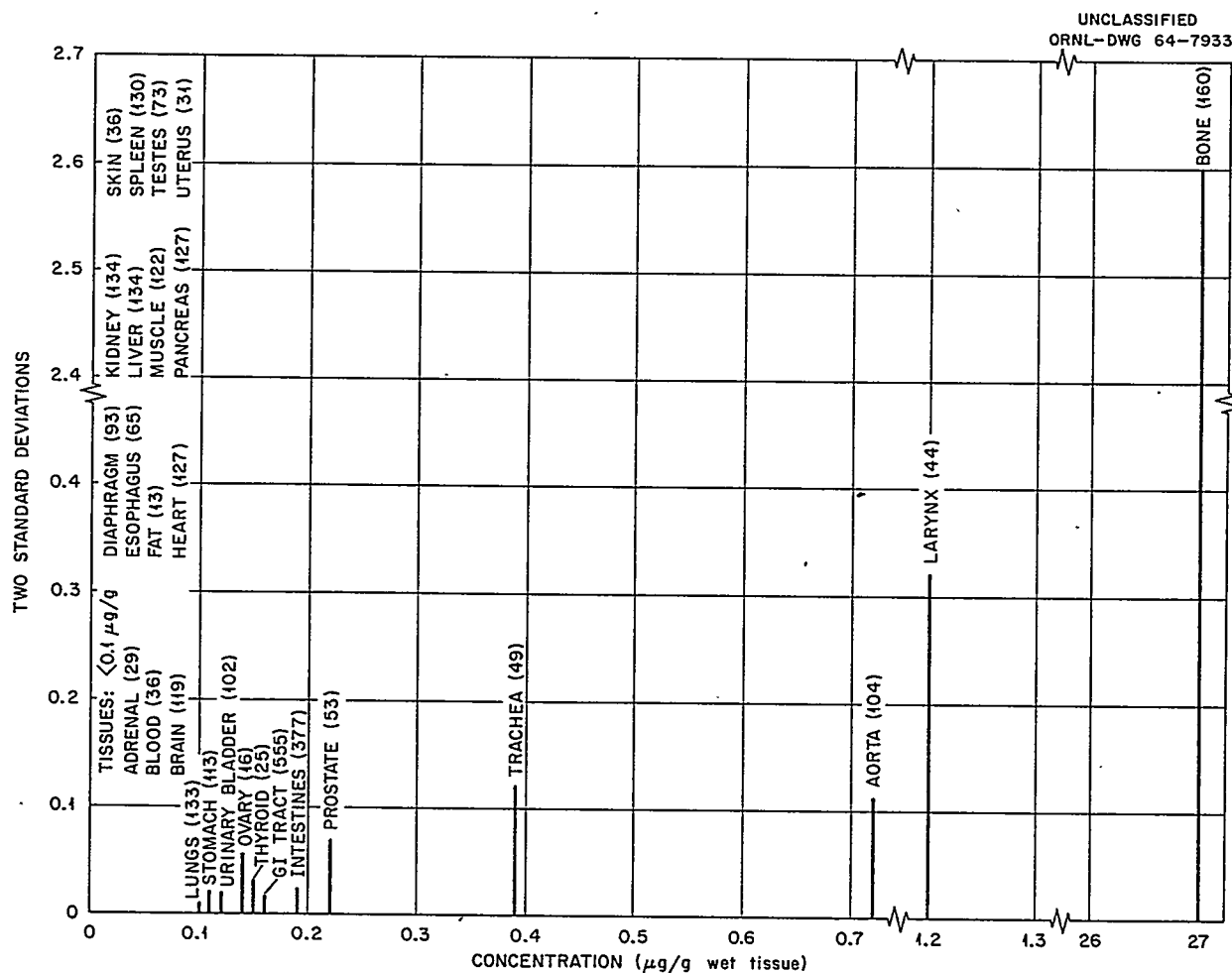


Fig. 21.6. Concentration of Stable Strontium in Wet Tissue.

almost half of the total weight of the body, muscle has the largest fraction of strontium of any of the soft tissues.

The dose which an organ receives from a radioactive element may be calculated from the concentration of this radionuclide in the tissues. A stable isotope of the same element should indicate, on the average, the pattern of distribution to be expected at near-equilibrium conditions for the radioactive element, provided suitable allowance is made for radioactive decay. Statistical methods given by Brunk¹² and by Dixon and Massey¹³ have been described and applied to the data for some elements¹⁴ and have now been applied to stable strontium in the bone. These data are

presented in Fig. 21.8. The small, dotted, center line is the cumulative sample distribution of strontium in wet bone for people in the United States between ages of 20–59. The two solid lines determine a band such that at each concentration value one may assert with 95% confidence that the true distribution function for the population being sampled lies below (above) the upper (lower)

¹²H. D. Brunk, *An Introduction to Mathematical Statistics*, Ginn and Co., New York, 1960.

¹³W. J. Dixon and F. J. Massey, Jr., *Introduction to Statistical Analysis*, McGraw-Hill, New York, 1957.

¹⁴W. S. Snyder and M. J. Cook, *Health Phys.* 9, 417–23 (1963).

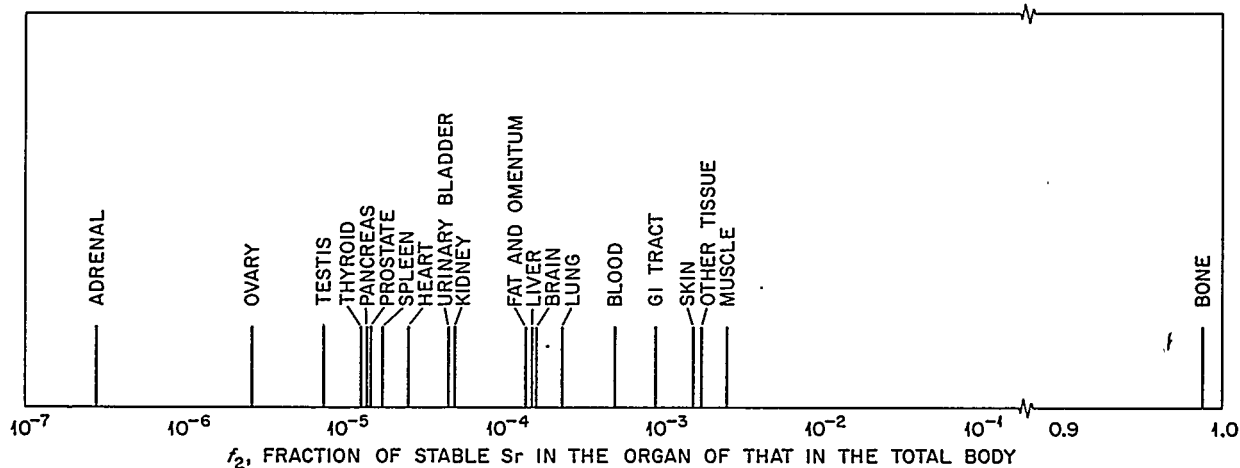
UNCLASSIFIED
ORNL-DWG 64-5095A

Fig. 21.7. f_2 - Fraction of Stable Strontium in the Organ of That in the Total Body.

boundary of the band. For example, at the sample mean, 27 μg of strontium per gram of wet bone, it can be asserted with 95% confidence that at least 32% of the individuals are above this value and 56% are below. For some estimates it is desirable to use the entire distribution function. This can be bracketed by use of a statistical method of Massey which defines a region bounded by the two outer curves in Fig. 21.8. It can be asserted with 95% confidence that the entire distribution curve of the population being sampled lies within this band.

Because the mean value exceeds the median value, the values are not normally distributed but are skewed to the right. Also, from this statistical analysis, 95% confidence intervals for different percentiles may be determined from the Brunk curves. As an example, the 10th percentile is between 10 and 13 $\mu\text{g/g}$ and the 90th percentile is between 45 and 55 $\mu\text{g/g}$. Thus, with 95% confidence one may say that the 80% range is above 10 $\mu\text{g/g}$ and, with the same confidence, that it does not extend beyond 55 $\mu\text{g/g}$.

Both strontium and calcium have been determined in each sample of tissue. However, many investigators have suggested and prefer studying strontium on the basis of the ratio of the concentrations of these elements. These ratios have been deter-

mined for 27 soft tissues and bone. The ratio of strontium to calcium in bone samples appears to be remarkably consistent, showing little dependence on age or bone type in the specimens analyzed for this study, and the study of these is continuing.

Although it is not possible to give an exact assessment of the distribution of dose in the body due to chronic exposure to ^{90}Sr , one can use these data to obtain rather good estimates of such exposure. For example, since man's exposure to ^{90}Sr in weapons fallout occurs largely via the diet, the ^{90}Sr would be expected to metabolize much as does the stable strontium of concern in this study. Because of radioactive decay, the levels of ^{90}Sr in various tissues that would occur after many years of exposure at a constant level might be expected to be somewhat less than the levels observed for comparable exposure to stable strontium. This reduction would be greatest in the tissue where the biological turnover is longest; thus the bone burden of ^{90}Sr would be relatively lower and soft tissues relatively higher than for stable strontium. However, the reduction in the bone burden cannot exceed 30% unless we postulate average turnover times in excess of 10 years. The decrease in the burden of the soft tissues would be expected to be much less.

As one illustration of the usefulness of this more detailed estimate of distribution in the body, we note that the concentration of strontium in bone is about 190 times greater than the concentration in the ovary. Even if we allow for a reduction in bone of 30% due to radioactive decay, this would indicate that the ovary gets no more than $\frac{1}{130}$ of the bone dose. Thus, if the average dose to bone does not exceed 0.5 rem/year, the radiation

protection guide recommended by the Federal Radiation Council, then the dose to the ovary should not exceed about 4 mrem/year and the dose to testes should be even less. This is much lower than estimates based on the values listed for the whole body which have sometimes been used, in the absence of anything better, as a basis for assessing genetic dose.

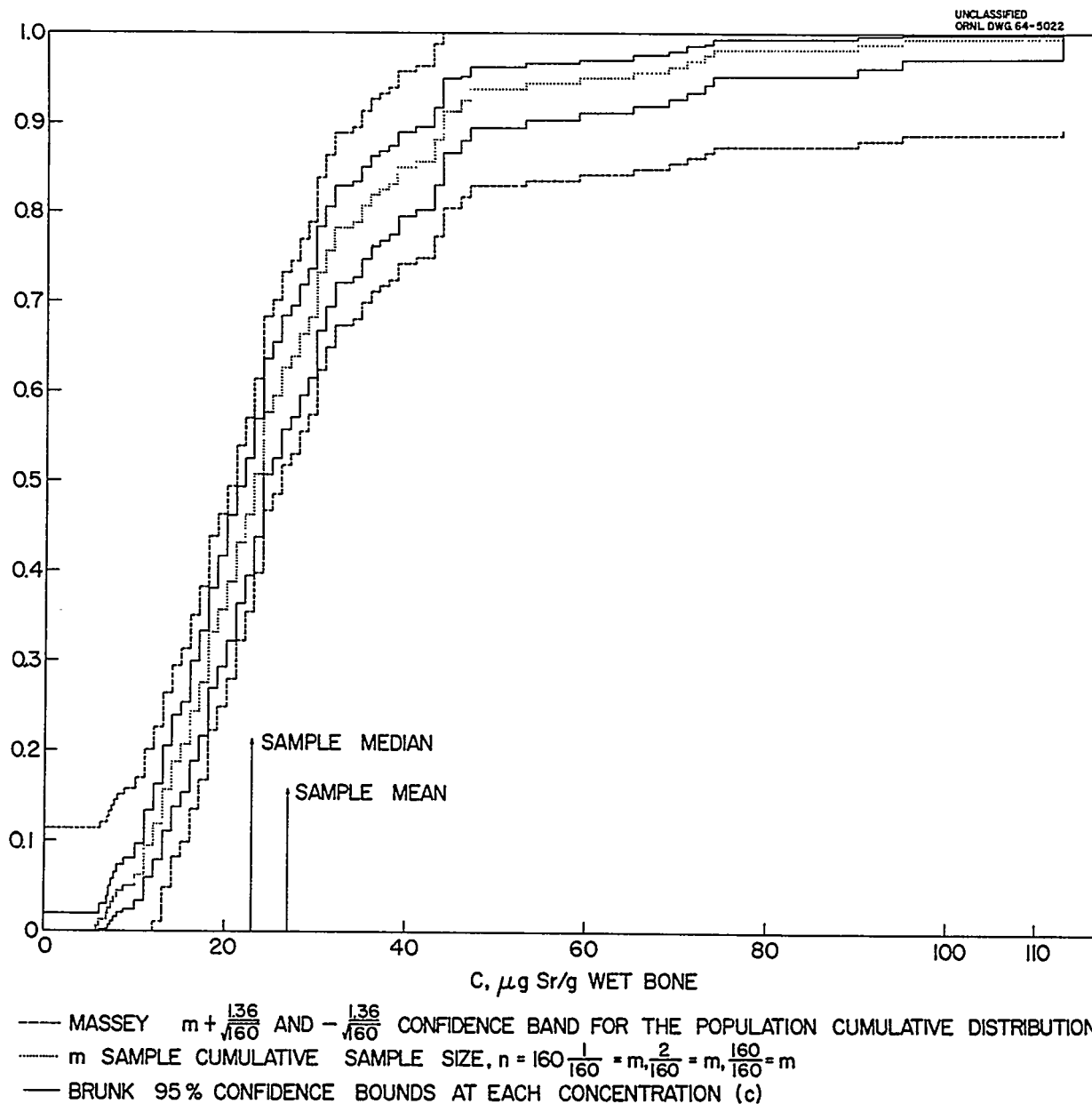


Fig. 21.8. Ninety-five Percent Confidence Bands for the Distribution of Stable Strontium in Human Bones (Ages 20-59) ORNL Trace Element Data.

22. A Two-Compartment Model with Random Variable Flows

S. R. Bernard

V. R. R. Uppuluri¹

The purpose of this section is to consider the problem of nonuniform distribution of bone-seeking radionuclides, such as the alkaline-earth elements, and the effect of age on retention of strontium by dogs via a mathematical study of a compartmental system in which the connections between the compartments are random variables. In most compartmental studies it is generally assumed that the contents of the compartments are uniformly distributed. This is not a realistic assumption for the case of bone-seeking elements such as radium, where it has been well demonstrated that hot spots of activity occur as many as 20 or 30 years after intake of ^{226}Ra by man.² Rowland states that the concentrations in the hot spots exist in regions of bone where new mineral was laid down at the time the radium was acquired and that in this mineral the original concentration of Ra, expressed as the ratio of Ra to Ca, was essentially the same as the Ra-to-Ca ratio that existed in the blood plasma at the time the new mineral was formed. There is also a second type of distribution which is much lower in concentration and rather uniform.² This is believed to be the result of an exchange process which continually transfers Ca and/or Ra atoms from blood to bone and back again and which is characterized by an unusually long time constant.

Also, there is a growing trend to consider turnover rates in bone in terms of at least two "sub-compartments," trabecular bone and compact bone. The turnover rates in these two types of bone are observed to be different — faster in trabecular bone and much slower in the compact bone. Lucas³ has suggested that the biological half-life for Ra in trabecular bone is ~7 to 14 years and twice as long in compact bone. Also, the hot spots of Ra would disappear from the bone after perhaps 200

years since by then the whole bone would be remodeled and turned over. How may we more adequately represent these phenomena in terms of a compartmental approach?

One way to gain more insight into this problem is to consider the bone-blood system as a set of j randomly connected compartments; let the first compartment represent blood, in which the element is uniformly mixed, and the other $j - 1$ compartments represent bone. Take a subset of r compartments, $r < j - 1$, and call these trabecular bone. Let the other $j - r + 1$ compartments be cortical bone. Assume that the flows between the blood and bone are random, that is, of the $j - 1$ compartments only l of them are connected to the blood in the interval 0 to t_1 , while in the interval t_1 to t_2 , l of them are also connected but not necessarily the same ones that were connected in the first interval of time, and so on for other intervals of time. Thus some of the $j - 1$ compartments trap the concentration that existed in the interval 0 to t_1 . (This represents the laying down of new bone.) They may release it at a later time (this represents the remodeling of bone), or they may never reopen and connect with the bloodstream (this represents a hot spot), thereby maintaining the same concentration that existed at time t_1 .

The above constitutes the general compartmental system we want to study. We need to determine the behavior of the system — what are the concentrations in a given compartment as a function of time — how long must one wait until a compartment releases the trapped material — how many randomly connected compartments are required to represent the available data on retention in bone? We find that these are difficult questions and that before we can get some answers to the general case we have to initiate our studies on a simpler system, namely, that of only two compartments with random flows. Here we gain some insight into the behavior of the general system and we find that the two-compartment system gives some information on the age effect on retention of ^{85}Sr by beagles. Thus we present the results of the study of this simpler model in this section.

¹Mathematics Division.

²R. E. Rowland, "Late Observations of the Distribution of Radium in the Human Skeleton," p. 339 in *A Symposium on Radioisotopes in the Biosphere*, ed. by R. S. Caldecott and L. A. Snyder, Univ. of Minnesota, Minneapolis, 1960.

³H. E. Lucas, personal communication, 1964.

TWO-COMPARTMENT MODEL

Let us suppose that we have two compartments of the same volume, with a gate between them which can be opened or closed at will (Fig. 22.1). Initially, say we have unit concentration in compartment 1 and zero concentration in compartment 2. Also, suppose that there is provision for an inlet and outlet through compartment 1 which will enable the concentration (in 1 only if the gate is closed or in both if the gate is open) to reduce by a factor of $e^{-\lambda \Delta t}$ in a time interval Δt . (Here λ is a constant.)

Take a fair coin, that is, with $P(H) = \frac{1}{2} = P(T)$, and toss it once. If a head appears, open the gate and assume that instantly the material in both the compartments becomes homogeneous, that is, of concentration $\frac{1}{2}$ in each. Wait for a time interval Δt and suppose that during the Δt the inlet and outlet through compartment 1 are functioning. After time Δt , the concentration in 1 and 2 will become $\frac{1}{2} e^{-\lambda \Delta t}$ each.

If a tail appears, keep the gate between compartments 1 and 2 closed, and after time Δt (during which the inlet and outlet through compartment 1 are functioning) the concentration in 1 will become $e^{-\lambda \Delta t}$ and of course the concentration in compartment 2 is still zero.

UNCLASSIFIED
ORNL-DWG 64-8617

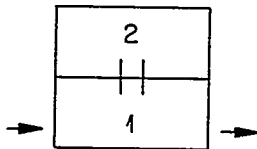


Fig. 22.1. A Two-Compartment Model.

The equations for this system are set up as follows:

Let $C_{0,1}$ denote the initial concentration in compartment 1 and $C_{0,2}$ denote the initial concentration in compartment 2, that is,

$$\begin{pmatrix} C_{0,1} \\ C_{0,2} \end{pmatrix} = \begin{pmatrix} 1 \\ 0 \end{pmatrix}.$$

This corresponds to an experiment where initially the gate is always closed. More generally, let $C_{n,i}$ denote the concentration at time t_n , $n = 1, 2, 3, \dots$, in compartment $i = 1, 2$.

Let X denote the binomial random variable, corresponding to the fair coin, that is,

$$X = \begin{cases} 1 & \text{if } H \text{ appears (with probability } \frac{1}{2}) \\ 0 & \text{if } T \text{ appears (with probability } \frac{1}{2}) \end{cases}.$$

Then, it is easily seen that

$$\begin{pmatrix} C_{1,1} \\ C_{1,2} \end{pmatrix} = \begin{pmatrix} \frac{1}{2} e^{-\lambda \Delta t} (C_{0,1} + C_{0,2}) & e^{-\lambda \Delta t} C_{0,1} \\ \frac{1}{2} e^{-\lambda \Delta t} (C_{0,1} + C_{0,2}) & C_{0,2} \end{pmatrix} \begin{pmatrix} X_1 \\ 1 - X_1 \end{pmatrix}$$

where X_1 denotes the binomial random variable at the first stage of the experiment, that is, more simply,

$$\begin{pmatrix} C_{1,1} \\ C_{1,2} \end{pmatrix} = \begin{pmatrix} \frac{1}{2} e^{-\lambda \Delta t} & e^{-\lambda \Delta t} \\ \frac{1}{2} e^{-\lambda \Delta t} & 0 \end{pmatrix} \begin{pmatrix} X_1 \\ 1 - X_1 \end{pmatrix}$$

which is a compact way of representing all the four possible outcomes, namely,

if heads, that is, $X_1 = 1$, $C_{1,1} = \frac{1}{2} e^{-\lambda \Delta t} = C_{1,2}$;

if tails, that is, $X_1 = 0$, $C_{1,1} = e^{-\lambda \Delta t}$; $C_{1,2} = 0$.

Next, we shall obtain a recursive relation between

$$\begin{pmatrix} C_{1,1} \\ C_{1,2} \end{pmatrix} \quad \text{and} \quad \begin{pmatrix} C_{0,1} \\ C_{0,2} \end{pmatrix},$$

connected through the random variable X_1 .

$$\begin{aligned}
\begin{pmatrix} C_{1,1} \\ C_{1,2} \end{pmatrix} &= C_{0,1} \begin{pmatrix} \frac{1}{2} e^{-\lambda \Delta t} & e^{-\lambda \Delta t} \\ \frac{1}{2} e^{-\lambda \Delta t} & 0 \end{pmatrix} \begin{pmatrix} X_1 \\ 1 - X_1 \end{pmatrix} \\
&+ C_{0,2} \begin{pmatrix} \frac{1}{2} e^{-\lambda \Delta t} & 0 \\ \frac{1}{2} e^{-\lambda \Delta t} & 1 \end{pmatrix} \begin{pmatrix} X_1 \\ 1 - X_1 \end{pmatrix} \\
&= C_{0,1} \begin{pmatrix} e^{-\lambda \Delta t} - \frac{1}{2} e^{-\lambda \Delta t} X_1 \\ \frac{1}{2} e^{-\lambda \Delta t} X_1 \end{pmatrix} \\
&+ C_{0,2} \begin{pmatrix} \frac{1}{2} e^{-\lambda \Delta t} X_1 \\ 1 - (1 - \frac{1}{2} e^{-\lambda \Delta t}) X_1 \end{pmatrix} \\
&= \begin{pmatrix} e^{-\lambda \Delta t} - \frac{1}{2} e^{-\lambda \Delta t} X_1 & \frac{1}{2} e^{-\lambda \Delta t} X_1 \\ \frac{1}{2} e^{-\lambda \Delta t} X_1 & 1 - (1 - \frac{1}{2} e^{-\lambda \Delta t}) X_1 \end{pmatrix} \\
&\quad \times \begin{pmatrix} C_{0,1} \\ C_{0,2} \end{pmatrix}
\end{aligned}$$

where we recall that

$$\begin{pmatrix} C_{0,1} \\ C_{0,2} \end{pmatrix} = \begin{pmatrix} 1 \\ 0 \end{pmatrix}.$$

By following the same reasoning we obtain, if X_m denotes the binomial random variable at the m th stage,

$$\begin{aligned}
\begin{pmatrix} C_{m,1} \\ C_{m,2} \end{pmatrix} &= \begin{pmatrix} e^{-\lambda \Delta t} - \frac{1}{2} e^{-\lambda \Delta t} X_m & \frac{1}{2} e^{-\lambda \Delta t} X_m \\ \frac{1}{2} e^{-\lambda \Delta t} X_m & 1 - (1 - \frac{1}{2} e^{-\lambda \Delta t}) X_m \end{pmatrix} \\
&\quad \times \begin{pmatrix} C_{m-1,1} \\ C_{m-1,2} \end{pmatrix} \quad m = 1, 2, \dots
\end{aligned}$$

If we assume that X_1, X_2, \dots, X_n are independent, identically distributed, random variables and E

denotes the expectation operator, then

$$E \begin{pmatrix} C_{n,1} \\ C_{n,2} \end{pmatrix} = \begin{pmatrix} \frac{3}{4} e^{-\lambda \Delta t} & \frac{1}{4} e^{-\lambda \Delta t} \\ \frac{1}{4} e^{-\lambda \Delta t} & \frac{1}{2} + \frac{1}{4} e^{-\lambda \Delta t} \end{pmatrix}^n \begin{pmatrix} 1 \\ 0 \end{pmatrix} \quad (1)$$

because $E(X_m) = \frac{1}{2}$; $m = 1, 2, \dots, n$; $\Delta t = t/n$.

Let $a_n = e^{-\lambda \Delta t}$ and μ_1, μ_2 denote the eigenvalues of the matrix

$$S = \begin{pmatrix} \frac{3}{4} a_n & \frac{1}{4} a_n \\ \frac{1}{4} a_n & \frac{1}{2} + \frac{1}{4} a_n \end{pmatrix} = \begin{pmatrix} s_{11} & s_{12} \\ s_{12} & s_{22} \end{pmatrix}. \quad (2)$$

It turns out that

$$\mu_1 = \frac{1}{4} [2 a_n + 1 + \sqrt{2 a_n^2 - 2 a_n + 1}]$$

and

$$\mu_2 = \frac{1}{4} [2 a_n + 1 - \sqrt{2 a_n^2 - 2 a_n + 1}],$$

and

$$\begin{aligned}
S &= \frac{1}{(\mu_2 - \mu_1) s_{12}} \begin{pmatrix} s_{12} & s_{12} \\ \mu_1 - s_{11} & \mu_2 - s_{11} \end{pmatrix} \\
&\quad \times \begin{pmatrix} \mu_1 & 0 \\ 0 & \mu_2 \end{pmatrix} \begin{pmatrix} \mu_2 - s_{11} & -s_{12} \\ -(\mu_1 - s_{11}) & s_{12} \end{pmatrix};
\end{aligned}$$

therefore

$$\begin{aligned}
S^n &= \frac{1}{(\mu_2 - \mu_1) s_{12}} \begin{pmatrix} s_{12} & s_{12} \\ \mu_1 - s_{11} & \mu_2 - s_{11} \end{pmatrix} \\
&\quad \times \begin{pmatrix} \mu_1^n & 0 \\ 0 & \mu_2^n \end{pmatrix} \begin{pmatrix} \mu_2 - s_{11} & -s_{12} \\ -(\mu_1 - s_{11}) & s_{12} \end{pmatrix}, \\
S^n \begin{pmatrix} 1 \\ 0 \end{pmatrix} &= \frac{1}{(\mu_2 - \mu_1) s_{12}} \\
&\quad \times \begin{pmatrix} s_{12} [\mu_1^n (\mu_2 - s_{11}) - \mu_2^n (\mu_1 - s_{11})] \\ (\mu_1 - s_{11}) (\mu_2 - s_{11}) (\mu_1^n - \mu_2^n) \end{pmatrix}. \quad (3)
\end{aligned}$$

It is of interest to determine the solution for $n \rightarrow \infty$, $\Delta t \rightarrow 0$. Now, as $n \rightarrow \infty$, we have:

$$a_n \rightarrow 1, s_{11} \rightarrow \frac{3}{4}, s_{12} \rightarrow \frac{1}{4}, \mu_1 \rightarrow 1, \mu_2 \rightarrow \frac{1}{2},$$

$$(\mu_2 - \mu_1) \rightarrow -\frac{1}{2}, \mu_1^n \rightarrow e^{-\frac{3}{4} \times \lambda t}, \text{ and } \mu_2^n \rightarrow 0.$$

Therefore

$$\lim_{n \rightarrow \infty} S^n \begin{pmatrix} 1 \\ 0 \end{pmatrix} = \frac{1}{2} e^{-\frac{3}{4} \times \lambda t} \begin{pmatrix} 1 \\ 1 \end{pmatrix}.$$

In Eqs. (1), (2), and (3) we see that the expected concentrations are functions of two parameters, λ and Δt , and the initial conditions. We investigate the effect of Δt on the concentrations by graphical techniques. Figure 22.2 presents a plot of the sum of the concentrations in both compartments for $\Delta t = 0, 1, 2, 4$, and $\lambda = 0.693$. As can be seen, when the interval width increases, the total concentrations decrease more rapidly, initially, but then it decreases more slowly along a second exponential component. Note also the intercept of this second exponential decreases with increasing Δt . It may be that the most appropriate value of Δt varies with the age of the animal, and thus the model might suggest an effect of age on the biological turnover time. It has been noted that the biological half-life for retention of Cs is larger for young than for old dogs.⁴ Now, if a second exponential component would occur, does it have a longer half-life and a smaller intercept in older dogs? In the case of ⁸⁵Sr retention in dogs of different ages, as observed by Glad, Mays, and Fisher,⁵ it appears that this model gives approximately the same quantitative picture as far as the intercept of the long-term component is concerned, but not the biological half-life, T_b . Figure 22.3 shows a plot of the data of Glad *et al.* Note the half-life of the second exponential component indicated in these figures is generally larger for young dogs that are injected than is the T_b for the second component fitting retention in old dogs. Note also that the intercept of that second component decreases with age. We find

⁴W. P. Norris, *Late Effects of Radiation Exposure*, presented at Radiation Research Society meeting, Miami Beach, Fla., May 18-20, 1964.

⁵B. W. Glad, C. W. Mays, and W. Fisher, *Radiation Res.* 12, 672-81 (1960).

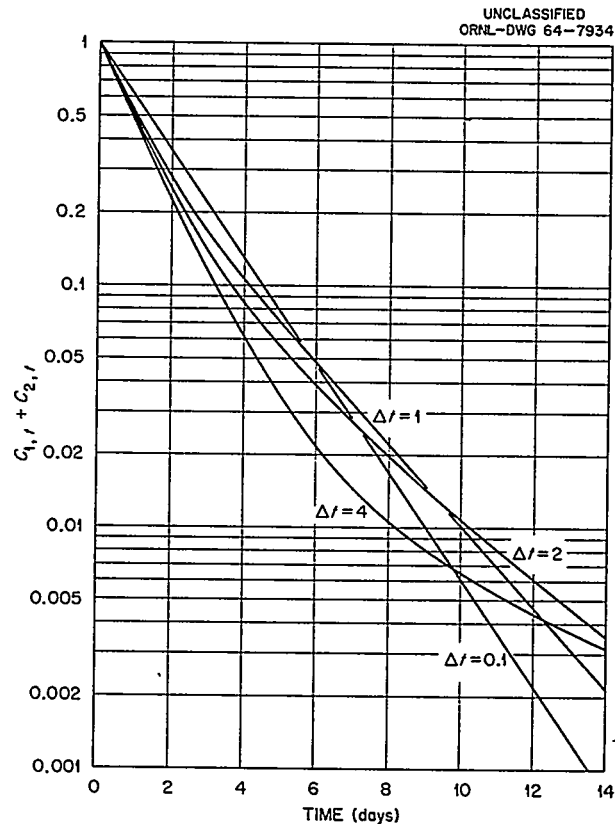


Fig. 22.2. Plot of the Sum of Concentrations in Compartments 1 and 2 vs Time for Case of Equally Spaced Subintervals of Time.

that we can get a better interpretation of these data in terms of increasing subinterval widths.

Also, Glad and Mays have shown that these data can also be represented with a power function. It is possible to obtain something akin to a power function from this two-compartment model with random flows simply by taking a partitioning of time intervals which increase monotonically. In this case we have to have a more general notation. Let

$$\Delta t_i = t_i - t_{i-1}$$

which are not necessarily equal intervals. Then, instead of Eq. (1), we have

$$E \begin{pmatrix} C_{t_i,1} \\ C_{t_i,2} \end{pmatrix} = \left(\prod_{i=n}^1 S(\Delta t_i) \right) \begin{pmatrix} 1 \\ 0 \end{pmatrix} \quad (4)$$

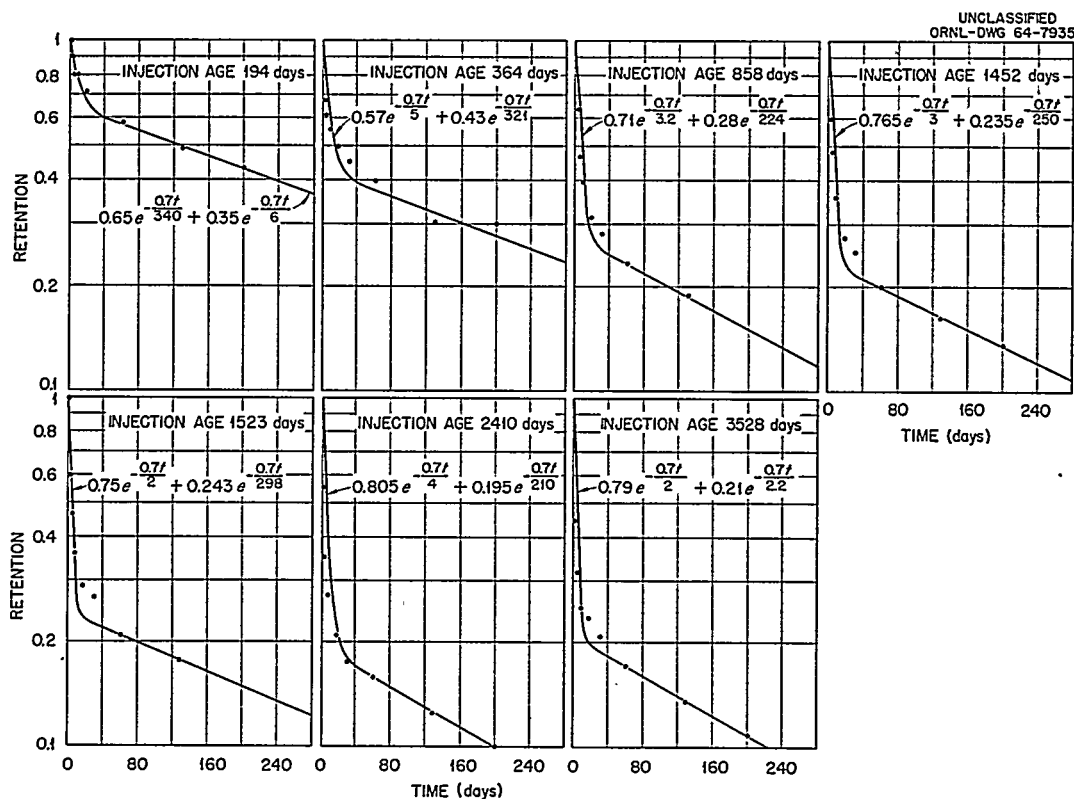


Fig. 22.3. Strontium-85 Retention in Dogs.

where S is the matrix which has already been defined in Eq. (2). When all Δt 's are equal, we recover Eq. (3) again. Now, taking a specific case, that is, $\Delta t_i = i$ and $i = 1, 2, \dots, 7$, and letting $\lambda = 0.693$, we insert into Eq. (4) and calculate the expected concentrations. Figure 22.4 presents a plot of the total concentrations, that is, $(C_{t,1} + C_{t,2})$, as a function of time. As can be seen, the slope of this function is monotonically decreasing. It can be seen from inspection of Eqs. (2) and (4) that as Δt_i gets larger

$$S(\Delta t_i) \rightarrow \begin{pmatrix} \sim 0 & \sim 0 \\ \sim 0 & \frac{1}{2} \end{pmatrix}$$

and hence the concentration in the second compartment decreases by $\frac{1}{2}$, but the time interval for this reduction to occur is larger the farther out we go. This behavior is similar to a power function.

To gain some further insight into the effect of age on retention from this model, consider the case

where we let $\Delta t_i = i + T$, $\Delta t_0 = 0$, and $i = 0, 1, 2, 3, \dots$. Here we let T correspond to the age of an animal at the time of injection. This corresponds to a simulation of aging. The gate opens and closes in a shorter time interval in a younger animal and in a longer time interval in an older animal. For example, in a newborn animal the gate first opens (or closes) after only one unit of time, while in a 3-year-old animal the gate first opens (or closes) after three units of time. We calculate the sum of the expected concentrations in compartments 1 and 2 for this case, and the results are presented graphically in Fig. 22.5. As can be seen, the curves are of the same qualitative shape as Glad and Mays observed in their experiments on ^{85}Sr retention in dogs of different ages.

It is to be pointed out here that the trend with age observed in Fig. 22.5 could be reversed by simply changing the initial conditions on the column vector. Recall that we dealt with the specific case where the gate between compartments 1 and 2 is initially closed. If we were to decide whether

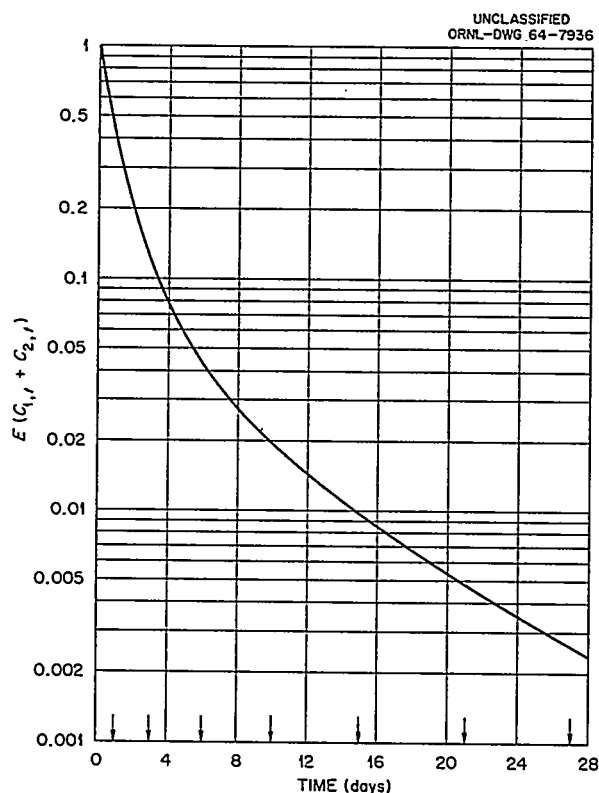


Fig. 22.4. Expected Sum of Concentrations in Compartments for Case of Increasing Subinterval Width.

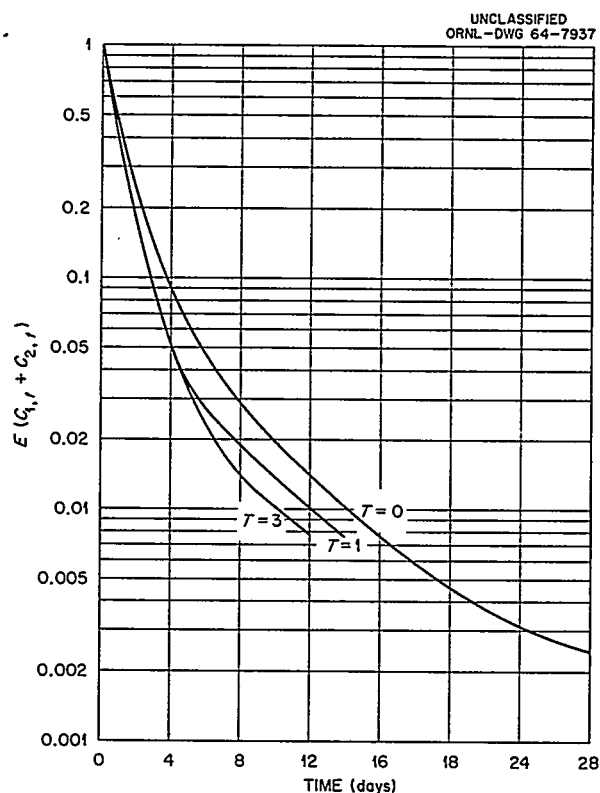


Fig. 22.5. Expected Sum of Concentrations for Case of Increasing Subinterval Width and for Different Ages.

this gate was initially opened or closed by a random toss of the coin, then the expected value of the initial concentrations would be

$$E \begin{pmatrix} C_{0,1} \\ C_{0,2} \end{pmatrix} = \begin{pmatrix} 3/4 \\ 1/4 \end{pmatrix}.$$

If we used this vector of initial concentrations, then the sum of the expected concentrations in

$$E \begin{pmatrix} C_{n,1} \\ C_{n,2} \end{pmatrix} = \begin{pmatrix} \frac{1}{8} (3 e^{-\lambda_1 \Delta t} + e^{-\lambda_2 \Delta t}) & \frac{1}{8} (e^{-\lambda_1 \Delta t} + e^{-\lambda_2 \Delta t}) \\ \frac{1}{8} (e^{-\lambda_1 \Delta t} + e^{-\lambda_2 \Delta t}) & \frac{1}{2} + \frac{1}{8} (e^{-\lambda_1 \Delta t} + e^{-\lambda_2 \Delta t}) \end{pmatrix}^n \begin{pmatrix} C_{0,1} \\ C_{0,2} \end{pmatrix}.$$

compartments 1 and 2 would behave differently for different interval widths of time. One would expect that as the interval was increased, then, since compartment 2 initially starts out with material in it, it would keep it longer the longer the

intervals. The chances for release would be greater the shorter the intervals.

Before closing, we list the equation for the two-compartment model, that is, the case where flows between compartments 1 and 2 are random and flow out of compartment 1 also is random. Let λ_1 denote one rate of flow and λ_2 the other rate of flow out of compartment 1. Assume these have equally probable occurrences. Then it can be shown that

This solution is only for the case where one flips two fair coins at the same time, that is, it is assumed that both gates are opened (or closed) in the equally spaced intervals of time according as the respective coins fall heads or tails.

23. Studies on the Internal Exposure/External Exposure Equivalence Relation

S. R. Bernard

Some data on the life-shortening effects of injected ^{239}Pu and ^{226}Ra in rats, rabbits, and dogs have been interpreted with the equivalence relation between internal exposure and external exposure, or what is really the same as the linear theory of life shortening by internal dose discussed in the previous progress report.¹ Also, by using this equivalence relation, an MPC is derived which would be related only to life shortening as an end point. This is offered as an illustration of a method which might be applied to other end points as well if appropriate data are available.

First, some familiarity with the approach outlined in the previous report is assumed. The argument in that report could be modified to show that if shortening of life is denoted by $S_0 - S$, where S_0 is the life span of uninjected (or non-irradiated) animals and S is the life span of injected (or radiated) animals, then life shortening is proportional to the total absorbed dose, denoted by D , that is,

$$S_0 - S = \alpha' D. \quad (1)$$

For an internal emitter, which is exponentially eliminated from the body,

$$D = \beta \int_0^S q_0 e^{-\lambda t} dt, \quad (2)$$

where β is the rem/unit time/ μc injected. From Eqs. (1) and (2) we find

$$S_0 - S = \frac{\alpha q_0}{\lambda} (1 - e^{-\lambda S}), \quad (3)$$

where $\alpha = \alpha' \beta$ with units of μc^{-1} . The dose to bone has been estimated on the basis of the reported data and the observed life shortening, $S_0 - S$, plotted against dose, and it was found that this linear theory was not obeyed. However, it was noted that when Eq. (3) was rearranged to read

$$q_0 = \frac{S_0 - S}{(\alpha/\lambda)(1 - e^{-\lambda S})} \quad (4)$$

and when an (S, q_0) plot of the data was made, then this function would fit the data fairly adequately if a suitable value of λ was used. We have estimated the parameters α and λ from the (S, q_0) data and have compared this λ with that estimated in metabolism studies. The two values of λ generally differed. Let us illustrate this point with the rat data of Moskalev.² Figure 23.1 shows a graph of his data — a plot of q_0/m , the microcuries of $^{239}\text{Pu}/\text{kg}$ injected into the rats vs S , the median life span in days. The equation and curve fitting the data are also shown. Note that the effective half-life is 36 days. Moskalev did not have any metabolic data from which to estimate a metabolic effective half-life (T). However, when we compared it with the T estimated from Fink's (S, q_0) data on rats,³ we found $T = 72$ days, differing by a factor of only 2.

When we attempt to interpret the data of Bukhtoyarova⁴ on rabbits or the Utah data on beagle dogs⁵ with this model, we find they are not really adequate as yet, because the studies are not complete. However, we can make some tentative calculations with these data. Figure 23.2 shows the ^{239}Pu injection data on rabbits, and the Utah data on dogs injected with ^{239}Pu and ^{226}Ra are shown in Figs. 23.3 and 23.4 respectively. (In these latter two figures, the mean life spans are estimated for dogs dying from osteosarcoma only and not the mean life span for all causes of death.) Note, however, that a linear fit of the long time data has been estimated and plotted together with the data in Figs. 23.2 to 23.4. From the estimated intercept, $\lambda S_0/\alpha m$, we can see that dogs are more sensitive to ^{239}Pu than rabbits which, in turn, are more sensitive than rats, that

²Yu. I. Moskalev, Joint Publications Research Service translation 16,900, p. 12, 1962 (Russian translation).

³R. M. Fink, *Biological Studies with Polonium, Radium, and Plutonium*, McGraw-Hill, New York, 1950.

⁴Z. M. Bukhtoyarova, Joint Publications Research Service translation 16,900, p. 65, 1962 (Russian translation).

⁵T. F. Dougherty et al., *Some Aspects of Internal Emitters*, Pergamon, New York, 1962.

¹W. S. Snyder et al., *Health Phys. Div. Ann. Progr. Rept. June 30, 1963*, ORNL-3492, pp. 163-65.

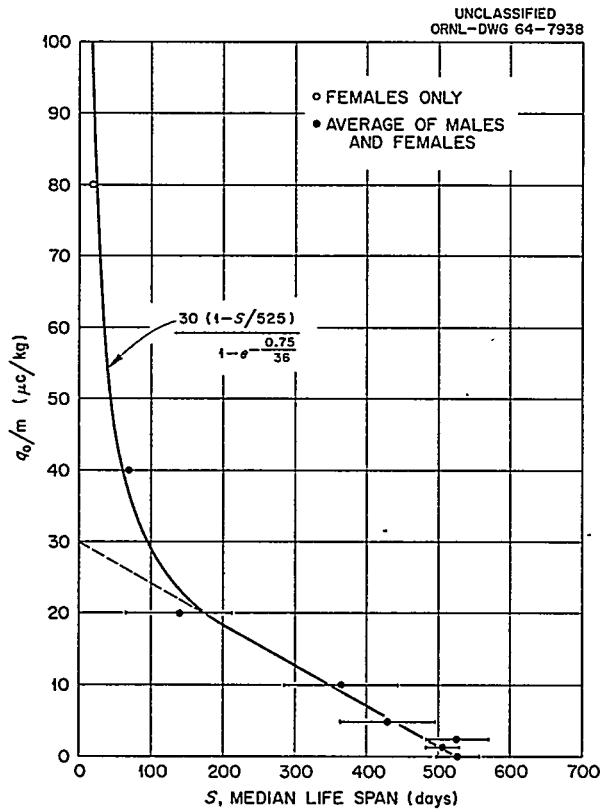
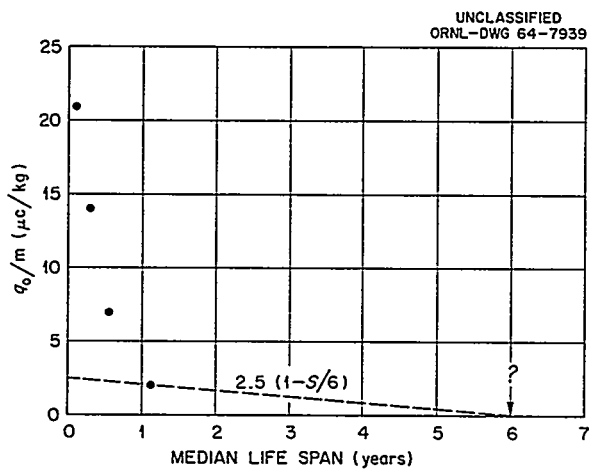
Fig. 23.1. Life Shortening by Injected ^{239}Pu - Rats.

Fig. 23.2. Life Shortening by Injected Plutonium - Rabbits.

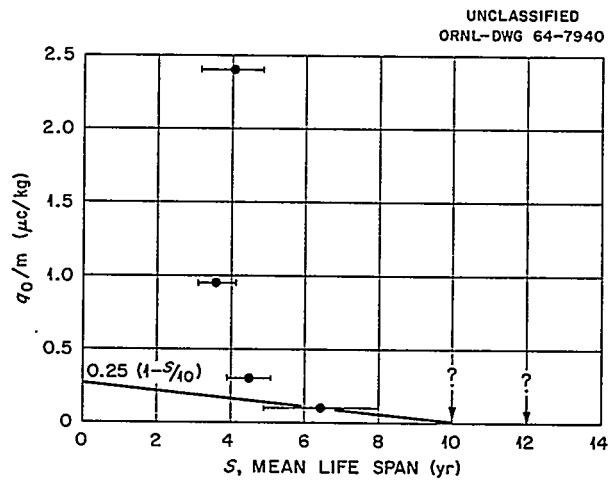


Fig. 23.3. Life Shortening by Injected Plutonium - Dogs.

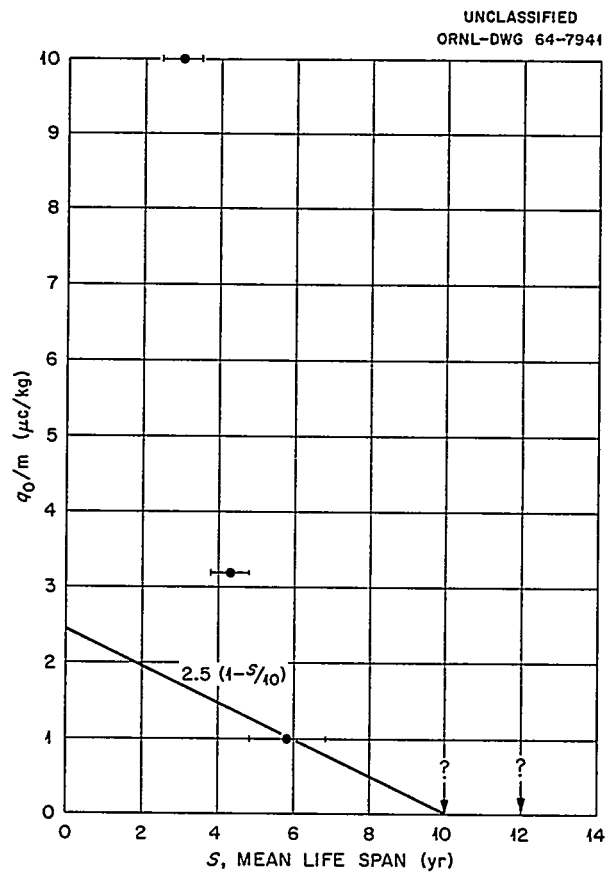


Fig. 23.4. Life Shortening by Injected Radium - Dogs.

is, the equations for the linear (or assumed-to-be-linear) regions are

$$\begin{aligned}
 q_0/m &\rightarrow 30 (1 - S/525 \text{ days}) \text{ rats} \\
 &\quad (\text{Fig. 23.1}), \\
 &\rightarrow 2.5 (1 - S/6 \text{ years}) \text{ rabbits} \\
 &\quad (\text{Fig. 23.2}), \\
 &\rightarrow 0.25 (1 - S/10 \text{ years}) \text{ dogs} \\
 &\quad (\text{Fig. 23.3}).
 \end{aligned} \tag{5}$$

What does this mean in terms of MPC values for man? Let us review the method we proposed for estimating MPC values.

Recall that in the previous report we noted that a plot of R , the daily whole-body dose rate in rads/day, to mice in the (S, R) plane became a linear function too for values of $S/S_0 \geq 0.5$; it was

$$R \sim 40 (1 - S/S_0) \tag{6}$$

in r/day (mice). Now, from Braestrup's data on American radiologists,⁶ we estimate

$$R \sim 5 (1 - S/S_0) \tag{7}$$

in r/day. Next we set up an equivalence between the whole-body external exposure data and the injection data by noting from Eq. (4) that

$$q_0 \rightarrow \left(\frac{\lambda S_0}{\alpha} \right) (1 - S/S_0) \tag{8}$$

and from Eqs. (7) and (8)

$$q_0 = \left(\frac{\lambda S_0/\alpha}{5} \right) R. \tag{9}$$

Now, the question is which value in Eq. (5) should be employed for the intercept $(\lambda S_0/\alpha)$ in Eq. (9). We attempt to answer this question by plotting the $(\lambda S_0/\alpha)$ in Eq. (5) vs the mean life span of the species. Figure 23.5 shows a log \times log graph of the intercept plotted vs the life span of the species. The power function $440 S^{-3}$ fits the data fairly well. Thus, if this function is used to extrapolate to the 70-year life span of man, we find

$$\frac{\lambda S_0}{\alpha m} = 0.00129 \mu\text{C/kg}.$$

Inserting this into Eq. (9) and letting $R = 0.02$ rad/day, then

$$q_0/m = 0.56 \times 10^{-5} \mu\text{C/kg}$$

and

$$q_0 \sim 39 \times 10^{-5} \mu\text{C}.$$

Recall that the interpretation of this is that a single injection of $39 \times 10^{-5} \mu\text{C}$ of ^{239}Pu into man would produce the same life shortening as the permissible whole-body external dose rate of 5 rads/year. What $(\text{MPI})_w$ does this correspond to? It turns out to be $\sim 0.07 \mu\text{C}/\text{quarter}$. The ICRP report⁷ recommends $\sim 10 \mu\text{C}/\text{quarter}$. This would imply that the ICRP report value is not a conservative value.

We interpret the ^{226}Ra rat data in the same manner and find from Fink's rat data $\lambda S_0/\alpha m = 350 \mu\text{C/kg}$, and from Fig. 23.4, on dogs, $\lambda S_0/\alpha m = 2.5 \mu\text{C/kg}$. Assuming the power function relation

⁷Report of Committee II on Permissible Dose for Internal Radiation (1959), "Health Phys. 3 (1960).

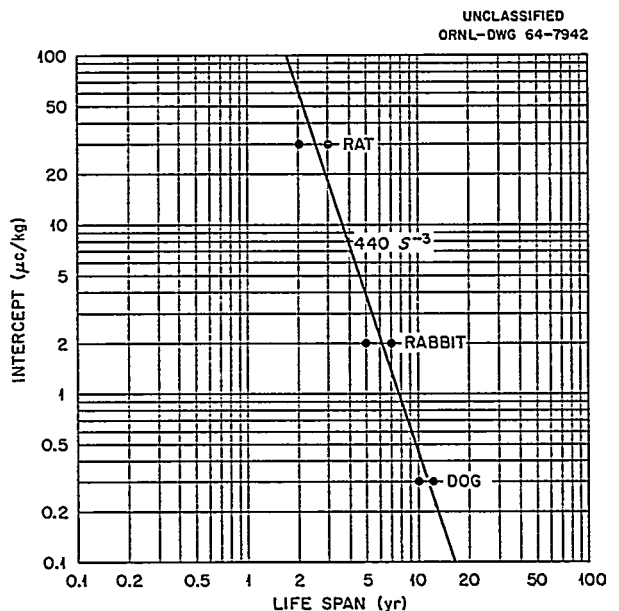


Fig. 23.5. Intercept of the Formula for Life Shortening $(\lambda S_0/\alpha)$ vs Life Span.

⁶Cited by P. R. J. Burch, *Nature* 185, 135-42 (1960).

between this intercept and mean life span of the species, we find $\lambda S_0/\alpha m \sim 7210 S^{-3.3}$. Extrapolating to man ($S = 70$ years), $(\lambda S_0/\alpha m)_{\text{man}} = 0.006 \mu\text{c/kg}$ for ^{226}Ra . Calculating Eq. (9) with $R = 0.02$ rad/day, we obtain $q_0/m \cong 3 \times 10^{-5} \mu\text{c/kg}$ and $q_0 \sim 210 \times 10^{-5} \mu\text{c}$. This is lower than the current permissible ^{226}Ra burden of $0.1 \mu\text{c}$ by a factor of ~ 500 , and it yields a correspondingly lower $(\text{MPI})_w$ too. This implies that if the $0.1\text{-}\mu\text{c}$ value is a valid body burden, then this method of estimating MPC values is either too conservative, or invalid, or perhaps the dog is equally as sensitive to internal exposure from ^{239}Pu and ^{226}Ra as man is. If we adopt the latter assumption and recalculate the $(\text{MPI})_w$, we find for ^{239}Pu , $(\text{MPI})_w \sim 14 \mu\text{c/quarter}$ (compared with ICRP

value of $10 \mu\text{c/quarter}$) and for ^{226}Ra , $(\text{MPI})_w \cong 0.01 \mu\text{c/quarter}$ (compared with ICRP value of $0.02 \mu\text{c/quarter}$).

The data on dogs are not adequate as yet, and hence it would be premature to draw any firm conclusions from these calculations. Also, we mention here that this estimation method should not be used without checking with data on more species of animals which were administered lower injection levels or which experience continuous feedings and inhalation of the radionuclides. In addition to the need for data to permit interspecies extrapolation, other biological effects should be considered also. When such data become available, a better basis for estimating body burdens and MPC's may evolve.

24. Comments on Intake Guides for Various Isotopes and Isotopic Mixtures of Uranium

Mary R. Ford

In the application of maximum permissible concentration (MPC) values, or intake guides, for uranium as provided by NCRP¹ and ICRP,^{2,3} questions arise frequently concerning a "curie" of natural uranium which has a special definition in these recommendations. Other questions relate to the fact that limiting values for some of the isotopes are based on considerations of chemical toxicity, while for other isotopes it is the radiological hazard that is limiting; thus, uncertainties in the computation of values for mixtures of the isotopes are encountered. In this study simple formulas, additional MPC values, and explanations are given as an aid in resolving these and other similar problems.

A CURIE OF NATURAL URANIUM

In the NCRP and ICRP Recommendations,^{1,2,3} a curie of natural uranium is considered to corre-

spond to 3.7×10^{10} dis/sec from ^{238}U , 3.7×10^{10} dis/sec from ^{234}U , and 1.7×10^9 dis/sec from ^{235}U . Even before 1962, when the curie was redefined as a unit of activity rather than a quantity of a radionuclide,⁴ this definition was confusing to many because a curie by the usual definition corresponded to only 3.7×10^{10} dis/sec. Evidence of this confusion is present in the Recommendations themselves, where the number of disintegrations per

¹"Maximum Permissible Body Burdens and Maximum Permissible Concentrations of Radionuclides in Air and Water for Occupational Exposure," *Natl. Bur. Std. (U.S.), Handbook 69*, GPO, Washington, 1959.

²Report of Committee II on Permissible Dose for Internal Radiation, ICRP Publication 2, Pergamon, London, 1959.

³Recommendations of the International Commission on Radiological Protection (as amended 1959 and revised 1962), ICRP Publication 6, Pergamon, London, 1964.

⁴"Radiation Quantities and Units," ICRU report 10a, *Natl. Bur. Std. (U.S.), Handbook 84*, GPO, Washington, 1962.

second from ^{235}U was listed incorrectly, but differently, in both the NCRP and ICRP texts. This has been corrected by errata, and fortunately it is of academic interest only, since ^{235}U is relatively unimportant in computations involving the natural mixture.

The first appearance of the special curie in internal dose recommendations was in the ICRP Recommendations of 1955.⁵ In that report the ICRP was influenced by the English, who for many years had used such a definition in industrial work. Since natural uranium is more than 99 wt % ^{238}U and since chemical toxicity is the principal concern, it was natural to neglect the ^{234}U and ^{235}U , which contribute very little to the total mass. Thus, the convention developed of computing the mass of ^{238}U that would correspond to 1 curie of activity of ^{238}U and calling this amount 1 curie of natural uranium. Since a counter, in measuring the disintegrations from such a curie of natural uranium, would register about twice the usual number of disintegrations, the "double curie" came into use.

CHEMICAL TOXICITY VS RADIATION DAMAGE AS A BASIS FOR ESTIMATING PERMISSIBLE INTAKE VALUES

It is quite generally known that natural uranium is very poisonous to the body chemically and that

kidney is the organ most severely injured.^{6,7} Therefore, it is not surprising to find kidney as an organ of reference for each of the uranium isotopes. As stated in the Recommendations, however, chemical toxicity is the limiting criterion only for the longer-lived isotopes; thus some of the kidney values are based on chemical toxicity and others on radioactivity, and no designations appear with the values as to which criterion was used in the estimations. Thus, confusion arises when intake guides for mixtures of the isotopes are needed, since values on both bases are needed in the computations.

MPC values computed by both criteria are given in Table 24.1. The pertinent biological and physical parameters as well as the computational methods of the NCRP and ICRP Recommendations were used in arriving at the values. Underscores indicate that these values, rounded to one significant place, are the ones appearing in the reports. As seen from this table, radiation damage results before the permissible chemical dose is reached in

⁵Recommendations of the International Commission on Radiological Protection, *Brit. J. Radiol. Suppl.* 6, Pergamon, London, 1955.

⁶Carl Voegtlin and H. C. Hodge, *Pharmacology and Toxicology of Uranium Compounds*, McGraw-Hill, New York, 1949.

⁷A. J. Luessenhop et al., *Am. J. Roentgenol.* 79(1), 83-100 (January 1958).

Table 24.1. Uranium MPC Values (in $\mu\text{c/cc}$) with Kidney as the Organ of Reference
(appropriate for an exposure of 168 hr/wk)

Isotope	Based on Radioactivity		Based on Chemical Toxicity	
	(MPC) _w	(MPC) _a	(MPC) _w	(MPC) _a
^{230}U	<u>2.4×10^{-5}</u>	<u>10^{-10}</u>	8.1×10^5	3.5
^{232}U	<u>4.4×10^{-5}</u>	<u>1.9×10^{-10}</u>	3.6×10^2	1.5×10^{-3}
^{233}U	<u>9.6×10^{-5}</u>	<u>4.2×10^{-10}</u>	0.16	7.0×10^{-7}
^{234}U	<u>9.8×10^{-5}</u>	<u>4.2×10^{-10}</u>	0.11	4.5×10^{-7}
^{235}U	10^{-4}	4.5×10^{-10}	<u>3.7×10^{-5}</u>	<u>1.6×10^{-10}</u>
^{236}U	<u>10^{-4}</u>	<u>4.4×10^{-10}</u>	1.1×10^{-3}	4.7×10^{-9}
^{238}U	1.1×10^{-4}	4.8×10^{-10}	<u>5.9×10^{-6}</u>	<u>2.5×10^{-11}</u>
^{240}U	<u>0.12</u>	<u>5.2×10^{-7}</u>	4.2×10^8	2.4×10^3

every case except for the very long-lived isotopes, ^{235}U and ^{238}U .

MAXIMUM PERMISSIBLE EXPOSURE VALUES FOR MIXTURES OF THE URANIUM ISOTOPES

In the isotopic separation plants, various enrichment processes result in the production and handling of many different mixtures of the uranium isotopes, both depleted and enriched, and reactors operating at a given enrichment of uranium result in a constant change in the isotopic mixture. Thus, a simple method of estimating maximum permissible exposure values for these various mixtures is needed. Since analyses of the isotopic composition of uranium resulting from these processes are routinely made and recorded as the fraction by weight (f) of each isotope in the mixture, it is convenient to begin the computation with these fractions. Considering that 1 g of a mixture contains f_i grams of isotope i , the microcuries of isotope i per gram of mixture is

$$\mu_i = \frac{f_i \times 6.02 \times 10^{23} \times \lambda_i}{A_i \times 3.7 \times 10^4 \times 3600 \times 24},$$

where

A = atomic weight,

λ = decay constant (days),

$3600 \times 24 \times 3.7 \times 10^4 = \text{dis day}^{-1} \mu\text{C}^{-1}$,

and the relative activities of the mixture, $\nu_i = \mu_i / \sum \mu_i$.

Since a concentration $(\text{MPC})_i \mu\text{C/cc}$ of isotope i produces the limiting concentration, C , in the critical organ, it follows that $1 \mu\text{C/cc}$ of isotope i produces the concentration $C/(\text{MPC})_i$ in the critical organ. Hence,

$$(\text{MPC})_{\text{mix}} \frac{\mu\text{C}}{\text{cc}} = \sum_i (\text{MPC})_{\text{mix}} \nu_i \frac{\mu\text{C}}{\text{cc}} \text{ produces}$$

$$\frac{\sum (\text{MPC})_{\text{mix}} \nu_i C}{(\text{MPC})_i} = C$$

and

$$(\text{MPC})_{\text{mix}} = \frac{1}{\sum_i [\nu_i / (\text{MPC})_i]}.$$

Figure 24.1 shows $(\text{MPC})_a$ values computed by this equation for mixtures of ^{234}U , ^{235}U , and ^{238}U , where the weight percentages of ^{234}U and ^{235}U were enriched or depleted by the same factor, with ^{238}U constituting the remaining percent by weight (i.e., mixtures which are somewhat analogous to those resulting from the gaseous diffusion process). These values, which are applicable for the 40-hr work week, are plotted in units of $\text{dis min}^{-1} \text{m}^{-3}$, and the point shows the position of natural uranium in the scheme. The curves are

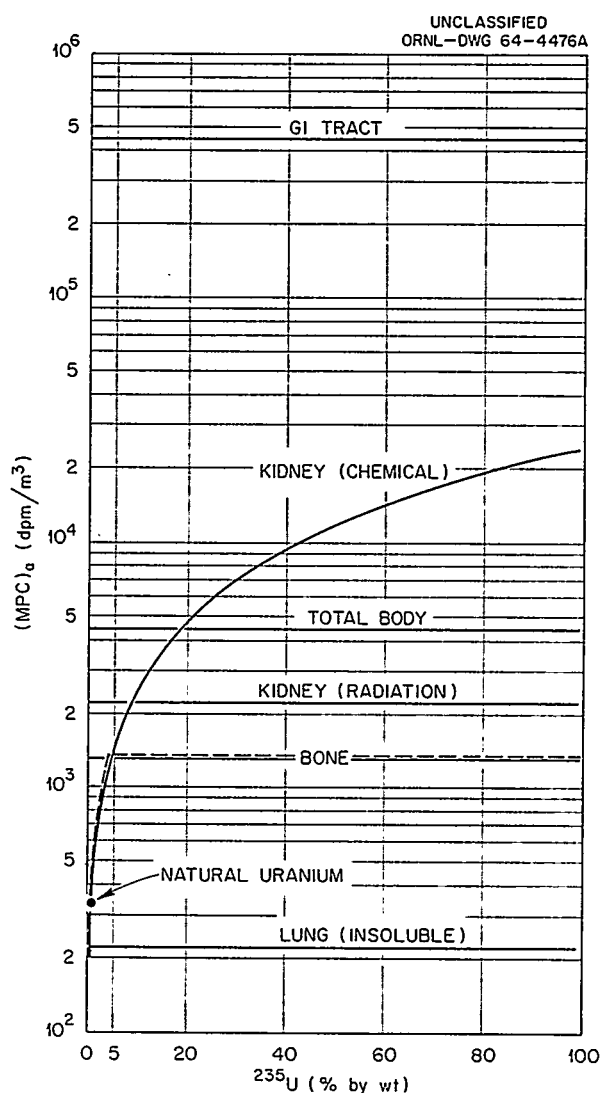


Fig. 24.1. MPC_a for Mixtures of ^{234}U , ^{235}U , and ^{238}U Appropriate for 40 hr/wk.

labeled according to the organ of reference used in the computation. The curve labeled "lung" applies to insoluble uranium, and all the others apply to the soluble form. As indicated by portions of curves overlaid with a dashed line, chemical toxicity is limiting for soluble mixtures up to an enrichment of about 5% ^{235}U . For higher enrichments, radioactivity is limiting, with bone as the critical organ. It should be noted, too, that unlike enriched uranium, the $(\text{MPC})_a$ for natural uranium is not acceptable for soluble depleted uranium.

This is more clearly discernible in Fig. 24.2, where the scale for mixtures up to 1% enrichment is enlarged. As shown in this figure, the limiting $(\text{MPC})_a$ values for soluble material decrease with depletion to about one-half the natural uranium values. In Fig. 24.3 the same values are plotted in mass units ($\mu\text{g}/\text{m}^3$). In these units the MPC values based on radioactivity decrease appreciably with enrichment. For example, values for a 90% enrichment are less than those for natural uranium by about two orders of magnitude. Thus, it becomes apparent that controlling the dust

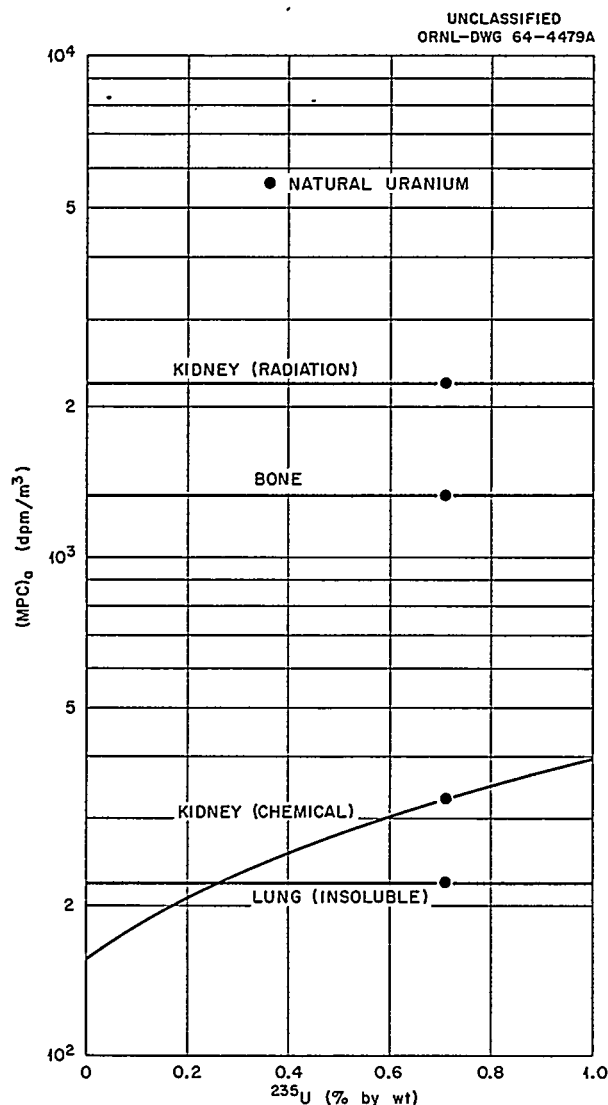


Fig. 24.2. MPC_a for Mixtures of ^{234}U , ^{235}U , and ^{238}U Appropriate for 40 hr/wk.

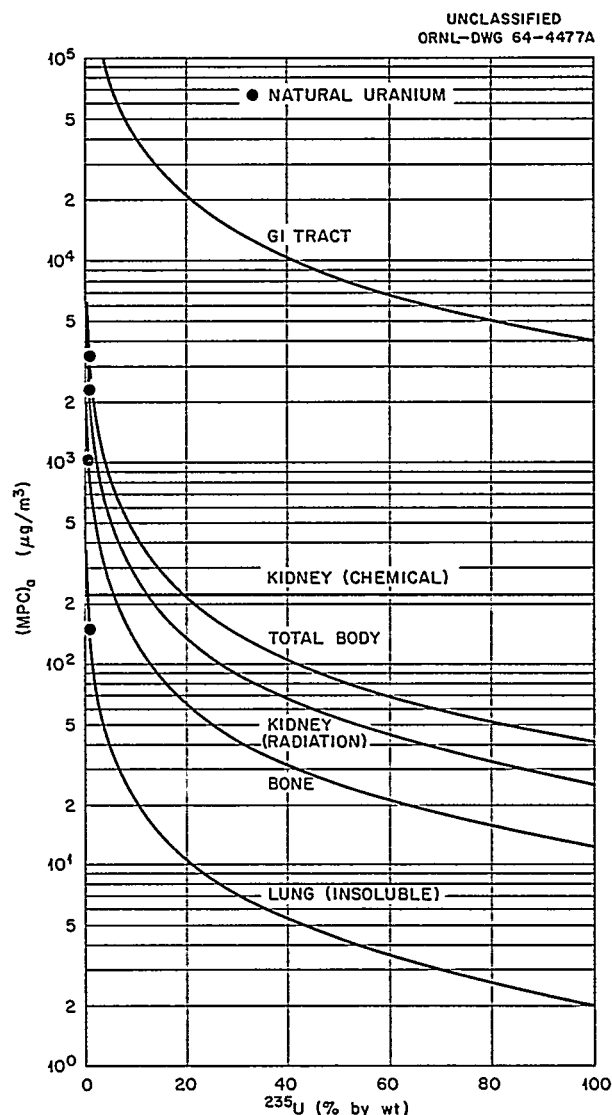


Fig. 24.3. MPC_a for Mixtures of ^{234}U , ^{235}U , and ^{238}U Appropriate for 40 hr/wk.

hazard is a much greater problem for enriched uranium than for natural or depleted mixtures even though the limiting $(MPC)_a$ values for enrichments greater than about 5% are all equal in units of $\text{dis min}^{-1} \text{m}^{-3}$.

SINGLE INTAKE GUIDES FOR URANIUM

Thus far, these comments have dealt with uncertainties of long standing concerning uranium values. Reference is made now to the recommendation released a short time ago in ICRP Publication 6 (ref. 3) regarding single-intake values of uranium. In this recommendation it is stated that because of the chemical toxicity of natural uranium, ^{238}U , ^{236}U , or ^{235}U , the inhalation of soluble uranium of any isotopic composition should not exceed 2.5 mg in 1 day, or the ingestion averaged over 2 days should not exceed 150 mg. Since these single-intake values are stated in units of mg/day, the question will arise as to whether or not they may be used every day, that is, for continuous exposure, without exceeding the permissible values based on radioactivity. Figure 24.4 shows the limiting $(MPC)_a$ in mg/day for continuous exposure based on radioactivity for these isotopes and for the same mixtures used in the previous examples. The levels for the individual isotopes are shown along the right-hand ordinate, and levels for the mixtures are shown by the curve on which natural uranium appears. A comparison of these MPC values with 2.5 mg/day reveals that many of them lie considerably below this value. Thus, 2.5 mg/day

would not be limiting for continuous exposure in every case. In like manner, it can be shown that one must be watchful that the radioactivity limit is not exceeded when applying the new single-intake value for ingestion.

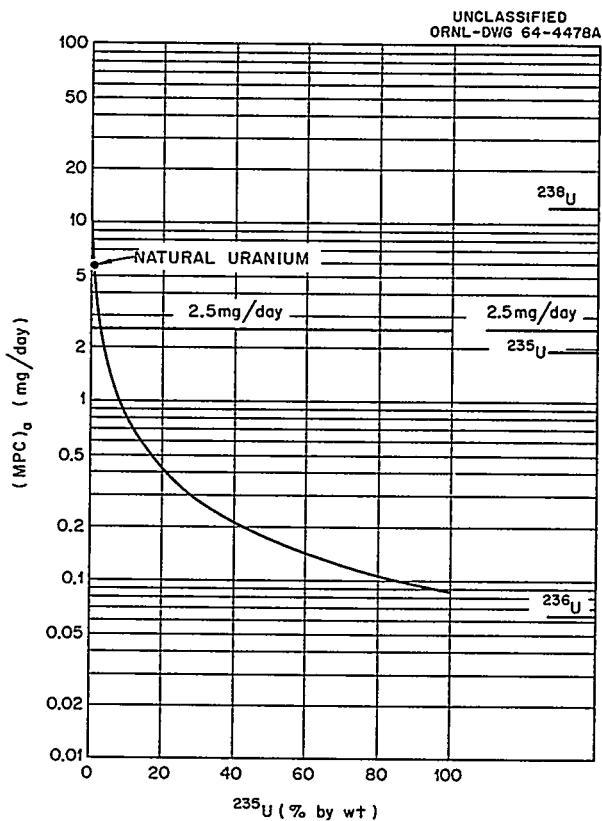


Fig. 24.4. $(MPC)_a$ Based on Radioactivity Compared with 2.5 mg/day.

25. On the Estimation of a Systemic Body Burden of Plutonium

W. S. Snyder

Employees exposed to plutonium generally excrete detectable amounts of the isotope in urine and feces. In fact, analysis of urine specimens is the more usual means of monitoring for possible exposure to ^{239}Pu . As the number of years of experience with processing of plutonium has increased, more and more cases have been found of employees who regularly show measurable amounts of ^{239}Pu in their urine. Often there is no known incident to which the exposure can be plausibly attributed, and the problem of estimating the employee's body burden is a very difficult one for the health physicist.

Computer codes have been designed^{1,2} which provide an estimate of the intake and/or retention on the basis of the urinalysis data of the employee. These codes assume that the ^{239}Pu reaching blood is retained and excreted from the body according to a metabolic model devised by Langham³ to fit the data on hospital patients given ^{239}Pu -citrate by intravenous injection. It is clear that all individuals do not follow the same metabolic model.⁴ Only one human case has come to autopsy,⁵ and, while the computer codes gave a rather accurate estimate in this case, the accuracy of these codes for estimation of body burden is not known in general.

During the past year the estimates of intake to blood as given by the code reported by Lawrence¹ have been used in an attempt to test the internal consistency of the model for metabolism of ^{239}Pu in the lung and also after reaching the blood. It is found that by postulating intakes via inhalation (which is considered to be the most likely mode of

exposure in this case⁶), and assuming a constant half-time for elimination from the lung, the pattern of intake to blood indicated by Lawrence's code can be realized. Also, by selection of appropriate constants to represent the fraction of an intake to the blood that deposits in liver and in bone, the distribution found at autopsy can be obtained. It is noteworthy that this distribution can be obtained only by changing some of the currently accepted constants of the metabolic model as given by ICRP Publication 2 (ref. 6). In particular, a half-time in lung of about 30 days must be used, and approximately equal fractions of the intake to blood must deposit in liver and in bone to obtain agreement with the autopsy data. These values are rather at variance with those currently given in ICRP Publication 2, although it must be recognized that it has been known that the half-time in lung might vary considerably depending on the size of the aerosol as well as on its physical and chemical form. It is concluded that, in view of the many unknown factors involved in the exposure (particle size, chemical form, time of exposure, etc.), the observed distribution in the body is not known to be grossly at variance with the metabolic model used as the basis for estimation of MPC values by ICRP and NCRP. For the same reason, it cannot be concluded that the model is validated by these data. The study does suggest that certain parameters involved in the model probably should have somewhat different values, namely, that deposits in liver and in bone should be approximately equal and that in some cases the half-time for elimination from the lung may be substantially less than 1 year. The detailed analysis which is the basis for these suggestions is being published in *Health Physics* as part of the proceedings of the Symposium on Inhaled Radioactive Particles and Gases, held at Hanford Laboratories on May 4-6, 1964.

A second attempt to check on the accuracy of currently available computer codes for estimation

¹J. N. P. Lawrence, *Health Phys.* 8(1), 61-66 (1962).

²W. S. Snyder, *Proceedings of 7th Annual Meeting on Bio-Assay and Analytical Chemistry, Held Oct. 12 and 13, 1961, at Argonne National Laboratory, ANL-6637*, p. 13.

³W. H. Langham et al., *Distribution and Excretion of Plutonium Administered Intravenously to Man*, LA-1151 (Sept. 20, 1950).

⁴W. S. Snyder, *Health Phys.* 8(6), 767-72 (1962).

⁵H. Foreman, W. Moss, and W. Langham, *Health Phys.* 2(4), 326-33 (1960).

⁶*Report of Committee II on Permissible Dose for Internal Radiation (1959)*, ICRP Publication 2, Pergamon, London, 1959.

of a systemic body burden of ^{239}Pu was undertaken, using data on dogs exposed intravenously and by inhalation to ^{239}Pu at Hanford Biology Laboratory. Bair *et al.*⁷ injected three dogs with plutonium nitrate (0.14 N HNO_3), and the dogs were sacrificed ~ 30 days postinjection. The urinary excretion data are plotted in Fig. 25.1 together with a curve representing an average of the data. It is apparent that there are very wide fluctuations from day to day and that the dogs differ rather markedly so far as day-to-day excretion is concerned. Nevertheless, the code mentioned above was used to estimate the intake. In Fig. 25.2 the daily intakes as estimated by the code are shown in the form of a bar histogram. It is clear that, despite the erratic character of the excretion data, the code did correctly find that the intake

⁷W. J. Bair *et al.*, *Health Phys.* 8(6), 639-49 (1962).

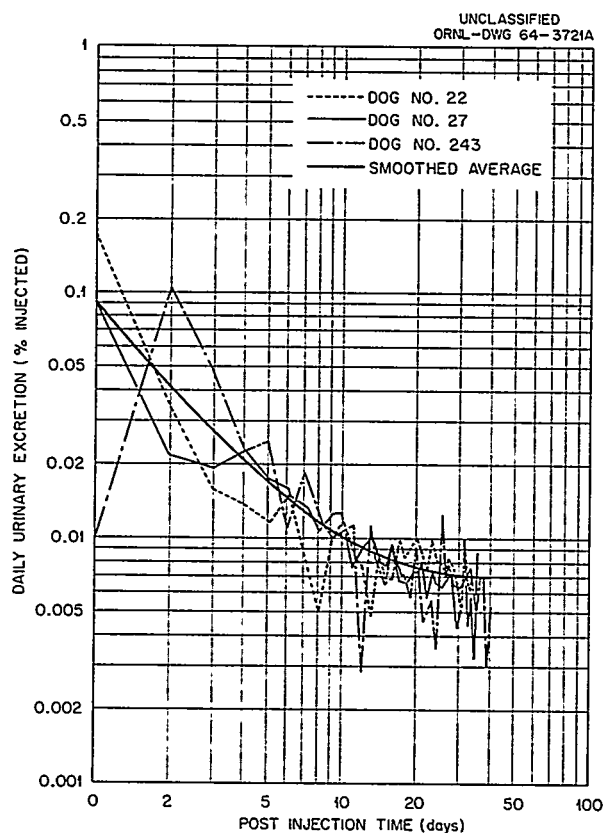


Fig. 25.1. Urinary Excretion Following Intravenous Injection of Plutonium Nitrate.

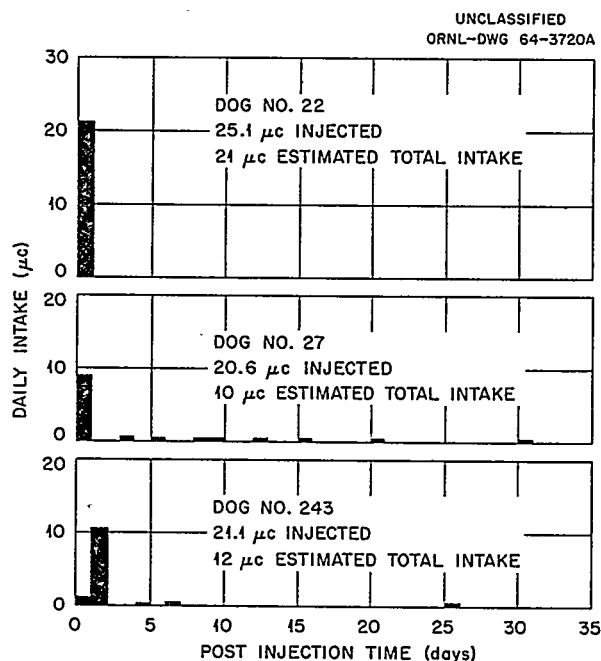


Fig. 25.2. Computer Estimates of Intake to Blood: Single Intravenous Injection Cases.

was confined largely to the first day or two. The small intakes to blood on succeeding days are the result of unusually high fluctuations of the excretion data. Thus, the code did give a qualitatively correct interpretation so far as time of intake is concerned. The estimated total intake is shown together with the injected amount, and it is evident that the estimates are within a factor of 2. In view of the erratic character of the data, this is considered to be encouraging.

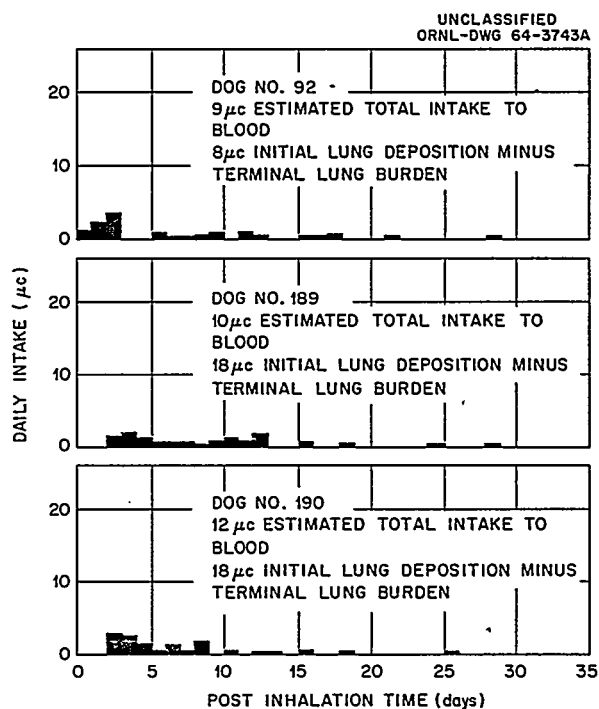
Bair *et al.*⁷ also exposed dogs to plutonium nitrate (0.14 N HNO_3) by inhalation. The urinary excretion data of those dogs exposed to the nitrate were analyzed by the code also, and the estimated intakes to blood are shown in Fig. 25.3. Although the time sequence is erratic, significant intakes to blood do seem to occur over a succession of days and tend to decrease with time. Thus, the qualitative aspects are as we might expect. However, the large number of days of no intake undoubtedly is an artifact produced by sporadic high excretions early in the period of observation. The estimated total intake to blood is shown also on Fig. 25.3, together with the difference of lung deposition and

the terminal lung burden as estimated by the experimenters. Again, the results generally agree within a factor of 2.

It seems clear that the present methods cannot be relied upon to give more than a very rough indication of the intake to blood. There are a number of possible improvements that suggest themselves. Some preliminary smoothing of data, perhaps by the computer, might reduce the error. However, it seems likely that marked improvements

will come only with a better understanding of the metabolic model and of the probable source of the wide individual differences and day-to-day fluctuations of the excretion data. It would seem that carefully controlled experiments might help in understanding these difficulties and that, even if the experiments did not enable us to overcome these difficulties, we might in this way obtain a firmer estimate of the uncertainty of our method of estimation.

Fig. 25.3. Computer Estimates of Intake to Blood: Inhalation Cases.



Part VI. Health Physics Technology

B. R. Fish

26. Aerosol Physics

B. R. Fish
G. W. Royster, Jr.
W. H. Wilkie, Jr.
F. G. Karioris¹
Georg Herrmann²

J. L. Thompson
R. L. Walker
Liliana Masironi³
C. F. Parrish⁴

Studies of particles and vapors and their dispersion in semi-isolated environments are the major areas emphasized by the aerosol physics program. These fundamental and engineering studies are directed primarily toward gaining an understanding of the mechanisms governing transport, deposition, redispersion, and measurement of radioactive surface contamination.

REDISPERSION OF SETTLED PARTICLES IN A ROOM

B. R. Fish
G. W. Royster, Jr.

R. L. Walker
J. L. Thompson

The accumulation of radioactive particles on surfaces in the working environment is of concern to the practicing health physicist for a variety of reasons. First, if the radiation is capable of penetrating the skin, the contaminating material may produce a radiation exposure hazard; in this case, monitoring to establish working time limits or to assess effectiveness of cleanup requires a rather straightforward application of radiation monitoring techniques. Radioactive surface contamination may also reflect recent conditions of airborne radioactivity, spills, and tracking. Fi-

nally, if radioactive particles are present on a surface at levels not constituting an external radiation hazard, they may sometime in the future be transferred to the surfaces of the skin or become redispersed in air and subsequently inhaled.

The estimation of the probability of future radiation exposure to be expected from a given level of surface contamination has led to a wide disparity in the contamination control practices of otherwise comparable nuclear energy facilities.⁵ It is quite possible that some of this disparity is warranted by differences in local conditions affecting redispersion. Thus the health physicist may be justified in exercising professional judgment in the setting of local control criteria. However, to provide a basis for professional judgment regarding resuspension of surface deposits, the various parameters that enter into the transport, deposition, and reentrainment of particles from surfaces should be considered. The release, transport, deposition, and redispersion of particles and their interactions with a sensitive target depend in a complex way upon the properties of the primary release mechanism, of the particles, of the surfaces, and of the local environment. It is not, in general, feasible to deduce the overall response of a room from fundamental principles; nevertheless, it is important to consider the basic parameters in any serious attempt to evaluate redispersion on a room-size scale.

¹Temporary summer employee, Marquette University, Milwaukee, Wisconsin.

²Eurochemic assignment, Mol, Belgium.

³NATO postdoctoral fellowship, citizen of Italy.

⁴Research participant, Indiana State College, Terra Haute.

⁵B. R. Fish, *Trip Report: Survey of Contamination Control Criteria, etc.*, May 12, 1960, ORNL-CF-60-5-118.

Studies in our aerosol physics program are directed toward the basic interactions of particles and surfaces,^{6,7} the actions of airstreams on deposited particles,^{8,9} and the techniques of measuring surface contamination.^{10,11} These and other laboratory studies are being used in an investigation of particle resuspension in a room.¹²

Two small demountable rooms were built for use in tracer studies of redispersion (see Fig. 26.1). Each room, 8 × 12 × 8 ft high, is constructed of painted wallboard and has an asphalt tile floor covering. Tracer dust is dispersed from a Wright

dust feed¹³ into a small mixing chamber outside the room and is introduced to the room through a short length of flexible hose. Four small oscillating fans are used to obtain a more homogeneous concentration in the room prior to settling. A typical dispersion operation, monitored simultaneously with air samplers in ten different locations in the room, resulted in a standard deviation of $\pm 1.9\%$ of the mean air concentration. In addition to particle concentration, the relative particle size distribution is monitored with a light-scattering particle size analyzer.¹⁴

After allowing the tracer dust to settle for two days, a man wearing coveralls, gloves, shoe covers, a cap, and a respirator enters the room to begin the redispersion test. New fans and air-sample heads are placed in the room, and contamination samples are obtained to determine the concentration of tracer dust deposited on the surface. The amount of tracer collected on the respirator filter is assumed to be related to the amount that would have been inhaled without a respirator.

⁶R. L. Walker et al., "Adhesion of Particles to Surfaces," this report.

⁷R. L. Walker and B. R. Fish, "Adhesion of Radioactive Glass Particles to Solid Surfaces," *Proceedings of the International Symposium on Surface Contamination*, June 8-12, 1964, Gatlinburg, Tennessee (in press).

⁸B. R. Fish et al., "Observation of Particle Re-entrainment from Surfaces," this report.

⁹L. A. Masironi and B. R. Fish, "Direct Observation of Particle Reentrainment from Surfaces," *Proceedings of the International Symposium on Surface Contamination*, June 8-12, 1964, Gatlinburg, Tennessee (in press).

¹⁰G. W. Royster, Jr., "Studies of Surface Contamination," *Health Phys. Div. Ann. Progr. Rept.* June 30, 1963, ORNL-3492, pp. 185-87.

¹¹G. W. Royster, Jr., and B. R. Fish, "Techniques for Assessing 'Removable' Surface Contamination," *Proceedings of the International Symposium on Surface Contamination*, June 8-12, 1964, Gatlinburg, Tennessee (in press).

¹²B. R. Fish et al., "Redispersion of Settled Particulates," *Proceedings of the International Symposium on Surface Contamination*, June 8-12, 1964, Gatlinburg, Tennessee (in press).

¹³B. M. Wright, *J. Sci. Instr.* 27, 12 (1950).

¹⁴Royco Instrument Co., model PC-202.

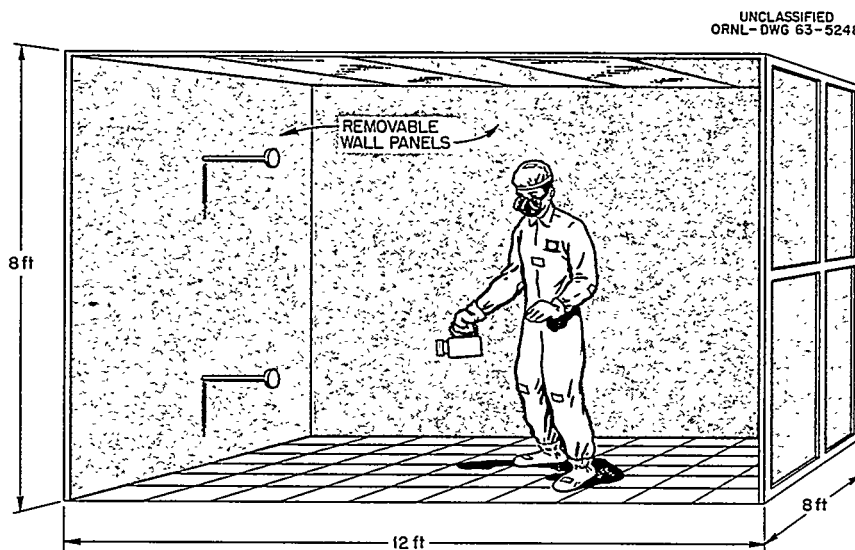


Fig. 26.1. Redispersion Room.

UNCLASSIFIED
ORNL-DWG 63-5248

Table 26.1. Redisperison of Settled Particles in a Room

Tracer	Run No.	Exposure Duration (min)	Particles Inhaled per hr per Particle per cm ²	Air Concentration (Fraction of Concentration Before Initial Settling)	Resuspension Factor [(Air Concentration)/(Surface Concentration)] (cm ⁻¹)
					$\times 10^{-7}$
ZnS ^a	Z-1	10	10	0.00096	19
	Z-2	20	3.2	0.00056	3.9
	Z-3	40	0.78	0.00048	0.94
CuO ^b	C-1	90	3.5	0.0098	71

^aMass median diameter, 3.1 μ ; σ_g , 1.9; ρ , 4.1 g/cm³.

^bMass median diameter, 2.0 μ ; σ_g , 2.3; ρ , 6.45 g/cm³.

Three redisperison tests were made with zinc sulfide¹⁵ (see Table 26.1). Particle concentrations were determined by direct particle counts with ultraviolet light and a microscope. The first test, simulating rather vigorous work activity including sweeping, was carried on for 10 min. The room was thoroughly cleaned, and a second dispersion was made. The second redisperison run employed only vigorous walking in order to simulate moderate work activity for a period of 20 min. The third run with ZnS lasted 40 min and was confined to the relatively light work activity of collecting contamination samples. There was no room exhaust, and no fans were used during the redisperison periods of the ZnS tests.

The current series of redisperison tests is being made with particles of cupric oxide. Nonradioactive CuO is detected by thermal neutron activation analysis of samples collected in the test. In the CuO study, there was no room exhaust; however, four clean fans were used to promote air circulation in the room. The fans did not blow directly on any surface but were directed upward at about 30° above a horizontal plane. During the 90-min redisperison run, there were two periods of 10 min each in which the floor was lightly swept with a broom; otherwise, the only human movement in the room was associated with sample

collection. Ten air samples collected concurrently during the 90-min redisperison period showed a standard deviation of $\pm 3.4\%$. Two battery-powered lapel air samplers, worn by the man in the room, differed only by 2.8% from their mean and indicated approximately 10% lower air concentration than the average of the ten fixed samplers.

Transforming the maximum permissible air concentration of unidentified radionuclides¹⁶ (4×10^{-13} $\mu\text{C/cc}$) to a 40-hr work week, the permissible intake rate is found to be 3.1 dis min⁻¹ hr⁻¹. On this basis, the data in Table 26.1 indicate that surface contamination levels greater than 30 to 400 dis/min per 100 cm² may result in air concentrations exceeding the permissible levels for occupational exposure.

MEASUREMENT OF AGGLOMERATE CONTAMINANTS ON SURFACES

G. W. Royster, Jr.

R. L. Walker

B. R. Fish

J. L. Thompson

On the basis of research reported in the literature, it is possible to predict grossly the ease of redisperison of single solid particles as a function

¹⁵U.S. Radium Corporation (New Jersey Zinc Co., NJZ-2210), zinc sulfide powder, Helecon fluorescent pigment No. 2210.

¹⁶Report of Committee II on Permissible Dose for Internal Radiation, ICRP publication 2, Pergamon, New York, 1959.

Table 26.2. Redispersion of Thorium Dioxide from Stainless Steel

Sample	Particle Size		
	Agglomerates (Up to 10 μ) (Unit Particle Size, 0.01–0.1 μ)	1.5- μ Single Particles	5- μ Single Particles
Smear ^a	49%	96%	86%
Smair ^a	10%	58%	75%
Sticky paper ^a	68%	96%	100%
Concentration, dis/min per 100 cm ²	299 ($\pm 7\%$)	2050 ($\pm 6\%$)	1370 ($\pm 2\%$)

^aSee text for explanation of sample types.

of particle size. However, the redispersibility of agglomerates is not readily inferred from published data. In order to explore the adhesion of agglomerates to surfaces, thorium dioxide particles were allowed to settle on a stainless steel test surface, and redispersion was sampled by three methods. The settling chamber and the sampling techniques are described by Royster and Fish.¹¹

Agglomerates were produced by electrically exploding wires of thorium metal¹⁷ and by allowing the resulting aerosol to coagulate. Thorium dioxide particles are produced primarily by oxidation and condensation of vaporized metal and secondarily by oxidation of molten metal droplets. The size distribution of primary particles is approximately log-normal, with particle diameters lying predominantly in the range 0.01 to 0.1 μ . Initial concentrations in the settling chamber exceed 10^8 particles per cm³, and coagulation is very rapid. Examination of the settled agglomerates shows that essentially all of the deposited mass is contained in rather tenuous-appearing aggregates having projected envelope areas with diameters in the range 1 to 10 μ . Table 26.2 summarizes the results of sampling ThO₂ agglomerates compared with single particles of the same material and in approximately the same size range as the aggregates.

The smear sample employs an abrasive mechanism in which a piece of filter paper is mechanically wiped over a fixed area of the surface while maintaining a constant contact pressure. Smair samples are obtained by collecting, on a filter paper, particles made airborne by the action of air jets impinging on the contaminated surface. The sticky-paper samples are obtained by pressing an adhesive-coated paper against the test surface. The sample consists of the particles that adhere to the paper when it is peeled off the surface.

Although there are obvious differences in redispersion of agglomerates compared with single particles, our results show that a significant fraction of deposited agglomerates can be redistributed by mechanical abrasion, by aerodynamic forces, and by adhesion to a contacting surface.

OBSERVATION OF PARTICLE REENTRAINMENT FROM SURFACES

B. R. Fish
Liliana Masironi

W. H. Wilkie, Jr.
J. L. Thompson

Reentrainment of particles from surfaces in a moving airstream is of interest from a number of different points of view. In addition to fundamental interest in the interactions of particles and surfaces, there are several applied problems in which reentrainment is of basic importance,

¹⁷F. G. Karioris, B. R. Fish, and G. W. Royster, Jr., *Proc. Conf. Exploding Wire Phenomenon* 2, 299–311 (1962).

including redispersion of particulate contamination,¹² blow-off in sampling devices,¹⁸ penetration of filters,^{19,20} and the dynamics of windblown sand and dust.²¹ The question of what happens physically just prior to, during, and immediately after a particle is reentrained in an airstream is one of considerable theoretical and practical interest.

A small wind tunnel was built for direct observation of particles during deposition, reentrainment, and rebound (Fig. 26.2). Compressed air is used to supply the wind tunnel. The first section has an inside diameter of 1 in. and contains two wire-mesh flow straighteners about 3 in. apart. Then, through an 8:1 convergent cone section, the diameter is reduced to match the diagonal of a $\frac{1}{4}$ -in. square. A coupling section provides a transition to the final $\frac{1}{4}$ -in. square cross section. The working section is formed by three microscope slides and an anodized brass surface. Three viewing ports permit visual and photographic observation.

A low-speed light chopper is used to resolve the motion of particles along a surface. A shutter disk mounted on a variable-speed motor chops the light from a xenon-mercury vapor lamp, yielding from 3 to 12.5 flashes per second. A photodiode and an oscilloscope monitor the flash rate. For the higher speed movement of particles after leaving the surface, a spinning disk with 22 mirror areas is being built and will be capable of providing up to 27,500 reflected flashes per second.

Soda-lime glass beads used in this study range in size from 10 to $38.3\ \mu$ in diameter. They are treated to narrow their size range and to reduce the number of beads containing air bubbles by microsieving followed by repeated settling in water. Size distribution data are obtained with a Zeiss particle size analyzer, which records the projected area diameter. Between $20\ \mu$ and the maximum size, $38.3\ \mu$, the diameters of the glass spheres are normally distributed about the count median, $28.9\ \mu$, with a standard deviation of $\pm 13\%$.

¹⁸D. W. Jordan, *J. Appl. Phys. Suppl.* 5, S194 (1954).

¹⁹T. Gillespie, *J. Colloid Sci.* 10, 266-98 (1955).

²⁰R. I. Larsen, *Am. Ind. Hyg. Assoc. J.* 19, 265 (1958).

²¹R. A. Bagnold, *Intern. J. Air Pollution* 2, 357 (1960).

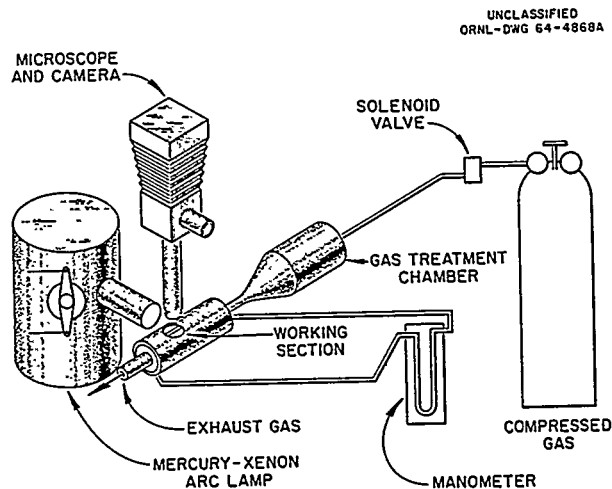


Fig. 26.2. Schematic Drawing of Wind Tunnel.

Visual observation of particle behavior on a glass surface in an airstream of 5300 cm/sec average velocity ($Re = 24,400$) shows three basically different types of response (Table 26.3). First, about half of the particles did not move during the test. Second, during a 2.5-sec exposure to the airstream, about 13% of the particles moved along the surface in straight lines parallel to the direction of air flow. (For simplicity, Table 26.3 refers to these particles as having "rolled"; however, as yet this has not been definitely established by observation, although consideration of the very high air velocity gradient near the surface strongly suggests that the spherical particles should, in fact, roll.²²) Finally, about one-third of the particles left the surface without first having "rolled."

The glass beads that "roll" present a very interesting pattern of movement. First, it is a characteristic of these particles that sometimes they will stop moving for a short time and then continue on in the same direction. The average distance moved is about four particle diameters per start, and the beads will start an average of 1.75 times per "rolling" particle. Some will stop as many as five or more times in their trajectory

²²N. A. Fuks, *The Mechanics of Aerosols* (1955) (Russian translation by MSP. E. Lachowicz), CWL special publication 4-12, Technical Information Division, U.S. Army Chemical Center, Maryland.

Table 26.3. Observed Movement of Soda-Lime Glass Spheres on the Glass Wall of a Wind Tunnel

Count median diameter of spheres: 28.9 μ with standard deviation of $\pm 13\%$
 Wind tunnel cross section: 0.64 cm²
 Average air velocity: 53 m/sec, Reynolds number: 24,400
 Spheres exposed to air for 2.5 sec
 Relative humidity <6%

Left the Surface		Did Not Leave Surface	
Did Not "Roll"	"Rolled"	"Rolled"	Did Not Move
32%	6.5%	6.5%	55%
38.5%		61.5%	

along the surface. A second flow of air with the same average velocity over the same field showed a few particles that "rolled" and left the surface, and a few that "rolled" and stopped, but none that left the surface without "rolling." Thus, there appears to be a time-dependent factor associated with the "rolling" phenomena. This observation confirms the findings of Corn²³ and of Becker²⁴ that increased time of exposure of particles to a high-velocity airstream results in increased particle removal. Corn²³ suggests that his findings indicate a fluctuation in air velocity in the vicinity of the particles; however, while our observations do not rule out the existence of local variations in air velocity, they do cast some doubt that this is the complete explanation of the time dependency. The gain or loss of discrete amounts of electrostatic charge on individual beads, along with a patchlike distribution of charge on the surface²⁵ and, perhaps, also fluctuations in air velocity, could account for the observed abrupt changes in particle motion on the surface.

Another rather striking observation is that the average velocity along the surface is only 180

²³M. Corn and F. Stein, "Reentrainment of Particles from a Plane Surface," presented at Annual Meeting of the American Industrial Hygiene Association, April 29, 1964, Philadelphia.

²⁴F. Becker, *Staub* 23, 60 (1963).

²⁵T. B. Owe Berg and N. Brunetz, *Arch. Environ. Health* 5, 22 (1962).

μ /sec. In contrast, based on classical boundary layer theory,²⁶ the air velocity at the top of a 28.9- μ -diam sphere is calculated to be greater than 10^5 times the observed particle velocity (1930 cm/sec). An analogous picture might be obtained by photographing a billiard ball being rolled along an adhesive tape by the action of an air jet applied to the top of the ball.

ADHESION OF PARTICLES TO SURFACES

R. L. Walker

B. R. Fish

J. L. Thompson

C. F. Parrish

Several factors have been reported to affect the adhesion of particles to plane surfaces. The major components of adhesion appear to be electrostatic forces, capillary forces in the presence of moisture layers, and the London van der Waals forces. In our studies of resuspension of settled particulates,¹² nonradioactive tracers are used to simulate radioactive particles. Thus it is important to examine the validity of making a direct comparison of the two types of particles.

There is justification for anticipating some difference in the adhesion of radioactive and of nonradioactive solid particles to solid surfaces. The radiation of the particle may affect the properties of the surface layers of the adhering particle and of the adherent surface. First, there may be sufficient energy deposited locally to desorb oxygen or other sorbed contaminants in the vicinity of the particle. This could greatly change the nature of the surface molecules in contact. In addition, the energy absorbed in the capillary layer of moisture between the particle and the surface may increase the rate of loss of moisture from the layer, potentially affecting a major factor of adhesion. Finally, radiation may produce a change in the electrostatic charge of the particle and of the adherent surface.

A method of applying known forces to remove particles by subjecting a surface to sonic vibrations was reported by Deryagin and Zimon.²⁷ A dynamic speaker is driven by a sine-wave input which causes it and the attached test surface to

²⁶M. Schlichting, *Boundary Layer Theory*, McGraw-Hill, New York, 1960.

²⁷B. V. Deryagin and A. D. Zimon, *Kolloidn. Zh.* 23, 454 (1961).

vibrate at a known frequency. If the displacement of the test specimen in a direction normal to its surface is given by

$$Y = A \sin 2\pi ft,$$

then the maximum acceleration a is

$$a = 4\pi^2 f^2 A.$$

Thus, the normal force, tending to remove a particle from the surface, is

$$F = 4\pi^2 f^2 Am.$$

The normal force, F , is in dynes when the mass of the particle, m , is in grams; the frequency of the speaker oscillation, f , is in cycles per second; and the amplitude of oscillation, A , is in cm ($A = \frac{1}{2}$ total displacement).

The apparatus is illustrated schematically in Fig. 26.3. A glove box is used to house the sonic shake table in order to control the humidity and temperature and also to keep the radioactive particles confined. Test surfaces are mounted on a magnesium block which is glued to the speaker cone. One microscope views a line scribed on the vibrating block to measure the amplitude. The force on the test surface is increased in steps by increasing the amplitude of the vibration while holding the frequency constant. Particles are photographed on the test surface through a second microscope. This arrangement allows the test surface to be observed without being disturbed during a series of observa-

tions. Also, in this arrangement, the same microscopic field on the test surface can be observed and photographed each time. All operations can be carried out without opening the box.

The particles used in the pilot runs were soda-lime glass beads (2.5 g/cm^3 density) with a count median diameter of 28.9μ . A sample of the beads was activated by thermal neutron irradiation to produce radioactive particles having a specific activity of approximately 0.4 curie/g. The surfaces used were 1×2 in. quartz slides that had been fire polished and cleaned. The average roughness height of the slides was less than 0.8% of the diameter of the particles.

A polonium source was used to eliminate the electrostatic charge on the test surfaces; then the particles were dispersed on them through a series of sieves. The surfaces were aged for 12 hr or more, after which there was no electrostatic charge detected on the test surface receiving the nonradioactive particles. The test surface with the radioactive particles, after aging for 2.5 days in a hot cell, had a positive electrostatic charge of approximately 7×10^{-10} coulomb/cm². For these trials the test chamber was held at 22°C and approximately 50% relative humidity.

In no case were any of the particles shaken off. The maximum g force which the present system is capable of producing is approximately 90 times gravity. This is equivalent to 2.8×10^{-3} dyne for $28.9\text{-}\mu$ -diam particles of density 2.5.

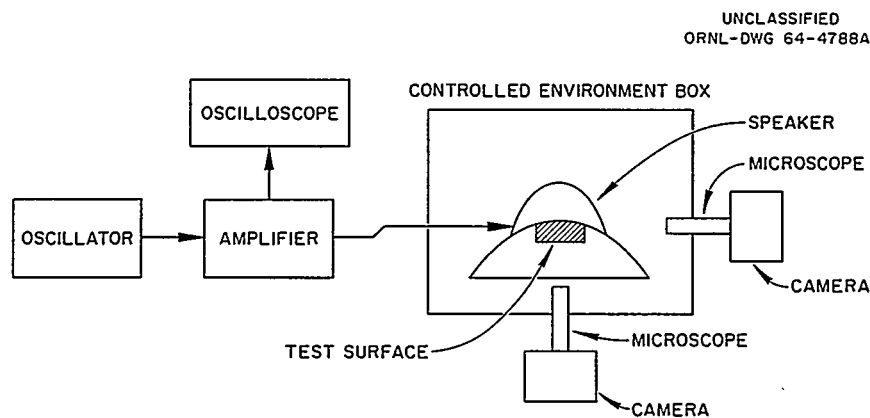


Fig. 26.3. Diagram of Sonic Vibration Force Apparatus.

PRODUCTION OF GOLD AND GOLD-PLATINUM AEROSOLS BY EXPLODING WIRES

F. G. Karioris B. R. Fish

Production of gold aerosols from the exploding-wire generator^{28,29} has been studied to elucidate the mechanisms of aerosol production by this method and in anticipation of the production of radioactive ¹⁹⁸Au aerosols. Gold-198 has several properties³⁰ that are desirable for surface contamination studies.

Electrical explosion of gold wire in the generator immediately produces a well-dispersed smoke. The particulate matter gives a matte black deposit when collected on membrane filters. Four different lengths of 0.010-in.-diam gold wires were exploded by using 2 to 14 kv on a 20- μ f capacitor bank, with the results shown in Fig. 26.4. For voltages above 4 kv, a significant fraction of the exploded wire can be collected from the solid disperse phase. Seven trials at 8 kv with the 2-cm length established that, at this point, the yield averages 87% and can be reproduced with a standard deviation of about 6%. Results for the longest wire (4 cm) were somewhat erratic.

The dependence of gold-aerosol yield on length of wire used and on initial capacitor voltage is shown in Fig. 26.5. Above 4 kv the yield is high and tends toward a rough maximum at a length of about 2 cm. This observation may be in accord with the optimization of physical and electrical parameters for maximum transfer of energy to the wire, as discussed by David.³¹ The behavior of exploding gold wires has been studied³² primarily to determine the dependence of resistance as a function of energy input at high current densities

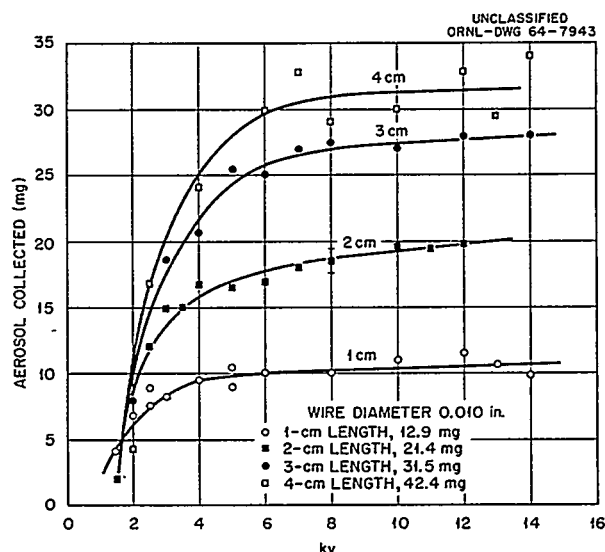


Fig. 26.4. Yield of Gold Aerosol from Wire Explosions with 20- μ f Capacitor.

and temperatures, rather than from the point of view of aerosol formation. In the theoretical treatment, consideration must be given to the electrical resistivity of the metal used, specific thermal capacity, temperature dependence of resistivity and heat capacity, melting point, boiling point, and heats of fusion and vaporization. Differences might be expected in the behavior of different metals. In our work the gold-aerosol yield curves are similar to those observed^{17,33} for copper, aluminum, and uranium. However, the behavior of tungsten wire seems to be considerably different from that of gold, as shown in Fig. 26.6. The yield data from 18 different metals reported previously³⁴ have been plotted vs the melting point and boiling point of each metal. Although

²⁸F. G. Karioris et al., *Health Phys. Div. Ann. Progr. Rept. July 31, 1960*, ORNL-2994, pp. 266-69.

²⁹F. G. Karioris and B. R. Fish, *J. Colloid Sci.* 17, 155-61 (1962).

³⁰L. Slack and K. Way, *Radiation from Radioactive Atoms*, p. 35, USAEC, Washington, D.C., U.S. Government Printing Office, Washington, D.C.

³¹E. David, *Proc. Conf. Exploding Wire Phenomenon* 1, 271-80 (1959).

³²T. J. Tucker, *J. Appl. Phys.* 32, 1894-1900 (1961).

³³F. G. Karioris, B. R. Fish, and A. J. Moll, *Health Phys. Div. Ann. Progr. Rept. June 30, 1963*, ORNL-3492, pp. 191-93.

³⁴F. G. Karioris and A. J. Moll, *Health Phys. Div. Ann. Progr. Rept. July 31, 1962*, ORNL-3347, pp. 145-47.

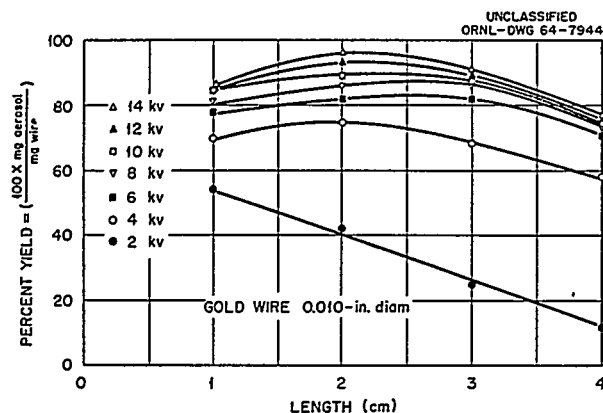


Fig. 26.5. Yield of Gold Aerosol from Wire Explosions as a Function of Wire Length.

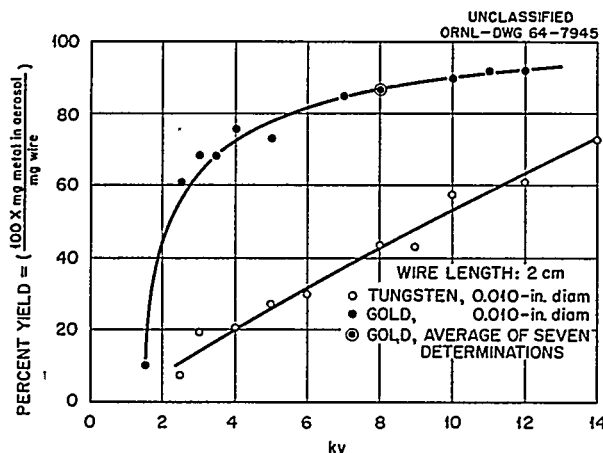


Fig. 26.6. Comparison of Gold and Tungsten Aerosol Yields from Wire Explosions.

there seems to be a trend for the percent aerosol yield to decrease with increasing melting point or boiling point, the correlation is poor.

There is some evidence that a wire is not always completely vaporized by an electrical explosion and that liquid droplets exist within the metal

vapor.³⁵ Tentatively, it is our hypothesis that the major portion of the aerosol particles represents condensation from the vapor phase, most of the liquid droplets having sufficient kinetic energy to reach and be deposited on the walls of the explosion chamber. The aerosol yield then represents rather closely the fraction of the wire vaporized. According to this hypothesis, the vapors of two different metals exploded simultaneously should mix homogeneously and condense to form a single alloy or intermetallic compound recoverable from the aerosol if the metals are properly chosen. A binary system is indicated which forms continuous solid solutions whose compositions can be determined from x-ray diffraction measurements of the lattice constant and from Vegard's law.³⁶

Gold and platinum wires were twisted together and exploded simultaneously in the aerosol generator. Several different ratios of wire diameters were used. The particulate matter in the aerosol from each explosion was examined by x-ray diffraction analysis to determine whether it consisted of a homogeneous Au-Pt alloy of definite composition. When the amount of platinum used was small compared with gold, the aerosol was essentially a homogeneous gold-rich alloy. Unfortunately, the Au-Pt constitutional diagram³⁷ shows an immiscibility gap from about 3.5 to 75% Au. Below about 1150°C, alloys within this composition range break down into two components. This two-component system was observed in the aerosol from exploded wires, so that it is not possible to deduce definitely that the metallic vapors mixed homogeneously.

In another test, the intermetallic compound Cu_5U was detected in the aerosol resulting from the simultaneous explosion of uranium and copper wires.

³⁵W. G. Chace, R. L. Morgan, and K. R. Saari, *Proc. Conf. Exploding Wire Phenomenon* 1, 59-72 (1959).

³⁶C. S. Barrett, *Structure of Metals*, p. 202, McGraw-Hill, New York, 1963.

³⁷R. F. Vines, *The Platinum Metals and Their Alloys*, p. 66, The International Nickel Company, Inc., New York, 1941.

INTERNATIONAL SYMPOSIUM ON SURFACE CONTAMINATION

B. R. Fish (Chairman)
G. W. Royster, Jr. (Treasurer)
D. D. Cowen (Local Arrangements Chairman)
Blanche Reed (Ladies Activities)

The first International Symposium on Surface Contamination was held in Gatlinburg, Tennessee, June 8-12, 1964. The meeting was sponsored jointly by the Oak Ridge National Laboratory, the American Association for Contamination Control, and the Health Physics Society.

There were 54 papers presented in 12 sessions. Four sessions were devoted to fundamental re-

search and development in the fields of aerosol physics, surfaces, adhesion-redispersion, and transport-deposition. Other administrative and technical problems were discussed in sessions on radioactive surface contamination control criteria, measurement techniques, environmental control of surface contamination, radioactive contamination control applications, dissemination of airborne microorganisms, biological and chemical surface contamination, insurance and economics, and decontamination.

The meeting was attended by 222 persons; 37 were from outside the United States. There were 14 attendees from France; 9 from the United Kingdom; 3 each from Canada, Germany, and Japan; 2 from Belgium; and 1 each from Australia, Austria, and Venezuela.

27. Applied Internal Dosimetry

B. R. Fish

ORNL IN VIVO GAMMA-RAY SPECTROMETRY FACILITY

P. E. Brown	L. B. Farabee
G. R. Patterson, Jr.	Rose J. McBath
W. H. Wilkie, Jr.	
L. S. Barden ¹	D. L. Mason ³
J. H. Dobkins ²	J. K. Eddy ⁴

The ORNL in vivo Gamma-Ray Spectrometer (IVGS) Facility continues to be used primarily as a monitoring device to aid in the detection and measurement of internal exposures. Additional improvements in instrumentation, schedul-

ing, and the operating program have made it possible to increase the rate of routine counting for monitoring purposes beyond the increase mentioned in the previous report.⁵ Emphasis is placed on the routine counting of persons suspected of having experienced an exposure or of having a potential for exposure and on obtaining base-line counts for persons prior to their entering new work involving potential internal exposure. The further increase in rate of counting people has made it possible to expand the base-line counting and obtain counts on essentially all persons with even a remote chance for exposure. During the past year, 1370 persons were counted for a total of 1568 human counts; 1159 of the counts or approximately 74% showed a normal human spectrum. By way of comparison, the totals for the period July 31, 1961, to July 31, 1962, were 142 human

¹ORINS trainee, Hendrix College, Conway, Ark.

²Temporary summer employee, North Carolina State College, Raleigh.

³Temporary summer employee, Austin Peay State College, Clarksville, Tenn.

⁴Temporary summer employee, West Virginia University, Morgantown.

⁵B. R. Fish *et al.*, *Health Phys. Div. Ann. Progr. Rept. June 30, 1963*, ORNL-3492, p. 194.

counts on 102 persons; the total for the period ending May 31, 1963, was 492 human counts. Table 27.1 summarizes the data for those cases in which measurable amounts of internal radioactive contamination were observed.

The current rate of counting is about 130 persons per month, excluding instrumentation downtime. Theoretically, one could count about 170 persons per month. This represents practically the maxi-

mum rate attainable with the present equipment operating 40 hr per week. We do not anticipate operating more than one shift per day, except when it is necessary to count persons regularly working only one of the night shifts. The increase of fiscal-year 1964 counting to more than three times the 1963 counts represents the realization of a number of improvements in equipment and operating program. Listed roughly in order of the favorable impact they have had, these improvements include installation of a second 512-channel analyzer, a paper-tape-to-typewriter data converter, the rolling scan bed, a new system for scheduling persons to be counted, and the computer program for data analysis. The rolling scan bed and the computer program were mentioned in some detail in the last report in this series;⁵ the other improvements were implemented during the present period.

Table 27.1. Measurable Radioactivity Found in Routine Whole-Body Monitoring Program, June 1, 1963-June 30, 1964

Isotope	Individuals Counted	Maximum Amount (μ c)	MPBB (μ c)
^{24}Na	1	^a	
^{51}Cr	10	0.042	800
^{58}Co	29	0.038	30
^{59}Fe	6	0.015	20
^{60}Co	34	0.220	10
^{64}Co	1	<0.005	10
^{65}Zn	32	0.016	60
^{75}Se	12	0.250	90
^{90}Sr - ^{90}Y	17	4.500	2
^{95}Zr - ^{95}Nb	67	0.047	20
^{106}Ru - ^{106}Rh	47	0.047	3
^{125}Sb	43	0.018	40
^{131}I	29	0.073	0.7
^{137}Cs	160	0.310	30
^{144}Ce - ^{144}Pr	17	≤ 0.007	5
^{155}Eu	3	Trace	70
^{198}Au	1	^a	
^{226}Ra	3	<0.005	0.1
U (enriched)	1	Trace	0.06

^aSkin contamination.

IN VIVO DETECTION AND MEASUREMENT OF ^{90}Sr - ^{90}Y INTERNAL CONTAMINATION

During this report period, the ORNL IVGS Facility was used to estimate the ^{90}Sr - ^{90}Y body burden of several ORNL employees who had been involved in airborne particulate contamination incidents. In two of the incidents the contamination was $^{90}\text{SrTiO}_3$; in the other incident the contaminant was $^{90}\text{SrCO}_3$. The practical limit of detection of ^{90}Sr for the ORNL in vivo counter is approximately one-tenth of the maximum permissible body burden (MPBB) or $\sim 0.20 \mu\text{c}$. In the observed cases the bremsstrahlung continuum was readily discernible at levels estimated to be around 5% of the MPBB. Of course, at these relatively low levels, estimation of ^{90}Sr internal contamination by in vivo counting is subject to large uncertainties, particularly when other contaminants may be present. In the first incident involving $^{90}\text{SrTiO}_3$, three persons were found to have obvious indications of bremsstrahlung in their spectra. Initial estimates of their whole-body strontium burden, based on the application of a strontium-in-skeleton calibration to whole-body scan counts, suggested 0.8, 0.9, and $6.2 \mu\text{c}$ for cases A, B, and C, respectively, as of three days postexposure. Figure 27.1 is a profile scan showing the relative counting rate as the body of employee C passed under the crystal. Note that even at this late date the largest fraction of the

deposit is in the lower abdomen. In view of this fact, the estimates were revised by using a combined GI tract-skeleton calibration. Revised estimates based on this calibration were 0.46, 0.55, and 4.5 μC for the three men. Figure 27.2 shows the net spectrum from 0 to 2.04 Mev for the initial scan count of case C. After much of

the abdominal deposit was eliminated, the chest counts taken with a lead-collimated 8×4 in. crystal were felt to provide a more accurate estimate of the strontium burden. Figure 27.3 shows the in vivo estimates of chest burden for case C up through the most recent count, 169 days post-exposure.

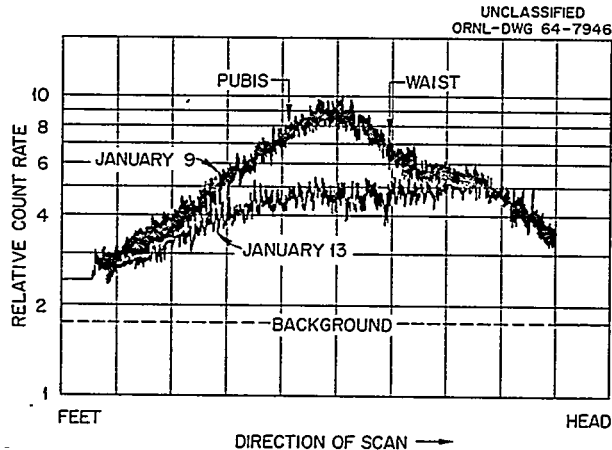


Fig. 27.1. Profile Scans of Two Whole Body Counts ($^{90}\text{SrTiO}_3$ exposure case C).

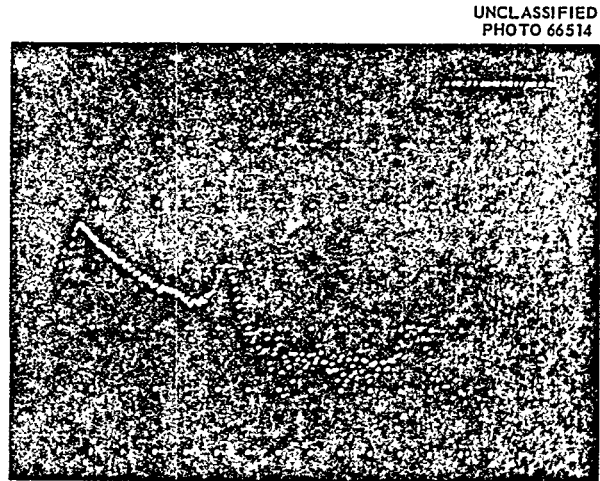


Fig. 27.2. Net Spectrum Whole Body Scan ^{90}Sr Inhalation Exposure.

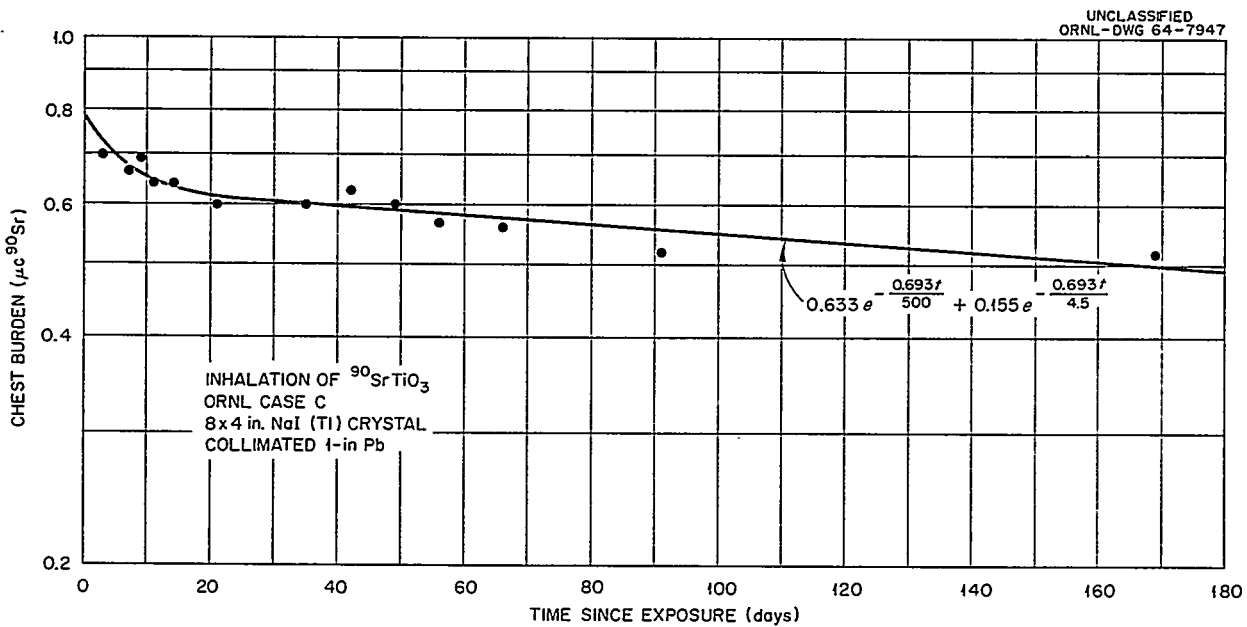


Fig. 27.3. Strontium-90-Yttrium-90 Chest Burden.

In both of the other incidents involving exposures to strontium compounds, the whole-body scan counts detected measurable amounts of ^{90}Sr , 0.50 μc in the $^{90}\text{SrTiO}_3$ incident and 0.60 μc in the $^{90}\text{SrCO}_3$ incident. However, in both cases the chest counts with the collimated crystal showed only small indications of bremsstrahlung, whereas profile scans show that the bulk of the deposit is in the abdominal region. These cases have adequately demonstrated that in vivo counting can give a rapid and positive indication of a serious intake of ^{90}Sr .

COMPUTER PROGRAM FOR IN VIVO COUNTING DATA

G. R. Patterson, Jr.
Barbara A. Flores⁶

M. T. Harkrider⁶
G. S. McNeilly

Program WBC,⁷ designed to analyze routine whole-body count data on the CDC 1604 computer, has been in limited use since March 1963. Some few changes have been made to correct minor flaws that became apparent or to make the program more flexible; for instance, it is no longer necessary to separate whole-body scan counts and chest counts and process them as separate groups of data. By providing rapid analysis of routine body count data with accurate estimates of total-body potassium and ^{137}Cs , the computer can handle approximately 75% of the data analysis load.

Computer plotting of raw and smoothed spectra has been discontinued as uneconomical and not significantly better than a Polaroid photograph of the oscilloscope spectrum display. The practice of circulating a written weekly report of in vivo counting activities and results was begun in March 1963. In the fall of 1963 it was decided that, with a slight change in format, the IBM cards that identify each punched paper tape for the computer program could be utilized to produce a machine tabulated weekly report of in vivo counts. M. T. Harkrider wrote the necessary computer program, and report No. 1 for the first week of January 1964 was the first in vivo counting weekly report that was machine tabulated.

⁶Mathematics Division.

⁷B. R. Fish et al., *Health Phys. Div. Ann. Progr. Rept.* June 30, 1963, ORNL-3492, pp. 202-4.

DEVELOPMENTS IN THE ORNL IN VIVO GAMMA-RAY SPECTROMETRY FACILITY

W. H. Wilkie, Jr.

During July and August 1963, a second 512-channel analyzer was installed at the IVGS Facility. In addition, new preamplifier cables were run from the iron room to the control room, and the divider network was rewired. Both analyzers and the associated electronic equipment were mounted in an integrated control complex of matching cabinets. A tape-to-typewriter data converter was installed, permitting direct coupling of the paper-tape reader to the typewriter. A master switching panel was installed which permits quick switching of any of the data readout equipment to either one of the two analyzers. These equipment changes have made it possible to use the facility more efficiently by reducing maintenance downtime and by providing off-line equipment for data processing.

The Saran webbing of the rolling scan bed was replaced by a stainless steel top and a foam mattress.

Various methods for calibrating whole-body counters are being studied. Differences between the results of calibrations using several phantom-source configurations and the actual situations they approximate are being examined. Preliminary data indicate that a whole-body scan calibration using a simple point source of ^{137}Cs positioned in the central portion of the abdomen of a bottle mannikin is comparable with a calibration in which a ^{137}Cs solution is uniformly distributed in the same type of phantom. Positioning of the point source in the single-source method is critical, and for this purpose a bottle mannikin was modified to allow reproducible positioning of the source. Neither method of calibration is expected to represent accurately all in vivo situations; in practice, distributions of source activity, and hence the overall detection efficiencies, vary considerably from case to case. It has been found also that nearly identical background spectra are obtained whether one uses a single container of distilled, demineralized water (size of the container determined empirically) or a multibottle phantom laid out under the crystal like a human subject. Here again, background for a human count is only an approximation of the actual perturbation of the radiation field as a result of scatter and absorption by the human body.

IODINE-131 IN MILK AND IN CATTLE THYROIDS

P. E. Brown

L. B. Farabee

In September 1963 the program for monitoring milk and cattle thyroids as indicators of the distribution of ^{131}I in this general geographical area was turned over to the Environmental Monitoring Section of Applied Health Physics. The program had been developed by the Health Physics Technology Section and tested during 1961–1963.^{8–10} An average of ten thyroid samples per week were tested during most of this time, and one or more milk samples were tested weekly for over a year. Under the Health Physics Technology program, the prepared samples had been counted by using either a 4×2 or a 3×3 in. NaI(Tl) crystal and a 200-channel analyzer, the original in vivo counting equipment. Transfer of the program to Environmental Monitoring necessitated revision of the techniques to make them compatible with presently available equipment – a 4×4 in. crystal and a single-channel analyzer. Detection efficiency for counting thyroid samples with the single-channel system was found to give a lower detection limit of 10 pc per 20 g of thyroid at the 95% confidence level.

BIOASSAY AND ENVIRONMENTAL MONITORING

L. B. Farabee

During the past year, one member of the Health Physics Technology Section participated in an International Atomic Energy Agency (IAEA) program aimed at improving the reliability and comparability of the results of low-level activity measurements in environmental samples. A panel

of representatives from 20 countries and world-wide organizations met in Vienna, Austria, October 28–31, 1963, for discussion and planning of an interlaboratory comparison program among nations associated with the IAEA. Representatives from the United States were: A. S. Goldin, U.S. Public Health Service, Bethesda, Maryland; M. F. Milligan, Los Alamos Scientific Laboratory; and L. B. Farabee, Oak Ridge National Laboratory. A paper entitled "Review of Existing Intercomparison and Interlaboratory Schemes in the United States" was presented by L. B. Farabee.

The need for greater accuracy in analytical data on the measurement of harmful radionuclides in the food supply of man was stressed, and guidelines for setting up an interlaboratory comparison program were discussed. Comprehensive reviews of interlaboratory comparison programs used in many countries were discussed by panel members. Statistical considerations for collection and analysis of environmental samples as a means for improvement in quality control were of interest. Although many radionuclides and many foods were suggested for use in the IAEA intercomparison program, it was expedient to limit the original program to only the more hazardous long-lived radionuclides. Therefore ^{90}Sr , ^{137}Cs , and ^{226}Ra were selected as having the most universal interest at present. A review of the panel discussion may be found in ORNL-CF-64-1-83, dated January 14, 1964.

⁸B. R. Fish et al., *Health Phys. Div. Ann. Progr. Rept. July 31, 1961*, ORNL-3189, pp. 232–34.

⁹B. R. Fish et al., *Health Phys. Div. Ann. Progr. Rept. July 31, 1962*, ORNL-3347, pp. 148–52.

¹⁰B. R. Fish et al., *Health Phys. Div. Ann. Progr. Rept. June 30, 1963*, ORNL-3492, p. 206.

Papers, Publications, and Lectures

Papers

- E. T. Arakawa, N. O. Davis, and R. D. Birkhoff
The Temperature and Thickness Dependence of Transition Radiation from Thin Silver Foils, American Physical Society, April 27–30, 1964, Washington, D.C.
- E. T. Arakawa, N. O. Davis, L. C. Emerson, and R. D. Birkhoff
The Angular and Spectral Distribution of Transition Radiation from Thin Silver Foils, Colloquium on the Optics of Solid Thin Layers, September 8–15, 1963, Marseilles, France.
- J. C. Ashley and R. H. Ritchie
Exchange Correction to the Mean Free Path of Hot Electrons and Holes in a Free Electron Gas, American Physical Society, April 27–30, 1964, Washington, D.C.
- J. A. Auxier
Health Physics Research at the DOSAR Facility, U.S. Army Nuclear Science Seminar, August 14, 1963, Oak Ridge, Tennessee.
Instrumentation for Neutron Detection, Ten-Week Course in Health Physics, Oak Ridge Institute of Nuclear Studies, October 1, 1963, Oak Ridge, Tennessee.
Hiroshima and Nagasaki: Their Role in the Effects of Nuclear Weapons, Office of Civil Defense, November 18, 1963, Oak Ridge, Tennessee.
Fast Pulsed Reactors and Their Application to Research, Environmental and Radiological Health Colloquia, December 2, 1963, New York, New York.
Density Interface Effects on Initial Radiation from Nuclear Weapons, National Academy of Sciences Shielding Sub-Committee on Civil Defense, April 2 and 3, 1964, San Francisco, California.
The Health Physics Research Reactor and Its Role at the DOSAR Facility, Health Physics Society, June 15–18, 1964, Cincinnati, Ohio.
- R. D. Birkhoff
Studies of Plasmas in Solids, American Physical Society, Southeastern Section, November 7–9, 1963, Lexington, Kentucky.
- R. L. Bradshaw
Demonstration Disposal of High-Level Radioactive Solids in Lyons, Kansas, Salt Mine, Health Physics Society, June 14–18, 1964, Cincinnati, Ohio.
- J. G. Carter, D. R. Nelson, and R. D. Birkhoff
Importance of Sample Environment in Thermoluminescence Measurements, American Physical Society, Southeastern Section, November 7–9, 1963, Lexington, Kentucky.
- L. G. Christophorou, G. S. Hurst, and J. A. Stockdale
Swarm Measurement of Cross Sections for Dissociative Electron Capture in Heavy Water, Chlorobenzene, and Bromobenzene, Radiation Research Society, May 18–20, 1964, Miami Beach, Florida.
- W. G. Connor and R. H. Ritchie
The Photoelectric Effect in Metals, Health Physics Society, June 15–18, 1964, Cincinnati, Ohio.

- D. A. Crossley, Jr.
Forest Soil Mites and Mineral Cycling, invited paper given at session on soil ecology, 1st International Conference on Acarology, September 3, 1963, Fort Collins, Colorado.
- D. A. Crossley, Jr.
Heterotrophic Production in the Grazing Food Chain of Terrestrial Vegetation, Symposium on Heterotrophic Production, August 22, 1963, International Congress of Zoology, Washington, D.C.
- D. A. Crossley, Jr.
Interdependence Between Arthropod Food Chains in a Tulip Poplar Forest, Annual Meeting of Ecological Society of America (with AIBS), August 27, 1963, Amherst, Massachusetts.
- Wallace de Laguna
Waste Disposal by Hydraulic Fracturing, Health Physics Society, June 14–18, 1964, Cincinnati, Ohio.
- P. B. Dunaway
Hematology of Wild Mammals, American Society of Mammalogists, Forty-Fourth Annual Meeting, June 14–18, 1964, Mexico City, Mexico.
- L. B. Farabee
Review of Existing Intercomparison and Interlaboratory Schemes in the United States, IAEA Panel on Standardization of Low-Level Activity Measurements, October 28–31, 1963, Vienna, Austria.
- B. R. Fish, R. L. Walker, G. W. Royster, Jr., and J. L. Thompson
Redispersal of Settled Particulates, International Symposium on Surface Contamination, June 8–12, 1963, Gatlinburg, Tennessee.
- F. F. Haywood
Health Physics Research Reactor, Navy Nuclear Sciences Seminar, December 5, 1963, Oak Ridge, Tennessee.
- R. J. Herickhoff, E. T. Arakawa, and R. D. Birkhoff
Detection of Plasma Radiation from Electron-Bombarded Al Foils, American Physical Society, April 27–30, 1964, Washington, D.C.
- R. H. Huebner, R. A. MacRae, E. T. Arakawa, and R. N. Hamm
The Optical Constants of Vacuum Evaporated Silver Films, American Physical Society, Southeastern Section, November 7–9, 1963, Lexington, Kentucky.
- G. S. Hurst
Interaction of Alpha Particles with the Argon Atom, Health Physics Society, June 15–18, 1964, Cincinnati, Ohio.
- D. G. Jacobs
The Effect of Lattice Collapse of Layer Alumino-Silicates on the Sorption of Cesium, 147th National Meeting of the American Chemical Society, April 5–10, 1964, Philadelphia, Pennsylvania.
- D. R. Johnson
An Experimental Calibration of Fission Foil Threshold Detectors, Health Physics Society, June 15–18, 1964, Cincinnati, Ohio.
- N. R. Kevern
Calcium and Strontium Uptake by the Alga, Oocystis, Health Physics Society, June 15–18, 1964, Cincinnati, Ohio.
- T. F. Lomenick and D. A. Gardiner
The Occurrence and Retention of Radionuclides in the Sediments of White Oak Lake, Health Physics Society, June 14–18, 1964, Cincinnati, Ohio.

- T. F. Lomenick and T. Tamura
Naturally Occurring Fixation of Cesium-137 on Sediments of Lacustrine Origin, Soil Science Society, November 18–21, 1963, Denver, Colorado.
- L. A. Masironi and B. R. Fish
Direct Observation of Particle Reentrainment from Surfaces, International Symposium on Surface Contamination, June 8–12, 1963, Gatlinburg, Tennessee.
- K. Z. Morgan
Teaching Health Physics to the Physics Student, American Physical Society, Southeastern Section, November 7–9, 1963, Lexington, Kentucky.
Maximum Permissible Internal Dose from Radioisotopes, Radiological Society of North America, November 17–23, 1963, Chicago, Illinois.
Panel Discussion on Lung Models, Symposium on Inhaled Radioactive Particles, May 4–6, 1964, Richland, Washington.
Graduate Programs for the Health Physicist in the United States, Ninth Annual Meeting of the Health Physics Society, June 15–18, 1964, Cincinnati, Ohio.
- J. Neufeld and Harvel Wright
Interaction of a Beam of Protons with Plasma, Sixth International Symposium on Ionization Phenomena in Gases, July 8–13, 1963, Paris, France.
- F. L. Parker, B. J. Frederick, P. H. Carrigan, Jr., and R. J. Pickering
Transport and Dispersion of Radioactive Materials in River, American Society of Civil Engineering, May 11–14, 1964, Salt Lake City, Utah.
- F. L. Parker, B. J. Frederick, P. H. Carrigan, Jr., and R. M. Richardson
Movement of Radionuclides in the Clinch River, Third Sanitary Engineering Conference, May 25, 1964, Vanderbilt University, Nashville, Tennessee.
- B. C. Patten
Some Experimental Characteristics of Dark and Light Bottles, Atlantic Estuarine Research Society, November 8–9, 1963, Beaufort, North Carolina.
- B. C. Patten
The Adaptive Significance of Diversity-Productivity Relationships in an Estuarine Phytoplankton Community, Conference on Estuaries, March 30–April 4, 1964, Jekyll Island, Georgia.
- R. H. Ritchie
The Effect of Surface Losses in Stopping Power Theory, Health Physics Society, June 15–18, 1964, Cincinnati, Ohio.
- A. K. Roecklein, Y. Nakai, E. T. Arakawa, J. L. Stanford, and R. D. Birkhoff
A New Technique for Measuring Ranges of Low Energy Charged Particles in Solids, Health Physics Society, June 15–18, 1964, Cincinnati, Ohio.
- G. W. Royster, Jr., and B. R. Fish
Techniques for Assessing "Removable" Surface Contamination, International Symposium on Surface Contamination, June 8–12, 1963, Gatlinburg, Tennessee.
- G. W. Royster, Jr., B. R. Fish, and L. B. Farabee
In Vitro Methods of Estimating Relative Solubility in Body Fluids, 9th Bioassay and Analytical Chemistry Conference, October 10 and 11, 1963, San Diego, California.
- Mohammad Unis Shaikh, D. G. Jacobs, and F. L. Parker
Movement of Radionuclides Through Saturated Porous Media, Health Physics Society, June 14–18, 1964, Cincinnati, Ohio.

A. F. Shinn

Transport of Radioactive Materials by Mud-Dauber Wasps, Health Physics Society, June 18, 1964, Cincinnati, Ohio.

W. S. Snyder

The LET Distribution of Dose in Various Tissue Cylinders, IAEA Symposium on the Biological Effects of Neutron Irradiations, October 7–11, 1963, Brookhaven National Laboratory, New York.

The Distribution of ^{239}Pu in the Body Following Exposure by Inhalation, Symposium on Inhaled Radioactive Particles and Gases, May 4–6, 1964, Richland, Washington.

On the Estimation of a Systemic Body Burden of Plutonium, IAEA, WHO, ILO Symposium on the Assessment of Radioactive Body Burden in Man, May 11–16, 1964, Heidelberg, Germany.

Internal Emitters, Health Physics Society Annual Meeting, June 15–18, 1964, Cincinnati, Ohio.

Distribution of Dose and Dose Equivalent Resulting from Broad-Beam Irradiation of a Man-Sized Cylindrical Phantom by Monoenergetic Neutrons, Health Physics Society Annual Meeting, June 15–18, 1964, Cincinnati, Ohio

W. S. Snyder and Mary Jane Cook

The Distribution of Stable Strontium in Bone and Soft Tissues of Man and Its Application to Metabolism of ^{90}Sr , Health Physics Society Annual Meeting, June 15–18, 1964, Cincinnati, Ohio.

T. D. Strickler, E. T. Arakawa, and G. S. Hurst

Optical Emission from Argon Excited by Alpha Particles: Quenching Studies, American Physical Society, Southeastern Section, November 7–9, 1963, Lexington, Kentucky.

Tsuneo Tamura

Clay Mineralogy and Waste Disposal, Conference on Water, Geology and the Future, April 27, 1964, University of Indiana, Bloomington.

Tsuneo Tamura

Selective Removal of Cesium-137 and Strontium-90 by Minerals, 147th National Meeting of the American Chemical Society, April 5–10, 1964, Philadelphia, Pennsylvania.

J. H. Thorngate

Neutron Dose Conversion Factors for PuBe and PoBe Sources, Health Physics Society, June 15–18, 1964, Cincinnati, Ohio.

G. M. Van Dyne, O. G. Thomas, and J. L. Van Horn

Diet of Cattle and Sheep Grazing on Winter Range, Symposium on Range Livestock Nutrition, July 13–14, 1964, Montana State College, Bozeman, Montana.

R. L. Walker and B. R. Fish

Adhesion of Radioactive Glass Particles to Solid Surfaces, International Symposium on Surface Contamination, June 8–12, 1963, Gatlinburg, Tennessee.

H. D. Waller and J. S. Olson

Landscape Studies Using Radioactive Tracers. III. Prompt Transfer of Cesium-137 to the Forest Floor and Soil of a Tagged Tulip Poplar Forest, Health Physics Society, June 14–18, 1964, Cincinnati, Ohio.

J. P. Witherspoon, Jr.

Glass Rod Dosimetry in Tree Tagging Experiments, Health Physics Society, June 18, 1964, Cincinnati, Ohio.

Harvel Wright and J. Neufeld

Multiple Instability in a Plasma-Beam System, American Physical Society, January 22–25, 1964, New York, New York.

Publications

- E. T. Arakawa
Trip Report, September 3-15, 1963: Colloquium on Optics of Thin Solid Layers; Visits to Institute of Optics, Paris; Technical University, Berlin, ORNL-CF-63-9-71 (Sept. 30, 1963).
- E. T. Arakawa, L. C. Emerson, D. C. Hammer, and R. D. Birkhoff
 "Transition Radiation and Optical Bremsstrahlung from Electron-Bombarded Thin Gold Foils," *Phys. Rev.* **131**, 719-22 (1963).
- E. T. Arakawa, N. O. Davis, L. C. Emerson, and R. D. Birkhoff
 "The Angular and Spectral Distribution of Transition Radiation from Thin Silver Foils," *J. Phys. (Paris)* **25**, 129-33 (1964).
- E. T. Arakawa, N. O. Davis, and R. D. Birkhoff
 "The Temperature and Thickness Dependence of Transition Radiation from Thin Silver Foils," *Phys. Rev.* **135**, A224-26 (1964).
- E. T. Arakawa, R. J. Herickhoff, and R. D. Birkhoff
 "Detection of Plasma Radiation from Electron-Bombarded Al and Mg Foils," *Phys. Rev. Letters* **12**, 319-20 (1964).
- J. C. Ashley and R. H. Ritchie
 "Photon Radiation from Irradiated Dielectric Slabs," to be published in the *Journal of Applied Physics*.
- S. I. Auerbach and J. S. Olson
 "Biological and Environmental Behavior of Ruthenium and Rhodium," pp. 509-19 in *Radioecology* (ed. by V. Schultz and A. W. Klement, Jr.), Reinhold, New York, and AIBS, Washington, 1963.
- S. I. Auerbach, J. S. Olson, and H. D. Waller
 "Landscape Investigations Using Cesium-137," *Nature* **201**(4921), 761-64 (1964).
- L. G. Augenstein, Jaynati Nag-Chaudhuri, DeVaghn Nelson, and Edward Yeagers
 "Comparison of Emission from Excited States Produced in Proteins and Amino Acids by Ultraviolet Light and Ionizing Radiation," to be published in *Physical Processes in Radiation Biology*, Academic, New York.
- J. A. Auxier
 "Dosimetry and Exposures in Nuclear Accidents," *Journal of Nuclear Safety* (in press).
 "The Health Physics Research Reactor," *Health Physics* (in press).
Ichiban: The Dosimetry Program for Nuclear Bomb Survivors of Hiroshima and Nagasaki - A Status Report as of April 1, 1964, CEX-64.3 (in press).
- J. A. Auxier and J. S. Cheka
Report of Trip Abroad by J. A. Auxier and J. S. Cheka During Period April 27, 1964-May 30, 1964, ORNL-CF-64-6-16 (June 15, 1964).
- J. A. Auxier, F. F. Haywood, and L. W. Gilley
General Correlative Studies - Operation BREN, CEX-62.03 (September 1963).
- S. R. Bernard, B. R. Fish, G. W. Royster, Jr., L. B. Farabee, P. E. Brown, and G. R. Patterson, Jr.
 "Human Thyroid Uptake and Bodily Elimination of I^{131} for the Case of Single and Continual Ingestion of Bound Iodine in Resin-Treated Milk," *Health Phys.* **9**, 1307-23 (1963).
- R. D. Birkhoff
 "Electron Spectroscopy in Health Physics Research," *Health Phys.* **9**, 973-86 (1963).
- R. D. Birkhoff
 "Energy Loss Spectra for Charged Particles Traversing Metal and Plastic Films," to be published in *Physical Processes in Radiation Biology*, Academic, New York.

- R. E. Blanco and F. L. Parker
Waste Treatment and Disposal Quarterly Progress Report, February–April 1963, ORNL-TM-603 (Dec. 16, 1963).
- B. G. Blaylock
 "Chromosomal Aberrations in a Natural Population of *Chironomus Tentans* Exposed to Chronic Low-Level Radiation," *Evolution* (in press).
- B. G. Blaylock, S. I. Auerbach, and D. J. Nelson
Chromosomal Aberrations in a Natural Population of Chironomus Tentans Exposed to Chronic Low-Level Environmental Radiation, ORNL-3531 (1963).
- J. O. Blomeke, J. J. Perona, H. O. Weeren, and R. L. Bradshaw
Evaluation of Ultimate Disposal Methods for Liquid and Solid Wastes. Part III. Interim Storage of Solidified Wastes, ORNL-3355 (Oct. 14, 1963).
- J. O. Blomeke, R. L. Bradshaw, J. J. Perona, and J. T. Roberts
 "Estimated Costs of Management of High-Activity Power Reactor Wastes," *Trans. Am. Nucl. Soc.* 6(1), 164 (June 1963).
- R. H. Boyett, T. G. Clark, and B. R. Fish
 β -Dosimetry Applications for Discrete Sources. I. Preliminary Review, ORNL-TM-802 (Feb. 26, 1964).
- R. L. Bradshaw, W. J. Boegly, Jr., F. M. Empson, H. Kubota, F. L. Parker, J. J. Perona, and E. G. Struxness
 "Ultimate Storage of High-Level Waste Solids and Liquids in Salt Formations," pp. 257–68 in *Retention and Migration of Radioactive Ions in Soils*, French University Press, Paris, 1963.
- R. L. Bradshaw, W. J. Boegly, Jr., F. M. Empson, H. Kubota, F. L. Parker, J. J. Perona, and E. G. Struxness
 "Ultimate Storage of High-Level Waste Solids and Liquids in Salt Formations," pp. 153–75 in *Treatment and Storage of High-Level Radioactive Wastes*, IAEA, Vienna, 1963.
- G. N. Brown
 "Cesium in Liriodendron and Other Woody Species: Organic Bonding Sites," *Science* 143(3604), 368–69 (1964).
- J. G. Carter, R. A. MacRae, D. R. Nelson, R. D. Birkhoff, and E. T. Arakawa
 "Interference Filter Spectrometer for Low Intensity Extended Sources," *Appl. Opt.* 3, 75–78 (1964).
- J. G. Carter, R. D. Birkhoff, and D. R. Nelson
 "Importance of Thermal Equilibrium in Thermoluminescence Measurements," *Health Phys.* 10, 539–42 (1964).
- J. S. Cheka
 "Stability of Radiophotoluminescence in Metaphosphate Glass," *Health Phys.* 10, 303–14 (1964).
- K. E. Cowser
Current Practices in the Release and Monitoring of I^{131} at NRTS, Hanford, Savannah River, and ORNL, NSIC-3 (1964).
- K. E. Cowser
 "Movement of Ruthenium in the ORNL Waste-Pit System," pp. 229–41 in *International Colloquium on Retention and Migration of Radioactive Ions in Soils, October 16–18, 1962*, Centre d'Etudes Nucleaires de Saclay, France (1963).
- K. E. Cowser and T. Tamura
 "Significant Results in Low-Level Waste Treatment at ORNL," *Health Phys.* 9, 687 (1963).
- K. E. Cowser, W. S. Snyder, and M. J. Cook
 "Preliminary Safety Analysis of Radionuclide Release to the Clinch River," pp. 17–38 in *Transport of Radionuclides in Fresh Water Systems*, TID-7664 (1963).

- D. A. Crossley, Jr.
 "Biological Elimination of Radionuclides," *Nucl. Safety* 5(3), 265-68 (1964).
- D. A. Crossley, Jr.
 "Consumption of Vegetation by Insects," pp. 427-30 in *Radioecology* (ed. by V. Schultz and A. W. Klement, Jr.), Reinhold, New York, and AIBS, Washington, 1963.
- D. A. Crossley, Jr.
 "Movement and Accumulation of Radiostrontium in Insects," pp. 103-5 in *Radioecology* (ed. by V. Schultz and A. W. Klement, Jr.), Reinhold, New York, and AIBS, Washington, 1963.
- D. A. Crossley, Jr.
 "Use of Radioisotopes in the Study of Insect-Plant Relationships," pp. 43-54 in *Radiation and Radioisotopes Applied to Insects of Agricultural Importance*, IAEA, Vienna, 1963.
- D. A. Crossley, Jr., and E. W. Baker
 "A New Species of Mite, *Fusoherecia lawrencei*, from an Artificial Tree Hole," *Publ. South African Museum* (in press).
- D. A. Crossley, Jr., and Martin Witkamp
 "Forest Soil Mites and Mineral Cycling," *Spec. Suppl., Acarologia* (in press).
- D. A. Crossley, Jr., with G. L. Plummer and D. A. Gardiner
 "A Growth Response of Two Sedges Inhabiting a Radioactive Waste Disposal Area," *Ecology* (in press).
- N. O. Davis, L. C. Emerson, E. T. Arakawa, and R. D. Birkhoff
Angular and Spectral Distribution of Light Emitted from Electron-Bombarded Silver Foils, ORNL-3485 (March 1964).
- Wallace de Laguna
Geology of Brookhaven National Laboratory and Vicinity, Suffolk County, New York, Geological Survey Bulletin 1156-A, U.S. Government Printing Office, Washington, D.C., 1963.
- P. B. Dunaway and S. V. Kaye
 "Effects of Ionizing Radiation on Mammal Populations on the White Oak Lake Bed," pp. 333-38 in *Radioecology* (ed. by V. Schultz and A. W. Klement, Jr.), Reinhold, New York, and AIBS, Washington, 1963.
- P. B. Dunaway and S. V. Kaye
 "Effects of Radiation on Mammalian Population Dynamics," pp. 141-49 in *Proc. 1st Inter. Conf. Wildl. Dis.*, Wildlife Disease Assoc., 1963.
- P. B. Dunaway and S. V. Kaye
 "Weights of Cotton Rats in Relation to Season, Breeding, and Environmental Radioactive Contamination," *Am. Midland Naturalist* 71, 141-55 (1964).
- L. C. Emerson, E. T. Arakawa, R. H. Ritchie, and R. D. Birkhoff
Emission Spectra of Electron Irradiated Metal Foils, ORNL-3450 (July 30, 1963).
- L. B. Farabee
Trip Report: IAEA Panel on Standardization of Low Level Activity Measurements, Vienna, Austria, October 26-November 19, 1963, ORNL-CF-64-1-83 (Jan. 14, 1964).
- B. R. Fish, S. R. Bernard, G. W. Royster, Jr., L. B. Farabee, P. E. Brown, and G. R. Patterson, Jr.
 "Human Uptake and Excretion of I^{131} : Single Inhalation Compared with Single and Continual Ingestion of Iodine in Milk," *Health Phys.* 9, 875 (August 1963).
- L. W. Gilley and L. B. Holland
Procedures Manual for the Health Physics Research Reactor (Including High-Level Gamma Facility), ORNL-3519 (Oct. 30, 1963).
- D. C. Hammer, E. T. Arakawa, L. C. Emerson, and R. D. Birkhoff
Optical Emission from Electron Irradiated Thin Gold Foils, ORNL-3468 (Aug. 26, 1963).

- D. C. Hammer, E. T. Arakawa, and R. D. Birkhoff
 "A Simple Grating Calibrator for the Visible and Vacuum Ultraviolet," *Appl. Opt.* 3, 79-81 (1964).
- F. F. Haywood
 "Spatial Dose Distribution in Air-Over-Ground Geometry," *Health Physics* (in press).
- F. F. Haywood, J. A. Auxier, and E. T. Loy
An Experimental Investigation of the Spatial Distribution of Dose in an Air-Over-Ground Geometry, CEX-62.14 (in press).
- H. H. Hubbell, Jr., W. J. McConnell, and R. D. Birkhoff
 "The Spherical Condenser as a High Transmission Particle Spectrometer-III. Construction and Calibration," submitted for publication in *Nuclear Instruments and Methods*.
- R. H. Huebner, E. T. Arakawa, R. A. MacRae, and R. N. Hamm
 "The Optical Constants of Vacuum Evaporated Silver Films," submitted for publication in the *Journal of the Optical Society of America*.
- G. S. Hurst and R. H. Ritchie
 "A Generalized Concept for Radiation Dosimetry," pp. 31-40 in *Neutron Dosimetry*, vol II, IAEA, Vienna, 1963.
- G. S. Hurst, L. B. O'Kelley, E. B. Wagner, and J. A. Stockdale
 "Time-of-Flight Investigations of Electron Transport in Gases," *J. Chem. Phys.* 39, 1341-45 (1963).
- D. G. Jacobs
 "Movement of Radionuclides Through the Ground," *Nucl. Safety* 5(1), 109-15 (1963).
 "The Effect of Collapse-Inducing Cations on the Cesium Sorption Properties of Hydrobiotite," pp. 239-48 in *Proceedings of International Clay Conference Held at Stockholm, Sweden, August 12-16, 1963*, Pergamon, London, 1963.
 "Ion Exchange in the Deep-Well Disposal of Radioactive Wastes," pp. 43-53 in *International Colloquium on Retention and Migration of Radioactive Ions in Soils, October 16-18, 1962*, Centre d'Etudes Nucleaires de Saclay, France, 1963.
- D. R. Johnson
Report of Trip Abroad by D. R. Johnson During the Period August 5-17, 1963, ORNL-CF-63-8-51 (Aug. 30, 1963).
- T. D. Jones
 "Neutron Dose Conversion Factors for PuBe and PoBe Sources," *Health Physics* (in press).
- S. V. Kaye
 "Use of Miniature Glass Rod Dosimeters in Radiation Ecology," *Ecology* (in press).
- S. V. Kaye and P. B. Dunaway
 "Estimation of Dose Rate and Equilibrium State from Bioaccumulation of Radioisotopes by Mammals," pp. 107-11 in *Radioecology* (ed. by V. Schultz and A. W. Klement, Jr.), Reinhold, New York, and AIBS, Washington, 1963.
- N. R. Kevem and R. C. Ball
 "Primary Productivity and Energy Relationships in Artificial Streams," *Limnology and Oceanography* (in press).
- D. A. LaBar, R. D. Birkhoff, and J. A. Harter
Time-of-Flight Electron Beam Monochromator, ORNL-3484 (April 1964).
- W. T. Lammers
 "Density Gradient Separation of Plankton and Clay from River Water: Theory and Applications," *Verh. Intern. Verein. Limnol.* 15, 1021-28 (1964).

- T. F. Lomenick
 "Movement of Ruthenium in the Bed of White Oak Lake," pp. 217-27 in *International Colloquium on Retention and Migration of Radioactive Ions in Soils, October 16-18, 1962, Centre d'Etudes Nucleaires de Saclay, France, 1963.*
 "Movement of Ruthenium in the Bed of White Oak Lake," *Health Phys.* 9, 835-45 (1963).
The Geology of a Portion of the Hutchinson Salt Member of the Wellington Formation in the Mine of The Carey Salt Company, Lyons, Kansas, ORNL-TM-597 (Sept. 3, 1963).
- R. E. Martin, S. I. Auerbach, and D. J. Nelson
Growth and Movement of Smallmouth Buffalo, Ictiobus bubalus (Rafinesque), in Watts Bar Reservoir, Tennessee, ORNL-3530 (Jan. 6, 1964).
- W. J. McConnell, H. H. Hubbell, Jr., and R. D. Birkhoff
Electron Slowing Down Spectrum in Cu of Beta Rays from Cu-64, ORNL-3463 (May 1964).
- K. Z. Morgan
 "Health Physics," chap. 8, p. 312 in *American Institute of Physics Handbook*, 2d ed., McGraw-Hill, New York, 1963.
 "Medical X-Ray Exposure," *Am. Ind. Hyg. Assoc. J.* 24(6) (November-December 1963).
 "Biomedical Considerations in Accidental Releases of Radioiodine," *Health Phys.* 9(12), 1423 (1963).
 "The Body Burden of Long-Lived Isotopes," *Arch. Environ. Health* 8(1), 86 (1964).
- K. Z. Morgan, W. S. Snyder, and M. R. Ford
 "Relative Hazard of the Various Radioactive Materials," *Health Phys.* 10(3), 151 (1964).
- D. J. Nelson
 "Deposition of Strontium in Relation to Morphology of Clam (Unionidae) Shells," *Verh. Internat. Verein. Limnol.* 15, 893-902 (February 1964).
- D. J. Nelson
 "Interpretation of Radionuclide Uptake from Aquatic Environments," *Nucl. Safety* 5(2), 196-99 (1964).
- D. J. Nelson
 "The Strontium and Calcium Relationships in Clinch and Tennessee River Mollusks," pp. 203-11 in *Radioecology* (ed. by V. Schultz and A. W. Klement, Jr.), Reinhold, New York, and AIBS, Washington, 1963.
- D. J. Nelson
Transport of Radionuclides in Fresh Water Systems: Role of Bottom Organisms, TID-7664, pp. 193-201 (July 1963).
- D. J. Nelson and B. G. Blaylock
 "The Preliminary Investigation of Salivary Gland Chromosomes of *Chironomus tentans* Fabr. from the Clinch River," pp. 367-72 in *Radioecology* (ed. by V. Schultz and A. W. Klement, Jr.), Reinhold, New York, and AIBS, Washington, 1963.
- D. J. Nelson and C. W. Wiser
 "Uptake and Elimination of Cobalt-60 by Crayfish," *American Midland Naturalist* (in press).
- J. Neufeld
 "Constitutive Equations for a Plasma-Like Medium," *J. Appl. Phys.* 34, 2549-52 (1963).
- J. Neufeld
 "Energy Density in a Dispersive Medium Formulated in Terms of Constitutive and Electromagnetic Parameters," *Phys. Letters* 6, 246-47 (1963).
- J. Neufeld
 "Interaction of a Stationary Plasma with an Electron Beam," *Phys. Fluids* 7, 306-10 (1964).

- J. Neufeld
 "Plasma-Beam Instability in the Hartree-Appleton Approximation," *Phys. Fluids* 6, 1750-56 (1963).
- J. Neufeld
Trip Report: July 8-26, 1963: International Conference on the Ionization Phenomena in Gases, Paris; Visit to Euratom-CEA Laboratories, Fontenay-aux-Roses; International Conference on the Physics of Electronic and Atomic Collisions, London, ORNL-CF-63-9-10 (Sept. 6, 1963).
- J. Neufeld and Harvel Wright
 "Generation of Whistler Waves by Helical Electron Beams," submitted for publication in *Nature*.
- J. Neufeld and Harvel Wright
 "Instabilities Produced in a Stationary Plasma by an 'Almost Circular' Electron Beam," submitted for publication in the *Physical Review*.
- J. Neufeld and Harvel Wright
 "Interaction of a Beam of Protons with Plasma," pp. 207-8 in *Proceedings of VIth International Conference on Ionization Phenomena in Gases*, North-Holland Publishing Co., Amsterdam, 1964.
- J. Neufeld and Harvel Wright
 "Interaction of a Plasma with a Helical Electron Beam," to be published in the *Physical Review*.
- J. Neufeld and Harvel Wright
 "Magnetodynamic Instabilities in a Plasma-Beam System," *Phys. Rev.* 131, 1395-1401 (1963).
- J. Neufeld and Harvel Wright
 "Multiple Instability in a Plasma-Beam System," to be published in the *Physics of Fluids*.
- J. S. Olson
 "Analog Computer Models for Measurement of Nuclides Through Ecosystems," pp. 121-26 in *Radioecology* (ed. by V. Schultz and A. W. Klement, Jr.), Reinhold, New York, and AIBS, Washington, 1963.
- J. S. Olson
 "Energy Storage and the Balance of Producers and Decomposers in Ecological Systems," *Ecology* 44(2), 322-32 (1963).
- J. S. Olson
 "Gross and Net Production of Terrestrial Vegetation," *J. Ecol.* 52 (Jubilee Supplement), 99-118 (1964).
- J. S. Olson and D. A. Crossley, Jr.
 "Tracer Studies of the Breakdown of Forest Litter," pp. 411-16 in *Radioecology* (ed. by V. Schultz and A. W. Klement, Jr.), Reinhold, New York, and AIBS, Washington, 1963.
- J. S. Olson with R. H. Whittaker and Neil Cohen
 "Net Production Relations of Three Tree Species at Oak Ridge, Tennessee," *Ecology* 44(4), 806-10 (1963).
- F. L. Parker
 "Clinch River Studies," pp. 161-91 in *Proceedings of Working Conference on Transport of Radio-nuclides in Fresh Water, Austin, Texas, January 30, 31, and February 1, 1963*, TID-7664 (January 1964).
- F. L. Parker
 "Ground Disposal of Radioactive Wastes," *Minutes of the National Technical Task Committee on Industrial Wastes Meeting, December 11-13, 1963*, St. Louis, Missouri (Mar. 16, 1964).
- F. L. Parker and R. E. Blanco
Waste Treatment and Disposal Progress Report for November-December 1962, and January 1963, ORNL-TM-516 (June 12, 1963).
- F. L. Parker and R. E. Blanco
Waste Treatment and Disposal Progress Report, May-October 1963, ORNL-TM-757 (April 1964).

- B. C. Patten
 "Information Processing Behavior of a Natural Plankton Community," *Am. Biol. Teacher* 25, 489–501 (1963).
- B. C. Patten
 "The Plankton Community," *Science* 144, 557–58 (1964).
- B. C. Patten
 "The Rational Decision Process in Salmon Migration," *J. du Cons.* 28, 410–17, 443–44 (1963).
- B. C. Patten, J. J. Norcross, D. K. Young, and C. L. Rutherford
 "Some Experimental Characteristics of Dark and Light Bottles," *J. du Cons.* 28, 335–53 (1963).
- J. J. Perona, J. O. Blomeke, R. L. Bradshaw, and J. T. Roberts
 "Effects of Fission Product Removal on Waste Management Costs," *Trans. Am. Nucl. Soc.* 6(1), 165 (June 1963).
- J. J. Perona, R. L. Bradshaw, and J. O. Blomeke
Comparative Costs for Final Disposal of Radioactive Solids in Concrete Vaults, Granite, and Salt Formations, ORNL-TM-664 (Oct. 23, 1963).
- J. J. Perona, R. L. Bradshaw, J. T. Roberts, and J. O. Blomeke
 "Economic Evaluation of Tank Storage and Pot Calcination of Power-Reactor Fuel-Reprocessing Wastes," pp. 309–35 in *Treatment and Storage of High-Level Radioactive Wastes*, International Atomic Energy Agency, Vienna, 1963.
- R. H. Ritchie and J. C. Ashley
 "Exchange Correction to the Mean Free Path of Hot Electrons and Holes in Metals," to be published in *Applied Physics Letters*.
- R. H. Ritchie, J. C. Ashley, and L. C. Emerson
 "Optical Bremsstrahlung and Transition Radiation from Irradiated Media," to be published in the *Physical Review*.
- G. W. Royster, Jr., and B. R. Fish
 "Studies of Surface Contamination. III. Effect of Particle Size on the Measurement and Redispersion of Particulates," *Health Phys.* 9, 896 (August 1963).
- H. A. Schroeder, J. J. Balassa, and Isabel H. Tipton
 "Abnormal Trace Metals in Man – Vanadium," *J. Chronic Diseases* 16, 1047 (1963).
- W. S. Snyder
Some Data on the Relationship of RBE and LET, TID-7652, p. 402.
 "The LET Distribution of Dose in Some Tissue Cylinders," p. 3 in *Biological Effects of Neutron and Proton Irradiations*, vol. 1, IAEA, Vienna, 1964.
- W. S. Snyder, M. J. Cook, and M. R. Ford
 "Estimates of $(MPC)_w$ for Occupational Exposure to ^{90}Sr , ^{89}Sr , and ^{85}Sr ," *Health Phys.* 10(3), 171 (1964).
- J. A. Stockdale and G. S. Hurst
 "Swarm Measurement of Cross Sections for Dissociative Electron Capture in Heavy Water, Chlorobenzene, and Bromobenzene," *J. Chem. Phys.* 41, 255–61 (1964).
- J. A. Stockdale, G. S. Hurst, and L. G. Christophorou
 "Capture of Low Energy Electrons in Chlorobenzene and Bromobenzene," *Nature* 202, 459–61 (1964).
- T. D. Strickler and E. T. Arakawa
 "Optical Emission from Argon Excited by Alpha Particles: Quenching Studies," to be published in the *Journal of Chemical Physics*.

Tsuneo Tamura

"Cesium Sorption Reactions as Indicator of Clay Mineral Structures," pp. 229-37 in *Proceedings of 1963 International Clay Conference*, Pergamon, London, 1963.

"Selective Sorption Reactions for Cesium and Strontium by Soil Minerals," pp. 95-104 in *International Colloquium on Retention and Migration of Radioactive Ions in Soils, October 16-18, 1962*, Centre d'Etudes Nucleaires de Saclay, France, 1963.

Tsuneo Tamura

"Selective Sorption Reactions of Cesium with Soil Minerals," *Nucl. Safety* 5(3), 262-65 (1964).

Tsuneo Tamura and E. G. Struxness

"Reactions Affecting Strontium Removal from Radioactive Wastes," *Health Phys.* 9, 697-704 (1963).

F. G. Taylor

"Supernumerary Incisors in *Lynx rufus* Schreber," *J. Mammal.* 45 (in press).

J. H. Thorngate

"Medium Speed Coincidence Circuit Using Tunnel Diodes," *Health Physics* (in press).

"The Response of a Neutron-Insensitive Gamma-Ray Dosimeter as a Function of Photon Energy," *Health Physics* (in press).

"A Versatile Frequency Divider," *Health Physics* (in press).

I. H. Tipton and J. J. Shafer

"Statistical Analysis of Lung Trace Element Levels," *Arch. Environ. Health* 8, 58 (January 1964).

J. E. Turner

"On the Experimental Verification and Determination of Parameters in Stopping Power Theory," to be published in *Studies on the Penetration of Charged Particles in Matter*, NAS-NRC Publication No. 1133.

J. E. Turner

"Values of I and I_{adj} , Suggested by Subcommittee," to be published in *Studies on the Penetration of Charged Particles in Matter*, NAS-NRC Publication No. 1133.

J. E. Turner and U. Fano

"Contributions to the Theory of Shell Corrections," to be published in *Studies on the Penetration of Charged Particles in Matter*, NAS-NRC Publication No. 1133.

J. E. Turner, C. D. Zerby, R. L. Woodyard, H. A. Wright, W. E. Kinney, W. S. Snyder, and J. Neufeld

"Calculation of Radiation Dose from Protons to 400 MeV," to be published in *Health Physics*.

W. H. Wilkie and R. D. Birkhoff

Measurement of Spectral Distribution of Positron Flux in an Infinite Copper Medium Containing Cu-64, ORNL-3469 (Dec. 10, 1963).

J. P. Witherspoon, Jr.

"Cycling of Cesium-134 in White Oak Trees," *Ecological Monographs* 34(4) (in press).

J. P. Witherspoon, Jr.

"Cycling of Cs^{134} in White Oak Trees on Sites of Contrasting Soil Type and Moisture. I. 1960 Growing Season," pp. 127-32 in *Radioecology* (ed. by V. Schultz and A. W. Klement, Jr.), Reinhold, New York, and AIBS, Washington, 1963.

Martin Witkamp

"First Year of Movement, Distribution, and Availability of Cs^{137} in the Forest Floor Under Tagged Tulip Poplars," *Radiation Botany* (in press).

Martin Witkamp

"Microbial Populations of Leaf Litter in Relation to Environmental Conditions and Decomposition," *Ecology* 44, 370-77 (1963).

Martin Witkamp and J. S. Olson

"Breakdown of Confined and Nonconfined Oak Litter," *Oikos* 14(2), 138-47 (1963).

Lectures

S. I. Auerbach

Radioactivity in Ecological System, Health Physics Course, ORINS, November 1963, Oak Ridge, Tennessee.

Recent Developments in Radiation Ecology and Environmental Behavior of Fission Derived Radionuclides, School of Medicine, University of Miami, December 11-12, 1963, Coral Gables, Florida. (Traveling Lecture)

Recent Developments in Radiation Ecology, Department of Zoology, Louisiana State University, December 13, 1963, Baton Rouge; Department of Biological Sciences, University of Delaware, January 17, 1964, Newark; Zoology Department, University of Arkansas, March 16, 1964, Fayetteville. (Traveling Lectures)

The Proposed Environmental Sciences Laboratory, American Society of Civil Engineers, February 13, 1964, Oak Ridge, Tennessee.

Responses of Field Populations to Ionizing Radiation, Biology Department, Tuskegee Institute, March 9, 1964, Tuskegee Institute, Alabama. (Traveling Lecture)

B. G. Blaylock

Cytogenetic Responses to Environmental Radiation, Institute in Radioecology, ORINS, July 23, 1963, Oak Ridge, Tennessee.

Effects of Chronic Low-Level Radiation on Natural Populations, Biology Department, Tennessee Polytechnic Institute, March 6, 1964, Cookeville, Tennessee.

W. J. Boegly, Jr.

Demonstration of the Disposal of Radioactive Waste in Salt, Tennessee Academy of Science, November 29-30, 1963, Chattanooga, Tennessee.

R. L. Bradshaw

Radioactive Waste Disposal in Natural Salt Formations, Long-Range Planning Group, Reactor Division, ORNL, October 18, 1963, Oak Ridge, Tennessee.

Ultimate Storage of High-Level Wastes in Salt Formations, U.S. Public Health Service Course on Reactor Safety and Hazards Evaluation, ORNL, March 17, 1964, Oak Ridge, Tennessee.

K. E. Cowser

Progress Report No. 3, Subcommittee on Safety Evaluation, Clinch River Study Steering Committee, December 4, 1963, Oak Ridge, Tennessee.

Current Practices in the Release and Monitoring of I^{131} at NRTS, Hanford, Savannah River, and ORNL, Nuclear Safety Seminar, May 14, 1964, Oak Ridge, Tennessee.

D. A. Crossley, Jr.

Use of Biological Half-Life as an Ecological Research Tool, Radioecology Institute, ORINS, July 8, 1963, Oak Ridge, Tennessee.

Radioecology, Third Army Nuclear Science Seminar, ORINS, August 21, 1963, Oak Ridge, Tennessee.

D. A. Crossley, Jr.

Use of Radioisotopes in the Study of Insect-Plant Relationships, International Short Course in Entomology, sponsored by IAEA, WHO, October 30, 1963, Gainesville, Florida.

Health Physics, Michigan State University, January 29, 1964, East Lansing, Michigan.

L. C. Emerson

Interaction of Radiation with Matter, ORSORT, ORNL, November 4, 6, 8, and 11, 1963, Oak Ridge, Tennessee.

Biological Effects of Radiation, ORSORT, ORNL, December 30, 1963, Oak Ridge, Tennessee.

Calculation of Maximum Permissible Flux for Fast and Thermal Neutrons, ORSORT, ORNL, January 3 and 6, 1964, Oak Ridge, Tennessee.

Interaction of Radiation with Matter, AEC Fellowship Course in Health Physics, University of Tennessee, January 8, 10, 15, 17, and 20, 1964, Knoxville.

Radiation Shielding, AEC Fellowship Course in Health Physics, University of Tennessee, May 1, 6, and 8, 1964, Knoxville.

Gamma-Ray Scattering, AEC Fellowship Course in Health Physics, University of Tennessee, May 13 and 15, 1964, Knoxville.

Radiation Sources, AEC Fellowship Course in Health Physics, University of Tennessee, May 20 and 22, 1964, Knoxville.

Calculation of Maximum Permissible Flux for Fast and Thermal Neutrons, AEC Fellowship Course in Health Physics, University of Tennessee, May 27 and 29, 1964, Knoxville.

Interaction of Radiation with Matter, AEC Fellowship Course in Health Physics, Vanderbilt University, February 3, 4, 10, and 11, 1964, Nashville, Tennessee.

Radiation Shielding, AEC Fellowship Course in Health Physics, Vanderbilt University, March 30 and April 1 and 6, 1964, Nashville, Tennessee.

Gamma-Ray Scattering, AEC Fellowship Course in Health Physics, Vanderbilt University, April 7, 1964, Nashville, Tennessee.

Radiation Sources, AEC Fellowship Course in Health Physics, Vanderbilt University, April 13, 1964, Nashville, Tennessee.

Calculation of Maximum Permissible Flux for Fast and Thermal Neutrons, AEC Fellowship Course in Health Physics, Vanderbilt University, April 14, 1964, Nashville, Tennessee.

H. H. Hubbell, Jr.

Radiological Units, Quantities, and Symbols, ORSORT, ORNL, November 13, 15, and 18, 1963, Oak Ridge, Tennessee.

Principles of Radiation Instrumentation, ORSORT, ORNL, November 20, 22, and 27, 1963, Oak Ridge, Tennessee.

Health Physics Instrumentation, ORSORT, ORNL, November 29 and December 2 and 4, 1963, Oak Ridge, Tennessee.

Radiological Units, Quantities, and Symbols, AEC Fellowship Course in Health Physics, University of Tennessee, January 29 and 31 and February 5, 1964, Knoxville.

Principles of Radiation Instrumentation, AEC Fellowship Course in Health Physics, University of Tennessee, February 7, 12, 14, and 19, 1964, Knoxville.

Health Physics Instrumentation, AEC Fellowship Course in Health Physics, University of Tennessee, February 21, 26, and 28, 1964, Knoxville.

Radiological Units, Quantities, and Symbols, AEC Fellowship Course in Health Physics, Vanderbilt University, February 17 and 18, 1964, Nashville, Tennessee.

Principles of Radiation Instrumentation, AEC Fellowship Course in Health Physics, Vanderbilt University, April 20, 21, 27, and 28, 1964, Nashville, Tennessee.

Statistics of Counting, AEC Fellowship Course in Health Physics, Vanderbilt University, May 4, 1964, Nashville, Tennessee.

Health Physics Instrumentation, AEC Fellowship Course in Health Physics, Vanderbilt University, May 5 and 11, 1964, Nashville, Tennessee.

Introduction to Health Physics, AEC Fellowship Course in Health Physics, ORNL, June 23, 1964, Oak Ridge, Tennessee.

Summary of Radiation Physics, AEC Fellowship Course in Health Physics, ORNL, June 23, 1964, Oak Ridge, Tennessee.

D. G. Jacobs

Radioisotopes in Soil-Plant Relations, ORINS Summer Institute in Radioecology, June 10–July 26, 1963, Oak Ridge, Tennessee.

Movement of Fission Products Through Soil and Rock, Fifth and Sixth Naval District Research Reserve group, Oak Ridge High School, September 18, 1963, Oak Ridge, Tennessee.

T. F. Lomenick

Disposal of Radioactive Wastes, USAEC-Sponsored 10-Week Course in Health Physics, ORINS, October 16, 1963, Oak Ridge, Tennessee.

Waste Disposal Activities, University of North Carolina School of Public Health Students, ORNL, September 4, 1963, Oak Ridge, Tennessee.

Radioactive Waste Disposal, 14th Annual Nuclear Science Seminar, Office of Naval Research, Department of the Navy, Washington, D.C., December 13, 1963, Oak Ridge, Tennessee.

Waste Management at ORNL, U.S. Public Health Service, Robert A. Taft Sanitary Engineering Center, Course on Reactor Safety and Hazards Evaluation, ORNL, March 17, 1964, Oak Ridge, Tennessee.

Waste Disposal Practices at Oak Ridge, ASEE-AEC Summer Institute at ORNL, August 16, 1963, Oak Ridge, Tennessee.

K. Z. Morgan

Future Progress in Studies of the Effects of Radiation on Man, ASEE-AEC Summer Institute, ORNL, August 12, 1963, Oak Ridge, Tennessee.

Internal Exposure Dose, AEC 10-Week Course, October 31, 1963, Oak Ridge, Tennessee.

Maximum Permissible Exposure to Ionizing Radiation, November 22, 1963, University of Miami, Coral Gables, Florida; 4th Ann. Space Technol. Seminar, November 26, 1963, Cape Canaveral, Florida.

Health Physics, ORSORT, December 11, 13, 16, 18, and 20, 1963; Navy Nuclear Sciences Seminar, ORINS, Dec. 12, 1963, Oak Ridge, Tennessee.

Maximum Permissible Exposure to Ionizing Radiation, Roanoke College, December 13, 1963, Salem, Virginia.

Health Physics, ORSORT, Jan. 8, 10, 13, 15, and 17, 1964, Oak Ridge, Tennessee; AEC Fellowship Students, Vanderbilt University, March 2–3, 1964, Nashville, Tennessee.

General Scope of Health Physics, Naval Reserve Research Company, March 2, 1964, Nashville, Tennessee.

Health Physics, AEC Fellowship Students, Vanderbilt University, March 2–3 and 9–10, 1964, Nashville, Tennessee.

Research Programs in Health Physics, Knoxville College, March 24, 1964, Knoxville, Tennessee.

K. Z. Morgan

Health Physics, University of Tennessee Health Physics Course, March 25, 1964; April 1, 3, 8, 10, 17, and 22, 1964, Knoxville, Tennessee.

Radiation Protection Criteria: ICRP, NCRP, and FRC, Health Physics Certification Course, ORINS, April 14, 1964, Oak Ridge, Tennessee.

Permissible Dose for Internal Radiation, Refresher Course, AIHA, April 27–29, 1964, Philadelphia, Pennsylvania.

Maximum Permissible Exposure to Ionizing Radiation, University of Ohio, May 14, 1964, Athens.

Permissible Allowable Exposure, Radiation Safety Training Program, ORNL, May 25, 1964, Oak Ridge, Tennessee.

D. J. Nelson

Uptake of Radionuclides by Aquatic Organisms and Distribution of Radionuclides in the Aquatic Environment, Robert A. Taft Sanitary Engineering Center, September 27, 1963, Cincinnati, Ohio.

Strontium, Strontium-90, and Calcium Relationships in Environmental Samples, Radiation Ecology Institute, Savannah River Plant, November 25, 1963, Aiken, South Carolina.

Interpretation of Radioisotope Tracer Studies Using Specific Activities and Biological Half-Lives, University of Georgia, November 26, 1963, Athens; Texas College of Arts and Industries, January 13, 1964, Kingsville, Texas.

Strontium, Strontium-90 and Calcium Relationships in Fresh-Water Mollusks, St. Louis University, December 6, 1963, St. Louis, Missouri; Institute of Marine Science, University of Miami, January 8, 1964, Coral Gables, Florida; School of Medicine, University of Miami, January 8, 1964, Coral Gables, Florida; Oklahoma State University, February 6, 1964, Stillwater.

The Inorganic Chemistry of Life, Spring Hill College, January 12, 1964, Mobile, Alabama; School of Medicine, University of Miami, January 9, 1964, Coral Gables, Florida; University of Missouri, February 6, 1964, Kansas City.

F. L. Parker

The Practice and Economics of Waste Disposal, Long-Range Planning Group, Reactor Division, ORNL, October 18, 1963, Oak Ridge, Tennessee.

Radioactive Waste Disposal, University of North Carolina School of Public Health Students, ORNL, September 4, 1963, Oak Ridge, Tennessee.

Radioactive Waste Disposal, U.S. Army Nuclear Science Seminar, ORINS, August 20, 1963, Oak Ridge, Tennessee.

Radioactive Waste Disposal, ASEE-AEC Summer Institute at ORNL, August 16, 1963, Oak Ridge, Tennessee.

Radioactive Wastes in River Systems, Gordon Research Conference: Environmental Science – Microchemical Contaminants in Water, June 17, 1964, New Hampton, New Hampshire.

Clinch River Studies, Civil Engineering Department, Harvard University, February 24, 1964, Cambridge, Massachusetts.

Clinch River Studies, Civil Engineering Department, Cornell University, February 25, 1964, Ithaca, New York.

B. C. Patten

Dynamics of Plankton Biomass and Diversity and Productivity in Plankton in Course, Biology of Plankton, at the University of Wisconsin, May 18–22, 1964, Madison.

The Adaptive Significance of Diversity-Productivity Relationships in an Estuarine Phytoplankton Community, in Zoology Colloquium at the University of Wisconsin, May 18–22, 1964, Madison.

Ecological Models: The Behavior of Coupled Exponential Systems, Radiation Ecology Institute, ORINS, June 9, 1964, Oak Ridge, Tennessee.

R. H. Ritchie

Theoretical Studies, AEC Fellowship Course in Health Physics, ORNL, June 23, 1964, Oak Ridge, Tennessee.

W. S. Snyder

Maximum Permissible Exposure for Fast and Thermal Neutrons, Health Physics Course, ORINS, October 18, 1963, Oak Ridge, Tennessee.

International Commission on Radiological Protection, National Committee on Radiation Protection, and the Federal Radiation Council, Health Physics Course, ORINS, November 19, 1963, Oak Ridge, Tennessee.

Estimation of Human Exposure to Neutrons or to Ingested Radionuclides in Accordance with Criteria of ICRP, UT-AEC Agricultural Research Laboratory, March 25, 1964, Oak Ridge, Tennessee.

Internal Dosimetry, Standard Man, Bioassay, and Whole Body Counting, Health Physics Certification Course, ORINS, June 2, 1964, Oak Ridge, Tennessee.

E. G. Struxness

Radioactive Waste Disposal, ORSORT, January 20 and 22, 1964, Oak Ridge, Tennessee.

Radioactive Waste Disposal, University of Tennessee, March 4 and 6, 1964, Knoxville.

Radioactive Waste Disposal, Vanderbilt University, March 23 and 24, 1964, Nashville, Tennessee.

Hydro-Fracturing Experiment for Disposal of Radioactive Waste, Course in Applied Health Physics, sponsored by AEC and ORINS, ORNL, June 9, 1964, Oak Ridge, Tennessee.

Radiation Waste Disposal, Summer Institute in Radioecology, ORINS, June 15, 1964, Oak Ridge, Tennessee.

Tsuneo Tamura

Clay Minerals in Waste Disposal, Conference on Water, Geology and the Future, University of Indiana, April 27, 1964, Bloomington.

Radioactive Waste Disposal Problems, University of Illinois, Geology Department, April 28, 1964, Urbana.

Selective Removal of ^{137}Cs and ^{90}Sr by Minerals, ACS Symposium, April 24, 1964, Philadelphia, Pennsylvania.

J. P. Witherspoon, Jr.

Cycling of ^{134}Cs in Forest, Radiation Ecology Institute, ORINS, July 1964, Oak Ridge, Tennessee.

Forest Studies at ORNL, Southern Trip of Syracuse University School of Forestry Seminar, August 26, 1963, Oak Ridge, Tennessee.

Plant Ecology at ORNL, Plant Ecology Class, University of Tennessee, October 6, 1963, Knoxville.

Forestry Studies at ORNL, Technical Committee of Southern Regional Foresters, S-26 Project, December 4, 1963, Oak Ridge, Tennessee.

Ecology and the Atomic Age, Biology Department, Tennessee Polytechnic Institute, May 5, 1964, Cookeville, Tennessee.

Radiation Ecology at ORNL, Health Physics Fellows, AEC Fellowship Program, June 23, 1964, Oak Ridge, Tennessee.

Martin Witkamp

Landscape Studies Using Radioactive Tracers: II. Behavior of Cesium-137 in the Floor of a Tulip Poplar Forest, 14th Annual AIBS Meeting, August 27, 1963, Amherst, Massachusetts.

ORNL-3697
UC-41 - Health and Safety
TID-4500 (34th ed.)

INTERNAL DISTRIBUTION

1. Biology Library
2. Reactor Division Library
- 3-5. Central Research Library
6. Laboratory Shift Supervisor
- 7-8. ORNL - Y-12 Technical Library,
Document Reference Section
- 9-59. Laboratory Records Department
60. Laboratory Records, ORNL R.C.
61. S. I. Auerbach
62. J. A. Auxier
63. S. E. Beall
64. S. R. Bernard
65. R. D. Birkhoff
66. W. J. Boegly
67. T. H. J. Burnett
68. R. L. Clark
69. W. E. Cohn
70. M. J. Cook
71. F. L. Culler
72. D. M. Davis
73. L. C. Emerson
74. B. R. Fish
75. J. L. Gabbard
76. J. H. Gillette
77. C. S. Harrill
78. J. A. Harter
79. A. Hollaender
80. L. B. Holland
81. A. S. Householder
82. G. S. Hurst
83. L. C. Johnson
84. W. H. Jordan
85. M. T. Kelley
86. J. A. Lane
87. C. E. Larson
88. T. A. Lincoln
89. S. C. Lind
90. R. S. Livingston
91. F. C. Maienschein
92. A. J. Miller
93. K. Z. Morgan
94. M. L. Nelson
95. J. S. Olson
96. F. L. Parker
- 97-98. R. B. Parker
99. R. W. Peelle
100. H. P. Raen
101. M. L. Randolph
102. R. M. Richardson
103. H. E. Seagren
104. M. J. Skinner
105. W. S. Snyder
106. E. G. Struxness
107. C. D. Susano
108. J. A. Swartout
109. N. Tarr
110. E. H. Taylor
111. O. D. Teague
112. A. C. Upton
113. A. D. Warden
114. A. M. Weinberg
115. G. C. Williams
116. G. Young
117. R. J. Morton (consultant)
118. T. E. Bortner (consultant)
119. P. H. Doyle (consultant)
120. U. Fano (consultant)
121. T. D. Strickler (consultant)
122. J. C. Frye (consultant)
123. J. B. Hursh (consultant)
124. J. L. Magee (consultant)
125. E. P. Odum (consultant)
126. H. O. Wyckoff (consultant)

EXTERNAL DISTRIBUTION

127. R. W. McNamee, Union Carbide Corporation, New York
128. Physics and Engineering Group, Balcones Research Center, RFD 4, Box 189, Austin, Texas
129. G. E. Thoma, St. Louis University Hospital, 135 South Grand Boulevard, St. Louis, Missouri
130. Vanderbilt University (Physics Library)
131. Paul Jones, U.S. Geological Survey, Washington, D.C.
132. Lola Lyons, Librarian, Olin Industries, Inc., East Alton, Illinois
133. Jack Story, Health Physicist, North Carolina State College, Raleigh, North Carolina
134. J. H. Ebersole, USS Nautilus, c/o Fleet Post Office, New York, New York
135. W. L. Templeton, Health and Safety Division, U.K. Atomic Energy Authority, Seascale, Cumberland, England
136. David S. Smith, Health and Safety Division, U.S. Atomic Energy Commission, Chicago Operations Office, P.O. Box 59, Lemont, Illinois
137. Research and Development Division, AEC, ORO
138. S. C. Sigoloff, Edgerton, Germeshausen and Grier, Inc., P.O. Box 98, Goleta, California
139. Robert Wood, Department of Physics, Memorial Center, 444 E. 68th St., New York 21, New York
140. John Wolfe, Division of Biology and Medicine, U.S. Atomic Energy Commission, Washington, D.C.
141. Orlando Park, Department of Biology, Northwestern University, Evanston, Illinois
142. W. T. Ham, Medical College of Virginia, Richmond, Virginia
143. F. H. W. Noll, Department of Physics, Berea College, Berea, Kentucky
144. Herbert E. Stokinger, Bureau of State Service, Department of Health, Education and Welfare, Penn 14 Broadway, Cincinnati 2, Ohio
145. J. B. Lackey, University of Florida, Gainesville, Florida
146. J. J. Davis, Biology Operation, Hanford Atomic Power Operations, Seattle, Washington
147. Robert B. Platt, Department of Biology, Emory University, Atlanta, Georgia
148. C. H. Bernard, Physics Department, Texas A&M, College Station, Texas
149. C. E. Dady, Watertown Arsenal, Ordnance Material Research Office, Watertown, Massachusetts
150. John I. Hopkins, Davidson College, Department of Physics, P.O. Box 327, Davidson, North Carolina
151. W. J. Lacy, Office of Civil Defense, Pentagon, Washington, D.C.
152. G. A. Andrews, Oak Ridge Institute of Nuclear Studies, Oak Ridge, Tennessee
153. E. P. Resner, States Marine Lines, c/o New York Shipbuilding Corp., Camden, New Jersey
- 154-158. Walter Belter, Division of Reactor Development, AEC, Washington, D.C.
159. H. J. Carey, Jr., The Carey Salt Company, Hutchinson, Kansas
160. C. Orr, Georgia Institute of Technology, Atlanta, Georgia
161. E. F. Gloyna, Department of Civil Engineering, University of Texas, Austin 12, Texas
162. J. S. Cragwall, Jr., U.S. Geological Survey, Surface Water Branch, 823 Edney Building, Chattanooga, Tennessee
163. H. H. Waesche, AEC Liaison Officer, Geochemical and Petrology Branch, U.S. Geological Survey, Naval Gun Factory, Building 213, Washington 25, D.C.
164. S. Leary Jones, Tennessee Department of Public Health, Cordell Hull Building, Nashville, Tennessee
165. H. C. Thomas, Chemistry Department, University of North Carolina, Chapel Hill, North Carolina
166. Glenn Gentry, Fish Management Division, Game and Fish Commission, Cordell Hull Building, Nashville, Tennessee
167. Vincent Schultz, Environmental Sciences Branch, Division of Biology and Medicine, U.S. Atomic Energy Commission, Washington 25, D.C.
168. O. W. Kochtitzky, Tennessee Valley Authority, 717 Edney Building, Chattanooga, Tennessee
169. Leslie Silverman, Industrial Engineering, Department of Industrial Hygiene, School of Public Health, Harvard University, 55 Shattuck Street, Boston 15, Massachusetts

170. J. Wade Watkins, U.S. Bureau of Mines, Washington, D.C.
171. Kansas State Board of Health, Topeka, Kansas (Lee Mayes)
172. Kansas State Geological Survey, Lawrence, Kansas (Frank Foley)
173. Linn Hoover, Executive Secretary, Division of Earth Sciences, National Academy of Sciences—National Research Council, Washington, D.C.
174. C. S. Shoup, Biology Division, U.S. Atomic Energy Commission, Oak Ridge, Tennessee
175. L. Garcia, Naval Research Laboratory, Washington, D.C.
176. J. A. Lieberman, Division of Reactor Development, AEC, Washington, D.C.
177. Conrad Straub, Robert A. Taft Sanitary Engineering Center, Cincinnati, Ohio
178. M. Vidmar, Boris Kidric Institute, Vinča, Yugoslavia
179. Warren J. Kaufman, University of California, Berkeley, California
180. Sakai Shimizu, Institute for Chemical Research, Kyoto University, Kyoto, Japan
181. Toshio Aoki, J. A. E. R. I., Tokai-Mura, Naka-Gun, Ibaraki-Ken, Japan
182. K. A. Mahmoud, Radiation Protection and Civil Defense Department, Atomic Energy Establishment, Abou-Zaabal Post Office, Cairo, U.A.R. (Egypt)
- 183-868. Given distribution as shown in TID-4500 (34th ed.) under Health and Safety category (100 copies - CFSTI)